# UNIVERSIDAD COMPLUTENSE DE MADRID

FACULTAD DE CIENCIAS QUÍMICAS
Departamento de Química Orgánica I

# TESIS DOCTORAL

## Nuevos sistemas de colorantes orgánicos para aplicaciones láser y biofotónicas

MEMORIA PARA OPTAR AL GRADO DE DOCTOR

PRESENTADA POR

**Gonzalo Durán Sampedro**

Directores

Inmaculada García-Moreno Gonzalo
Mª Josefa Ortiz García
Antonia Rodríguez Agarrabeitia

**Madrid, 2015**

© **Gonzalo Durán Sampedro, 2015**

**UNIVERSIDAD COMPLUTENSE DE MADRID**
**FACULTAD DE CIENCIAS QUÍMICAS**
**DEPARTAMENTO DE QUÍMICA ORGÁNICA I**

# *NUEVOS SISTEMAS DE COLORANTES ORGÁNICOS PARA APLICACIONES LÁSER Y BIOFOTÓNICAS*

Memoria presentada por

**GONZALO DURÁN SAMPEDRO**

Para optar al grado de Doctor en Ciencias Químicas

**Directores:**

**Prof. Inmaculada García-Moreno Gonzalo**

**Prof. Dra. Mª Josefa Ortiz García**

**Prof. Dra. Antonia Rodríguez Agarrabeitia**

**Madrid, 2015**

*“La locura es hacer una y otra vez la misma cosa*
*esperando diferentes resultados”*

*“Quien nunca ha cometido un error*
*nunca ha probado nada nuevo”*

Albert Einstein

# ÍNDICE

# ABREVIATURAS Y ACRÓNIMOS

**AcOEt:** Acetato de etilo

**AcOH:** Ácido acético

**BLA:** Alternancia en las longitudes de enlace ("*Bond Length Alternation*")

**BODIPY:** 4,4-Difluoro-4-bora-3a,4a-diaza-*s*-indaceno

**CuTc:** Tiofencarboxilato de cobre

**DCE:** 1,2-Dicloroetano

**DCM:** Diclorometano

**DDQ:** 2,3 diciano-5,6- Dicloro-1,4-benzoquinona

**DEA:** *N*,*N*-Dietilamina

**DIPA:** Diisopropilamina

**DME:** Dimetoxietano

**DMF:** *N*,*N*-Dimetilformamida

**DMSO:** Dimetilsulfóxido

**$\Delta\upsilon_{St}$:** Desplazamiento de Stokes

**EET:** Transferencia de energía de excitación ("*Excitation Energy Transfer*")

**$\varepsilon_{max}$:** Coeficiente de extinción molar

**equiv:** Equivalentes

| | |
|---|---|
| **EtOH:** | Etanol |
| **$\phi_\Delta$:** | Rendimiento de generación de oxígeno singlete |
| **FRET:** | Transferencia de energía Förster "*Förster Resonance Energy Transfer"* |
| **HMBC:** | "*Heteronuclear Multiple Bond Correlation experiment"* |
| **HOMO:** | Orbital ocupado de mayor energía ("*Highest Ocuppied Molecular Orbital*") |
| **HRMS:** | Espectroscopía de alta resolución (*"High Resolution Mass Spectroscopy"*) |
| **ISC:** | Cruce entre sistemas ("*Intersystem crossing")* |
| **ICT** | Transferencia de carga ("*Intersystmen charge transfer*") |
| **$k_{fl}$:** | Constante de desactivación radiativa |
| **$\lambda_{abs}$:** | Longitud de onda en el máximo de absorbancia |
| **$\lambda_{exc}$:** | Longitud de onda de excitación |
| **$\lambda_{fl}$:** | Longitud de onda en el máximo de fluorescencia |
| **$\lambda_{láser}$:** | Longitud de onda de emisión láser |
| **LUMO:** | Orbital vacío de menor energía ("*Lowest Unocuppied Molecular Orbital*") |
| **MeOH:** | Metanol |
| **MW:** | Radiación microondas ("*micro-wave*") |
| **NBS:** | *N*-Bromosuccinimida |
| **NCS:** | *N*-Clorosuccinimida |
| **NIS** | *N*-Yodosuccinimida |
| **$^1O_2$:** | Oxígeno singlete |

| | |
|---|---|
| **OLED:** | Diodo orgánico emisor de luz ("*Organic Light-Emitting Diode*") |
| **PTCDA** | Perilentetracarboxidianhidrido |
| **PDI:** | Perilendiimida |
| **PET:** | Transferencia electrónica fotoinducida ("*Photoinduced Electron Transfer*") |
| **PMMA:** | Polimetacrilato de metilo |
| **PN:** | Fenalenona |
| **RB:** | Rosa de bengala |
| **$S_EAr$:** | Sustitución electrófila aromática |
| **Selectfluor™:** | Bis(tetrafluoroborato) de 1-clorometil-4-fluoro-1,4-diazobisciclo[2,2,2]octano |
| **$S_nAr$:** | Sustitución nucleófila aromática |
| **$S_0$:** | Estado energético fundamental singlete |
| **$S_1$:** | Estado energético excitado singlete |
| **TBET:** | Transferencia de energía a través de enlace ("*Through-Bond Energy Transfer*") |
| **TFA:** | Ácido trifluoroacético ("*Trifluoroacetic acid*") |
| **TFD:** | Terapia fotodinámica |
| **TFP:** | Trifurilfosfina |
| **THF:** | Tetrahidrofurano |
| **TMS:** | Tetrametilsilano |
| **TMSCl:** | Cloruro de trimetilsilano |
| **TMSCN:** | Cianuro de trimetilsilano |

| | |
|---|---|
| **TMSOAc:** | Acetato de trimetilsilano |
| **t. a.:** | Temperatura ambiente |
| **UV:** | Ultravioleta |
| **UV-Vis** | Ultravioleta-Visible |
| **u. a.:** | Unidades arbitrarias |

# RESUMEN

La presente Tesis Doctoral titulada "***NUEVOS COLORANTES ORGÁNICOS PARA APLICACIONES LÁSER Y BIOFOTÓNICAS***" está dirigida al diseño y síntesis de nuevos colorantes orgánicos, principalmente BODIPYs, con propiedades fotofísicas optimizadas para la generación de emisión láser altamente estable y eficiente.

Los 4,4-difluoro-4-bora-3a,4a-diaza-*s*-indacenos o complejos dipirrometano·$BF_2$, conocidos comercialmente como BODIPYs, constituyen un área de investigación emergente, que ha experimentado un desarrollo exponencial en las dos últimas décadas debido a su versatilidad química, sus buenas y fácilmente modulables propiedades fotofísicas y a sus numerosas e importantes aplicaciones, dentro de las cuales se enmarca el objetivo principal de esta Tesis Doctoral.

La Memoria consta de una introducción general y un breve resumen de los antecedentes más relevantes relacionados con los objetivos de la misma. Seguidamente, se recogen los aspectos claves planteados en este trabajo para conseguir dichos objetivos, así como la estructura de la Memoria y las técnicas empleadas para su desarrollo.

A continuación, se divide la Tesis en cinco capítulos, recogiéndose en los cuatro primeros una serie de artículos publicados sobre los resultados obtenidos agrupados según su temática, y en el cuarto también se recoge parte del trabajo de investigación pendiente de publicación. Finalmente, en el quinto capítulo de la Tesis se resume el trabajo desarrollado en la estancia pre-doctoral realizada en la Universidad de Guanajuato, México, bajo la dirección del Prof. Peña-Cabrera.

El Capítulo 1 consiste en una recopilación de tres artículos en los cuales se describe el diseño y síntesis de una serie de nuevos colorantes halogenados y la evaluación de sus propiedades fotofísicas y de sus aplicaciones. A través de reacciones de sustitución electrófila aromática en diferentes cromóforos comerciales (BODIPYs, perilenos, cumarinas y rodaminas) se han logrado obtener nuevos colorantes fluorados que presentan mayor fotoestabilidad y mejor emisión láser

que sus precursores no fluorados. En los otros dos artículos se detalla la halogenación selectiva de BODIPYs, para obtener cloro- y yodo-BODIPYs mono-, di- y polihalogenados. Este estudio demuestra que estos derivados, además de ser versátiles precursores sintéticos, han resultado ser eficientes láseres de colorante (derivados clorados) o excelentes generadores de oxígeno singlete (derivados yodados), lo que abre la posibilidad de que sean usados como sensibilizadores en terapia fotodinámica.

En el Capítulo 2 se detalla la síntesis de tres nuevos colorantes BODIPY, obtenidos por reacciones de acoplamiento C-C y reacciones de Knoevenagel, con emisión en la zona roja del espectro, por extensión de la conjugación a través de las posiciones 3 y 5. Estos nuevos cromóforos presentan una emisión láser centrada en torno a 620 nm y una fotoestabilidad superior a la de otros colorantes comerciales con emisión en la misma región espectral.

El Capítulo 3 consta de dos artículos, en los que se aborda la síntesis de nuevos *O*- y *E*-BODIPYs por la introducción de diferentes grupos carboxilatos y acetilenos, respectivamente, en el átomo de boro de una serie colorantes comerciales. De forma general, estos nuevos derivados presentan una fotoestabilidad y emisión láser muy superior a sus precursores, tanto en líquido como incorporados en matrices poliméricas, lo que potencia su uso en diferentes aplicaciones.

En el Capítulo 4 se describe la síntesis de una serie de cassettes con absorción pancromática y alta eficiencia láser, por combinación, en una misma molécula, de varios colorantes orgánicos como perilenos, cumarinas y BODIPYs. De esta forma, se han sintetizado sistemas multicromofóricos que, tras excitación a 355 nm, presentan una mejor fotoestabilidad y emisión láser en la región roja del espectro que algunos colorantes comerciales empleados como referencia en la misma región espectral. Además, la disposición ortogonal entre los fragmentos de BODIPYs que forman uno de los complejos multicromofóricos, permite que dicho sistema presente un comportamiento dual, pudiendo utilizarse como sonda fluorescente y generador de oxígeno singlete.

El trabajo desarrollado tiene un carácter marcadamente multidisciplinar y no hubiera sido posible sin la colaboración de otros grupos de investigación, tanto de nuestra propia Universidad (Prof. Santiago de la Moya Cerero), como de otros centros nacionales (Prof. Iñigo López-Aberloa y Prof. Jorge Bañuelos Prieto de la Universidad del País Vasco, y Dr. José Luis Chiara del CSIC)

e internacionales (Prof. Eduardo Peña-Cabrera de la Universidad de Guanajuato, México, y Prof. Prof. Norman A. García de la Universidad de Rio Cuarto, Argentina).

## SUMMARY

The present Doctoral Thesis entitled as "***NEW ORGANIC DYES FOR LASER AND BIOPHOTONICS APPLICATIONS***" is focused on the development of new compounds' based on BODIPYs crhomophore. Its main objective is the design of new systems with optimized applications for efficient and stable laser emission.

The 4,4,-difluoro-4-bora-3a,4a-diaza-*s*-incadene or dipyrromethene·BF2 complex commercially known as BODIPYs, are an emerging area of research that has increased exponentially over the past two decades, due to its good and easily modulated photophysical properties and their many important applications, in which the goal of this thesis is framed.

The Thesis consists of a general introduction and a brief summary of the most important records that keep a relationship to the purpose of the thesis. The two next chapters expose the objectives to achieve the goals and the structure of the Memory, as the techniques used its development.

In the next four chapters consist of a compilation of eight articles grouped by theme. The first three articles (Chapter 1) are about of direct halogenation of commercial dye. Using direct monofluorination of the most outstanding laser dyes from the blue to the red edge of the visible spectrum (BODIPYs, perylen, coumarins and rhodamines) we synthesized new fluorinated dyes with enhanced phtotostabily and laser efficiencies with respect to their non-fluorinated analogues. In the other two articles was carried out the design and synthesis of a new series of polihalogenated BODIPY (chloride- and iodine-BODIPYs). These new halogenated compounds are excellent synthetic tools or efficient singlet oxygen generators, may be used in Photodynamic Therapy.

Chapter 2 shows the design and synthesis of three new BODIPYs with emission in red region of spectrum by extension conjugation via positions 3 and 5, by Suzuki and Knoevenagel reactions. These new dyes present a laser emission centered around 620 nm and high photostability, superior to other commercial dyes with emission in the same spectral region.

The Chapter 3 consists of two articles, where the synthesis of new *O*- and *E*-BODIPYs addressed by introducing different carboxylate groups and acetylenes, respectively, in the boron atom of commercial dyes. In general, these new derivatives are more efficient and photostable that their commercials analogues, in liquid or incorporated into polymer matrices.

Chapter 4 is about the synthesis of a series of cassettes with panchromatic absorption by linking of different dyes (BODIPYs, coumarins and perylenes). These new dyes exhibit a laser emission centered in red region of spectrum under pumping in the UV (355 nm) or in the Vis (532 nm) spectral region. Furthermore, some of these new systems show a better laser efficiency than other commercial dyes with emission in the same spectral region.

Finally, last chapter we describe the synthesis work carried out during a pre-doctoral stay in the University of Guanajuato, Mexico. This work has focused on obtaining new BODIPY-boron-diketonates and BODIPY-triphenylthiopheneamine systems through the *meso* position of BODIPY, with possible applications as dye lasers or solar cells, respectively.

The work has a distinctly multidisciplinary and would not have been possible without the collaboration of other researches groups, both our own University (Prof. Santiago de la Moya Cerero) and other national centers (Prof. Iñigo López Arbeloa and Prof. Jorge Bañuelos Prieto of UPV), and international centers (Prof. Eduardo Peña Cabrera of the University o Guanajuato Mexico and Prof. Norman A. García of University Rio Cuarto, Argentina).

# INTRODUCCIÓN

# INTRODUCCIÓN

A lo largo de las últimas décadas, los láseres han pasado de ser un tema competitivo de investigación entre grupos científicos especializados, a ser herramientas de trabajo habituales e imprescindibles en un buen número de campos relacionados con la vida cotidiana. Sus aplicaciones son numerosas: se usan en medicina, industria, telecomunicaciones, en el ocio, etc. Atendiendo a su medio activo, los láseres pueden ser de fase gaseosa, de estado sólido y de fase líquida, y es dentro de este últimos grupo donde se encuadran los láseres de colorante, objeto de estudio de la presente Memoria.

## Emisión láser

El término láser proviene del acrónimo inglés "*Light Amplification by Stimulated Emission of Radiation*", es decir, amplificación de luz por emisión estimulada de radiación. En la figura 1 se muestran los tres elementos esenciales de un láser. Estos elementos son:

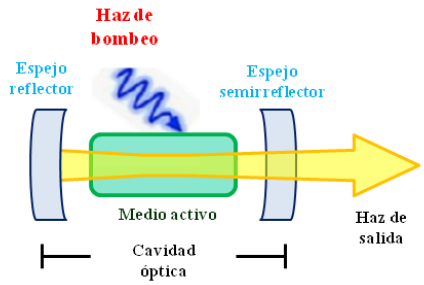


**Figura 1**. Esquema de los elementos que conforman un láser.

- El medio activo, en el que se genera la emisión láser, formado por un conjunto adecuado de moléculas, átomos o iones.

- La fuente de excitación o bombeo.
- La cavidad óptica o resonador, de geometría y dimensiones adecuadas.

Para conseguir emisión láser se necesita, en primer lugar, excitar las especies que forman el medio activo, desde el estado fundamental a otro de mayor energía, mediante la energía suministrada por una fuente de bombeo, consiguiendo así una inversión de población, es decir, que haya más átomos, moléculas o iones en el estado excitado que en el fundamental. Cuando un electrón en uno de estos estados excitados decae espontáneamente al estado fundamental, se emite un fotón. Este puede, por el principio de resonancia, provocar la emisión estimulada de un segundo fotón desde otro estado excitado en el medio. Esta emisión presenta algunas propiedades especiales: los fotones emitidos tienen la misma longitud de onda que el fotón original (monocromaticidad), están en fase con el mismo (coherencia temporal y espacial) y se propagan en la misma dirección.

El medio activo se coloca en una cavidad en cuyos extremos hay espejos paralelos entre sí. Los fotones emitidos en una dirección diferente a la del eje de la cavidad salen del sistema y no participan en la acción láser. Aquellos que se emiten según el eje de la cavidad viajan una y otra vez entre los espejos y estimulan la emisión de más fotones con la misma longitud de onda y la misma fase. Se produce un efecto “cascada” por el cual muchos fotones con la misma longitud de onda y la misma fase se propagan según el eje de la cavidad. Los espejos constituyen por tanto una cavidad óptica resonante, en la cual crece un modo de onda estacionaria. Típicamente, uno de los espejos de la cavidad es parcialmente transparente o posee un pequeño orificio para permitir que parte de la radiación pueda salir de dicha cavidad.

Los láseres de colorante en fase líquida son fuentes de radiación visible, coherente y sintonizable muy atractivas, dadas sus características y propiedades: energías láser habitualmente elevadas, excelente calidad óptica y espacial, sintonizabilidad de la emisión desde el UV hasta el IR con pequeña anchura de banda, posibilidad de generación de pulsos ultracortos por acoplamiento de modos, etc. A pesar de todas estas interesantes características, el uso de estos láseres se ve limitado en la práctica por la dificultad y los

riesgos que entraña trabajar con disoluciones de colorantes en fase líquida: grandes volúmenes de disolventes que pueden ser tóxicos e inflamables, colorantes orgánicos potencialmente peligrosos para la salud, complejidad del sistema y necesidad de personal especializado.[1]

Una alternativa atractiva es utilizar colorantes incorporados a matrices sólidas, lo que permite disponer de láseres que combinan todas las ventajas del estado sólido, manteniendo las ya mencionadas en fase líquida, pero eliminando los inconvenientes. Así, los sistemas en fase sólida son más respetuosos con el medioambiente, significativamente más económicos y tecnológicamente más sencillos, por lo que podrían ser manejados por personal no especializado. Además, su posible compacidad y versatilidad los hacen muy apropiadas para su aplicación en la medicina y la industria.[2]

Durante estos últimos años se han conseguido materiales láser con excelentes características, pero cuya emisión está limitada a la región espectral entre 550 y 600 nm. Para lograr que estos sistemas puedan competir con los actualmente comercializados en fase líquida hay que sintetizar y desarrollar nuevos materiales láser eficientes y estables, extendiendo su emisión a las regiones extremas del visible: 400-550 nm y 600-700 nm.

**Colorantes orgánicos**

Un colorante es un compuesto orgánico que presenta dobles enlaces conjugados en su estructura y recibe su nombre por poseer una intensa banda de absorción en la región visible del espectro, a la que debe su fuerte coloración. Los colorantes empleados como láseres deben presentar una serie de características para un buen funcionamiento:

- Mínimo solapamiento entre las bandas de absorción y emisión.
- Altos rendimientos cuánticos de fluorescencia (0.5-1.0).
- Buena estabilidad química y fotoquímica.
- Baja absorción desde estados excitados.

- Baja probabilidad de cruce intersistemas (ISC).

Los colorantes se agrupan en familias con estructuras químicas similares y pueden clasificarse en función de su estructura como: cumarinas, xantenos, oxacinas, cianinas, hidrocaburos policonjugados y dipirrometenos, entre otras. Todas estas familias de colorantes orgánicos permiten cubrir un rango de emisiones que van desde los 350 hasta los 850 nm, ocupando de esta manera toda la región del espectro visible[3] (Figura 2).

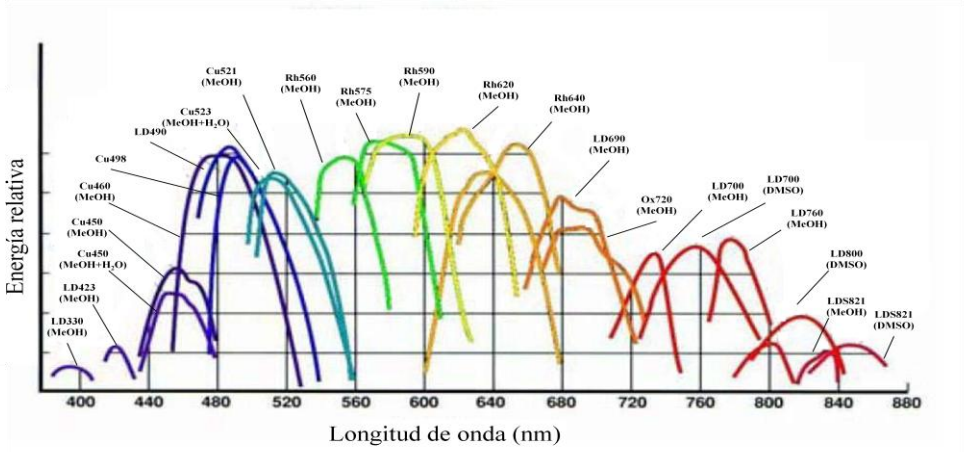


**Figura 2.** Espectro de emisión de varios colorantes láser comerciales

*Cumarinas*

Las cumarinas son benzopironas que se encuentran principalmente en las plantas y aceites esenciales. La molécula de cumarina sin sustituyentes no presenta fluorescencia pero la presencia de grupos electrodadores en la posición 7, tales como hidroxilo, amino o alcoxi, provoca una intensa fluorescencia debido a que sufren un proceso interno de transferencia de carga (ICT) inducido por absorción de luz (efecto "*push-pull*") ( Figura 3).[2,4]

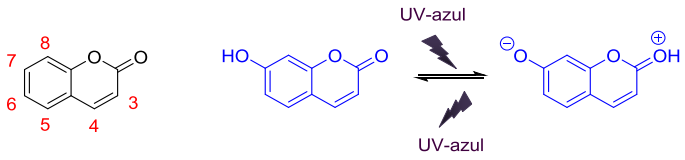


**Figura 3.** Estructuras de las cumarinas.

Sus bandas de absorción y emisión se centran en la región azul-verde del espectro visible (400-540 nm), con rendimientos cuánticos de fluorescencia relativamente altos, por lo que son empleadas para el desarrollo de colorantes láser con emisión en la zona azul del espectro.[3,4] Como desventaja, las cumarinas presentan baja estabilidad química y baja fotoestabilidad ya que sufren una rápida fotodegradación bajo bombeo con luz UV.[4]

*Xantenos*

Desde el punto de vista químico, estos colorantes son derivados de las dibenzo-4*H*-pironas y pueden clasificarse en: (1) tipo rodamina, con grupos amino en las posiciones 2 y 7 del anillo xanténico y (2) tipo fluoresceína, que presentan grupos hidroxilo en esas mismas posiciones (Figura 4).

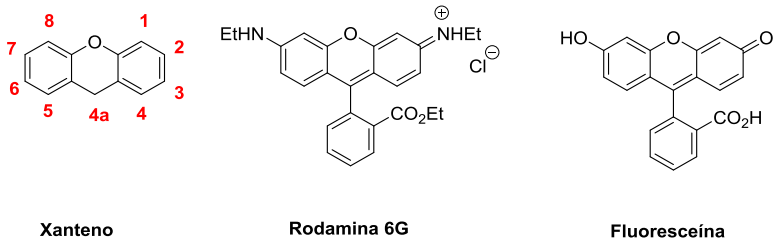


**Figura 4.** Estructuras de la rodamina y fluoresceína.

Sus bandas de absorción y emisión se centran en la región amarillo-roja (550-650 nm) del espectro visible, en función de los sustituyentes que se incorporen a su estructura. Entre ellos destaca la Rodamina 6G (**Rh 6G**), como uno de los colorantes láser más empleados. Se caracterizan por tener elevados rendimientos cuánticos de fluorescencia, bajos rendimientos de ISC, bajas constantes de velocidad de los procesos no radiativos y bajas eficiencias de absorción desde sus estados excitados. Como desventaja, sufren procesos de agregación en concentraciones superiores a $10^{-3}$ M, tanto en disolución acuosa como en disolventes orgánicos.[2c,3,4a]

*Oxacinas*

Las oxacinas presentan una estructura rígida similar a los xantenos, en donde se ha sustituido el átomo de carbono en la posición 4a por un átomo de nitrógeno. Además de ser utilizadas como colorantes láser, también se usan como colorantes textiles. Los colorantes más representativos de la familia de las oxacinas son el Violeta de cresilo y el Azul Nilo (Figura 5).

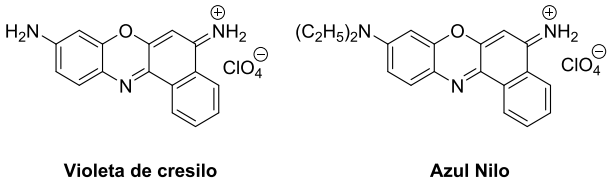


**Figura 5.** Estructuras del Violeta de cresilo y Azul Nilo.

La posición de sus bandas de emisión se centra en la región roja del espectro visible, concretamente entre 650 y 750 nm, presentan bajos rendimientos de fluorescencia, baja absorción a las longitudes de onda habituales de bombeo (355 y 532 nm), baja fotoestabilidad y problemas de solubilidad a altas concentraciones.[3]

*Cianinas*

Los colorantes de la familia de la cianinas presentan en su estructura cadenas de dobles enlaces conjugados con grupos heterocíclicos al final de la cadena hidrocarbonada (Figura 6). Su emisión se localiza en la zona roja-infrarrojo del espectro, presentan bajos rendimientos de fluorescencia, tiempos de vida muy cortos, inferiores en algunos casos al nanosegundo, baja absorción a las longitudes de bombeo habituales (355 y 532 nm), baja fotoestabilidad y baja solubilidad a altas concentraciones.[2c]

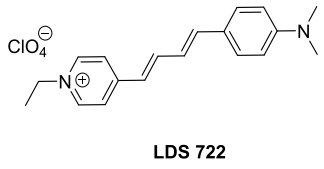


**Figura 6.** Estructura de la cianina LDS 722.

*Hidrocarburos policonjugados*

A esta familia pertenecen los polifenilos y estilbenos, que presentan emisión en la región azul del espectro. Estos colorantes tienen baja solubilidad en los disolventes orgánicos más habituales, en parte debido al apilamiento inducido por la presencia de anillos policonjugados en su estructura.

En este grupo de colorantes también se incluyen los derivados de las perilendicarboxidiimidas (PDI) cuya emisión se encuentra en la zona del naranja-rojo y, al igual que muchos otros colorantes, presentan baja absorción a las longitudes de onda de las radiaciones habituales de bombeo (355 y 532 nm), así como problemas de solubilidad debido al apilamiento de sus anillos aromáticos (Figura 7).[2c,5]

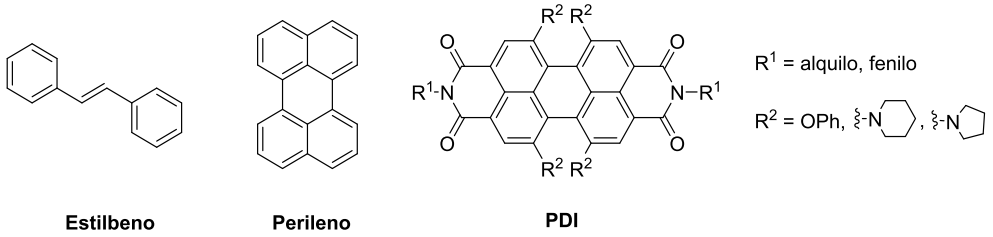


**Figura 7.** Estructuras del perileno, estilbeno y PDI.

*Dipirrometenos*

Los colorantes de la familia de los complejos dipirrometenos·$BF_2$, conocidos comercialmente como BODIPYs, constituyen un importante grupo de colorantes orgánicos debido a sus buenas propiedades fotofísicas y a su elevada versatilidad química, que permite, seleccionando el sustituyente adecuado, cubrir todo el espectro de emisión desde el azul al IR cercano. Esta familia de cromóforos ha solucionado, en parte, algunas de las desventajas y problemas que presentan el resto de los colorantes.[2c,4a,6]

El trabajo desarrollado en esta Memoria se centra fundamentalmente en el diseño, síntesis y caracterización de nuevos colorantes BODIPY con propiedades optimizadas para aplicaciones avanzadas, por lo que, a continuación, se presenta una visión más detallada de estos cromóforos.

## Colorantes BODIPY

Estos compuestos están formados por dos núcleos pirrólicos y un grupo $BF_2$, constituyendo un complejo dipirrometénico·$BF_2$. Su sistema de numeración IUPAC es el que se emplea en los carbociclos análogos (*s*-indaceno), siendo por tanto diferente del utilizado para los dipirrometenos. Sin embargo, los términos α-, β- y *meso*- se utilizan para indicar las mismas posiciones en los núcleos de BODIPY y de dipirrometeno (Figura 8).[6a]

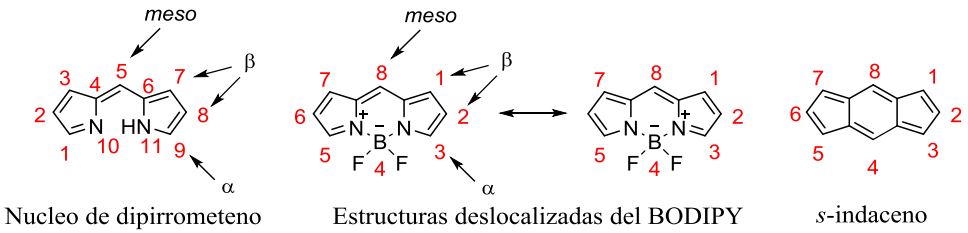


**Figura 8.** Esqueleto de BODIPY.

### *Síntesis de BODIPYs*

Los BODIPYs se describieron por primera vez por Treibs y Kreuzer[7] como resultado inesperado en la reacción del 2,4-dimetilpirrol y el trifluoruro de boroeterato en presencia de anhídrido acético, en un intento de α-acetilar el anillo pirrólico. La reacción dio lugar a los compuestos **I** y **II** a través del correspondiente acetato de 2,2´-dipirrometeno **III** (Esquema 1).

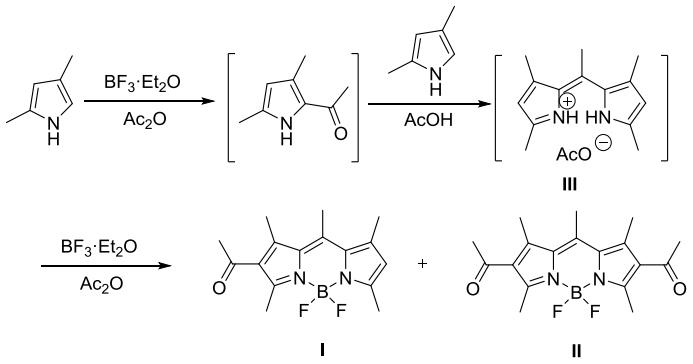


**Esquema 1**

Décadas más tarde (principios de los años 90), estos colorantes se redescubrieron debido a sus altos rendimientos cuánticos de fluorescencia, su alta estabilidad química, buena fotoestabilidad, su eficiente emisión láser en disolución[8] y, sobre todo, a su versatilidad química, que permite modular sus propiedades fotónicas y, por tanto, sus aplicaciones.

La síntesis del BODIPY más sencillo, formado exclusivamente por el esqueleto básico, se realizó a finales de los años setenta,[9] aunque este compuesto no volvió a adquirir interés hasta el año 2009,[10] en el que a través de dos rutas diferentes lo sintetizaron de nuevo dos grupos de investigación. Este BODIPY tan sencillo es un compuesto con una inestabilidad notable, puesto que al carecer de sustituyentes es altamente reactivo.

En general, los colorantes BODIPY son relativamente fáciles de preparar a partir de pirroles comerciales, siguiendo fundamentalmente tres estrategias sintéticas generales:

*A partir de pirroles y aldehídos*

La condensación de aldehídos aromáticos con pirroles, en medio ácido, conduce a un intermedio dipirrometano (**IV**), el cual se utiliza inmediatamente ya que suele ser inestable (sensible a la luz y al aire). Su posterior oxidación conduce a dipirrometenos o dipirrinos (**V**), que por adición sucesiva de una base (normalmente $Et_3N$) y $BF_3{\cdot}Et_2O$ da lugar a los BODIPYs deseados (**VI**). Los agentes oxidantes empleados normalmente son DDQ (2,3-diciano-5,6-dicloro-1,4-benzoquinona) y, para condiciones más suaves, *p*-cloranilo (tetracloro-1,4-benzoquinona) (Esquema 2).[6a] Mediante esta metodología se han preparado BODIPYs simétricos sustituidos en la posición 8.[11]

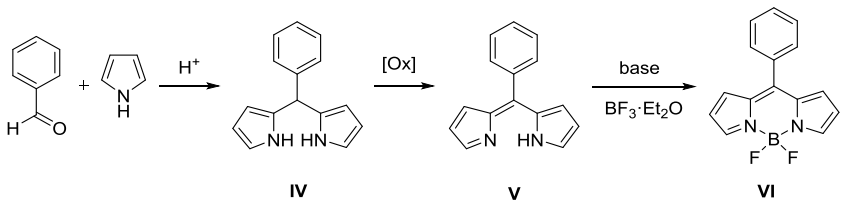


**Esquema 2**

Si se trabaja con pirrol sin sustituir, es necesario utilizar un gran exceso de pirrol (100 equivalentes). Sin embargo, más recientemente, se ha descrito la formación de estos dipirrometanos en medio acuoso ácido, utilizando menor exceso de pirrol que en el caso anterior.[12]

*A partir de pirroles y cloruros de ácido o anhídridos*

La forma más directa de preparar BODIPYs simétricos sustituidos es la condensación entre cloruros de ácido y α-*H* pirroles. Los hidrocloruros de dipirrometeno intermedios (**VII)** se hacen reaccionar *in situ* con $BF_3 \cdot Et_2O$ en presencia de una base, para formar el correspondiente colorante (**VIII**) (Esquema 3).[6a]

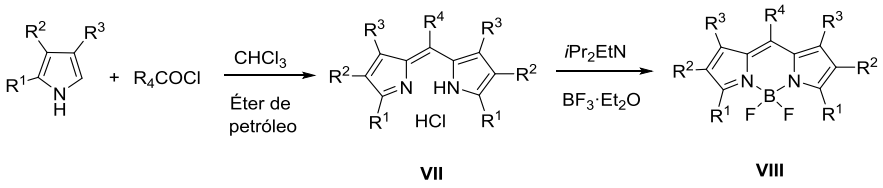


**Esquema 3**

En esta reacción también pueden usarse anhídridos (Esquema 4). Cabe destacar que, en este caso, se obtienen BODIPYs con un grupo carboxilo en posición *meso* (**IX**), que pueden ser utilizados para incorporar el colorante como sonda a una molécula diana.[13]

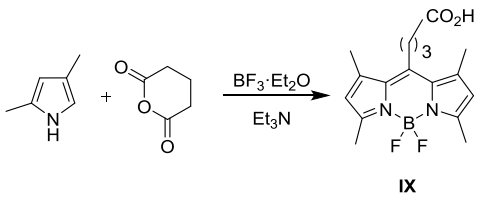


**Esquema 4**

*A partir de cetopirroles*

Este método permite la síntesis de BODIPYs asimétricos, y consiste en la reacción de 2-formilpirrol o un cetopirrol con otro fragmento de pirrol en presencia de un ácido (Esquema 6). Este procedimiento se conoce como acoplamiento de MacDonald, por

analogía con una reacción similar de la química de porfirinas desarrollada por este químico canadiense.[14] Los catalizadores ácidos más comúnmente utilizados en esta condensación son el ácido bromhídrico[15] y oxicloruro de fósforo.[16] Empleando esta metodología, nuestro grupo de investigación ha descrito la síntesis de una serie de BODIPYs asimétricos **(X**) análogos al colorante comercial **PM567** (2,6-dietil-4,4-difluoro-1,3,5,7,8-pentametil-4-bora-3a,4a-diaza-*s*-indaceno) por condensación de 2-acetil-4-etil-3,5-dimetilpirrol y pirroles diferentemente sustituidos en posición α (**XI**) (Esquema 5).[17]

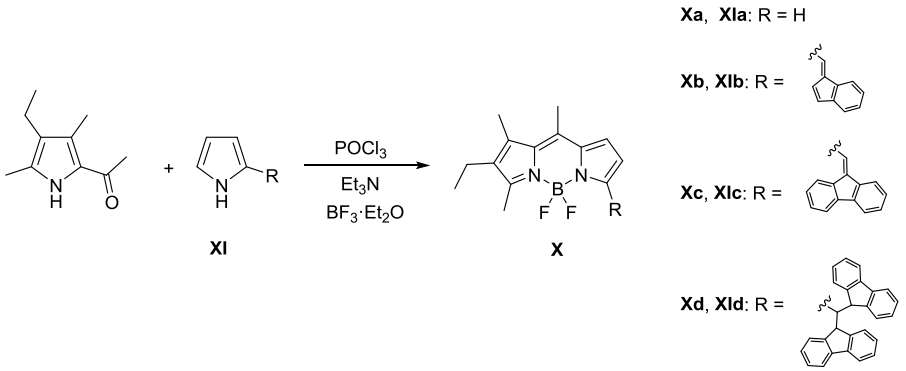


**Esquema 5**

***Funcionalización del núcleo de BODIPY***

Una de las principales razones por las que los BODIPYs han sido objeto de números trabajos de investigación es, sin duda, la versatilidad química del núcleo de BODIPY, que permite su fácil y casi infinita derivatización. La Figura 9 muestra la evolución del número de publicaciones sobre BODIPYs en revistas científicas a lo largo de los últimos 20 años.[18]

A través de reacciones de menor o mayor complejidad, un gran número de grupos funcionales pueden ser introducidos en el núcleo del BODIPY.[6]

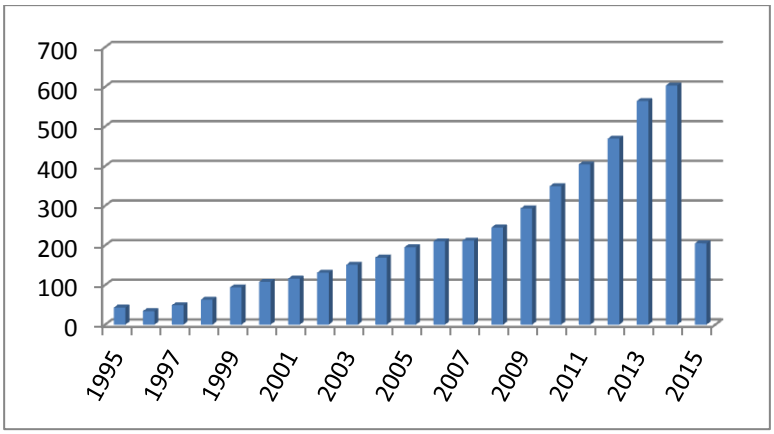


**Figura 9**. Publicaciones relacionadas con síntesis de BODIPYs en los últimos años.

Los estudios descritos en la bibliografía hasta este momento demuestran que estos sistemas son extremadamente reactivos y experimentan distintos tipos de reacciones en todas las posiciones de su núcleo, tal y como se muestra en la Figura 10.[6] Esto permite la post-funcionalización del núcleo de BODIPY, para obtener nuevos fluoróforos de esta familia con propiedades fotofísicas adecuadas para sus diferentes aplicaciones.

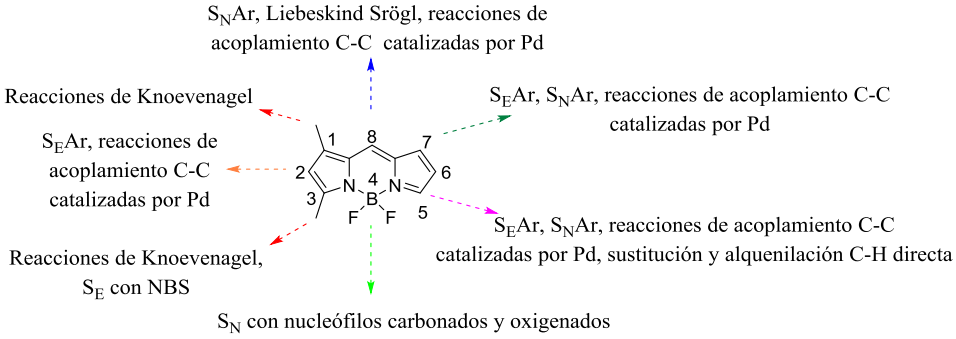


**Figura 10.** Reactividad del núcleo de BODIPY.

Los BODIPYs son compuestos ricos en electrones y experimentan fácilmente diferentes reacciones de sustitución electrófila aromática (halogenación,[19] sulfonación,[20] nitración[8b,21] y formilación[22]), fundamentalmente en las posiciones 2 y 6 del núcleo, aunque, en los últimos años, se han descrito también reacciones de este tipo, principalmente nitración y halogenación, en otras posiciones del BODIPY.[21,23] Los

sistemas halogenados son intermedios versátiles para posteriores transformaciones, experimentando reacciones de sustitución con diferentes tipos de reactivos nucleófilos ($S_NAr$) en las posiciones 1, 3, 5 y 7.[24] Estas reacciones pueden detenerse en la etapa de monosustitución, o bien conducir a productos disustituidos, difíciles de obtener por otras rutas.[24] Además, estos derivados halogenados experimentan también reacciones de acoplamiento C-C catalizadas por paladio (Sonogashira, Suzuki, Stille, Heck,...).[24b, 25]

Una reactividad similar ($S_NAr$ o reacciones de acoplamiento con metales de transición vía reacción Liebeskind-Srögl) ha sido descrita para 8-tiometilBODIPYs, con un grupo tioéter actuando como un pseudohalógeno[26] y, más recientemente, se han empleado 8-haloBODIPYs en este mismo tipo de reacciones.[27] La sustitución de los átomos de flúor por nucleófilos carbonados y oxigenados ha demostrado ser otro método versátil para la introducción de diferente funcionalidad en estos fluoróforos.[28]

Por otra parte, las posiciones 2 y 6 del núcleo del BODIPY son susceptibles de experimentar reacciones de sustitución directa de hidrógeno por grupos alquenilo.[29] Análogamente, BODIPYs sin sustituyentes en las posiciones $\alpha$ de los anillos pirrólicos (posiciones 3 y 5), incorporan en un solo paso diferentes sustituyentes en dichas posiciones a través de una reacción de sustitución nucleófila en condiciones oxidativas (atmósfera de oxígeno).[30] Estas funcionalizaciones directas C-H también pueden llevarse a cabo a través de reacciones de acoplamiento empleando metales de transición.[31]

Además, debido a la acidez de los grupos metilo en posiciones 1, 3, 5 y 7 del esqueleto del colorante, éstos pueden experimentar reacciones de condensación con aldehídos aromáticos a través de reacciones de Knoevenagel, permitiendo la obtención de los correspondientes mono-, di-, tri- y tetraestirilBODIPYs,[32] extendiendo así la conjugación del sistema.

Recientemente, nuestro grupo de investigación ha ampliado esta metodología a los metilos situados en la posición *meso* del BODIPY, obteniendo 8-alquenilderivados de forma selectiva y demostrando que los metilos en esta posición presentan una mayor acidez que los restantes metilos unidos al esqueleto de BODIPY.[33]

***Propiedades espectroscópicas del cromóforo BODIPY***

Los compuestos de la familia de los BODIPYs presentan bandas de absorción y emisión en la zona visible del espectro, tienen altos coeficientes de absorción molar, con valores de entre 40000 y 110000 $M^{-1}\cdot cm^{-1}$, altos rendimientos cuánticos de fluorescencia, a veces cercanos a la unidad, un tiempo de vida de fluorescencia entre 1 y 10 ns, buena estabilidad química y fotoquímica tanto en disolución como en estado sólido, y sus espectros de absorción/emisión son relativamente insensibles al cambio de polaridad y pH del disolvente.[6] El espectro de absorción de estos cromóforos muestra, en general, una banda principal intensa correspondiente a la transición al primer estado excitado ($S_0$-$S_1$), con un hombro asociado a la estructura vibracional. El proceso de emisión de fluorescencia siempre parte de $S_1$ y su espectro es la imagen especular del de absorción, poniendo de manifiesto que las conformaciones de los estados fundamentales ($S_0$) y excitado ($S_1$) son muy similares (Figura 11).

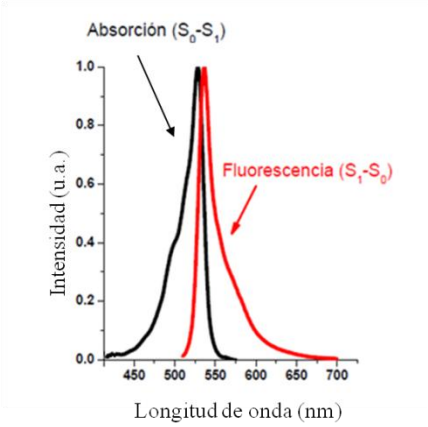


**Figura 11**. Espectro típico de absorción y emisión de un BODIPY.

Los BODIPYs suelen emitir con elevados rendimientos cuánticos de fluorescencia y la excitación del cromóforo BODIPY genera muy poca concentración de estados triplete, aunque en la bibliografía existente varios ejemplos de BODIPYs con un alto ISC debido a la presencia de átomos pesados en su estructura.[34] Una de las características más importantes del cromóforo BODIPY es la modulación de sus propiedades espectroscópicas

modificando el número, posición y estructura de los sustituyentes que se incorporen a su núcleo.

### *Aplicaciones de los BODIPYs*

Desde el redescubrimiento del cromóforo BODIPY a principios de los años 90, el número de aplicaciones de estos colorantes ha aumentado de modo exponencial durante la última década, incluyendo usos tan diferentes como láseres de colorante,[35] marcado fluorescente en moléculas de interés en Biología,[36] sondas de imagen,[37] sensores de cationes metálicos y aniones,[38] sensores de pH y de potenciales redox,[6f, 39] interruptores fluorescentes,[40] células solares,[41] dispositivos electroluminiscentes[42] y terapia fotodinámica (TFD),[34] entre otros. Estos y otros aspectos de estos interesantes fluoróforos están detallados en varias revisiones bibliográficas.[6] A continuación, se muestran algunos ejemplos significativos del uso del cromóforo BODIPY como colorante láser, por ser la aplicación principal de este cromóforo en el trabajo aquí desarrollado.

### *BODIPYs como colorantes láser*

Los cromóforos tipo BODIPY presentan emisión láser, incluso algunos de ellos superior a la de la Rodamina 6G, considerada hasta hace poco como un colorante de referencia.[6e,8,43]

Los primeros trabajos donde se describe el comportamiento láser de los BODIPYs fueron realizados por Boyer y col., que sintetizaron una serie de BODIPYs para estudiar la relación entre su estructura y su emisión láser.[8,43] En este estudio se determinó que la introducción de cadenas alquílicas en las posiciones 2 y 6 del BODIPY producía un desplazamiento de las bandas espectrales hacia mayores longitudes de onda (desplazamiento batocrómico), siendo el compuesto con grupos *terc*butilo el que presenta un mayor desplazamiento. No se observó una clara relación entre los rendimientos cuánticos de fluorescencia y la eficiencia láser, pero se comprobó que la presencia de un átomo de hidrógeno en la posición *meso* producía una drástica disminución de la eficiencia láser.

Muchos de los BODIPYs descritos por Boyer han sido posteriormente comercializados,[44] siendo los más utilizados los que se recogen en la Figura 12. Aunque presentan una buena eficiencia láser y una fotoestabilidad aceptable, su emisión está centrada generalmente en la zona amarilla-naranja (530-595 nm) del espectro visible.

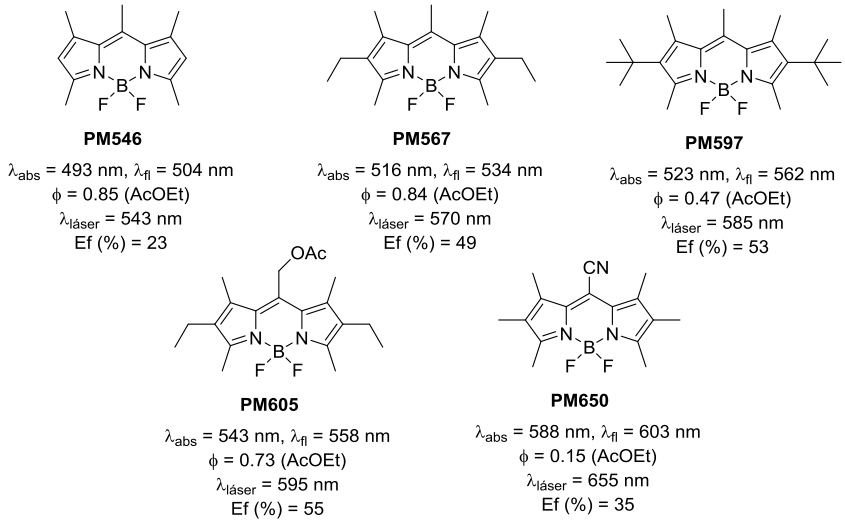


**Figura 12**. Estructuras, propiedades fotofísicas y láser de BODIPYs comerciales.

Nuestro grupo de investigación es, desde finales de los 90, el que ha desarrollado un trabajo más sistemático en este campo. Así, buscando sistemas láser más eficientes y estables, ha estudiado el comportamiento láser, en fase líquida y en matrices sólidas poliméricas, de diversos colorantes de la familia de los BODIPYs, tanto comerciales como BODIPYs modificados sintéticamente (**IX** y **X**). Un ejemplo del trabajo desarrollado se recoge en la Figura 13.[45]

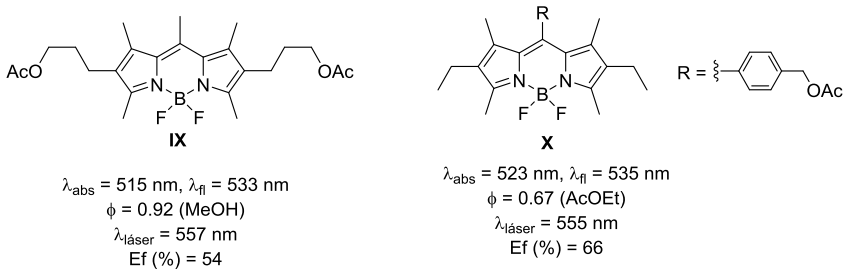


**Figura 13**. Estructuras, propiedades fotofísicas y láser de los BODIPYs **IX** y **X**.

Recientemente, el grupo de investigación del Prof. Peña Cabrera ha desarrollado una metodología para sintetizar una serie de BODIPYs (**XI-XIV**) con emisión láser en la región azul del espectro visible con eficiencias láser entre el 10 y 60%, mediante la introducción de grupos amino en la posición 8 del cromóforo (Figura 14).[26b,46]

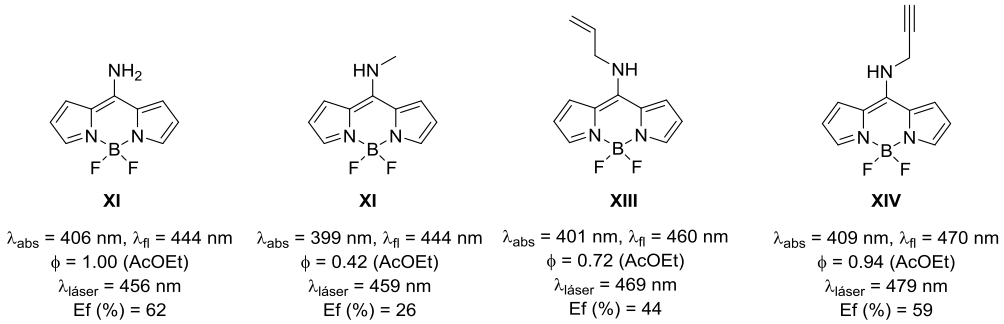


**Figura 14** Estructuras, propiedades fotofísicas y láser de los BODIPYs **XI-XIV**.

Estos nuevos BODIPYs presentan una eficiencia láser mayor y una mejor solubilidad que otros colorantes comerciales con emisión en esta región espectral. Sin embargo, aún presentan una baja fotoestabilidad, similar a la de las cumarinas en las mismas condiciones de bombeo.

Siguiendo esta misma metodología, este grupo de investigación ha obtenido otra serie de nuevos BODIPYs (**XV-XVIII**) con emisión láser desde la región azul hasta la zona naranja del espectro visible (Figura 15).[47]

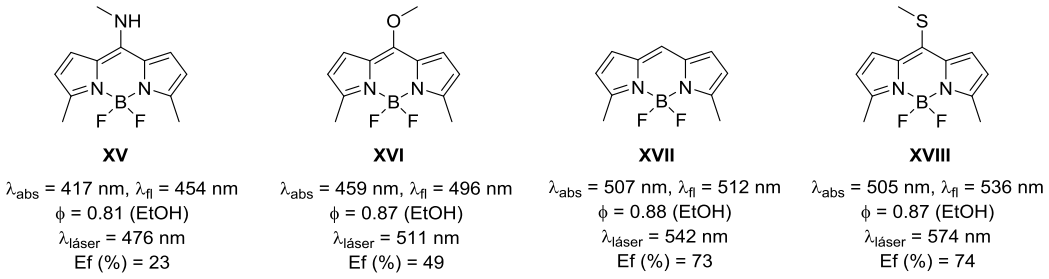


**Figura 15.** Estructuras, propiedades fotofísicas y emisión láser de los BODIPYs **XV-XVIII**.

Por lo que se refiere a la región roja del espectro visible, nuestro grupo ha descrito también BODIPYs con emisión láser en esa zona, sintetizados fundamentalmente a través de reacciones de condensación de Knoevenagel (Figura 16).[48]

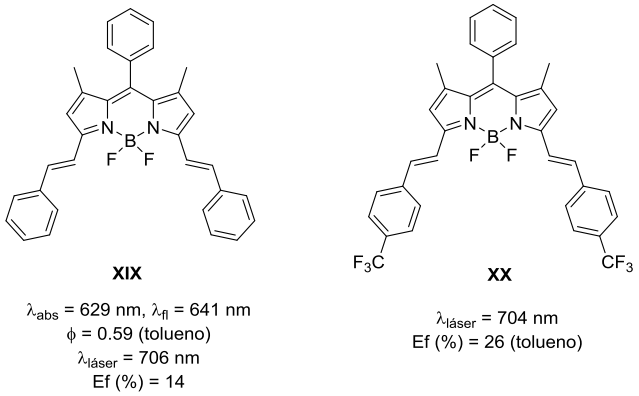


**Figura 16.** Estructuras, propiedades fotofísicas y emisión láser de los BODIPYs **XIX** y **XX**.

En resumen, los trabajos publicados ponen de manifiesto que se pueden conseguir colorantes láser basados en BODIPYs con emisión en toda la zona del espectro visible, sin embargo, es necesario desarrollar nuevos derivados con propiedades optimizadas que mejoren las de los actualmente existentes.

**Bibliografía**


[1] F. J. Duarte, L. W. Hillman, en *Dye Laser Principles* (Ed.: F. J. Duarte), Academic Press, New York, **1990**.

[2] a) A. Costela, I. García-Moreno, R. Sastre, en *Handbook of Advanced Electronic and Photonic Materials and Devices* (Ed.: H. S. Nalwa), Academic Press, **2001**, Vol. 7, Cap. 4, pp. 161-208; b) A. Costela, I. García-Moreno, R. Sastre, en *Tunable Laser Applications*, (Ed.: F. J. Duarte), CRC Press, 2ª Ed., **2009**, pp. 97-120 y 227-244; c) A. Costela, I. García-Moreno, en Ciencia y Sociedad: Aplicaciones recientes de la luz en medicina, mediambiente y nuevos materiales (Eds.: D. Armesto, R. Sastre), Editorial Complutense, **2010**, Cap. 4, pp. 81-174.

[3] G. S. Shankarling, K. J. Jarag, *Resonance*, **2010**, 804-810.

[4] a) F. López Arbeloa, T. López Arbeloa, I. López Arbeloa, en *Handbook of Advanced Electronic and Photonic Materials and Devices* (Ed.: H. S. Nalwa), Academic Press, **2001**, Vol. 7, Cap. 5, pp. 209-245; b) S. R. Trenor, A. R. Shultz, B. J. Love, T. E. Long, *Chem. Rev.*, **2004**, *104*, 3059-3077; c) B. D. Wagner, *Molecules* **2009**, *14*, 210-237; d) X. Liu, Z. Xu, J. M. Cole, *J. Phys. Chem. C* **2013**, *117*, 16584-16595.

[5] N. Soh, T. Ueda, *Talanta*, **2011**, *85*, 1233-1237.

[6] a) A. Loudet, K. Burgess, *Chem. Rev*. **2007**, *107*, 4891-4932; b) R. Ziessel, G. Ulrich, A. Harriman, *New J. Chem.* **2007**, *31*, 496-501; c) G. Ulrich, R. Ziessel, A. Harriman, *Angew. Chem., Int. Ed.* **2008**, *47*, 1184-1201; d) A. C. Benniston, G. Copley, *Phys. Chem. Chem. Phys.* **2009**, *11*, 4124-4131; e) M. Benstead, G. H. Mehl, R. W. Boyle, *Tetrahedron* **2011**, *67*, 3573-3601; f) N. Boens, V. Leen, W. Dehaen, *Chem. Soc. Rev.* **2012**, *41*, 1130-1172; g) H. Lu, J. Mack, Y. Yang, Z. Shen, *Chem. Soc. Rev.* **2014**, *43*, 4778-4823.

[7] A. Treibs, F. H. Kreuzer, *Liebigs Ann. Chem.* **1968**, *718*, 208-223.

[8] a) M. Shah, K. Thangaraj, M.-L. Soong, L. T. Wolford, J. H. Boyer, I. R. Politzer, T. G. Pavlopoulos, *Heteroatom Chem.* **1990**, *1*, 389-399; b) J. H. Boyer, A. M. Haag, G. Sathyamoorthi, M.-L. Soong, K. Thangaraj, T. G. Pavlopoulos, *Heteroatom Chem.* **1993**, *4*, 39-49.

[9] A. R. Holzwarth, H. Lehner, S. E. Braslavsky, K. Schaffner, *Liebigs Ann. Chem.* **1978**, 2002-2017.

[10] a) I. J. Arroyo, R. Hu, G. Merino, B. Z. Tang, E. Peña-Cabrera, *J. Org. Chem.* **2009**, *74*, 5719-5722; b) A. Schmitt, B. Hinkeldey, M. Wild, G. Jung, *J. Fluoresc.* **2009**, *19*, 755-758.

[11] M. Baruah, W. Qin, N. Basarić, W. M. De Borggraeve, N. Boens, *J. Org. Chem.* **2005**, *70*, 4152-4157.

[12] T. Rohand, E. Dolusic, T. H. Ngo, W. Maes, W. Dehaen, *Arkivoc*, **2007**, 307-324.

[13] Z. Li, E. Mintzer, R. Bittman, *J. Org. Chem.* **2006**, *71*, 1718-1721.

[14] G. P. Arsenault, E. Bullock, S. F. MacDonald, *J. Am. Chem. Soc.* **1960**, *82*, 4384-4389.

[15] A. Al-Sheikh-Ali, K. S. Cameron, T. S. Cameron, K. N. Robertson, A. Thompson, *Org. Lett.* **2005**, *7*, 4773-4775.

[16] C.-W. Wan, A. Burghart, J. Chen, F. Bergström, L. B.-Å. Johansson, M. F. Wolford, T. G. Kim, M. R. Topp, R. M. Hochstrasser, K. Burgess, *Chem. Eur. J.* **2003**, *9*, 4430-4441.

[17] J. Bañuelos-Prieto, A. R. Agarrabeitia, I. Garcia-Moreno, I. Lopez-Arbeloa, A. Costela, L. Infantes, M. E. Perez-Ojeda, M. Palacios-Cuesta, M. J. Ortiz, *Chem. Eur. J.* **2010**, *16*, 14094-14105.

[18] Datos obtenidos de SciFinder a 26/5/2015 empleando BODIPY como palabra clave para la búsqueda.

[19] a) L. Bonardi, G. Ulrich, R. Ziessel, *Org. Lett.* **2008**, *10*, 2183-2186; b) Ö. A. Bozdemir, O. Büyükcakir, E. U. Akkaya, *Chem. Eur. J.* **2009**, *15*, 3830-3838; c) K. Krumova, G. Cosa, *J. Am. Chem. Soc.* **2010**, *132*, 17560-17569; d) S. Rihn, M. Erdem, A. De Nicola, P. Retailleau, R. Ziessel, *Org. Lett.* **2011**, *13*, 1916-1919; e) L. Wang, J.-W. Wang, A.-j. Cui, X.-X. Cai, Y. Wan, Q. Chen, M.-Y. He, W. Zhang, *RSC Adv.* **2013**, *3*, 9219-9222.

[20] L. Li, J. Han, B. Nguyen, K. Burgess, *J. Org. Chem.* **2008**, *73*, 1963-1970.

[21] I. Esnal, J. Bañuelos, I. López Arbeloa, A. Costela, I. Garcia-Moreno, M. Garzón, A. R. Agarrabeitia, M. J. Ortiz, *RSC Adv.* **2013**, *3*, 1547-1556.

[22] a) L. Jiao, C. Yu, J. Li, Z. Wang, M. Wu, E. Hao, *J. Org. Chem.* **2009**, *74*, 7525-7528; b) C. Yu, L. Jiao, H. Yin, J. Zhou, W. Pang, Y. Wu, Z. Wuang, J. Yang, E. Hao, *Eur. J. Chem*, **2011**, 5460-5468.

[23] L. Jiao, W. Pang, J. Zhou, Y. Wei, X. Mu, G. Bai, E. Hao, *J. Org. Chem.* **2011**, *76*, 9988-9996.

[24] a) T. Rohand, M. Baruah, W. Qin, N. Boens, W. Dehaen, *Chem. Commun.* **2006**, 266-268; b) V. Leen, D. Miscoria, S. Yin, A. Filarowski, J. M. Ngongo, M. Van der Auweraer, N. Boens, W. Dehaen, *J. Org. Chem.* **2011**, *76*, 8168-8176.

[25] a) G. Ulrich, R. Ziessel, *J. Org. Chem.* **2004**, *69*, 2070-2083. b) S. Rihn, P. Retailleau, N. Bugsaliewicz, A. De Nicola, R. Ziessel, *Tetrahedron Lett*. **2009**, *50*, 7008-7013. c) J. Han, G. Gonzalez, A. Aguilar-Aguilar, E. Peña-Cabrera, K. Burgess, *Org. Biomol. Chem.* **2009**, *7*, 34-36. d) S. Niu, G. Ulrich, P. Retailleau, R. Ziessel, *Tetrahedron Lett.* **2011**, *52*, 4848-4853. e) E. Heyer, R. Ziessel, *Tetrahedron Lett.* **2013**, *54*, 3388-3393.

[26] a) E. Peña-Cabrera, A. Aguilar-Aguilar, M. González-Domínguez, E. Lager, R. Zamudio-Vázquez, J. Godoy-Vargas, F. Villanueva-García, *Org. Lett.* **2007**, *9*, 3985-3988; b) C. F. A. Gómez-Duran, I. García-Moreno, A. Costela, V. Martin, R. Sastre, J. Bañuelos, F. López Arbeloa, I. López Arbeloa, E. Peña-Cabrera, *Chem. Commun.* **2010**, *46*, 5103-5105; c) J. Bañuelos, V. Martín, C. F. A. Gómez-Durán, I. J. Arroyo Córdoba, E. Peña-Cabrera, I. García-Moreno, A. Costela, M. E. Pérez-Ojeda, T. Arbeloa, I. López Arbeloa, *Chem. Eur. J.* **2011**, *17*, 7261-7270; d) J. O. Flores-Rizo, I. Esnal, C. A. Osorio-Mártinez, C. F. A. Gómez-Durán, J. Bañuelos, I. López Arbeloa, K. H. Pannell, A. J. Metta-Magaña, E. Peña-Cabrera, *J. Org. Chem.* **2013**, *78*, 5867-5877; e) R. I. Roacho, A. J. Metta-Magaña, E. Peña-Cabrera, K. H. Pannell, *J. Phys. Org. Chem.* **2013**, *26*, 345-351.

[27] a) V. Leen, P. Yuan, L. Wang, N. Boens, W. Dehaen, *Org. Lett.* **2012**, *14*, 6150-6153; b) H. Wang, M. G. H. Vicente, F. R. Fronczek, K. M. Smith, *Chem. Eur. J.* **2014**, *20*, 5064-5074.

[28] a) R. Ziessel, G. Ulrich, A. Haefele, A. Harriman, *J. Am. Chem. Soc.* **2013**, *135*, 11330-11344; b) B. Brizet, C. Bernhard, Y. Volkova, Y. Rousselin, P. D. Harvey, C. Goze, F. Denat, *Org. Biomol. Chem.* **2013**, *11*, 7729-7737; c) A. M. Courtis, S. A.

Santos, Y. Guan, J. A. Hendricks, B. Ghosh, D. M. Szantai-Kis, S. A. Reis, J. V. Shah, R. Mazitschek, *Bioconjugate Chem.* **2014**, *25*, 1043-1051; d) E. M. Sánchez-Carnerero, F. Moreno, B. L. Maroto, A. R. Agarrabeitia, M. J. Ortiz, B. G. Vo, G. Muller, S. de la Moya, *J. Am. Chem. Soc.* **2014**, *136*, 3346-3349.

[29] a) C. Thivierge, R. Bandichhor, K. Burgess, *Org. Lett.* **2007**, *9*, 2135-2138; b) J. Chen, M. Mizumura, H. Shinokubo, A. Osuka, *Chem. Eur. J.* **2009**, *15*, 5942-5949.

[30] a) V. Leen, M. Van der Auweraer, N. Boens, W. Dehaen, *Org. Lett.* **2011**, *13*, 1470-1473; b) B. Verbelen, S. Boodts, J. Hofkens, N. Boens, *Angew. Chem. Int. Ed.* **2015**, *54*, 4612-4616.

[31] a) B. Verbelen, V. Leen, L. Wang, N. Boens, W. Dehaen, *Chem. Commun.* **2012**, *48*, 9129-9131; b) L. Wang, B. Verbelen, C. Tonnelé, D. Beljonne, R. Lazzaroni, V. Leen, W. Dehaen, N. Boens, *Photochem. Photobiol. Sci.* **2013**, *12*, 835-847; c) L. Luo, D. Wu, W. Li, S. Zhang, Y. Ma, S. Yan, J. You, *Org. Lett.* **2014**, *16*, 6080-6083.

[32] a) K. Rurack, M. Kollmannsberger, J. Daub, *Angew. Chem. Int. Ed.* **2001**, *40*, 385-387; b) O. Buyukcakir, O. A. Bozdemir, S. Kolemen, S. Erbas, E. U. Akkaya, *Org. Lett.* **2009**, *11*, 4644-4647; c) T. Bura, P. Retailleau, G. Ulrich, R. Ziessel, *J. Org. Chem.* **2011**, *76*, 1109-1117; d) Z. Kostereli, T. Ozdemir, O. Buyukcakir, E. U. Akkaya, *Org. Lett.* **2012**, *14*, 3636-3639; e) S. Zhu, J. Zhang, G. Vegesna, A. Tiwari, F.-T. Luo, M. Zeller, R. Luck, H. Li, S. Green, H. Liu, *RSC Adv.* **2012**, *2*, 404-407; f) X. Zhang, Y. Xiao, J. Qi, J. Qu, B. Kim, X. Yue, K. D. Belfield, *J. Org. Chem.* **2013**, *78*, 9153-9160.

[33] E. Palao, A. R. Agarrabeitia, J. Bañuelos-Prieto, T. Arbeloa Lopez, I. Lopez-Arbeloa, D. Armesto, M. J. Ortiz, *Org. Lett.* **2013**, *15*, 4454-4457.

[34] a) S. G. Awuah, Y. You, *RSC Adv.* **2012**, *2*, 11169-11183. b) A. Kamkaew, S. H. Lim, H. B. Lee, L. V. Kiew, L. Y. Chung, K. Burguess, *Chem. Soc. Rev.* **2013**, *42*, 77-88.

[35] L. Gartzia-Rivero, H. Yu, J. Bañuelos, I. López-Arbeloa, A. Costela, I. García-Moreno, Y. Xiao, *Chem. Asian J.* **2013**, *8*, 3133-3141.

[36] a) T. Ehrenschwender, H.-A. Wagenknecht, *Synthesis* **2008**, *22*, 3657-3662; b) J. A. Key, C. Li, C. W. Cairo, *Bioconjugate Chem.* **2012**, *23*, 363-371; c) L.-Y. Niu, Y.-S.

Guan, Y.-Z. Chen, L.-Z. Wu, C.-H. Tung, Q.-Z. Yang, *J. Am. Chem. Soc.* **2012**, *134*, 18928-18931; d) D. Dziuba, R. Pohl, M. Hocek, *Bioconjugate Chem.* **2014**, *25*, 1984-1995.

[37] a) J.-S. Lee, N.-y. Kang, Y. K. Kim, A. Samanta, S. Feng, H. K. Kim, M. Vendrell, J. H. Park, Y.-T. Chang, *J. Am. Chem. Soc.* **2009**, *131*, 10077-10082; b) J.-J. Lee, S.-C. Lee, D. Zhai, Y.-H. Ahn, H. Y. Yeo, Y. L. Tan, Y.-T. Chang, *Chem. Commun.* **2011**, *47*, 4508-4510; c) M. Ono, H. Watanabe, H. Kimura, H. Saji, *ACS Chem. Neurosci.* **2012**, *3*, 319-324; d) F. Wang, Z. Guo, X. Li, X. Li, C. Zhao, *Chem. Eur. J.* **2014**, *20*, 11471-11478; e) R. Mazitschek, A. M. Courtis, J. A. Hendricks, *Patent, WO2014055505*, **2014**.

[38] a) M. Baruah, W. Qin, R. A. L. Vallee, D. Beljonne, T. Rohand, W. Dehaen, N. Boens, *Org. Lett.* **2005**, *7*, 4377-4380; b) X. Zhang, Y. Xiao, X. Qian, *Angew. Chem. Int. Ed.* **2008**, *47*, 8025-8029; c) A. Ojida, T. Sakamoto, M.-a. Inoue, S.-h. Fujishima, G. Lippens, I. Hamachi, *J. Am. Chem. Soc.* **2009**, *131*, 6543-6548; d) Q. Li, Y. Guo, S. Shao, *Analyst* **2012**, *137*, 4497-4501; e) X. Jia, X. Yu, G. Zhang, W. Liu, W. Qin, *J. Coord. Chem.* **2013**, *66*, 662-670.

[39] a) Z. Yuan, T. W. Hanks, *Polymer* **2008**, *49*, 5023-5026; b) T. Hirata, T. Terai, T. Komatsu, K. Hanaoka, T. Nagano, *Bioorg. Med. Chem. Lett.* **2011**, *21*, 6090-6093; c) M. Hecht, W. Kraus, K. Rurack, *Analyst* **2013**, *138*, 325-332; d) M. M. Salim, E. A. Owens, T. Gao, J. H. Lee, H. Hyun, H. S. Choi, M. Henary, *Analyst* **2014**, *139*, 4862-4873.

[40] a) H. Son, H. Y. Lee, J. M. Lim, D. Kang, W. S. Han, S. S. Lee, J. H. Jung, *Chem. Eur. J.* **2010**, *16*, 11549-11553; b) H. Song, S. Rajendiran, N. Kim, S. K. Jeong, E. Koo, G. Park, T. D. Thangadurai, S. Yoon, *Tetrahedron Lett.* **2012**, *53*, 4913-4916.

[41] a) S. Erten-Ela, M. D. Yilmaz, B. Icli, Y. Dede, S. Icli, E. U. Akkaya, *Org. Lett.* **2008**, *10*, 3299-3302; b) S. Kolemen, Y. Cakmak, S. Erten-Ela, Y. Altay, J. Brendel, M. Thelakkat, E. U. Akkaya, *Org. Lett.* **2010**, *12*, 3812-3815; c) J. Lu, H. Fu, Y. Zhang, Z. J. Jakubek, Y. Tao, S. Wang, *Angew. Chem. Int. Ed.* **2011**, *50*, 11658-11662; d) Y. Ooyama, Y. Hagiwara, T. Mizumo, Y. Harima, J. Ohshita, *RSC Adv.* **2013**, *3*, 18099-18106; e) M. Mao, X.-L. Zhang, X.-Q. Fang, G.-H. Wu, Y. Ding, X.-L. Liu, S.-Y. Dai, Q.-H. Song, *Organic Electronics* **2014**, *15*, 2079-2090.

[42] a) A. Nagai, K. Kokado, J. Miyake, Y. Cyujo, *J. Polym. Sci. Part A: Polym. Chem.* **2010**, *48*, 627-634; b) S. Xiao, Q. Cao, F. Dan, *Curr. Org. Chem.* **2012**, *16*, 2970-2981; c) Y. Rong, C. Wu, J. Yu, X. Zhang, F. Ye, M. Zeigler, M. E. Gallina, I. C. Wu, Y. Zhang, Y.-H. Chan, W. Sun, K. Uvdal, D. T. Chiu, *ACS Nano* **2013**, *7*, 376-384; d) C.-L. Liu, Y. Chen, D. P. Shelar, C. Li, G. Cheng, W.-F. Fu, *J. Mater. Chem. C* **2014**, *2*, 5471-5478.

[43] T. G. Pavlopoulos, J. H. Boyer, M. Shah, K. Thangaraj, M. L. Soong, *Appl. Opt.* **1990**, *29*, 3885-3886.

[44] http://www.photonicsolutions.co.uk/Exciton%20dyes.asp.

[45] a) I. García-Moreno, F. Amat-Guerri, M. Liras, A. Costela, L. Infantes, R. Sastre, F. López Arbeloa, J. Bañuelos Prieto, I. López Arbeloa, *Adv. Funct.Mater.* **2007**, *17*, 3088-3098; b) M. Alvarez, A. Costela, I. García-Moreno, F. Amat-Guerri, M. Liras, R. Sastre, F. López Arbeloa, J. Bañuelos Prieto, I. López Arbeloa, *Photochem. Photobiol. Sci.* **2008**, *7*, 802-813; c) J. Bañuelos, F. L. Arbeloa, V. Martinez, M. Liras, A. Costela, I. G. Moreno, I. L. Arbeloa, *Phys. Chem. Chem. Phys.* **2011**, *13*, 3437-3445

[46] a) R. I. Roacho, A. Metta-Magana, M. M. Portillo, E. Peña-Cabrera, K. H. Pannell, *J. Org. Chem.* **2013**, *78*, 4245-4250.

[47] I. Esnal, I. Valois-Escamilla, C. F. A. Gomez-Duran, A. Urias-Benavides, M. L. Betancourt-Mendiola, I. López-Arbeloa, J. Bañuelos, I. García-Moreno, A. Costela, E. Peña-Cabrera, *Chem. Phys. Chem.* **2013**, *14*, 4134-4142.

[48] I. Garcia-Moreno, D. Zhang, A. Costela, V. Martin, R. Sastre, Y. Xiao, *J. Appl. Phys.* **2010**, *107*, 73105-73107.

# OBJETIVOS

# OBJETIVOS

El presente trabajo pretende dar respuesta a la creciente demanda de nuevos materiales fotónicos avanzados, funcionales y eficaces, con aplicación inmediata en el campo de la energía y biomedicina. Los objetivos concretos de esta Tesis Doctoral son los siguientes:

- Diseñar y sintetizar nuevos colorantes con propiedades láser optimizadas respecto a los actualmente comercializados, atendiendo a uno o varios de estos parámetros: absorción a las longitudes de onda de bombeo más usuales (355 y 532 nm), eficiencia, fotoestabilidad y sensibilidad en medios de interés (disolventes orgánicos y matrices poliméricas).
- Generar un cuerpo de conocimiento sobre la relación estructura-propiedad de colorantes orgánicos que simplifique el diseño y la síntesis de colorantes con propiedades optimizadas para aplicaciones avanzadas.

Las estrategias de síntesis seguidas en el desarrollo de estos nuevos colorantes se engloban en:

- Halogenación de colorantes.
- Reacciones de acoplamientos C-C catalizadas por paladio en haloBODIPYs para extensión de la conjugación.
- Sustitución nucleófila sobre el átomo de boro en diferentes BODIPYs comerciales.
- Formación de sistemas multicromofóricos (cassettes o antenas).

Posteriormente, se aborda la evaluación de las propiedades fotofísicas y de emisión láser de los nuevos colorantes obtenidos para su posible aplicación en los diferentes campos de la fotónica.

## ESTRUCTURA DE LA MEMORIA

## ESTRUCTURA DE LA MEMORIA

Esta Memoria se ha redactado siguiendo el formato de recopilación de artículos científicos ya publicados, los cuales, para facilitar su lectura, se han agrupado en cuatro capítulos atendiendo a los objetivos perseguidos:

Capítulo 1: síntesis de nuevos colorantes halogenados mediante reacciones de sustitución electrófila aromática.
Capítulo 2: síntesis de nuevos colorantes BODIPY con emisión en la zona roja del espectro mediante extensión de la conjugación.
Capítulo 3: síntesis de nuevos colorantes BODIPY por introducción de diferentes sustituyentes en el átomo de boro de una serie de BODIPY comerciales.
Capítulo 4: diseño y síntesis de una serie de nuevos sistemas multicromofóricos basados fundamentalmente en BODIPYs.

En todos los capítulos se incluyen, por este orden, una introducción general en la que se detallan los objetivos del trabajo, un breve resumen de cada uno de los artículos, discutiendo: i) la estrategia de síntesis, ii) las propiedades fotofísicas, iii) las propiedades láser y iv) conclusiones.

En el capítulo 4 se recoge, además, el trabajo que está pendiente de ser publicado y esta parte se presenta según el formato convencional, dividiendo cada uno de los apartados en: i) introducción, ii) resultados y discusión, iii) conclusiones y iv) materiales y métodos/parte experimental.

Finalmente, se incluye un último capítulo en donde se recoge el trabajo desarrollado durante la estancia pre-doctoral en el grupo de investigación del Profesor Peña Cabrera de la Facultad de Ciencias de la Universidad de Guanajuato (México).

# TÉCNICAS EXPERIMENTALES

# TÉCNICAS EXPERIMENTALES

Común a toda la Memoria son las técnicas experimentales seleccionadas para la caracterización de los nuevos colorantes, de sus propiedades fotofísicas y de sus propiedades láser. Aunque todas ellas están detalladas en los correspondientes artículos, con el fin de facilitar la lectura de esta Memoria se incluye a continuación una breve descripción de las mismas:

*Caracterización de colorantes:*

Los espectros de RMN de $^{1}H$ y $^{13}C$ se han realizado en el servicio de Resonancia Magnética Nuclear de la Universidad Complutense de Madrid y de la Universidad de Guanajuato (México). Estos espectros se han registrado en un espectrómetro Varian Germini 200 (200 MHz para $^{1}H$ y 50 MHz para $^{13}C$), Inova-500 MHz (500 MHz para $^{1}H$ y 125 MHz para $^{13}C$) y Bruker Avance DPX-300 (300 MHz para $^{1}H$ y 75 MHz para $^{13}C$) y espectrómetro Bruker Avance III (700 MHz para $^{1}H$ y 176 MHz para $^{13}C$), utilizando como disolventes $CDCl_3$ o $CD_3OD$. Los desplazamientos químicos de $^{1}H$ se dan en ppm con relación a tetrametilsilano ($\delta$ = 0.00 ppm), utilizando la señal de disolvente residual como referencia interna. Los desplazamientos químicos en $^{13}C$ se dan en ppm con $CDCl_3$ ($\delta$ = 77.67 ppm) o $CD_3OD$ ($\delta$ = 49.2 ppm) como patrón interno. Las multiplicidades de los desplazamientos químicos se indican como s = singlete, d = doblete, t = triplete, c = cuadruplete, q = quintuplete y m = multiplete. Los espectros de IR (en $cm^{-1}$) se han registrado en un espectrómetro Bruker Tensor-27-FTIR.

Los espectros de masas de alta resolución se han realizado en el servicio de Espectroscopía de Masas de la Universidad Complutense de Madrid, utilizando un espectrofotómetro ThermoFisher MAT XP 95. La determinación estructural por difracción de Rayos X se ha realizado en un difractómetro Agilent SuperNova Cu, equipado con detector de tipo CCD modelo Atlas, a una temperatura de 100 K, usando un Cryostream

700 de Agilent Cryosystems alimentado con nitrógeno líquido. Todos los átomos de hidrógeno se han localizado en el mapa de densidad residual y se han refinado con el modelo "*riding*" de SHELXL97.

*Propiedades fotofisicas*

Estos estudios se han realizado en el Grupo del Profesor López Arbeloa de la Universidad del País Vasco. Los espectros de absorción y de fluorescencia se han llevado a cabo utilizando un espectrofotómetro UV/Vis Perkin Elmer, modelo Lambda 16, y los espectrofluorímetros Perkin Elmer LS20B, y Perkin Elmer LS55. El rendimiento cuántico de fluorescencia, $\phi$, (cociente entre el número de fotones emitidos como fluorescencia y el número de fotones absorbidos por el sistema) se determinó usando como referencia el colorante láser comercial **PM567** en metanol ($\phi$ = 0.91).

*Cálculos teóricos*

Todos los cálculos de mecánica cuántica fueron realizados por el grupo del Prof. López Arbeloa empleando el programa Gaussian 03. Las geometrías de los estados fundamental y excitado fueron optimizadas por los métodos ab-initioDFT ("*Density Functional Theory*") y CIS ("*Configuration Interaction Singles*") con una base de doble valencia (6-31G), respectivamente. Las transiciones de absorción y fluorescencia fueron simuladas por el método DFT dependiente del tiempo (TD-DFT) para las geometrías de los estados fundamental y excitado, respectivamente.

*Medidas de oxígeno singlete*

Las medidas de oxígeno singlete se han llevado a cabo en dos grupos de investigación: el grupo del Prof. Norman A. García de la Universidad de Rio Cuarto Argentina y del Prof. Iñigo López Arbeloa de la UPV.

La producción de oxigeno singlete se determinó mediante la medida directa de su luminiscencia a 1270 nm, con un detector para NIR integrado en el espectrofluorímetro (detector IngaAs, Hamamatsu G8605-23). Las medidas de emisión de oxígeno singlete se llevaron a cabo en configuración frontal (*front face*), a 40º y 50º con respecto a los haces de excitación y emisión, respectivamente y con muestra inclinada 30º respecto al plano

formado por la dirección de incidencia y de registro, en cubetas de 1 cm. La señal de emisión se por medio de un filtro de corte bajo (*cut-off*) de 850 nm. Se registraron al menos 5 disoluciones de concentraciones comprendidas entre $1 \cdot 10^{-6}$ M y $5 \cdot 10^{-5}$ M. La longitud de onda de excitación se elige teniendo en cuenta los máximos de absorción de los sensibilizadores a estudiar. Se utilizaron como referencias sustancias con rendimientos cuánticos de producción de oxígeno singlete conocidos (estándar). Dependiendo de la longitud de onda de excitación elegida se emplearon diferentes referencias: Fenalenona (PN), para la región UV, con un rendimiento de 1, independiente del disolvente (*J. Photochem. Photobiol. A* **1994**, *79*, 11-17); Rosa de Bengala (RB), para la región visible concretamente en el verde, con un rendimiento de 0.55 (medido respecto a la Fenalenona).

Una vez recogidas las señales de las muestras y de las referencias a la misma longitud de onda de excitación, se determinaron los rendimientos cuánticos de generación de oxígeno singlete por diferencia, empleando la siguiente ecuación:

$$\phi_\Delta = \phi_\Delta(R) \cdot \left(\frac{\alpha_R}{\alpha_{Ps}}\right) \cdot \left(\frac{Se_{Ps}}{Se_R}\right) \cdot \left(\frac{\tau_R}{\tau_{Ps}}\right)$$

donde $\phi_\Delta(R)$ es el rendimiento cuántico de generación de oxígeno singlete de la referencia. El factor $\alpha = 1\text{-}10^{-Abs}$, corrige la diferente cantidad de fotones absorbidos por la muestra ($\alpha_{Ps}$) y por la referencia ($\alpha_R$), $Se_{ps}$ y $Se_R$ es la señal de oxigeno singlete de la muestra y de la referencia a 1276 nm y $\tau$ es el tiempo de vida de oxigeno singlete en cada disolvente.

*Propiedades láser*

Estos estudios se han realizado en el Grupo de Materiales Láser e Interacción Láser-Metriales del Instituto de Química-Física "Rocasolano" del CSIC. El sistema experimental (Figura 17) consta esencialmente de un sistema de excitación (bombeo) de las muestras, otro de focalización, una cavidad óptica resonante, y sistemas de detección y análisis de la emisión láser.

Como fuente de bombeo se utiliza un láser de Nd:YAG a 532 nm y/o a 355 nm (segundo y tercer armónico, respectivamente) con una energía: 5.5 mJ; duración temporal del pulso (FWHM): 6 ns; divergencia: <4.5 mrad; razón de polarización: >1000:1; sección transversal circular. La velocidad de repetición seleccionada para las medidas de

fotoestabilidad de las muestras es de 10 Hz. La cavidad utilizada es plano-paralela, formada por un espejo plano de aluminio de reflectividad 90% y diámetro 2.5 cm (E2 en la Figura 17) y por un acoplador de salida, que es la cara de la célula. La longitud de la cavidad resonante es de 2 cm (1 cm de muestra y 1 cm de distancia entre el extremo de la muestra y el espejo) y no se utilizan otros elementos para sintonizar la longitud de onda.

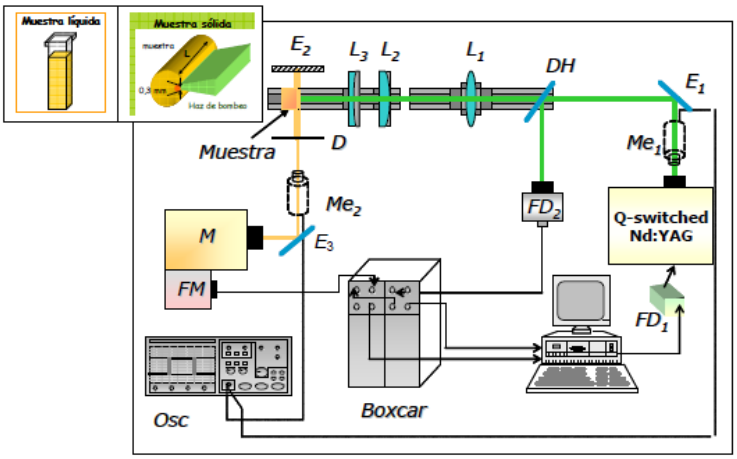


**Figura 17.** Sistema experimental: DH: divisor de haz; Me: medidor de energía; $L_1$: lente esférica; $L_{2,3}$: lentes cilíndricas; M: monocromador; $E_{1,2,3}$: espejos planos de aluminio; D: diafragma; $FD_{1,2}$: fotodiodos; FM: tubo fotomultiplicador.

La velocidad de repetición seleccionada para las medidas de fotoestabilidad de las muestras es de 10 Hz. La cavidad utilizada es plano-paralela, formada por un espejo plano de aluminio de reflectividad 90% y diámetro 2.5 cm (E2 en la Figura 17) y por un acoplador de salida, que es la cara de la célula. La longitud de la cavidad resonante es de 2 cm (1 cm de muestra y 1 cm de distancia entre el extremo de la muestra y el espejo) y no se utilizan otros elementos para sintonizar la longitud de onda.

La acción láser de cada colorante se analiza en base a tres parámetros: longitud de onda de emisión láser ($\lambda_{láser}$), registrada con un sistema monocromador-CCD; eficiencia (Ef en %) definida como el coeficiente entre la energía de excitación que incide sobre la superficie de la muestra y la de emisión láser inducida en la misma; y fotoestabilidad, analizada como la pérdida de emisión que experimenta el colorante (I en %), con respecto a su intensidad inicial ($I_0$) después de n pulsos de excitación.

# CAPÍTULO 1. COLORANTES HALOGENADOS

# 1. COLORANTES HALOGENADOS

## 1.1. INTRODUCCIÓN

En los últimos años se ha realizado un gran esfuerzo en el diseño y síntesis de colorantes orgánicos fluorescentes. A pesar de los numerosos avances, no se ha conseguido establecer una regla general que permita obtener fluoróforos más eficientes y fotoestables, con aplicaciones en los diversos campos de la fotónica.

Por lo tanto, actualmente, un desafío importante es el desarrollo de una única metodología sintética que mejore las propiedades de emisión de los fluoróforos comerciales en la zona del espectro visible, bajo drásticas condiciones de bombeo láser. Esta tarea puede abordarse mediante modificaciones estructurales adecuadas en los esqueletos de los diferentes cromóforos.

En este sentido, la fluoración es una buena alternativa, ya que el enlace C-F está muy polarizado y presenta un componente electrostático significativo, lo que hace que sea considerado como un enlace fuerte desde el punto de vista de la Química Orgánica. Como consecuencia, los compuestos organofluorados poseen una mayor estabilidad química y térmica que sus análogos no fluorados. Más interesante aún es el hecho de que los cromóforos fluorados presentan mayor fotoestabilidad,[1] menor reactividad hacia el oxígeno singlete,[2] mayores rendimientos cuánticos de fluorescencia[2] y menores procesos de agregación que los sistemas no fluorados.[3]

Existen en la bibliografía ejemplos de colorantes fluorados obtenidos a través de diferentes metodologías: (a) sustitución de átomos de cloro o bromo por flúor, (b) empleo de precursores fluorados y (c) fluoración directa del esqueleto del colorante por transformación de un enlace C-H en C-F mediante la utilización de un agente electrofílico

de fluoración. Así, se han obtenido perilenos fluorados por intercambio de cloro y/o bromo (Esquema 6a),[2c] rodaminas fluoradas a partir de bencenos fluorados (Esquema 6b)[1c] y fluorocumarinas por fluoración directa del cromóforo (Esquema 6c).[4]

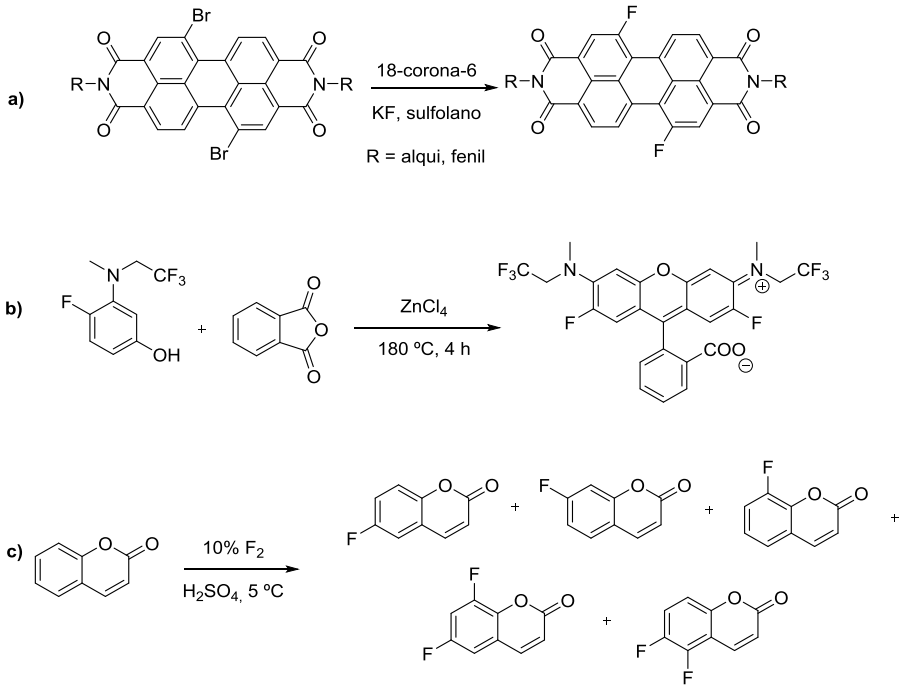


**Esquema 6**

Además, existe una patente japonesa en donde se recoge un ejemplo de BODIPY fluorado, aunque no se detalla ni su síntesis ni sus datos espectroscópicos (Figura 18).[5]

**Figura 18**. Estructura del 2,6-difluoroBODIPY.

Teniendo en cuenta estas consideraciones, en el primer artículo de este Capítulo se describe una estrategia sintética de monofluoración directa de una serie de colorantes comerciales con emisión láser en las diferentes zonas del espectro visible, en donde se

demuestra que, efectivamente, la incorporación de un átomo de flúor en el núcleo del cromóforo induce una notable mejora del comportamiento láser.

Por otra parte, en este estudio se pudo comprobar la dificultad que supone la fluoración directa de BODIPYs y la inesperada incorporación de átomos de cloro cuando se llevaron a cabo las reacciones en un disolvente orgánico clorado, al intentar optimizar las condiciones de reacción. Sorprendentemente, estos derivados clorados son altamente fluorescentes, por lo que, a continuación, se realizó un estudio detallado de reacciones de cloración de BODIPYs y se estudió su comportamiento láser. Los resultados obtenidos, recogidos en el segundo artículo de este Capítulo, demostraron que es posible halogenar BODIPYs de forma selectiva, dando lugar a mono-, di- o policloro-BODIPYs, con alta eficiencia y fotoestabilidad láser. Hasta este momento todos los BODIPYs clorados ólo se habían obtenido y caracterizado como intermedios de reacción, sin prestar mayor atención a sus propiedades fotofísicas y ópticas.

Mucho más estudiados como intermedios de reacción y como fotosensibilizadores en terapia fotodínámica son los BODIPYs bromados y yodados. Sin embargo, no se ha referenciado ningún estudio sistemático que demuestre el potencial que ofrece la polihalogenación selectiva de BODIPYs. Por ello, en el tercer artículo del presente Capítulo se presenta un estudio detallado de la reacción de yodación de BODIPYs con diferente grado de sustitución, a través de reacciones de sustitución electrófila aromática. Así, se ha confirmado la generalidad de la polihalogenación en BODIPYs, ya que en esa fecha no existía ningún estudio referible. Estos nuevos yodoBODIPYs, lógicamente, no estaban orientados a ser empleados como colorantes láser, pues es bien conocido que la presencia de átomos de yodo unidos directamente al núcleo de indaceno provoca una disminución notable de la fluorescencia y un incremento de ISC debido al efecto de átomo pesado, lo que potencia su utilización como fotosensibilizadores en terapia fotodinámica.

## 1.2. COLORANTES FLUORADOS

**Artículo 1: "Increased laser action in comercial dyes from fluorination regardless of their skeleton"** *Laser Physics Letters* **2014**, *11*, 115818(7 pp)

### 1.2.1. Introducción

Para estudiar el efecto de fluoración sobre las propiedades ópticas de los BODIPYs se abordó la reacción de fluoración directa sobre el dipirrometeno comercial **PM546**. Una vez demostrada la viabilidad de esta metodología en este BODIPY, se estudió la posibilidad de extender este protocolo a otros colorantes comerciales con independencia de sus estructuras, y cuyas emisiones permitieran cubrir todo el espectro visible. Por ello, los colorantes comerciales seleccionados fueron: Cumarina 460 (**Cu460**), Rodamina 6G (**Rh6G**) y Perileno Rojo (**PerRed**) (Figura19).

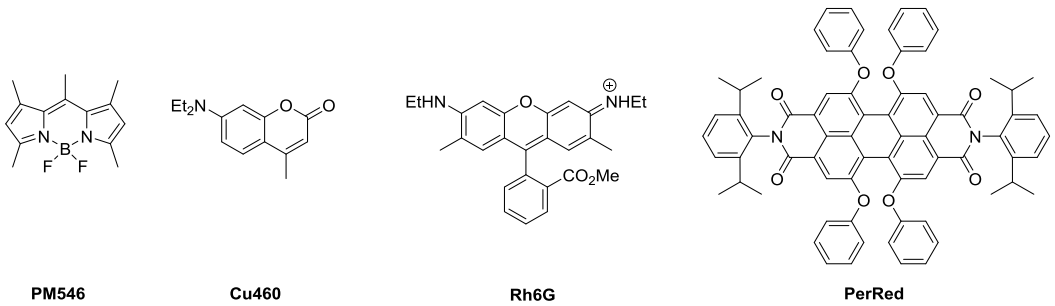


**Figura 19.** Estructura de los colorantes comerciales dipirrometeno 546 (**PM546**), Cumarina 460 (**Cu460**), Rodamina 6G (**Rh6G**) y Perileno Rojo (**PerRed**).

### 1.2.2. Síntesis

El estudio se inició con la reacción de fluoración del dipirrometeno **PM546**, empleando Selectfluor™ como agente de fluoración bajo irradiación en microondas o reflujo de $CH_3CN$. En ambas condiciones se producía la descomposición del compuesto de partida. Por ello, se empleó $XeF_2$ (2.5 equiv) bajo irradiación en microondas, conduciendo a la formación del compuesto **1a** con un 11% de rendimiento. Un mayor número de equivalentes de $XeF_2$ no dio lugar ni a la formación del derivado difluorado ni a una mejora del rendimiento de la reacción. Sorprendentemente, cuando se llevó a cabo la

reacción en las mismas condiciones anteriores pero utilizando $CH_2Cl_2$ (DCM) como disolvente se observó la formación de un nuevo compuesto fluorescente que resultó ser el derivado monoclorado **1b** (Esquema 7).

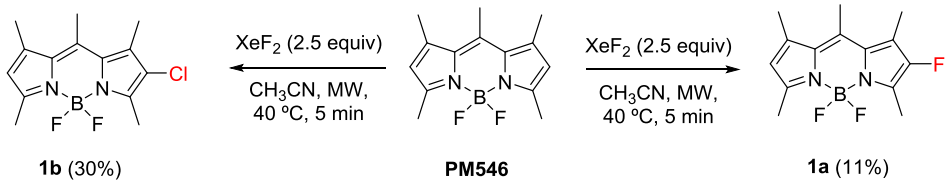


**Esquema 7**

Esta reactividad inesperada, según estudios recogidos en la bibliografía, puede deberse a la reacción del $XeF_2$ con el disolvente clorado, para generar subproductos de cloro-fluoración (Esquema 9).[6] Así, por ejemplo, Zupna y Pollack describen la síntesis de derivados clorados en la reacción de sistemas heterocíclicos empleando $XeF_2$ en presencia de disolventes como $CH_2Cl_2$ o $CHCl_3$ (Esquema 9).[7]

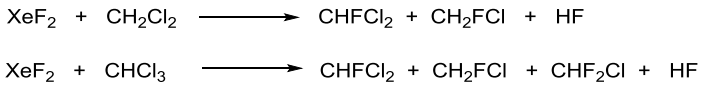


**Esquema 8**

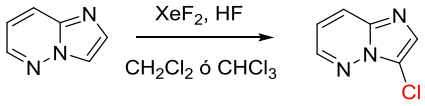


**Esquema 9**

A continuación, se llevó a cabo la fluoración de los colorantes comerciales seleccionados, empleando $CH_3CN$ como disolvente para evitar la formación de los productos clorados. Así, la reacción de **Cu460** en presencia de $XeF_2$, en la mismas condiciones de reacción empleadas para la monofluoración de **PM546**, condujo a la descomposición del producto de partida, por lo que se optó por emplear Selectfluor™

como agente de fluoración, obteniéndose una mezcla de las fluorocumarinas **2a** y **2b**, separables por cromatografía en columna (Esquema 10).

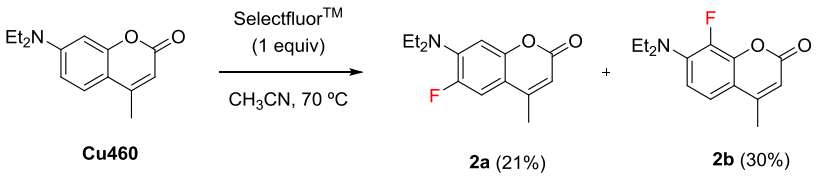


**Esquema 10**

La síntesis de la rodamina monofluorada **3** se llevó a cabo bajo irradiación en microondas, empleando Selectfluor™ ya que el empleo $XeF_2$ dio lugar a la descomposición de la rodamina de partida (Esquema 11).

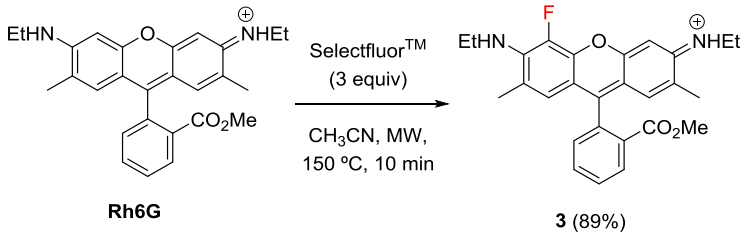


**Esquema 11**

En el caso del **PerRed**, la reacción con $XeF_2$ dio lugar a un nuevo compuesto al que, en base a sus datos espectroscópicos, se le asignó la estructura **4** (Esquema 12).

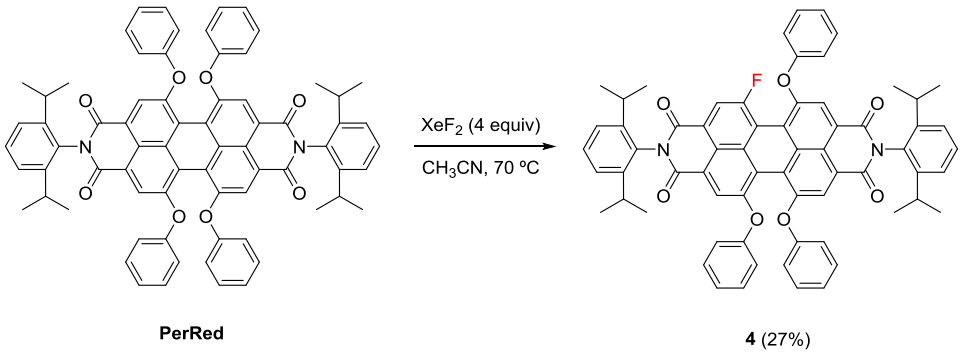


**Esquema 12**

Por espectroscopía de masas de alta resolución, HRMS, se observó el pico molecular *z* 1005.7236 que corresponde a la sustitución de un grupo fenoxi por un átomo de flúor. Por $^{19}$F-RMN se demostró la presencia de un átomo de fluor unido al núcleo de perileno. Tambíen se observó una diferencia en el desplazamiento de las señales en $^{1}$H RMN de los protones unidos a los carbonos C-2, C-5, C-8 y C-11 con respceto a los singletes que aparecen en el producto de partida (Figura 20).

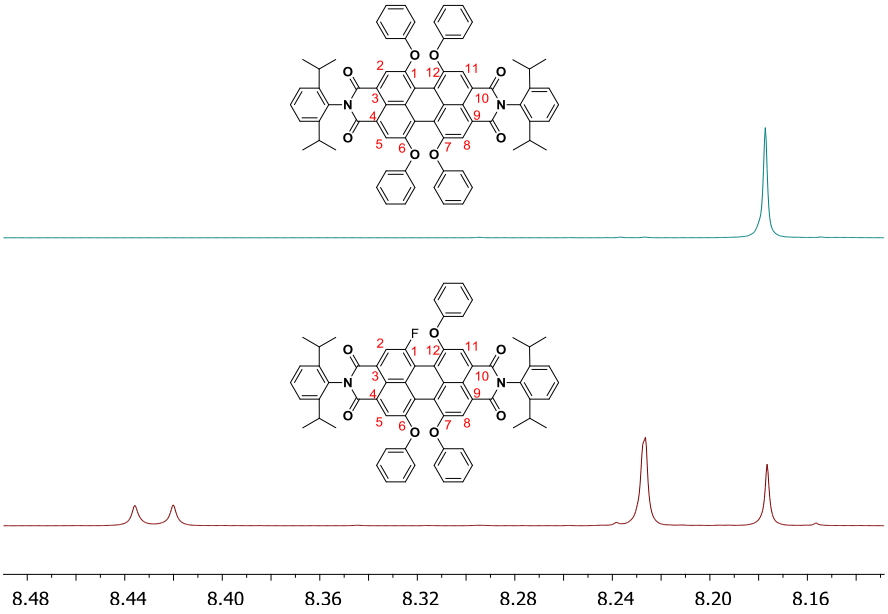


**Figura 20**. Ampliación de $^{1}$H-RMN del **PerRed** y **4.**

Por otro lado, el experimento HMBC muestra una correlación entre H-2 y el C-1 que soporta el átomo de F ($\delta$159.7, d, $^{1}J_{CF}$ = 262 Hz, C-F). La formación de **4** implica la ruptura de un enlace éter que, de forma general, son estables en reaciones de fluoración, aunque existen algunos ejemplos de cambio de grupos alcoxi por átomos de flúor.[8]

### 1.2.3. Propiedades fotofísicas

Los nuevos colorantes fluorados poseen unas propiedades fotofísicas similares a las de sus precursores no fluorados, tal y como se recoge en la Tabla 1.

**Tabla 1**. Propiedades fotofísicas de colorantes comerciales y de sus derivados fluorados en AcOEt.

| Compuesto | $\lambda_{abs}$ (nm) | $\varepsilon_{max}$· ($10^4$ $M^{-1}$·$cm^{-1}$) | $\lambda_{fl}$ (nm) | $\phi$ |
|---|---|---|---|---|
| **PM546** | 494.0 | 8.1 | 504.0 | 0.85 |
| **1a** | 504.0 | 2.7 | 514.5 | 0.80 |
| **Cu460** | 360.5 | 2.4 | 451.5 | 1.00 |
| **2a** | 357.0 | 1.8 | 418.5 | 0.78 |
| **2b** | 359.0 | 0.7 | 415.5 | 1.00 |
| **Rh6G**[a] | 527.0 | 8.4 | 549.5 | 1.00 |
| **3** | 531.0 | 5.8 | 555.5 | 0.90 |
| **PerRed** | 568.2 | 4.9 | 597.5 | 1.00 |
| **4** | 554.0 | 5.4 | 584.5 | 0.89 |

[a] medido en acetona

El derivado monofluorado **1a** presenta un rendimiento cuántico de fluorescencia inferior al de su precursor no fluorado, ya que la introducción en la posición 2 del BODIPY de un átomo fuertemente electroactractor, como el átomo de flúor, produce una asimetría en la distribución de densidad de carga entre las unidades de pirrol. Como resultado, se produce una disminución de los procesos de desactivación radiantes, lo que justifica que el compuesto **1a** presente un menor rendimiento cuántico de fluorescencia que el **PM546**.

En el caso de las fluorocumarinas **2a-b**, existe una clara dependencia entre sus propiedades fotofísicas y la posición del átomo de flúor en su estructura. Como se puede observar en la Tabla 1, la cumarina **2b** mantiene su rendimiento cuántico de fluorescencia, mientras que en la cumarina **2a** se produce una disminución de este parámetro. Este comportamiento se debe a que la presencia del átomo de flúor en la posición 6 de la cumarina interrumpe el efecto "*push-pull*" entre el grupo dador de la posición 7 y el anillo de benzopirona (Figura 21).

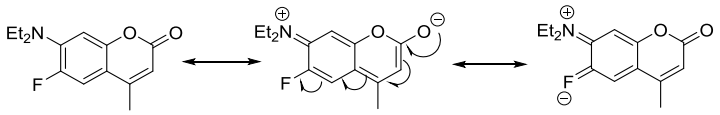

**Figura 21**. Estructuras resonantes de **2a**.

Este efecto es menos pronunciado en la rodamina, ya que la presencia de dos grupos electrodadores en el anillo de xanteno minimiza este efecto y, en consecuencia, no se produce una gran disminución del rendimiento cuántico de fluorescencia.

El **PerRed** se caracteriza por la deslocalización del sistema π por todo el núcleo de perilendiimida. La sustitución de un grupo metoxi por un átomo de flúor, más electroatractor, provoca la retirada de densidad de carga del sistema π, lo que justifica que el derivado monofluorado **4** posea un rendimiento cuántico de fluorescencia menor que su cromóforo precursor.

### 1.2.4. Propiedades láser

Las propiedades láser de estos colorantes, sin embargo, resultaron ser más dependientes de la fluoración que las propiedades fotofísicas. De acuerdo con sus bandas de absorción, los derivados de **Cu460** y de **PM546** fueron bombeados a 355 nm (Tabla 2) mientras que el resto de los colorantes fueron excitados bajo irradiación a 532 nm (Tabla 3).

Como se muestra en ambas tablas, y con excepción del derivados **2a**, todos estos nuevos colorantes fluorados presentan mejor eficiencia láser que sus correspondientes precursores no fluorados debido a que el enlace C-F posee una mayor fortaleza que el enlace C-H, aumentado así la estabilidad de la molécula, y reduciendo, con respecto a sus sistemas no fluorados, tanto sus procesos de fotoblanqueo como su reactividad frente al oxígeno singlete. Como resultado, los nuevos colorantes presentan una fotoestabilidad muy superior a la de sus precursores no fluorados, que reducía drásticamente su aplicabilidad. En este sentido, cabe señalar la elevada fotoestabilidad de la cumarina **2b**, que aumenta cinco veces con respecto a la cumarina comercial.

**Tabla 2.** Propiedades láser de los nuevos colorantes fluorados respecto a los comerciales no fluorados, bombeados a 355 nm y disueltos en AcOEt.

| Compuesto | Conc. (mM) | Ef (%) | $\lambda_{láser}$ (nm) | I (%) |
|---|---|---|---|---|
| **PM546** | 20 | 23 | 541 | 60 |
| **1a** | 20 | 38 | 556 | 95 |
| **Cu460** | 2 | 30 | 456 | 20 |
| **2a** | 5 | 20 | 466 | 0 |
| **2b** | 2 | 46 | 460 | 100 |

**Tabla 3.** Propiedades láser de los nuevos colorantes fluorados respecto a los comerciales no fluorados, bombeados a 532 nm y disueltos en AcOEt.

| Compuesto | Conc. (mM) | Ef (%) | $\lambda_{láser}$ (nm) | I (%) |
|---|---|---|---|---|
| **1a** | 3.5 | 46 | 558 | 95 |
| **Rh6G** | 0.9 | 42 | 580 | 20 |
| **3** | 1.5 | 65 | 582 | 70 |
| **PerRed** | 0.5 | 23 | 624 | 66 |
| **4** | 0.8 | 38 | 615 | 100 |

### 1.2.5. Conclusiones

Se ha desarrollado una metodología que permite la monofluoración directa de una serie de colorantes comerciales, con independencia de su esqueleto. Además, estos nuevos colorantes fluorados presentan una mayor eficiencia y estabilidad láser que sus precursores no fluorados, con la excepción del compuesto **2a** en que el átomo de flúor se localiza en el eje longitudinal de la molécula, reduciendo sus propiedades fotofísicas y su emisión láser.

Este aumento de eficiencia y fotoestabilidad láser se debe a que el enlace C-F presenta una mayor fortaleza que el enlace C-H, otorgando de esta manera una mayor estabilidad tanto química como fotoquímica a la molécula. Por lo tanto, la monofluoración resulta ser un protocolo sencillo de funcionalización directa para la mejora de las propiedades fotofísicas y de emisión láser de colorantes comerciales, con independencia de su estructura.

## 1.3. BODIPYS CLORADOS

**Artículo 2: "Chlorinated BODIPYs: Surprisingly Efficient and Highly Photostable Laser Dyes"** *Eur. J. Org. Chem.* **2012**, 6335-6350.

**Patente:** *Novel chlorinated derivatives of BODIPY as fluorescent markers and dyes*. ES201230486, **2012**.

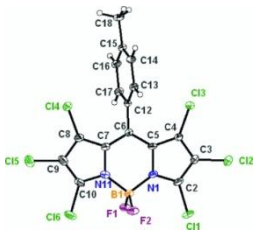


### 1.3.1. Introducción

En el estudio de fluoración de colorantes descrito anteriormente, se había observado la obtención del 2-cloroderivado del **PM546** al llevar a cabo la reacción del colorante comercial con $XeF_2$ en presencia de DCM como disolvente, manteniendo este derivado clorado la alta fluorescencia del **PM546**. Hasta este momento, los BODIPYs clorados se han utilizado como intermedios sintéticos en reacciones de $S_NAr$ o reacciones de acoplamiento C-C catalizadas por Pd en las posiciones 3 y 5,[9] y solamente existen algunos ejemplos descritos en la bibliografía en los que se ha medido el rendimiento cuántico de fluorescencia de estos intermedios clorados.[9d,10] Teniendo en cuenta estos resultados, se pensó que los derivados clorados podrían tener unas propiedades fotofísicas y láser interesantes, y no analizadas hasta ese momento.

Los BODIPYs son compuesto ricos en electrones y experimentan fácilmente reacciones de sustitución electrófila aromática. En las estructuras resonantes clásicas del núcleo de BODIPY, la densidad de carga positiva se sitúa con preferencia sobre las posiciones 1, 3, 5 y 7, lo que deja a las posiciones 2 y 6 como las más susceptibles de ataque electrófilo (Figura 22).[11]

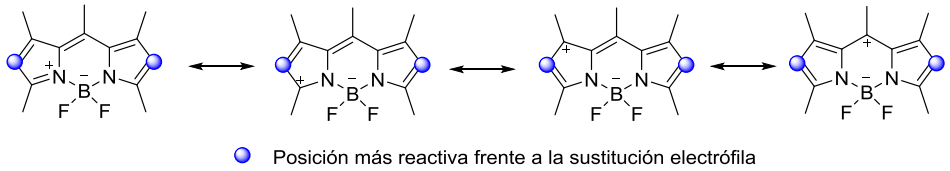


**Figura 22.** Estructuras resonantes del BODIPY.

Sin embargo, hasta ese momento no existía un estudio definitivo sobre la regioselectividad de la reacción de halogenación sobre BODIPYs no sustituidos, ya que en la mayoría de los casos estudiados las otras posiciones se encontraban ocupadas por otros sustituyentes. Por ello, se planteó el diseño y síntesis de una serie de cloroBODIPYs, así como el estudio teórico de sus estructuras y distribuciones de carga, y de sus propiedades fotofísicas y emisión láser. Para este estudio se eligieron tres BODIPYs con diferentes estructuras y grado de sustitución (Figura 23).

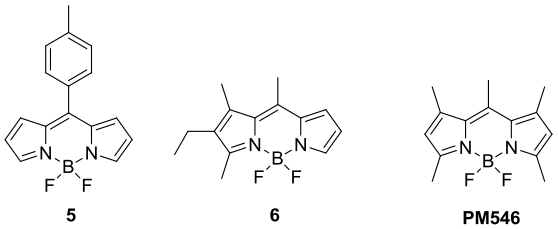


**Figura 23**. Estructuras de los BODIPYs **5**, **6** y **PM546**.

### 1.3.2. Síntesis

Para la obtención de los nuevos BODIPYs clorados se siguieron tres estrategias generales descritas previamente en la síntesis de otros BODIPYs halogenados por sustitución electrófila:

- Halogenación directa de BODIPYs.
- Halogenación de dipirrometanos intermedios.
- Halogenación de los pirroles precursores.

El estudio se inició con la reacción del BODIPY **5** con diferentes proporciones de *N*-clorosuccinimida (NCS) en THF a temperatura ambiente (Esquema 13). El empleo de dos equivalentes de reactivo condujo a la obtención de **7a** con un 80 % de rendimiento, mientras que para la obtención del derivado diclorado **7b** fue necesario el empleo de tres equivalentes. Los compuestos tri- y tetra-clorados **7c** y **7d** se obtuvieron por la reacción de **5** con cuatro y diez equivalentes de NCS, respectivamente.

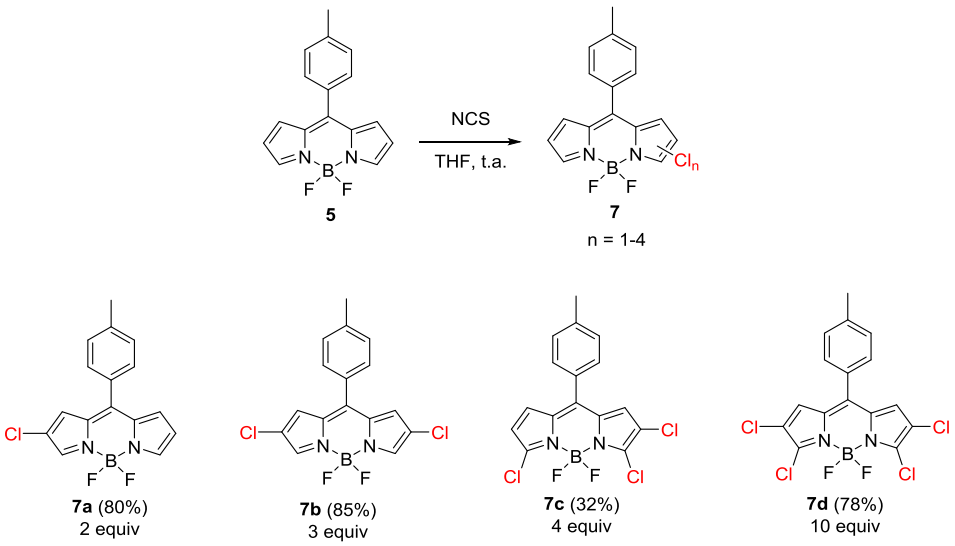


**Esquema 13**

El intento de obtención del BODIPY hexaclorado **7e**, por cloración directa de **5** empleando un gran exceso de NCS, no dio resultado ya que únicamente se obtuvo el derivado tetraclorado **7d**, por lo que se empleó el método descrito por Boens y col.[12] en el que la cloración tiene lugar sobre el dipirrometano precursor. Así, con un exceso de NCS (14 equiv), y a temperatura ambiente, se consiguió obtener el derivado hexaclorado **7e**, mientras que cuando se emplearon 2.2 equivalentes del agente halogenante a -78 ºC de temperatura se obtuvo el derivado 3,5-diclorado **7f**[12] (Esquema 14).

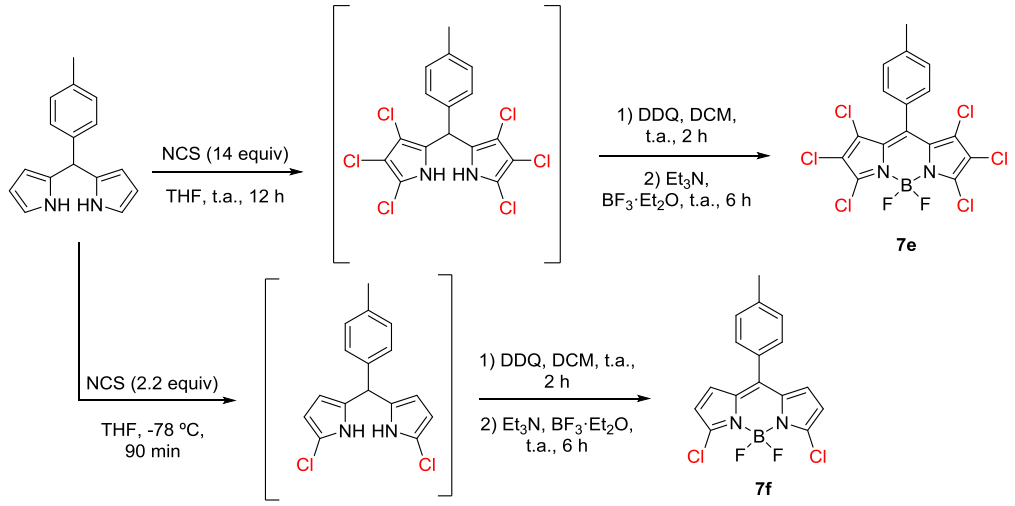


**Esquema 14**

Por otra parte, la halogenación directa del BODIPY asimétrico **6** tuvo como resultado la obtención de una mezcla compleja de productos, muy difícil de purificar por cromatografía. Por ello, se optó por la cloración de sus pirroles precursores. De esta forma, la cloración del 2-acetilpirrol con 1.1 equiv de NCS condujo a la obtención del pirrol **8a**,[9d] mientras que una mayor cantidad del reactivo (3 equiv) dio lugar a una mezcla de los pirroles **8b** y **8c**,[13] separables por cromotografía en columna (Esquema 15).

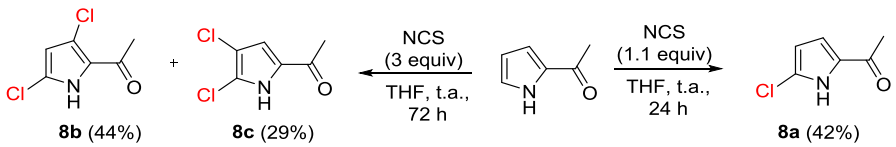


**Esquema 15**

Posteriormente, la reacción de los derivados **8a-c** con 3-etil-2,4-dimetilpirrol en presencia de $POCl_3$, seguida de la adición de $Et_3N$ y $BF_3{\cdot}Et_2O$ condujo a la formación de los BODIPYs **9a-c**, con rendimientos moderados (Esquema 16).

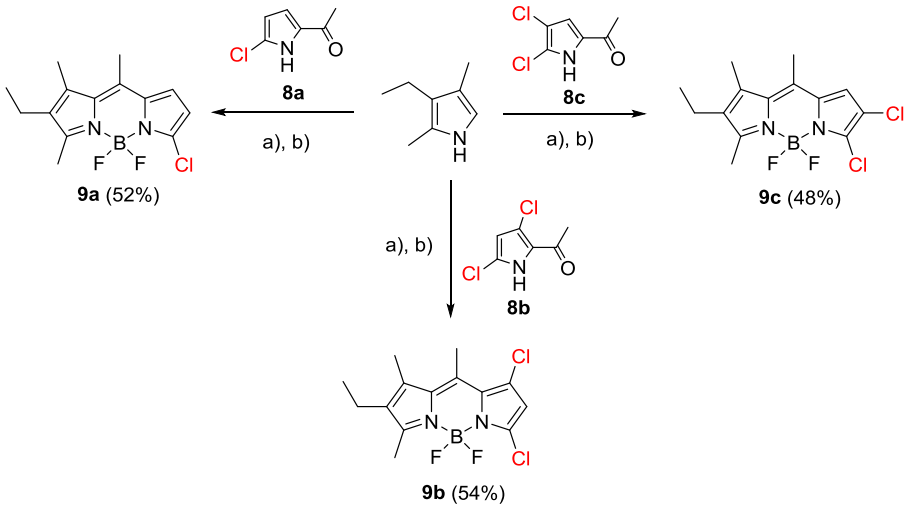


**Esquema 16**.Condiciones de reacción: a) $POCl_3$, DCM, t.a., 30 min. b) $Et_3N$, $BF_3{\cdot}Et_2O$, t.a., 3-4 h.

La cloración del **PM546** se realizó siguiendo un protocolo similar al del compuesto **5**, obteniéndose así los derivados **1b** y **1c** con un 73 y 67% de rendimiento, respectivamente, en función de la cantidad de NCS empleada (Esquema 17).

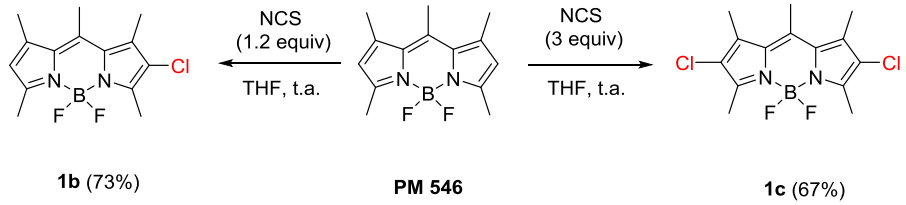


**Esquema 17**

Por último, se planteó la síntesis de un BODIPY clorado con emisión en la región roja del espectro visible. El compuesto elegido fue el derivado **10**, que se había obtenido de forma paralela en esta Tesis dentro del Capítulo de síntesis de nuevos BODIPYs con emisión en la zona roja del espectro. Para ello, se hizo reaccionar el compuesto **10** con 2 y 4 equivalentes de NCS para obtener los derivados clorados **11a** y **11b**, con rendimientos moderados (Esquema 18).

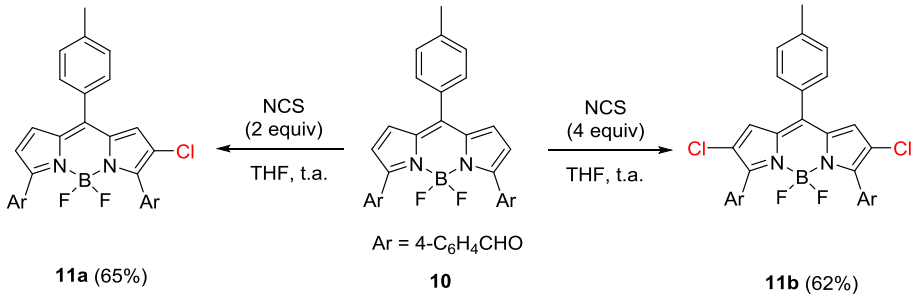


**Esquema 18**

### 1.3.3. Estudio teórico

Para una mayor comprensión de la regioselectividad observada en la reacción de cloración sobre BODIPYs, se realizó un estudio teórico de la distribución de cargas (CHelpg) del compuesto no halogenado **5** y de sus derivados clorados.

Los resultados obtenidos reflejan que las posiciones 2 y 6 son las que poseen mayor densidad de carga negativa, por lo que serán las más susceptibles de sufrir reacciones de sustitución electrófila, justificando la obtención de los compuestos mono y diclorados **7a** y **7b**. El carácter electronegativo del átomo de cloro perturba la distribución de carga, induciendo una disminución de carga negativa en las posiciones sustituidas y un aumento en el carbono adyacente. Por tanto, las posiciones más susceptibles de una ulterior sustitución electrofílica serían los carbonos 1 y 7. Sin embargo, la obtención del compuesto tetraclorado **7d** pone de manifiesto que las posiciones más reactivas a la sustitución electrófila, cuando las posiciones 2 y 6 se encuentran ocupadas, son las 3 y 5, probablemente por el impedimento estérico que el grupo fenilo en la posición 8 del BODIPY impone a los carbonos adyacentes 1 y 7 (Figura 24 y Tabla 4).

El estudio teórico también revela que, en la geometría optimizada, el grupo fenilo en la posición 8 se encontraría girado 55º con respecto al núcleo de indaceno cuando las posiciones 1 y 7 están libres, mientras que la incorporación de cloro en estas posiciones (compuesto **7e**) provoca un impedimento estérico suficiente para obligar al grupo fenilo a una disposición casi perpendicular (en un ángulo de 89º).

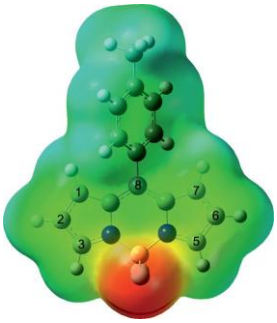

**Figura 24.** Mapa de potencial electroestático de **5**.

**Tabla 4.** Distribución de carga (CHelpg) de **5** y de sus derivados clorados

| | **Átomo de carbono del BODIPY** | | | | | |
|---|---|---|---|---|---|---|
| | **1** | **2** | **3** | **5** | **6** | **7** |
| **5** | -0.109 | -0.180 | 0.041 | 0.041 | -0.179 | -0.111 |
| **7a** | -0.107 | -0.181 | 0.046 | 0.036 | 0.064 | -0.150 |
| **7b** | -0.135 | 0.055 | 0.061 | 0.039 | 0.061 | -0.131 |
| **7c** | -0.078 | -0.181 | 0.189 | 0.168 | 0.055 | -0.129 |
| **7d** | -0.112 | 0.043 | 0.171 | 0.173 | 0.040 | -0.144 |
| **7e** | 0.084 | 0.004 | 0.190 | 0.171 | 0.028 | 0.066 |
| **7f** | -0.081 | -0.201 | 0.200 | 0.197 | -0.198 | -0.082 |

Estos datos teóricos concuerdan con los experimentales, ya que las estructuras de rayos X de los compuestos **7d** y **7e** indican que el anillo de fenilo en la posición 8 se sitúa en ángulos de 45º y 86º, respectivamente, respecto al esqueleto de indaceno (Figura 25).

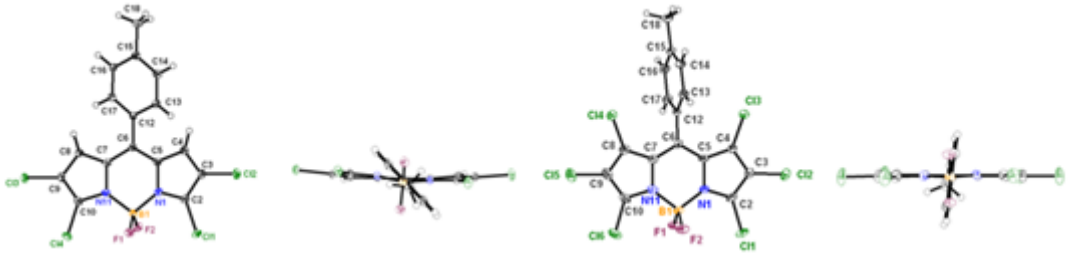

**7d** **7e**

**Figura 25**. Estructuras de rayos X de los compuestos **7d** y **7e**.

### 1.3.4. Propiedades fotofísicas

#### *1.3.4.1. Propiedades fotofísicas de los 8-arilBODIPYs clorados*

En el BODIPY **5**, el giro libre del grupo fenilo en la posición *meso* induce un aumento de los procesos de desactivación no radiativos y, en consecuencia, una drástica reducción del rendimiento de fluorescencia (Tabla 5).

**Tabla 5.** Propiedades fotofísicas del 8-arilBODIPY **5** y de sus derivados **7a-f** en AcOEt.

| BODIPY | $\lambda_{abs}$ (nm) | $\varepsilon_{max}$ ($10^4$ $M^{-1}\cdot cm^{-1}$) | $\lambda_{fl}$ (nm) | $\phi$ |
|---|---|---|---|---|
| **5** | 500.5 | 6.9 | 516.0 | 0.036 |
| **7a** | 518.5 | 6.5 | 534.5 | 0.093 |
| **7b** | 538.0 | 1.4 | 555.0 | 0.153 |
| **7c** | 530.0 | 10.5 | 542.0 | 0.560 |
| **7d** | 546.5 | 8.3 | 557.5 | 0.460 |
| **7e** | 537.0 | 9.5 | 548.5 | 0.450 |
| **7f**[a] | 514.0 | 8.7 | 551.0 | 0.30 |

[a] medido en c-hexano

La retirada de densidad electrónica del sistema π, por la introducción de átomos de cloro, conlleva una disminución de los procesos de desactivación no radiativos asociados al giro libre del anillo en la posición 8, lo que determina un aumento del rendimiento cuántico de fluorescencia, más acusado a mayor número de átomos de cloro unidos al núcleo del BODIPY.

Asimismo, el estudio teórico confirma que no sólo el número de átomos de cloro, sino también la posición que ocupan en la estructura, son factores determinantes en las propiedades fotofísicas de estos nuevos colorantes. Concretamente, la introducción de átomos cloro en las posiciones terminales del sistema π (posiciones 3 y 5) induce una mayor deslocalización de la densidad de carga por efecto "*push-pull*",[14] reduciendo aún más el giro libre del grupo fenilo y aumentando, en consecuencia, tanto las probabilidades de absorción como de emisión de fluorescencia observadas en los derivados **7c-7e**.

Esta hipótesis se ve confirmada analizando an las propiedades fotofísicas del compuesto **10** y de sus derivados clorados (compuestos **11a** y **11b**) (Tabla 6). La presencia de grupos electroaceptores, como 4-formilfenilo, en las posiciones 3 y 5 reduce la densidad electrónica en la posición *meso*, disminuyendo significativamente la rotación libre del grupo fenilo, lo que explica el elevado rendimiento de fluorescencia del compuesto **10** (0.54) comparado con el compuesto **5**, no sustituido en posiciones 3 y 5, que es no

fluorescente (0.036). La cloración del compuesto **10** retira aún más densidad de carga del sistema π, reduciendo la probabilidad de absorción y de emisión.

**Tabla 6.** Propiedades fotofísicas del colorante **10** y de sus derivados clorados **11a** y **11b** en AcOEt.

| BODIPY | $\lambda_{abs}$ (nm) | $\varepsilon_{max}$ ($10^4 \cdot M^{-1} \cdot cm^{-1}$) | $\lambda_{fl}$ (nm) | $\phi$ |
|---|---|---|---|---|
| **10** | 558.0 | 3.0 | 599.0 | 0.54 |
| **11a** | 559.5 | 4.0 | 596.5 | 0.29 |
| **11b** | 564.0 | 1.0 | 599.5 | 0.22 |

Además, la cloración reduce también la separación energética entre estados excitados, lo que incrementa procesos no-radiativos de conversión interna, que contribuyen a reducir aún más la capacidad de emisión de los colorantes **11a** y **11b**.

### *1.3.4.2. Propiedades fotofísicas de los alquilBODIPYs clorados*

Las propiedades fotofísicas del alquilBODIPY **6** están gobernadas por la asimetría en la distribución de densidad de carga entre sus unidades de pirrol. Por tanto, las propiedades fotofísicas de sus derivados clorados van a mostrar una mayor dependencia con el número y posición de los átomos de cloro que los derivados clorados del BODIPY **5** (Tabla 7).

**Tabla 7.** Propiedades fotofísicas del alquilBODIPY **6** y de sus derivados clorados **9a-c** en AcOEt.

| BODIPY | $\lambda_{abs}$ (nm) | $\varepsilon_{max}$ ($10^4\ M^{-1} \cdot cm^{-1}$) | $\lambda_{fl}$ (nm) | $\phi$ |
|---|---|---|---|---|
| **6** | 504.0 | 3.3 | 515.0 | 0.96 |
| **9a** | 510.5 | 5.1 | 520.5 | 0.78 |
| **9b** | 504.0 | 3.3 | 526.0 | 0.57 |
| **9c** | 521.0 | 3.3 | 531.0 | 0.91 |

La introducción de un átomo de cloro en la posición 5 del BODIPY **6**, compuesto **9a**, incrementa aún más la asimetría en la distribución de densidad de carga entre las unidades

de pirrol, lo que justifica que el compuestos **9a** posea un menor rendimiento cuántico de fluorescencia que su precursor no clorado.

Esta asimetría en la distribución de densidad de carga depende del número y de las posiciones sustituidas por átomos de cloro. Así, el compuesto **9c**, con átomos de cloro en las posiciones 5 y 6 del BODIPY, posee unas propiedades fotofísicas similares a las del BODIPY **6**. Por otro lado, la introducción de átomos de cloro en las posiciones 5 y 7 produce una fuerte asimetría, lo que justifica que el compuesto **9b** presente peores propiedades fotofísicas que su homólogo no clorado.

En cuanto a los derivados clorados del **PM546**, el compuestos monoclorado **1b** posee unas propiedades fotofísicas muy similares a las de su precursor (Tabla 8).

**Tabla 8.** Propiedades fotofísicas del alquilBODIPYs **PM546**, y de sus derivados **1b** y **1c** en AcOEt

| **BODIPY** | $\lambda_{abs}$ **(nm)** | $\varepsilon_{max}$ **($10^4 \cdot M^{-1} \cdot cm^{-1}$)** | $\lambda_{fl}$ **(nm)** | $\phi$ |
|---|---|---|---|---|
| **PM546** | 499.5 | 9.7 | 512.0 | 0.91 |
| **1b** | 512.0 | 5.5 | 525.5 | 0.91 |
| **1c** | 527.0 | 7.1 | 542.5 | 0.87 |

Sin embargo, el derivado diclorado **1c** presenta un rendimiento cuántico de fluorescencia ligeramente inferior al del **PM546** debido a que se produce una mayor retirada de densidad de carga del sistema $\pi$ del BODIPY. En resumen, se demuestra que las posiciones 2 y 6 no son muy sensibles a los efectos de sustitución.

### 1.3.5. Propiedades láser

El comportamiento láser de los 8-arilBODIPYs **7a-f** presenta una buena concordancia con las propiedades fotofísicas descritas anteriormente. Como puede observarse en la Tabla 9, la eficiencia láser aumenta al aumentar el número de átomos de cloro unidos al BODIPY, desde un 30% en el derivado monoclorado **7a** hasta un 60% en el derivado hexaclorado **7e**. Al igual que sus propiedades fotofísicas, la eficiencia láser también

depende de la posición en la que se encuentre el átomo de cloro, ya que el compuesto 3,5-diclorado **7f** presenta una mayor eficiencia láser que el derivado 2,6-diclorado **7b**.

**Tabla 9**. Propiedades láser de los compuestos **7a-f** en AcOEt.

| | BODIPY | | | | | |
|---|---|---|---|---|---|---|
| | **7a** | **7b** | **7c** | **7d** | **7e** | **7f** |
| **$\lambda_{láser}$ (nm)** | 572 | 575 | 573 | 575 | 571 | 572 |
| **Ef (%)** | 30 | 44 | 58 | 57 | 60 | 48 |
| **I (%)** | 90 | 95 | 100 | 100 | 100 | 100 |

En cuanto a sus fotoestabilidades, los derivados clorados **7a-f** resultaron ser más fotoestables que su precursor no clorado **5** y, además, la fotoestablidad aumenta al aumentar el número de átomos de cloro (Figura 26), comportamiento que también puede explicarse en relación a sus propiedades fotofísicas, ya que la cloración disminuye los procesos no radiativos de desactivación.

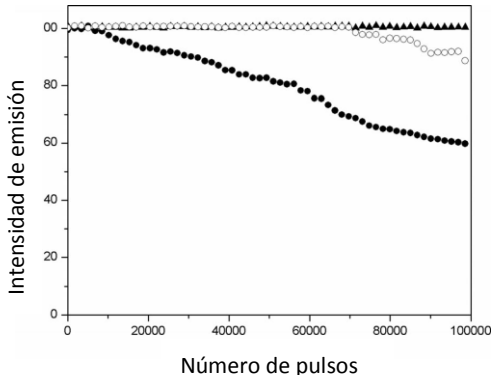


**Figura 26.** Fotoestabilidad de los BODIPYs **5** (●), **7a** (○) y **7e** (▲) en AcOEt.

Este aumento de la eficiencia láser y de la fotoestabilidad observada en los nuevos 8-arilBODIPYs clorados también se observa en el resto de los BODIPYs clorados descritos en este Capítulo (Tabla 10). Sin embargo, no existe una correlación entre las propiedades fotofísicas y la eficiencia láser, ya que la incorporación de átomos de cloro al BODIPY **6**, **10** y **PM546** empeora sus propiedades fotofísicas, pero aumenta su eficiencia y estabilidad láser.

**Tabla 10.** Propiedades láser de los colorantes **6**, **10** y **PM546**, y sus derivados clorados **9-11** y **1b-c** en AcOEt.

| | BODIPY | | | | | | | | | |
|---|---|---|---|---|---|---|---|---|---|---|
| | **6** | **9a** | **9b** | **9c** | **PM546** | **1b** | **1c** | **10** | **11a** | **11b** |
| **Ef (%)** | 34 | 38 | 46 | 36 | 23 | 40 | 51 | 14 | 28 | 30 |
| **$\lambda_{laser}$ (nm)** | 530 | 561 | 566 | 562 | 541 | 558 | 562 | 615 | 612 | 618 |
| **I (%)** | 80 | 100 | 100 | 100 | 60 | 90 | 100 | 50 | 85 | 100 |

De hecho, un análisis detallado de la dependencia de las propiedades láser con la cloración plantea otras importantes cuestiones, como por ejemplo: a) un colorante como el tetracloroBODIPY **7d**, con un rendimiento de fluorescencia bajo (0.46), tiene una eficiencia laser del 57%; b) sin embargo, un colorante como el BODIPY monoclorado **9a**, con un mayor rendimiento de fluorescencia (0.78), presenta menor eficiencia láser (38%). Para explicar este comportamiento hay que considerar los efectos de la polarización del láser de bombeo en la emisión láser de los nuevos colorantes.

La presencia de átomos de cloro unidos al núcleo de BODIPY determina un momento dipolar, cuyo módulo y orientación depende del número y posición del átomo de cloro en el BODIPY. El alineamiento entre el momento dipolar de la molécula y la polarización del láser de excitación incrementa significativamente la eficiencia fotónica del sistema. Por ello, aquellos colorantes con mayor momento dipolar y totalmente alineado (o paralelo) a lo largo del eje transversal de la molécula, como el compuesto tetraclorado **7d**, (Figura 27) presentan una elevada eficiencia láser, con independencia de su rendimiento de fluorescencia. Sin embargo, otros derivados, como el BODIPY monoclorado **9a**, tienen un momento dipolar menor y girado con respecto al eje transversal de molécula (Figura 27), lo que reduce su eficiencia en la absorción del bombeo y, en consecuencia, en su emisión. De ahí que, aunque siendo colorantes láser eficientes, no lo sean tanto como cabría esperar de colorantes con rendimientos de fluorescencia tan altos como 0.94.

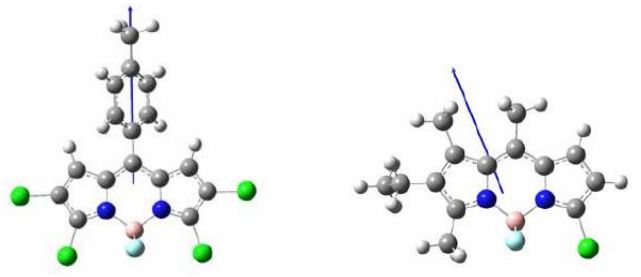

**7d** **9a**

**Figura 27**. Momentos dipolares de los compuestos **7d** y **9a**

### 1.3.6. Conclusiones

La cloración de BODIPYs es un protocolo de síntesis directo, barato y sencillo para mejorar significativamente las propiedades fotofísicas y, especialmente, el comportamiento láser de colorantes tanto comerciales como de síntesis. La metodología de síntesis aquí desarrollada permite controlar tanto el grado como la posición de cloración, modulando las propiedades ópticas del BODIPY de partida, permitiendo establecer relación entre la estructura del colorante y sus propiedades de emisión.

Los cálculos teóricos predicen las posiciones más accesibles a la halogenación, así como la variación del módulo y orientación del momento dipolar en la molécula final. De hecho, las elevadas eficiencias láser registradas con algunos de estos nuevos BODIPYs clorados no sólo están tanto relacionadas con unos rendimientos cuánticos de fluorescencia elevados como con el hecho de que la cloración, dependiendo del número de átomos de cloro y la posición a la que estos se incorporan en el cromóforo BODIPY, induce momentos dipolares altos con la orientación adecuada para alinearse con la polarización del láser de bombeo, lo que incrementa significativamente la eficiencia cuántica del sistema.

## 1.4. BODIPYS YODADOS

**Artículo 3: "Synthesis and functionalization of new polyhalogenated BODIPY dyes. Study of their photophysical properties and singlet oxygen generation"** *Tetrahedron*, **2012**, *68*, 1153-1162.

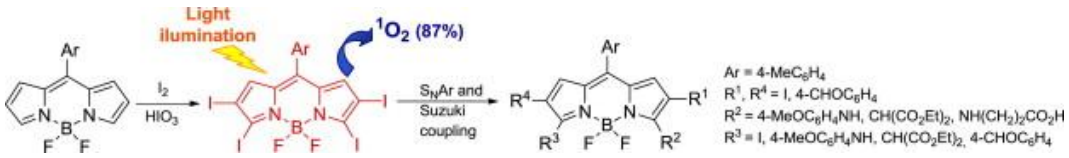


### 1.4.1. Introducción

Paralelamente al estudio de cloración de BODIPYs con diferente grado de sustitución, se llevó a cabo un estudio teórico, experimental y fotofísico sobre la reacción de yodación selectiva de una serie de BODIPYs (Figura 28) análogos a los empleados en la cloración.

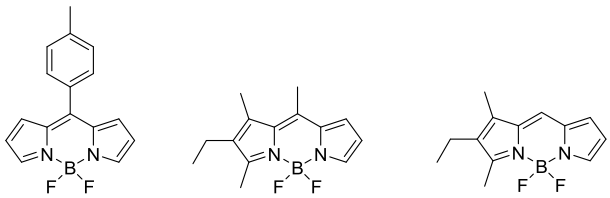


**Figura 28**. Estructuras de los BODIPYs **5**, **6** y **12**.

Una interesante observación es que los yodoBODIPYs obtenidos en este estudio pueden considerarse también como precursores sintéticos valiosos para la incorporación selectiva de diferentes grupos funcionales en posiciones específicas del BODIPY.

Además, la presencia de átomos pesados, como el yodo, unidos directamente al núcleo de indaceno, incrementa la probabilidad de ISC, y por tanto, su capacidad para generar oxígeno singlete.

### 1.4.2. Estudio teórico

El estudio teórico, cuyos resultados están recogidos en el artículo, demuestra que, en principio, todas las posiciones del BODIPY son susceptibles de ser yodadas, siendo dependiente de factores estéricos en el BODIPY **5** y de factores electrónicos en los BODIPYs **6** y **12**. Así, en el BODIPY **5** no se observa la yodación de las posiciones 1 y 7 debido al impedimento estérico del grupo fenilo junto con el gran tamaño del átomo de yodo. En el caso del BODIPY **12**, tampoco se observa la yodación de la posición *meso*, ya que los mapas de potencial electroestático muestran carga positiva en el entorno de dicha posición, lo que está de acuerdo con la orientación del momento dipolar a lo largo del eje transversal de la molécula, situando una mayor densidad de carga negativa en los átomos de flúor y carga positiva en la posición *meso*. Además, cabe esperar que en los BODIPYs **6** y **12** la yodación tenga lugar en primer lugar en las posiciones 5 y 6, ya que el átomo de yodo puede acceder de una forma más fácil a estas posiciones, aunque presentan menor carga negativa que las posiciones 7 y 8.

### 1.4.3. Síntesis

En este estudio se emplearon como agentes de yodación ICl o el sistema $I_2/HIO_3$. En primer lugar se llevó a cabo la reacción sobre el BODIPY **5** empleando ICl como agente de halogenación, lo que permitió obtener los derivados **13a-g** (Esquema 19).

Así, la reacción de halogenación con cantidades equimolares del reactivo dio lugar al derivado monoyodado **13a**. El empleo de 2.5 equivalentes de ICl condujo al correspondiente derivado diyodado **13b**. También fue posible la obtención del derivado triyodado **13c**, aunque con menor rendimiento debido a que se encontraba acompañado de los di- y tetrayodado derivados, **13b** y **13d**, respectivamente, difícilmente separables por cromatografía. Mayores proporciones de ICl condujeron a mezclas complejas de derivados polihalogenados (**13d-g**) con átomos de yodo y cloro en diferentes posiciones del BODIDY (Tabla 11). La reactividad que presenta el BODIPY **5** en presencia de ICl y DCM como disolvente, concuerda con los datos bibliográficos sobre la reactividad de

compuestos aromáticos con este reactivo, que ponen de manifiesto que es posible obtener cloro o yodo derivados en función de las condiciones de reacción.[15]

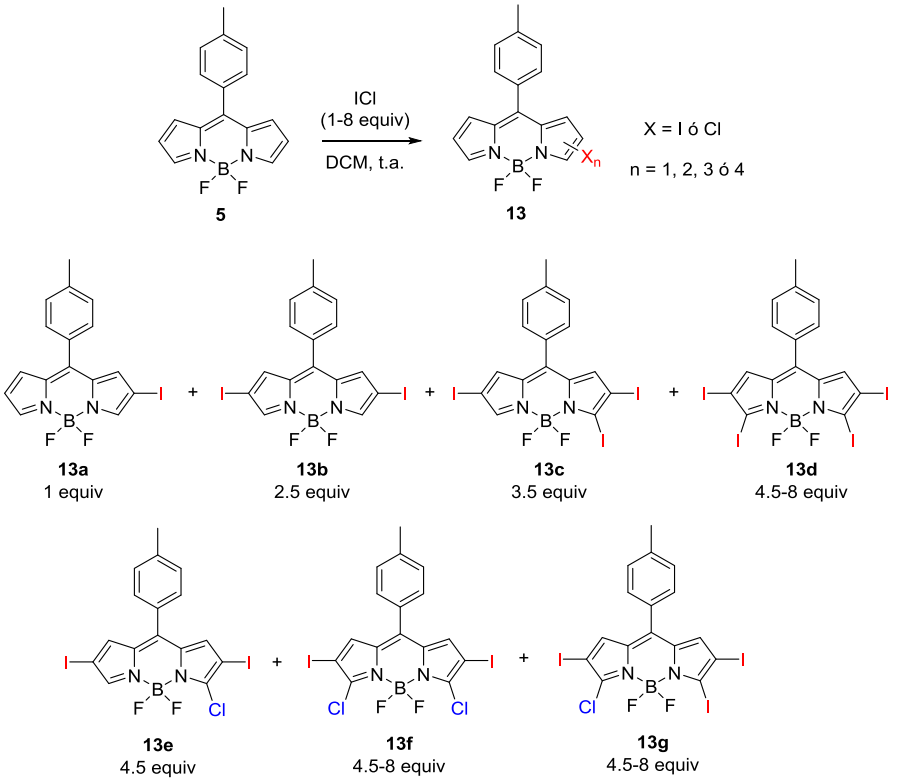


**Esquema 19**

**Tabla 11.** Condiciones de reacción y productos de la reacción de yodación de **5**. En rojo se detaala los compuestos que se obtienen con un mayor rendimiento.

| **Condiciones** | **Equiv**[a] | **Tiempo (min)** | **BODIPY (%)** |
|---|---|---|---|
| ICl | 1:1 | 30 | **13a** (75) |
| ICl | 1:2.5 | 60 | **13a** (14), **13b** (72) |
| ICl | 1:3.5 | 120 | **13b** (22), **13c** (54), **13d** (8) |
| ICl | 1:4.5 | 180 | **13d** (10), **13e** (5), **13f** (21) **13g** (40) |
| ICl | 1:8 | 360 | **13d** (25), **13f** (24), **13g** (20) |
| $I_2/HIO_3$ | 1:1:0.8 | 30 | **13a** (70) |
| $I_2/HIO_3$ | 1:2.5:2 | 60 | **13a** (15), **13b** (69) |
| $I_2/HIO_3$ | 1:3.5:3 | 60 | **13b** (15), **13c** (30), **13d** (30) |
| $I_2/HIO_3$ | 1:4.5:4 | 180 | **13d** (64) |

[a] relación molar BODIPY/ICl o BODIPY/$I_2$/$HIO_3$

Para evitar la formación de los derivados clorados, se llevó a cabo la reacción de yodación de **5** usando el sistema $I_2/HIO_3$ como agente de yodación en diferentes cantidades, lo que permitió obtener los compuestos **13a-d** con buenos rendimientos, aunque el resultado más interesante con este reactivo es la formación de **13d**, que se obtenía como una mezcla de compuestos difícil de separar cuando la reacción se llevaba a cabo en presencia de ICl.

Análogamente, la reacción de los BODIPYs **6** y **12** con ICl en proporciones prácticamente estequiométricas permitió la obtención de los monoyododerivados **14a** y **15a**, respectivamente, con excelentes rendimientos (Esquema 20), aunque cuando la reacción se llevó a cabo con un mayor número de equivalentes de ICl se obtuvo también una mezcla de los mono-, di- y trihaloBODIPYs (**14a-e** y **15a-e**). Por ello, se empleó de nuevo el sistema $I_2/HIO_3$ para obtener de forma exclusiva o mayoritaria los correspondientes triyododerivados con rendimientos moderados (Tabla 12).

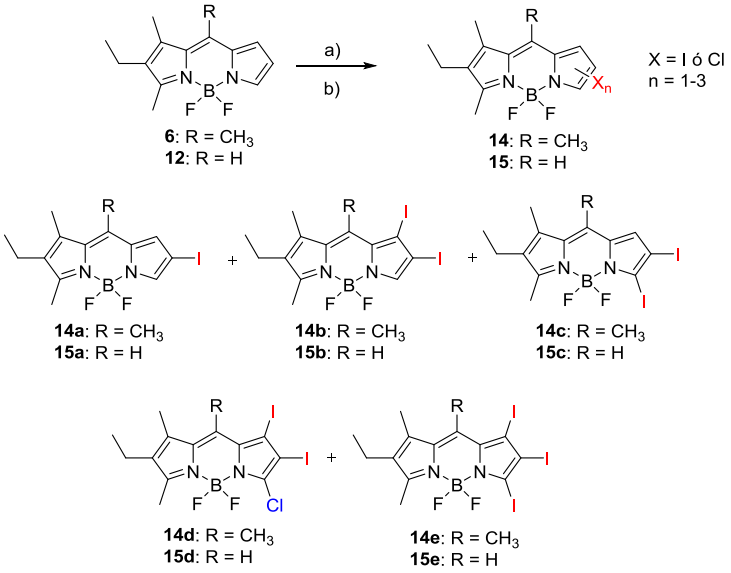


**Esquema 20**. Condiciones de reacción: a) ICl en DCM, t.a. b) $I_2/HIO_3$, EtOH, reflujo.

**Tabla 12.** Condiciones de reacción y productos de la reacción de yodación de **6** y **12**.

| BODIPY | Condiciones | Equiv[a] | Tiempo (min) | BODIPY (%) |
|---|---|---|---|---|
| **6** | ICl | 1:1.3 | 30 | **14a** (95) |
| | ICl | 1:1.25 | 60 | **14a** (8), **14b** (10), **14c** (67) |
| | ICl | 1:6 | 180 | **14c** (6), **14d** (35), **14e** (20) |
| | $I_2/HIO_3$ | 1:4.5:4 | 180 | **14c** (5), **14e** (48) |
| **12** | ICl | 1:0.8 | 30 | **15a** (81) |
| | ICl | 1:2.5 | 90 | **15a** (13), **15b** (34), **15c** (35) |
| | ICl | 1:8 | 300 | **15d** (30), **15e** (35) |
| | $I_2/HIO_3$ | 1:5:4.5 | 300 | **15e** (54) |

[a] relación molar BODIPY/ICl ó BODIPY/$I_2/HIO_3$

Los resultados obtenidos indican que cualquier posición del BODIPY es susceptible de sufrir reacciones de sustitución electrófila, a excepción de la posición 8 debido a su baja densidad de carga negativa (Figura 29).

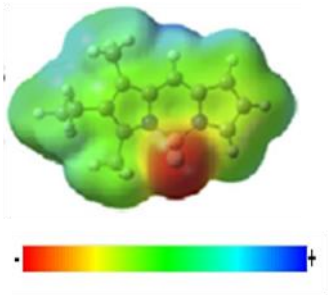

**Figura 29.** Distribución de densidad de carga del BODIPY **12**.

### 1.4.4. Funcionalización selectiva

Como ha quedado reflejado en la introducción de este capítulo, los BODIPYs halogenados son precursores sintéticos para una funcionalización selectiva del núcleo de indaceno, permitiendo la obtención de una gran variedad de BODIPYs que son difíciles de obtener por procedimientos alternativos. Está descrito que los 3,5-dihaloBODIPYs experimentan fácilmente reacciones de sustitución de los átomos de halógeno por un gran número de nucleófilos oxigenados, carbonados, nitrogenados o sulfurados y, además, las condiciones de reacción pueden controlarse para la obtención de productos mono- o

disustituidos.[12] Teniendo en cuenta estas consideraciones, en este estudio se llevó a cabo la reacción del compuesto tetrayodado **13d** con varios nucleófilos, lo que permitió obtener, dependiendo de las condiciones de reacción, los derivados **16**-**20**, en los que se ha introducido una o dos unidades del reactivo nucleófilo (Esquema 21).

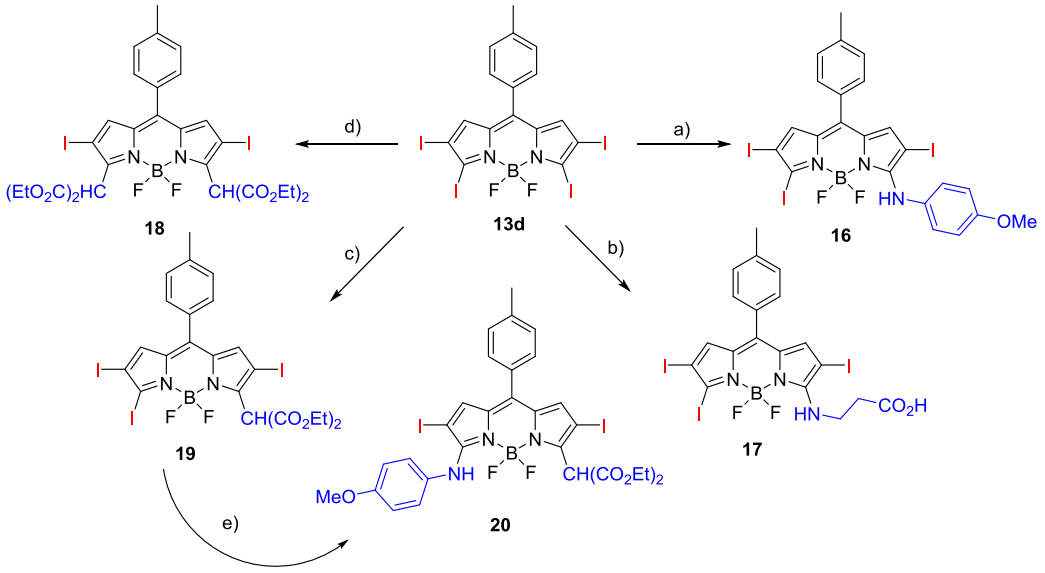


**Esquema 21.** a) *p*-anisidina (2 equiv), $CH_3CN$, Δ; b) β-alanina, (5 equiv), $CH_3CN$, Δ; c) malonato de dietilo (1.1 equiv), NaH, $CH_3CN$, Δ; d) malonato de dietilo (4 equiv), NaH, $CH_3CN$, Δ; e) *p*-anisidina (1.1 equiv), $CH_3CN$, Δ.

Además, estos nuevos yodoBODIPYs pueden experimentar también reacciones de acoplamiento C-C catalizadas por paladio, lo que incrementa el valor añadido de los mismos como intermedios sintéticos, pudiendo obtenerse derivados como el compuesto **21**, con emisión en la zona roja del espectro visible (Esquema 22).

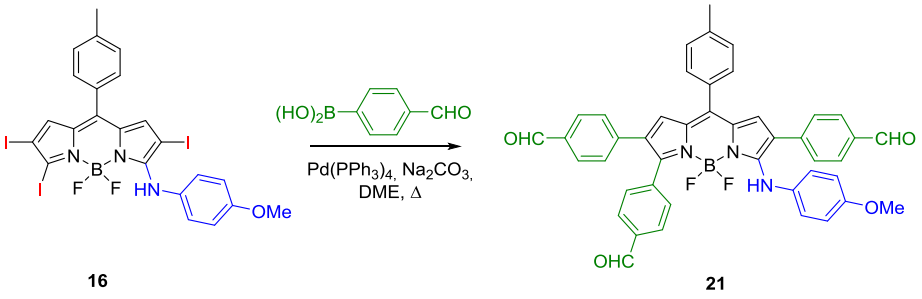


**Esquema 22**

### 1.4.5. Propiedades fotofísicas

Como se refleja en la Tabla 13, la progresiva introducción de átomos de yodo en los BODIPYs **5**, **6** y **12** produce un desplazamiento batocrómico en sus bandas de absorción y emisión y, de forma general, una disminución significativa del rendimiento cuántico de fluorescencia por efecto del átomo pesado, fundamentalmente en los derivados yodados de **6** y **12**.

**Tabla 13**. Propiedades fotofísicas de los derivados yodados del **5**, **6** y **12** en c-hexano.

| **BODIPY** | $\lambda_{abs}$ **(nm)** | $\varepsilon_{max}$ **($10^4$ $M^{-1}\cdot cm^{-1}$)** | $\lambda_{fl}$ **(nm)** | $\phi$ |
|---|---|---|---|---|
| **5** | 500.5 | 6.9 | 516.0 | 0.036 |
| **13a** | 523.5 | 2.2 | 540.0 | 0.034 |
| **13b** | 548.5 | 4.3 | 567.5 | 0.012 |
| **13c** | 563.5 | 4.8 | 577.5 | 0.060 |
| **13d** | 581.0 | 11.6 | 593.0 | 0.099 |
| **6** | 504.0 | 3.3 | 515.0 | 0.96 |
| **14a** | 517.5 | 4.6 | 532.0 | 0.13 |
| **14b** | 515.5 | 2.9 | 538.5 | 0.05 |
| **14c** | 532.0 | 9.8 | 546.0 | 0.20 |
| **14e** | 531.5 | 1.7 | 554.5 | 0.10 |
| **12** | 512.5 | 2.9 | 517.5 | 0.70 |
| **15a** | 528.0 | 6.3 | 538.5 | 0.11 |
| **15b** | 527.5 | 5.6 | 537.0 | 0.05 |
| **15c** | 542.0 | 7.6 | 550.5 | 0.26 |
| **15e** | 543.5 | 6.9 | 551.5 | 0.07 |

Esta disminución del rendimiento cuántico de fluorescencia tiene lugar, salvo que:

- Los átomos de halógeno ocupen las posiciones 3 y/o 5 del cromóforo, lo que induce un efecto *"push-pull"* ya comentado en el caso de los BODIPYs clorados y que conlleva un incremento del rendimiento de fluorescencia al disminuir los procesos no radiantes. De ahí que los 6,7-diyododerivados (**14b** y **15b**) presenten

un rendimiento de fluorescencia muy inferior a los 5,6-diyododerivados (**14c** y **15c**).

- Exista una alta homogeneidad en la distribución de carga electrónica del sistema. De ahí que el derivado tetrayodado **13d** presente un rendimiento cuántico de fluorescencia tres veces superior al de su BODIPY precursor.

Los resultados obtenidos en este estudio concuerdan con los observados para los correspondientes derivados clorados en los que quedó demostrado que el número y posición del átomo de halógeno modula las propiedades fotofísicas del colorante final.

### 1.4.6. Generación de oxígeno singlete

Una vez realizado el estudio fotofísico de estos nuevos BODIPYs yodados, se evaluó la capacidad de los compuestos **13b-d** como generadores de oxígeno singlete, utilizando como referencia el Rosa de Bengala (RB) con un $\phi_\Delta$ para la generación de $^1O_2$ de 0.71 (Figura 30).

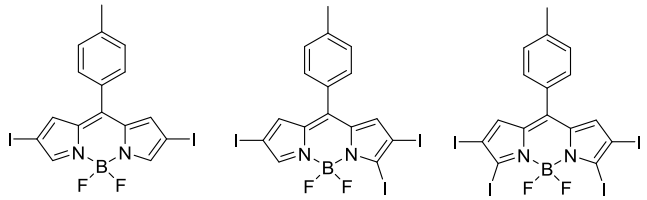


**Figura 30**. Estructuras de **13b-d** y sus rendimientos de generación de $^1O_2$

Los resultados obtenidos indican que los nuevos BODIPYs yodados son unos buenos generadores de oxígeno singlete, con valores superiores a los descritos para fotosensibilizadores de $^1O_2$ utilizados como referencia, y que la incorporación de átomos de yodo en las posiciones 3 y 5 no produce un incremento significativo en dicha generación.

### 1.4.7. Conclusiones

Se ha desarrollado una nueva y sencilla metodología sintética para la obtención de derivados poliyodados de forma regioselectiva, que permite, en función del número y posición de los átomos de yodo introducidos, modular fácilmente sus propiedades fotofísicas. Estos nuevos BODIPYs yodados, aparte de ser unos intermedios sintéticos muy versátiles para reacciones más complejas, pueden comportarse como excelentes generadores de oxígeno singlete.

## 1.5. BIBLIOGRAFÍA


[1] a) C. Vijila, A. Ramalingam, *J. Mater. Chem.* **2001**, *11*, 749-755; b) C. C. Spagnuolo, R. J. Vermeij, E. A. Jares-Erijman, *J. Am. Chem. Soc.* **2006**, *128*, 12040-12041; c) G. Y. Mitronova, V. N. Belov, M. L. Bossi, C. A. Wurm, L. Meyer, R. Medda, G. Moneron, S. Bretschneider, C. Eggeling, S. Jakobs, S. W. Hell, *Chem. Eur. J.* **2010**, *16*, 4477-4488.

[2] a) F. Wuerthner, P. Osswald, R. Schmidt, T. E. Kaiser, H. Mansikkamaeki, M. Koenemann, *Org. Lett.* **2006**, *8*, 3765-3768; b) G. L. Silva, V. Ediz, D. Yaron, B. A. Armitage, *J. Am. Chem. Soc.* **2007**, *129*, 5710-5718; c) R. Schmidt, P. Osswald, M. Koenemann, F. Wuerthner, *Z. Naturforsch., B: J. Chem. Sci.* **2009**, *64*, 735-746.

[3] a) B. R. Renikuntla, H. C. Rose, J. Eldo, A. S. Waggoner, B. A. Armitage, *Org. Lett.* **2004**, *6*, 909-912; b) K. Hamada, E. Miyawaki, J.-Y. Jaung, *Color Technol.* **2005**, *121*, 127-131.

[4] D. Holling, G. Sandford, A. S. Batsanov, D. S. Yufit, J. A. K. Howard, *J. Fluorine Chem.* **2005**, *126*, 1377-1383.

[5] T. Suzuki, T. Tanaka, I. Higashiguchi, A. Oda, JP11176572A, **1999**.

[6] a) W. W. Dukat, J. H. Holloway, E. G. Hope, P. J. Townson, R. L. Powell, *J. Fluorine Chem.* **1993**, *62*, 293-296; b) M. A. Tius, *Tetrahedron* **1995**, *51*, 6605-6634.

[7] M. Zupan, A. Pollak, *J. Fluorine Chem.* **1976**, *8*, 275-278.

[8] Z. Suzuki, K. Morita, *Bull. Chem. Soc. Jap.* **1968**, *41*, 1724-1725.

[9] a) A. Ojida, T. Sakamoto, M.-a. Inoue, S.-h. Fujishima, G. Lippens, I. Hamachi, *J. Am. Chem. Soc.* **2009**, *131*, 6543-6548; b) Y. Xiao, D. Zhang, X. Qian, A. Costela, I. Garcia-Moreno, V. Martin, M. E. Perez-Ojeda, J. Bañuelos, L. Gartzia, I. L. Arbeloa, *Chem. Commun.* **2011**, *47*, 11513-11515; c) S. Yin, V. Leen, S. Van Snick, N. Boens, W. Dehaen, *Chem. Commun.* **2010**, *46*, 6329-6331; d) V. Leen, T. Leemans, N. Boens, W. Dehaen, *Eur. J. Org. Chem.* **2011**, *2011*, 4386-4396; e) L. Jiao, W. Pang, J. Zhou, Y. Wei, X. Mu, G. Bai, E. Hao, *J. Org. Chem.* **2011**, *76*, 9988-9996; f) V. Leen, D. Miscoria, S. Yin, A. Filarowski, J. M. Ngongo, M. Van der Auweraer, N. Boens, W. Dehaen, *J. Org. Chem.* **2011**, *76*, 8168-8176; g) Y.

Chen, J. Zhao, L. Xie, H. Guo, Q. Li, *RSC Adv.* **2012**, *2*, 3942-3953; h) X. Li, S. Huang, Y. Hu, *Org. Biomol. Chem.* **2012**, *10*, 2369-2372.

[10] a) W. Qin, T. Rohand, W. Dehaen, J. N. Clifford, K. Driesen, D. Beljonne, B. Van Averbeke, M. Van der Auweraer, N. Boens, *J. Phys.Chem. A* **2007**, *111*, 8588-8597; b) S. Rihn, P. Retailleau, N. Bugsaliewicz, A. De Nicola, R. Ziessel, *Tetrahedron Lett.* **2009**, *50*, 7008-7013; ) L. Jiao, C. Yu, M. Liu, Y. Wu, K. Cong, T. Meng, Y. Wang, E. Hao, *J. Org. Chem.* **2010**, *75*, 6035-6038; d) K. Krumova, G. Cosa, *J. Am. Chem. Soc.* **2010**, *132*, 17560-17569; e) T.-I. Kim, S. Park, Y. Choi, Y. Kim, *Chem. Asian J.* **2011**, *6*, 1358-1361.

[11] A. Loudet, K. Burgess, *Chem. Rev*. **2007**, *107*, 4891-4932.

[12] T. Rohand, M. Baruah, W. Qin, N. Boens, W. Dehaen, *Chem. Commun.* **2006**, 266-268.

[13] R. A. Rane, V. N. Telvekar, *Bioorg. Med. Chem. Lett.* **2010**, *20*, 5681-5685.

[14] A. Cui, X. Peng, J. Fan, X. Chen, Y. Wu, B. Guo, *J. Photochem. Photobiol. A* **2007**, *186*, 85-92.

[15] a) S. M. Hubig, W. Jung, J. K. Kochi, *J. Org. Chem.* **1994**, *59*, 6233-6244; b) L. Eberson, M. P. Hartshorn, F. Radner, O. Persson, *J. Chem. Soc., Perkin Trans. 2* **1998**, 59-70; c) V. K. Chaikovskii, V. D. Filimonov, *Russ. J. Org. Chem.* **2001**, *37*, 1130-1133.

# CAPÍTULO 2. COLORANTES CON EMISIÓN EN EL ROJO

# 2. COLORANTES CON EMISIÓN EN EL ROJO

## 2.1. INTRODUCCIÓN

Existe un interés creciente en el desarrollo de nuevos colorantes fluorescentes que emitan en la zona de baja energía, con longitudes de onda superiores a 600 nm.[1] Estos colorantes muestran varias ventajas sobre los que emiten a longitud de onda más corta: presentan mayor penetrabilidad en los tejidos y presentan menor interferencia con la emisión auto-fluorescente (UV) de las biomoléculas.

En la actualidad existen colorantes comerciales con emisión centrada en la zona roja del espectro visible, tales como rodaminas y perilenos, aunque ambos presentan problemas relacionados con la agregación y la solubilidad, además de poseer bajos coeficientes de absorción a las longitudes de onda de bombeo más comunes (355 y 532 nm), como se mencionó en el Capítulo 1. Existen también BODIPYs comerciales con emisión en dicha zona,[2] aunque hay pocos que presenten buenas propiedades fotofísicas y adecuada solubilidad en medios polares, ya que la mayoría tienen bajos rendimientos cuánticos de fluorescencia, bandas espectrales anchas, y lo que es más limitante, poca fotoestabilidad y baja solubilidad en disolventes polares como alcoholes o agua. Por todo ello, el diseño y síntesis de BODIPYs con emisión optimizada en la región roja del espectro sigue siendo un reto actual.

Hay varias estrategias sintéticas para desplazar la longitud de onda de los BODIPYs hacia el rojo, basadas en la extensión de la conjugación del sistema $\pi$.[3] Algunas de ellas implican la post-funcionalización del BODIPY (Figura 31) mediante:

- Reacciones de sustitución nucleófila en los átomos de halógeno de BODIPYs 3,5-dihalogenados.[4]

- Reacciones de acoplamiento catalizadas por metales de transición, tales como reacciones de Suzuki, Stille, Heck o Sonogashira.[5]
- Condensaciones tipo Knoevenagel con los metilos del núcleo de BODIPY.[6]

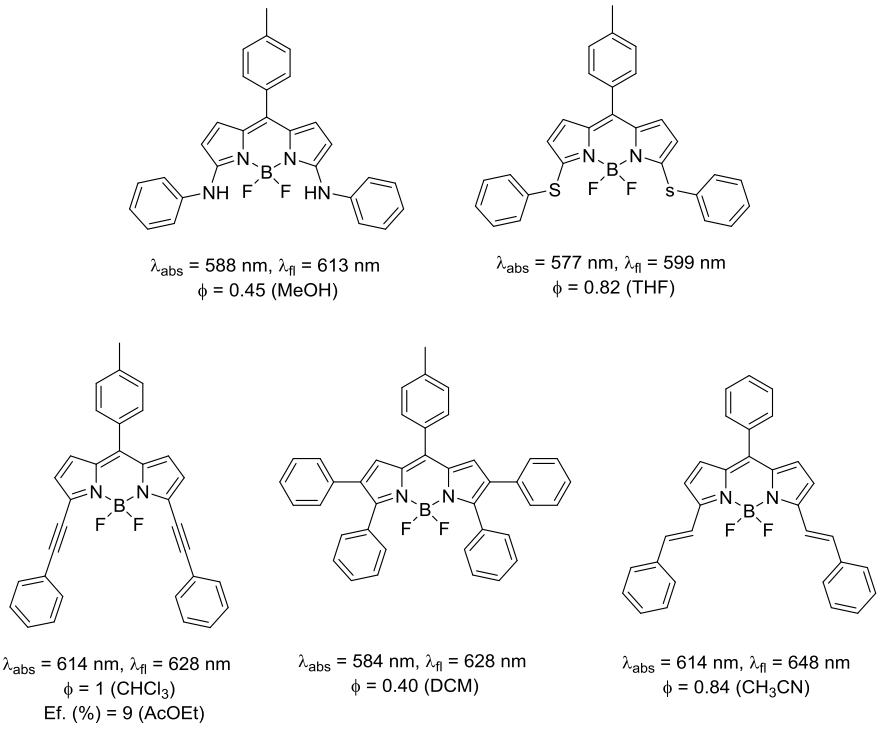


**Figura 31**. Estructuras de BODIPYs con emisión en la zona roja y sus propiedades fotofísicas.

Otra metodología es la rigidificación del sistema mediante la introducción de anillos fusionados (Figura 32). La síntesis de BODIPYs benzofusionados implica el uso de pirroles modificados a través de la síntesis de Paal-Knor,[7] que reaccionarán con aldehídos aromáticos o cloruros de ácido en las condiciones típicas de síntesis de BODIPYs.[8]

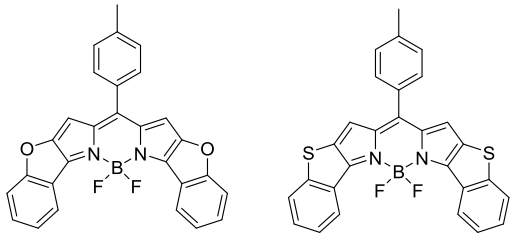


**Figura 32**. Estructuras de BODIPYs benzocondensados y sus propiedades fotofísicas.

También se pueden obtener BODIPYs con emisión en la zona roja del espectro mediante la sustitución del carbono en posición *meso* por un átomo de nitrógeno tipo imina (aza-BODIPYs) (Figura 33).[9]

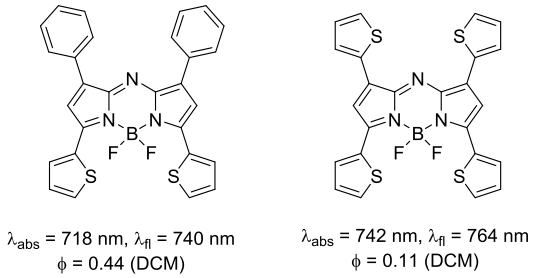


**Figura 33**. Estructuras de azaBODIPYs y sus propiedades fotofísicas.

Una última estrategia para generar un desplazamiento batocrómico en las bandas de emisión y absorción del BODIPY es la construcción de estructuras multicromofóricas que presenten eficientes procesos de transferencia de carga o energía[10] (transferencia de carga intramolecular, ICT "*intramolecular charge transfer*"; transferencia de energía a través del espacio, FRET "*Förster resonance energy transfer*" o a través del enlace, TBET[11] "*through-bond energy transfer*").[3] Todas ellas persiguen una disminución de la diferencia de energía entre los orbitales moleculares HOMO y LUMO, que se traduzca en un incremento de la longitud de onda de emisión.[12]

## 2.2. BODIPYs CON EMISIÓN EN LA ZONA ROJA

**Artículo 4: "Red-edge-wavelength finely-tunable laser action from new BODIPY dyes"** *Phys. Chem. Chem. Phys.* **2010**, *12*, 6335-6350.

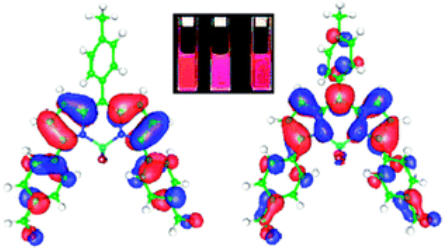

### 2.2.1. Introducción

En los trabajos anteriormente comentados, se recogen algunos ejemplos de BODIPYs con emisión en la zona roja del espectro visible, aunque son muy pocos en los que se haya realizado un estudio de su comportamiento láser, comprobando, en general, que no poseen una alta eficiencia láser y estabilidad.[13]

Para responder a la creciente demanda de nuevos colorantes con emisión en la zona roja del espectro visible, se planteó la síntesis de tres nuevos BODIPYs con una emisión superior a 600 nm mediante la extensión de la conjugación por reacciones de acoplamiento C-C catalizadas por paladio (Figura 34).

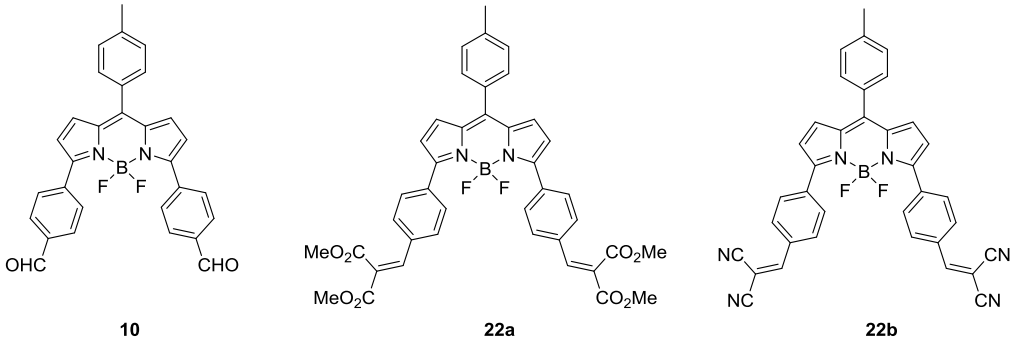


**Figura 34.** Estructuras de los compuestos **10** y **22a-b**.

### 2.2.2. Síntesis

Para la obtención de estos tres nuevos BODIPYs se empleó el compuesto **7f**[4a] como producto de partida. En primer lugar, la reacción de acoplamiento de Suzuki entre **7f** y el ácido 4-formilborónico (2.5 equiv), bajo irradiación en microondas, condujo a la formación del compuesto **10** con un 46% de rendimiento (Esquema 25).

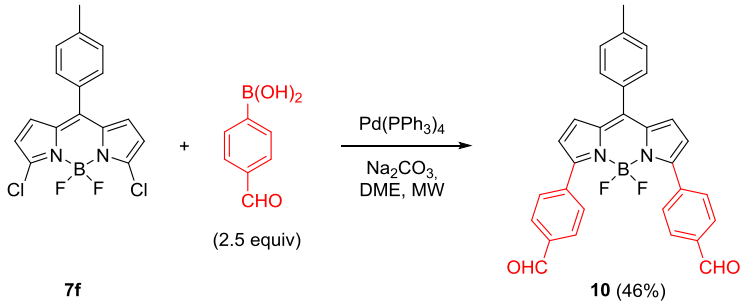


**Esquema 25**

A continuación, la reacción de Knoevenagel del compuesto **10** con malonato de dimetilo o malononitrilo, siguiendo las condiciones previamente descritas en nuestro laboratorio,[14] dio como resultado la obtención de **22a** y **22b** con un 47 y 21%, respectivamente (Esquema 26).

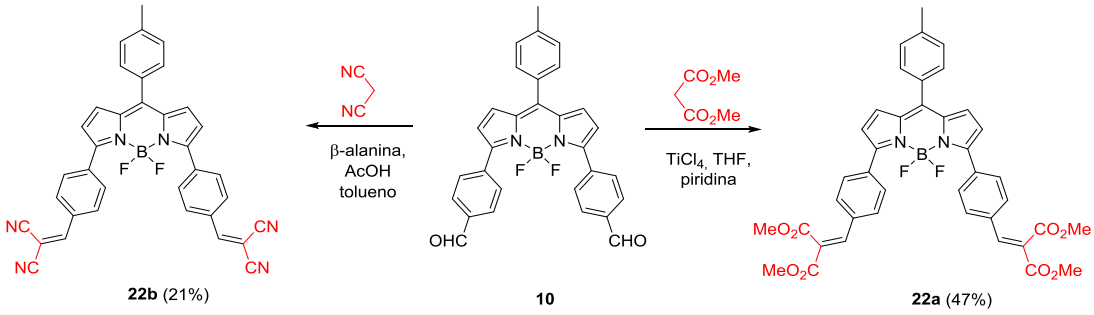


**Esquema 26**

### 2.2.3. Propiedades fotofísicas

Los nuevos BODIPYs **10** y **22a-b** se caracterizan por tener sus bandas de absorción y emisión en la zona roja del espectro visible, con valores de desplazamientos de Stokes muy

altos ($\Delta\nu_{St} \approx 1200\text{-}1800\ cm^{-1}$), concretamente tres veces superior al de los alquilBODIPYs, como por ejemplo **PM546** o **PM567** (Figura 35). Este factor es clave ya que supone una disminución de los procesos de reabsorción y de reemisión, que reducen la eficiencia de emisión tanto de fluorescencia como láser, especialmente a altas concentraciones.

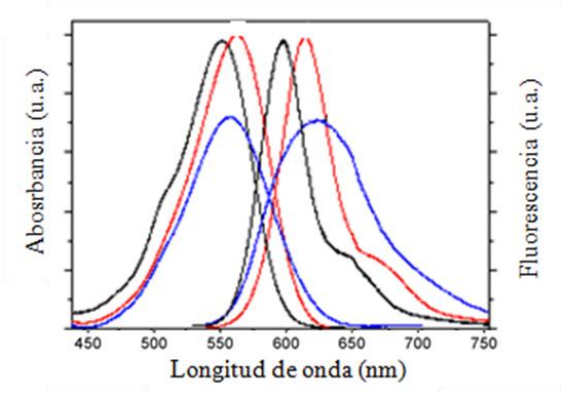


**Figura 35**. Espectros de absorción y emisión de los BODIPYs **10** (línea negra), **22a** (línea roja) y **22b** (línea azul) en AcOEt.

Este desplazamiento hacia el rojo se debe a que ahora la densidad electrónica del sistema π no está confinada únicamente en el núcleo, sino que está extendida por los anillos aromáticos en la posiciones 3 y 5, tal y como se observa en el mapa de densidad electrónica del BODIPY **10** (Figura 36).

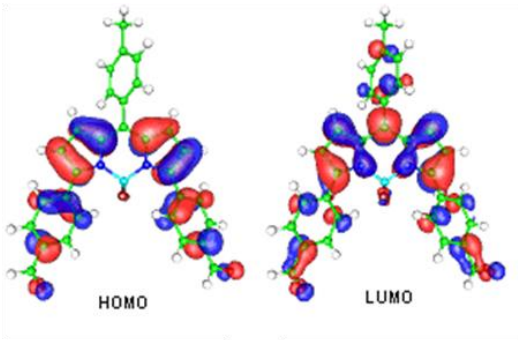


**Figura 36**. Mapa de densidad electrónica de los orbitales HOMO y LUMO del BODIPY **10**.

Los compuestos **22a-b** presentan un desplazamiento batocrómico mayor que el compuesto **10** debido a una mayor extensión de la conjugación por la presencia de sustituyentes dimetoxicarbonilvinil y dicianovinil, respectivamente, en la posición *para* de los fenilos situados en las posiciones 3 y 5 del BODIPY (Tabla 15).

**Tabla 15.** Propiedades fotofísicas de los compuestos **10** y **22a-b** en AcOEt y F3-EtOH.

| BODIPY | $\lambda_{abs}$ (nm) | $\varepsilon_{max}$ ($10^4$ $M^{-1}\cdot cm^{-1}$) | $\lambda_{fl}$ (nm) | $\phi$ | $\Delta\nu_{St}$ ($cm^{-1}$) | $k_{fl}$ ($10^{-8}$ $s^{-1}$) |
|---|---|---|---|---|---|---|
| **10** | | | | | | |
| **F3-EtOH** | 551.5 | 3.0 | 595.5 | 0.58 | 1365 | 1.28 |
| **AcOEt** | 558.0 | 3.0 | 599.0 | 0.57 | 1240 | 1.55 |
| **22a** | | | | | | |
| **F3-EtOH** | 562.5 | 1.8 | 613.5 | 0.59 | 1470 | 1.18 |
| **AcOEt** | 572.0 | 1.9 | 620.0 | 0.64 | 1355 | 1.40 |
| **22b** | | | | | | |
| **F3-EtOH** | 558.0 | 0.6 | 622.0 | 0.42 | 1845 | 0.87 |
| **AcOEt** | 563.0 | 0.6 | 617.5 | 0.54 | 1570 | 1.16 |

Como se recoge en la literatura, los colorantes con emisión en la zona roja del espectro suelen poseer un bajo rendimiento cuántico de fluorescencia debido a que la baja diferencia energética entre los niveles $S_0$ y $S_1$ favorece los procesos de conversión interna.[15] En estos nuevos BODIPYs, con emisión en el rojo, la incorporación de grupos fenilos en las posiciones 3 y 5 del BODIPY no solo provoca un desplazamiento batocrómico de las bandas de absorción y emisión sino que, además, reduce los procesos de conversión interna, por lo que sus rendimientos cuánticos de fluorescencia son relativamente altos.

### 2.2.4. Propiedades láser

Las propiedades láser de los nuevos colorantes BODIPY **10** y **22a-b** muestran una buena correlación con sus propiedades fotofísicas, ya que el desplazamiento batocrómico de las bandas de absorción y emisión también se observa en la banda de emisión láser

(Tabla 16 y Figura 37). Los compuestos **22a-b** presentan menores constantes de desactivación radiativas que el compuesto **10**, lo que justifica que sus eficiencias de emisión láser también sean menores.

**Tabla 16.** Propiedades láser de los compuestos **10** y **22a-b** bombeados a 532 nm en AcOEt.

| BODIPY | $\lambda_{láser}$ (nm) | Ef (%) | I (%) |
|---|---|---|---|
| **10** | 615 | 12 | 60 |
| **22a** | 632 | 2 | 80 |
| **22b** | 648 | 4 | 90 |

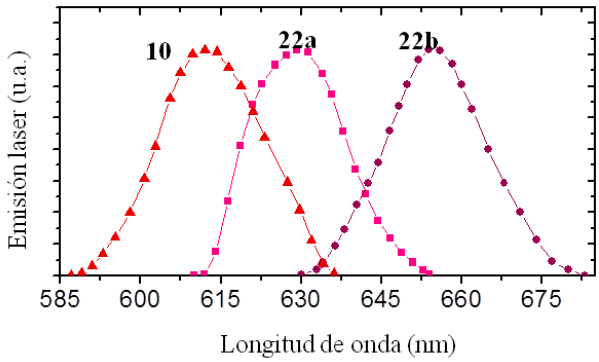


**Figura 37**. Espectros de emisión láser de los compuestos **10** y **22a-b** en AcOEt.

En cuanto a su fotoestabilidad, el compuesto **10** mantiene un 60% de su eficiencia láser tras 100 000 pulsos bombeado a 532 nm, mientras que los compuestos **22a** y **22b** mantienen, respectivamente, un 80 y 90% de su emisión inicial. Estos nuevos BODIPYs resultan ser más fotoestables que algunos colorantes comerciales con emisión en la misma región de espectro, como la Rodamina 640 (**Rh640**) y el Perileno rojo (**PerRed**), bombeados bajo idénticas condiciones experimentales (Figura 38).

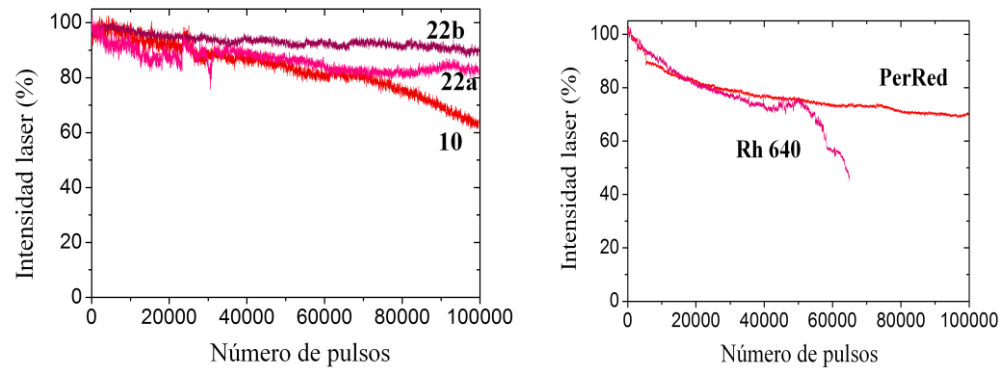


**Figura 38**. Fotoestabilidad láser de los compuestos **10** y **22a-b**, y de los colorantes comerciales **Rh640** y **PerRed** bombeados a 532 nm en AcOEt.

### 2.2.5. Conclusiones

Un diseño racional de derivación del sistema BODIPY permite obtener, con sólo modificar los sustituyentes en las posiciones 3 y 5 del BODIPY, una serie de colorantes con una emisión láser sintonizable en la región de 590-700 nm. Estos nuevos colorantes resultaron ser más estables que algunos de los actualmente comercializados con emisión láser en la misma región espectral.

## 2.3. BIBLIOGRAFÍA


[1] F. J. Duarte, L. W. Hillman, en *Dye Laser Principles* (Ed.: F. J. Duarte), Academic Press, New York, **1990**.

[2] a) L. Yuan, W. Lin, K. Zheng, L. He, W. Huang, *Chem. Soc. Rev.* **2013**, *42*, 622-661; b) K. Umezawa, D. Citterio, K. Suzuki, *Anal. Sci.* **2014**, *30*, 327-349.

[3] H. Lu, J. Mack, Y. Yang, Z. Shen, *Chem. Soc. Rev.* **2014**, *43*, 4778-4823.

[4] a) T. Rohand, M. Baruah, W. Qin, N. Boens, W. Dehaen, *Chem. Commun.* **2006**, 266-268; b) E. Fron, E. Coutino-Gonzalez, L. Pandey, M. Sliwa, M. Van der Auweraer, F. C. De Schryver, J. Thomas, Z. Dong, V. Leen, M. Smet, W. Dehaen, T. Vosch, *New J. Chem.* **2009**, *33*, 1490-1496; c) W. Qin, V. Leen, W. Dehaen, J. Cui, C. Xu, X. Tang, W. Liu, T. Rohand, D. Beljonne, B. Van Averbeke, J. N. Clifford, K. Driesen, K. Binnemans, M. Van der Auweraer, N. Boens, *J. Phys. Chem. C* **2009**, *113*, 11731-11740.

[5] a) T. Rohand, W. Qin, N. Boens, W. Dehaen, *Eur. J. Org. Chem.* **2006**, 4658-4663; b) V. Leen, E. Braeken, K. Luckermans, C. Jackers, M. Van der Auweraer, N. Boens, W. Dehaen, *Chem. Commun.* **2009**, 4515-4517; c) S. Yin, V. Leen, S. Van Snick, N. Boens, W. Dehaen, *Chem. Commun.* **2010**, *46*, 6329-6331; d) L. Jiao, C. Yu, T. Uppal, M. Liu, Y. Li, Y. Zhou, E. Hao, X. Hu, M. G. H. Vicente, *Org. Biomol. Chem.* **2010**, *8*, 2517-2519.

[6] a) K. Rurack, M. Kollmannsberger, J. Daub, *Angew. Chem. Int. Ed.* **2001**, *40*, 385-387; b) O. Buyukcakir, O. A. Bozdemir, S. Kolemen, S. Erbas, E. U. Akkaya, *Org. Lett.* **2009**, *11*, 4644-4647; c) T. Bura, P. Retailleau, G. Ulrich, R. Ziessel, *J. Org. Chem.* **2011**, *76*, 1109-1117; d) S. Zhu, J. Zhang, G. Vegesna, A. Tiwari, F.-T. Luo, M. Zeller, R. Luck, H. Li, S. Green, H. Liu, *RSC Adv.* **2012**, *2*, 404-407.

[7] a) D. H. R. Barton, J. Kervagoret, S. Z. Zard, *Tetrahedron* **1990**, *46*, 7587-7598; b) N. Ono, H. Kawamura, M. Bougauchi, K. Maruyama, *Tetrahedron* **1990**, *46*, 7483-7496.

[8] a) M. Shah, K. Thangaraj, M.-L. Soong, L. T. Wolford, J. H. Boyer, I. R. Politzer, T. G. Pavlopoulos, *Heteroatom Chem.* **1990**, *1*, 389-399; b) Z. Li, E. Mintzer, R. Bittman, *J. Org. Chem.* **2006**, *71*, 1718-1721.

[9] a) J. Killoran, L. Allen, J. F. Gallagher, W. M. Gallagher, D. F. O'Shea, *Chem. Commun.* **2002**, 1862-1863; b) A. Gorman, J. Killoran, C. O'Shea, T. Kenna, W. M. Gallagher, D. F. O'Shea, *J. Am. Chem. Soc.* **2004**, *126*, 10619-10631; c) S. O. McDonnell, M. J. Hall, L. T. Allen, A. Byrne, W. M. Gallagher, D. F. O'Shea, *J. Am. Chem. Soc.* **2005**, *127*, 16360-16361; d) J. Killoran, D. F. O'Shea, *Chem. Commun.* **2006**, 1503-1505.

[10] A. P. de Silva, H. Q. N. Gunaratne, T. Gunnlaugsson, A. J. M. Huxley, C. P. McCoy, J. T. Rademacher, T. E. Rice, *Chem. Rev.* **1997**, *97*, 1515-1566.

[11] Y. Zhao, Y. Zhang, X. Lv, Y. Liu, M. Chen, P. Wang, J. Liu, W. Guo, *J. Mater. Chem.* **2011**, *21*, 13168-13171.

[12] G. Qian, Z. Y. Wang, *Chem. Asian J.* **2010**, *5*, 1006-1029.

[13] a) I. Garcia-Moreno, D. Zhang, A. Costela, V. Martin, R. Sastre, Y. Xiao, *J. Appl. Phys.* **2010**, *107*, 73101-73107; b) Y. Xiao, D. Zhang, X. Qian, A. Costela, I. Garcia-Moreno, V. Martin, M. E. Perez-Ojeda, J. Bañuelos, L. Gartzia, I. L. Arbeloa, *Chem. Commun.* **2011**, *47*, 11513-11515; c) D. Zhang, V. Martin, I. Garcia-Moreno, A. Costela, M. E. Perez-Ojeda, Y. Xiao, *Phys. Chem. Chem .Phys.* **2011**, *13*, 13026-13033.

[14] M. Martin-Fontecha, A. R. Agarrabeitia, M. J. Ortiz, D. Armesto, *Org. Lett.* **2010**, *12*, 4082-4085.

[15] a) P. O. Andersson, S. M. Bachilo, R.-L. Chen, T. Gillbro, *J. Phys. Chem.* **1995**, *99*, 16199-16209; b) C. E. M. Carvalho, I. M. Brinn, A. V. Pinto, M. D. C. F. R. Pinto, *J. Photochem. Photobiol. A* **2000**, *136*, 25-33; c) J. Bañuelos Prieto, F. Lopez Arbeloa, V. Martinez Martinez, T. Arbeloa Lopez, F. Amat-Guerri, M. Liras, I. Lopez Arbeloa, *Chem. Phys. Lett.* **2004**, *385*, 29-35.

# CAPÍTULO 3. FUNCIONALIZACIÓN SOBRE EL ÁTOMO DE BORO

# 3. FUNCIONALIZACIÓN SOBRE EL ÁTOMO DE BORO

## 3.1. INTRODUCCIÓN

Se ha demostrado que una apropiada funcionalización del núcleo de indaceno de los BODIPYs conduce a la obtención de nuevos colorantes con interesantes propiedades fotofísicas. En los últimos años, una de las principales modificaciones sintéticas sobre el núcleo de BODIPY es la sustitución de los átomos de flúor unidos al boro. Así, una amplia variedad de nuevos dipirrometenos se han sintetizado mediante el empleo de alquiboranos en lugar de $BF_3 \cdot Et_2O$, lo que ha permitido obtener derivados de esta familia de colorantes con grupos alquilo unidos al átomo de boro (*C*-BODIPYs), en los que el aumento del volumen del grupo alquilo produce una disminución del rendimiento cuántico de fluorescencia (Figura 39).[1]

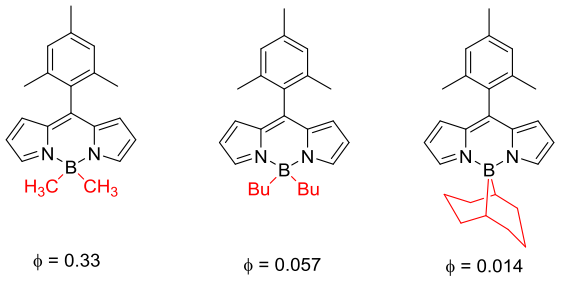


**Figura 39**. Estructuras de *C*-BODIPYs.

El empleo de otros halogenuros de boro, como $BCl_3$, $PhBCl_2$ o $BH_3 \cdot SMe_2$, conduce a la formación de los denominados *Cl*-BODIPYs[2] y *H*-BODIPYs[3] (Figura 40). Sin embargo, estos compuestos presentan una mayor inestabilidad con respecto a los BODIPYs con átomos de flúor unidos al boro (*F*-BODIPYs).

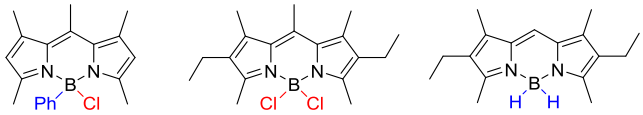


**Figura 40**. Estructuras de *Cl*-BODIPYs y *H*-BODIPYs.

Otras modificaciones sobre el átomo de boro, ampliamente estudiadas por Ziessel y col., implican el desplazamiento de los átomos de flúor por *C*-nucleófilos, como son los reactivos de Grignard u organolíticos. Así, se han sintetizado varios BODIPYs análogos al dipirrometano comercial **PM567** con grupos arilo (*C*-BODIPYs) y alquinos (*E*-BODIPYs) unidos al átomo de boro (Figura 41).[4]

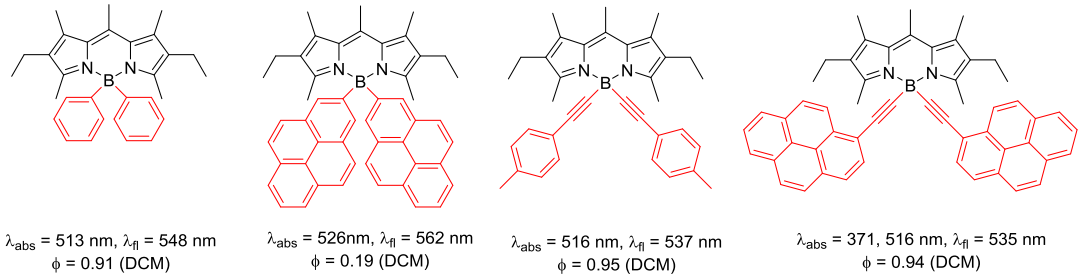


**Figura 41**. Estructuras de diferentes *C*- y *E*-BODIPYs.

El desplazamiento de los átomos de flúor por grupos arilo produce un desplazamiento batocrómico de las bandas de emisión, mientras que la introducción de grupos acetilenos no provoca desplazamiento de las bandas espectrales. Además, la introducción de grupos que puedan excitarse en la región del UV, como el pireno, incrementa el rango de absorción en el espectro visible con respecto a sus homólogos *F*-BODIPYs, por lo que se comportan como cassettes susceptibles de experimentar transferencia de energía.

Otros sustituyentes que se pueden incorporar en el átomo de boro son grupos alcoxi o ariloxi (*O*-BODIPYs)[2b, 4d, 5] como tales grupos e incluso formando un quelato con el átomo de boro (Figura 42).[6] La incorporación de estos grupos no produce un desplazamiento significativo de las bandas de absorción y emisión, aunque la introducción

de grupos ariloxi provoca una drástica disminución del rendimiento cuántico de fluorescencia.

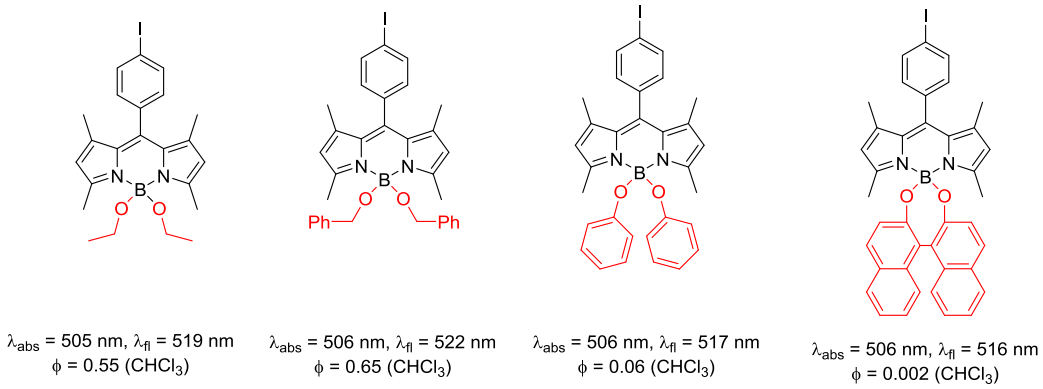


**Figura 42**. Estructuras de *O*-BODIPYs.

En una reciente publicación, Zhao y col. describen la sustitución de uno o ambos átomos de flúor en el 4,4-difluoro-1,3,5,7-tetrametil-4-bora-3a,4a-diaza-*s*-indaceno por grupos acetoxi para estudiar el efecto de dicha sustitución sobre el átomo de boro, observando que los nuevos derivados obtenidos (Figura 43) presentan mayor rendimiento cuántico de fluorescencia y fotoestabilidad, así como una mejor solubilidad en agua que su BODIPY precursor.[7]

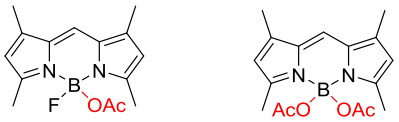

**Figura 43**. Estructuras de boroacetoxi BODIPYs.

## 3.2. NUEVOS DERIVADOS DE *O*-BODIPYs

**Artículo 5: "Carboxylates versus Fluorines: Boosting the Emission Properties of Commercial BODIPYs in Liquid and Solid Media".** *Adv. Funct. Mater.* **2013**, *23*, 4195-4205.

**Patente:** *Nuevos O-BODIPYs como láseres de colorantes*. ES201200871, **2012**.

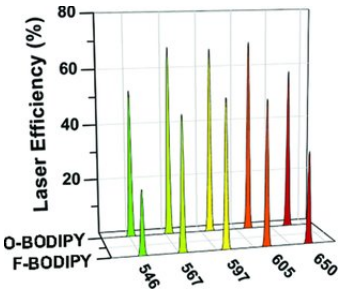


### 3.2.1. Introducción

Basándonos concretamente en los resultados observados por Zhao y col. se planteó el diseño y síntesis de una serie de *O*-BODIPYs mediante la introducción de diferentes grupos carboxilato en el átomo de boro de BODIPYs comerciales (Figura 44), con emisión en diferentes zonas del espectro visible.

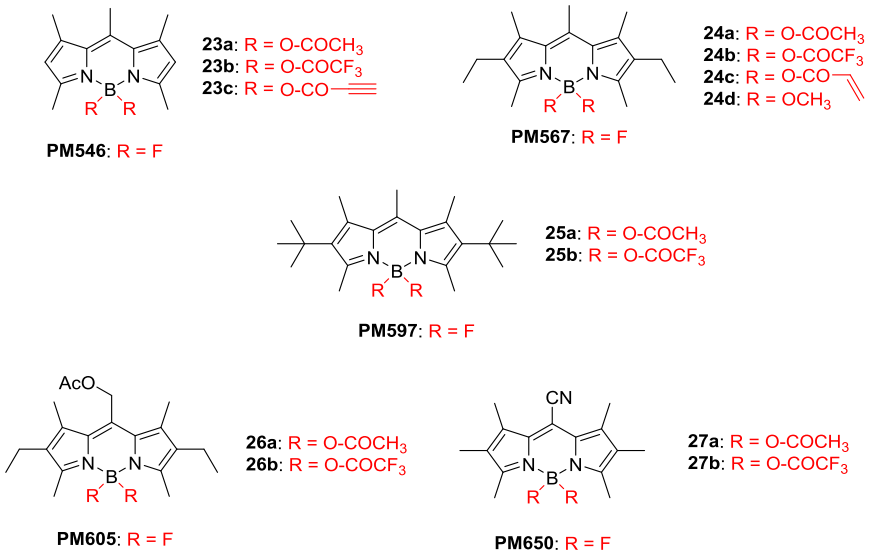


**Figura 44**. Estructuras de los nuevos *O*-BODIPYs y sus precursores comerciales.

Con ello, se pretendió aprovechar las buenas propiedades fotofísicas que, como se ha comentado, conlleva es tipo de sustitución para desarrollar una fácil estrategia de sintética que permitiera el acceso a nuevos colorantes láser con propiedades optimizadas

### 3.2.2 Síntesis

Para la obtención de estos nuevos colorantes se emplearon dos rutas sintéticas: la ruta A implica el uso de un ácido de Lewis, como el $AlCl_3$, y un exceso de *O*-nucleófilo, mientras que en la ruta B se utilizan las mismas condiciones pero en ausencia de $AlCl_3$.

De esta forma, por la ruta A se obtuvieron los BODIPYs **23a**, **24a**, **26a** y **27a** con rendimientos moderados a partir de los BODIPYs comerciales **PM546**, **PM567**, **PM605** y **PM650,** respectivamente (Esquema 27) y acetato de trimetilsililo (TMSOAc).


**Esquema 27**

La utilización de esta misma metodología, pero empleando ácido trifluoroacético y cloruro de trimetilsililo para generar *in situ* el trifluoracatetato de trimetilsililo, permitió la obtención de los derivados **25b** y **27b** con un 22 y 37% de rendimiento, respectivamente (Esquema 28).

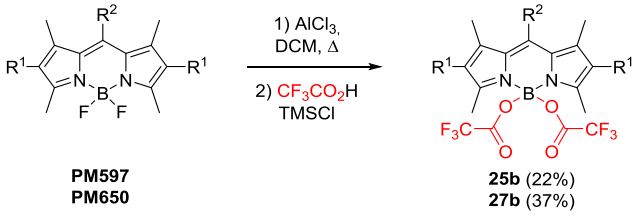


**Esquema 28**

Por otro lado, el compuesto **25a** no se pudo sintetizar mediante esta ruta ya que se producía la perdida de los grupos *terc*-butilos, generándose de esta manera el compuesto **23a**. Por tanto, se optó por emplear la ruta B, utilizando ácido acético y cloruro de trimetilsililo, obteniéndose de esta manera **25a** con un 19% de rendimiento (Esquema 29).

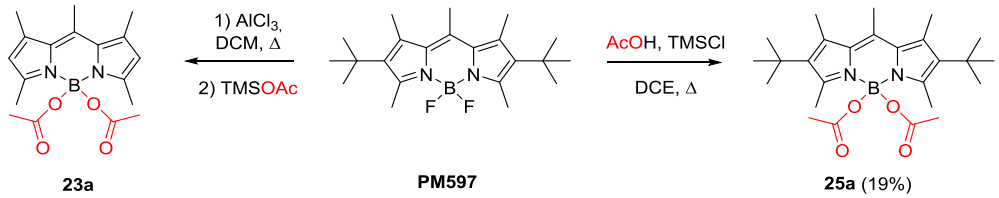


**Esquema 29**

El empleo de esta última metodología permitió obtener también los compuestos **23b**, **24b** y **26b**, por tratamiento de los correspondientes BODIPYs comerciales con un exceso de $CF_3CO_2TMS$, generado *in situ* a partir de ácido trifluoroacético y cloruro de trimetilsililo, en ausencia de $AlCl_3$ (Esquema 30).

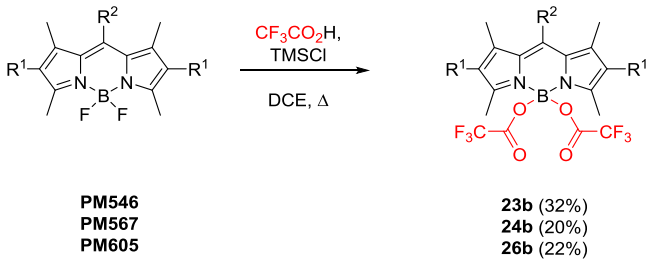


**Esquema 30**

Por otro lado, la reacción entre el propargilato o acrilato de trimetilsililo, generados *in situ* por el tratamiento del correspondiente ácido carboxílico con el cloruro de trimetilsilano, y el **PM546** o **PM567** dio lugar a los compuestos **23c** y **24c** respectivamente, con rendimientos moderados (Esquema 31).

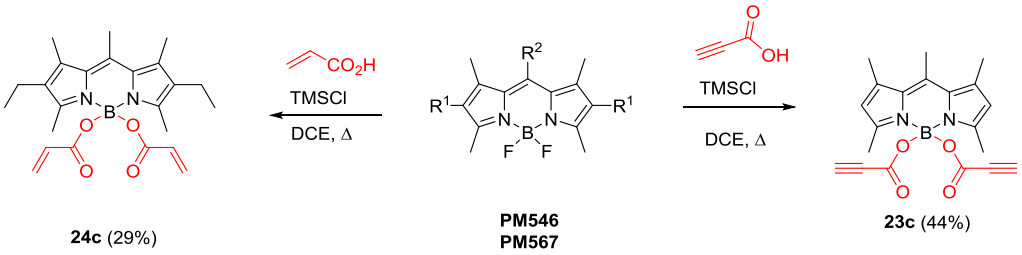


**24c** (29%) **PM546** **PM567** **23c** (44%)

**Esquema 31**

Finalmente, mediante el procedimiento descrito en la bibliografía, se llevo a cabo la síntesis de **24d**,[8] mediante el tratamiento de **PM567** con metóxido sódico en metanol, con un 38% de rendimiento (Esquema 32).

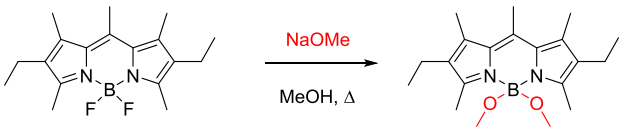


**PM567** **24d** (38%)

**Esquema 32**

### 3.2.3. Propiedades fotofísicas

La incorporación de grupos alcoxi en el átomo de boro tiene una influencia mínima en el desplazamiento de las bandas de absorción y emisión de estos nuevos colorantes con respecto a sus BODIPYs precursores, ya que el grupo $BF_2$ no participa en la deslocalización del sistema π (Tabla 17). Estos nuevos *O*-BODIPYs presentan rendimientos cuánticos de fluorescencia similares o superiores a los de sus precursores comerciales. En cualquier caso, el rendimiento de fluorescencia depende de la naturaleza del sustituyente en el átomo de boro. Así, la introducción de grupos fuertemente electroatractores (compuestos **23b**, **24b**, **25b**, **26b** y **27b**) como el trifluoroacetato, induce un aumento significativo del rendimiento cuántico de fluorescencia, mientras que la incorporación de grupos dadores (compuesto **24d**), como metoxi, tiene el efecto contrario.

**Tabla 17. Propiedades fotofísicas de los BODIPYs comerciales PM546, PM567, PM597, PM605 y PM650 y su correspondientes *O*-BODIPYs en c-hexano.**

| BODIPY | $\lambda_{abs}$ (nm) | $\varepsilon_{max}$ ($10^4$ $M^{-1}\cdot cm^{-1}$) | $\lambda_{fl}$ (nm) | $\phi$ |
|---|---|---|---|---|
| **PM546** | 499.5 | 9.7 | 509.5 | 0.91 |
| **23a** | 501.0 | 9.5 | 508.0 | 0.91 |
| **23b** | 502.0 | 10.2 | 509.5 | 0.95 |
| **23c** | 502.0 | 8.2 | 511.0 | 0.99 |
| **PM567** | 522.5 | 9.3 | 537.0 | 0.88 |
| **24a** | 522.0 | 8.5 | 537.0 | 0.84 |
| **24b** | 525.5 | 7.8 | 541.5 | 0.94 |
| **24c** | 523.5 | 8.1 | 541.0 | 0.90 |
| **24d** | 522.0 | 8.0 | 539.5 | 0.81 |
| **PM597** | 529.0 | 8.1 | 571.0 | 0.43 |
| **25a** | 530.5 | 7.0 | 573.0 | 0.58 |
| **25b** | 532.5 | 5.4 | 571.0 | 0.76 |
| **PM605** | 547.5 | 8.6 | 561.0 | 0.74 |
| **26a** | 548.5 | 8.0 | 563.0 | 0.76 |
| **26b** | 551.0 | 7.8 | 564.0 | 0.80 |
| **PM650** | 589.5 | 5.3 | 599.5 | 0.36 |
| **27a** | 588.5 | 4.5 | 600.5 | 0.39 |
| **27b** | 591.0 | 3.8 | 599.0 | 0.47 |

Este comportamiento está relacionado con la reorganización de la distribución de carga del cromóforo, inducida por el desplazamiento de los átomos de flúor por sustituyentes con diferente carácter electrónico. Así, tomando como ejemplo los derivados del **PM567**, la presencia de un grupo electroatractor incrementa la carga positiva sobre el boro, adquiriendo el oxigeno más carga negativa que la que tenía el átomo de flúor, y la carga negativa de los átomos de nitrógeno disminuye, lo que sugiere que su par de electrones está más deslocalizado y, en consecuencia, se suaviza la alternancia de carga sobre los carbonos con respecto al colorante de partida (Figura 45). Sin embargo, la sustitución de flúor por grupos electrodonadores tiene el efecto contrario, es decir, disminuye la carga

positiva sobre el boro y la negativa sobre los átomos de oxigeno. Esta variación en la deslocalización del sistema π provoca un cambio del carácter aromático del cromóforo.

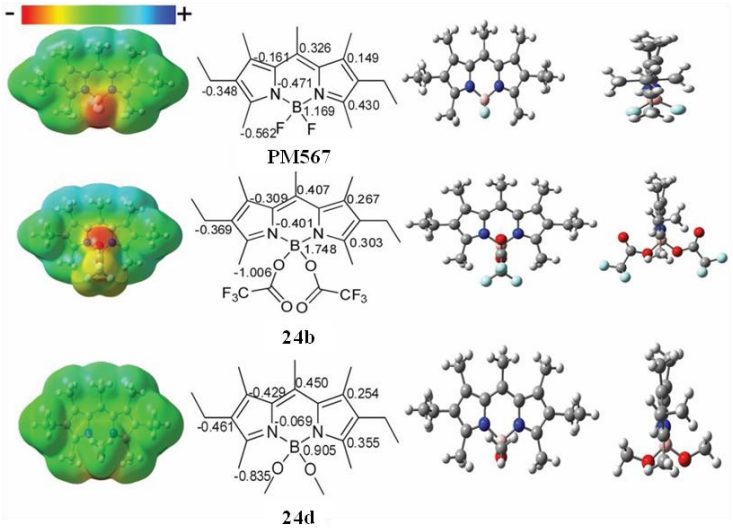


**Figura 45**. Mapas de potencial electroestático y distribución de carga de **PM567**, **24b** y **24d**.

El carácter aromático puede determinarse por la diferencia entre la longitudes medias de enlace carbono-carbono en la alternancia del enlace sencillo-doble del sistema π del cromóforo.[9] Este parámetro se conoce como BLA ("*Bond Length Alternation*"). Un valor elevado de BLA indica una menor aromaticidad del sistema, mientras que un bajo valor conlleva una mayor aromaticidad. Los valores de BLA de los nuevos *O*-BODIPYs y sus colorantes precursores se recogen la Tabla 18.

Los compuestos con grupos electroactractores, como los acetatos, unidos al átomo de boro presentan valores de BLA similares a sus precursores comerciales y, en consecuencia, valores también similares en rendimientos de fluorescencia

El aumento del carácter electroatractor del grupo unido al átomo de boro induce una disminución significativa del valor de BLA, lo que justifica que los BODIPYs en los que se han sustituido los átomos de flúor por grupos como el trifluoroacetato presenten rendimientos cuánticos de fluorescencia superiores a los de sus BODIPYS precursores.

**Tabla 18. Valores de BLA de los nuevos *O*-BODIPYs y sus precursores comerciales**

| BODIPY | BLA | BODIPY | BLA |
|---|---|---|---|
| **PM546** | 0.0245 | **PM597** | 0.0225 |
| **23a** | 0.0251 | **25a** | 0.0217 |
| **23b** | 0.0218 | **25b** | 0.0181 |
| **23c** | 0.0240 | **PM605** | 0.0242 |
| **PM567** | 0.0222 | **26b** | 0.0205 |
| **24a** | 0.0227 | **PM650** | 0.0223 |
| **24b** | 0.0192 | **27a** | 0.0236 |
| **24c** | 0.0225 | **27b** | 0.0194 |
| **24d** | 0.0260 | | |

Por otro lado, la unión al átomo de boro de grupos dadores, como el grupo metoxi en el compuesto **24d**, produce un aumento del valor de BLA, y por lo tanto, una menor aromaticidad, lo que conlleva a que este compuesto presente menor rendimiento cuántico de fluorescencia que el **PM567**.

Este comportamiento es más pronunciado en los derivados del **PM597**, ya que la introducción de grupos acetato en el átomo de boro, además de provocar un cambio en su aromaticidad, produce un aumento de su planaridad, lo que conlleva a un incremento aún más significativo del rendimiento cuántico de fluorescencia.

### 3.2.4. Propiedades láser

Las propiedades láser de los derivados del **PM546** se determinaron bombeando a 355 nm, mientras que el resto de los compuestos fueron bombeados a 532 nm. Las propiedades láser de los nuevos *O*-BODIPYs muestran buena concordancia con sus propiedades fotofísicas. Así, estos nuevos derivados presentan eficiencia láser superior a sus correspondientes BODIPYs precursores (Tabla 19). En cuanto a sus fotoestabilidades, estos nuevos *O*-BODIPYs resultaron ser más fotoestables que sus precursores, con excepción de los derivados del **PM650**. Especial atención merecen los derivados del **PM567**, en los que su fotoestabilidad aumenta de forma drástica

**Tabla 19.** Propiedades láser y fotoestabilidad de los BODIPYs comerciales **PM546**, **PM567**, **PM597**, **PM605** y **PM650** y su correspondientes *O*-BODIPY en AcOEt.

| BODIPY | Conc. (mM) | Ef (%) | $\lambda_{láser}$ (nm) | I (%) |
|---|---|---|---|---|
| **PM546** | 2.5 | 23 | 541 | 60 |
| **23a** | 3.8 | 43 | 544 | 100 |
| **23b** | 7.5 | 53 | 541 | 100 |
| **23c** | 2.5 | 59 | 542 | 100 |
| **PM567** | 1.5 | 48 | 566 | 17 |
| **24a** | 1.5 | 63 | 566 | 98 |
| **24b** | 0.6 | 68 | 562 | 100 |
| **24c** | 1.5 | 65 | 563 | 90 |
| **24d** | 9 | 59 | 565 | 30 |
| **PM597** | 0.5 | 53 | 588 | 85 |
| **25a** | 0.9 | 59 | 586 | 100 |
| **25b** | 0.9 | 65 | 587 | 100 |
| **PM605** | 0.6 | 55 | 586 | 20 |
| **26a** | 0.6 | 60 | 591 | 65 |
| **26b** | 0.6 | 67 | 592 | 91 |
| **PM650** | 0.9 | 35 | 657 | 80 |
| **27a** | 1.4 | 50 | 655 | 30 |
| **27b** | 0.5 | 55 | 661 | 50 |

A la vista de los excelentes resultados, se decidió estudiar en estado sólido la acción láser del **PM567** y sus derivados **24a-c**, por ser los que presentan la mayor eficiencia de emisión y estabilidad láser. Para ello, dichos compuestos se incorporaron a una matriz polimérica de PMMA, polímero que se asemeja al disolvente AcOEt. En la Tabla 20 se recogen los datos obtenidos de la acción láser inducida en estos materiales bombeados a 532 nm a una frecuencia de repetición de 10 Hz.

**Tabla 20.** Propiedades de emisión láser y fotoestabilidad de **PM567** y **24a-c** en una matriz polimérica de PMMA.

| BDP | Ef (%) | $\lambda_{láser}$ (nm) | I (%) |
|---|---|---|---|
| **PM567** | 34 | 566 | 30 |
| **24a** | 49 | 568 | 80 |
| **24b** | 56 | 568 | 100 |
| **24c** | 47 | 567 | 100 |

Al igual que en disolución, los nuevos colorantes presentan una eficiencia y estabilidad láser mayor que la de sus precursores comerciales (Figura 46). Cabe destacar que las eficiencias láser obtenidas en medio sólido son inferiores a las obtenidas en disolución, probablemente debido al acabado de las caras de la muestra sólida. Mejorando el pulido de las mismas se conseguiría un incremento de sus ya buenas propiedades láser.

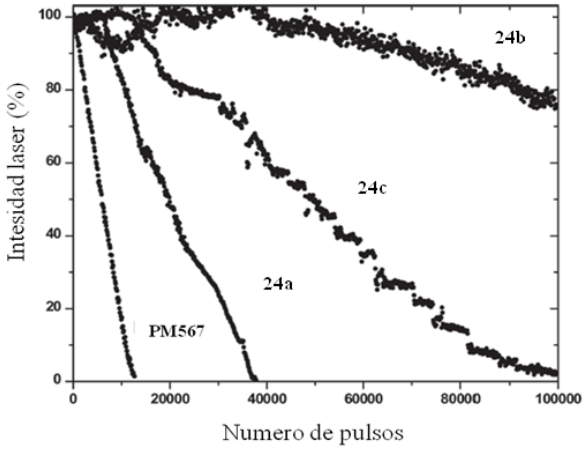


**Figura 46**. Estabilidad láser del **PM567** y **24a-c** en PMMA.

Especial interés muestra el compuesto **24c**, donde el grupo acrilato permite, durante la polimerización, su unión covalente a la matriz polimérica. Este colorante mejora la fotoestabilidad del **PM567** y del **24a**, que están simplemente disueltos en la matriz, a pesar de tener un rendimiento de fluorescencia menor y, por tanto, una constante de desactivación no radiativa mayor. Sin embargo, la unión covalente del colorante a la matriz

incrementa las vías de disipación de calor asociado a la energía de excitación no convertida en emisión, lo que conlleva a un significativo incremento de su fotoestabilidad.

### 3.2.5. Conclusiones

El desarrollo de nuevos *O*-BODIPYs a partir de BODIPYs comerciales es una estrategia directa, sencilla y barata para la optimización de las propiedades fotofísicas y del comportamiento láser de estos colorantes, tanto en fase líquida como en estado sólido. La sustitución de átomos de flúor por grupos carboxilato incrementa el rendimiento cuántico de fluorescencia, que en algunos casos llega a alcanzar el 100% y las eficiencias láser, que llegan a ser hasta tres veces superior a la de los correspondientes colorantes comerciales.

Además, presentan elevadas fotoestabilidades, ya que, en general, estos nuevos colorantes mantienen un 80% de su emisión tras 100 00 pulsos de bombeo, sin embargo, la acción láser del correspondiente colorante comercial se destruye completamente después de tan sólo 12000 pulsos. Por lo tanto, estos nuevos *O*-BODIPYs son unos buenos candidatos para conseguir una emisión láser eficiente, estable y sintonizable en todas las regiones del espectro visible.

## 3.3. NUEVOS DERIVADOS DE *C*- Y *E*-BODIPYs

**Artículo 6: "First Highly Efficient and Photostable *E* and *C* Derivates of 4,4,-Difluoro-4-bora-3a,4a-diaza-*s*-indacene (BODIPY) as Dye Lasers in the Liquid Phase, Thin Films, and Solid-State Rods"**. *Chem. Eur. J.* **2014**, *20*, 2646-2653.

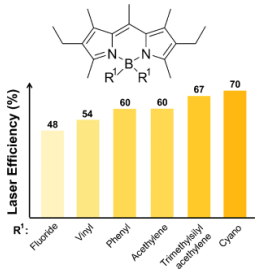


### 3.3.1. Introducción

A la vista de los excelentes resultados obtenidos en el artículo anterior, se propuso la síntesis de una nueva serie de *C*- y *E*-BODIPYs (**28-34**) (Figura 47) a partir de sus precursores comerciales y el estudio de las propiedades fotofísicas y comportamiento láser de los compuestos obtenidos

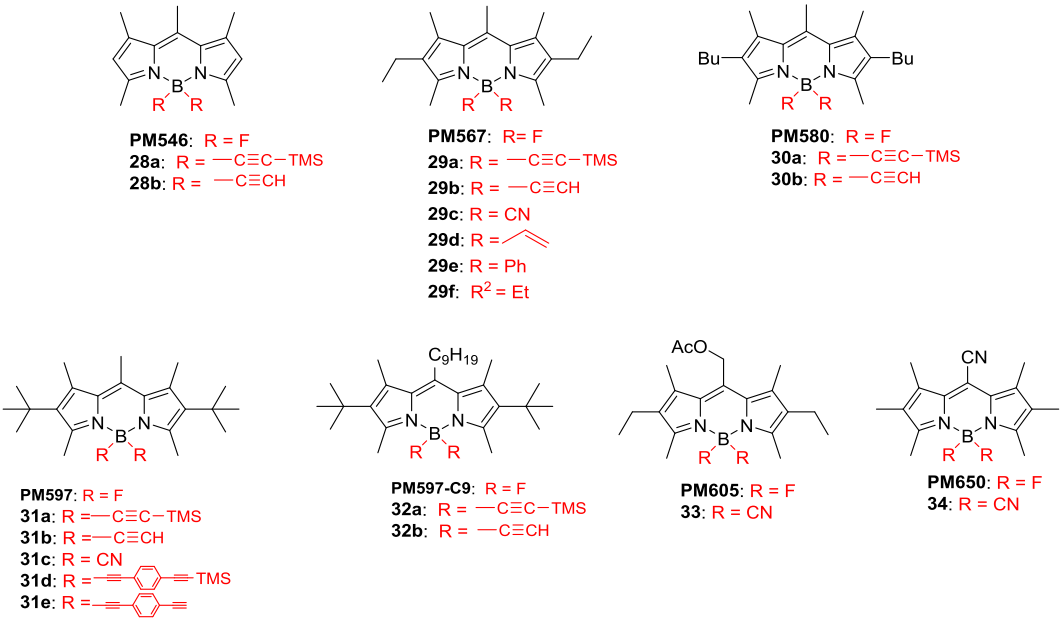


**Figura 47**. Estructuras de los nuevos *C* y *E*-BODIPYs y sus precursores comerciales.

### 3.3.2. Síntesis

Para la síntesis de los nuevos *C*- y *E*-BODIPYs se emplearon los colorantes comerciales **PM546**, **PM567**, **PM580**, **PM597**, **PM597-C9**, **PM605** y **PM650** como material de partida y diferentes organolíticos, reactivos de Grignard o TMSCN como nucleófilos, dependiendo del grupo funcional que se quiera introducir en el átomo de boro. Los compuestos **29a-b**[10] y **29e**[8] fueron sintetizados por los procedimientos descritos en la bibliografía a partir del BODIPY comercial **PM567**.

Los derivados **28a** y **30a-32a** se prepararon por reacción entre el BODIPY comercial y el trimetilsilil acetiluro de litio, generado *in situ* por reacción del trimetilsililacetileno y *n*-BuLi. A continuación, la eliminación del grupo trimetilsililo se llevó a cabo por el tratamiento del correspondiente *E*-BODIPY con exceso de NaOH, dando lugar a los BODIPYs **28b** y **30b-32b** (Esquema 33).

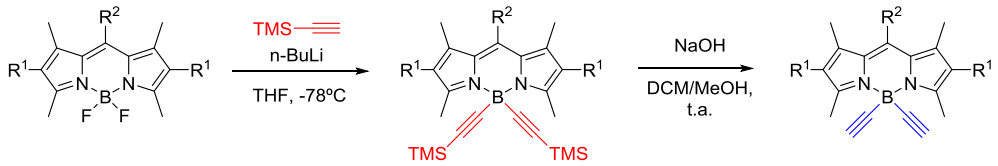


**PM546**
**PM580**
**PM597**
**PM597-C9**

**28a** (89%)
**30a** (70%)
**31a** (63%)
**32a** (57%)

**28b** (78%)
**30b** (62%)
**31b** (90%)
**32b** (60%)

**Esquema 33**

Con esta metodología también se obtuvieron los compuestos **31d-e** con un rendimiento del 65 y 80% respectivamente, a partir del **PM597** (Esquema 34). Cabe destacar que fue necesario el empleo de un gran exceso de NaOH para la desprotección del grupo trimetilsililo, ya que la utilización cantidades estequiométricas en la obtención de los anteriores compuestos, producía una mezcla de productos mono- y di-desprotegidos.

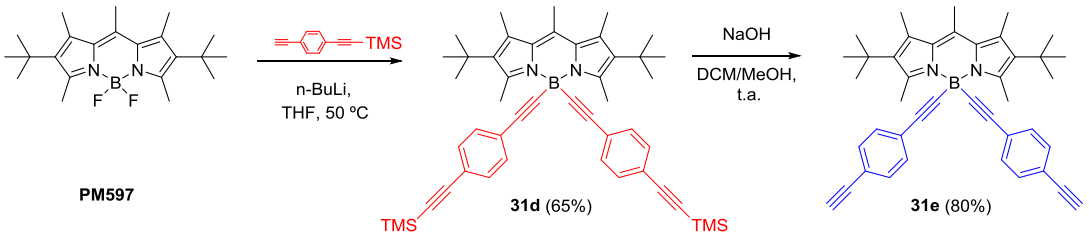


**Esquema 34**

Para el desplazamiento de los átomos de flúor por grupo ciano, se siguió una estrategia similar a la utilizada para la introducción de grupos acetato, recogida en el anterior artículo, empleando en este caso TMSCN como nucleófilo en presencia (compuestos **29c** y **33**) o en ausencia de $AlCl_3$ (compuestos **31c** y **34**) (Esquema 35).

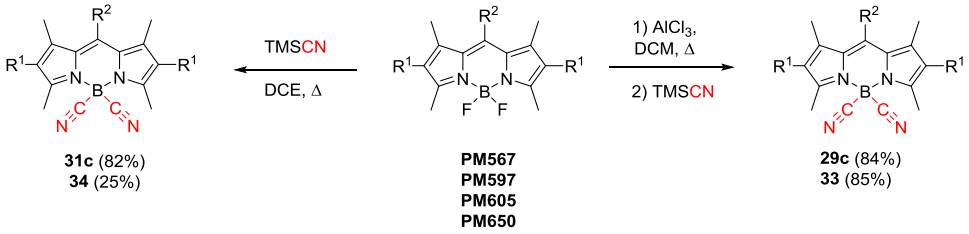


**Esquema 35**

Por último, los compuestos **29d** y **29f** se obtuvieron por reacción del **PM567** y bromuro de vinilmagnesio o etilmagnesio, respectivamente, con rendimientos moderados (Esquema 36).

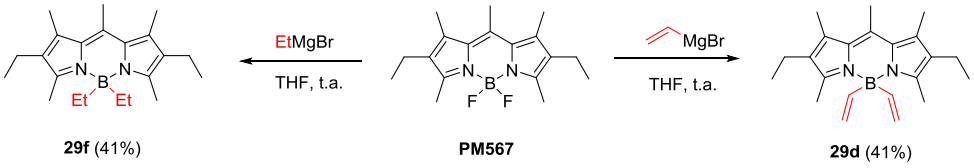


**Esquema 36**

### 3.3.3. Propiedades fotofísicas

Al igual que ocurre en los *O*-BODIPYs, el desplazamiento de los átomos de flúor del grupo $BF_2$ por grupos acetileno, ciano, vinilo o etilo, no produce un desplazamiento de las bandas de absorción y emisión, ya que, como se ha comentado anteriormente, el grupo $BF_2$ no participa en la deslocalización del sistema $\pi$ (Tabla 21).

La elección de los diferentes grupos introducidos en el átomo de boro permite establecer una correspondencia entre estructura y propiedades fotofísicas de los nuevos BODIPYs:

a) La incorporación de grupos acetileno en el átomo de boro no produce una gran redistribución de carga en la estructura del BODIPY debido al leve carácter electroatractor de dicho grupo.

b) Un aumento del carácter electroatractor del sustituyente unido al boro, como grupos ciano, induce un incremento del rendimiento cuántico de fluorescencia debido a una reorganización de la distribución de carga que conlleva a un aumento del carácter aromático del cromóforo. Este incremento es más llamativo en los derivados del **PM650**, ya que la presencia de grupos ciano unidos directamente al átomo de boro contrarresta el proceso de ICT generado por la presencia del grupo ciano en la posición *meso*.

c) La presencia de grupos electrodadores, como los grupos fenilo, unidos directamente al átomo de boro provoca una disminución del rendimiento cuántico de fluorescencia. Además, en el compuesto **29e** se produce una distorsión de la planaridad del cromóforo, ya que los anillos de fenilo se sitúan de forma ortogonal con respecto al anillo de indaceno. Esta pérdida de planaridad induce un proceso de conversión interna, lo que justifica el bajo rendimiento cuántico de fluorescencia de dicho compuesto.

d) Un comportamiento similar se observa también en función del grado de insaturación de la cadena alquílica unida al átomo de boro. De esta manera, la disminución del grado de insaturación, desde acetileno a etilo para **29b**, **29d** y **29f**, respectivamente, provoca una distorsión en la geometría molecular y una disminución de la aromaticidad del compuesto

(BLA = 0.027, 0.029 y 0.031, respectivamente) y, en consecuencia, disminución del rendimiento cuántico de fluorescencia.

**Tabla 21.** Propiedades fotofísicas de los BODIPYs comerciales precursores y su correspondientes *C*- y *E*-BODIPYs.

| BODIPY | $\lambda_{abs}$ (nm) | $\varepsilon_{max}$ ($10^4$ $M^{-1}\cdot cm^{-1}$) | $\lambda_{fl}$ (nm) | $\phi$ |
|---|---|---|---|---|
| **PM546** | 494.0 | 8.1 | 504.0 | 0.85 |
| **29a** | 49.5 | 5.5 | 504.0 | 0.96 |
| **29b** | 493.0 | 7.9 | 503.5 | 0.95 |
| **PM567** | 516.5 | 8.0 | 531.5 | 0.84 |
| **30a** | 513.5 | 7.4 | 530.5 | 0.86 |
| **30b** | 513.0 | 8.4 | 531.0 | 0.86 |
| **30c** | 515.5 | 6.7 | 530.5 | 0.88 |
| **30d** | 510.0 | 8.4 | 531.5 | 0.70 |
| **30e** | 512.0 | 6.9 | 550.0 | 0.51 |
| **30f** | 507.5 | 4.8 | 538.0 | 0.45 |
| **PM580** | 518.5 | 8.5 | 536.5 | 0.94 |
| **31a** | 515.0 | 10.0 | 533.0 | 0.90 |
| **31b** | 514.5 | 11.3 | 532.0 | 0.93 |
| **PM597** | 523.0 | 7.7 | 562.5 | 0.47 |
| **32a** | 521.5 | 7.0 | 565.5 | 0.54 |
| **32b** | 521.0 | 7.2 | 566.5 | 0.61 |
| **32c** | 522.0 | 6.4 | 567.0 | 0.57 |
| **32d** | 521.5 | 6.2 | 565.0 | 0.57 |
| **32e** | 526.0 | 6.7 | 567.0 | 0.62 |
| **PM597-C9** | 523.0 | 8.6 | 595.5 | 0.10 |
| **33a** | 520.5 | 8.2 | 606.0 | 0.13 |
| **33b** | 519.5 | 7.0 | 604.5 | 0.18 |
| **PM605** | 543.0 | 7.5 | 558.0 | 0.73 |
| **34** | 541.5 | 7.6 | 557.0 | 0.80 |
| **PM650** | 588.0 | 4.2 | 603.0 | 0.15 |
| **35** | 587.0 | 4.7 | 602.0 | 0.29 |

### 3.3.4. Propiedades láser

Atendiendo a sus bandas de absorción, los derivados del **PM546** se excitaron a 355 nm, mientras que el resto de los compuestos fueron excitados a 532 nm (Tabla 22).

**Tabla 22.** Eficiencia de emisión láser y fotoestabilidad de los BODIPYs comerciales seleccionados y su *C*- y *E*-BODIPYs derivados.

| BODIPY | Conc. (mM) | Ef. (%) | $\lambda_{láser}$ (nm) | I (%) |
|---|---|---|---|---|
| **PM546** | 2.5 | 23 | 541 | 60 |
| **28a** | 3.5 | 58 | 543 | 92 |
| **28b** | 3.5 | 52 | 542 | 76 |
| **PM567** | 3.5 | 58 | 566 | 17 |
| **29a** | 3.5 | 67 | 565 | 55 |
| **29b** | 3.5 | 60 | 567 | 70 |
| **29c** | 1.5 | 68 | 566 | 100 |
| **29d** | 2.5 | 54 | 564 | - |
| **29e** | 2.5 | 60 | 562 | 100 |
| **29f** | 5.0 | 30 | 562 | 50 |
| **PM580** | 1.5 | 57 | 573 | 48 |
| **30a** | 1.5 | 65 | 572 | 84 |
| **30b** | 1.5 | 63 | 571 | 70 |
| **PM597** | 0.5 | 53 | 588 | 85 |
| **31a** | 0.8 | 70 | 586 | 100 |
| **31b** | 0.8 | 63 | 587 | 94 |
| **31c** | 0.8 | 73 | 589 | 65 |
| **31d** | 0.8 | 68 | 588 | 42 |
| **31e** | 1.0 | 73 | 586 | 100 |
| **PM597-C9** | 1.5 | 55 | 606 | 30 |
| **32a** | 1.5 | 62 | 603 | 100 |
| **32b** | 1.5 | 59 | 604 | 100 |
| **PM605** | 0.7 | 55 | 586 | 20 |
| **33** | 0.8 | 68 | 588 | 100 |
| **PM650** | 0.9 | 35 | 657 | 80 |
| **34** | 0.9 | 45 | 655 | 75 |

Las propiedades de emisión láser muestran una buena concordancia con las propiedades fotofísicas de estos nuevos *C*- y *E*-BODIPYs ya que, de forma general, los compuestos con mayores rendimientos cuánticos de fluorescencia y menores constantes de desactivación no radiativas son los que presentan mayores eficiencias láser

A la vista de estos excelentes resultados se decidió realizar un estudio de los compuestos con mejor emisión láser (**29c**, **31c** y **33**) incorporados en una matriz polimérica de PMMA. Al igual que en disolución, los nuevos BODIPYs presentaron una mayor eficiencia láser y estabilidad que sus precursores comerciales (Tabla 23).

**Tabla 23.** Propiedades de emisión laser y fotoestabilidad del **PM567**, **PM597**, **PM605**, **29c**, **31c** y **33** en una matriz polimérica de PMMA.

| BODIPY | Ef. (%) | $\lambda_{láser}$ (nm) | I (%) |
|---|---|---|---|
| **PM567** | 34 | 566 | 30 |
| **29c** | 49 | 568 | 96 |
| **PM597** | 36 | 585 | 85 |
| **31c** | 53 | 588 | 100 |
| **PM605** | 37 | 595 | 0 |
| **33** | 51 | 597 | 80 |

### 3.3.5. Conclusiones

Se ha diseñado un protocolo de síntesis fácil, barato y "universal" para mejorar las propiedades fotofísicas y de emisión láser de una serie de BODIPYs comerciales. La sustitución de los átomos de flúor sobre el boro por sustituyentes con diferente carácter eletroatractor/dador permite concluir que la presencia de grupos electroatractores mejora las propiedades fotofísicas y láser de estos colorantes. Sin embargo, sustituyentes con un fuerte carácter electrodador inducen una distorsión tanto en la geometría como en la distribución de carga, incrementando los procesos no radiativos que disminuyen tanto la eficiencia de fluorescencia como de emisión láser.

## 3.4. BIBLOGRAFÍA


[1] H. L. Kee, C. Kirmaier, L. Yu, P. Thamyongkit, W. J. Youngblood, M. E. Calder, L. Ramos, B. C. Noll, D. F. Bocian, W. R. Scheidt, R. R. Birge, J. S. Lindsey, D. Holten, *J. Phys. Chem. B* **2005**, *109*, 20433-20443.

[2] a) T. W. Hudnall, T.-P. Lin, F. P. Gabbai, *J. Fluorine Chem.* **2010**, *131*, 1182-1186; b) T. Lundrigan, S. M. Crawford, T. S. Cameron, A. Thompson, *Chem. Commun.* **2012**, *48*, 1003-1005.

[3] C. Bonnier, W. E. Piers, M. Parvez, T. S. Sorensen, *Chem. Commun.* **2008**, 4593-4595.

[4] a) C. Goze, G. Ulrich, L. J. Mallon, B. D. Allen, A. Harriman, R. Ziessel, *J. Am. Chem. Soc.* **2006**, *128*, 10231-10239; b) A. Harriman, G. Izzet, R. Ziessel, *J. Am. Chem. Soc.* **2006**, *128*, 10868-10875; c) R. Ziessel, C. Goze, G. Ulrich, *Synthesis* **2007**, 936-949; d) R. Ziessel, G. Ulrich, A. Harriman, *New J. Chem.* **2007**, *31*, 496-501.

[5] a) A. Loudet, K. Burgess, *Chem. Rev.* **2007**, *107*, 4891-4932; b) G. Ulrich, R. Ziessel, A. Harriman, *Angew. Chem. Int. Ed.* **2008**, *47*, 1184-1201; c) S. M. Crawford, A. Thompson, *Org. Lett.* **2010**, *12*, 1424-1427.

[6] a) A. K. Parhi, M.-P. Kung, K. Ploessl, H. F. Kung, *Tetrahedron Lett.* **2008**, *49*, 3395-3399; b) C. Ikeda, S. Ueda, T. Nabeshima, *Chem. Commun.* **2009**, 2544-2546; c) Y. Kubo, Y. Minowa, T. Shoda, K. Takeshita, *Tetrahedron Lett.* **2010**, *51*, 1600-1602; d) S. Rausaria, A. Kamadulski, N. P. Rath, L. Bryant, Z. Chen, D. Salvemini, W. L. Neumann, *J. Am. Chem. Soc.* **2011**, *133*, 4200-4203; e) Y. Tomimori, T. Okujima, T. Yano, S. Mori, N. Ono, H. Yamada, H. Uno, *Tetrahedron* **2011**, *67*, 3187-3193.

[7] X.-D. Jiang, J. Zhang, T. Furuyama, W. Zhao, *Org. Lett.* **2012**, *14*, 248-251.

[8] L. Yang, R. Simionescu, A. Lough, H. Yan, *Dyes Pigm.* **2011**, *91*, 264-267.

[9] G. Bourhill, J.-L. Bredas, L.-T. Cheng, S. R. Marder, F. Meyers, J. W. Perry, B. G. Tiemann, *J. Am. Chem. Soc.* **1994**, *116*, 2619-2620.

[10] C. Goze, G. Ulrich, R. Ziessel, *Org. Lett.* **2006**, *8*, 4445-4448.

# CAPÍTULO 4. CASSETTES BASADOS EN FLUORÓFOROS ORGÁNICOS

# 4. CASSETTES BASADOS EN FLUORÓFOROS ORGÁNICOS

## 4.1. INTRODUCCIÓN

Los colorantes orgánicos, como se ha comentado en el capítulo de Introducción de esta Memoria, presentan una serie de desventajas, entre ellas pequeños rendimientos de Stokes (normalmente menos de 25 nm) lo que limita en la práctica su aplicación en técnicas de detección por fluorescencia. Una de las principales estrategias que se ha desarrollado para superar las mismas se basa en la síntesis de complejos multicromofóricos en los que poder inducir eficientes procesos de transferencia de energía de excitación (EET "*Excitation Energy Transfer*") entre un cromóforo dador y otro aceptor.[1]

De forma general, se denomina cassette a todo compuesto formado por la unión de dos o más cromóforos en el que uno de ellos actúa como dador, que tras ser excitado a una cierta longitud de onda, transfiere la energía a otro cromóforo que actúa como aceptor. Fundamentalmente, el proceso EET tiene lugar por dos mecanismos: transferencia de energía por resonancia de fluorescencia (FRET "*Fluorescence Resonance Energy Transfer*") o por transferencia de energía a través de enlace (TBET "*Through-Bond Energy Transfer*") (Figura 47).

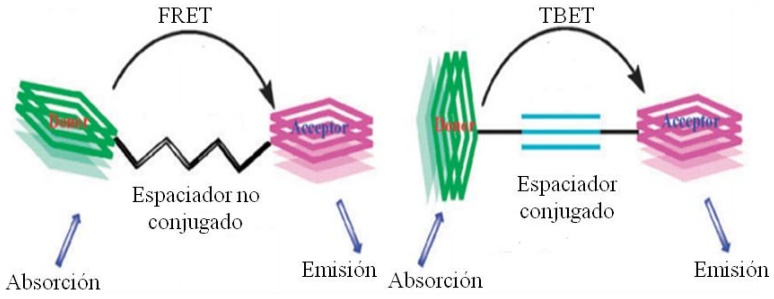


**Figura 47**. Procesos FRET y TBET.

En el proceso FRET, la transferencia de energía se produce a través del espacio, ya que los cromóforos no se encuentran conectados por un espaciador conjugado. En este caso, la eficiencia del proceso depende, esencialmente, de tres factores: a) el solapamiento entre la banda de emisión del donador y la de absorción del aceptor; b) el alineamiento de los correspondientes momentos dipolares de transición y c) la distancia entre cromóforos, que debería ser siempre inferior a los 10 nm. Por otro lado, la transferencia de energía en el proceso TBET se produce a través de un espaciador que une los cromóforos involucrados en el proceso (Figura 47). Por lo tanto, la eficiencia de este proceso no está ya tan controlada por el solapamiento de las bandas de emisión y absorción de los cromóforos aceptor y dador. En este caso los mayores requerimientos son: a) elevada absorbancia del donador a la longitud de onda de excitación; b) aceptor altamente fluorescente y c) un espaciador que evite que los colorantes estén coplanares, lo que nos llevaría a un colorante simplemente conjugado.

En la bibliografía existen múltiples ejemplos de cassettes,[2] algunos de los cuales están basados en el esqueleto de BODIPY, tanto unido a otros colorantes como rodamina, cumarina o perileno, o bien a unidades del mismo cromóforo. Una serie de cassettes sencillos están basados en la unión de un BODIPY con diferentes sistemas policíclicos, como antraceno, pireno o perileno (Figura 48).[3] En estos sistemas queda patente la importancia de la orientación ortogonal entre ambos cromóforos, manteniéndose así la individualidad electrónica de cada uno de ellos.

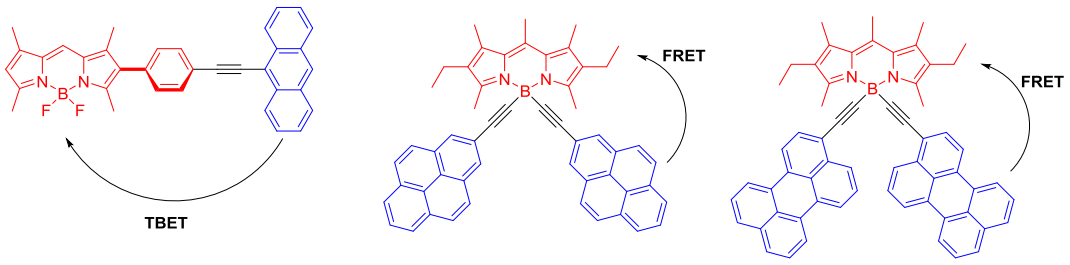


**Figura 48**. Estructuras de cassettes basado en BODIPY y compuestos policíclicos.

Otros ejemplos de cassettes son los sintetizados por Akkaya y col., basados en diadas de BODIPYs (Figura 49),[1c] en los que, modulando la distancia entre los cromóforos, es posible variar la eficiencia de proceso de transferencia de energía. Así, un aumento de la distancia entre ambos cromóforos conlleva una menor eficiencia de EET.

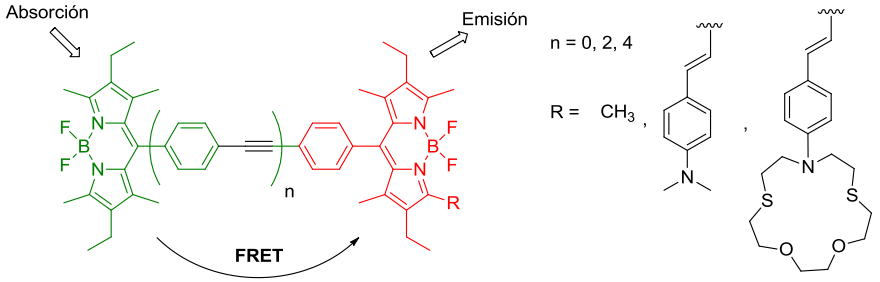


**Figura 49**. Estructuras de cassettes BODIPY-BODIPY.

Como se recoge en el capítulo de Introducción, la extensión de la conjugación a través de las posiciones 3 y/o 5 constituye una de las principales estrategias para la obtención de BODIPYs con emisión en la zona roja del espectro visible. Así, mediante reacciones de Knoevenagel, Akkaya y col. sintetizaron, además de los cassettes mencionados en la figura anterior, sistemas de triadas basados en 3,5-diestirilBODIPY con una eficiente transferencia de energía entre ambos cromóforos y una emisión fluorescente a 670, nm tras excitación a 525 nm (Figura 50).[4]

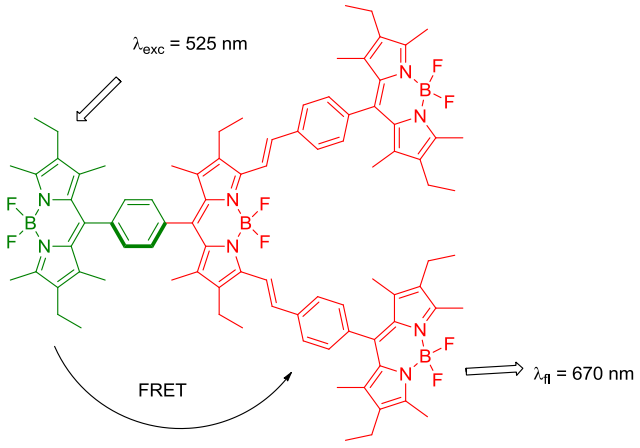


**Figura 50**. Estructura de un cassette multicromofórico formado por unidades de BODIPY.

También existen ejemplos de cassettes formados por dos cromóforos de diferente naturaleza, como los obtenidos por Burguess y col., basados en la combinación de BODIPYs y diferentes cianinas, y en los que se ha modulado la longitud de emisión en función de la longitud de la cadena hidrocarbonada de la cianina (Figura 51).[5] De esta manera, es posible obtener colorantes con una emisión centrada a 794 nm.

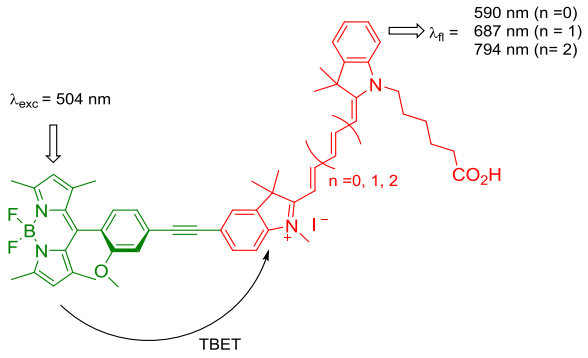


**Figura 51.** Estructuras de un cassette BODIPY-cianina.

Otro tipo de cassette formado por dos cromóforos con distinta estructura son los que contienen unidades de BODIPY y cumarina. Por lo que nosotros conocemos, hasta este momento existen pocos ejemplos de este tipo de sistemas. Así, Guo y col. [6] describen la formación de una serie de cassettes de este tipo que presentan las bandas típicas de emisión de los BODIPYs bajo excitación a 340 nm, consiguiéndose, en algunos casos, desplazamientos de Stokes de hasta 410 nm y eficiencias en la transferencia de energía de hasta un 98.6% (Figura 52).

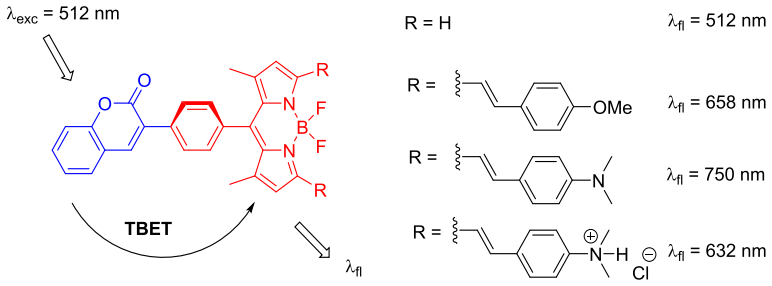


**Figura 52**. Estructuras de cassettes BODIPY-cumarina.

Además, la presencia de grupos ionizables, como el dimetilamino, permite modular la fluorescencia en función del pH mediante un proceso de transferencia electrónica fotoinducida (PET "*Photoinduced Electron Transfer*").

Análogamente, Kang y col.[7] sintetizaron una serie de cassettes BODIPY-cumarina muy similares a los anteriores, que poseen además determinados grupos funcionales para interaccionar con ciertas biomoléuclas. Estos sistemas fueron utilizados como sensores de viscosidad en mitocondrias, demostrando una relación directa entre la fluorescencia y la viscosidad (Figura 53).

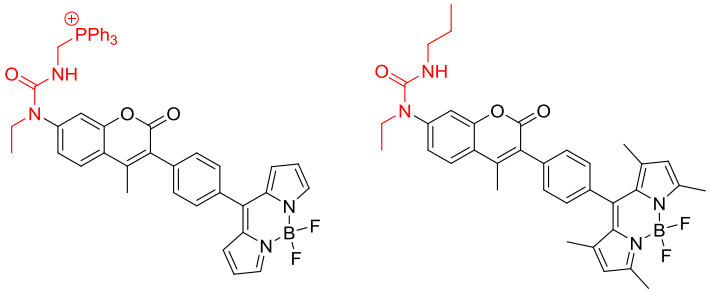


**Figura 53**. Estructuras de sistemas BODIPY-cumarina utilizados como sensores.

Por otro lado, Lin y col.[8] desarrollaron un sistema basado en BODIPY-cumarina que actúa como sensor de aniones fluoruro debido a la eliminación de grupo triisopropilsililo de la posición 7 de la cumarina, en presencia de este ión, induce un desplazamiento hipsocrómico de la banda de fluorescencia (Figura 54).

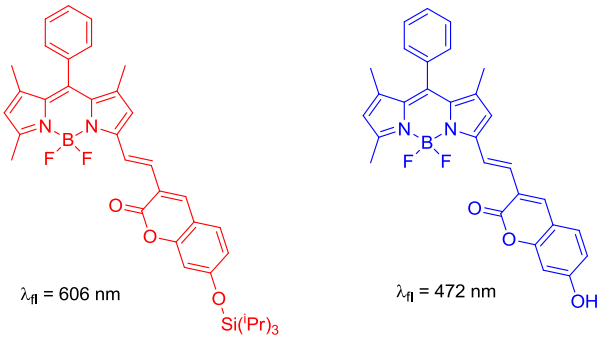


**Figura 54**. Estructuras de sistemas BODIPY-cumarinas como sensores de fluoruro.

También están descritos en la bibliografía cassettes formados por la unión de BODIPYs y perilendiimida (PDI). Así, Akkaya y col., diseñaron un cassette de este tipo (Figura 55) donde, bajo excitación a 526 nm, se registra emisión a 618 nm inducida por un proceso FRET, con una eficiencia del 99%.[9] Este sistema fue la primera demostración de una eficiente transferencia de energía en un cassette BODIPY-PDI de estructura tipo dendrímero, obtenida con alto rendimiento a través de una reacción "click".

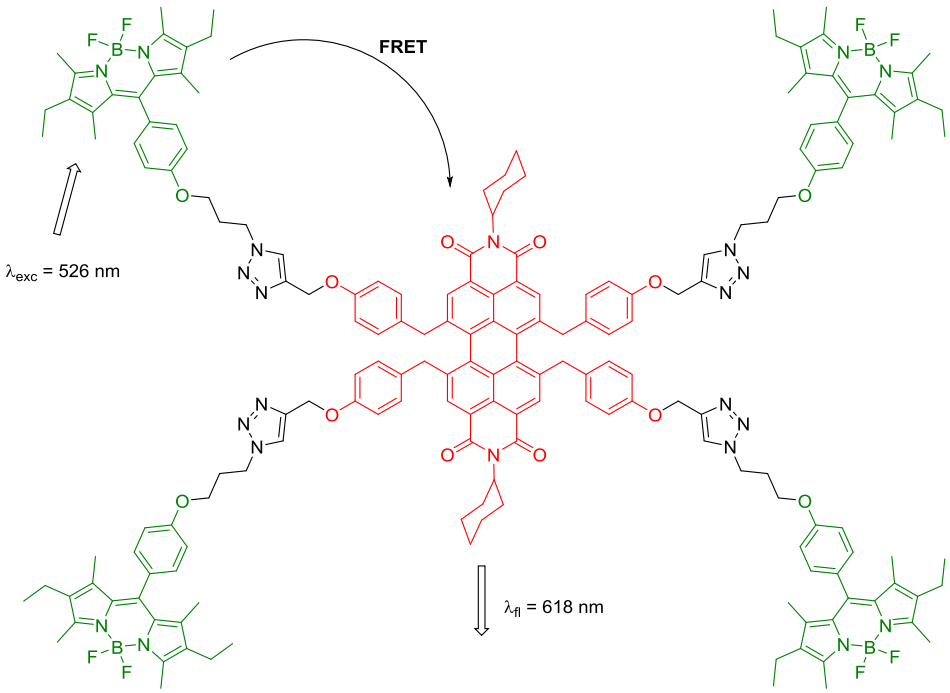


**Figura 55**. Estructura del dendrímero BODIPY-PDI.

Algunos de los cassettes anteriormente comentados resultan ser unas útiles herramientas en el campo de la bioimagen, en el diagnóstico clínico o en la detección de iones y moléculas pequeñas. Sin embargo, existen pocos ejemplos de cassettes empleados como colorantes láser basados en la combinación de varios cromóforos (Figura 56).[10]

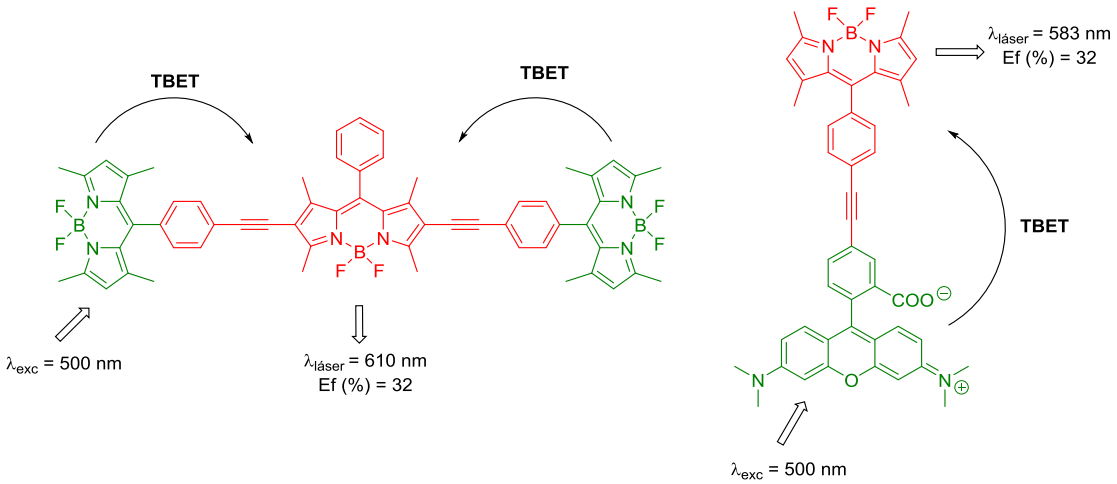


**Figura 56**. Estructuras de cassettes basados en BODIPYs y su comportamiento láser.

Estos cassettes fueron desarrollados por nuestro grupo de investigación mediante la incorporación de dos unidades BODIPYs a través de las posiciones 2 y 6, o por la unión de una molécula de rodamina a través de la posición *meso* del BODIPY. Ambos sistemas presentan una emisión láser entorno a 600 nm con una eficiencia del 32% pero bajo excitación a 500 nm, ya que excitando a la longitud de onda estándar (532 nm) su eficiencia láser disminuye significativamente.

## 4.2. CASSETTES BASADOS EN TRÍMEROS DE BODIPYs

**Artículo 7: "Asymmetric BODIPY triad for panchromatic absorption and red-edge laser emission"**. **(Aceptado *Chem. Commun.*)**

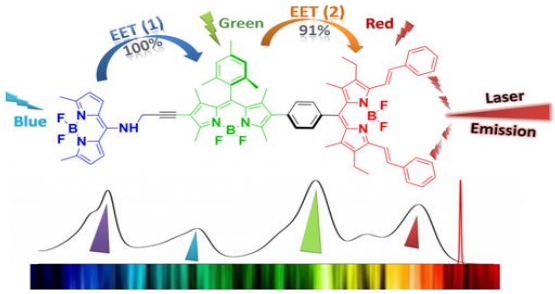


### 4.2.1. Introducción

El diseño y síntesis de concentradores de luz (antenas) para aplicaciones fotovoltaicas sigue siendo una demanda actual del sector energético. Por ello, es importante desarrollar sistemas cromofóricos que tengan fuerte absorción en toda la región UV-visible. Más relevantes resultan estos sistemas en los que, además de conseguir absorción pancromática, se puede conseguir eficiente emisión de luz monocromática en la región roja del espectro. La combinación de todas estas propiedades puede conseguirse por la unión de varios cromóforos para construir un cassette o "antena". Una vez más, la versatilidad química y las excelentes propiedades de emisión de los BODIPYs les hacen excelentes candidatos para alcanzar este objetivo.

En el presente artículo se planteó el diseño, síntesis y estudio tanto de sus propiedades fotofísicas como del comportamiento láser del complejo multicromofórico **35**, formado por la unión de tres BODIPYs, cada uno con emisión en diferentes zonas del espectro visible (Figura 57).

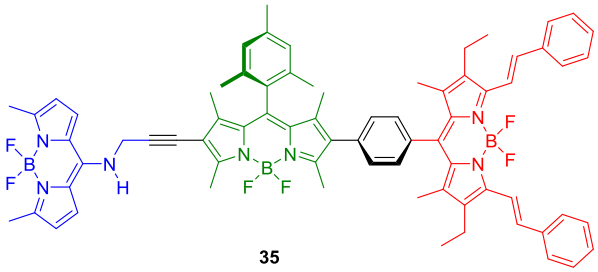


**Figura 57**. Estructura del compuesto **35**.

Se trata de un cassette asimétrico, lo que implica una mayor dificultad de síntesis que los cassettes simétricos, que pueden conseguirse más fácilmente a partir de pirroles funcionalizados de forma adecuada. Los BODIPYs que integran este nuevo cassette (compuestos **36**, **37** y **38**) fueron seleccionados en función de sus propiedades fotofísicas (Figura 58). El fragmento lateral de 8-aminoBODIPY se caracteriza por poseer absorción y emisión en la región azul del espectro visible (400-500 nm).[11] Por otro lado, el fragmento central fue seleccionado por presentar bandas de absorción/emisión en la zona verde-naranja del espectro visible (490-600 nm),[12] además de permitir una fácil funcionalización asimétrica. Finalmente, el fragmento de 3,5-diestirilBODIPY posee absorción y emisión centrada en la región roja del espectro (600-750 nm).[13]

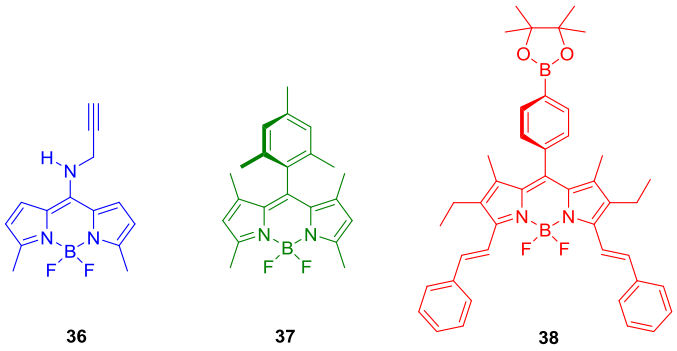


**Figura 58**. Estructuras de los compuestos **36-38**.

Los conectores entre los diferentes fragmentos son rígidos y cortos. En el extremo rojo el conector es un grupo fenilo que evita la coplanaridad molecular, y por tanto, su posible

apliamiento, proceso que conlleva siempre una reducción de la eficiencia láser. En el extremo azul, se seleccionó como conector un fragmento de propalgilamina. En este caso, se evita la conjugación entre ambos cromóforos con el fin de mantener la absorción y la emisión del fragmento de 8-aminoBODIPY en la región azul del espectro.

### 4.2.2. Síntesis

El cassette **35** se obtuvo mediante la secuencia de reacciones que se muestran en el Esquema 37. En primer lugar, la reacción de **37**[14] con NIS como agente de reacción a temperatura ambiente dio como resultado la obtención del diyodo derivado **39**,[14] con un 80% de rendimiento.

Por otra parte, el BODIPY **36** se sintetizó a través de una reacción de sustitución nucleófila entre el 8-tiometilBODIPY **40**[15] y la propargilamina en $CH_3CN$, empleando la metodología descrita por Peña-Cabrera y col.[11] Destacar que la presencia de un grupo amino unido directamente a la posición *meso* del BODIPY provoca que las bandas de absorción y emisión del cromóforo se localicen en la región azul de espectro visible, por lo que el compuestos **36** actuará como el fragmento donador del cassette.

Posteriormente, la reacción de Knoevenagel entre el BODIPY **41**[16] y benzaldehído, en presencia de piperidina y ácido acético a reflujo de tolueno, dio como resultado una mezcla compleja de los productos mono-y di-sustituidos. Para la obtención de forma exclusiva del 3,5-diestirilBODIPY **38** se optó por llevar a cabo la reacción bajo irradiación en microondas, empleando en esta ocasión DMF como disolvente, obteniéndose así de forma selectiva el compuesto **38** con un 60% de rendimiento.

A continuación, la reacción de Sonogashira entre los BODIPYs **36** y **39** en cantidades equimolares no condujo a la formación del compuesto **42**. Para su obtención fue necesario emplear 3 equiv del compuesto **36**, en idénticas condiciones de reacción, observándose la formación del dímero **42** con un 64 % de rendimiento.

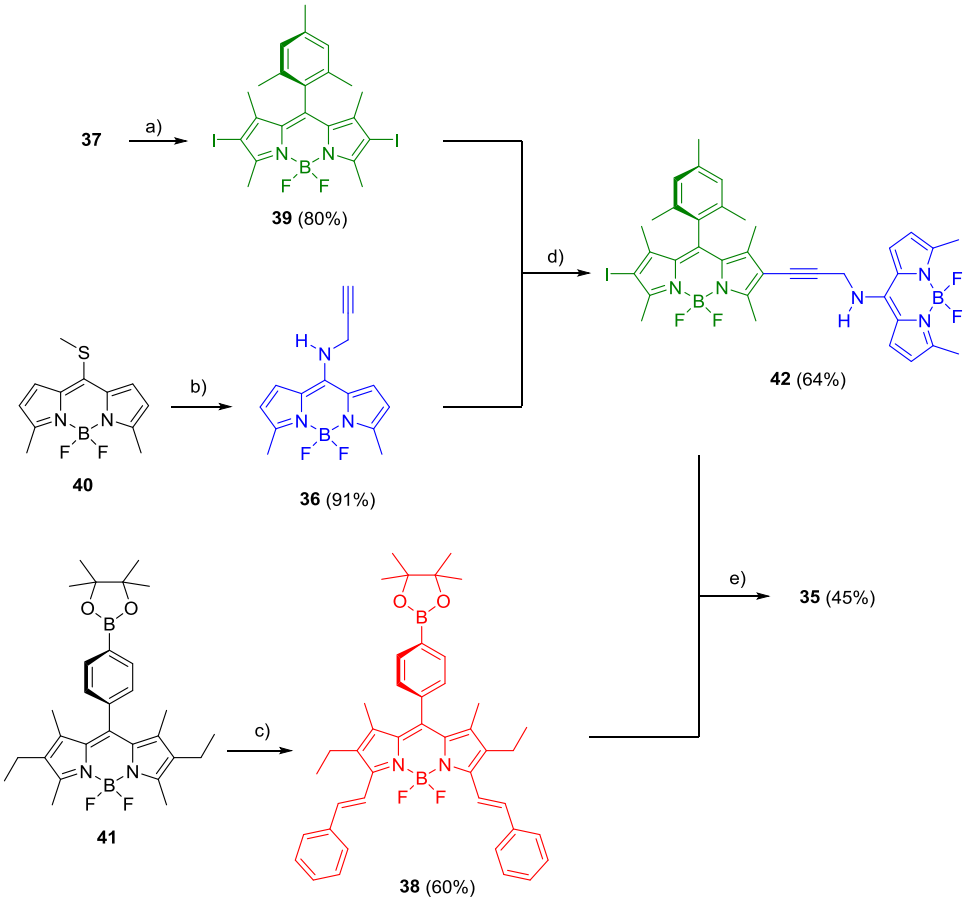


**Esquema 37**. Condiciones de reacción: a) NIS (2.2 equiv), DCM, t.a.; b) propalgilamina (1.2 equiv), $CH_3CN$, t.a.; c) benzaldehído (4 equiv), piperidina, AcOH, DMF, MW, 150 ºC, 30 min; d) **36** (3 equiv), CuI, THF/$Et_3N$ (4:1, v/v), $Pd(PPh_3)_2Cl_2$; e) **38** (2 equiv), $K_2CO_3$, $Pd(PPh_3)_4$, tolueno/EtOH/$H_2O$ (4:4:2, v/v/v).

Finalmente, la síntesis de **35** se realizó mediante una reacción de Suzuki entre el dímero **42** y el fragmento **38**. Destacar que el rendimiento de esta última reacción fue moderado, debido a que la reactividad bispinacolato de boro no es tan buena como la de los ácidos borónicos en este tipo de acoplamientos.

### 4.2.3. Propiedades fotofísicas

En cuanto a sus propiedades fotofísicas, el espectro de absorción del compuesto **35** corresponde a la suma de cada uno de los espectros de los fragmentos que constituyen este cassette (Figura 59 y Tabla 24).

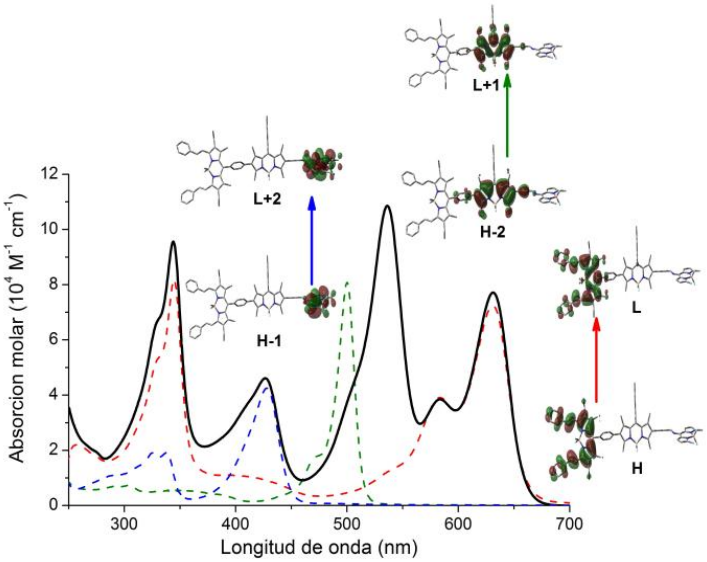


**Figura 59**. Espectro de absorción de **35** (línea negra) y de los fragmentos **36** (línea azul), **37** (línea verde) y **38** (línea roja) en AcOEt y simulación de sus orbitales moleculares HOMO (H) y LUMO (L).

**Tabla 24**. Propiedades fotofísicas de los compuestos **35**-**38** en AcOEt

| BODIPY | $\lambda_{abs}$ (nm) | $\varepsilon_{max}$ ($10^4$ $M^{-1}$ $cm^{-1}$) | $\lambda_{fl}$ (nm) | $\phi$ |
|---|---|---|---|---|
| **35** | 344 | 9.8 | - | - |
| | 426 | 4.8 | 450.5 | 0.01 |
| | 536 | 11.2 | 560.0 | 0.08 |
| | 631 | 8.0 | 645.0 | 0.72 |
| **36** | 428 | 4.6 | 488.0 | 0.90 |
| **37** | 500 | 8.7 | 508.5 | 0.94 |
| **38** | 631 | 7.8 | 647.0 | 0.68 |

Cabe destacar que la excitación en cada uno de los cromóforos que constituyen el cassette **35** produce una emisión centrada en 645 nm y un rendimiento cuántico de fluorescencia del 72% (Figura 60).

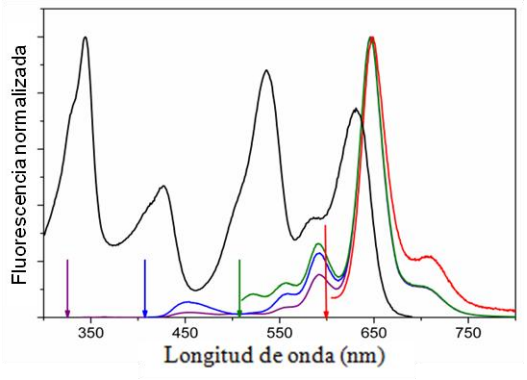


**Figura 60**. Espectro de fluorescencia de **35** bajo excitación a diferentes longitudes de onda (indicadas con flechas).

Además, en el cassette se observa un desplazamiento batocrómico de la banda de absorción del fragmento BODIPY **37** (536 nm) debido a la extensión de la conjugación del sistema π, inducida por la incorporación de los grupos fenilo y acetileno en las posiciones 2 y 6, así como la aparición de una nueva banda a 344 nm asociada a los grupos estirilos del BODIPY **38** (Figura 61).

La eficiencia del proceso de transferencia de energía puede cuantificarse por la atenuación de la fluorescencia del fragmento donador en presencia del fragmento aceptor. Así, este proceso tiene un eficiencia del 100% entre los fragmentos azul y verde, mientras que la transferencia entre los fragmentos verde y rojo es del 91%. Destacar que la transferencia entre los fragmentos azul y verde tiene lugar mediante un mecanismo FRET, altamente eficiente, debido al fuerte solapamiento de sus bandas de absorción y emisión (Figura 61). Por otro lado, existe un proceso TBET entre los fragmentos central y rojo, ya que la presencia del anillo de fenilo entre ambos permite la interacción electrónica entre los orbitales de ambos cromóforos.

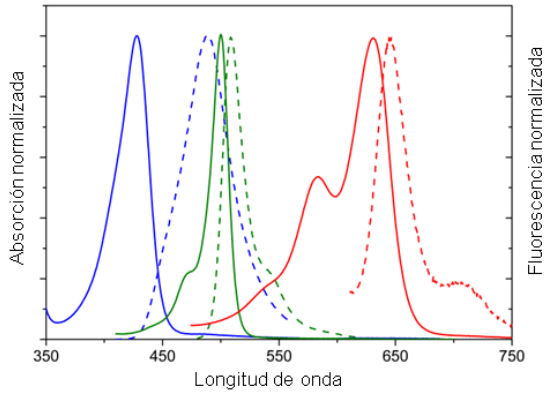


**Figura 61**. Espectros de absorción (línea gruesa) y fluorescencia (línea punteada) de los compuestos **36** (línea azul), **37** (línea verde) y **38** (línea roja) en AcOEt.

### 4.2.4. Propiedades láser

El nuevo cassette **35** presenta un mejor comportamiento láser que sus fragmentos cuando estos son tratados de forma individual, debido a que la apropiada unión covalente entre los cromóforos provoca un aumento de los coeficientes de absorción molar a las longitudes de bombeo convencionales (355 y 532 nm) con respecto a los fragmentos **36-38**. Así, la excitación de **35** bajo bombeo a 355 ó 532 nm genera una emisión láser centrada en 665 nm con un 49% de eficiencia, mientras que el BODIPY **38** posee un 30% de eficiencia láser en las mismas condiciones de bombeo. En cuanto a la fotoestabilidad del compuesto **35**, mantiene prácticamente el 100% de su eficiencia láser tras un bombeo de 100 000 pulsos.

El compuesto **35** posee un mejor comportamiento láser que el de otros cromóforos comerciales con una emisión láser en la misma región espectral, como el del BODIPY comercial **PM650**. De hecho, este colorante no puede ser bombeado a 355 nm, debido a su baja absorbancia a esa longitud. Bajo bombeo a 532 nm presenta una eficiencia láser del 35% y muy baja fotoestabilidad, ya que pierde el 40% de emisión tras 100 000 pulsos. Esta fotoestabilidad es muy inferior a la del cassette **35**, sobre todo considerando que el BODIPY comercial **PM650** se bombea con fotones a 532 nm “menos agresivos” que los de 355 nm con los que se bombearon el nuevo cassette.

### 4.2.5. Conclusiones

En resumen, gracias a la gran versatilidad sintética del cromóforo BODIPY y al óptimo diseño de la ruta de síntesis, se obtuvo un nuevo cassette basado en este tipo de cromóforo con una mayor eficiencia y estabilidad láser que otros colorantes comerciales referibles como el **PM650**.

## 4.3. CASSETTE ORTOGONAL BASADO EN BODIPYs CON COMPORTAMIENTO DUAL. **(Trabajo pendiente de publicación).**

### 4.3.1. Introducción

Uno de los principales requerimientos para la aplicación de la terapia fotodinámica es el empleo de fotosensibilizadores que transfieran la energía a las moléculas de oxígeno. Por otro lado, existen fotosensibilizadores para la visualización de tumores mediante la técnica de detección de fluorescencia del fotosensilizador (PFD, "*Photosensitizer Fluorescence Detectión*"), debido a su buena acumulación en tejidos tumorales y a su emisión fluorescente, lo que permite ayudar en la cirugía para la extirpación más precisa de tumores con el mínimo daño al tejido no afectado.[17]

Los fotosensibilizadores comúnmente empleados en TFD son las porfirinas, ya que muestran un buen rendimiento de generación de oxígeno singlete, una baja citotoxicidad, aunque su baja capacidad fluorescente limita su uso en las técnicas de detección por fluorescencia.[18] Por ello, la obtención de nuevos fotosensibilizadores con una baja citotoxicidad, alto rendimiento de generación de oxígeno singlete y una buena fluorescencia supone un reto actual, dado que ambos procesos compiten en la desactivación del estado excitado.

Unos buenos candidatos para la síntesis de fotosensibilizadores con un comportamiento dual son los compuestos derivados del cromóforo BODIPY, ya que debido a sus altos rendimientos cuánticos de fluorescencia son empleados en las técnicas de detección por imagen,[12a, 13, 19] y además la incorporación de átomos pesados en su estructura hace que muestren buenos rendimientos cuánticos de generación de oxígeno singlete, aunque se ha demostrado que estos compuestos resultan ser citotóxicos en ausencia de luz.[19-20]

Por ello, una de las actuales tendencias es la obtención de BODIPYs con un buen rendimiento de generación de oxígeno singlete sin la incorporación de átomos pesados en su estructura lo que incrementaría de fluorescencia y disminuiría su citotoxicidad. Teóricamente, cualquier sustituyente con orbitales moleculares que tenga niveles de multiplicidad y de energía apropiados podría comportarse de igual misma manera que los

BODIPYs que incorporan átomos pesados. Se ha demostrado que dímeros de BODIPY en los que la unión directa de dos unidades del cromóforo es de tipo ortogonal, dan una mayor eficiencia de ISC que los correspondientes monómeros. Los primeros estudios que pusieron de manifiesto la eficiencia de dímeros de BODIPY como generadores de oxígeno singlete fueron los descritos por Flamigni y col.[21] Estos autores sintetizaron dímeros con unión a través de las posiciones 3-3, observando una marcada influencia del disolvente sobre la generación de $^1O_2$ (Figura 62).

En esta línea, Akkaya y col.[22] llevaron a cabo un estudio computacional de una serie de dímeros unidos por posiciones 2-8 y 8-8, explicando, desde un punto de vista teórico, el comportamiento de estos sistemas como generadores de oxígeno singlete. Así, el dímero unido por las posiciones 8-8 es el que presenta el mayor rendimiento de generación de $^1O_2$ ($\phi_\Delta$ = 0.51 con respecto al azul de metileno), mientras que el dímero con unión 2-8 mantiene un significativo rendimiento cuántico de fluorescencia ($\phi$ = 0.31 con respecto a la Rodamina 6G) junto a un buen rendimiento de generación de oxígeno singlete ($\phi_\Delta$ = 0.46 con respecto al azul de metileno), lo que permite su uso dual, como agente terapéutico y como sonda en bioimagen (Figura 62).

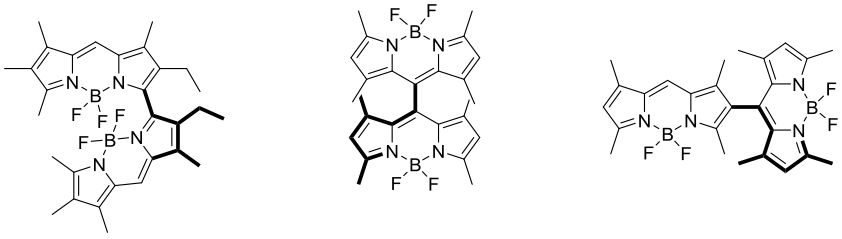

$\lambda_{abs}$ = 559 nm (DCM)
$\phi$ = 0.56 (DCM)
$\phi_\Delta$ = 0.5 (DCM)
Ref. 21

$\lambda_{abs}$ = 514 nm ($CHCl_3$)
$\phi$ = 0.03
$\phi_\Delta$ = 0.51 (DCM)
Ref. 22

$\lambda_{abs}$ = 515 nm ($CHCl_3$)
$\phi$ = 0.31
$\phi_\Delta$ = 0.46 (DCM)
Ref. 22

**Figura 62** Dímeros de BODIPY unidos por diferentes posiciones

Considerando estos antecedentes, se diseño y sintetizó un nuevo sistema multicromofórico **43** mediante unión de cromóforos tipo BODIPY, con una unión ortogonal entre ellos, y con emisión en las diferentes regiones del espectro visible, lo que

podría permitir el acceso a un sistema multicromofórico con un potencial comportamiento dual (Figura 63).

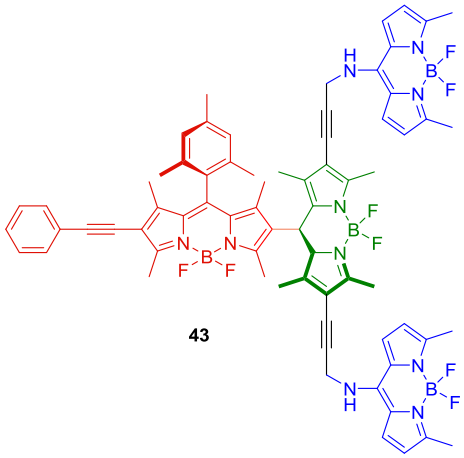


**Figura 63**. Estructura del cassette ortogonal **43**.

Los fragmentos que integran el cassette **43** se muestran en la figura 61, y fueron seleccionados en función de sus propiedades fotofísicas. Como se observó en el anterior artículo, la presencia de un grupo amino unido directamente a la posición *meso* del BODIPY **36** induce el desplazamiento de las bandas de absorción y emisión a la zona azul de espectro, por lo que actuará como fragmento donador (Figura 64).

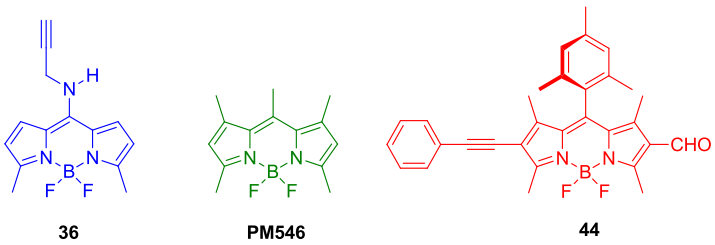


**Figura 64**. Estructuras de los fragmentos **36**, **PM546** y **44**.

El BODIPY comercial **PM546** se seleccionó como fragmento central debido a que sus bandas están en la región amarilla-verde del espectro y presenta sus posiciones 2 y 6 libres, lo que permitirá su posterior funcionalización con los conectores adecuados para lograr la

unión a los fragmentos azul y rojo. En cuanto al fragmento rojo, se eligió el compuesto **44**, ya que la presencia de un grupo fenilacetileno en la posición 2 produce un desplazamiento batocrómico de las bandas de absorción y emisión. Destacar, que la disposición ortogonal entre el fragmento central y rojo evita la interacción orbitalaria entre ambos, y como se comentó anteriormente, este es un requisito necesario para la generación de $^1O_2$ en ausencia de átomos pesados incorporados a la estructura del BODIPY.

### 4.3.2. Síntesis

La síntesis del cassette **43** se ha llevado a cabo mediante la secuencia de reacciones que se muestran en el esquema 38. El primer paso fue la reacción de formilación del BODIPY **37**[14] por tratamiento con $POCl_3$ (3 equiv) y DMF (6 equiv) durante 30 min, dando lugar al monoaldehído **45** (95%). Destacar que, a pesar de que el BODIPY **37** posee dos posiciones susceptibles de ser formiladas, solamente se obtuvo el derivado monoformilado, aun en presencia de exceso de reactivo.[23] La posterior yodación de **45**, empleando ICl como agente de halogenación, permitió aislar el derivado asimétrico difuncionalizado **46** con un rendimiento del 64%. Posteriormente, a partir de **46** se obtuvo el fragmento **44** (64%) mediante una reacción tipo Sonogashira empleando fenilacetileno como reactivo y $Pd(PPh_3)_2Cl_2$ como catalizador.

A continuación, la reacción entre **44** y el 2,4-dimetilpirrol, en las condiciones típicas de formación de dipirrometanos a partir de aldehídos aromáticos y pirroles sustituidos,[12a] condujo a la formación del dipirrometano **47** (56%). Posteriormente, la oxidación del dipirrometano empleando DDQ, seguida del tratamiento con $Et_3N$ y $BF_3{\cdot}Et_2O$ permitió aislar el dímero **48** con un 60% de rendimiento.

La yodación posterior de **48** en presencia de ICl como agente de halogenación, empleando 2.2 equiv de reactivo, permitió obtener el derivado diyodado **49** (50%), que mediante un acoplamiento de Sonogashira con el fragmento **36**, sintetizado previamente para la obtención del cassette **35** (Figura 55 y Pag. 122), condujo a la obtención del cassette **43** con un 35% de rendimiento. Destacar que este bajo rendimiento refleja la

dificultad de este tipo de acoplamientos, ya observado en el artículo anterior, a pesar de emplear un gran exceso de reactivo.

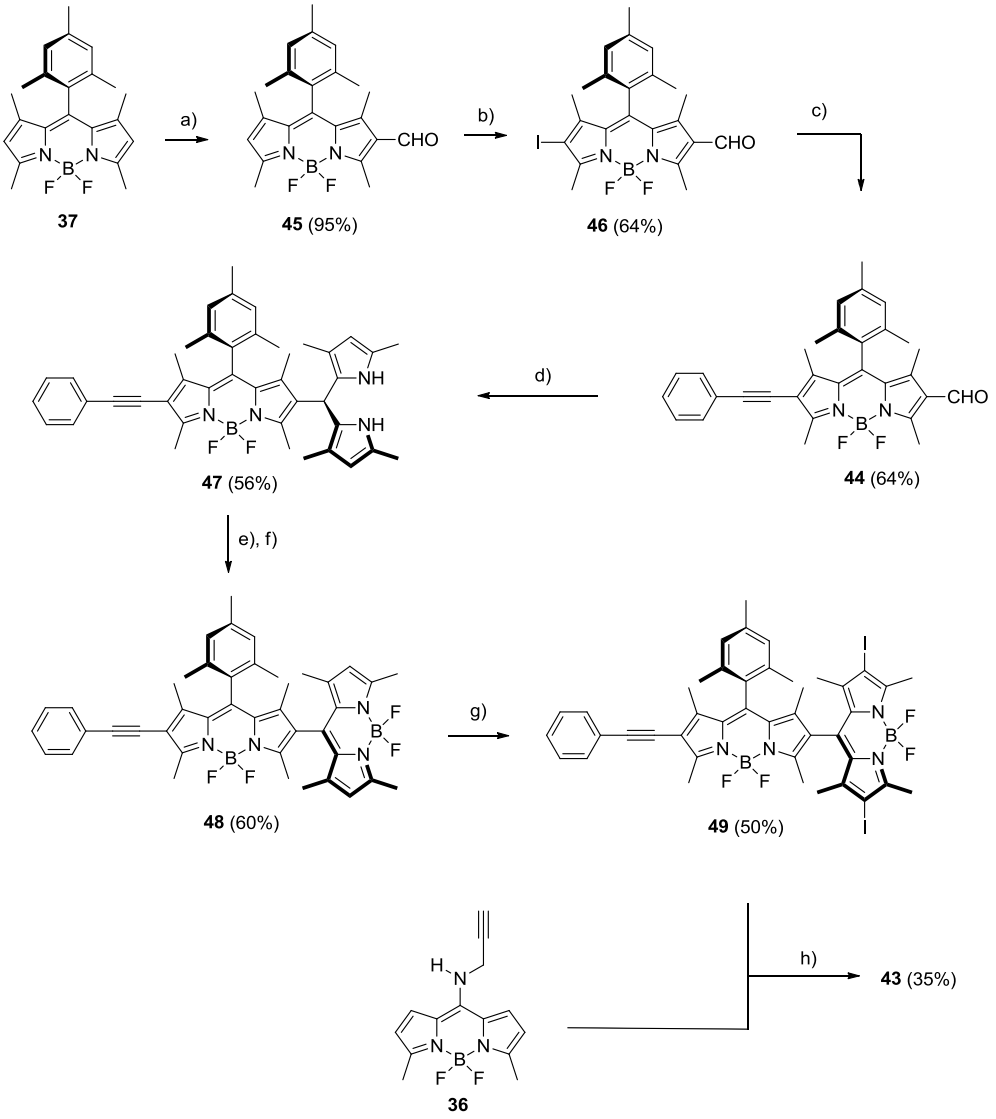


**Esquema 38**. Condiciones de reacción: a) (i) $POCl_3$ (3 equiv), DMF (6 equiv), 0 ºC, 30 min, (ii) **37** (1 equiv), 50 ºC, 30 min, DCM; b) ICl (1.1 equiv) (1 M en DCM), t. a., 15 min, DCM; c) fenilacetileno (2 equiv), CuI, $Pd(PPh_3)_2Cl_2$, 70 ºC, 1 h, THF, diisopropilamina; d) 2,4-dimetilpirrol (2.2 equiv), TFA, t.a., 30 min, DCM; e) DDQ, t.a., DCM; f) $Et_3N$, $BF_3{\cdot}Et_2O$, t.a., DCM; g) ICl (2.2 equiv) (1 M en DCM), t. a., 15 min, DCM; h) **36** (3 equiv), CuI, $Pd(PPh_3)_2Cl_2$, 70 ºC., 1 h, THF, diisopropilamina.

### 4.3.3. Propiedades fotofísicas

En primer lugar, se llevó a cabo el estudio de las propiedades fotofísicas de los fragmentos recogidos en la figura 65.

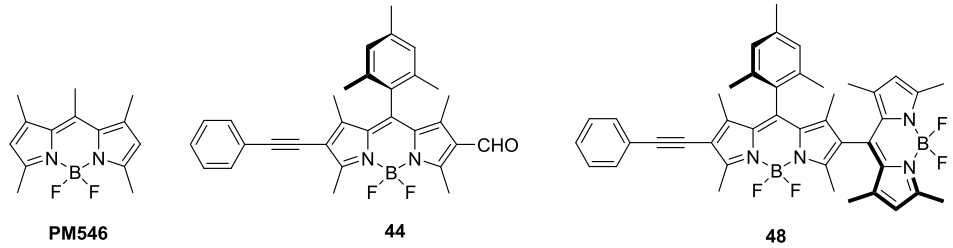


**Figura 65**. Estructuras de los compuestos **PM456**, **44** y **48**.

El espectro de absorción del intermedio **48** corresponde a la suma de los espectros del **PM546** y del **44**, ya que la disposición ortogonal de los fragmentos permite que cada cromoforo mantenga su identidad (Figura 66). Sin embargo, puesto que la separación espectral es moderada, la absorción de ambos cromóforos está muy solapada, por lo que es difícil excitar selectivamente cada uno de ellos. El espectro de fluorescencia muestra de forma exclusiva la emisión de **48** sin rastro de la emisión del **PM546**, aunque se excite a 470 nm. Por tanto, existe un eficiente proceso de transferencia de energía intramolecular, aunque hay que señalar que parte de la emisión de **48** se debe a la excitación directa de **44**.

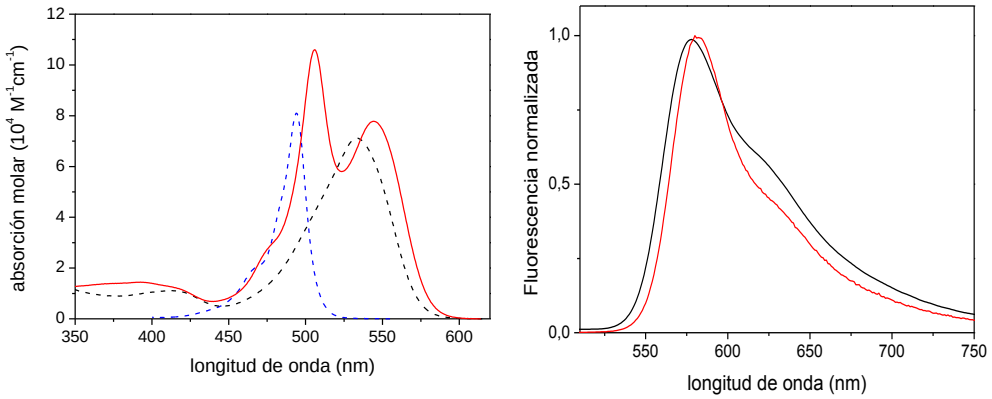


**Figura 66**. Espectros de absorción y emisión del **PM546** (azul), **44** (negro) y **48** (rojo) en AcOEt.

La extensión de la deslocalización del sistema π por introducción del fenilacetileno en **44** induce un desplazamiento batocrómico en las bandas de absorción y emisión (Tabla 25) con respecto a **37**, tal y como era de esperar en base a los resultados observados en los compuestos similares **50a**[24] y **50b**[25] publicados previamente (Figura 67).

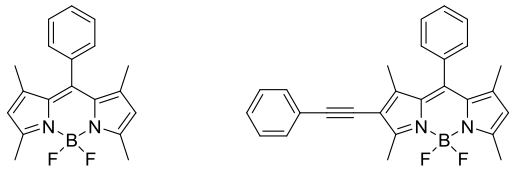


**Figura 67**. Estructura de los compuestos **50a**-**b**.

**Tabla 25. Propiedades fotofísicas de PM546, 37, 44, 48 y 50 en AcOEt**

| BODIPY | $\lambda_{abs}$ (nm) | $\varepsilon_{max}$ ($10^4$ $M^{-1}\cdot cm^{-1}$) | $\lambda_{flu}$ (nm) | ϕ |
|---|---|---|---|---|
| **PM546** | 494 | 8.1 | 506 | 0.85 |
| **37** | 500 | 8.7 | 508 | 0.94 |
| **44** | 533 | 7.1 | 577 | 0.26 |
| **48** | 506<br>545 | 7.8<br>10.6 | 580 | 0.2 |
| **50a** | 498 | 9.1 | 508 | 0.65 |
| **50b** | 530 | 5.4 | 567 | 0.44 |

La presencia adicional del aldehído en la posición 6 de **44** reduce la capacidad fluorescente e induce un mayor desplazamiento batocrómico de la banda de emisión con respecto al BODIPY **50b**. Este comportamiento se debe a la asimetría del patrón de sustitución, ya que el carácter electroatractor del grupo aldehído, unido con el carácter electrodador del grupo fenilacetileno en la posición 2, provoca un efecto "*push-pull*". Este mismo efecto se observa en el cassette **48**, en el que también la sustitución asimétrica reduce la capacidad fluorescente. En cuanto al espectro de absorción de **43** (Figura 68), este consta de dos bandas solapadas en la región menos energética (idénticas a las del

compuesto **48** pero desplazadas batocrómicamente por la presencia de dos acetilenos en el fragmento central) y una banda a mayores energías análoga a la del 8-aminoBODIPYs.[26]

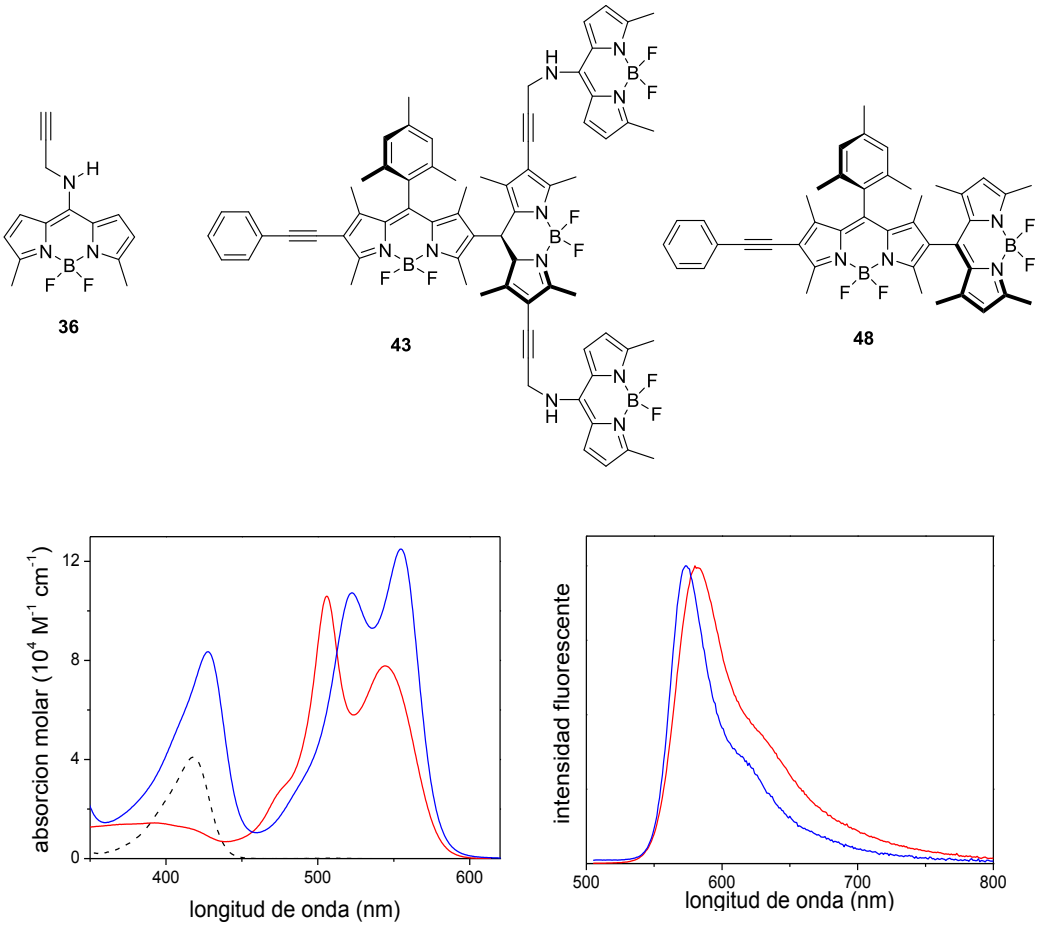


**Figura 68**. Estructuras de los compuestos **36** (negro), **43** (azul) y **48** (rojo) en AcOEt .y sus espectros de absorción y emisión.

En el cassette **43**, el grupo propargilo asegura que el par de electrones de la amina vaya al BODIPY **36**, constituyendo la forma hemicianina, y evitando que se deslocalicen en el resto de la estructura.[26] Por lo tanto, la unión entre **36** y el BODIPY **48** es adecuada, ya que se mantiene la identidad de cada fragmento y, además, se consigue ampliar la zona de absorción hacía el azul, lo que permite un mayor rango espectral para seleccionar la excitación. De hecho, la excitación a 400 nm de **43** provoca una emisión a una longitud de

onda similar a cuando se excita **48** a 500 nm (Tabla 26). Por tanto, existe un proceso de transferencia de energía altamente eficiente.

**Tabla 26. Propiedades fotofísica de 36, 43 y 48 en AcOEt.**

| BODIPY | $\lambda_{abs}$ (nm) | $\varepsilon_{max}$ ($10^4$ $M^{-1}\cdot cm^{-1}$) | $\lambda_{flu}$ (nm) | $\phi$ |
|---|---|---|---|---|
| **36** | 428 | 4.6 | 488 | 0.90 |
| **43** | 554 | 12.5 | 573 | 0.19 |
| | 522 | 10.7 | | |
| | 427 | 8.4 | | |
| **48** | 544 | 7.8 | 580 | 0.20 |
| | 506 | 10.6 | | |

La capacidad fluorescente de los cassettes **43** y **48** es aproximadamente del 20% como cabía esperar considerando la disposición ortogonal entre el fragmento central y el rojo en ambos sistemas, lo que evita la interacción electrónica entre dichos cromóforos e induce un aumento del ISC, reduciendo así su rendimiento cuántico de fluorescencia.

### 4.3.4. Generación de oxígeno singlete

La eficiencia de generación de oxígeno singlete para los compuestos **43** y **48** se registró en $CH_3CN$ y empleando Rosa de Bengala (**RB**) ($\phi_\Delta$ = 0.42) o Fenalenona (**PN**) ($\phi_\Delta$ = 1) como referencias. Los resultados obtenidos se muestran en la tabla 27.

**Tabla 27. Propiedades fotofísica de 43 y 48 en AcOEt**

| BODIPY | $\lambda_{exc}$ (nm) | $\phi_\Delta$ |
|---|---|---|
| **43** | 400 | 0.38 |
| | 522 | 0.52 |
| **48** | 545 | 0.31 |

Como puede observarse, el cassette **48** muestra un rendimiento de generación de oxígeno singlete del 31% bajo excitación a 545 nm y empleando **RB** como referencia (Figura 69).

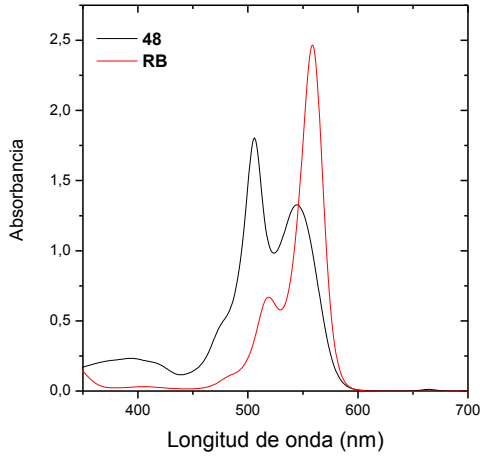


**Figura 69**. Espectro de absorción de **48** y **RB** en $CH_3CN$ bajo excitación a 545 nm.

En cuanto al cassette **43**¸ este posee dos bandas de absorción, lo que le permite cubrir un mayor rango espectral. Así, este cassette posee una eficiencia de generación de oxígeno singlete del 38% bajo irradiación a 400 nm (empleando **PN** como referencia,) mientras que esta eficiencia es del 52% excitando a 545 nm y usando en este caso **RB** como referencia (Figura 70).

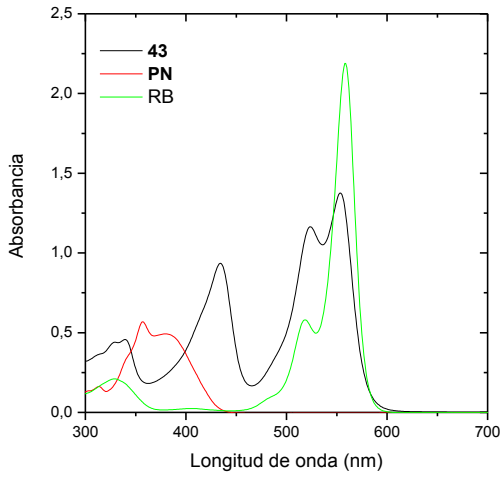


**Figura 70**. Espectro de absorción de **43**, **PN** y **RB** en $CH_3CN$ bajo excitación a 400 nm

### 4.3.5. Propiedades láser

El comportamiento láser de los cassettes **43** y **48** se analizo bajo bombeo a 355 nm en AcOEt. El cassette **43** presenta una emisión láser centrada a 600 nm con un eficiencia de 6%, mientras que el cassette **48** posee una eficiencia del 18% y una emisión a 610 nm. Este comportamiento bajo condiciones drásticas de bombeo asegura su potencial uso como sondas fluorescentes a parte de su capacidad de actuación como fotosensibilizador, lo que garantizaría el comportamiento dual para el que fueron diseñados.

### 4.3.6. Conclusiones

El diseño racional desarrollado ha permitido la obtención de un nuevo sistema multicromofórico basado en BODIPYs que presenta un comportamiento dual Así, el tetrámero **43** tiene un rendimiento cuántico de fluorescencia de 0.2 y es a la vez un buen generador de oxígeno singlete con una eficiencia del 38% cuando se irradia a 400 nm y del 52% si se excita a 545 nm, potenciando su aplicabilidad dual: como agente terapéutico (TFD) y como sonda de diagnóstico (bioimagen).

### 4.3.7. Parte experimental

#### *4.3.7.1. Procedimientos generales*

##### *4.3.7.1.a. Reacción de yodación de BODIPYs*

En un matraz de dos bocas provisto de entrada y salida de gases y agitación magnética, se introduce, en atmósfera de argón, el BODIPY (1 equiv) disuelto en la mínima cantidad de una mezcla DCM/MeOH (5:5). A continuación, se añade ICl (1.1-2 equiv) y la mezcla de reacción se agita a temperatura ambiente hasta que por cromatografía en capa fina se observe que no queda producto de partida (15-30 minutos). Pasado este tiempo, se añade DCM y se lava con una disolución saturada de $Na_2S_2O_3$. La fase orgánica se seca sobre $MgSO_4$ anhidro, se filtra y se elimina el disolvente a presión reducida. El compuesto

obtenido se purifica por cromatografía flash en columna sobre gel de sílice, indicándose en cada caso la mezcla de disolventes utilizada.

*4.3.7.1.b. Reacción de acoplamiento tipo Sonogashira*

En un matraz de dos bocas provisto de entrada y salida de gases y agitación magnética, se introduce, bajo atmósfera de argón, el BODIPY (1 equiv) en THF/DIPA (10:5). A continuación, se añade el alquino (2 equiv) y una punta de espátula de CuI, manteniéndose la agitación a temperatura ambiente durante 5 min. Pasado este tiempo, se añade una punta de espátula del catalizador de Pd y se sigue la reacción hasta que por cromatografía en capa fina se observe que no queda producto de partida. El crudo de reacción se extrae con DCM y se lava con una disolución de HCl al 10%. La fase orgánica se seca sobre $MgSO_4$ anhidro, se filtra y se elimina el disolvente a presión reducida. El crudo de reacción se purifica por cromatografía flash en columna sobre gel de sílice, indicándose en cada caso la mezcla de disolventes utilizada.

***4.3.7.2. Síntesis de BODIPYs***

*4.3.7.2.a. Síntesis del BODIPY **45***

En un matraz de dos bocas y 50 mL de capacidad, provisto de entrada y salida de gases, refrigerante de reflujo y agitación magnética, se introduce a 0 ºC, y en atmósfera inerte, DMF (6 mL) y se añade gota a gota $POCl_3$ (3 mL). La reacción se mantiene a esa temperatura durante 30 min y, a temperatura ambiente, se añade el BODIPY **37** (100 mg, 0,273 mmol) disuelto en DCM (10 mL), calentando a 50 ºC durante otros 30 min. La reacción se deja enfriar y se hidroliza con $K_2CO_3$. A continuación, se extrae con DCM. Los extractos orgánicos se secan sobre $MgSO_4$ anhidro, se elimina el desecante mediante filtración y el disolvente a presión reducida. Por último, los restos de DMF se eliminan mediante destilación a vacío. El crudo de reacción se purifica por cromatografía flash en columna (hexano/AcOEt 9:1), obteniéndose el BODIPY **45** (210 mg, 95%) como un sólido naranja oscuro.

$^{1}$H-RMN (300 MHz, $CDCl_3$): δ 9.94 (s, 1H, CHO), 6.91 (s, 2H), 6.07 (s, 1H), 2.75 (s, 3H), 2.54 (s, 3H), 2.28 (s, 3H), 2.01 (s, 6H), 1.62 (s, 3H), 1.35 (s, 3H); $^{13}$C-RMN (75 MHz, $CDCl_3$): δ 186.0 (CHO), 161.4, 156.3, 146.3, 143.8, 142.0, 139.3, 134.7 , 133.5, 130.3, 129.4 (CH), 128.8, 126.0, 123.7 (CH), 21.2 ($CH_3$), 19,.5 ($CH_3$), 15.1 ($CH_3$), 13.9 ($CH_3$), 13.0 ($CH_3$), 10.4 ($CH_3$); IR (puro): 2925, 2859, 2740, 1670, 1545, 1310, 1100, 1034, 986 $cm^{-1}$; HRMS-EI: calculado para ($C_{23}H_{25}BF_2N_2O$) 394.2026, encontrado 394.2019.

*4.3.7.2.b. Síntesis del BODIPY **46***

Siguiendo el procedimiento general de síntesis *4.3.7.1.a*, se hace reaccionar el BODIPY **45** (210 mg, 0.533 mmol) disuelto en la mínima cantidad de una mezcla DCM/MeOH (5:5) con ICl (0.58 mL, 1 M en DCM, 0.58 mmol). El crudo de reacción se purifica mediante cromatografía flash en columna (hexano/AcOEt 9:1), obteniéndose el BODIPY **46** (200 mg, 64%) como un sólido naranja.

$^{1}$H-RMN (300 MHz, $CDCl_3$): δ 9.95 (s, 1H, CHO), 6.93 (s, 2H), 2.76 (s, 3H), 2.63 (s, 3H), 2.30 (s, 3H), 2.00 (s, 6H), 1.62 (s, 3H), 1.38 (s, 3H); $^{13}$C-RMN (75 MHz, $CDCl_3$): δ 185.8 (CHO), 160.3, 157.8, 147.1, 144.5, 144.3, 139.7, 134.6, 132.8, 130.3, 129.5 (CH), 126.8, 100.0, 87.9, 21.3 ($CH_3$), 19.5 ($CH_3$), 16.4 ($CH_3$), 16.2 ($CH_3$), 13.3 ($CH_3$), 10.6 ($CH_3$); IR (puro): 2946, 2860, 2741, 1671, 1554, 1300, 1151, 1020, 976 $cm^{-1}$; HRMS-EI: calculado para ($C_{23}H_{24}BF_2IN_2O$) 520.0992, encontrado 520.0988

*4.3.7.2.c. Síntesis del BODIPY **44***

Siguiendo el procedimiento general de síntesis *4.3.7.1.b.*, se hace reaccionar el BODIPY **46** (110 mg, 0.21 mmol) en THF/DIPA (2:1), fenilacetileno (0.42 mmol. 0.045 mL), una punta de espátula de CuI y otra de $Pd(PPh_3)_2Cl_2$ durante 30 min. El crudo de reacción se purifica mediante cromatografía flash en columna (hexano/AcOEt 95:5), obteniendose el compuesto **44** (66 mg, 64%) como un sólido rojizo.

$^{1}$H-RMN (300 MHz, $CDCl_3$): δ 9.95 (s, 1H, CHO), 7.41-7.37 (m, 2H), 7.26-7.24 (m, 3H), 6.93 (s, 2H), 2.77 (s, 3H), 2.68 (s, 3H), 2.29 (s, 3H), 2.02 (s, 6H), 1.64 (s, 3H), 1.48 (s,

3H); $^{13}$C-RMN (75 MHz, $CDCl_3$): δ 185.8 (CHO), 161.9, 157.6, 145.9, 144.8, 143.7, 139.6, 134.6, 132.2, 131.4 (CH), 130.2, 129.7, 129.5, 129.4 (CH), 128.5 (CH), 128.4 (CH), 126.6, 123.0, 118.1, 97.7 (C≡C), 80.8 (C≡C), 21.3 ($CH_3$), 19.5 ($CH_3$), 14.1 ($CH_3$), 13.3 ($CH_3$), 12.8 ($CH_3$), 10.6 ($CH_3$); IR (puro): 2917, 2859, 2736, 2212, 1676, 1528, 1317, 1181, 1086 $cm^{-1}$; HRMS-EI: calculado para ($C_{31}H_{29}BF_2N_2O$) 494.2341, encontrado 494.2335.

*4.3.7.2.d. Síntesis del BODIPY **47***

En un matraz de dos bocas provisto de agitación magnética, entrada y salida de gases, se introduce, bajo atmósfera de argón, el BODIPY **44** (232 mg, 0.47mmol), 2.4-dimetilpirrol (0.1 mL, 1.03 mmol) y 2 gotas de ácido trifluoroacético. La mezcla de reacción de agita durante 30 min a temperatura ambiente y, pasado este tiempo, se lava con HCl al 10%. La fase orgánica se seca sobre $MgSO_4$ anhidro, se filtra y se elimina el disolvente a presión reducida. El crudo de reacción se purifica por cromatografía en columna (hexano/AcOEt 95:5), obteniéndose el compuesto **47** (250 mg, 56%) como un sólido naranja.

$^1$H-RMN (300 MHz, $CDCl_3$): δ 7.39-7.36 (m, 2H), 7.24-7.22 (m, 3H), 6.87 (s, 2H), 5.60 (s, 2H), 5.25 (s, 1H), 2.63 (s, 3H), 2.25 (s, 6H), 2.08 (s, 6H), 2.00 (s, 6H), 1.70 (s, 6H), 1.42 (s, 3H), 1.07 (s, 3H); $^{13}$C-RMN (75 MHz, $CDCl_3$): δ 157.0, 156.2, 141.8, 141.7, 140.2, 138.9, 134.8, 131.3 (CH), 131.2, 131.1, 130.5, 129.4; 129.2 (CH), 128.3 (CH), 128.0 (CH), 125.3, 123.8, 123.7, 114.9, 114.7, 114.7, 109.0 (CH), 95.9 (C≡C), 82.1 (C≡C), 31.8 (CH), 21.2 ($CH_3$), 19.6 ($CH_3$), 13.6 ($CH_3$), 13.1 ($CH_3$), 13.0 ($CH_3$), 12.3 ($CH_3$), 10.9 ($CH_3$), 10.7 ($CH_3$); IR (puro): 3435, 2922, 2210, 1535, 1397, 1318, 1192, 1083, 1007 $cm^{-1}$; HRMS-EI: calculado para ($C_{43}H_{45}BF_2N_4$) 666.3705, encontrado 666.3711.

*4.3.7.2.e. Síntesis del BODIPY **48***

En un matraz de dos bocas provisto de agitación magnética, entrada y salida de gases, se introduce, bajo atmósfera de argón, el compuesto **47** (100 mg, 0.31 mmol) y DDQ

(113.5 mg, 0.5 mmol) en DCM (20 mL), agitando la reacción durante 30 min. Pasado este tiempo, se añade $Et_3N$ (0.3 mL) y tras 5 min $BF_3{\cdot}Et_2O$ (0.51mL) manteniendo la agitación durante 20 min más. El crudo de reacción se purifica por cromatografía flash en columna (hexano/AcOEt 95:5), obteniéndose el dímero **48** (190 mg, 60%) como un sólido naranja.

$^1$H-RMN (300 MHz, $CDCl_3$): δ 7.40-7.37 (m, 2H), 7.23-7.16 (m, 3H), 6.89 (s, 2H), 5.90 (s, 2H), 2.67 (s, 3H), 2.45 (s, 6H), 2.36 (s, 3H), 2.24 (s, 3H), 2.02 (s, 6H), 1.62 (s, 6H), 1.48 (s, 3H), 1.16 (s, 6H); $^{13}$C-RMN (75 MHz, $CDCl_3$): δ 15.,3, 155.9, 152.2, 144.1, 143.1, 142.3, 139.4, 139.1, 134.5, 133.3, 131.8, 131,4 (CH), 130.9, 130.6, 130.5, 129.4 (CH), 128.4 (CH), 128.3 (CH), 126.1, 123.3, 121.4 (CH), 116.4, 96.8 (C≡C), 81.4 (C≡C), 21.3 ($CH_3$), 19.4 ($CH_3$), 14.7 ($CH_3$), 14.0 ($CH_3$), 13.8 ($CH_3$), 12.9 ($CH_3$), 12.5 ($CH_3$), 11.3 ($CH_3$); IR (puro): 2922, 2856, 2221, 1539, 1313, 1190, 1083, 1009, 978 $cm^{-1}$; HRMS-EI: calculado para ($C_{43}H_{42}B_2F_4N_4$) 712.3522, encontrado 712.3552.

*4.3.7.2.f. Síntesis del BODIPY **49***

Siguiendo el procedimiento general de síntesis *4.3.7.1.a*, se hace reaccionar el BODIPY **48** (180 mg, 0.25 mmol) y ICl (1 M en DCM, 0.6 mL, 0.6 mmol) disuelto en una mezcla DCM/MeOH (5:5) durante 15 min. El crudo de reacción se purifica por cromatografía flash en columna (hexano/DCM 7:3), obteniéndose el compuesto **49** (120 mg, 50%) como un sólido rojo.

$^1$H-RMN (300 MHz, $CDCl_3$): δ 7.35-7.23 (m, 5H), 6.93 (s, 2H), 2.62 (s, 3H), 2.55 (s, 6H), 2.35 (s, 3H), 2.27 (s, 3H), 2.09 (s, 3H), 2.06 (s, 3H) 1.67 (s, 6H), 1.42 (s, 3H), 1.16 (s, 3H); $^{13}$C-RMN (75 MHz, $CDCl_3$**)**: δ 157.2, 156.3, 151.4, 144.5, 144.0, 141.5, 139.5, 138.5, 134.8, 134.5, 134.4, 133.5, 131.7, 130.9, 130.7, 130.4, 129.6 (CH), 129.5 (CH), 128.8 (CH), 128.4 (CH), 128.2, 127.8, 127.5, 125.6, 123.8, 101.0 (C≡C), 85.9 (C≡C), 21.3 ($CH_3$), 19.6 ($CH_3$), 19.5 ($CH_3$), 16.4 ($CH_3$), 16.3 ($CH_3$), 16.1 ($CH_3$), 13.6 ($CH_3$), 13.0 ($CH_3$), 12.2 ($CH_3$), 11.4 ($CH_3$); IR (puro): 2921, 2215, 1532, 1311, 1178, 1094, 999 $cm^{-1}$; HRMS-EI: calculado para ($C_{43}H_{40}B_2F_4I_2N_4$) 964.2291, encontrado 954.2283.

*4.3.7.2.g. Síntesis del BODIPY **43***

Siguiendo el procedimiento general de síntesis *4.3.7.1.b.,* se hace reaccionar **49** (50 mg, 0,081 mmol), **36** (66 mg, 0,243 mmol) en 10 mL de una mezcla THF/DIPA (2:1 v:v), una punta de espátula de CuI y otra de $Pd(PPh_3)_2Cl_2$. La mezcla de reacción se mantiene a reflujo durante 1 h. El crudo de reacción se purifica por cromatografía flash en columna (hexano/AcOEt 9:1), obteniéndose **43**, (35 mg, 35 %) como un sólido rojo.

$^1$H-RMN (700 MHz, $CDCl_3$): δ 7.54-7.46 (m, 1H), 7.44–7.40 (m, 2H), 7.38-7.31 (m, 2H), 7.02 (s, 4H), 7.01 (s, 2H), 4.66 (d, *J* = 5.3 Hz, 4H), 2.76 (d, *J* = 41.5 Hz, 3H), 2.62 (s, 6H), 2.60 (s, 12H), 2.44 (d, *J* = 15.9 Hz, 3H), 2.36 (d, *J* = 3.6 Hz, 3H), 2.17 (d, *J* = 18.0 Hz, 3H), 1.79 (s, 3H), 1.60 (s, 3H), 1.52 (s, 2H), 1.24 (d, *J* = 14.9 Hz, 3H); $^{13}$C-RMN (176 MHz, $CDCl_3$): δ 160.7, 159.3, 159.2, 156.5, 150.9, 150.40, 148.5, 145.1, 144.7, 144.0, 143.4, 141.7, 141.4, 139.6, 139.5, 138.0, 135.6, 134.5, 134.3, 134.2, 131.5, 131.4 (CH), 130.6, 130.3, 130.2, 129.6, 129.5 (CH), 128.9, 128.8 (CH), 128.4 (CH), 128.3 (CH), 123.7, 123.1, 122.9, 115.5, 114.7, 101.1, 97.2 (C≡C), 89.3 (C≡C), 37.7 ($CH_2$), 21.3 ($CH_3$), 19.6 ($CH_3$), 19.5 ($CH_3$), 14.2 ($CH_3$), 13.8 ($CH_3$), 13.7 ($CH_3$), 13.6 ($CH_3$), 13.0 ($CH_3$), 12.9 ($CH_3$), 12.8 ($CH_3$), 12.7 ($CH_3$), 12.6 ($CH_3$), 12.2 ($CH_3$), 11.3 ($CH_3$); IR (puro): 3276, 2917, 2141, 1589, 1413, 1209, 1014, 977 $cm^{-1}$; HRMS-EI: calculado para ($C_{71}H_{98}B_4F_8N_{10}$) 1256.6222, encontrado 1256.5873.

## 4.4. CASSETTES BASADOS EN BODIPY-CUMARINA

**Artículo 7: "Coumarin-BODIPY hybrids by heteroatom linkage: versatile, tunable and photostable dye lasers for UV irradiation".** *Phys. Chem. Chem. Phys.* **2015**, *17*, 8239-8247.

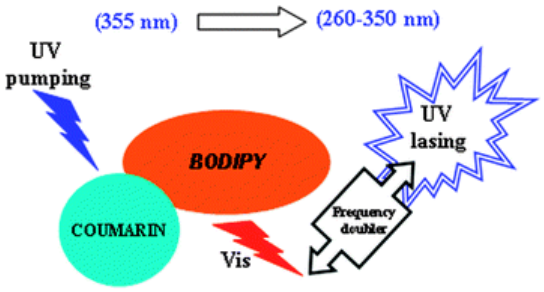


### 4.4.1. Introducción

Los BODIPY y las cumarinas poseen excelentes propiedades fotofísicas y espectralmente complementarias, sin embargo, tal y como se ha comentado en la introducción de este capítulo, hay pocos ejemplos de cassettes BODIPY-cumarina (ver Figuras 49-51 y Pag. 116 y 117)[6-8] y en ellos la unión de ambos cromóforos se establece entre la posición 3 del anillo de cumarina y la posición 3 u 8 del BODIPY. También se han obtenido sistemas de este tipo en los que ambos cromóforos se encuentran fusionados o bien muy alejados espacialmente, mostrando todos ellos unas propiedades fotofísicas interesantes, útiles para el desarrollo de ciertas herramientas fotónicas.[7-8, 27] Sin embargo, es importante señalar que ninguno de estos sistemas ha sido evaluado como colorante láser. Por otro lado, híbridos BODIPY-cumarina en los que ambos cromóforos estén unidos a través del grupo amino o hidroxilo de la cumarina (involucrados en el efecto "*push-pull*" de este cromóforo) son desconocidos.

Teniendo en cuenta estos antecedentes, en el presente artículo se planteó la síntesis de una serie de sistemas BODIPY-cumarina (**51**-**55**) unidos por el heteroátomo de la cumarina (Figura 71), con el fin de incrementar significativamente la absorción en la región UV de los BODIPY manteniendo, e incluso incrementando su eficiencia y estabilidad láser en la región entre 520-680 nm. Un sistema láser de este tipo es el único que permitiría generar,

por doblado de frecuencia, radiación láser eficiente, estable y sintonizable en la región UV entre 250-340 nm, dando respuesta a una demanda actual y creciente tanto de la comunidad científica como de la industria optoelectrónica. Esta radiación láser sintonizable en el UV es la única radiación que permite estudiar en profundidad los mecanismos de fotodegradación de moléculas biológicas esenciales, como los ácidos nucleicos, inducida por la acción de la radiación solar UV, y que son sin duda, desencadenantes de procesos cancerígenos y metastásicos.

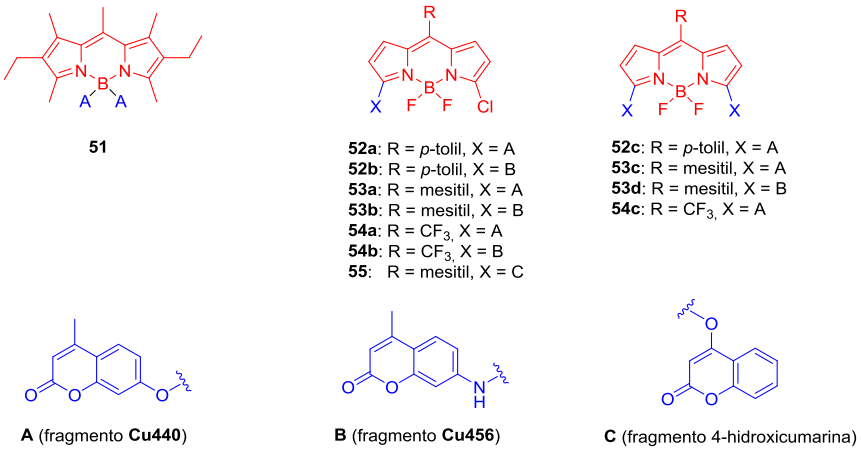


**Figura 71**. Estructuras de los híbridos **51**-**55**

### 4.4.2. Síntesis

El compuesto **51** se obtuvo fácilmente por introducción de los grupos hidroxilo de la cumarina comercial **Cu456** en el átomo de boro del BODIPY comercial **PM567** en presencia del $AlCl_3$ (Esquema 91).

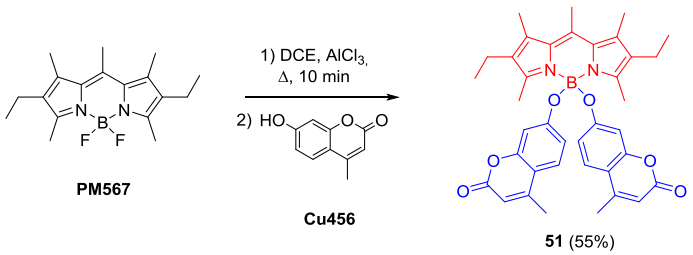


**Esquema 39**

A continuación, para la obtención de **52-54** fue necesario sintetizar en primer lugar los BODIPYs precursores **7f**,[28] **56**[29] y **57**.[30] La síntesis de **7f** se recoge en el esquema 14 de la página 52 de esta Memoria, mientras que los compuestos **56** y **57** se obtuvieron a través de las secuencias de reacción que se recogen en el esquema 40.

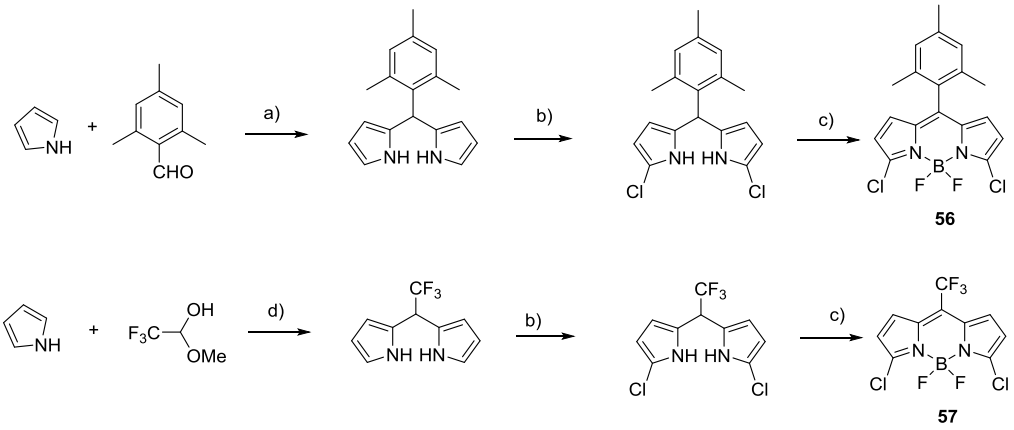


**Esquema 40**. Condiciones de reacción: a) $HCl/H_2O$, t.a. 4 h; b) NCS (2.2 equiv), -78 ºC, THF, 90 min; c) DDQ (1.1 equiv), DCM, t.a.; c) (i) $Et_3N$, DCM, t.a. 30 min; (ii) $BF_3 \cdot Et_2O$, t.a. 30 min; d) HCl (35%), THF, Δ, 4 h.

Una vez obtenidos los BODIPYs precursores, la reacción de sustitución nucleófila aromática de los 3,5-dicloroBODIPYs **7f** y **56** con la 7-aminocumarina (**Cu440**) y la 7-hidroxicumarina (**Cu456**), controlando las condiciones de reacción, permitió obtener los correspondientes mono- y di-derivados **52a-c** y **53a-d** con rendimientos de moderados a excelentes (Esquema 41). Señalar que, aunque se observó la formación del derivado disustituido con dos restos de 7-aminocumarina a partir de **6f**, fue solamente a nivel de trazas, lo que impidió su caracterización. En cuanto a los cassettes derivados del BODIPY **57**, se modificó la metodología anteriormente empleada para la introducción de 7-hidroxicumarinas, ya que el uso de $K_2CO_3$ como base producía la descomposición del BODIPY de partida, no siendo posible por ello la obtención del derivado disustituido.

Por último, se sintetizó el compuesto **55**, en donde se ha modificado la unión entre ambos cromóforos (posición 3 del BODIPY y 4 de la cumarina), con la finalidad de estudiar la influencia sobre las propiedades fotofísicas y el comportamiento láser del

cambio en la posición de unión. Esta síntesis se realizó en colaboración con el grupo del Prof. Peña-Cabrera y se llevó a cabo entre el BODIPY **56** y la 4-hidroxicumarina empleando NaH como base (Esquema 41).

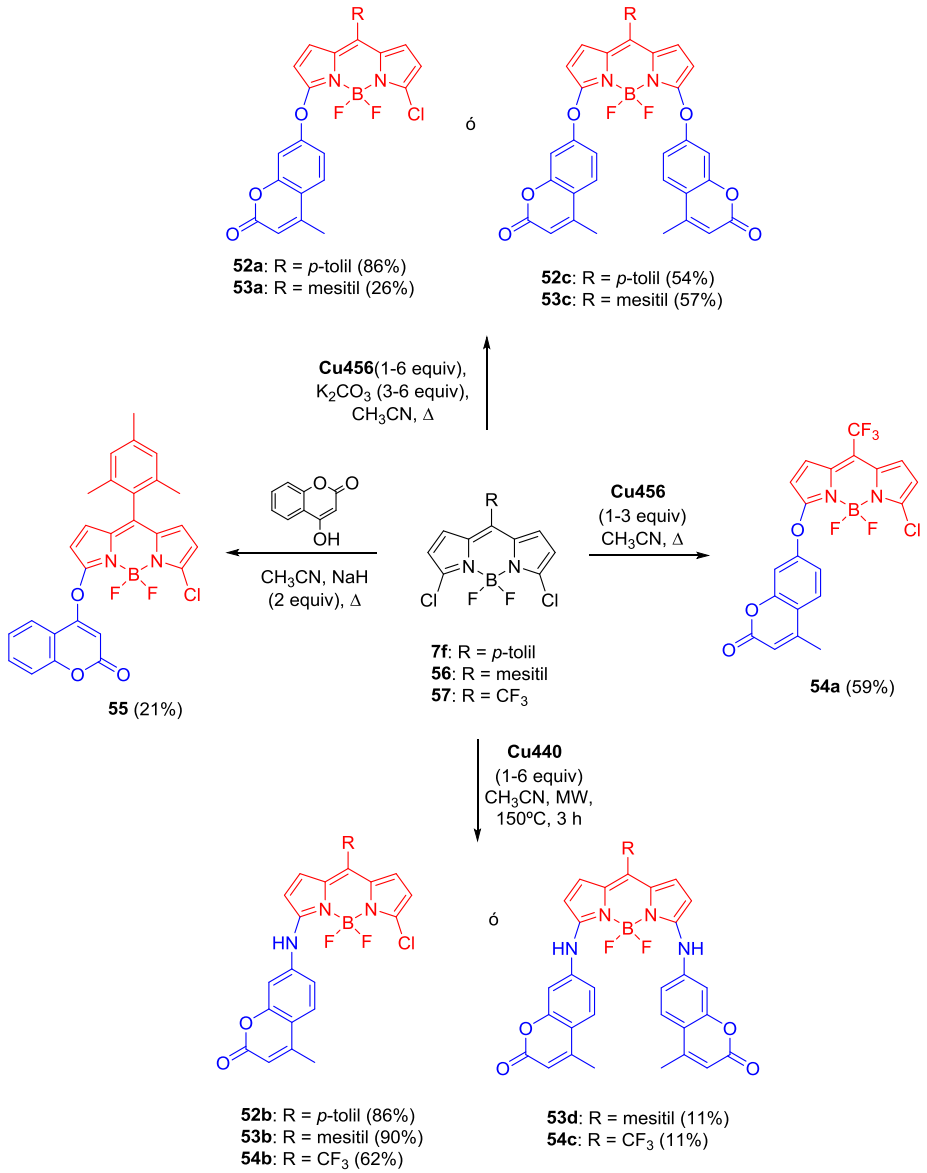


**Esquema 41**

### 4.4.3. Propiedades fotofísicas

Las propiedades fotofisicas de los nuevos sistemas dependen del esqueleto de BODIPY, del carácter electrónico del espaciador, y del número y posición de la cumarina unida al mismo. Por claridad, estas propiedades se van a describir para cada uno de los BODIPYs seleccionados.

Así, con respecto al cassette **51**, sus espectros de absorción y emisión resultan ser la suma de los espectros de ambos cromóforos, **PM567** y **Cu456** (Figura 72), ya que no hay acoplamiento electrónico entre los mismos, porque el átomo de boro no participa en la deslocalización del sistema π.

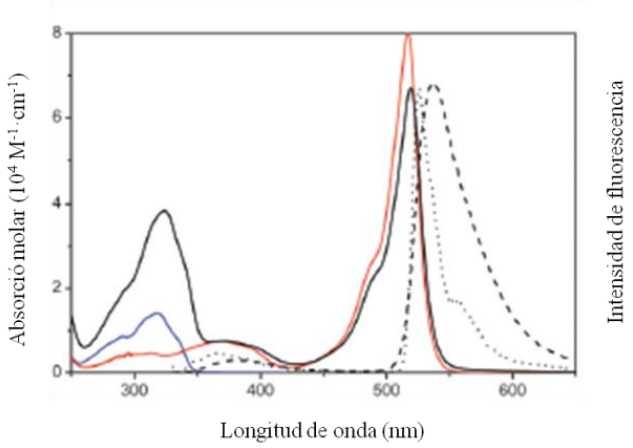


**Figura 72**. Espectros de absorción (línea sólida) de **51** (línea negra), **PM567** (línea roja), **Cu456** (línea azul) y de fluorescencia a temperatura ambiente (línea punteada) y a 77 k (línea rayada) de **51**.

En este caso, el mecanismo de transferencia es tipo FRET y la eficiencia del mismo es prácticamente del 100%, ya que no se registra emisión desde el fragmento cumarina, por lo que las propiedades fotofísicas del compuesto **51** bajo irradiación UV son muy similares a las del BODIPY de partida (Tabla 28).

Las propiedades fotofísicas de los BODIPYs **7f** y **56** están determinadas por el giro libre del anillo en la posición *meso* que induce importantes procesos de desactivación no radiante. Este proceso es mayor en el BODIPY **7f** (con un grupo *p*-metilfenilo) que en su

homólogo **56** (con un grupo mesitilo), por lo que sus derivados presentarán menores rendimientos cuánticos de fluorescencia que los cassettes derivados del BODIPY **56** (Tabla 29).

**Tabla 28**. Propiedades fotofísicas de **Cu456**, **PM567** y **51** en AcOEt.

| Compuesto | $\lambda_{abs}$ (nm) | $\varepsilon_{max}$ ($10^4$ $M^{-1}\cdot cm^{-1}$) | $\lambda_{fl}$ (nm) | $\phi$ |
|---|---|---|---|---|
| **Cu456**[a] | 323.0 | 1.4 | 380.0 | 0.28 |
| **PM567** | 516.5 | 8.0 | 531.5 | 0.84 |
| **51** | 519.0 | 6.7 | 537.0 | 0.82 |
| | 323.5 | 3.9 | | |

[a]: medido en EtOH

La introducción de una 7-hidroxi (**52a** y **53a**) o 7-aminocumarina (**52b** y **53b**) en la posiciones 5 del BODIPY provoca un leve desplazamiento batocrómico de sus bandas espectrales, siendo mayor en los cassettes formados por 7-aminocumarinas. Además, en estos últimos cassettes, **52b** y **53b**, se produce una drástica disminución del rendimiento cuántico de fluorescencia debido a que existe una fuerte interacción electrónica entre los cromóforos, inducida por la naturaleza electrodonadora del nitrógeno, es decir, el sistema π se encuentra deslocalizado por toda la molécula Por otro lado, la presencia en la misma molécula de un átomo de cloro induce un eficaz proceso intramolecular de transferencia de carga ("*push-pull*") que reduce significativamente la eficiencia de emisión. Este efecto se reduce en los cassettes basados en 7-hidroxicumarina, **52a** y **53a**, ya que la mayor electronegatividad del átomo de oxígeno hace que la densidad de carga se localice principalmente sobre el BODIPY. En la figura 73 se muestran los HOMO de las 7-hidroxicumarina **53a** y de la 7-aminocumarina **53b**.

**Tabla 29**. Propiedades fotofísicas de nuevos híbridos **BODIPY-cumarina** en AcOEt.

| Compuesto | $\lambda_{abs}$ (nm) | $\varepsilon_{max}$ ($10^4$ $M^{-1}\cdot cm^{-1}$) | $\lambda_{fl}$ (nm) | $\phi$ |
|---|---|---|---|---|
| **Cu456** | 323.0 | 1.4 | 380.0 | 0.28 |
| **Cu440** | 340.0 | 2.0 | 400.0 | 0.82 |
| **7f** | 509.5 | 10.3 | 522.0 | 0.25 |
| **52a** | 510.0 | 4.6 | 525.0 | 0.16 |
| **52b** | 524.0 | 4.5 | 577.0 | 0.04 |
| **52c** | 517.5 | 4.2 | 532.0 | 0.36 |
| **56** | 511.5 | 10.7 | 521.5 | 0.94 |
| **53a** | 510.5 | 8.0 | 522.5 | 0.95 |
| **53b** | 519.5 | 9.6 | 569.0 | 0.07 |
| **53c** | 519.5 | 7.5 | 530.0 | 0.90 |
| **53d** | 607.0 | 13.0 | 623.5 | 0.70 |
| **55** | 510.5 | 7.5 | 521.5 | 0.93 |

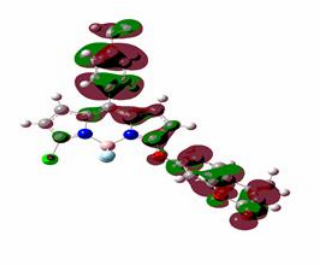

**53a**

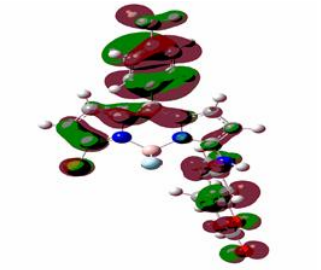

**53b**

**Figura 73**. Orbitales HOMO de **53a-b**

La introducción de una segunda molécula de 7-hidroxicumarina (**52c** y **53c**) aumenta el rendimiento cuántico de fluorescencia, tal y como ya se ha explicado anteriormente en otros capítulos de la Memoria, donde se describe el efecto que la presencia de grupos electronegativos en las posiciones 3 y 5 de 8-arilBODIPYs tiene sobre sus propiedades fotofísicas (ver Pag. 45).

La sustitución del átomo de cloro en el compuesto **53b** por una segunda molécula de 7-aminocumarina, compuesto **53d**, conduce a una disminución de los mencionados procesos de transferencia intramolecular de carga, lo que conlleva a un incremento significativo de los rendimientos de fluorescencia y a un fuerte desplazamiento batocrómico de las bandas espectrales. En estos sistemas derivados de los BODIPYs **6f** y **56** el mecanismo de transferencia de energía no puede ser descrito como FRET debido al fuerte acoplamiento electrónico entre los cromóforos. De hecho, de forma rigurosa no pueden denominarse como cassettes aunque su irradiación UV conduce a la emisión visible del BODIPY. En realidad, en estos sistemas el mecanismo de transferencia de energía es un proceso coherente, en el cual la energía de excitación oscila entre donador y aceptor, y resulta un proceso extremadamente rápido y eficaz. Señalar que el compuestos **55** presenta un comportamiento análogo al de **53a**, por lo tanto la posición de unión de la cumarina no es un factor determinante en las propiedades fotofísicas.

En cuanto al compuesto **57**, sus propiedades fotofisicas están determinadas por la presencia del grupo electroatractor como es el trifluorometilo en posición *meso*, que induce un efecto "*push-pull*", acentuado por la sustitución en posiciones 3 y/o 5 de 7-hidroxi o 7-aminocumarinas, compuestos **54a-c** (Tabla 30). De hecho, el derivado con una 7-aminocumarina (**54b**) no es fluorescente y el resto siguen el comportamiento ya descrito anteriormente para los otros cassettes.

**Tabla 30. Propiedades fotofísicas de 54a-c y 57 en AcOEt.**

| BODIPY | $\lambda_{abs}$ (nm) | $\varepsilon_{max}$ ($10^4$ $M^{-1}\cdot cm^{-1}$) | $\lambda_{fl}$ (nm) | $\phi$ |
|---|---|---|---|---|
| **57** | 545.0 | 6.8 | 552.0 | 0.82 |
| **54a** | 537.0 | 6.4 | 555.0 | 0.41 |
| **54b** | 520.5 | 3.7 | - | 0 |
| **54c** | 642.5 | 5.3 | 665.0 | 0.73 |

### 4.4.4. Propiedades láser

Las propiedades láser de los nuevos cassettes, determinadas en disolución de AcOEt y bajo irradiación a 355 nm (Tabla 31), concuerdan con las propiedades fotofísicas de los mismos: mayores rendimientos de fluorescencia determinan mayores eficiencias láser, longitudes de onda de fluorescencia más largas determinan emisión láser "mas en el rojo" y menores constantes de desactivación no radiativas determinan mayores fotoestabilidades.

**Tabla 31. Propiedades láser de los compuestos PM567, 7f, 56 y 57 y su cassettes derivados en AcOEt.**

| | Ef (%) | $\lambda_{láser}$ (nm) | I (%) |
|---|---|---|---|
| **PM567** | 20 | 575 | 0 |
| **51** | 46 | 565 | 25 |
| **7f** | - | - | - |
| **52a** | 21 | 552 | 20 |
| **52b** | 14 | 610 | 0 |
| **52c** | 35 | 562 | 35 |
| **56** | 22 | 590 | 0 |
| **53a** | 46 | 555 | 40 |
| **53b** | 8 | 615 | 20 |
| **53c** | 51 | 575 | 55 |
| **53d** | 25 | 645 | 30 |
| **55** | 45 | 540 | 55 |
| **57** | - | - | - |
| **54a** | 30 | 615 | 35 |
| **54b** | - | - | - |
| **54c** | 40 | 680 | 55 |

Con excepción del compuesto **54b**, que no presenta fluorescencia, los nuevos cassettes BODIPY-cumarina presentan una eficiencia y fotoestabilidad láser muy superior a la de sus BODIPYs precursores bajo las mismas condiciones de bombeo. Especial interés muestran los compuestos **52a-b** y **53b**, que a pesar de presentar rendimientos de fluorescencia bajos, entre el 4 y 16%, presentan eficiencias láser de hasta el 21%. Este

comportamiento está relacionado con la arquitectura de estos cassettes que induce: a) altos desplazamientos de Stokes (superiores a 1700 $cm^{-1}$), lo que minimiza los procesos de re-absorción; b) tiempos de vida de fluorescencia muy cortos (inferiores a 0.2 ns), lo que conduce a constantes radiativas muy similares a las de otros BODIPY a pesar de tener rendimientos de fluorescencia muy inferiores y c) altos momentos dipolares, que permiten una correcta alineación de los mismos con la polarización del haz de excitación, incrementando la eficiencia fotónica del sistema.

### 4.4.5. Conclusiones

Mediante un sencillo procedimiento de síntesis directo, barato y eficaz, se ha obtenido una serie de cassettes basados en BODIPYs y cumarinas, consiguiendo una elevada absorción en la región UV del espectro y una emisión láser altamente eficiente y estable en la región 520-700 nm del espectro visible. Además, estos nuevos colorantes, mediante un doblado de la frecuencia, permitirían obtener radiación láser en la región de UV, aproximadamente entre 260 y 350 nm. Esta radiación es fundamental para un mejor estudio de los mecanismos de fotodegradación de ciertas moléculas biológicas, como los ácido nucleicos, bajo la radiación solar.

El sistema final, cuyas propiedades ópticas quedan moduladas por la posición, número, estructura y tipo de unión entre ambos cromóforos, mejora las propiedades fotofísicas y láser de cada uno de los cromóforos en las mismas condiciones de trabajo.

## 4.5. CASSETTES BASADOS EN PERILENDIIMIDAS (Trabajo pendiente de publicación)

### 4.5.1. Introducción

Las perilen-3,4,9,10-tetracarboxidiimidas (comúnmente llamadas perilendiimidas y abreviadamente PDIs) han recibido una considerable atención desde el punto de vista tanto industrial como de la investigación.[31] Desde el descubrimiento de estos compuestos en el año 1913 por Kardos,[32] se han utilizado como pigmentos industriales durante muchos años, aunque más recientemente los derivados de PDI han encontrado nuevas aplicaciones en el campo de la optoelectrónica.

En la figura 74 se muestra la estructura del perilen-3,4,9,10-tetracarboxidianhídrido (PTCDA), considerado el precursor de esta clase de compuestos y de un colorante genérico PDI, indicando la numeración y nomenclatura de sus posiciones.

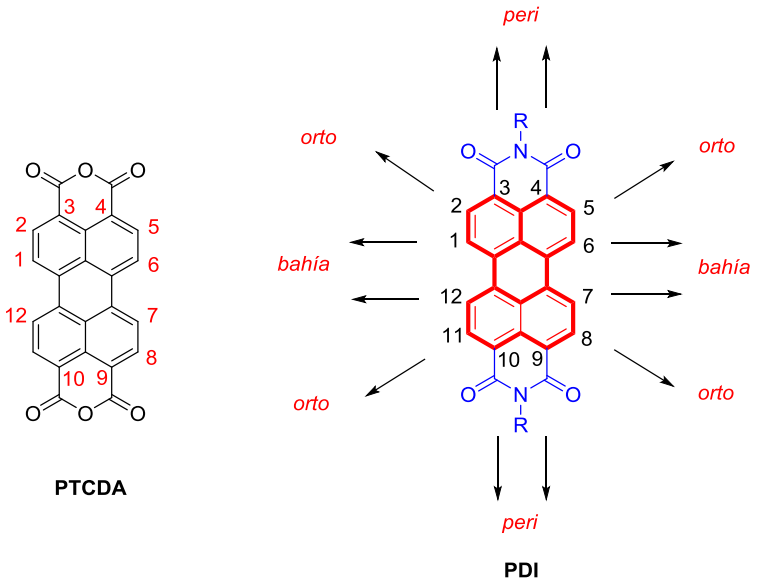


**Figura 74**. Estructura y numeración de **PTCDA** y **PDI**.

### *4.5.1.1. Funcionalización del núcleo de perileno*

La sustitución del esqueleto de **PDI** tiene una significativa influencia sobre sus propiedades químicas y físicas, lo que permite una fácil modulación de las mismas en función de las diversas aplicaciones. Debido a la simetría del núcleo de perileno, se pueden distinguir tres posiciones con diferente reactividad:

- Sustitución en el nitrógeno imídico de las posiciones *peri*
- Sustitución en las posiciones *bahía*
- Sustitución en las posiciones *orto*

La introducción de diferentes grupos, tales como alquil, bencil o fenil en el nitrógeno imídico de la posición *peri*, permite obtener diferentes derivados con una absorción y emisión indistinguibles, debido a la presencia de nodos de energía en los orbitales HOMO y LUMO en dicha posición, lo que minimiza la interacción entre el grupo de la posición imida con el núcleo de perileno.[33] Por lo tanto, una adecuada funcionalización en esta posición permite modular la solubilidad o los procesos de agregación de los derivados de perileno sin que se modifiquen sus propiedades fotofísicas (Figura 75).

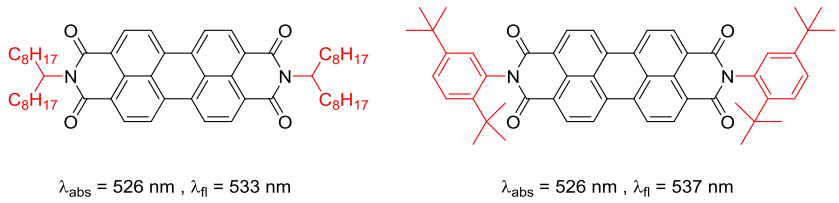


**Figura 75**. Estructuras de PDIs.

Por otro lado, las posiciones *bahía* se caracterizan por poseer una alta densidad de carga negativa,[34] por lo que son susceptibles de sufrir reacciones de sustitución electrófila tales como cloración o bromación. Así, en la bibliografía existen ejemplos de derivados de perilendiimidas en donde las posiciones 1, 6, 7 y/ó 12 están ocupadas por átomos de cloro o bromo, en función de las condiciones de reacción.[35] Además, estos cloro- o

bromoderivados son útiles precursores sintéticos, ya que pueden reaccionar con diferentes nucleófilos, como aminas,[36] alcoholes[37], cianuros,[38] o intercambiarse por átomos de flúor,[39] además de sufrir diferentes reacciones de acoplamiento C-C, tales como Suzuki-Miyaura [35d, 40] o Sonogashira[41] (Esquema 42).

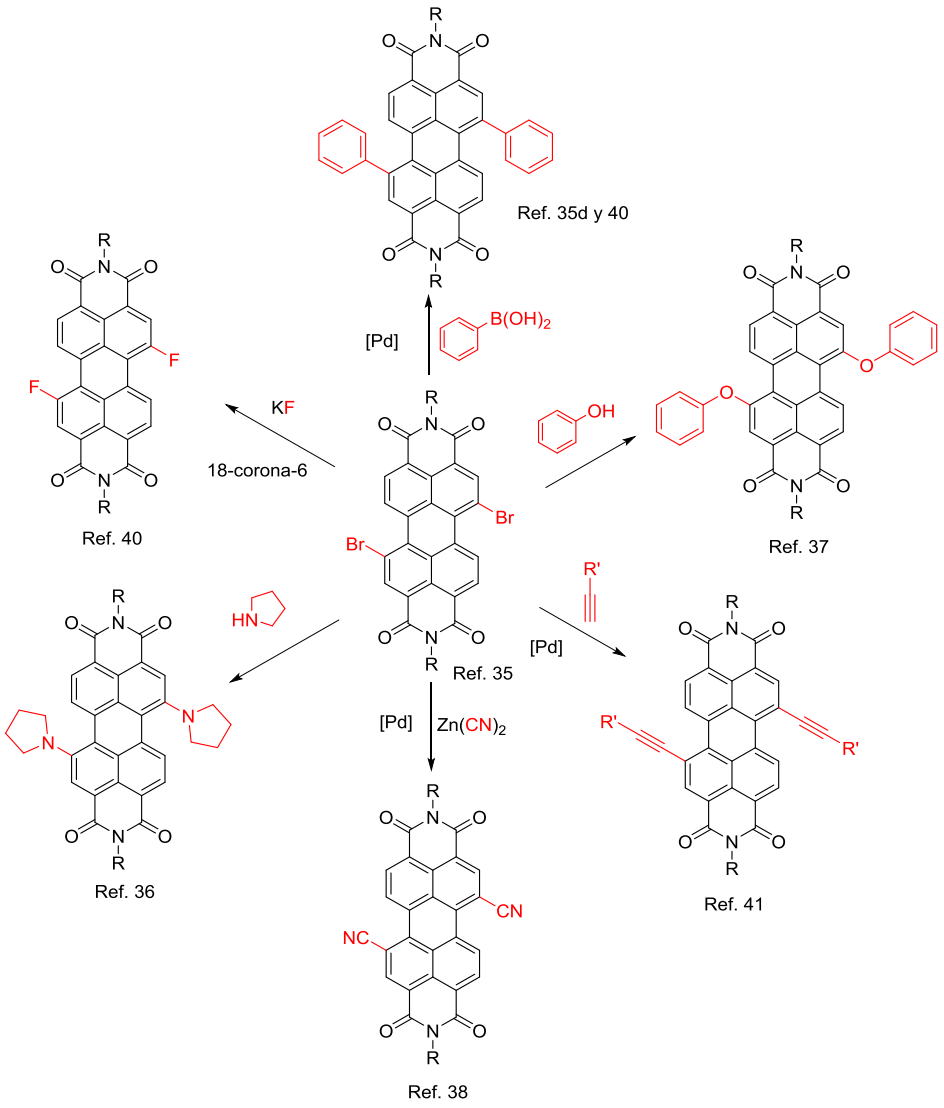


**Esquema 42**

En cuanto a la posiciones *orto*, éstas pueden funcionalizarse mediante una activación de C-H catalizada por rutenio, siendo este el principal método para la obtención de aril- o

alquilderivados.[42] La introducción de grupos alquilo o arilo en estas posiciones produce una gran distorsión de la planaridad, aumentando de forma significativa el rendimiento cuántico de fluorescencia en estado sólido con respecto a sus homólogos no sustituidos (Figura 76).

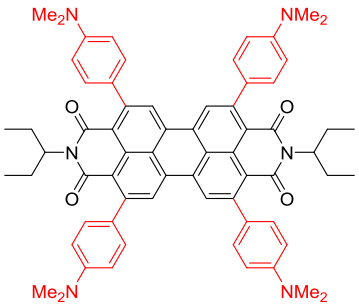


**Figura 76**. Estructura de un PDI con posiciones *orto* sustituidas.

#### *4.5.1.2. Aplicaciones de los derivados de las perilendiimidas*

Desde su descubrimiento a principios del siglo XX, estos compuestos se han usado como pigmentos en diferentes sectores de la industria. Sin embargo, gracias a su gran versatilidad sintética y a sus interesantes propiedades fotofísicas, tales como rendimientos cuánticos de fluorescencia cercanos a la unidad, alta estabilidad y fuerte carácter electroatractor, hace que sean utilizados actualmente en la obtención de dispositivos electrónicos orgánicos,[43] como sensibilizadores en células solares,[44] en la fabricación de OLEDs[45] o como colorantes láser[46] entre otras aplicaciones.

### 4.5.2. Perilendiimidas como sistemas antena

Una de las aplicaciones más atractivas de los compuestos derivados de las perilendiimidas es su empleo en el desarrollo de sistemas antena con una eficiente transferencia de energía, por lo que en los últimos años varios grupos de investigación están trabajando activamente en este campo.[2] Así, Akkaya y col.[9, 47] han sintetizado a través de una reacción “click” varios sistemas antena con una estructura dendrimérica basados en perilendiimidas a las que se han unido 4 ó 8 unidades de BODIPYs,

obteniéndose de esta manera un sistema con hasta un 99% de eficiencia en la transferencia de energía (Figura 77).

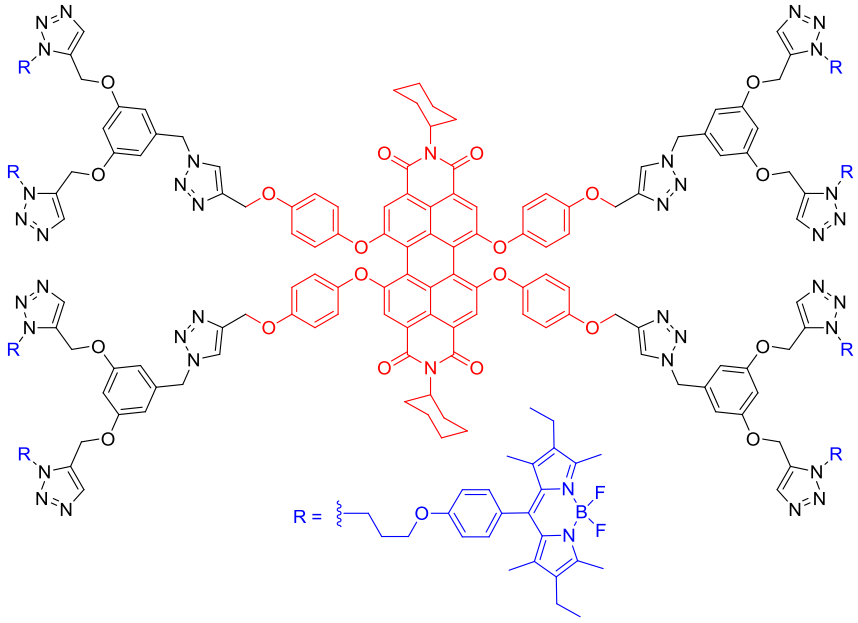

**Figura 77**. Estructura de una antena BODIPY-perilendiimida.

Los autores indican que aunque el cassette con 8 unidades de BODIPY presenta una mayor capacidad fluorescente, su eficiencia es algo menor (95% frente 99% del sistema con 4 unidades de BODIPY). Esto es debido a que un mayor número de unidades de BODIPY genera un mayor impedimento estérico, lo que conlleva una mayor distancia con el núcleo de perilendiimida y una menor eficiencia en el proceso EET.

También existen ejemplos de complejos antena formados por cumarinas y perilendiimidas, en las que las moléculas de cumarina se unen a través de la posición imídica de núcleo de perileno (Figura 78),[48] consiguiéndose cassettes que tras excitación en el UV logran emitir en la región roja del espectro con una eficiente transferencia de energía.

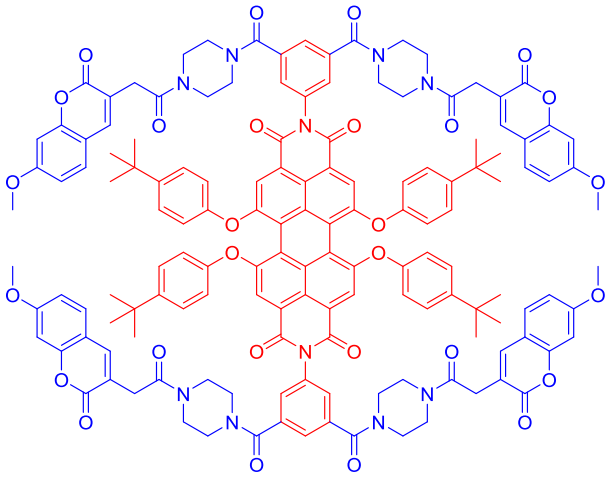

**Figura 78**. Estructura de una antena cumarina-perilendiimida.

Sin embargo, no existen ejemplos de sistemas antenas basados en PDIs en los que se haya estudiado su comportamiento como colorantes láser, hecho que pone de manifiesto la necesidad de profundizar en dicha área. Por ello, se planteó el diseño, síntesis y estudio láser de cassettes formados por la combinación de un núcleo de perilendiimida y cromóforos comerciales, como las cumarinas y los BODIPYs. En la Figura 79 se recogen las estructuras diseñadas para abordar el objetivo planteado.

En el sistema **58** la unión entre los cromóforos se produce de forma directa, ya que el átomo de nitrógeno de la 7-aminocumarina (**Cu440**) se encuentra formando parte de uno de los grupos carboxiimida de perileno comercial (**PerRed**). En los complejos **59a-c**, unión se produce a través del grupo fenilo de la posición *peri* del núcleo de perileno. En este caso se varía la posición de unión de la cumarina, ya que puede unirse a través de la posición 7 (**59a-b**) o a través de la posición 8 (**59c**), lo que nos permitiría determinar qué tipo de unión es la más eficiente en el proceso de transferencia de enrgía. En el caso de los compuestos **60a-b,** el fragmento donador es un BODIPY con un grupo amino en la posición *meso* unido al núcleo de PDI a través de un cadena de dos carbonos. Finalmente, en el sistema **61**, se combinan tres cromóforos (perileno, BODIPY y cumarina) con absorción en diferentes zonas del espectro visible, lo que hace que este sistema puede ser

excitado a tres longitudes de onda diferentes. Además destacar que la unión seleccionada entre los fragmentos hace que se mantenga la identidad de cada cromóforo.

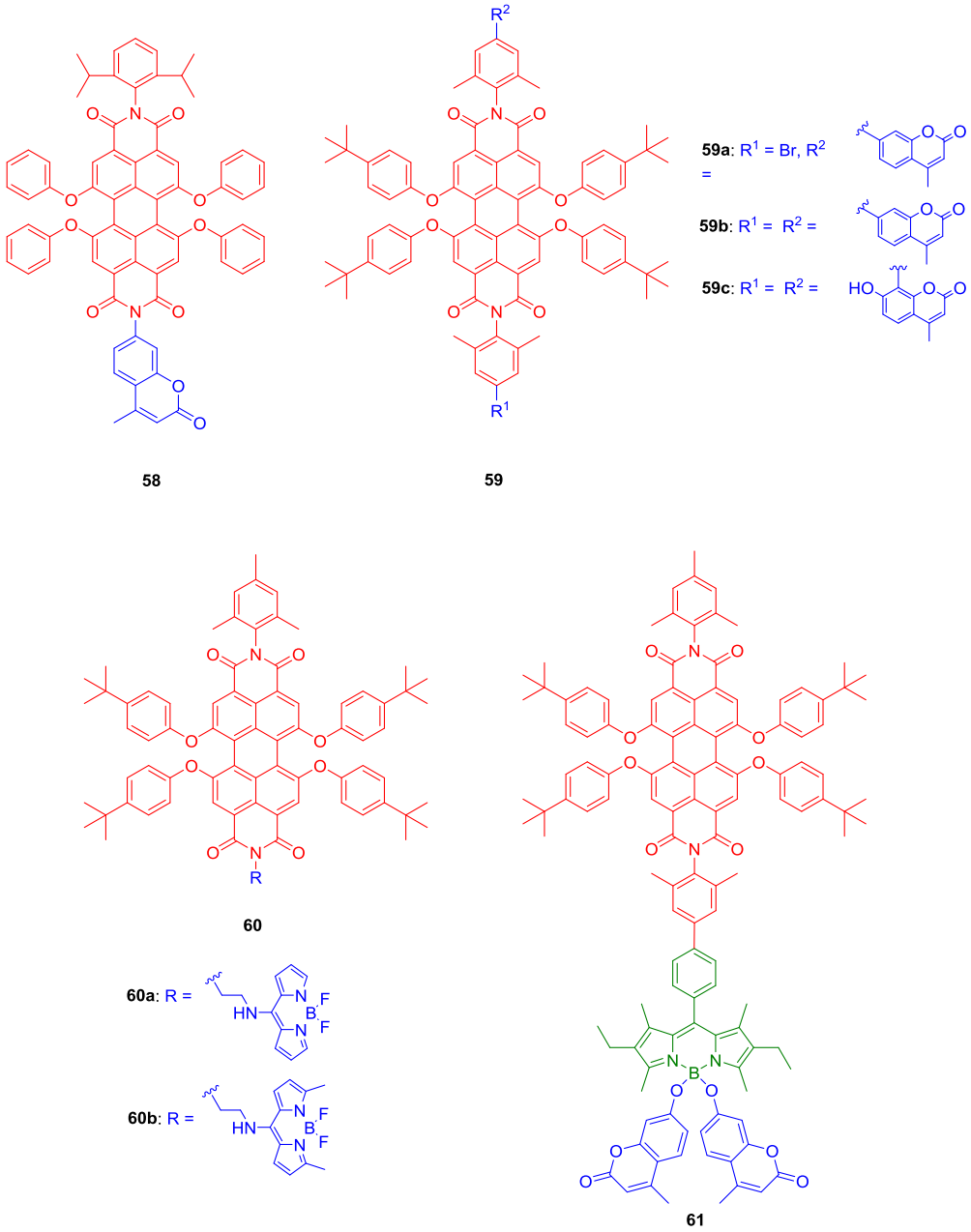


**Figura 79**. Estructuras de las antenas **58-61**.

### 4.5.3. Síntesis

Para la obtención de la antena **58** se emplearon los colorantes comerciales **PerRed** y la 7-aminocumarina **Cu440**. Un primer paso implica la ruptura de uno de los grupos imida del PDI mediante reacción con exceso de 15 equiv de KOH, siguiendo el procedimiento habitual para la obtención de este tipo de derivados.[49] Así, se obtuvo la perilen-monoimida **62**[49] con un 36% de rendimiento (Esquema 44). Posteriormente, la reacción de **62** con la cumarina **Cu440** en ácido propiónico, condujo a la obtención del sistema **58** aunque con bajo rendimiento, debido probablemente a la baja nucleofilia del grupo amino de la cumarina **Cu440** ya que sus electrones están deslocalizados por el efecto "*push-pull*" (Esquema 43).

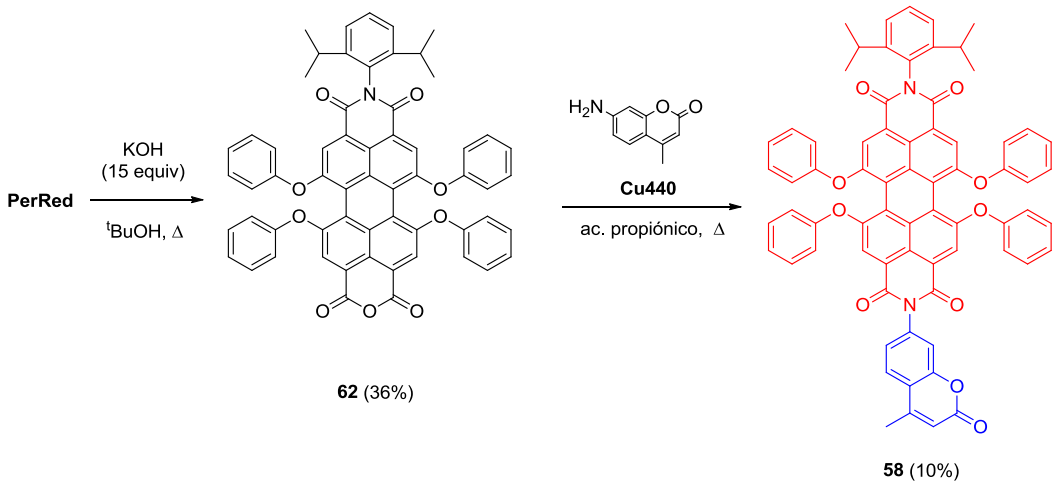


**Esquema 43**

Por otro lado, para la síntesis de las antenas **59a-c** se siguió la secuencia de reacciones que se muestra en el esquema 44. Así, la reacción del **PTCDA** con ácido clorosulfónico en presencia de cantidades catalíticas de yodo, condujo a la obtención del derivado tetraclorado **63**[50] que se usó en el siguiente paso de reacción sin purificación. Su posterior reacción con la 4-bromo-2,6-dimetilanilina en ácido propiónico a reflujo permitió aislar la diimida **64**[51] con un 85% de rendimiento. A continuación, la perilendiimida **65** se obtuvo, con un 36%, por el tratamiento de **64** con 4-*terc*butilfenol en presencia de $K_2CO_3$. Mencionar que fue necesario emplear 10 equiv de fenol para evitar la formación de los

derivados mono-, di- o tri-sustituidos. Posteriormente, la perilendiimida **66** se obtuvo mediante la reacción de Suzuki-Miyahura sobre **65**, siendo también necesario el uso de un gran exceso de reactivo para obtener de forma exclusiva el compuesto di-sustituido.

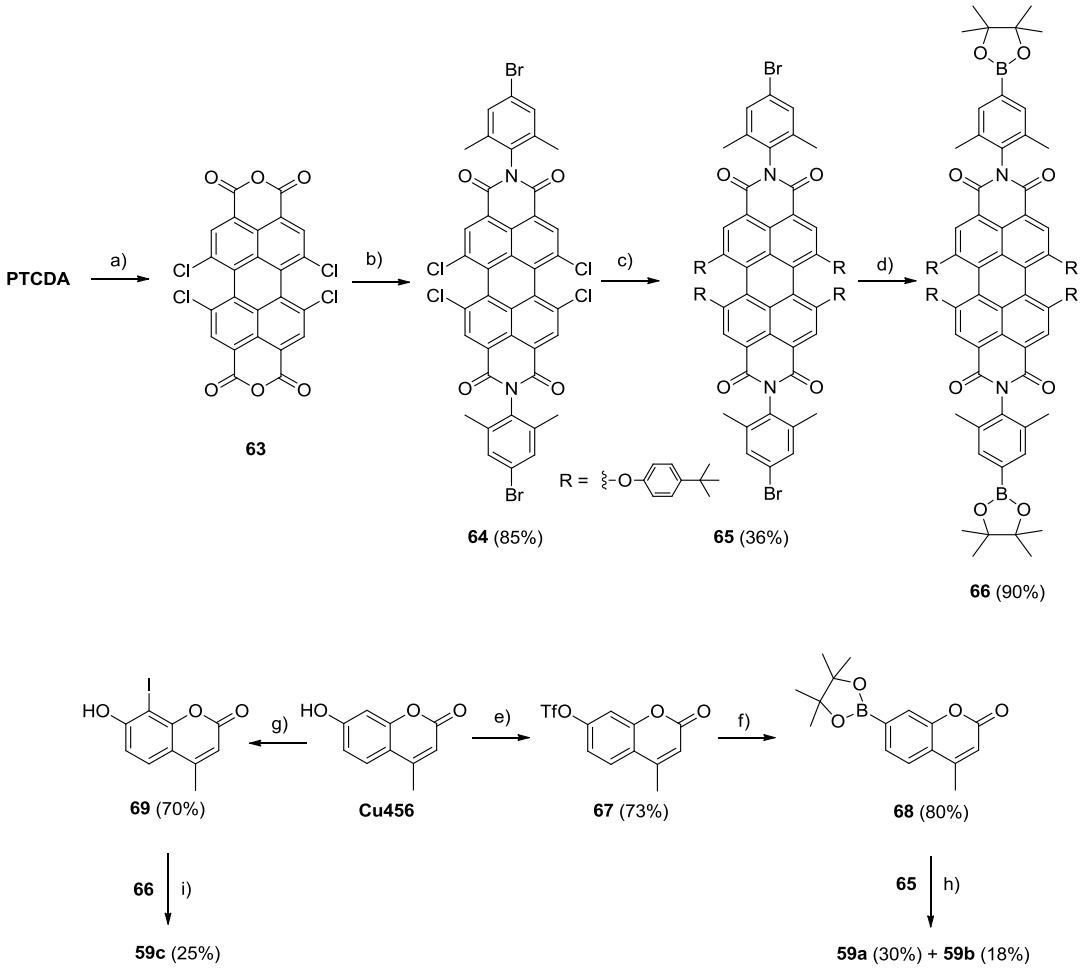


**Esquema 44**. Condiciones de reacción: a) $ClSO_3H$, $I_2$, 70ºC, 24 h; b) 4-bromo-2,6-dimetilanilina, ac. propiónico, 160º C, 16 h; c) 4-*terc*butilfenol (10 equiv), $K_2CO_3$ (5 equiv), DMF, 90ºC, 5 h; d) bispinacolato de boro, AcOK, Pd(dppf)$Cl_2$, DME, Δ; e) $Tf_2O$, $Et_3N$, DCM, t.a.; f) bispinacolato de boro, AcOK, Pd(dppf)$Cl_2$, DME, Δ; g) $I_2$/KI, $NH_4 \cdot H_2O$; h) **68** (8 equiv), $K_2CO_3$ (4 equiv), $Pd(PPh_3)_4$, tolueno/EtOH/$H_2O$ (4:4:2 v/v/v), Δ; i) **69** (8 equiv), $K_2CO_3$ (4 equiv), $Pd(PPh_3)_4$, tolueno/EtOH/$H_2O$ (4:4:2 v/v/v), Δ.

Paralelamente, se abordó la obtención de las cumarinas **68** y **69** a partir de la cumarina comercial **Cu456**. Así, la reacción de esta cumarina con anhídrido tríflico en presencia de $Et_3N$ condujo la formación de la cumarina **67**,[52] que por tratamiento con bispinacolato de boro en la condiciones de acoplamiento Suzuki-Miyahura dio lugar a la cumarina **68** con un buen rendimiento. La obtención del derivado de cumarina **69**[53] se realizó según el procedimiento descrito en la bibliografía a través de una reacción de yodación de la cumarina comercial **Cu456** empleando el sistema $I_2$/KI en $NH_4 \cdot H_2O$

Una vez sintetizadas las PDIs y las cumarinas adecuadamente funcionalizadas, se llevaron a cabo las correspondientes reacciones de acoplamiento entre ellas. Así, la reacción de Suzuki entre los fragmentos **65** y **68** dio lugar a la mezcla de las antenas **59a-b**, separables por cromatografía, con rendimientos del 30 y 18%, respectivamente. Finalmente, la reacción entre **66** y **69**, en las mismas condiciones de reacción empleadas para la obtención de **59a-b**, condujo a la antena **59c** con un 25% de rendimiento, observándose trazas del producto de monosustitución.

En cuanto a la síntesis de los sistemas **60a-b** fue necesaria seguir la ruta propuesta en el esquema 45. Por reacción del dianhidrido **63** con la 2,4,6-trimetilanilina a reflujo de ácido propiónico dio como resultado la obtención de la perilendiimida simétrica **70** con un 80% de rendimiento. Posteriormente, la reacción de sustitución nucleófila de los átomos de cloro de las posiciones *bahía* por 4-*terc*butilfenol en presencia de $K_2CO_3$, condujo a la formación del compuesto **71** con buen rendimiento. La posterior hidrólisis de un grupo imida de **71** por tratamiento con exceso de KOH en $^t$BuOH, condujo a la obtención del monoanhídrido **72** (77%). Sin embargo, la reacción de **72** con 1,2-etilendiamina en las condiciones habituales para este tipo de condensaciones, es decir, ácido propiónico a 160 ºC, no condujo a la obtención del derivado esperado **73**, sino que se observó la formación de un nuevo compuesto al que, en base a sus datos espectroscópicos de RMN-$^1$H y $^{13}$C, se le asignó la estructura **74** (Esquema 45). La formación de este compuesto puede justificarse por la reacción de ciclación favorecida por la alta temperatura utilizada en el proceso y la estabilidad del ciclo que se forma. Esta reactividad está de acuerdo con estudios similares recogidos en la bibliografía.[54]

Para evitar la formación de este nuevo compuesto se modificaron las condiciones de reacción, empleando tolueno como disolvente a 90 ºC, lo que permitió obtener el compuesto deseado **73** con un 63% de rendimiento.

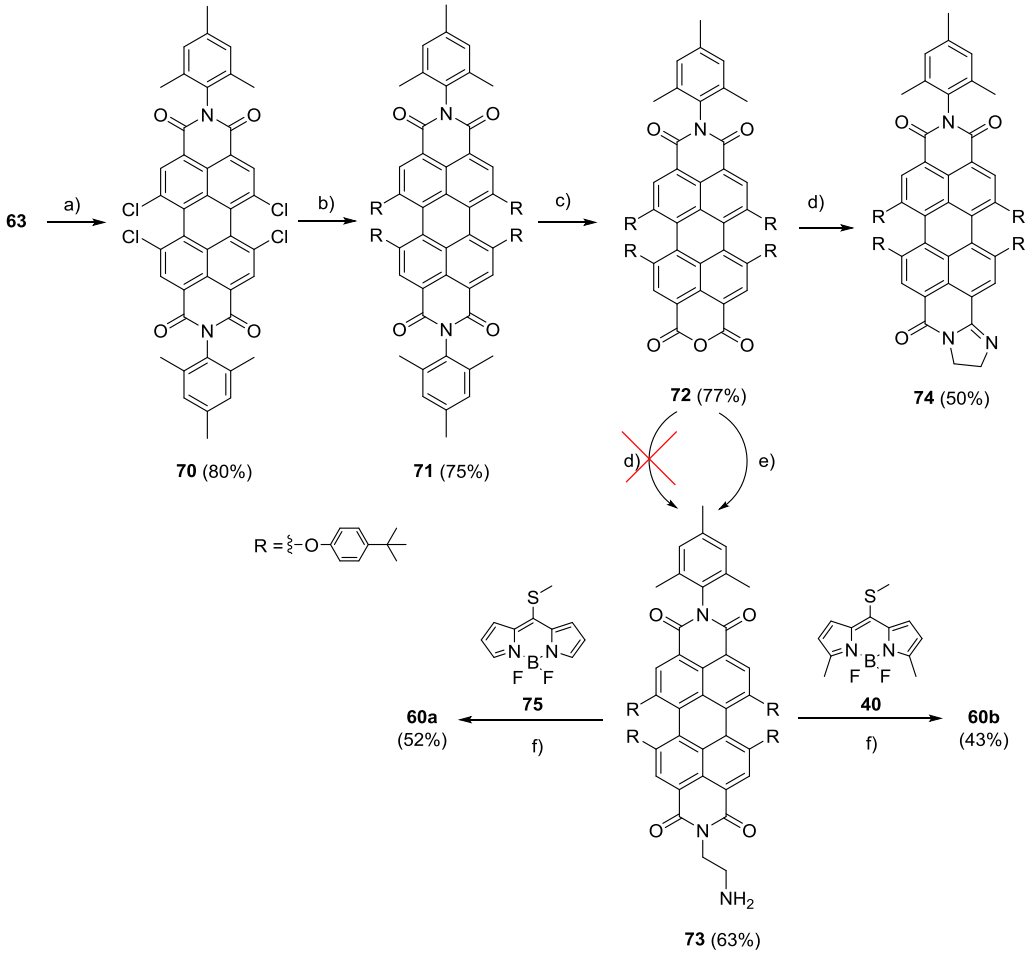


**Esquema 45**. Condiciones de reacción: a) 2,4,6-trimetilanilina (10 equiv), ac. propiónico, 160 ºC, 16 h; b) 4-*terc*butilfenol (10 equiv), $K_2CO_3$ (5 equiv), DMF, 90 ºC, 4 h; c) KOH (3 equiv), $^tBuOH$, Δ; d) 1,2-etilendiamina (5 equiv), ac. propiónico, 160 ºC, 16 h; e) 1,2-etilendiamina (5 equiv), tolueno, 90 ºC, 1 h; f) $CH_3CN$, t.a. 1 h.

Por último, a través de una reacción de sustitución nucleófila del grupo tiometilo en la posición *meso* de los BODIPYs **40**[15] y **75**[55] (BODIPYs comercializados por Cuántico de

México) se obtuvieron los cassettes **60a-b** con un 52 y 43% de rendimiento, respectivamente.

Para la obtención de la triada **61** se abordó la ruta sintética se muestra en el esquema 46. El primer paso fue la obtención de la perilendiimia asimétrica **76** mediante la reacción de **72** con 5 equiv de 4-bromo-2,6-dimetilanilina en ácido propiónico. Posteriormente, mediante una reacción de Suzuki-Miyaura, en idénticas condiciones a las empleadas anteriormente, se obtuvo el compuesto **77** con un excelente rendimiento.

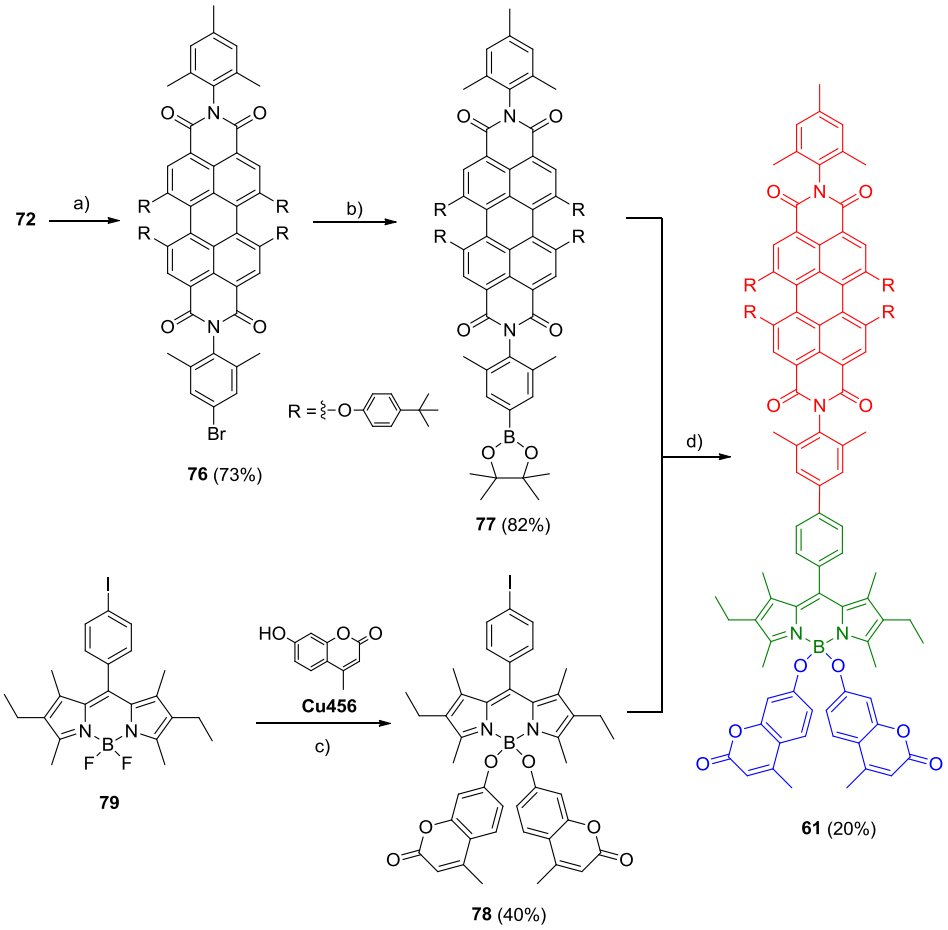


**Esquema 46**. Condiciones de reacción: a) 4-bromo-2,6-dimetilanilina, ac. propiónico, 160 ºC, 16 h; b) bispinacolato de boro, AcOK, $Pd(dppf)Cl_2$, DME, Δ; c) $AlCl_3$ (2 equiv), **Cu456** (5 equiv), DCE, Δ; d) **77** (3 equiv), $K_2CO_3$ (2 equiv), $Pd(PPh_3)_4$, tolueno/EtOH/$H_2O$ (4:4:2 v/v/v), Δ.

Por otro lado, la síntesis de la diada BODIPY-cumarina **78** se llevó a cabo mediante la metodología desarrollada para la obtención de *O*-BODIPYs con grupos ariloxi unidos al átomo de boro (ver Pag. 91). Así, la reacción del BODIPY **79**[56] y la cumarina comercial **Cu456** en presencia de $AlCl_3$ condujo a la obtención de **78** con un 40% de rendimiento (Esquema 46). Destacar que el BODIPY **79** fue necesario sintetizarlo previamente por reacción del cloruro de 4-yodobenzoilo y 3-etil-2,4-dimetilpirrol a través del procedimiento descrito.[56] Finalmente, la reacción de acoplamiento de Suzuki entre los fragmentos **77** y **78** dio como resultado la obtención de la antena **61** con un 20% de rendimiento (Esquema 46).

### 4.5.4. Propiedades fotofísicas y comportamiento láser

Las propiedades fotofísicas de los sistemas **58**-**61** se han registrado en disolución de AcOEt a una concentración de $10^{-5}$ M. En la tabla 32 se recogen los datos de absorción y fluorescencia de los mismos, comparados con los del perileno rojo comercial (**PerRed**).

En cuanto al comportamiento láser, basándonos en los resultados previos obtenidos por nuestro grupo de investigación en la construcción de sistemas multicromofóricos con absorción pancromática, podemos postular que la incorporación de restos de cumarina a la estructura de diferentes perilendiimas permitiría excitar los sistemas **58**-**60** a dos longitudes de onda, una correspondiente a la cumarina y la otra al **PDI**. Además, la incorporación de un tercer cromóforo, como el BODIPY en la antena **61**, abre la posibilidad de que este compuesto presente absorción en toda la región del espectro visible.

Para demostrar esta teoría se realizó una primera evaluación de sus propiedades láser bajo bombeo a 355 nm. En la tabla 32 se presentan los resultados más relevantes atendiendo a su eficiencia láser y longitud de onda de emisión.

Estos datos ponen una vez más de manifiesto que la acción láser es dependiente de la estructura y composición del cassette. Todos estos nuevos sistemas presentan absorción pancromática y emisión monocromática en la región roja del espectro, lo que demuestra la presencia de una eficiente transferencia de energía dentro del sistema. Además, algunos de

ellos, como los compuestos **59b** y **61**, presentan una eficiencia láser (32 y 27%, respectivamente) superior al colorante comercial perileno rojo (**PerRed)**, con emisión en la misma región espectral y cuya eficiencia no supera el 22% bajo bombeo a 532 nm.

**Tabla 32. Propiedades espectroscópicas y de emisión láser de los cassettes 58-61 en AcOEt bajo bombeo a 355 nm.**

| Compuesto | $\lambda_{abs}$ (nm) | $\lambda_{fl}$ (nm) | Ef. (%) | $\lambda_{láser}$ (nm) |
|---|---|---|---|---|
| **PerRed** | 568 | 597 | 23 | 624 |
| **58** | 428<br>578 | 598 | 13 | 626 |
| **59a** | 437<br>572 | 601 | 22 | 625 |
| **59b**[a] | 444<br>571 | 602 | 32 | 623 |
| **59c** | 441<br>569 | 599 | 10 | 624 |
| **60a** | 423<br>571 | 607 | 12 | 625 |
| **60b** | 402<br>573 | 598 | 14 | 627 |
| **61** | 445<br>523<br>569 | 607 | 27 | 628 |

[a] medido en DCM

### 4.5.5. Conclusiones

Mediante un diseño racional de las rutas sintéticas se obtuvieron una serie de nuevos cassettes basados en la combinación de perilendiimidas con BODIPY y/o cumarinas a través de diferentes tipos de unión. Todos estos nuevos sistemas pueden ser excitados a 355 nm, presentando alguno de ellos una eficiencia láser superior a la del colorante comercial perileno rojo que, además, no puede ser excitado a esa longitud de onda. Actualmente, se está evaluando la fotoestabilidad de los mismos así como la eficiencia del proceso de transferencia de energía entre los diferentes fragmentos.

## 4.5.6. Parte experimental

### *4.5.6.1. Métodos generales*

#### *4.5.6.1.a. Hidrólisis de perilendiimidas*

En matraz de dos bocas, provisto de agitación magnética, refrigerante de reflujo y tubo de $CaCl_2$, se añade la perilendiimida correspondiente (1 equiv) y KOH (3-15 equiv) en $^tBuOH$. La mezcla se reacción se agita a reflujo durante 1 h. Transcurrido este tiempo, se añade ácido acético, calentando la mezcla a reflujo durante 30 min. Paso este tiempo, se deja alcanzar la temperatura ambiente y se añade agua. El precipitado formado se filtra a vacío, lavándolo con varias porciones de agua. El crudo de reacción se purifica por cromatografía en columna con gel de sílice, empleando como eluyente una mezcla hexano/AcOEt, en las proporciones que se especifican en cada caso.

#### *4.5.6.1.b. Formación de perilenimidas a partir de anhidrido*

En matraz de dos bocas, provisto de agitación magnética, refrigerante de reflujo y tubo de $CaCl_2$, se añade el perilenanhidrido (1 equiv) y la correspondiente amina (5-10 equiv) en ácido propiónico o tolueno. La mezcla se reacción se agita a reflujo durante 5-16 h. Transcurrido este tiempo, se deja alcanzar la temperatura ambiente y se añade agua. El precipitado formado se filtra a vacío, lavándolo con varias porciones de agua. El crudo de reacción se purifica por cromatografía en columna con gel de sílice, empleando como eluyente una mezcla hexano/DCM, en las proporciones que se especifican en cada caso.

#### *4.5.6.1.c. Sustitución nucleófila aromática de 1,6,7,12-tetracloroperilendiimidas*

En matraz de dos bocas, provisto de agitación magnética, refrigerante de reflujo y tubo de $CaCl_2$, se añade la correspondiente 1,6,7,12-tetracloroperilendiimida (1 equiv), 4-*terc*butilfenol (10 equiv) y $K_2CO_3$ (5 equiv) en DMF. La mezcla se reacción se agita a reflujo durante 24 h. Transcurrido este tiempo, se deja alcanzar la temperatura ambiente y se añade una disolución acuosa de HCl al 50%. El precipitado formado se filtra a vacío,

lavándolo con varias porciones de agua. El crudo de reacción se purifica por cromatografía en columna con gel de sílice, empleando como eluyente una mezcla hexano/DCM, en las proporciones que se especifican en cada caso.

*4.5.6.1.d. Reacción de Suzuki-Miyaura*

En matraz de dos bocas, provisto de agitación magnética y refrigerante de reflujo, se introduce bajo atmósfera de argón, el derivado halogenado o el triflato (1 equiv), bispinacolato de boro (2-8 equiv), AcOK (2-8 equiv) y Pd(pddf)$Cl_2$ (10% mol) en DME anhidro (10 mL). La mezcla se reacción se agita a reflujo durante el tiempo indicado en cada caso. Una vez concluida la reacción, se lleva a temperatura ambiente y se elimina el disolvente a presión reducida. El crudo de reacción se purifica por cromatografía en columna con gel de sílice, empleando como eluyentes una mezcla hexano/DCM o hexano/AcOEt en las proporciones que se especifican en cada caso.

*4.5.6.1.e. Reacción de Suzuki*

En matraz de dos bocas, provisto de agitación magnética, y refrigerante de reflujo, se introduce bajo atmósfera de argón, el derivado halogenado (1 equiv), el correspondiente ácido borónico (2-8 equiv), $Na_2CO_3$(2-8 equiv) y Pd($PPh_3$)$_4$ (10% mol) en 10 mL de una mezcla tolueno/EtOH/$H_2O$ (4:4:2, v:v:v). La mezcla se reacción se agita a reflujo durante el tiempo indicado en cada caso. Una vez concluida la reacción, se lleva a temperatura ambiente y se elimina el disolvente a presión reducida. El crudo de reacción se purifica por cromatografía en columna con gel de sílice, empleando como eluyentes una mezcla hexano/DCM o hexano/AcOEt en las proporciones que se especifican en cada caso.

*4.5.6.1.f. Formación de 8-amino BODIPYs*

En matraz de dos bocas, provisto de agitación magnética, se introduce, bajo atmósfera de argón, el 8-tiometil BODIPY (1.2 equiv) y la amina primaria (1 equiv) en $CH_3CN$ (10 mL). La mezcla se reacción se agita a temperatura ambiente el tiempo indicado en cada

caso. Una vez finalizada la reacción, se elimina el disolvente a presión reducida y el crudo de reacción se purifica por cromatografía en columna con gel de sílice, empleando como eluyentes una mezcla hexano/AcOEt en las proporciones que se especifican en cada caso.

### *4.5.6.2. Síntesis de 58*

#### *4.5.6.2.a. Síntesis de **62***

Siguiendo el método general *4.5.6.1.a*, se hace reaccionar **PerRed** (200 mg, 0.2 mmol) y KOH (50 mg, 0.9 mmol) en $^{t}$BuOH (30 mL). El crudo de reacción se purifica por cromatografía en columna, empleando una mezcla de hexano/AcOEt 95:5. Se obtiene **62**[49] (60 mg, 36%) como un sólido morado.

$^{1}$H-RMN (300 MHz, $CDCl_3$): δ = 8.16 (s, 2H), 8.15(s, 2H), 7.47 (t, *J* = 7.2 Hz, 1H), 7.35 (d , 2H), 7.33-7.28 (m, 8H), 7.21-7.13 (m, 4H), 7.03-6.97(m, 8H), 2.73-2.62 (sept, *J* = 6.9 Hz, 2H), 1.08 (d, *J* = 6.9 Hz, 12H).

#### *4.5.6.2.b Síntesis de **58***

Siguiendo el método general *4.5.6.1.a*, se hace reaccionar **62** (60 mg, 0.065 mmol) y la cumarina **Cu440** (57 mg, 0.33 mmol) en ácido propiónico (10 mL). El crudo de reacción se purifica por cromatografía en columna, empleando una mezcla de hexano/AcOEt 5:5. Se obtiene **58** (7 mg, 10%) como un sólido rojo.

$^{1}$H-RMN (300 MHz, $CHCl_3$): δ 8.19 (s, 2H), 8.18 (s, 2H), 7.66 (d, *J* = 8.4 Hz, 1H), 7.59-7.40 (m, 2H), 7.44-7.26 (m, 2H), 7.27-7.16 (m, 8H), 7.14 (dd, *J* = 8.4 y 1.9 Hz, 1H), 7.06-7.04 (m, 4H), 6.89 (d, *J* = 7.8 Hz, 8H), 6.29 (s, 1H), 2.62 (q, *J* = 6.8 Hz, 2H), 2.41 (s, 3H), 1.05 (d, *J* = 6.8 Hz, 12H); $^{13}$C-RMN (176 MHz, $CDCl_3$): δ 163.2, 163.1, 161.1, 160.3, 156.1, 155.8, 155.3, 155.2, 153.9, 151.8, 145.6, 138.1, 133.2, 133.1, 130.0 (CH), 129.5 (CH), 125.3 (CH), 125.2 (CH), 124.8 (CH), 124.7 (CH), 124.6 (CH), 123.9 (CH), 123.1, 122.3, 121.3, 120.6 (CH), 120.3 (CH), 120.2, 119.9 (CH), 119.8 (CH), 117.8 (CH), 115.8 (CH), 113.5, 110.0, 24.0 ($\underline{CH}(CH_3)_2$), 18.8 ($CH_3$), 14.2 ($CH_3$); IR (puro): 2963, 2868,

1725, 1353, 1172, 895 $cm^{-1}$; HRMS-EI calculado para ($C_{70}H_{48}N_2O_{10}$) 1077.1589, encontrado 1077.0939.

### *4.5.6.3. Síntesis de 59a-c*

#### *4.5.6.3.a. Síntesis de **63***

En un matraz de dos bocas, provisto de agitación magnética y refrigerante de reflujo, se introduce **PTCDA** (1 g, 2.5 mmol) y $I_2$ (127 mg, 0.68 mmol) en $ClSO_3H$ (10 mL). La mezcla de reacción se calienta a 70 ºC durante 24 h. Pasado este tiempo, se deja alcanzar la temperatura ambiente y se añade agua, observándose la formación de un precipitado rojo. El precipitado se filtra a vacío, lavando con tres porciones de agua. El sólido se seca a 70 ºC, obteniéndose **63**,[50] que se emplea en la siguiente etapa de reacción sin purificación previa.

$^1$H-RMN (300 MHz, $CHCl_3$): δ = 8.80 (s, 4 H).

#### *4.5.6.3.b. Síntesis de **64***

Según el método *4.5.6.1.a* se hicieron reaccionar **63** (1g, 1.89 mmol) y 4-bromo-2,6-dimetilanilina (3.8 g, 18.9 mmol) en ácido propiónico (50 mL). El crudo de reacción se purificó por cromatografía en columna, empleando DCM como eluyente. Se obtiene **64**[51] (1.5 g, 85%) como un sólido naranja.

$^1$H-RMN (300 MHz, $CDCl_3$): δ 8.80 (s, 4H), 7.30 (s, 4H), 2.19 (s, 12H).

#### *4.5.6.3.c. Síntesis de **65***

Según el método *4.5.6.1.d* se hicieron reaccionar **64** (1.5 g, 1.60 mmol), 4-*terc*butilfenol (2.4 g, 16.2 mmol) y $K_2CO_3$ (1.2 g, 8.1 mmol) en DMF (50 mL). El crudo de reacción se purificó por cromatografía en columna, empleando como eluyente una mezcla hexano/AcOEt 9:1. Se obtiene **65** (780 mg, 36%) como un sólido rojo.

$^1$H-RMN (300 MHz, $CDCl_3$): δ 8.32 (s, 4H), 7.38 (s, 4H), 7.30 (d, *J* = 8.7 Hz, 8H), 6.93 (d, *J* = 8.7 Hz, 8H), 2.14 (s, 12H), 1.33 (s, 36 H); $^{13}$C-RMN (75 MHz, $CDCl_3$): δ 162.6, 156.2, 152.6, 147.62 137.8, 133.3, 133.0, 131.3 (CH1), 126.8 (CH), 122.5, 122.4, 120.8, 120.1 (CH), 119.4 (CH), 34.4 ($\underline{C}(CH_3)_3$), 31.5 ($CH_3$), 17.8 ($CH_3$); IR (puro): 2976, 2850, 1731, 1452, 1351, 1154, 965 cm$^{-1}$; HRMS-EI calculado para ($C_{80}H_{72}Br_2N_2O_8$) 1349.2701, encontrado 1349.2735.

*4.5.6.3.d. Síntesis de **66***

Según el método *4.5.6.1.e* se hicieron reaccionar **65** (50 mg, 0.037 mmol), bispinacolado de boro (76 mg, 0.3 mmol), AcOK (30 mg, 0.3 mmol) y una punta de espátula de $Pd(dppf)Cl_2$. El crudo de reacción se purificó por cromatografía en columna, empleando como eluyente una mezcla hexano/AcOEt 6:4. Se obtiene **66** (48 mg, 90%) como un sólido rojo.

$^1$H-RMN (300 MHz, $CDCl_3$): δ 8.19 (s, 4H), 7.55 (s, 4H), 7.16 (d, *J* = 8.7 Hz, 8H), 6.79 (d, *J* = 8.7 Hz, 8H), 2.04 (s, 12H), 1.19 (s, 48H); $^{13}$C-RMN (75 MHz, $CDCl_3$): δ 162.6, 156.1, 152.7, 147.4, 136.6, 134.9 (CH), 134.8, 133.2, 126.7 (CH), 122.5, 120.8, 120.1 (CH), 119.4 (CH), 83.9, 83.5, 34.4 ($\underline{C}(CH_3)_3$), 31.5 ($CH_3$), 25.1 ($CH_3$), 24.9 ($CH_3$), 17.7 ($CH_3$); IR (puro): 2998, 2865, 1728, 1437, 1365, 1159, 921 cm$^{-1}$; HRMS-EI calculado para ($C_{92}H_{96}B_2N_2O_{12}$) 1442.7109, encontrado 1442.7129.

*4.5.6.3.e. Síntesis de **67***

En matraz de dos bocas, provisto de agitación magnética, se añade, bajo atmósfera de argón, la cumarina **Cu440** (1 g, 5.7 mmol), anhídrido tríflico (1.9 mL, 11.3 mmol) y $Et_3N$ (1.6 mL, 11.3 mmol en $CH_3CN$ anhidro (15 mL). La mezcla de reacción se agita a temperatura ambiente durante 2 h. Una vez concluida la reacción, el disolvente se elimina a presión reducida y el crudo de reacción se purifica por cromatografía en columna, empleando una mezcla de hexano/AcOEt 7:3. Se obtienen **67**[52] (1.3 g, 73%) de  como un sólido amarillo

$^1$H-RMN (300 MHz, $CDCl_3$): δ 7.74 (d, *J* = 8.6 Hz, 1H), 7.31-7.26 (m, 2H), 6.39 (d, *J* = 1.1 Hz, 1H), 2.50 (d, *J* = 1.1 Hz, 3H).

*4.5.6.3.g. Síntesis de **68***

Según el método *4.5.6.1.e* se hicieron reaccionar **67** (500 mg, 1.6 mmol), bispinacolado de boro (825 mg, 3.3 mmol), AcOK (320 mg, 303 mmol) y una punta de espátula de $Pd(dppf)Cl_2$. El crudo de reacción se purificó por cromatografía en columna, empleando como eluyente una mezcla hexano/AcOEt 7:3. Se obtiene **68** (366 mg, 80%) de como un sólido blanco.

$^1$H-RMN (300 MHz, $CDCl_3$): δ 7.77 (s, 1H), 7.73 (dd, *J* = 7.9, 0.7 Hz, 1H), 7.61 (d, *J* = 7.8 Hz, 1H), 2.48 (d, *J* = 1.1 Hz, 4H), 1.40 (s, 14H); $^{13}$C-RMN (75 MHz, $CDCl_3$): δ 152.1, 130.0 (CH), 123.7 (CH), 123.1 (CH), 116.1 (CH), 84.4, 83.5, 83.4, 25.0 ($CH_3$), 24.9, 18.7 ($CH_3$); IR (puro): 2979, 1726, 1353, 1142, 969 $cm^{-1}$; HRMS-EI calculado para ($C_{16}H_{19}BO$) 286.1467, encontrado 286.1441.

*4.5.6.3.h. Síntesis de **69***

En matraz de dos bocas, provisto de agitación magnética, refrigerante de reflujo y tubo de $CaCl_2$, se añaden **Cu440** (200 mg, 1.14 mmol) en $NH_4OH$ 28 % aq. (5 mL) de. Posteriormente, y a temperatura ambiente, se añade $I_2$ (289 mg, 1.14 mmol) disuelto en 5 mL de una disolución acuosa de KI 5%. La mezcla se reacción se agita a temperatura ambiente durante 90 min y a continuación se añade una disolución 1 M de $H_2SO_4$ hasta observarse la formación de un sólido amarillo. El precipitado formado se colecta por filtración a vacio, lavándolo con varias porciones de agua, obteniéndose 240 mg (70%) de **69**[53] como un sólido amarillo.

$^1$H-RMN (300 MHz, acetona-$d^6$): δ 7.51 (d, *J* = 8.8 Hz, 1H), 6.86 (d, *J* = 8.7 Hz, 1H), 6.01 (d, *J* = 1.4 Hz, 1H), 2.31 (d, *J* = 1.4 Hz, 3H).

*4.5.6.3.i. Síntesis de **59a-b***

Según el método *4.5.6.1.f* se hicieron reaccionar **65** (200 mg, 0.15 mmol), **68** (255 mg, 0.89 mmol), $K_2CO_3$ (123 mg, 0.89 mmol) y una punta de espátula de $Pd(PPh_3)_4$. El crudo de reacción se purificó por cromatografía en columna, empleando como eluyente una mezcla hexano/AcOEt 7:3, obteniéndose por orden de elución **59a** (27 mg, 30%) y **59b** (35 mg, 18%), ambos como un sólido rojo.

*Compuesto **59a**:* $^1$H-RMN (700 MHz, $CDCl_3$): δ 8.30 (s, 2 H), 8.29 (s, 2 H), 7.67 (d, *J* = 8.2 Hz, 1H), 7.59 (d, *J* = 1.1 Hz, 1H), 7.57 (d, *J* = 8.2 Hz, 1H), 7.45 (s, 2H), 7.35 (s, 2H), 7.28 (d, *J* = 8.9 Hz, 8H), 6.91 (d, *J* = 7.5 Hz, 8H), 6.32 (s, 1H), 2.49 (s, 3H), 2.22 (s, 6H), 2.11 (s, 6H), 1.30 (s, 18 H), 1.29 (18 H); $^{13}$C-RMN (176 MHz, $CDCl_3$): δ 162.8, 162.6, 160.9, 156.2, 156.1, 153.9, 152.6, 152.2, 147.6, 144.5, 139.1, 137.5, 136.4, 134.2, 133.2, 133.0, 131.3 (CH), 127.5 (CH), 127.1 (CH), 126.8 (CH), 124.9 (CH), 123.3 (CH), 122.5, 122.4, 122.3, 120.9, 120.9, 120.1 (CH), 120.1 (CH), 119.4 (CH), 119.4 (CH), 115.4 (CH), 114.9 (CH), 34.4 ($\underline{C}(CH_3)_3$), 31.4 ($CH_3$), 18.7 ($CH_3$), 18.2 ($CH_3$), 17.8 ($CH_3$); IR (puro): 2977, 2847, 1748, 1432, 1355, 1167, 955 $cm^{-1}$; HRMS-EI calculado para ($C_{90}H_{79}BrN_2O_{10}$) 1426.4918, encontrado 1426.4962.

*Compuesto **59b***: $^1$H-RMN (300 MHz, $CDCl_3$): δ 8.34 (s, 4H), 7.69 (d, *J* = 8.1 Hz,2 H), 7.63-7.57 (m, 4H), 7.47 (s, 4H), 7.30 (d, *J* = 8.8 Hz, 8H), 6.94 (d, *J* = 8.8 Hz, 8H), 6.34 (d, *J* = 1.2 Hz, 2H), 2.51 (d, *J* = 1.1 Hz, 6H), 2.25 (s, 12H), 1.31 (s, 36H); $^{13}$C-RMN (75 MHz, $CDCl_3$) δ 162.8, 160.9, 156.20, 153.9, 152.7, 152.2, 147.6, 144.5, 139.6, 136.4, 134.2, 133.3, 127.5 (CH), 126.8 (CH), 124.9 (CH), 123.3 (CH), 122.4, 120.9, 120.2 (CH), 119.4 (CH), 119.0, 115.4 (CH), 114.9 (CH), 34.4 ($\underline{C}(CH_3)_3$), 31.5 ($CH_3$), 18.7 ($CH_3$), 18.2 ($CH_3$); IR (puro): 2988, 2810, 1745, 1449, 1367, 1150, 963 $cm^{-1}$; HRMS-EI calculado para ($C_{100}H_{86}N_2O_{12}$) 1506.6181, encontrado 1506.6103.

*4.5.6.3.j. Síntesis de **59c***

Según el método *4.5.6.1.f* se hicieron reaccionar **66** (65 mg, 0.045 mmol), **69** (92 mg, 0.36 mmol), $K_2CO_3$ (50 mg, 0.36 mmol) y una punta de espátula de $Pd(PPh_3)_4$. El crudo de reacción se purificó por cromatografía en columna, empleando como eluyente una mezcla hexano/AcOEt 7:3, obteniéndose **59c** (17 mg, 25%) como un sólido rojo.

$^1$H-RMN (700 MHz, $CDCl_3$): δ 8.24 (s, 4H), 7.45 (d, *J* = 8.8 Hz, 2H), 7.21-7.17 (m, 12H), 6.91 (d, *J* = 8.8 Hz, 2H), 6.82 (d, *J* = 8.8 Hz, 8H), 6.06 (s, 8H), 2.36 (s, 6H), 2.12 (s, 12H), 1.21 (s, 36H); $^{13}$C-RMN (176 MHz, $CDCl_3$): δ 162.72 161.0, 156.5, 156.1, 152.7, 152.50, 151.8, 147.6, 137.3, 134.5, 133.2, 132.1, 130.6 (CH), 126.8 (CH), 125.0 (CH), 122.4, 120.9, 120.2 (CH), 120.1, 119.3 (CH), 115.8, 113.6, 112.5, 111.9 (CH), 34.4 ($\underline{C}(CH_3)_3$), 31.5 ($CH_3$), 18.9 ($CH_3$), 18.1($CH_3$); IR (puro): 2988, 2853, 1728, 1451, 1358, 1157, 976 cm$^{-1}$; HRMS-EI calculado para ($C_{100}H_{86}N_2O_{14}$) 1538.7880, encontrado 1538.7813.

***4.5.6.4. Síntesis de 60a-b***

*4.5.6.4.a. Síntesis de **70***

Según el método *4.5.6.1.a* se hicieron reaccionar **65** (750 mg, 1.41 mmol) y 2,4,6-trimetilanilina (1.9 g, 14.1 mmol) en ácido propiónico (50 mL). El crudo de reacción se purificó por cromatografía en columna, empleando DCM como eluyente. Se obtiene **70** (1 g, 80%) como un sólido naranja.

$^1$H-RMN (300 MHz, $CDCl_3$): δ 8.81 (s, 4H), 7.13 (s, 4H), 2.43 (s, 12H), 2.19 (s, 6H); $^{13}$C-RMN (75 MHz, $CDCl_3$): δ 161.7, 139.2, 135.6, 135.1, 133.8 (CH), 131.7, 130.1, 129.6 (CH), 128.9, 123.9, 123.3, 21.3 ($CH_3$), 17.89 ($CH_3$); IR (puro): 2995, 2832, 1758, 1447, 1350, 1136, 964 cm$^{-1}$; HRMS-EI calculado para ($C_{42}H_{26}Cl_4N_2O_4$) 762.0574, encontrado 762.0535.

*4.5.6.4.b. Síntesis de **71***

Según el método *4.5.6.1.*d se hicieron reaccionar **70** (1.2 g, 1.6 mmol), 4-*terc*butilfenol (2.4 g, 16 mmol) y $K_2CO_3$ (690 mg, 8 mmol) en DMF (50 mL). El crudo de reacción se purificó por cromatografía en columna, empleando como eluyente una mezcla hexano/AcOEt 9:1. Se obtiene **71** (1.5 g, 75%) como un sólido rojo.

$^1$H-RMN (300 MHz, $CDCl_3$): δ 8.19 (s, 4H), 7.16 (d, *J* = 8.7 Hz, 8H), 6.89 (s, 4H), 6.79 (d, *J* = 8.7 Hz, 8H), 2.23 (s, 6H), 1.98 (s, 12H), 1.18 (s, 36H); $^{13}$C-RMN (75 MHz, $CDCl_3$): δ 163.3, 156.5, 153.2, 147.8, 138.8, 135.4, 133.6, 131.4, 129.7 (CH), 128.6, 128.2, 127.9, 127.2, 123.0, 121.1, 120.6, 120.5 (CH), 119.8 (CH), 34.8 ($\underline{C}(CH_3)_3$), 31.9 ($CH_3$), 21.6 ($CH_3$), 18.3($CH_3$); IR (puro): 2976, 2878, 1732, 1489 1367, 1114, 923 cm$^{-1}$; HRMS-EI calculado para ($C_{82}H_{72}N_2O_8$) 1218.5758, encontrado 1218.5720.

*4.5.6.4.c. Síntesis de **72***

Según el método *4.5.6.1.b* se hicieron reaccionar **70** (200 mg, 0.16 mmol) y KOH (27.6 mg, 0.48 mmol) en $^t$BuOH (30 mL). El crudo de reacción se purificó por cromatografía en columna, empleando una mezcla de hexano/AcOEt 95:5, obteniéndose **72** (100 mg, 77%) como un sólido rojo.

$^1$H-RMN (300 MHz, $CDCl_3$): δ 8.28 (s, 4H), 7.31-7.27 (m, 8H), 7.01 (s, 2H), 6.91-6.7 (m, 8H), 2.35 (s, 3H), 2.09 (s, 6H), 1.34 (s, 18H), 1.31 (s, 18H); $^{13}$C-RMN (75 MHz, $CDCl_3$): δ 163.1, 160.4, 157.1, 156.3, 153.0, 152.8, 148.2, 148.1, 138.9, 135.3, 133.9, 133.6, 131.3, 129.7 (CH), 128.53, 128.21, 127.3 (CH), 127.2 (CH), 123.5, 122.6, 122.2, 122.0 (CH), 120.3, 120.2 (CH), 119.9 (CH), 119.7 (CH), 118.5, 34.84 ($\underline{C}(CH_3)_3$), 34.8 ($CH_3$), 31.9 ($CH_3$), 31.8 ($CH_3$), 21.6 ($CH_3$), 18.2 ($CH_3$); IR (puro): 2979, 2850, 1731, 1452, 1351, 1154, 965 cm$^{-1}$; HRMS-EI calculado para ($C_{73}H_{67}NO_9$) 1101.4816, encontrado 1101.4870.

*4.5.6.4.d. Síntesis de **73***

Según el método *4.5.6.1.c* se hicieron reaccionar **72** (100 mg, 0.1 mmol) y etilendiamina (30 mg, 0.5 mmol) en tolueno (10 mL) a 60ºC. El crudo de reacción se purificó por cromatografía en columna, empleando una mezcla de DCM/MeOH 95:5. Se obtienen **73** (43 mg, 63%) de como un sólido rojo.

$^{1}$H-RMN (300 MHz, $CDCl_3$): δ 8.18 (s, 2H), 8.16 (s, 2H), 7.94 (s, 1H, NH), 7.18-7.14 (m, 8H), 6.89 (s, 2H), 6.80-674 (m, 8H), 4.15 (t, *J* = 6.4 Hz, 2H), 2.95 (t, *J* = 6.4 Hz, 2H), 2.23 (s, 3H), 1.97 (s, 6H), 1.21 (s, 18H), 1.19 (s, 18H); $^{13}$C-RMN (75 MHz, $CDCl_3$): δ 163.7, 162.9, 162.5, 156.1, 155.9, 152.9, 152.7, 147.4, 147.3, 138.4, 135.0, 133.1, 131.00 129.3 (CH), 126.7 (CH), 122.6 (CH), 122.4, 120.8 (CH), 120.6, 120.2 (CH), 112.0 (CH), 119.4 (CH), 119.3 (CH), 43.17 ($CH_2$), 40.44 ($CH_2$), 34.5 ($\underline{C}(CH_3)_3$), 34.4 ($\underline{C}(CH_3)_3$), 31.5 ($CH_3$), 31.4 ($CH_3$), 21.2 ($CH_3$), 17.8($CH_3$); IR (puro): 2979, 2878, 1732, 1448, 1323, 1110, 917 $cm^{-1}$; HRMS-EI calculado para ($C_{75}H_{73}N_3O_8$) 1143.5398, encontrado 1143.5320.

*4.5.6.4.e. Síntesis de **74***

Según el método *4.5.6.1.c* se hicieron reaccionar **72** (50 mg, 0.05 mmol) y etilendiamina (15 mg, 0.25 mmol) en ácido propiónico (10 mL) a 160ºC. El crudo de reacción se purificó por cromatografía en columna, empleando una mezcla de hexano/AcOEt 8:2. Se obtienen **74** (28 mg, 50%) de como un sólido rojo.

$^{1}$H-RMN (300 MHz, $CDCl_3$): δ 8.15 (s, 1H), 8.13 (s, 1H), 8.11 (s, 1H), 8.07 (s, 1H), 7.23 - 7.01 (m, 8H), 6.89 (s, 4H), 6.86-6.61 (m, 8H), 4.13- 4.01 (m, 4H), 2.23 (s, 4H), 1.98 (s, 6H), 1.21 (s, 9H), 1.20 (s, 9H), 1.19 (s, 18H); $^{13}$C-RMN (75 MHz, CDCl3): δ 162.9, 159.6, 156.0, 155.7, 155.6, 155.6, 154.3, 153.2, 153.1, 153.0, 152.8, 152.3, 147.2, 147.1, 147.0, 135.0, 133.6, 131.1, 129.2 (CH), 126.6 (CH), 124.8, 122.0, 121.9, 121.1, 121.0, 120.7 (CH), 120.2, 120.1 (CH), 119.5 (CH), 119.4 (CH), 119.2 (CH), 119.0 (CH), 118.3 (CH), 116.2 (CH), 54.3 ($CH_2$), 44.1 $CH_2$, 34.3, 31.5 ($\underline{C}(CH_3)$), 31.4 ($CH_3$), 21.2 ($CH_3$), 17.8 ($CH_3$); IR (puro): 2999, 2920, 1732, 1438, 1302, 1131, 917 $cm^{-1}$; HRMS-EI calculado para ($C_{75}H_{71}N_3O_8$) 1125.5391, encontrado 1125.5363.

*4.5.6.4.f. Síntesis de **60a***

Según el método *4.5.6.1.g* se hicieron reaccionar **73** (43 mg, 0.037 mmol) y **36** (7 mg, 0.025 mmol) en $CH_3CN$ (5 mL). El crudo de reacción se purificó por cromatografía en columna, empleando una mezcla de hexano/DCM 7:3 como eluyente. Se obtienen **60a** (25 mg, 52%) como un sólido rojo.

$^1$H-RMN (300 MHz, $CDCl_3$); δ 8.33 (t, *J* = 3.8 Hz, 1H, $\underline{NH}CH_2$), 8.27 (s, 2H), 8.13 (s, 2H), 7.60 (s, 1H), 7.38 (s, 1H), 7.20 (d, *J* = 8.9 Hz, 4H), 7.15 (d, *J* = 8.8 Hz, 4H), 7.02 (d, *J* = 6.5 Hz, 4H), 6.89 (s, 2H), 6.80 (d, *J* = 8.8 Hz, 4H), 6.71 (d, *J* = 8.7 Hz, 4H), 6.42 (s, 1H), 6.25 (s, 1H), 4.65 (s, 2H), 3.98 (s, 2H), 2.23 (s, 3H), 1.96 (s, 6H), 1.24 (s, 18H), 1.19 (s, 18H); $^{13}$C-RMN (75 MHz, $CDCl_3$) δ 165.0, 162.7, 156.7, 155.6, 153.1, 152.4, 148.4, 147.7, 147.4, 135.8 (CH), 134.9, 133.1, 132.9, 132.4, 130.9, 125.1, 123.0 (CH), 122.2 (CH), 121.1 (CH), 119.9, 119.8, 119.7 (CH), 119.5 (CH), 115.8 (CH), 113.7 (CH), 48.6 ($CH_2$), 39.3 ($CH_2$), 34.5 ($\underline{C}(CH_3)_3$), 31.4 ($CH_3$), 21.2 ($CH_3$), 17.8 ($CH_3$); IR (puro): 3125, 2988, 2823, 1796, 1502, 1333, 1147, 966 $cm^{-1}$; HRMS-EI calculado para ($C_{84}H_{78}BF_2N_3O_8$) 1333.5219, encontrado 1333.5279.

*4.5.6.4.g. Síntesis de **60b***

Según el método *4.5.6.1.g* se hicieron reaccionar **73** (60 mg, 0.05 mmol) y **75** (28 mg, 0.1 mmol) en $CH_3CN$ (5 mL). El crudo de reacción se purificó por cromatografía en columna, empleando una mezcla de hexano/DCM 7:3 como eluyente. Se obtienen **60b** (27 mg, 43%) como un sólido rojo.

$^1$H-RMN (300 MHz, $CDCl_3$); δ 8.26 (s, 2H), 8.13 (s, 2H), 7.74 (s, 1H, NH), 7.20 (d, *J* = 8.5 Hz, 4H), 7.15 (d, *J* = 8.8 Hz, 4H), 6.89 (s, 2H), 6.87 (s, 2H), 6.81 (d, *J* = 8.8 Hz, 4H), 6.71 (d, *J* = 8.8 Hz, 4H), 6.05 (s, 1H), 4.60 (s, 2H), 3.91 (s, 2H), 2.45 (s, 6H), 2.23 (s, 3H), 1.97 (s, 6H), 1.24 (s, 18H), 1.19 (s, 18H); $^{13}$C-RMN (75 MHz, $CDCl_3$): δ 164.9, 162.8, 156.6, 155.6, 153.2, 152.46, 147.6, 147.4, 146.0, 138.5, 134.9, 133.1, 132.9, 130.9, 129.3 (CH), 126.8 (CH), 123.0, 122.1, 121.3, 121.1 (CH), 120.0, 119.9, 119.8, 119.7 (CH), 119.6 (CH), 119.0 (CH), 48.3 ($CH_2$), 39.5 ($CH_2$), 34.5 ($\underline{C}(CH_3)_3$), 34.4 ($\underline{C}(CH_3)_3$), 31.5 ($CH_3$),

31.4 ($CH_3$), 21.2 ($CH_3$), 17.8 ($CH_3$), 14.1($CH_3$); IR (puro): 3102, 2988, 2857, 1736, 1463, 1311, 1121, 897 $cm^{-1}$; HRMS-EI calculado para ($C_{86}H_{82}BF_2N_3O_8$) 1361.6225, encontrado 1361.6258.

### *4.5.6.5. Síntesis de 61*

#### *4.5.6.5.a. Síntesis de **76***

Según el método *4.5.6.1.c* se hicieron reaccionar **72** (100 mg, 0.1 mmol) y 4-bromo-2,6-dimetilanilina (100 mg, 0.5 mmol) en ácido propiónico (10 mL). El crudo de reacción se purificó por cromatografía en columna, empleando una mezcla de hexano/AcOEt 9:1, obteniéndose **76** (90 mg, 73%) de como un sólido rojo.

$^1$H-RMN (300 MHz, $CDCl_3$): δ 8.19 (s, 1H), 7.26 (s, 2H), 7.18-7.15 (m, 8H), 6.90 (s, 2H), 6.81-6.78 (m, 8H), 2.24 (s, 3H), 2.00 (s, 6H), 1.98 (s, 6H), 1.19 (s, 18H), 1.18 (s, 18H); $^{13}$C-RMN (75 MHz, $CDCl_3$): δ 162.8, 162.6, 156.2, 156.1, 152.7, 147.5, 147.5, 138.5, 137.8, 13 133.27, 133.2, 133.0, 131.3 (CH), 131.0, 129.3 (CH), 128.2, 127.8, 127.5, 126.8 (CH), 122.8, 122.5, 122.2, 121.0, 120.6, 120.2 (CH), 120.0 (CH), 119.4 (CH), 119.3 (CH), 34.42 ($\underline{C}(CH_3)_3$), 31.5 ($CH_3$), 21.2 ($CH_3$), 17.8 ($CH_3$), 17.8 ($CH_3$); IR (puro): 2989, 2844, 1731, 1412, 1378, 1198, 922 $cm^{-1}$; HRMS-EI calculado para ($C_{81}H_{75}BrN_2O_8$) 1482.4704, encontrado 1482.4710.

#### *4.5.6.5.b. Síntesis de **77***

Según el método *4.5.6.1.e* se hicieron reaccionar **76** (80 mg, 0.066 mmol), bispinacolado de boro (50 mg, 0.2 mmol), AcOK (20 mg, 0.2 mmol) y una punta de espátula de $Pd(dppf)Cl_2$. El crudo de reacción se purificó por cromatografía en columna, empleando como eluyente una mezcla hexano/AcOEt 9:1. Se obtienen **77** (72 mg, 82%) como un sólido rojo.

$^1$H-RMN (300 MHz, $CDCl_3$): δ 8.19 (s, 2H), 8.18 (s, 2H), 7.54 (s, 2H), 7.16 (d, *J* = 8.9 Hz, 8H), 6.90 (s, 2H), 6.79 (d, *J* = 8.7 Hz, 8H), 2.23 (s, 3H), 2.04 (s, 12H), 1.98 (s, 12H), 1.14

(s, 48H); $^{13}$C-RMN (75 MHz, $CDCl_3$): δ 162.9, 162.6, 156.1, 156.1, 152.7, 147.4, 138.4, 136.6, 135.0, 134.9 (CH), 134.8, 133.2, 131.0, 129.3 (CH), 126.7 (CH), 122.6, 122.5, 120.8, 120.7, 120.2, 120.1 (CH), 120.0 (CH), 119.4 (CH), 119.3 (CH), 83.9 (C-B), 75.1 (C-O), 34.4 ($\underline{C}(CH_3)_3$), 31.5 ($CH_3$), 24.8 ($CH_3$), 24.6 ($CH_3$), 24.1 ($CH_3$), 17.8 ($CH_3$), 17.7 ($CH_3$); IR (puro): 2999, 2856, 1747, 1436 1352, 1155, 989 $cm^{-1}$; HRMS-EI calculado para ($C_{81}H_{75}BrN_2O_8$) 1330.6454, encontrado 1330.6490.

*4.5.6.5.c. Síntesis de **79***

En un matraz de dos bocas, provisto de agitación y refrigerante de reflujo, se hacen reaccionar bajo atmósfera de argón, cloruro de 4-yodobenzoilo (1g, 3.8 mmol) y 3-etil-2,4-dimetilpirrol (1.1 mL, 8.3 mmol) en DCM (20 mL) a reflujo durante 3h. Pasado este tiempo, y a temperatura ambiente, se añaden $Et_3N$ (2 mL) y $BF_3{\cdot}Et_2O$ (2 mL) manteniendo la agitación durante 30 min. La reacción se hidroliza con agua, y el crudo de reacción se extrae varias veces lavando con porciones de DCM. Las fases orgánicas se secan sobre $MgSO_4$ y se elimina el desecante por filtración. El crudo de reacción se purificó en cromatografía en columna empleando como eluyente una mezcla hexano/DCM 7:3, obteniéndose **79**[1i] (700 mg, 45%) como un sólido naranja.

$^1$H-RMN (300 MHz, $CDCl_3$): δ 7.89 (d, *J* = 8.2 Hz, 2H), 7.42 (d, *J* = 8.3 Hz, 2H), 2.36 (s, 6H), 2.15 (q, *J* = 7.5 HZ, 4H), 1.31 (s, 6H), 0.78 (t, *J* = 7.5 Hz, 6H).

*4.5.6.5.d. Síntesis de **78***

En un matraz de dos bocas, provisto de agitación y refrigerante de reflujo, se añaden bajo atmósfera de argón, **79** (100 mg, 0.2 mmol) y $AlCl_3$ (53 mg, 0.4 mmol) en DCE (10 mL). La mezcla de reacción se calentó a reflujo durante 30 min y pasado este tiempo se añadió la **Cu456** (176 mg, 1 mmol). La mezcla de reacción se agitó a reflujo durante otros 30 min más y a continuación se deja que alcance la temperatura ambiente. La reacción se hidroliza con agua, y el crudo de reacción se extrae varias veces lavando con porciones de DCM. Las fases orgánicas se secan sobre $MgSO_4$ y se elimina el desecante por filtración.

El crudo de reacción se purificó en cromatografía en columna empleando como eluyente una mezcla DCM/MeOH 9:1, obteniéndose **78** (40 mg, 40%) de como un sólido naranja.

$^{1}$H-RMN (300 MHz, $CDCl_3$): δ 7.86 (d, *J* = 8.2 Hz, 2H), 7.31 (d, *J* = 8.8 Hz, 2H), 7.13 (d, *J* = 8.3 Hz, 2H), 6.71 (dd, *J* = 8.8, 2.4 Hz, 2H), 6.36 (d, *J* = 2.4 Hz, 2H), 5.98 (d, *J* = 1.1 Hz, 2H), 2.38 (s, 6H), 2.27 (d, *J* = 1.0 Hz, 6H), 2.15-208 (m, 7H), 1.32 (s, 6H), 0.78 (t, *J* = 7.5 Hz, 6H). $^{13}$C-RMN (75 MHz, $CDCl_3$): δ 161.9, 160.1, 155.2, 154.9, 152.9, 139.7, 139.4, 138.6 (CH), 134.6, 134.2, 131.2, 130.2 (CH), 125.3 (CH), 116.5 (CH), 113.0, 111.3, 105.2 (CH), 94.8 (C-I), 18.6 ($CH_3$), 17.1 ($CH_2$), 14.4 ($CH_3$), 12.8 ($CH_3$), 12.3($CH_3$). IR (puro): 2976, 2840, 1738, 1457, 1381, 1166, 879 cm$^{-1}$; HRMS-EI calculado para ($C_{43}H_{40}BIN_2O_6$) 818.2024, encontrado 818.2055.

*4.5.6.5.e. Síntesis de **61***

Según el método se hicieron reaccionar **77** (340 mg, 0.26 mmol), **78** (70 mg, 0.085 mmol), $K_2CO_3$ (50 mg, 0.5mmol) y una punta de espátula de $Pd(PPh_3)_4$. El crudo de reacción se purificó por cromatografía en columna, empleando como eluyente una mezcla hexano/AcOEt 7:3, obteniéndose **61** (32 mg, 20%), ambos como un sólido rojo.

$^{1}$H-RMN (300 MHz, $CDCl_3$): δ 8.24 (s, 2H), 8.20 (s, 2H), 7.79 (d, *J* = 8.2 Hz, 2H), 7.46 (s, 2H), 7.42 (d, *J* = 8.2 Hz, 2H), 7.32 (d, *J* = 8.8 Hz, 2H), 7.2-7.17 (m, 12H), 6.91 (s, 2H), 6.83 (d, *J* = 3.3 Hz, 4H), 6.80 (d, *J* = 3.3 Hz, 4H), 6.70 (dd, *J* = 8.8, 2.4 Hz, 2H), 6.44 (d, *J* = 2.4 Hz, 2H), 5.99 (d, *J* = 1.1 Hz, 2H), 2.39 (s, 6H), 2.27 (d, *J* = 1.1 Hz, 6H), 2.25 (s, 3H), 2.17-2.07 (m, 10H), 2.00 (s, 6H), 1.34 (s, 6H), 1.20 (s, 18H), 1.18 (s, 18H), 0.78 (t, *J* = 7.3 Hz, 6H); $^{13}$C-RMN (75 MHz, $CDCl_3$): δ 162.9, 162.8, 161.9, 160.2, 156.2, 156.1, 155.2, 154.5, 152.8, 152.7, 147.5, 141.4, 140.0, 138.4, 136.2, 135.0, 133.9, 133.2, 131.5, 131.0, 129.3 (CH), 128.7 (CH), 128.0 (CH), 127.3 (CH), 126.7 (CH), 125.2 (CH), 122.7, 120.9, 120.2 (CH), 120.1 (CH), 119.4 (CH), 116.3 (CH), 113.0, 111.3 (CH), 105.4 (CH), 34.4 ($\underline{C}(CH_3)_3$), 31.5 ($CH_3$), 29.7 ($CH_2$), 18.6 ($CH_3$), 18.1 ($CH_3$), 17.8 ($CH_3$), 14.5 ($CH_3$), 12.6 ($CH_3$), 12.3 ($CH_3$); IR (puro): 2996, 2870, 1777, 1497, 1289, 1188, 936 cm$^{-1}$; MADLI-TOF: calculado para ($C_{124}H_{115}BN_4O_{14}$) 1894.8503, encontrado 1894.8543.

## 4.6. BIBLIOGRAFÍA


[1] a) T. Komatsu, K. Kikuchi, H. Takakusa, K. Hanaoka, T. Ueno, M. Kamiya, Y. Urano, T. Nagano, *J. Am. Chem. Soc.* **2006**, *128*, 15946-15947; b) A. Coskun, E. U. Akkaya, *J. Am. Chem. Soc.* **2006**, *128*, 14474-14475; c) J. Han, J. Jose, E. Mei, K. Burgess, *Angew. Chem. Int. Ed.* **2007**, *46*, 1684-1687; d) X. Zhang, Y. Xiao, X. Qian, *Angew. Chem. Int. Ed.* **2008**, *47*, 8025-8029; e) M. H. Lee, H. J. Kim, S. Yoon, N. Park, J. S. Kim, *Org. Lett.* **2008**, *10*, 213-216; f) V. Balzani, A. Credi, M. Venturi, *ChemSusChem* **2008**, *1*, 26-58; g) M. Suresh, S. Mishra, S. K. Mishra, E. Suresh, A. K. Mandal, A. Shrivastav, A. Das, *Org. Lett.* **2009**, *11*, 2740-2743; h) R. Guliyev, A. Coskun, E. U. Akkaya, *J. Am. Chem. Soc.* **2009**, *131*, 9007-9013.

[2] J. Fan, M. Hu, P. Zhan, X. Peng, *Chem. Soc. Rev.* **2013**, *42*, 29-43.

[3] a) C.-W. Wan, A. Burghart, J. Chen, F. Bergstroem, L. B. A. Johansson, M. F. Wolford, T. G. Kim, M. R. Topp, R. M. Hochstrasser, K. Burgess, *Chem. Eur. J.* **2003**, *9*, 4430-4441; b) C. Goze, G. Ulrich, L. J. Mallon, B. D. Allen, A. Harriman, R. Ziessel, *J. Am. Chem. Soc.* **2006**, *128*, 10231-10239; c) A. Harriman, G. Izzet, R. Ziessel, *J. Am. Chem. Soc.* **2006**, *128*, 10868-10875.

[4] G. Barin, M. D. Yilmaz, E. U. Akkaya, *Tetrahedron Lett.* **2009**, *50*, 1738-1740.

[5] Y. Ueno, J. Jose, A. Loudet, C. Perez-Bolivar, P. Anzenbacher, K. Burgess, *J. Am. Chem. Soc.* **2011**, *133*, 51-55.

[6] Y. Zhao, Y. Zhang, X. Lv, Y. Liu, M. Chen, P. Wang, J. Liu, W. Guo, *J. Mater. Chem.* **2011**, *21*, 13168-13171.

[7] Z. Yang, Y. He, J.-H. Lee, N. Park, M. Suh, W.-S. Chae, J. Cao, X. Peng, H. Jung, C. Kang, J. S. Kim, *J. Am. Chem. Soc.* **2013**, *135*, 9181-9185.

[8] X. Cao, W. Lin, Q. Yu, J. Wang, *Org. Lett.* **2011**, *13*, 6098-6101.

[9] M. D. Yilmaz, O. A. Bozdemir, E. U. Akkaya, *Org. Lett.* **2006**, *8*, 2871-2873.

[10] a) Y. Xiao, D. Zhang, X. Qian, A. Costela, I. Garcia-Moreno, V. Martin, M. E. Perez-Ojeda, J. Bañuelos, L. Gartzia, I. L. Arbeloa, *Chem. Commun.* **2011**, *47*, 11513-11515; bL. Gartzia-Rivero, H. Yu, J. Bañuelos, I. Lopez-Arbeloa, A. Costela, I. Garcia-Moreno, Y. Xiao, *Chem. Asian J.* **2013**, *8*, 3133-3141.

[11] a) C. F. A. Gomez-Duran, I. Garcia-Moreno, A. Costela, V. Martin, R. Sastre, J. Bañuelos, F. Lopez Arbeloa, I. Lopez Arbeloa, E. Peña-Cabrera, *Chem. Commun.* **2010**, *46*, 5103-5105; b) J. Bañuelos, V. Martin, C. F. A. Gomez-Duran, I. J. A. Cordoba, E. Peña-Cabrera, I. Garcia-Moreno, A. Costela, M. E. Perez-Ojeda, T. Arbeloa, I. L. Arbeloa, *Chem. Eur. J.* **2011**, *17*, 7261-7270.

[12] a) A. Loudet, K. Burgess, *Chem. Rev.* **2007**, *107*, 4891-4932; b) G. Ulrich, R. Ziessel, A. Harriman, *Angew. Chem, Int. Ed.* **2008**, *47*, 1184-1201.

[13] H. Lu, J. Mack, Y. Yang, Z. Shen, *Chem. Soc. Rev.* **2014**, *43*, 4778-4823.

[14] L. Fu, F.-L. Jiang, D. Fortin, P. D. Harvey, Y. Liu, *Chem. Commun.* **2011**, *47*, 5503-5505.

[15] Comercializado por Cuántico de México

[16] M. Koepf, A. Trabolsi, M. Elhabiri, J. A. Wytko, D. Paul, A. M. Albrecht-Gary, J. Weiss, *Org. Lett.* **2005**, *7*, 1279-1282.

[17] J. P. Celli, B. Q. Spring, I. Rizvi, C. L. Evans, K. S. Samkoe, S. Verma, B. W. Pogue, T. Hasan, *Chem. Rev.* **2010**, *110*, 2795-2838.

[18] H. Kobayashi, M. Ogawa, R. Alford, P. L. Choyke, Y. Urano, *Chem. Rev.* **2010**, *110*, 2620-2640.

[19] A. Kamkaew, S. H. Lim, H. B. Lee, L. V. Kiew, L. Y. Chung, K. Burgess, *Chem. Soc. Rev.* **2013**, *42*, 77-88.

[20] T. Yogo, Y. Urano, Y. Ishitsuka, F. Maniwa, T. Nagano, *J. Am. Chem. Soc.* **2005**, *127*, 12162-12163.

[21] a) M. Bröering, R. Krüeger, S. Link, C. Kleeberg, S. Köehler, X. Xie, B. Ventura, L. Flamigni, *Chem. Eur. J.* **2008**, *14*, 2976-2983; b) B. Ventura, G. Marconi, M. Bröering, R. Krïger, L. Flamigni, *New J. Chem.* **2009**, *33*, 428-438.

[22] Y. Cakmak, S. Kolemen, S. Duman, Y. Dede, Y. Dolen, B. Kilic, Z. Kostereli, L. T. Yildirim, A. L. Dogan, D. Guc, E. U. Akkaya, *Angew. Chem. Int. Ed.* **2011**, *50*, 11937-11941

[23] a) L. Jiaho, C. Yu, J. Li, Z. Wang, M. Wu, E. Hao, *J. Org. Chem.***2009**, *74*, 7525-7528; b) C. Yu, L. Jiao, H. Yin, J. Zhou, W. Pang, Y. Wu, Z. Wang, G. Yang, E. Hao, *Eur. J. Org. Chem.* **2011**, *2011*, 5460-5468.

[24] D. Zhang, Y. Wen, Y. Xiao, G. Yu, Y. Liu, X. Qian, *Chem. Commun.* **2008**, 4777-4779.

[25] I. Garcia-Moreno, L. Wang, A. Costela, J. Bañuelos, A. I. Lopez, Y. Xiao, *Chem. Phys.Chem* **2012**, *13*, 3923-3931.

[26] I. Esnal, I. Valois-Escamilla, C. F. A. Gomez-Duran, A. Urias-Benavides, M. L. Betancourt-Mendiola, I. Lopez-Arbeloa, J. Bañuelos, I. Garcia-Moreno, A. Costela, E. Peña-Cabrera, *Chem. Phys. Chem* **2013**, *14*, 4134-4142.

[27] a) S. Lin, W. S. Struve, *Photochem. Photobiol.* **1991**, *54*, 361-365; b) A. Y. Bochkov, I. O. Akchurin, O. A. Dyachenko, V. F. Traven, *Chem. Commun.* **2013**, *49*, 11653-11655; c) Y. Qian, B. Yang, Y. Shen, Q. Du, L. Lin, J. Lin, H. Zhu, *Sens. Actuators, B* **2013**, *182*, 498-503; dA. K. Bhoi, S. K. Das, D. Majhi, P. K. Sahu, A. Nijamudheen, A. N, A. Rahaman, M. Sarkar, *J. Phys. Chem. B* **2014**, *118*, 9926-9937; e) D. Majhi, S. K. Das, P. K. Sahu, S. M. Pratik, A. Kumar, M. Sarkar, *Phys. Chem. Chem. Phys.* **2014**, *16*, 18349-18359.

[28] T. Rohand, M. Baruah, W. Qin, N. Boens, W. Dehaen, *Chem. Commun.* **2006**, 266-268.

[29] T. Sakida, S. Yamaguchi, H. Shinokubo, *Angew. Chem, Int. Ed.* **2011**, *50*, 2280-2283.

[30] L. Li, B. Nguyen, K. Burgess, *Bioorg. Med. Chem. Lett.* **2008**, *18*, 3112-3116.

[31] H. Zollinger, *Color Chemistry: Syntheses, Properties, and Applications of Organic Dyes and Pigments*, Wiley, **2003**.

[32] a) M. Kardos, German Patent, DE 276357, **1913**; bM. Kardos, German Patent, DE 276956, **1913**.

[33] F. Wüerthner, *Chem. Commun.* **2004**, 1564-1579.

[34] P. M. Kazmaier, R. Hoffmann, *J. Am. Chem. Soc.* **1994**, *116*, 9684-9691.

[35] a) H. Eilingsfeld, M. Patsch, BASF A.-G., Fed. Rep. Ger. **1976**, p. 9 pp; bR. Iden, G. Seybold, BASF A.-G., Fed. Rep. Ger. . **1985**, p. 16 pp; c) M. Sadrai, L. Hadel, R. R. Sauers, S. Husain, K. Krogh-Jespersen, J. D. Westbrook, G. R. Bird, *J. Phys. Chem.* **1992**, *96*, 7988-7996; d) W. Qiu, S. Chen, X. Sun, Y. Liu, D. Zhu, *Org. Lett.* **2006**,

*8*, 867-870; eM. Queste, C. Cadiou, B. Pagoaga, L. Giraudet, N. Hoffmann, *New J. Chem.* **2010**, *34*, 2537-2545.

[36] Y. Zhao, M. R. Wasielewski, *Tetrahedron Lett.* **1999**, *40*, 7047-7050.

[37] H. Langhals, *Heterocycles* **1995**, *40*, 477-500.

[38] a) M. J. Ahrens, M. J. Fuller, M. R. Wasielewski, *Chem. Mater.* **2003**, *15*, 2684-2686; b) B. A. Jones, M. J. Ahrens, M.-H. Yoon, A. Facchetti, T. J. Marks, M. R. Wasielewski, *Angew. Chem. Int. Ed.* **2004**, *43*, 6363-6366.

[39] R. Schmidt, M. M. Ling, J. H. Oh, M. Winkler, M. Köenemann, Z. Bao, F. Wuerthner, *Adv. Mater.* **2007**, *19*, 3692-3695.

[40] V. Sivamurugan, K. Kazlauskas, S. Jursenas, A. Gruodis, J. Simokaitiene, J. V. Grazulevicius, S. Valiyaveettil, *J. Phys. Chem. B* **2010**, *114*, 1782-1789.

[41] U. Rohr, C. Kohl, K. Müllen, A. van de Craats, J. Warman, *J. Mater. Chem.* **2001**, *11*, 1789-1799.

[42] a) S. Nakazono, S. Easwaramoorthi, D. Kim, H. Shinokubo, A. Osuka, *Org. Lett.* **2009**, *11*, 5426-5429; b) S. Nakazono, Y. Imazaki, H. Yoo, J. Yang, T. Sasamori, N. Tokitoh, T. Cedric, H. Kageyama, D. Kim, H. Shinokubo, A. Osuka, *Chem. Eur. J.* **2009**, *15*, 7530-7533.

[43] aT. M. Wilson, T. A. Zeidan, M. Hariharan, F. D. Lewis, M. R. Wasielewski, *Angew. Chem. Int. Ed.* **2010**, *49*, 2385-2388; b) J. Lambrecht, T. P. I. Saragi, J. Salbeck, *J. Mater. Chem.* **2011**, *21*, 18266-18270.

[44] a) W. Chen, X. Yang, G. Long, X. Wan, Y. Chen, Q. Zhang, *J. Mater. Chem. C* **2015**, *3*, 4698-4705; b) P. E. Hartnett, A. Timalsina, H. S. S. R. Matte, N. Zhou, X. Guo, W. Zhao, A. Facchetti, R. P. H. Chang, M. C. Hersam, M. R. Wasielewski, T. J. Marks, *J. Am. Chem. Soc.* **2014**, *136*, 16345-16356; c) F. Pekdemir, S. Kurnali, A. Sengul, A. Altindal, A. Riza Ozkaya, B. Salih, O. Bekaroglu, *Dalton Trans.* **2015**, *44*, 158-166.

[45] a) C. Karapire, C. Zafer, S. Icli, *Synth. Met.* **2004**, *145*, 51-60; b) F. J. Cespedes-Guirao, S. Garcia-Santamaria, F. Fernandez-Lazaro, A. Sastre-Santos, H. J. Bolink, *J. Phys. D: Appl. Phys.* **2009**, *42*, 105101-105106; c) I. Oner, C. Varlikli, S. Icli, *Appl. Surf. Sci.* **2011**, *257*, 6089-6094.

[46] a) E. M. Calzado, J. M. Villalvilla, P. G. Boj, J. A. Quintana, R. Gomez, J. L. Segura, M. A. Diaz-Garcia, *J. Phys. Chem. C* **2007**, *111*, 13595-13605; ) bM. G. Ramirez, M. Morales-Vidal, V. Navarro-Fuster, P. G. Boj, J. A. Quintana, J. M. Villalvilla, A. Retolaza, S. Merino, M. A. Diaz-Garcia, *J. Mater. Chem. C* **2013**, *1*, 1182-1191; c) T. Ribeiro, S. Raja, A. S. Rodrigues, F. Fernandes, C. Baleizao, J. P. S. Farinha, *Dyes Pigm.* **2014**, *110*, 227-234.

[47] O. A. Bozdemir, M. D. Yilmaz, O. Buyukcakir, A. Siemiarczuk, M. Tutas, E. U. Akkaya, *New J. Chem.* **2010**, *34*, 151-155.

[48] J. H. Hurenkamp, W. R. Browne, R. Augulis, A. Pugžlys, P. H. M. van Loosdrecht, J. H. van Esch, B. L. Feringa, *Org. Biomol. Chem.* **2007**, *5*, 3354-3362.

[49] K. Peneva, G. Mihov, F. Nolde, S. Rocha, J.-i. Hotta, K. Braeckmans, J. Hofkens, H. Uji-i, A. Herrmann, K. Muellen, *Angew. Chem, Int. Ed.* **2008**, *47*, 3372-3375.

[50] A. S. Nia, C. Enders, W. H. Binder, *Tetrahedron* **2012**, *68*, 722-729.

[51] C. Addicott, I. Oesterling, T. Yamamoto, K. Müllen, P. J. Stang, *J. Org. Chem.* **2005**, *70*, 797-801.

[52] D. R. Breed, R. Thibault, F. Xie, Q. Wang, C. J. Hawker, D. J. Pine, *Langmuir* **2009**, *25*, 4370-4376.

[53] S. S. Lele, S. Sethna, *J. Org. Chem.* **1958**, *23*, 1731-1734.

[54] a) J. Fortage, M. Severac, C. Houarner-Rassin, Y. Pellegrin, E. Blart, F. Odobel, *J. Photochem. Photobiol., A* **2008**, *197*, 156-169; bJ. Schoenamsgruber, H. Maid, W. Bauer, A. Hirsch, *Chem. Eur. J.* **2014**, *20*, 16969-16979; c) J. Schoenamsgruber, A. Hirsch, *Eur. J. Org. Chem.* **2015**, *2015*, 2167-2174.

[55] T. V. Goud, A. Tutar, J.-F. Biellmann, *Tetrahedron* **2006**, *62*, 5084-5091.

[56] A. Burghart, H. Kim, M. B. Welch, L. H. Thoresen, J. Reibenspies, K. Burgess, F. Bergstroem, L. B. A. Johansson, *J. Org. Chem.* **1999**, *64*, 7813-7819.

# CAPÍTULO 5. NUEVOS DERIVADOS DE BODIPYs POR FUNCIONALIZACIÓN EN POSICIÓN 8

# 5. NUEVOS DERIVADOS DE BODIPYs POR FUNCIONALIZACIÓN EN POSICIÓN 8

## 5.1. INTRODUCCIÓN

A lo largo del trabajo desarrollado en la presente Tesis, ha quedado demostrado que los BODIPYs son una familia de colorantes con propiedades únicas fácilmente modulables para su utilización en diferentes áreas. Muchas de sus aplicaciones requieren la derivatización de la posición *meso* del cromóforo, lo que permite obtener BODIPYs difícilmente accesibles por otras rutas sintéticas. Varias aproximaciones han sido descritas en la literatura para la funcionalización de esta posición. Así, la síntesis de BODIPYs a partir de pirroles adecuadamente funcionalizados y aldehídos aromáticos o cloruros de ácido permite la incorporación de diferentes sustituyentes en posición 8, aunque esta ruta presenta algunas limitaciones[1] (Esquema 47).

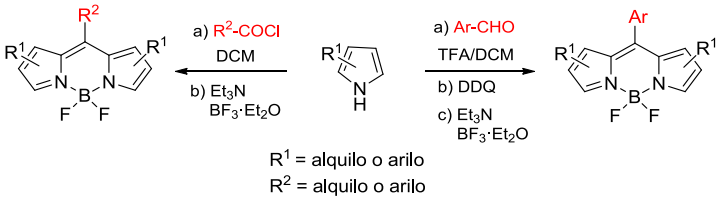


**Esquema 47**

Una de las metodologías alternativas más utilizadas actualmente se basa en la utilización del llamado BODIPY de Biellman,[2] que presenta un grupo tioéter en *meso*. Este derivado se obtiene por tratamiento del pirrol con tiofosgeno, aislándose un derivado de tiocetona precursor de dicho BODIPY (Esquema 48). Este 8-tiometilBODIPY es capaz

de experimentar una amplia variedad de reacciones sobre la posición *meso*, lo que le confiere una gran versatilidad sintética.

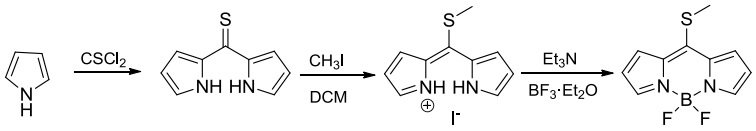


**Esquema 48**

A partir de este tiometil BODIPY, el grupo del Prof. Peña-Cabrera ha desarrollado con éxito la funcionalización del mismo a través de reacciones de sustitución nucleófila aromática[3] o reacciones de acoplamiento C-C catalizadas por paladio,[4] lo que ha permitido preparar nuevos BODIPYs diferentemente sustituidos en posición 8 con emisión en toda la región del espectro visible (400-650 nm) (Esquema 49).

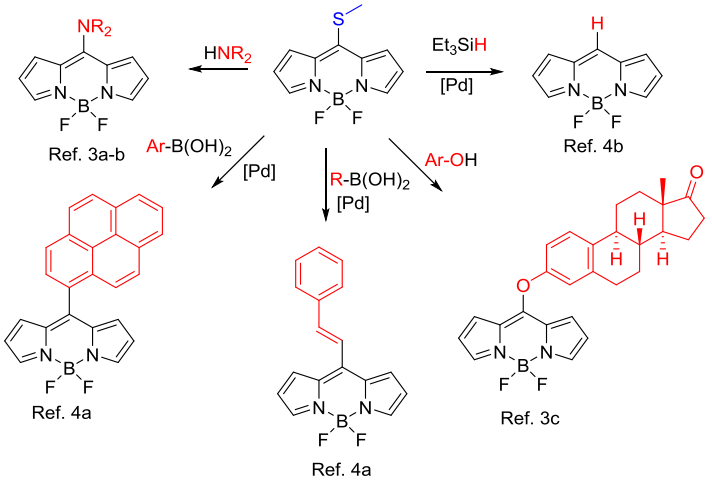


**Esquema 49**

De forma análoga, el grupo del Prof. Dehaen[5] ha utilizado 2-(*N*,*N*-dimetilaminocarbonil)pirrol para la preparación de un colorante funcionalizado en la posición *meso*, que es interesante debido al elevado número de reacciones posibles que se pueden realizar sobre el átomo de halógeno que presenta en dicha posición. En este caso, en vez de tiofosgeno se utiliza un método más sencillo como es la reacción de este

compuesto con pirrol, formando el intermedio de tipo dipirrolilcetona, que evoluciona al tratarlo con $POCl_3$ al dipirrometeno halogenado, precursor del BODIPY *meso*-halogenado (Esquema 50). Los haloBODIPYs obtenidos son valiosos intermedios en diferentes reacciones de sustitución nucleófila aromática y acoplamiento C-C catalizadas por paladio.[5] Este tipo de intermedios ha permitido también la formación de dímeros de BODIPY mediante la reacción con difenoles y dianilinas.[6] Una variante de esta última metodología, empleando pirroles sustituidos y tiofosgeno, ha sido empleada recientemente por Smith y col.[7] dando lugar a 8-haloBODIPYs similares

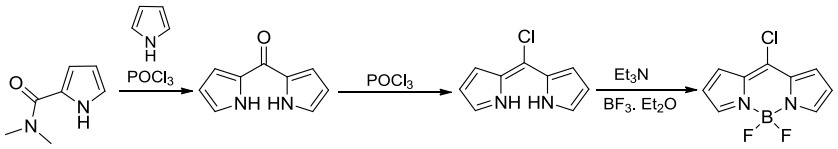


**Esquema 50**

En esta misma línea, nuestro grupo de investigación ha descrito recientemente reacciones de funcionalización selectiva en posición 8 basadas en la mayor acidez de los hidrógenos de los grupos metilos en dicha posición. Así, se han obtenido 8-estirilBODIPYs por condensación de Knoevenagel[8] y nuevos derivados *meso* funcionalizados por litiación selectiva de 8-metilBODIPYs[9] (Esquema 51).

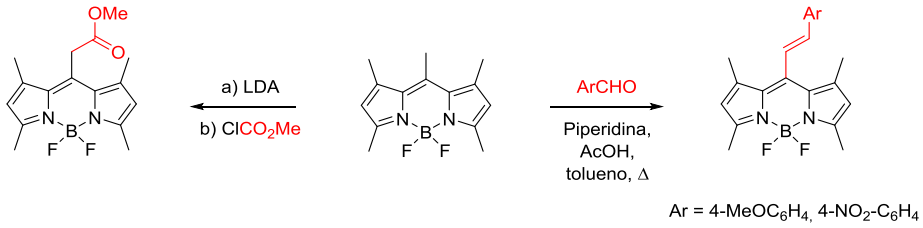


**Esquema 51**

Teniendo en cuenta estos antecedentes, durante la estancia pre-doctoral realizada en el grupo del Prof. Peña-Cabrera, y dentro de la colaboración que mantiene con nuestro grupo de investigación, se plantearon dos objetivos que implican la obtención de nuevos derivados de BODIPY mediante funcionalización en posición 8 (Figura 80):

a) Síntesis de sistemas basados en BODIPYs y dicetonatos de boro

b) Síntesis de sistemas basados en BODIPYs y tiofentrifenilaminas

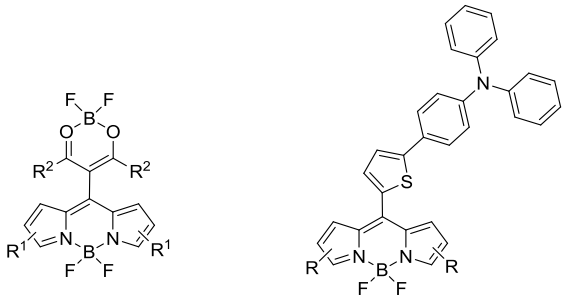

**Figura 80**. Estructuras de sistemas basados en BODIPYs con dicetonatos de boro y tiofentrifenilaminas.

La síntesis de estos sistemas tiene como finalidad el estudio posterior de sus propiedades fotofísicas y de sus posibles aplicaciones como láseres de colorante o como células solares, respectivamente.

## 5.2. SÍNTESIS DE SISTEMAS BODIPY-DICETONATO·$BF_2$

### 5.2.1. Introducción

Los derivados de las 1,3-dicetonas poseen un gran interés en el campo de los sensores y la química supramolecular gracias a sus buenas propiedades quelantes[10] y, más concretamente, a las excelentes propiedades fluorescentes de estos sistemas cuando se encuentran formando 1,3-dicetonatos de boro (Figura 81).[11]

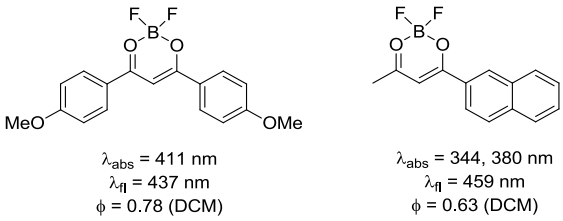


**Figura 81.** Estructuras y propiedades fotofísicas de 1,3-dicetonatos de boro

En la bibliografía existen varios ejemplos de BODIPYs con acetilacetonas (AcAc) en su estructura, lo que ha permitido su incorporación en nanopartículas de $TiO_2$ para su potencial uso en células solares (Figura 82).[12]

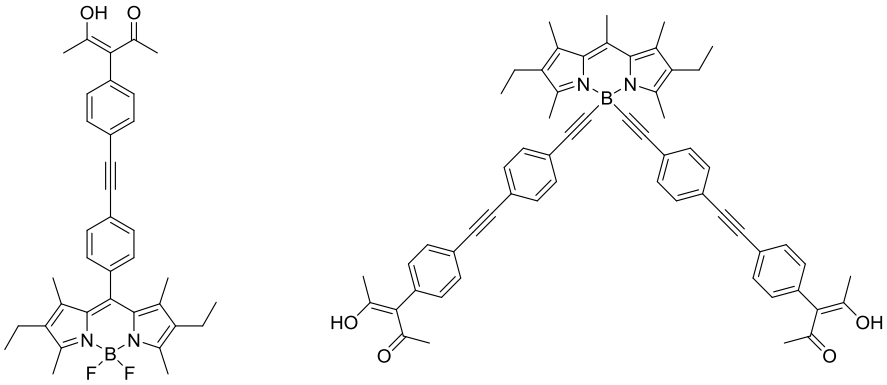


**Figura 82**. Estructuras de BODIPYs-AcAc.

Sin embargo, no existen ejemplos de sistemas formados por la unión entre un BODIPY y un dicetonato de boro, en los que, además, los derivados de la 1,3-dicetona se encuentren unidos directamente al núcleo de indaceno.

Teniendo en cuenta la metodología desarrollada por el grupo del Prof Peña-Cabrera y los recientes resultados obtenidos en la incorporación de 1,3-dicetonas en posición 8 de un BODIPY,[13] pareció conveniente utilizar esta estrategia para lleva a cabo la síntesis de BODIPYs-dicetonatos de boro. En la figura 83 se recogen los sistemas diseñados para abordar el primer objetivo planteado.

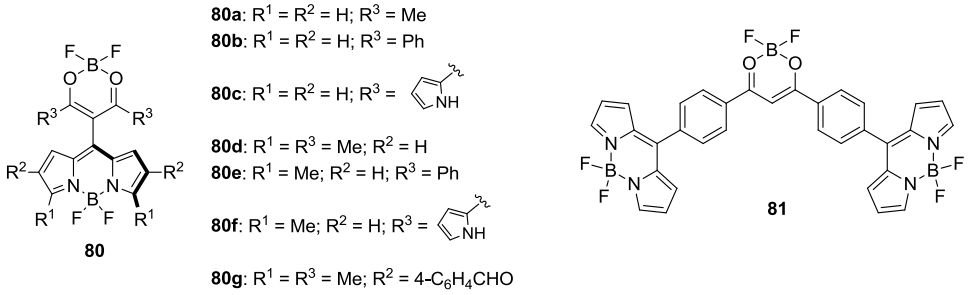


**Figura 83**. Estructuras de BODIPYs-dicetonato·$BF_2$.

### 5.2.2. Síntesis

Las 1,3-dicetonas seleccionadas fueron la acetilacetona comercial (**82a**), la 1,5-difenil-2,4-pentanodiona (**82b**) y la 1,5-dipirrolidil-2,4-pentanodiona (**82c**), siendo estas dos últimas sintetizadas según los procedimientos descritos en la literatura. Así, la reacción entre la acetofenona y el cloruro de benzoilo en presencia del eterato del bromuro de magnesio y diisopropilamina dio como resultado la obtención de **82b**[14] con un 62% de rendimiento (Esquema 48). De forma análoga, por reacción entre el dicloruro del ácido malónico y pirrol se obtuvo la dicetona **82c**[15] como una mezcla de isómeros en proporción 4:1, con un 70% de rendimiento (Esquema 52).

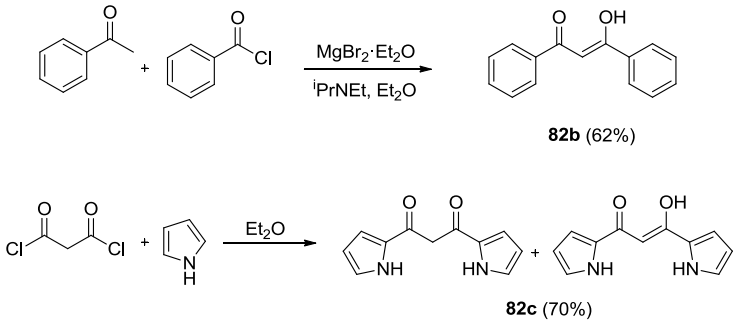


**Esquema 52**

A continuación, se llevó a cabo la reacción de los 8-tiometilBODIPYs **40**[16] y **75**[2] con las diferentes 1,3-dicetonas **82a-c** en presencia de 2-tiofencarboxilato de cobre (I) (CuTc) y $Na_2CO_3$, lo que permitió obtener los sistemas **83a-d** con rendimientos de moderados a buenos. Sin embargo, cuando se hizo reaccionar el BODIPY **40** con las dicetonas **82b-c** no se consiguió aislar los derivados deseados (Esquema 53).

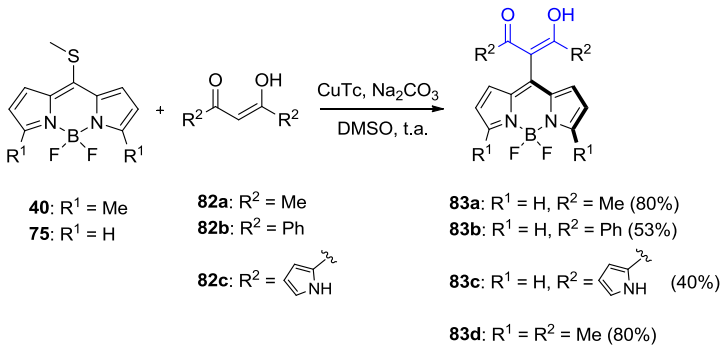


**Esquema 53**

Una vez sintetizados los sistemas **83a-d** se llevó a cabo la reacción de complejación de los mismos por tratamiento con $BF_3{\cdot}Et_2O$ en tolueno a reflujo. Sorprendentemente, la reacción solo tuvo lugar en el caso de las dicetonas **83a** y **83d**, lo que permitió obtener los cassettes **80a** y **80d** con un 14 y 17% de rendimiento, respectivamente (Esquema 54). Señalar, que en los otros dos casos solo se observó la descomposición del material de partida.

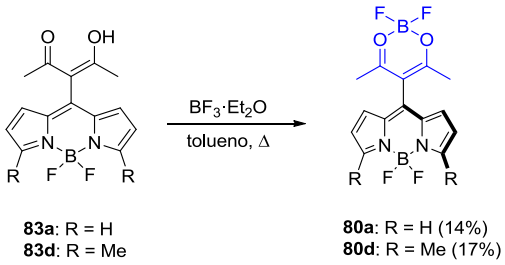


**Esquema 54**

En cuanto a la síntesis del compuesto **80g**, se diseñó una ruta sintética que se detalla en el esquema 51. La reacción de **40** con 2.1 equiv de NBS condujo a la formación del BODIPY dibromado **84**, con un 90% de rendimiento. Posteriormente, la reacción de **84** con acetilacetona,

en las condiciones anteriormente empleadas, dio como resultado la obtención del intermedio **85**, que tras un acoplamiento de Suzuki con el ácido 4-formilfenilborónico originó el derivado **83g**. Sin embargo, la reacción de **83** con $BF_3{\cdot}Et_2O$ no tuvo como resultado la formación de **80g**, observándose únicamente la descomposición del material de partida.

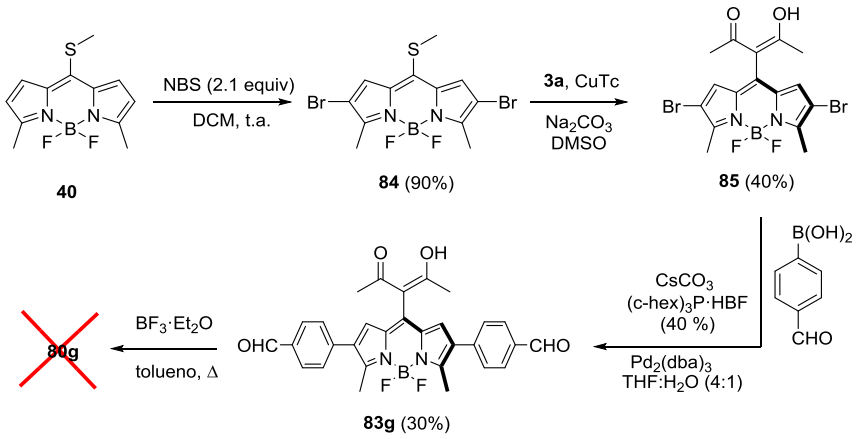


**Esquema 55**

A continuación, se abordó la obtención del cassette **81**, a través de la ruta sintética que se describe en el esquema 56.

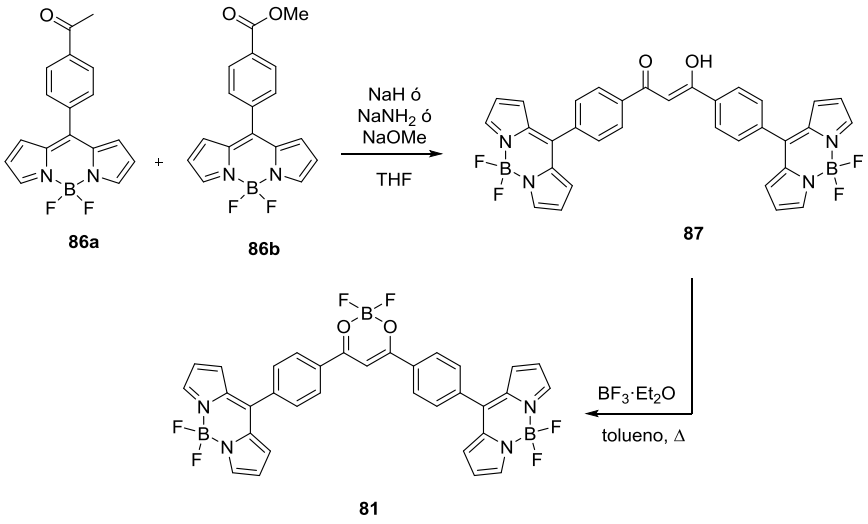


**Esquema 56**

En primer lugar, se llevó a cabo la obtención de los precursores **86a-b** mediante el procedimiento habitual empleado por el grupo del Prof. Peña-Cabrera.[4a] Así, la reacción del BODIPY **75** con los ácidos 4-acetilfenil- o 4-carboximetilfenilborónico, en presencia de $Pd_2(dba)_3$, condujo a la obtención de los compuestos **86a** y **86b**[17] con excelentes rendimientos (Esquema 57).

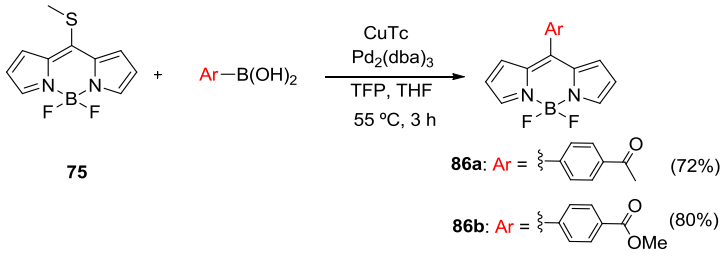


**Esquema 57**

Una vez obtenidos los BODIPYs precursores **86a-b**, se llevó a cabo la reacción de condensación de Claisen entre ambos derivados empleando como base NaH, $NaNH_2$ o NaOMe. En ninguno de los casos se obtuvo el producto deseado, recuperándose de forma exclusiva los materiales de partida

A la vista de estos resultados, se optó por modificar la ruta sintética anteriormente planteada. Para esta nueva ruta se obtuvo el BODIPY **86c**[18] con un grupo carboxílico en la posición *meso*, que podría convertirse en un cloruro de ácido (**86d**) por tratamiento con $SOCl_2$, para reaccionar posteriormente con el BODIPY **86a** en la misma condiciones de obtención que la dicetona **82b**. Sin embargo, esta reacción tampoco dio resultado positivo, recuperándose únicamente el compuesto **86a** inalterado (Esquema 58).

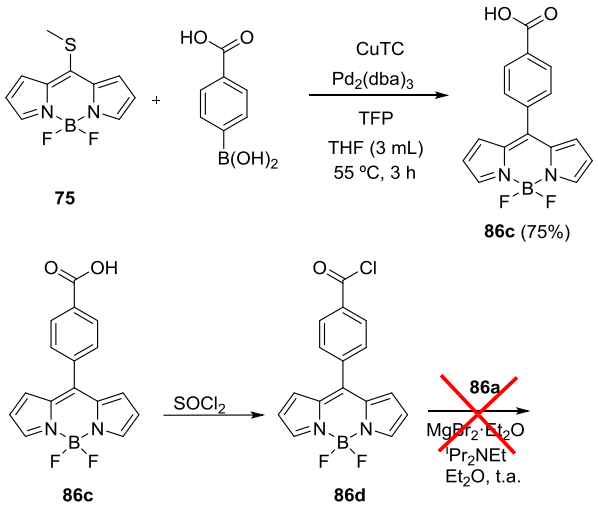


**Esquema 58**

En resumen, por lo que se refiere al primer objetivo planteado, se ha conseguido obtener dos nuevos compuestos basados en dicetonatos de boro. El estudio fotofísico y de comportamiento láser de estos sistemas se realizará posteriormente, aunque será necesario profundizar más en este tipo de reactividad con interesantes perspectivas.

## 5.3. CASSETTES BASADOS EN BODIPYs Y TIOFENTRIFENILAMINAS

### 5.3.1. Introducción

Durante los últimos años, una de las tendencias actuales en la comunidad científica es la construcción de dispositivos capaces de convertir la energía solar en energía eléctrica. Para lograr este objetivo, una de las principales estrategias es la obtención de sistemas que absorban dicha energía solar (dador) y la transfieran a una segunda unidad que se va a encargar de generar el flujo de electrones (aceptor).

Dentro de los colorantes orgánicos, los compuestos de la familia de los BODIPYs han alcanzado importancia dentro de este campo debido a sus excelentes propiedades ópticas y redox, además de por su gran versatilidad química. Por ello, podemos encontrar ejemplos de BODIPYs empleados en la construcción de células solares, en los que la parte dadora es un fragmento de trifenilamina (Figura 84).[19]

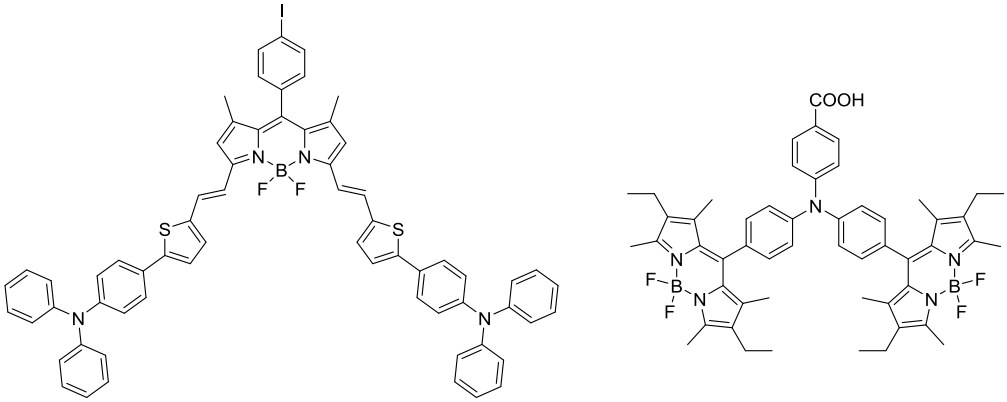


**Figura 84**. Estructuras de BODIPYs empleados en la construcción de células solares.

Sin embargo, la obtención de estos sistemas no es trivial, ya que suele implicar muchos pasos de reacción o estrategias sintéticas complejas. Por ello, como segundo objetivo de la estancia, se planteó acceder a este tipo de sistemas empleando el 8-tiometilBODIPY **40** como precursor y aplicando la metodología desarrollada en el grupo. En la figura 85 se muestran las estructuras de los sistemas elegidos para este estudio.

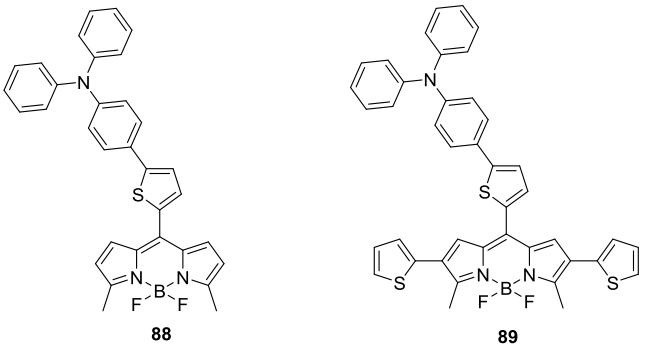


**Figura 85**. Estructuras de los BODIPYs **88** y **89**.

El compuesto **88** se eligió como compuesto patrón para los posteriores estudios sobre el comportamiento de estos sistemas como células solares. El compuesto **89** se propuso para intentar desplazar la emisión hacia la zona roja del espectro.

### 5.3.2. Síntesis

En primer lugar, se llevó a cabo la reacción entre el BODIPY **40** y el ácido 5-bromo-2-tiofenborónico, obteniéndose el BODIPY intermedio **90** con un 78% de rendimiento (Esquema 59). Se seleccionó este ácido borónico ya que la presencia de un átomo de bromo en la posición 5 del anillo de tiofeno permite realizar el posterior acoplamiento con el ácido borónico de la trifenilamina. Así, el posterior acoplamiento de Suzuki entre **90** y el ácido borónico correspondiente permitió obtener el compuesto **88** con un excelente rendimiento (Esquema 59).

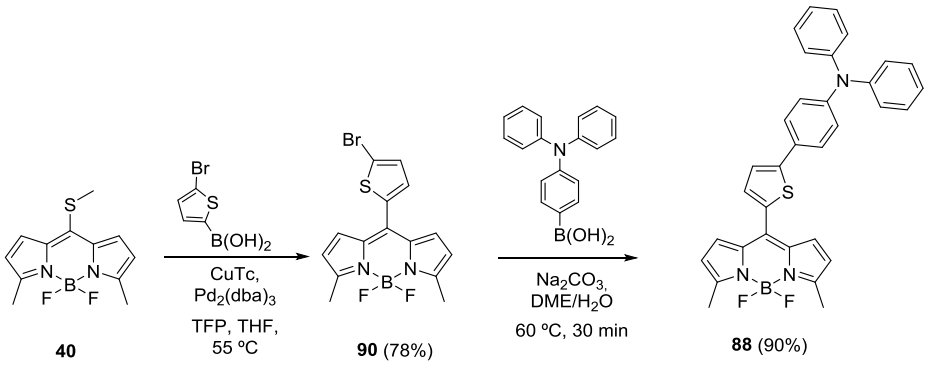


**Esquema 59**

A continuación, se abordó la síntesis de **89** a partir del compuesto **88**. La reacción de bromación de este derivado, empleando inicialmente 2 equivalentes de NBS como agente de halogenación, no dio lugar al 2,6-dibromoBODIPY esperado, recuperándose únicamente el compuesto de partida. El uso de más equivalentes de NBS tampoco condujo a la formación del derivado dibromado, sino a la obtención del derivado tetrabromado **91**. En este punto, se consideró conveniente llevar a cabo el acoplamiento planteado con el ácido 2-tiofenborónico, obteniéndose el derivado **92** con un rendimiento del 70%. Este derivado presenta un desplazamiento batocrómico considerable hacia la zona roja del espectro, lo que le hace un candidato ideal para los estudios propuestos (Esquema 60).

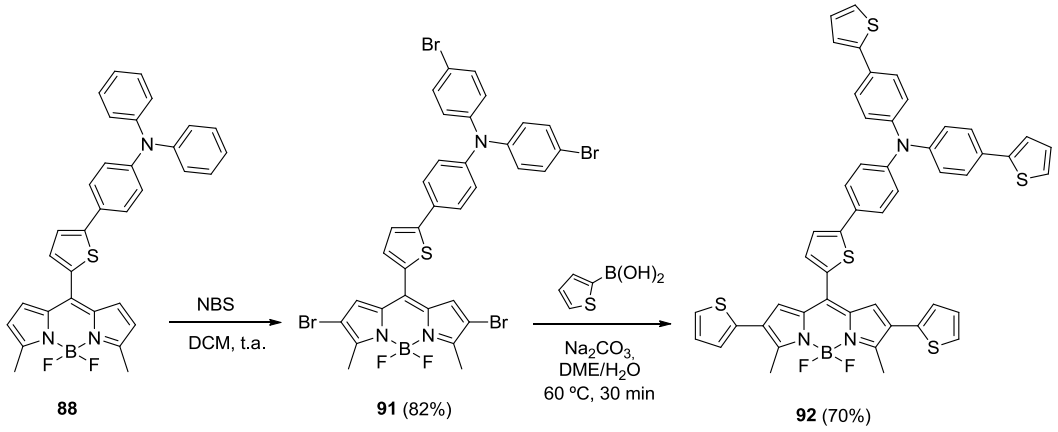


**Esquema 60**

En resumen, en estos nuevos compuestos se pone de manifiesto que la metodología empleada para su obtención resulta ser una herramienta sencilla y muy versátil, que simplifica de forma significativa las rutas de síntesis descritas previamente. En estos momentos se están llevando a cabo estudios preliminares sobre su evaluación como fotosensibilizadores para células solares.

## 5.4. PARTE EXPERIMENTAL

### 5.4.1. Procedimientos generales

#### *5.4.1.1. Síntesis de BODIPYs-1,3-dicetona*

En un matraz de dos bocas provisto de agitación magnética, se introduce bajo atmósfera de argón, el 8-tiometilBODIPY derivado (1 equiv) y CuTc (1.1 equiv) en DMSO (2 mL), agitando la reacción a temperatura ambiente durante 5 min. Pasado este tiempo, se añade bajo atmósfera de argón, la 1,3-dicetona (2 equiv) y $Na_2CO_3$ (2 equiv). La reacción se sigue por cromatografía en capa fina hasta observarse que se ha consumido todo el material de partida Una vez concluida la reacción, se hidroliza con 5 mL de un tampón de fosfatos (pH 7 y 0.2 M), y se extrae con AcOEt. Los extractos orgánicos se juntan y se secan sobre $MgSO_4$, se filtra y se elimina el disolvente a presión reducida. El crudo de reacción se purifica por cromatografía flash en columna sobre gel de sílice, indicándose en cada caso la mezcla de disolventes utilizada.

#### *5.4.1.2. Síntesis de BODIPYs-dicetonatos de boro*

En un matraz dos bocas provisto de agitación magnética y refrigerante de reflujo, se introduce el BODIPY-1,3-dicetona derivado (1 equiv) y $BF_3 \cdot Et_2O$ (3 equiv) en tolueno (3 mL), calentando la mezcla a 80º C. La reacción se sigue por cromatografía en capa fina hasta observarse que se ha consumido todo el material de partida. El disolvente se elimina a presión reducida y el crudo de reacción se purifica por cromatografía flash en columna sobre gel de sílice, indicándose en cada caso la mezcla de disolventes utilizada.

#### *5.4.1.3. Reacción de bromación de BODIPYs*

En un matraz de dos bocas provisto de agitación magnética, se introduce bajo atmósfera de argón, el BODIPY (1 equiv) y NBS (2.1 equiv) en DCM (10 mL), agitando la mezcla a temperatura ambiente. La reacción se sigue por cromatografía en capa fina hasta observarse que se ha consumido todo el material de partida. El disolvente se elimina a presión reducida y el crudo de reacción se purifica por cromatografía flash en columna sobre gel de sílice, indicándose en cada caso la mezcla de disolventes utilizada.

#### *5.4.1.4. Reacción de acoplamiento de Suzuki*

En un matraz dos bocas provisto de agitación magnética y refrigerante de reflujo, se introduce el BODIPY (1 equiv), el ácido borónico correspondiente (3-8 equiv), $Na_2CO_3$ (6-12 equiv) y una punta de espátula de $Pd(PPh_3)_4$ en una mezcla DME/$H_2O$ (4:1 mL), calentando la reacción a 80 ºC. La reacción se sigue por cromatografía en capa fina hasta observarse que se ha consumido todo el material de partida. El disolvente se elimina a presión reducida y el crudo de reacción se purifica por cromatografía flash en columna sobre gel de sílice, indicándose en cada caso la mezcla de disolventes utilizada.

#### *5.4.1.5. Reacción de acoplamiento de Liesbeskind-Srölg*

En un matraz dos bocas provisto de agitación magnética y refrigerante de reflujo, se introduce, bajo atmósfera de argón, el BODIPY (1equiv), el ácido borónico (3 equiv), CuTc (3 equiv) y una punta de espátula de TFP y $Pd_2(dba)_3$ en THF anhidro (3mL), calentando mezcla a 55 ºC. La reacción se sigue por cromatografía en capa fina hasta observarse que se ha consumido todo el material de partida. El disolvente se elimina a presión reducida y el crudo de reacción se purifica por cromatografía flash en columna sobre gel de sílice, indicándose en cada caso la mezcla de disolventes utilizada.

### 5.4.2. Síntesis de 1,3-dicetonas

#### *5.4.2.1. Síntesis de 82b*

En un matraz de dos bocas, provisto de agitación magnética y tubo de $CaCl_2$, se introduce el cloruro de benzoilo (0.2 mL, 1.74 mmol), acetofenona (0.24 mL, 2.06 mmol), $MgBr_2 \cdot Et_2O$ (630 mg, 2.44 mmol) y etildiisopropilamina (0.61 mL, 3.44 mmol) en DCM (6 mL) La mezcla de reacción se agita a temperatura ambiente durante 24 h, observándose la desaparición del material de partida. Posteriormente, se hidroliza con una disolución de HCl al 10 % v/v, agitando el crudo de reacción durante 20 min. Pasado este tiempo, se extrae la fase acuosa varias veces con DCM. La fase orgánica se seca sobre $MgSO_4$, se filtra y se elimina el disolvente a presión reducida. El crudo de

reacción se purifica por cromatografía en columna sobre gel de sílice empleando como eluyente una de mezcla de hexano/AcOEt (95:5) obteniéndose **82b**[14] (264 mg, 68 %) como un sólido blanco.

$^1$H-RMN (200 MHz, $CDCl_3$): δ 7.99 (d, *J* = 7.3 Hz, 4H), 7.56 (m, 2H), 7.56-7.48 (m, 4H), 6.86 (s, 1H).

#### *5.4.2.2. Síntesis de 82c*

En un matraz de dos bocas provisto de agitación magnética y tubo de $CaCl_2$, se introducen el pirrol (0.97 mL, 10 mmol) y el cloruro de maloilo (1.4 mL, 20 mmol) en DCM (20 mL) a 0 ºC. Se deja que la reacción alcance la temperatura ambiente, agitando a esta temperatura durante 3 h. Pasado este tiempo, se hidroliza con una disolución de $Na_2CO_3$ saturada y se extrae varias veces con DCM. Las fases orgánicas se secan sobre $MgSO_4$, se filtra y se elimina el disolvente a presión reducida. El crudo se purifica por cromatografía en columna empleando con eluyente DCM hasta llegar a una mezcla DCM/MeOH (95:5), obtiéndose **82c** (2.8 g, 70 %) como una mezcla de isómeros en proporción 4:1.

$^1$H-RMN (200 MHz, DMSO-$d^6$): forma ceto δ = 11.86 (s ancho, 2H, NH), 7.14-7.09 (m, 2 H), 7.06-7.03 (m, 2 H), 6.23-6.15 (m, 2 H), 4.22 (s, 2 H); forma enol: δ = 16.75 (s, ancho, 1H, OH), 11.81 (s ancho, 2H, NH), 7.15-7.11 (m,2 H), 6.98-6.93 (m, 2 H), 6.65 (s, 1H), 6.27-6.24 (m,2H).

### 5.4.3. Síntesis de BODIPYs 80a y 80d

#### *5.4.3.1. Síntesis de 83a*

Siguiendo el método *5.4.1.1* se hace reaccionar **75**[16] (50 mg, 0.21 mmol), **82a** (0.043 mL, 0.42 mmol), $Na_2CO_3$ (45 mg, 0.42 mmol) y CuTc (44 mg, 23 mmol) en DMSO (2 mL). El crudo de reacción se purificó por cromatografía en columna, empleando como eluyente una mezcla hexano/AcOEt (9:1). Se obtienen **83a**[13] (72 mg, 80%) como un sólido naranja.

$^1$H-RMN (200 MHz, $CDCl_3$): δ 16.94 (s, OH, 1H), 7.94 (s ancho, 2H), 7.07 (s ancho, 2H), 6.57(s ancho, *2*H), 2.03 (s, 6H).

#### *5.4.3.2. Síntesis de 83b*

Siguiendo el método *5.4.1.1* se hace reaccionar **75**[2] (50 mg, 0.21 mmol), **82b** (94 mg, 0.42 mmol), $Na_2CO_3$ (45 mg, 0.42 mmol) y CuTc (44 mg, 0.23 mmol) en DMSO (2 mL). El crudo de reacción se purifica por cromatografía en columna, empleando como eluyente una mezcla hexano/AcOEt (5:5). Se obtiene **83b** (49 mg, 53%) como un sólido naranja.

$^1$H-RMN (200 MHz, $CDCl_3$): δ 18.31 (s, OH, 1H), 7.64 (s ancho, 2H), 7.43 (s ancho, 2H), 7.42 (s ancho, 2H), 7.23-7.19 (m, 6H), 6.85 (s, 2H), 6.24 (s, 2H); HRMS-EI: calculado para ($C_{26}H_{21}BF_2N_2O_2$) 442.1674, encontrado 442.1632.

#### *5.4.3.3. Síntesis de 83c*

Siguiendo el método *5.4.1.1* se hace reaccionar **75**[2] (50 mg, 0.21 mmol), **82c** (85 mg, 0.42 mmol), $Na_2CO_3$ (45 mg, 0.42 mmol) y CuTc (44 mg, 0.23 mmol) en DMSO (2 mL). El crudo de reacción se purifica por cromatografía en columna, empleando como eluyente una mezcla hexano/AcOEt (5:5). Se obtiene **83c** (33 mg, 40%) como un sólido naranja.

$^1$H-RMN (200 MHz, $CDCl_3$): δ 18.90 (s, 1H), 9.40 (s, NH, 2H), 7.89 (s, 2H), 7.04 (s, 2H), 6.88 (s, 2H), 6.36 (s, 2H), 6.27 (s, 2H), 6.05 (s, 2H); $^{13}$C-RMN (76 MHz, $CDCl_3$): δ 174.9, 145.2 (CH), 137.2, 130.5(CH), 126.5, 126.4, 123.6 (CH), 118.9 (CH), 118.0 (CH), 112.5 (CH); IR (puro): 3125, 2978, 1742, 1555, 1481, 1387, 987 $cm^{-1}$; HRMS-EI: calculado para ($C_{20}H_{15}BF_2N_2O_4$) 392.1253, encontrado 392.1293.

#### *5.4.3.4. Síntesis de 83d*

Siguiendo el método *5.4.1.1* se hace reaccionar **40**[16] (50 mg, 0.19 mmol), **82a** (0.04 mg, 0.38 mmol), $Na_2CO_3$ (40 mg, 0.38 mmol) y CuTc (39 mg, 0.21 mmol) en DMSO (2 mL). El crudo de reacción se purificó por cromatografía en columna, empleando como eluyente una mezcla hexano/AcOEt (5:5). Se obtiene **83d**[13] (61 mg, 80%) como un sólido naranja.

$^1$H-RMN (200 MHz, $CDCl_3$): δ 16.88 (s, OH, 1H), 6.85 (s ancho, 2H), 6.29 (s ancho, 2H), 2.65 (s, 6H), 2.01 (s, 6H).

#### *5.4.3.5. Síntesis de 80a*

Siguiendo el método *5.4.1.2* se hace reaccionar **83a** (30 mg, 0.10 mmol) y $BF_3 \cdot Et_2O$ (0.04 mL, 0.31 mmol) en tolueno (3 mL) a 80 ºC. El crudo de reacción se purifica por cromatografía en columna, empleando como eluyente una mezcla hexano/AcOEt (7:3). Se obtiene **80a** (5 mg, 14%) como un sólido naranja.

$^1$H-RMN (200 MHz, $CDCl_3$): δ 8.01 (s ancho, 2H), 7.00 (s ancho, 2H), 6.63 (s ancho, 2H), 2.28 (s, 6H); HRMS-EI: calculado para ($C_{14}H_{12}B_2F_4N_2O_2$) 338.1321, encontrado 338.1345.

#### *5.4.3.6. Síntesis de 80d*

Siguiendo el método *5.4.1.2* se hace reaccionar **83d** (40 mg, 0.13 mmol) y $BF_3 \cdot Et_2O$ (0.05 mL, 0.38 mmol) en tolueno (3 mL) a 80 ºC. El crudo de reacción se purifica por cromatografía en columna, empleando como eluyente una mezcla hexano/AcOEt (7:3). Se obtiene **80d** (9 mg, 17%) como un sólido naranja.

$^1$H.RMN (200 MHz, $CDCl_3$): δ 6.71 (s ancho, 2H), 6.27 (s ancho, 2H), 2.59 (s, 6H), 2.19 (s, 6H); $^{13}$C-RMN (76 MHz, $CDCl_3$): δ 191.9, 160.7, 135.8, 134.9, 128.7 (CH), 128.4, 121.1 (CH), 15.1 ($CH_3$), 14.8 ($CH_3$); IR (puro): 2979, 1789, 1445, 1325, 1114, 897 $cm^{-1}$; HRMS-EI: calculado para ($C_{16}H_{16}B_2F_4N_2O_2$) 365.9269, encontrado 365.9223.

### 5.4.4. Síntesis del BODIPYs 83g

#### *5.4.4.1. Síntesis de 84*

Siguiendo el método *5.4.1.3* se hace reaccionar **40**[16] (100 mg, 0.38 mmol) y NBS (141 mg, 0.8 mmol) en DCM (10 mL) a temperatura ambiente. El crudo de reacción se purifica por cromatografía en columna, empleando como eluyente una mezcla hexano/AcOEt (95:5). Se obtiene **84** (144 mg, 90%) como un sólido rojo.

$^1$H-RMN (200 MHz, CDCl3): δ 6.89(s ancho, 2H), 2.98 (s, 3H), 2.45 (s, 6H); HRMS-EI: calculado para ($C_{12}H_{11}BBr_2F_2N_2S$) 421.8071, encontrado 421.8032.

#### *5.4.4.2. Síntesis de 85*

Siguiendo el método *5.4.1.3* se hace reaccionar **84** (160 mg, 0.38 mmol), **82a** (0.08 mg, 0.75 mmol), $Na_2CO_3$ (80 mg, 0.75 mmol) y CuTc (79 mg, 0.41 mmol) en DMSO (2 mL). El crudo de reacción se purifica por cromatografía en columna, empleando como eluyente una mezcla hexano/AcOEt (5:5). Se obtienen **85d** (72 mg, 40%) como un sólido naranja.

$^1$H-RMN (200 MHz, $CDCl_3$): δ 16.85 (s, OH, 1H), 6.96 (s ancho, 2H), 2.63 (s, 6H), 2.02 (s, 6H); $^{13}$C-RMN (76 MHz, $CDCl_3$): δ 190.2, 156.4, 134.7, 133.5, 127.7 (CH), 108.7, 105.1, 23.1 ($CH_3$), 12.6 ($CH_3$); IR (puro): 3115, 2977, 1729, 1565, 1423, 1387, 1023 $cm^{-1}$; HRMS-EI: calculado para ($C_{16}H_{15}BBr_2F_2N_2O_2$) 475.9328, encontrado 475.9290.

#### *5.4.4.3. Síntesis de 83g*

En un matraz de dos bocas provisto de agitación magnética y refrigerante de reflujo se introduce, bajo atmósfera de argón, **85** (20 mg, 0.042 mmol), ácido 4-formilborónico (15 mg, 0.1 mmol), $CsCO_3$ (55 mg, 0.17 mmol) y una punta de espátula de (c-hex)$_3$P·$HBF_4$ y $Pd_2(dba)_3$ en una mezcla de THF /$H_2O$ (5 mL, 4:1 v/v), calentando la reacción a 55 ºC. La reacción se sigue por cromatografía en capa fina hasta observarse que todo el material de partida se ha consumido. Posteriormente, se hidroliza con una disolución de $Na_2CO_3$ saturada y se extrae varias veces con DCM. Las fases orgánicas se secan sobre $MgSO_4$, se filtra y se elimina el disolvente a presión reducida. El crudo se purifica en cromatografía en columna empleando cuna mezcla hexano/AcOEt (95:5). Se obtiene **83g** (7 mg, 30 %) como un sólido rojo.

$^1$H-RMN (200 MHz, $CDCl_3$): δ 16.85 (s, OH, 1H), 9.98 (s, CHO, 2H), 7.88 (d, *J* = 8.1 Hz, 4H), 7.51 (d, *J* = 8.1 Hz, 4H), 6.99 (s, 2H), 2.74 (s, 6 H), 2.03 (s, 6 H); $^{13}$C-RMN (76 MHz, $CDCl_3$): δ 191.4 (CHO), 156.9, 139.7, 135.3, 135.2, 133.6, 130.1 (CH), 128.5 (CH), 126.6 (CH), 106.5, 29.7 ($CH_3$), 24.2 ($CH_3$); IR (puro): 3105, 2979, 2753 1736, 1502, 1443, 1355, 987 $cm^{-1}$; HRMS-EI: calculado para ($C_{30}H_{25}BF_2N_2O_4$) 526.1985, encontrado 526.1979.

### 5.4.5. Síntesis del BODIPYs 86a-c

#### *5.4.5.1. Síntesis de 86a*

Siguiendo el método *5.4.1.5* se hace reaccionar **75**[2] (50 mg, 0.21 mmol), ácido 4-acetofenil borónico (103 mg, 0.63 mmol), CuTc (120 mg, 0.63 mmol) y una punta de espátula de TFP y $Pd_2(dba)_3$ en THF (2 mL). El crudo de reacción se purifica por cromatografía en columna, empleando como eluyente una mezcla hexano/AcOEt (9:1). Se obtiene **86a** (47 mg, 72%) como un sólido naranja.

$^1$H-RMN (200 MHz, $CDCl_3$): 8.09 (d, *J* = 8.4 Hz, 2H), 7.89 (s, 2H), 7.73 (d, *J* =8.4 Hz, 2H) 6.93 (d, *J* = 4.2 Hz, 2H), 6.38 (d, *J* = 4.2 Hz, 2H), 2.02 (s, 3H); HRMS-EI: calculado para ($C_{17}H_{13}BF_2N_2O$) 310.1073, encontrado 310.1065.

#### *5.4.5.2. Síntesis de 86b*

Siguiendo el método *5.4.1.5* se hicieron reaccionar **75**[2] (50 mg, 0.21 mmol), ácido 4-(carboximeti)lfenil borónico (113 mg, 0.63 mmol), CuTc (120 mg, 0.63 mmol) y una punta de espátula de TFP y $Pd_2(dba)_3$ en THF (2 mL). El crudo de reacción se purifica por cromatografía en columna, empleando como eluyente una mezcla hexano/AcOEt (9:1). Se obtiene **86b**[18] (66 mg, 80%) como un sólido naranja.

$^1$H-RMN (200 MHz, $CDCl_3$): 8.28 (d, *J* = 8.7 Hz, 2H), 7.91 (s, 2H), 7.72 (d, *J* =8.7 Hz, 2H) 6.90 (d, *J* = 4.5 Hz, 2H), 6.37 (d, *J* = 4.5 Hz, 2H), 3.81 (s, 3H).

#### *5.4.5.3. Síntesis de 86c*

Siguiendo el método *5.4.1.5* se hicieron reaccionar **75**[2] (50 mg, 0.21 mmol), ácido 4-carboxilfenil borónico (104 mg, 0.63 mmol), CuTc (120 mg, 0.63 mmol) y una punta de espátula de TFP y $Pd_2(dba)_3$ en THF (2 mL). El crudo de reacción se purifica por cromatografía en columna, empleando como eluyente una mezcla hexano/AcOEt (8:2). Se obtienen **86c**[17] (61 mg, 75%) como un sólido naranja.

$^1$H-RMN (200 MHz, $CDCl_3$): 10.92 (s, ancho, OH, 1H), 8.31 (d, *J* = 8.4 Hz, 2H), 7.93 (s, 2H), 7.72 (d, *J* =8.4Hz, 2H) 6.95 (d, *J* = 4.3 Hz, 2H), 6.39 (d, *J* = 4.3 Hz, 2H).

### 5.4.6. Síntesis del BODIPYs 88

#### *5.4.6.1. Síntesis de 90*

Siguiendo el método *5.4.1.5* se hicieron reaccionar **40**[16] (40 mg, 0.15 mmol), ácido 5-bromo-2-tiofenborónico (100 mg, 0.45 mmol), CuTc (83 mg, 0.45 mmol) y una punta de espátula de TFP y $Pd_2(dba)_3$ en THF (2 mL). El crudo de reacción se purificó por cromatografía en columna, empleando como eluyente una mezcla hexano/AcOEt 8:2. Se obtienen **90** (44 mg, 78%) como un sólido naranja.

$^1$H-RMN (200 MHz, $CDCl_3$): δ 7.08 (s, 2H), 6.95 (d, *J* = 3.3 Hz, 2H), 6.22 (d, *J* = 3.6 Hz, 2H), 2.56 (s, 6H); $^{13}$C-RMN (76 MHz, $CDCl_3$) δ 158.2, 136.1, 133.9, 133.2, 131.7 (CH), 130.6 (CH), 130.1 (CH), 119.7 (CH), 116.9, 14.97 ($CH_3$); IR (puro): 2989, 1736, 1555, 1423, 1328, 987 $cm^{-1}$; HRMS-EI: calculado para ($C_{15}H_{12}BBrF_2N_2S$) 379.9866, encontrado 379.9731.

#### *5.4.6.2. Síntesis de 88*

Siguiendo el método *5.4.1.4* se hicieron reaccionar **40**[16] (70 mg, 0.18 mmol), ácido (4-fenil)difenilaminoborónico (160 mg, 0.55 mmol), $Na_2CO_3$ (117 mg, 1.1 mmol) y una punta de espátula de $Pd(PPh_3)_4$ en una mezclaDME/$H_2O$ (5 mL, 4:1 v/v). El crudo de reacción se purificó por cromatografía en columna, empleando como eluyente una mezcla hexano/AcOEt (8:2). Se obtiene **88** (88 mg, 90%) como un sólido naranja.

$^1$H-RMN (200 MHz, $CDCl_3$): δ 7.39 (d, *J* = 8.5 Hz, 2H), 7.28 (d, *J* = 3.9 Hz, 1H), 7.16-7.12 (m, 5H), 7.05-704 (m, 7H), 6.97-6.94 (m, 4H), 6.19 (d, *J* = 3.9 Hz, 1H), 2.55 (s, 6H); HRMS-EI: calculado para ($C_{33}H_{26}BF_2N_3S$) 545.1919, encontrado 545.1942.

### 5.4.7. Síntesis del BODIPYs 92

#### *5.4.7.1. Síntesis de 91*

Siguiendo el método *5.4.1.3* se hicieron reaccionar **88** (50 mg, 0.09 mmol) y NBS (34 mg, 0.19 mmol) en DCM (10 mL) a temperatura ambiente. El crudo de reacción se purifica por cromatografía en columna, empleando como eluyente una mezcla hexano/AcOEt (95:5). Se obteniene **91** (63 mg, 82%) como un sólido rojo.

$^{1}$H-RMN (200 MHz, $CDCl_3$): δ 7.45 (d, *J* = 8.6 Hz, 2H), 7.36 (d, *J* = 3.9 Hz, 1H), 7.33 (d, *J* = 8.8 Hz, 4H), 7.27 (s, 1H), 7.16 (s, 2H), 7.00 (d, *J* = 8.6 Hz, 1H), 6.92 (d, *J* = 8.8 Hz, 4H), 2.56 (s, 6H); $^{13}$C-RMN (76 MHz, $CDCl_3$): δ 155.2, 150.3, 147.7, 145.8, 134.5, 134.0 (CH), 132.6 (CH), 132.3, 130.1 (CH), 127.5, 127.3 (CH), 126.2 (CH), 123.6 (CH), 116.6, 108.8, 13.42 ($CH_3$); IR (puro): 2979, 1748, 1533, 1401, 1317, 987 $cm^{-1}$; HRMS-EI: calculado para ($C_{33}H_{22}BBr_4F_2N_3S$) 856.8429, encontrado 856.8399.

### *5.4.7.2. Síntesis de 92*

Siguiendo el método *5.4.1.4* se hicieron reaccionar **91** (40 mg, 0.05 mmol), ácido 2-tiofenborónico (47 mg, 0.37 mmol), $Na_2CO_3$ (59 mg, 0.56 mmol) y una punta de espátula de $Pd(PPh_3)_4$ en una mezclaDME/$H_2O$ (5 mL, 4:1 v/v). El crudo de reacción se purifica por cromatografía en columna, empleando como eluyente una mezcla hexano/AcOEt (8:2). Se obtiene **92** (30 mg, 70%) como un sólido azul.

$^{1}$H-RMN (200 MHz, $CDCl_3$): δ 7.50-7.74 (m, 5H), 7.42 (d, *J* = 3.7 Hz, 1H), 7.31 (d, *J* = 3.8 Hz, 1H), 7.21-7.17 (m, 8H), 7.10-7.07 (m, 6H), 7.06-7.05 (m, 3H), 7.02-6.98 (m, 4H), 2.76 (s, 6H); $^{13}$C-RMN (76 MHz, $CDCl_3$): δ 154.8, 149.7, 147.8, 146.2, 143.9, 136.1, 134.4, 133.6 (CH), 132.9, 132.8, 129.9, 128.1 (CH), 127.7 (CH), 127.6, 127.36, 127.1 (CH), 127.0 (CH), 126.8 (CH), 124.9 (CH), 124.8 (CH), 124.7 (CH), 124.4 (CH), 124.3, 123.8, 123.6 (CH), 123.3 (CH), 122.6 (CH), 14.27 ($CH_3$); IR (puro): 2989, 1798, 1505, 14398, 1317, 989 $cm^{-1}$; HRMS-EI: calculado para ($C_{49}H_{34}BF_2N_3S5$) 873.1415, encontrado 873.1452.

## 5.5. BIBLIOGRAFÍA


[1] a) A. Loudet, K. Burgess, *Chem. Rev.* **2007**, *107*, 4891-4932; b) R. Ziessel, G. Ulrich, A. Harriman, *New J. Chem.* **2007**, *31*, 496-501; c) G. Ulrich, R. Ziessel, A. Harriman, *Angew. Chem. Int. Ed.* **2008**, *47*, 1184-1201; d) A. C. Benniston, G. Copley, *Phys. Chem. Chem. Phys.* **2009**, *11*, 4124-4131; e) M. Benstead, G. H. Mehl, R. W. Boyle, *Tetrahedron* **2011**, *67*, 3573-3601; f) N. Boens, V. Leen, W. Dehaen, *Chem. Soc. Rev.* **2012**, *41*, 1130-1172; g) H. Lu, J. Mack, Y. Yang, Z. Shen, *Chem. Soc. Rev.* **2014**, *43*, 4778-4823.

[2] T. V. Goud, A. Tutar, J.-F. Biellmann, *Tetrahedron* **2006**, *62*, 5084-5091.

[3] a) C. F. A. Gomez-Duran, I. Garcia-Moreno, A. Costela, V. Martin, R. Sastre, J. Bañuelos, F. Lopez Arbeloa, I. Lopez Arbeloa, E. Pena-Cabrera, *Chem. Commun.* **2010**, *46*, 5103-5105; b) J. Bañuelos, V. Martin, C. F. A. Gomez-Duran, I. J. A. Cordoba, E. Peña-Cabrera, I. Garcia-Moreno, A. Costela, M. E. Perez-Ojeda, T. Arbeloa, I. L. Arbeloa, *Chem. Eur. J.* **2011**, *17*, 7261-7270; c) J. O. Flores-Rizo, I. Esnal, C. A. Osorio-Martinez, C. F. A. Gomez-Duran, J. Banuelos, I. Lopez Arbeloa, K. H. Pannell, A. J. Metta-Magana, E. Peña-Cabrera, *J. Org. Chem.* **2013**, *78*, 5867-5877.

[4] a) E. Peña-Cabrera, A. Aguilar-Aguilar, M. Gonzalez-Dominguez, E. Lager, R. Zamudio-Vazquez, J. Godoy-Vargas, F. Villanueva-Garcia, *Org. Lett.* **2007**, *9*, 3985-3988; b) I. J. Arroyo, R. Hu, G. Merino, B. Z. Tang, E. Peña-Cabrera, *J. Org. Chem.* **2009**, *74*, 5719-5722.

[5] V. Leen, P. Yuan, L. Wang, N. Boens, W. Dehaen, *Org. Lett.* **2012**, *14*, 6150-6153.

[6] R. Misra, B. Dhokale, T. Jadhav, S. M. Mobin, *New J. Chem.* **2014**, *38*, 3579-3585.

[7] H. Wang, M. G. H. Vicente, F. R. Fronczek, K. M. Smith, *Chem. Eur. J.* **2014**, *20*, 5064-5074.

[8] E. Palao, A. R. Agarrabeitia, J. Banuelos-Prieto, T. A. Lopez, I. Lopez-Arbeloa, D. Armesto, M. J. Ortiz, *Org. Lett.* **2013**, *15*, 4454-4457.

[9] E. Palao, S. de la Moya, A. R. Agarrabeitia, I. Esnal, J. Banuelos, I. Lopez-Arbeloa, M. J. Ortiz, *Org. Lett.* **2014**, *16*, 4364-4367.

[10] a) R. C. Mehrotra, *Pure Appl. Chem.* **1988**, *60*, 1349-1356; bP. C. Andrews, T. Beck, B. H. Fraser, P. C. Junk, M. Massi, B. Moubaraki, K. S. Murray, M.

Silberstein, *Polyhedron* **2009**, *28*, 2123-2130; c) P. A. Vigato, V. Peruzzo, S. Tamburini, *Coord. Chem. Rev.* **2009**, *253*, 1099-1201.

[11] a) X. Zhang, R. Lu, J. Jia, X. Liu, P. Xue, D. Xu, H. Zhou, *Chem. Commun.* **2010**, *46*, 8419-8421; b) L. Kersten, S. Roesner, G. Hilt, *Org. Lett.* **2010**, *12*, 4920-4923; c) A. Chaicham, S. Kulchat, G. Tumcharern, T. Tuntulani, B. Tomapatanaget, *Tetrahedron* **2010**, *66*, 6217-6223; dY. Haketa, S. Sakamoto, K. Chigusa, T. Nakanishi, H. Maeda, *J. Org. Chem.* **2011**, *76*, 5177-5184; e) Y. Terashima, T. Sakurai, Y. Bando, S. Seki, H. Maeda, *Chem. Mater.* **2013**, *25*, 2656-2662; f) M. Tanaka, E. Ohta, A. Sakai, Y. Yoshimoto, K. Mizuno, H. Ikeda, *Tetrahedron Lett.* **2013**, *54*, 4380-4384.

[12] J.-H. Olivier, A. Haefele, P. Retailleau, R. Ziessel, *Org. Lett.* **2010**, *12*, 408-411.

[13] B. D. Gutierrez-Ramos, J. Bañuelos, T. Arbeloa, I. L. Arbeloa, P. E. Gonzalez-Navarro, K. Wrobel, L. Cerdan, I. Garcia-Moreno, A. Costela, E. Peña-Cabrera, *Chem. Eur. J.* **2015**, *21*, 1755-1764.

[14] D. Lim, G. Zhou, A. E. Livanos, F. Fang, D. M. Coltart, *Synthesis* **2008**, *2008*, 2148-2152.

[15] H. Maeda, Y. Kusunose, *Chemistry – A European Journal* **2005**, *11*, 5661-5666.

[16] Comercializado por Cuántico de México.

[17] A. Cui, X. Peng, J. Fan, X. Chen, Y. Wu, B. Guo, *J. Photochem. Photobiol. A* **2007**, *186*, 85-92.

[18] J. A. Melanson, D. A. Smithen, T. S. Cameron, A. Thompson, *Can. J. Chem.* **2014**, *92*, 688-694.

[19] S. Erten-Ela, M. D. Yilmaz, B. Icli, Y. Dede, S. Icli, E. U. Akkaya, *Org. Lett.* **2008**, *10*, 3299-3302.

# CAPÍTULO 6. CONCLUSIONES

# 6. CONCLUSIONES

1. Se ha desarrollado y sintetizado un serie de nuevos sistemas de colorantes orgánicos que han resultado ser, en su mayoría, colorantes láser con mejor eficiencia y estabilidad que los actualmente comercializados.

2. Se han sintetizado nuevos colorantes fluorados a través de la fluoración directa de colorantes comerciales, obteniéndose láseres más eficientes y estables que los precursores no fluorados.

3. Se ha desarrollado una metodología que implica reacciones de sustitución electrófila aromática que ha permitido acceder selectivamente a mono-, di- y poli-halo-BODIPYs (derivados clorados y yodados).

4. Los nuevos cloroBODIPYs han resultado ser unos excelentes colorantes láser, cuya eficiencia y estabilidad está modulada por el número y posición de los átomos de cloro unidos al núcleo de BODIPY.

5. Esta misma metodología ha permitido obtener también poli-yodoBODIPYs que son eficientes generadores de oxígeno singlete, y, como tales, potenciales sensibilizadores para terapia fotodinámica.

6. A través de un diseño racional y sencillo se han sintetizado una nueva serie de colorantes con emisión láser sintonizable en la región 590-700 nm. Estos nuevos colorantes han resultado ser más estables que algunos de los actualmente comercializados con emisión láser en la misma región espectral.

7. Se ha diseñado un protocolo de síntesis fácil, barato y universal que ha permitido mejorar las propiedades fotofísicas y de emisión láser de una serie de BODIPYs comérciales. Este protocolo se basa en la sustitución de los átomos de flúor sobre el boro por diferentes sustituyentes con carácter electroatractor obtiéndose así nuevos *O*- y *E*-BODIPYs.

8. Se han diseñado y sintetizado una serie de cassettes con absorción pancromática pero emisión monocrómatica, mediante la combinación de varios colorantes orgánicos (BODIPYs, perileno y cumarinas).

9. Los sistemas multicromofóricos obtenidos presentan, tras excitación a 355 nm, una mejor fotoestabilidad y emisión láser en la región roja del espectro que algunos colorantes comerciales empleados como referencia en la misma región espectral.

10. Se ha sintetizado un complejo multicromofórico constituido por BODIPYs con emisión en diferentes regiones del espectro y con una disposición ortogonal entre los fragmentos, lo que ha permitido obtener un sistema que presenta un comportamiento dual, pudiendo utilizarse como sonda fluorescente y generador de oxígeno singlete.

11. Se han diseñado y sintetizado nuevos sistemas de dicetonatos de boro-BODIPYs y sistemas trifeniltiofenamina-BODIPY a través de la posición *meso* del BODIPYs, con posibles aplicaciones como láseres de colorante como células solares.

12. Como conclusión general puede indicarse que el trabajo realizado en esta Tesis ha permitido la obtención de nuevos sistemas de colorantes con propiedades fotofísicas optimizadas para diferentes aplicaciones fotónicas y biofotónicas. El trabajo ha quedado recogido, hasta este momento, en 8 artículos publicados en revistas de alto índice de impacto y 3 artículos más en fase de redacción en estos momentos.

# ANEXOS

IOP Publishing | Astro Ltd
Laser Physics Letters
Laser Phys. Lett. **11** (2014) 115818 (7pp)
doi:10.1088/1612-2011/11/11/115818

# Increased laser action in commercial dyes from fluorination regardless of their skeleton

**G Duran-Sampedro[1], A R Agarrabeitia[1], T Arbeloa Lopez[2], J Bañuelos[2,5], I López-Arbeloa[2], J L Chiara[3], I Garcia-Moreno[4,5] and M J Ortiz[1,5]**

[1] Departamento de Química Orgánica, Facultad de Ciencias Químicas, Universidad Complutense de Madrid, Ciudad Universitaria, 28040 Madrid, Spain
[2] Departamento de Química Física, Universidad del País Vasco-EHU, Aptdo. 644, 48080 Bilbao, Spain
[3] Instituto de Química Orgánica General, IQOG-CSIC, Juan de la Cierva 3, 28006 Madrid, Spain
[4] Instituto de Química-Física "Rocasolano", IQFR-CSIC, Serrano 119, 28006 Madrid, Spain

E-mail: mjortiz@quim.ucm.es

Received 17 March 2014, revised 17 August 2014
Accepted for publication 18 August 2014
Published 29 September 2014

**Abstract**
The direct and simple fluorination of representative organic laser dyes with emission covering the entire visible spectrum, from blue to red, including Coumarin 460, Pyrromethene 546, Rhodamine 6G and Perylene Red, enhances laser efficiencies by a factor up to 1.8 with respect to the corresponding non-fluorinated parent dyes. More importantly, fluorination also significantly enhances the photostability of the dyes, even under drastic laser pumping conditions.

Keywords: laser dye, direct monofluoration, fluorinated dyes, photostability

S Online supplementary data available from stacks.iop.org/LPL/11/115818/mmedia

(Some figures may appear in colour only in the online journal)

## 1. Introduction

Optical imaging approaches are emerging as promising non-invasive, real-time, high-resolution platforms in cancer detection and prognosis determination in the disease's early stages [1–7]. The reliability and sensitivity of modern biological fluorescence microscopy such as fluorescence correlation spectroscopy, fluorescence intensity distribution analysis or photon-counting histogram analysis, rely on the brightness and photostability of fluorescent probes, which allows the acquisition of as much fluorescence signal as possible in the shortest time [8–14]. Compared to wide-field fluorescence microscopy, these new optical techniques require excitation conditions that are several orders of magnitude more severe, thus demanding fluorophores with improved photostability since irradiation with a focused laser beam at high power density significantly increases the photobleaching rate of the fluorescent probes, which, in practice, reduces the resolution of the experimental technique.

In recent years, increased efforts have been witnessed regarding the design and synthesis of organic fluorescent dyes with enhanced photostability [15–23]. Despite the numerous advances in fluorescent dye synthesis, fluorescent probe development is limited by a lack of knowledge of the specific molecular properties responsible for producing optimum emission characteristics. In addition, design rules are not sufficiently understood and are thus not helpful as a guide for the development of more efficient and photostable fluorophores performance under the demanding excitation conditions of modern fluorescence microscopy. As a result, the number of fluorophores that have found widespread use in these optical techniques is a limited subset of the many thousands that have been synthesized.

Therefore, a major challenge is designing a synthesis strategy to improve the emission properties of commercial fluorophores throughout the visible spectrum under drastic laser pumping conditions regardless of their structure and composition, thus overcoming restrictions imposed by the physical properties of the fluorophores. This task can be addressed by making suitable structural modifications on scaffolds of

[5] Authors to whom any correspondence should be addressed.

 © 2014 Astro Ltd Printed in the UK

well-known chromophores. In this regard, fluorination arises as a good alternative since the C–F bond is highly polarized and thus presents a significant electrostatic component that makes it the strongest bond in organic chemistry. As a consequence, organofluorine molecules normally have higher chemical and thermal stability and lower polarizability than analogous non-fluorinated molecules as they are generally more hydrophobic and more lipophilic [24, 25]. More interestingly, fluorine-substituted chromophores generally show higher photostability [26–28] and exhibit greater resistance to photobleaching and reduced reactivity towards singlet oxygen. They also display enhanced fluorescence quantum yields [29–31] and reduced aggregation [32, 33] compared to their non-fluorinated counterparts.

In this paper, we describe a synthetic route for the monofluorination of a number of representative chromophores as a general strategy to improve the performance of dyes regardless of their structure and composition as well as the photophysical and laser characteristics of these novel fluorophores by looking for improved tunable laser dyes from the blue to red parts of the visible spectrum under drastic pumping conditions. Among the wide variety of existing laser dyes covering the entire visible spectrum, coumarins, borondipyrromethenes (BODIPY), rhodamines and perylenes (figure 1) stand out due to their strong absorption profile and bright fluorescence and laser emission. In particular, within each laser dye family we have chosen a candidate, namely Coumarin 460 (Cu460, compound **1**), Pyrromethene 546 (PM546, **4**), Rhodamine 6G (Rh6G, **6**) and Perylene Red (Per Red, **8**), to be fluorinated. The particular dyes were chosen because they can be considered benchmarks in terms of laser performance in their respective spectral regions.

## 2. Experiment

### 2.1. Materials

Laser dyes Coumarin 460, Pyrromethene 546, Rhodamine 6G and Perylene Red were purchased from Exciton and used as received. Solvents for laser and photophysical studies were of spectroscopic grade (Merck, Aldrich or Sigma) and were used without purification.

### 2.2. Synthesis

New fluorinated dyes were synthesized by direct fluorination of commercially available laser dyes using Selectfluor™ or $XeF_2$ as fluorination reagents. Synthetic procedures and characterization of the new dyes are described in detail in the supporting information (SI) (stacks.iop.org/LPL/11/115818/mmedia).

### 2.3. Photophysical properties

Photophysical properties in diluted solutions (around $2 \times 10^{-6}$M) were registered by adding the corresponding solvent (spectroscopic grade) to the residue from the adequate amount of a concentrated stock solution in acetone after vacuum evaporation of this solvent. UV-Vis absorption and fluorescence spectra were recorded on a Varian model CARY 4E spectrophotometer and a SPEX Fluorolog 3–22 spectrofluorimeter, respectively. Fluorescence quantum yield ($\phi$) was obtained from corrected spectra, to account for detector sensitivity with the monochromator wavelength using diluted dye solutions of standard references in each spectral region as follows: quinine sulphate ($\phi^r = 0.54$ in 0.5 M $H_2SO_4$), fluorescein ($\phi^r = 0.93$ in 0.1 M NaOH) and cresyl violet ($\phi^r = 0.54$ in methanol). Radiative decay curves were measured by the time correlated single-photon counting technique (Edinburgh Instruments, model FL920, equipped with a microchannel plate detector, Hamamatsu C4878) with picosecond time-resolution. Fluorescence emission was monitored at the maximum emission wavelength after excitation at 370 nm, 470 nm and 530 nm by means of a diode laser (PicoQuant, model LDH370, 470 and 530) with 150 ps FWHM pulses. The fluorescence lifetime ($\tau$) was obtained after the deconvolution of the instrumental response signal from the recorded decay curves by means of an iterative method. The goodness of the exponential fit was controlled by statistical parameters (chi-square, Durbin-Watson and the analysis of the residuals). The radiative ($k_{fl}$) and non-radiative ($k_{nr}$) rate constants were calculated from the fluorescence quantum yield and lifetime: $k_{fl} = \phi/\tau$ and knr = $(1- \phi)/\tau$. Ground state geometry, charge distribution, and molecular orbitals were calculated by means of the density functional theory (B3lYP/6–31 G) as implemented in the Gaussian 09.

### 2.4. Laser properties

Liquid solutions of dyes were contained in 1 cm optical-path quartz cells carefully sealed to avoid solvent evaporation during the experiments. The solutions of the newly synthesized dyes were transversely pumped at different wavelengths matching the maximum absorption of the corresponding dyes: at 355 nm, with 5 mJ $pulse^{-1}$, 8 ns FWHM pulses from the third-harmonic of Q-switched Nd:YAG laser (Spectron SL282G) and at 532 nm with 5.5 mJ, 6 ns FWHM pulses from a frequency-doubled Q-switched Nd:YAG laser (Monocrom OPL-10), both at a repetition rate of 10 Hz. The exciting pulses were line-focused onto the cell, providing pump fluences on the active medium of 110 mJ $cm^{-2}$. The oscillation cavity (2 cm length) consisted of a 90% reflectivity aluminium mirror with the lateral face of the cell as output coupler.

The photostability of the dyes was evaluated by irradiating 10 $\mu$L of a solution in ethyl acetate or ethanol under lasing conditions. The solutions were contained in a cylindrical Pyrex tube (1 cm height, 1 mm internal diameter) carefully sealed to avoid solvent evaporation during the experiments. Although the low optical quality of the capillary tube prevented laser emission from the dyes, information about photostability was obtained by monitoring the decrease in laser-induced fluorescence intensity, excited transversally to the capillary tube, as a function of the number of pump pulses at 10 Hz repetition rate. The fluorescence emission was monitored perpendicular to the exciting beam, collected by an optical

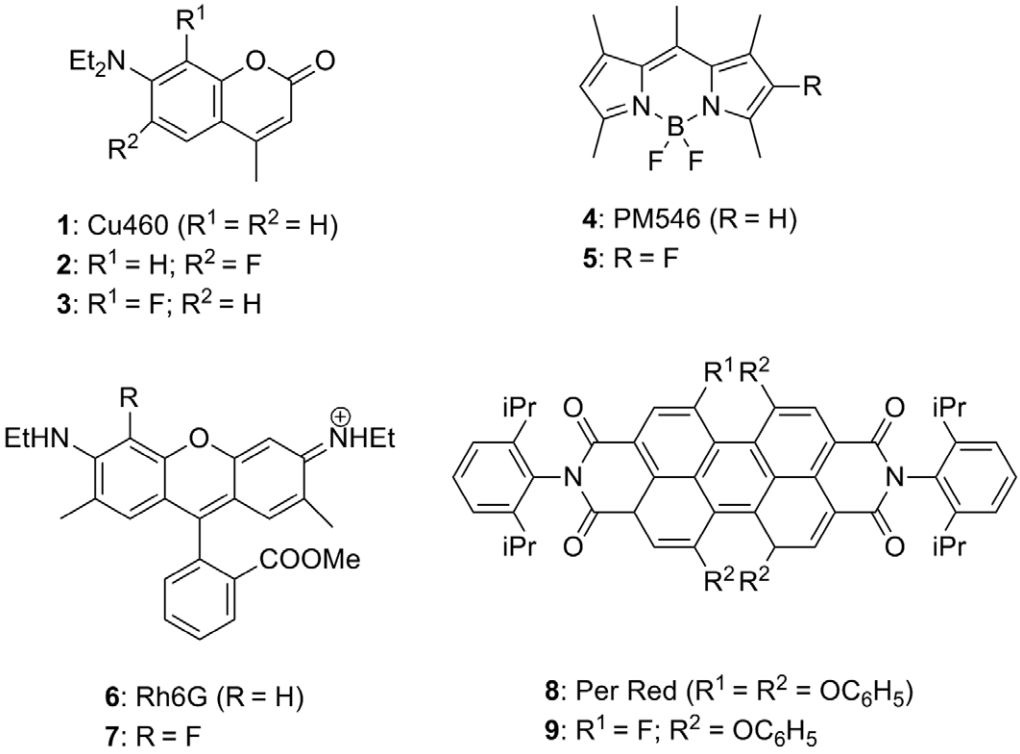


**Figure 1.** Structures of commercially available dyes and their monofluorinated derivatives.

fiber, and imaged onto the input slit of a monochromator (Acton Research corporation) for detection with a charge-coupled device (CCD) (SpectruMM:GS128B). The fluorescence emission was recorded by feeding the signal to the boxcar (Stanford Research, model 250) to be integrated before being digitized and processed by a computer. Each experiment was repeated at least three times. The estimated error in the energy and photostability measurements was 10%.

## 3. Results and discussion

### *3.1. Synthesis*

Synthetic procedures for the preparation of fluorinated heteroaromatic systems include cyclisation strategies involving fluorinated building blocks, substitution of chlorine or bromine (halogen exchange) by fluorine, or direct fluorination of heteroaromatic derivatives by selective transformation of carbon-hydrogen bonds to carbon-fluorine bonds in reactions involving electrophilic fluorination reagents, along with a number of outstanding recently described fluorination processes mediated by transition metals [34–37]. Various approaches have been described in the literature for the direct fluorination of coumarins from electrophilic addition of acetyl hypofluorite [38], Selectfluor™ [39], or fluorine in acid media [40, 41]. Regarding BODIPY dyes, there is only one example of core-fluorinated BODIPY in a discontinued Japanese patent, but neither its synthesis nor spectroscopic data have been described [42]. However, it should be noted that direct fluorination of rhodamines and perylenes bisimides have not been reported.

Here we have carried out direct fluorination of commercially available laser dyes using Selectfluor™ or $XeF_2$ as fluorination reagents with the aim of facilitating access to fluorinated fluorophores. Thus, reaction of **1** (Cu460) with Selectfluor™ gave a complex mixture of products from which 6-fluoro coumarin **2** (21%) and 8-fluoro coumarin **3** (20%) were isolated by column chromatography (figure 1).

Fluorination of **4** (PM546) with $XeF_2$ under microwave irradiation resulted in 2-fluoro-BODIPY **5** in low yield (11%). Similarly, fluorinated rhodamine **7** was prepared in a microwave synthesizer from **6** (Rh6G) and Selectfluor™ under microwave irradiation in 89% isolated yield. Interestingly, fluorination of **8** (Per Red) using $XeF_2$ as the fluorinating reagent afforded a complex mixture from which a major product **9** (27%) was identified (figure 1). The structure elucidation of **9** was carried out by extensive spectroscopic analysis using one- and two-dimensional (1D- and 2D-) NMR spectroscopic and MS-FAB experiments. MS-FAB revealed a molecular ion peak at m/z 1005.7 $[M]^+$, suggesting that the compound is a monofluoro-triphenoxy-substituted perylene bisimide, which obviously originates from the substitution of one phenoxy group by a fluorine atom. $^{19}F$ NMR confirmed the presence of one fluorine atom, and the analysis of the $^1H$ spectrum demonstrated that the protons at C-2, C-5, C-8 and C-11 positions, which appeared as singlets in the starting Per Red **8**, were modified ($\delta$ 8.27, d, $^3J_{HF}$ = 11.2 Hz, 1 H, H-2; 8.07, s, 2 H, H-5 and H-8; 8.02, s, 1 H, H-11). On the other hand, the HMBC correlation between H-2 and C-1 ($\delta$ 159.7, d, $^1J_{CF}$ = 262 Hz, C-F) confirmed the presence of a perylene core proton in an adjacent position to the fluorine atom at C-1. The formation of **9** involved the breaking of ether linkage that is generally stable towards most fluorinating agents; however, some examples of substitution of the alcoxy group by fluorine atoms are known [43].

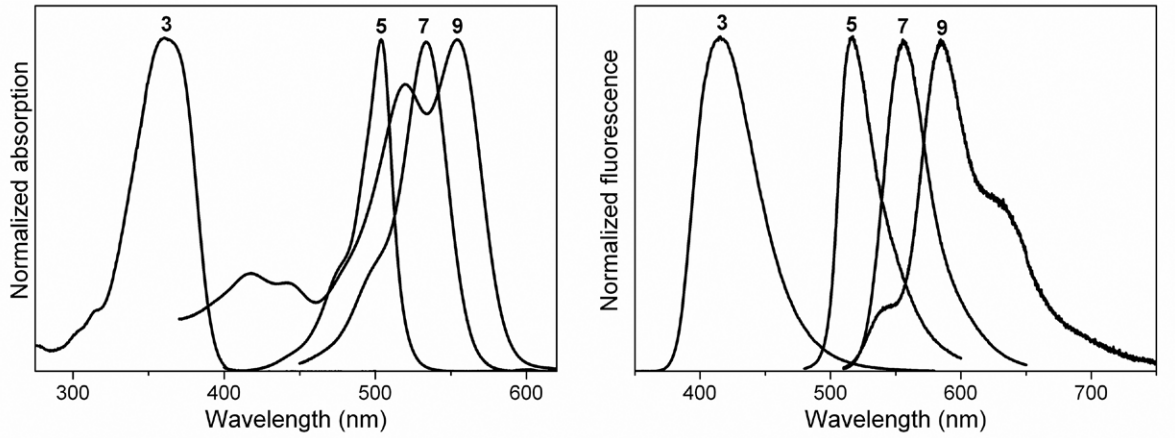


**Figure 2.** Absorption and fluorescence spectra of the fluorinated derivatives of commercially available Cu460, PM546, Rh6G and Per Red in a common solvent (ethanol).

### *3.2. Photophysical properties*

The new dyes exhibit photophysical properties similar to their respective reference compounds. The spectral bands of **1** (Cu460) are located in the more energetic part of the visible spectrum (figure 2), according to a chromene delocalyzed $\pi$-system, which can be described by two main resonance structures (scheme S1). The interaction of the aromatic amine with the benzopyrone core and the specific interactions of the former group with the solvent molecules determine the photophysical properties of the coumarin [44, 45]. The position in which the fluorine atom is attached to the benzopyrone plays a fundamental role. Thus, its grafting along the molecular transversal axis (compound **3**) exerts little influence and the photophysical properties remain similar to those of the reference Cu460, i.e. high fluorescence efficiency in the more apolar media (table 1) and progressive decrease in polar/protic solvents (table S1 (stacks.iop.org/LPL/11/115818/mmedia)). Such evolution can be described by two main theories. The first suggests the presence of a quenching twisted intramolecular charge transfer state (TICT [46, 47]) from the donor amine to the acceptor benzopyrone, which is stabilized in polar media by specific interactions that locate the negative charge at oxygen (scheme S2).

The second is related to the internal conversion processes with hybridization change $sp^2$–$sp^3$ of the amino group (Umbrella Like Motion, ULM [48]). Thus, the interactions described above favour and increase the electronic density at the amino-coumarine bond ($sp^2$), enhancing non-radiative deactivation. On the other hand, the presence of fluorine along the longitudinal axis (**2**) limits the fluorescence efficiency of coumarin (table 1), mainly in the most polar media, in which the decline is very pronounced (table S1 and figure S1 (stacks.iop.org/LPL/11/115818/mmedia)). Indeed, the incorporation of electron donor or acceptor groups (as is the case of the electronegative fluorine atom) aligned in the direction in which the charge transfer takes place enhances the push-pull effect and hence fluorescence quenching (scheme S3 [49]).

BODIPY **4** laser dyes presented spectral bands in a less energetic part of the visible spectrum due to its cyanine-like delocalized $\pi$-system (figure 2). This dye stands out due to its strong spectral bands that are rather independent of the physicochemical properties of the environment. The monofluorination of commercial PM546 (compound **5**) led to a slight decrease in fluorescence efficiency and a more marked diminution in absorption probability (table 1). The gathering of electronic density by the electronegative fluorine at position 2 led to an asymmetric charge transfer distribution between the pyrroles (figure S2 (stacks.iop.org/LPL/11/115818/mmedia)). As result, molar absorption decreases, which correlates with a lower radiative deactivation probability and thereby explains the slightly lower fluorescence quantum yield and longer lifetimes of the fluorinated derivative with respect to the commercial dyes [50].

At lower energies, the spectral bands of **6** (Rh6G) are characterized by a xanthene-like chromophore (figure 1). Its photophysical properties are also controlled by aromatic amine, as in coumarines [51, 52]. Nonetheless, the push-pull effect in rhodamines is less important because the donor and acceptor fragments are interchangeable (scheme S4), while in coumarines, the donor and acceptor parts are clearly differentiated (amine and carbonyl, respectively, table S1 (stacks.iop.org/LPL/11/115818/mmedia)). Thus, the charge transfer character and the influence of the non-radiative pathways (TICT or ULM) described above is lesser, as reflected in the lower dependence of the fluorescence quantum yield on the solvent properties (table S3 (stacks.iop.org/LPL/11/115818/mmedia)). Overall, the photophysical signatures of monoethylated rhodamines are not very sensitive to the surrounding environment. In agreement with the above conclusions for coumarines, the attachment of fluorine in the transversal vertical axis (**7**) has scarce influence of the photophysical properties of xanthene (table 1 [28]) because the charge separation takes place mainly through the longitudinal horizontal axis.

Finally, in the less energetic part of the visible spectrum we considered **8** (Per Red), which is characterized by an extended perylenimide-like delocalized $\pi$-system. One of the main signatures of this dye is its low tendency to aggregate due to the sterical hindrance provided by the side *ortho* isopropyls at the imides (figure S3 (stacks.iop.org/LPL/11/115818/mmedia) [53]). The replacement of a phenoxy by a fluorine atom (**9**)

**Table 1.** Photophysical properties of commercial dyes and their fluorinated derivatives in ethyl acetate (with the exception of rhodamine, where the data are in acetone): absorption ($\lambda_{ab}$) and fluorescence ($\lambda_{fl}$) wavelengths, Stokes shift ($\Delta\nu_{St}$), molar absorption coefficient ($\varepsilon_{max}$), fluorescence quantum yield ($\phi$) and lifetime ($\tau$), radiative ($k_{fl}$) and non-radiative ($k_{nr}$) rate constants. Full photophysical data are listed in tables S1–S4 (stacks.iop.org/LPL/11/115818/mmedia).

| | $\lambda_{ab}$(nm) | $\varepsilon_{max}\cdot10^{-4}$ ($M^{-1}cm^{-1}$) | $\lambda_{fl}$(nm) | $\Delta\nu_{St}$($cm^{-1}$) | $\phi_{fl}$ | $\tau$(ns) | $k_{fl}\cdot10^{-7}$ ($s^{-1}$) | $k_{nr}\cdot10^{-7}$ ($s^{-1}$) |
|---|---|---|---|---|---|---|---|---|
| 1 (Cu460) | 360.5 | 2.4 | 415.5 | 3670 | 1.00 | 3.52 | 28.4 | 0.00 |
| 2 | 357.0 | 1.8 | 418.5 | 4115 | 0.78 | 3.56 | 21.9 | 6.18 |
| 3 | 359.0 | 0.7 | 415.5 | 3780 | 1.00 | 3.50 | 28.6 | 0.00 |
| 4 (PM546) | 494.0 | 8.1 | 504.0 | 400 | 0.85 | 5.58 | 15.2 | 2.70 |
| 5 | 504.0 | 2.7 | 514.5 | 405 | 0.80 | 6.47 | 12.3 | 3.09 |
| 6 (Rh6G) | 527.0 | 8.4 | 549.5 | 775 | 1.00 | 3.90 | 25.6 | 0.00 |
| 7 | 531.0 | 5.8 | 555.5 | 830 | 0.90 | 3.86 | 23.3 | 2.59 |
| 8 (Per Red) | 568.2 | 4.9 | 597.5 | 865 | 1.00 | 6.16 | 16.2 | 0.00 |
| 9 | 554.0 | 5.4 | 584.5 | 940 | 0.89 | 5.92 | 15.0 | 1.86 |

**Table 2.** Lasing properties of commercial laser dyes and their new fluorinated derivatives at dye concentrations for optimization of their laser action. [c]: dye concentration; Eff: lasing efficiency (ratio between the energy of the laser output and the pump energy incident on the sample surface); $\lambda_l$: peak wavelength of the laser emission; intensity of the laser-induced fluorescence emission ($I_n$) after $n$ pump pulses for dyes in ethyl acetate solution; $\lambda_{exc}$: pumping wavelength.

| | $\lambda_{exc}$ = 355 nm, 10 Hz | | | | | $\lambda_{exc}$ = 532 nm, 10 Hz | | | | |
|---|---|---|---|---|---|---|---|---|---|---|
| | Cu460 | 2 | 3 | PM546 | 5 | 5 | Rh6G | 7 | PerRed | 9 |
| [c]/mM | 2 | 5 | 2 | 20 | 20 | 3.5 | 0.9 | 1.5 | 0.5 | 0.8 |
| Eff(%) | 30 | 20 | 46 | 23 | 38 | 46 | 42 | 65 | 23 | 38 |
| $\lambda_{la}$/nm | 456 | 466 | 460 | 541 | 556 | 558 | 580 | 582 | 624 | 615 |
| $I_n$(%)[a] | 20 | 0 | 100 | 60 | 95 | 100 | 20 | 70 | 66 | 100 |
| n/1000 | 8 | 5 | 25 | 100 | 100 | 100 | 100 | 100 | 100 | 100 |

[a] $I_n$ (%) = 100 ($I_n$ / $I_0$), with $I_0$ being the initial intensity.

produces a moderate decrease in the fluorescence efficiency, which is likely due to its electron withdrawing character (table 1 and S4 (stacks.iop.org/LPL/11/115818/mmedia)). Indeed, the contribution of the pendant aryls to the frontier orbitals is rather low (figure S3 (stacks.iop.org/LPL/11/115818/mmedia)) and the same holds true when replacing one of them with fluorine, thereby explaining its low influence. As a consequence, fluorescence efficiency is still very high, approaching 100% in the most apolar media [54–56].

### 3.3. Lasing properties

The laser behavior of the selected dyes exhibits a stronger dependence on fluorine presence than that shown by the photophysical properties. According to their absorption properties, the lasing properties of Cu460 and PM546 and their fluorinated derivatives were studied under pumping at 355 nm, whereas all the other dyes were studied under pumping at 532 nm. The dye concentrations in lasing studies were in the millimolar range, as required by our experimental conditions of transversal excitation and strong focusing of the incoming pump radiation. In this way, the pump radiation was totally absorbed within the first millimeter of the solution in order to obtain an emitted laser beam with near-circular cross-section and section and optimize the lasing efficiency (ratio between the energy of the dye laser output and the pump energy incident on the sample surface). To determine the dye concentration that optimizes laser emission for the different derivatives, the dependence of their laser emission on the corresponding dye concentrations was first analyzed in ethyl acetate by varying the optical densities from 4 to 40, while keeping all other experimental parameters constant. The low solubility in ethyl acetate of compounds **6** and **7** forced us to conduct the corresponding studies in ethanol. Table 2 summarizes the concentrations that produced the highest lasing efficiencies in each case as well as the corresponding lasing wavelengths. The optimum value of the dye concentration was determined in this manner and then used to prepare dye solutions in a number of polar protic and polar aprotic solvents in order to analyze the effect of the nature of the solvent on the laser properties of the different derivatives. The results obtained are listed in table 2.

Under the described experimental conditions, the fluorination of the commercial dyes led to laser efficiencies improved by a factor of up to 1.8 with respect to the value reached with the non-fluorinated parent dyes pumped under otherwise identical experimental conditions. For instance, monofluorination of Rh6G increased its laser efficiency from 42% to an impressive 65%. In addition, monofluorination of PM546 induced a bathochromic shift of its absorption band, allowing it to be pumped at 532 nm, which is not possible for the commercial dye even at concentrations approaching its limit of solubility. However, pumping an ethyl acetate solution (3.5 mM) of compound **5** at 532 nm reached laser efficiency as high as 46%. The only exception to this laser efficiency enhancement is compound **2,** where the presence of fluorine along the longitudinal axis of Cu460 significantly worsened its photophysical properties and consequently, its laser action.

Following photophysical analysis, the actual effect of solvent on dye laser action was analyzed in solutions of polar protic and polar aprotic solvents. Although the photophysical studies showed that the new derivatives exhibited their highest

**Table 3.** Lasing efficiencies for the commercial dyes and their new fluorinated derivatives in different solvents. $\lambda_{exc}$: pumping wavelength.

| | $\lambda_{exc}$ = 355 nm | | | | | $\lambda_{exc}$ = 532 nm | | | | |
|---|---|---|---|---|---|---|---|---|---|---|
| Solvent | Cu460 | 3 | PM546 | 5 | 5 | Rh6G | 7 | PerRed | **9** | |
| Ethyl acetate | 30 | 46 | 24 | 38 | 46 | | | 24 | 38 | |
| Acetone | 30 | 44 | 23 | 33 | 41 | 44 | 65 | 24 | 34 | |
| Ethanol | 28 | 44 | 20 | 30 | 40 | 42 | 64 | | | |
| Methanol | 25 | 36 | 18 | 25 | 35 | 38 | 58 | | | |
| $F_3$-Ethanol[a)] | 20 | 32 | | | | 45 | 68 | | | |
| c-hexane | | | | | | | | 22 | 42 | |

[a] $F_3$-Ethanol: 2,2,2,-trifluoroethanol.

fluorescence capacity when dissolved in the apolar solvent c-hexane, the low solubility of the synthesized dyes in this solvent prevented preparation of solutions at the concentrations required for laser experiments under the pumping conditions selected in the present work. The lasing properties of the new dyes exhibit dependence on solvent similar to that exhibited by the commercial dyes, with higher lasing efficiencies in polar aprotic solvents than in polar protic ones (table 3), which is in good agreement with their photophysical properties (tables S1–S4 (stacks.iop.org/LPL/11/115818/mmedia)). In compounds **4–9** the photophysics and lasing efficiency change little in the different solvents. It can be seen in table 3 that, with the exception of dye **2**, in all cases, the lasing efficiency of the fluorinated derivatives is higher than that of the commercial parent dye.

An important parameter for any practical application of the dye lasers is their lasing photostability under repeated pumping. Table 2 shows data on the decrease of laser-induced fluorescence intensity of capillary containing dye solutions under transversal excitation (see experimental section) after a given number n of pump pulses, for both the commercial dyes and their fluorinated derivatives. Dyes Cu460 and PM546 and their derivatives **3** and **5**, respectively, were pumped at 355 nm with a 10 Hz repetition rate. The other dyes were pumped at 532 nm with a 10 Hz repetition rate. The pump energy in all cases was 5 mJ. Similarly, the photostability of these dyes are significantly improved by monofluoration, with the effect on the behaviour of Cu460 being particularly remarkable; the emission of the commercial dye disappears completely after just 10,000 pulses but its monofluorination is sufficient to maintain emission at 100% of its initial value after 25,000 pump pulses, with more than 55,000 pulses required to completely stop its emission. This photostability enhancement provides further support for our initial hypothesis: the strength of the C–F bond provides greater stability to the entire molecular structure in fluorinated dyes, which exhibit greater resistance to photobleaching and reduced reactivity towards singlet oxygen than their parent non-fluorinated counterparts.

## 4. Conclusions

Direct monofluorination, using Selectfluor or $XeF_2$ as fluorination reagents, of the most outstanding laser dyes from the blue to the red edge of the visible spectrum, including Cu460, PM546, Rh6G and Per Red, is a successful strategy to optimize their laser action regardless of their structure and composition. However, for this enhancement, it is required that the position in which the fluorine atom is grafted neither significantly distorts the electronic distribution of the chromophore framework nor interferes with its emission mechanism that increases the non-radiative processes. The new fluorinated dyes exhibit, under drastic pumping laser conditions, enhanced laser efficiencies with high photostability with respect to their non-fluorinated analogues. In this way, monofluorination becomes a facile protocol for overcoming important shortcomings exhibited by commercial laser organic dyes and should heighten their practical applications in optical and sensing fields.

## Acknowledgements

This work was supported by projects MAT2010-20646-C04-01, C04-02, C04-03 and C04-04 of the Spanish Ministerio de Economia y Competitividad (MINECO). Furthermore, the authors wish to thank Gobierno Vasco (IT339-10) for financial support. Gonzalo Durán-Sampedro wishes to thank MICINN for a predoctoral scholarship (FPI, cofinanced by Fondo Social Europeo).

## References

[1] Alivasatos A P 1996 *Science* **271** 933
[2] Weissleder R and Ntziachristos V 2003 *Nat. Med.* **9** 123
[3] Ferrari M 2005 *Nat. Rev. Cancer* **5** 161
[4] Kondepati V R, Heise H M and Backhaus J 2008 *Anal. Bioanal. Chem.* **390** 125
[5] Smith A M, Duan H, Mohs A M and Nie S 2008 *Adv. Drug Deliv. Rev.* **60** 1126
[6] Luo S, Zhang E, Su Y, Cheng T and Shi C 2011 *Biomaterials* **32** 7127
[7] Kobayashi H, Ogawa M, Alford R, Choyke P L and Urano Y 2010 *Chem. Rev.* **110** 2620
[8] Moerner W E 2007 *Proc. Natl Acad. Sci. USA* **104** 12596
[9] Hell S W 2007 *Science* **316** 1153
[10] Bates M, Huang B, Dempsey G T and Zhuang X 2007 *Science* **317** 1749
[11] Evanko D 2009 *Nat. Methods* **6** 19
[12] Bossi M, Fölling J, Belov V N, Boyarskiy V P, Medda R, Egner A, Eggeling C, Schönle A and Hell S W 2008 *Nano Lett.* **8** 2463
[13] Zhuang X 2009 *Nat. Photon.* **3** 365
[14] Fitzpatrick J A, Yan Q, Sieber J J, Dyba M, Scwarz U, Szent-Gyorgyi C, Woolford C A, Berget P B, Waggoner A S and Bruchez M P 2009 *Bioconjug. Chem.* **20** 1843
[15] Loudet A and Burgess K 2007 *Chem. Rev.* **107** 4891
[16] Ulrich G, Ziessel R and Harriman A 2008 *Angew. Chem. Int. Edn* **47** 1184
[17] Resch-Genger U, Grabolle M, Cavaliere-Jaricot S, Nitschke R and Nann T 2008 *Nat. Methods* **5** 763
[18] Fischer G M, Isomäki-Krondall M, Gottker-Schnetmann I, Daltrozzo E and Zumbusch A 2009 *Chem. Eur. J.* **15** 4857
[19] Kolmakov K, Belov V N, Bierwagen J, Ringemann C, Müller V, Eggeling C and Hell S W 2010 *Chem. Eur. J.* **16** 158

[20] Perez-Ojeda M E, Trastoy B, Lopez-Arbeloa I, Banuelos J, Costela A, Garcia-Moreno I and Chiara J L 2011 *Chem. Eur. J.* **17** 13258
[21] Duran-Sampedro G, Agarrabeitia A R, Garcia-Moreno I, Costela A, Banuelos J, Arbeloa T, Lopez Arbeloa I, Chiara J L and Ortiz M J 2012 *Eur. J. Org. Chem.* 6335
[22] Duran-Sampedro G, Agarrabeitia A R, Cerdán L, Pérez-Ojeda M E, Costela A, Garcia-Moreno I, Esnal I, Banuelos J, Lopez Arbeloa I and Ortiz M J 2013 *Adv. Funct. Mater.* **23** 4195
[23] Duran-Sampedro G, Esnal I, Agarrabeitia A R, Banuelos Prieto J, Cerdán L, Garcia-Moreno I, Costela A, Lopez Arbeloa I and Ortiz M J 2014 *Chem. Eur. J*. **20** 2646
[24] Biffinger J C, Kim H W and DiMagno S G 2004 *Chem. Bio. Chem.* **5** 622
[25] O'Hagan D 2008 *Chem. Soc. Rev*. **37** 308
[26] Spagnuolo C C, Vermeij R J and Jares-Erijman E A 2006 *J. Am. Chem. Soc.* **128** 12040
[27] Vijila C and Ramalingam A 2001 *J. Mater. Chem.* **11** 749
[28] Mitronova G Y *et al* 2010 *Chem. Eur. J*. **16** 4477
[29] Schmidt R, Osswald P, Koenemann M and Wuerthner F Z 2009 *Naturf. B J. Chem. Sci.* **64** 735
[30] Wuerthner F, Osswald P, Schmidt R, Kaiser T E, Mansikkamaeki H and Koenemann M 2006 *Org. Lett.* **8** 3765
[31] Silva G L, Ediz V, Yaron D and Armitage B A 2007 *J. Am. Chem. Soc.* **129** 5710
[32] Renikuntla B R, Rose H C, Eldo J, Waggoner A S and Armitage B A 2004 *Org. Lett.* **6** 909
[33] Hamada K, Miyawaki E and Jaung J-Y 2005 *Color. Technol.* **121** 127
[34] Baasner B, Hagemann H and Tatlow J C (ed) 1999 Methods of organic chemistry *E 10b/Part 1*: *Organo-Fluorine Compounds* (New York: Thieme Stuttgart)
[35] Liang T, Neumann C N and Ritter T 2013 *Angew. Chem. Int. Edn* **52** 8214
[36] Fier P S and Hartwig J F 2013 *Science* **342** 956
[37] Lee E, Kamlet A S, Powers D C, Neumann C N, Boursalian G B, Furuya T, Choi D C, Hooker J M and Ritter T 2011 *Science* **334** 639
[38] Rozen R, Lerman O, Kol M and Hebel D 1985 *J. Org. Chem.* **50** 4753
[39] Heindel N D, Jabin I, Rapp R D and Laskin J D 2000 *J. Heterocycl. Chem.* **37** 31
[40] Rozen S and Brand M 1986 *J. Org. Chem.* **51** 3607
[41] Holling D, Sandford G, Batsanov A S, Yufit D S and Howard J A K 2005 *J. Fluor. Chem.* **126** 1377
[42] Suzuki T, Tanaka T, Higashiguchi I and Oda A 1999 *Jpn. Kokai Tokkyo Koho JP 11176572 A 19990702*
[43] Suzuki Z and Morita K 1968 *Bull. Chem. Soc. Japan* **41** 1724
[44] López Arbeloa T, López Arbeloa F, Tapia M J and López Arbeloa I 1993 *J. Phys. Chem.* **97** 4704
[45] López Arbeloa F, López Arbeloa I and López Arbeloa T 2001 *Handbook of Advanced Electronic and Photonic Materials and Devices* vol 7 ed H S Nalwa (New York: Academic) 209
[46] Rettig W 1982 *J. Phys. Chem.* **86** 1970
[47] Grabowski Z R, Rotkiewicz K and Rettig W 2003 *Chem. Rev.* **103** 3899
[48] López Arbeloa F, López Arbeloa T and López Arbeloa I 1994 *Trends Photochem. Photobiol.* **3** 145
[49] Liu X, Cole J M, Waddell P G, Lin T-C, Radia J and Zeidler A 2012 *J. Phys. Chem.* A **116** 727
[50] Bañuelos J, Agarrabeitia A R, García-Moreno I, López Arbeloa I, Costela A, Infantes L, Pérez-Ojeda M E, Palacios-Cuesta M and Ortiz M J 2010 *Chem. Eur. J.* **16** 14094
[51] López Arbeloa F, López Arbeloa T M Tapia J and López Arbeloa I 1991 *J. Phys. Chem.* **95** 2203
[52] López Arbeloa T, López Arbeloa F, Hernández P and López Arbeloa I 1992 *Chem. Phys.* **160** 123
[53] Al-Kaysi R O, Ahn T S, Müller A M and Bardeen C J 2006 *Phys. Chem. Chem. Phys.* **8** 3453
[54] Langhals H 1994 *Chimia* **48** 503
[55] Langhals H, Karolin J and Johansson L B-A 1998 *J. Chem. Soc. Faraday Trans.* **94** 2919
[56] Castiglione F, Lanzani G, Mele A, Monguzzi A, Pasarello M, Ruggirello A, Scotognella F and Liveri V T 2011 *J. Mater. Sci.* **46** 6402

## Supporting Information

# Increased laser action in commercial dyes from fluorination regardless of their skeleton

**G Duran-Sampedro[1], A R Agarrabeitia[1], T Arbeloa Lopez[2], J Bañuelos[2]*, I López Arbeloa[2], J L Chiara[3], I Garcia-Moreno[4]* and M J Ortiz[1]***

[1] Departamento de Química Orgánica, Facultad de Ciencias Químicas, Universidad Complutense de Madrid, Ciudad Universitaria, 28040 Madrid, Spain
[2] Departamento de Química Física, Universidad del País Vasco-EHU, Aptdo. 644, 48080 Bilbao, Spain
[3] Instituto de Química Orgánica General, IQOG-CSIC, Juan de la Cierva 3, 28006 Madrid, Spain
[4] Instituto de Química-Física "Rocasolano", IQFR-CSIC, Serrano 119, 28006 Madrid, Spain

E-mail: mjortiz@qium.ucm.es

## Table of Contents Page

## General

*Synthesis*: Starting materials and reagents used in the preparation of BODIPYs are commercially available unless synthesis is described. The solvents were dried and distilled before use. Flash column chromatography was performed using silica gel Merck 60 (230-400 mesh). $^{1}H$ and $^{13}C$ NMR spectra were recorded on a Bruker Avance-DPX-300 (300 MHz for $^{1}H$ and 75 MHz for $^{13}C$) and Avance III (700 MHz for $^{1}H$ and 176 MHz for $^{13}C$) spectrometers. The spectra were recorded in $CDCl_3$ or $C_2D_6O$. $^{1}H$ chemical shifts are reported in ppm relative to tetramethylsilane ($\delta$ = 0.00 ppm), using the residual solvent signal as the internal reference. $^{13}C$ chemical shifts are reported in ppm with $CDCl_3$ or $C_2D_6O$ as the internal standard. Chemical shift multiplicities are reported as s = singlet, d = doublet, t = triplet, q = quartet and m = multiplet. IR spectra (in $cm^{-1}$) were recorded a Bruker Tensor-27-FTIR spectrophotometer. Mass spectra (MS) and high resolution mass spectra (HRMS) were recorded on a Thermofisher MAT 95 XP, by using the EI or FAB techniques.

## Synthesis of core-fluorinated derivatives

6-Fluorocoumarin **2** and 8-fluorocoumarin **3**:

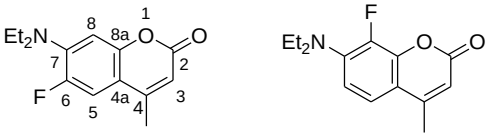


A solution of Coumarin 460 (**1**) (183 mg, 0.79 mmol) and Selectfluor™ (280 mg, 0.79 mmol) in MeCN anhydrous (10 mL) and under an argon atmosphere, was sonicated at 70 ºC for 2 h. The mixture was diluted with EtOAc, washed with $H_2O$, dried over $MgSO_4$, filtered and concentrated to dryness. Flash chromatography using hexane/EtAcO (8:2) afforded, by order of elution, 6-fluorocoumarin **2** (41 mg, 21%) as a yellow solid, 8-fluorocoumarin **3** (39 mg, 20%) as a yellow solid and starting coumarin **1** (29 mg, 16%).

*Compound **2***: $^{1}H$ NMR (700 MHz, $CDCl_3$): $\delta$ 7.05 (d, $^{3}J_{HF}$ = 14.0 Hz, 1H, H-5), 6.58 (d, $^{4}J_{HF}$ = 7.7 Hz, 1H, H-8), 5.97 (s, 1H, H-3), 3.29 (q, *J* = 7.0 Hz, 4H, 2C$\underline{H}_2$CH$_3$), 2.24 (s, 3H, $CH_3$), 1.11 (t, *J* = 7.0 Hz, 6H, 2CH$_2$C$\underline{H}_3$); $^{13}C$ NMR (176 MHz, $CDCl_3$): $\delta$ 161.6

(C=O), 152.0 (d, $^{4}J_{CF}$ = 1.8 Hz, C-4), 151.2 (C-8a), 149.8 (d, $^{1}J_{CF}$ = 241.1 Hz, C-6), 141.3 (d, $^{2}J_{CF}$ = 10.6 Hz, C-7), 110.9 (d, $^{2}J_{CF}$ = 24.6 Hz, CH-5), 110.8 (CH-3), 110.3 (d, $^{3}J_{CF}$ = 8.8 Hz, C-4a), 103.9 (d, $^{3}J_{CF}$ = 3.5 Hz, CH-8), 46.1 ($\underline{C}H_2CH_3$), 46.0 ($\underline{C}H_2CH_3$), 18.4 ($CH_3$), 12.8 ($CH_2\underline{C}H_3$); $^{19}$F NMR (282 MHz, $CDCl_3$): δ -139.78 (s, C6-F); IR (neat): 2971, 1704, 1592, 1523, 1407, 1353, 1267, 1170, 1141, 1066 cm$^{-1}$; HRMS-EI: calcd for ($C_{14}H_{16}FNO_2$) 249.1162 found 249.1158.

*Compound **3***: $^{1}$H NMR (300 MHz, $CDCl_3$): δ 7.10 (dd, *J* = 9.0, 1.5 Hz, 1H, H-5), 6.64 (app t, *J* = 9.0 Hz, 1H, H-6), 5.97 (d, *J* = 0.9 Hz, 1H, H-3), 3.33 (q, *J* = 7.2 Hz, 2H, $C\underline{H}_2CH_3$), 3.32 (q, *J* = 7.2 Hz, 2H, $C\underline{H}_2CH_3$), 2.28 (d, *J* = 0.9 Hz, 3H, $CH_3$), 1.13 (t, *J* = 7.2 Hz, 6H, $2CH_2C\underline{H}_3$); $^{13}$C NMR (176 MHz, $CDCl_3$): δ 159.5 (C=O), 151.5 (C-4), 142.8 (d, $^{2}J_{CF}$ = 12.3 Hz, C-8a), 139.4 (d, $^{2}J_{CF}$ = 17.6 Hz, C-7), 138.8 (d, $^{1}J_{CF}$= 246.4 Hz, C-8), 118.2 (CH-5), 111.5 (CH-6), 111.0 (C-4a), 109.5 (CH-3), 45.1 ($\underline{C}H_2CH_3$), 17.6 ($CH_3$), 12.2 ($CH_2\underline{C}H_3$); $^{19}$F NMR (282 MHz, $CDCl_3$): δ -127.0 (s, C8-F); IR (neat): 2970, 1710, 1582, 1520, 1400, 1357, 1254, 1165, 1140, 1054 cm$^{-1}$; HRMS-EI: calcd for ($C_{14}H_{16}FNO_2$) 249.1162 found 249.1155.

<u>2-FluoroBODIPY **5**:</u>

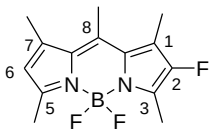


A solution of BODIPY **4** (100 mg, 0.38 mmol) and $XeF_2$ (161 mg, 0.95 mmol) in MeCN anhydrous (10 mL) and under an argon atmosphere, was placed in a sealed vessel and was reacted in a Biotage® Initiator Classic microwave synthesizer at 40 ºC for 5 min. After cooling to room temperature, the mixture was filtered through of Celite® and the filtrate was concentrated under reduced pressure. Column chromatography on silica gel using hexane/DCM (7:3) afforded, by order of elution, 2-fluoroBODIPY **5** (12 mg, 11%) as an orange solid and starting BODIPY **4** (40 mg, 40%).

*Compound **5***: $^{1}$H NMR (300 MHz, $CDCl_3$): δ 6.03 (s, 1H, CH), 2.53 (s, 3H, $CH_3$-C8), 2.46 (s, 6H, $CH_3$-C3 and $CH_3$-C5), 2.36 (s, 3H, $CH_3$-C7), 2.34 (s, 3H, $CH_3$-C1); $^{13}$C NMR (176 MHz, $CDCl_3$): δ 154.4 (C-5), 152.7 (d, $^{1}J_{CF}$ = 242.9 Hz, C-2), 141.1 (C-8a), 141.0 (C-7a), 137.6 (d, $^{2}J_{CF}$ = 24.6 Hz, C-3), 131.5 (C-7), 125.8 (C-8), 120.4 (CH-6), 119.6 (d, $^{2}J_{CF}$ = 10.6 Hz, C-1), 16.3 ($CH_3$-C7), 15.3 ($CH_3$-C8), 13.5 ($CH_3$-C5), 10.4

($CH_3$-C1), 9.2 ($CH_3$-C3); $^{19}$F NMR (282 MHz, $CDCl_3$): δ -147.0 (m, $BF_2$), -163.7 (s, C2-F); IR (neat): 2953, 2925, 2860, 1553, 1203, 1140, 1001 $cm^{-1}$; HRMS-EI: calcd for ($C_{14}H_{16}BF_3N_2$) 280.1356 found 280.1349.

4-Fluororhodamine **7**:

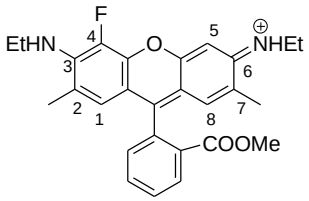


A solution of rhodamine **6** (50 mg, 0.107 mmol) and Selectfluor™ (110 mg, 0.312 mmol) in MeCN anhydrous (2.5 mL) and under an argon atmosphere, was placed in a sealed vessel and was reacted in a Biotage® Initiator Classic microwave synthesizer at 150 ºC for 10 min. The mixture was diluted with DCM, washed with saturated aqueous NaCl solution, dried over $MgSO_4$, filtered and concentrated to dryness. The resulting precipitate was dissolved in MeOH and the filtrate gave pure fluororhodamine **7** (46 mg, 89%) as a red solid.

$^1$H NMR (300 MHz, $CDCl_3$): δ 8.36 (dd, *J* = 7.5 and 0.9 Hz, 1H, CH), 7.94-7.82 (m, 2H, 2CH), 7.45 (d, *J* = 7.2 Hz, 1H, CH), 6.91 (broad s, 2H, 2CH), 6.88 (s, 1H, CH), 3.63 (s, 3H, $CH_3$), 3.53 (q, *J* = 7.2 Hz, 4H, $2CH_2$), 2.14 (s, 6H, $2CH_3$), 1.39 (t, *J* = 7.2 Hz, 6H, $2CH_3$); $^{13}$C NMR (75 MHz, $CDCl_3$): δ 167.0 (COO), 159.5 (C), 158.9 (C), 157.6 (C), 135.5 (C), 135.1 (C), 134.2 (CH), 132.3 (CH), 131.6 (CH), 131.5 (CH), 131.4 (C), 131.3 (C), 129.9 (CH), 128.4 (C), 127.9 (C), 127.5 (C), 126.8 (C), 125.6 (CH), 114.8 (C), 94.9 (CH), 52.9 ($CH_3$), 39.5 ($CH_2$), 17.6 ($CH_3$), 14.1 ($CH_3$); $^{19}$F NMR (282 MHz, $CDCl_3$): δ -154.9 (s, ArF); IR (neat): 3193, 1721, 1649, 1604, 1498, 1301, 1268, 1243, 1185, 1020 $cm^{-1}$; MS-EI *m*/*z* (%): 446 ($M^+$-1, 41), 431 (100), 413 (62).

1-Fluoroperylene bisimide **9**:

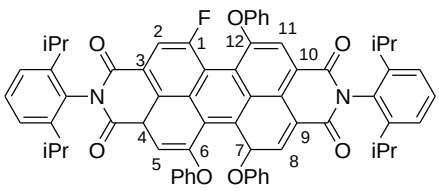


A solution of perylene bisimide **8** (55 mg, 0.05 mmol) and $XeF_2$ (70 mg, 0.40 mmol) in MeCN anhydrous (10 mL) and under an argon atmosphere, was sonicated at 70 ºC for 3

h. The mixture was diluted with EtOAc, washed with $H_2O$, dried over $MgSO_4$, filtered and concentrated to dryness. Flash chromatography using hexane/EtOAc (9:1) afforded, by order of elution, 1-fluoroperylene bisimide **9** (14 mg, 27%) as a red solid and starting perylene **8** (7 mg, 13%). $^1$H NMR (700 MHz, $C_2D_6O$): δ 8.27 (d, $^3J_{HF}$ = 11.2 Hz, 1H, CH), 8.07 (s, 2H, 2CH), 8.02 (s, 1H, CH), 7.32-6.98 (m, 21H, 21CH), 2.74-2.66 (m, 4H, 4CH), 1.00-0.94 (m, 24H, 8$CH_3$); $^{13}$C NMR (176 MHz, $C_2D_6O$): δ 162.87 (C), 162.84 (C), 162.79 (C), 162.63 (C), 159.74 (d, $^1J_{CF}$ = 262 Hz, C-F), 156.41 (C), 156.15 (C), 155.87 (C), 155.51 (C), 155.21 (C), 155.18 (C), 145.92 (C), 145.85 (C), 132.77 (C), 132.71 (C), 131.05 (C), 131.03 (C), 130.53 (CH), 130.19 (CH), 129.29 (CH), 129.26 (CH), 125.26 (CH), 124.97 (CH), 124.31 (C), 123.75 (CH), 123.72 (CH), 123.52 (C), 123.30 (C), 121.27 (C), 120.28 (C), 120.25 (CH), 120.18 (CH), 120.15 (CH), 120.03 (C), 119.96 (CH), 119.51 (CH), 119.36 (CH), 118.81 (CH), 118.64 (CH), 28.80 (CH), 23.37 ($CH_3$)23.34 ($CH_3$); $^{19}$F NMR (282 MHz, $CDCl_3$): δ -92.3 (m, ArF); IR (neat): 2963, 1705, 1672, 1586, 1487, 1408, 1385, 1340, 1284, 1198, 876 cm$^{-1}$; MS-FAB *m*/*z* (%): 1005 ($M^+$, 100).

**Table S1**. Photophysical properties of coumarine Cu460 and its fluorinated derivatives (**2** and **3**) under an inert atmosphere (samples flushed with argon) in several solvents: absorption ($\lambda_{ab}$) and fluorescence ($\lambda_{fl}$) wavelengths, Stokes shift ($\Delta\nu_{St}$), molar absorption coefficient ($\varepsilon_{max}$), fluorescence quantum yield ($\phi$) and lifetime ($\tau$), radiative ($k_{fl}$) and non-radiative ($k_{nr}$) rate constants.

| | $\lambda_{ab}$ (nm) | $\varepsilon_{max} \cdot 10^{-4}$ $M^{-1}cm^{-1}$ | $\lambda_{fl}$ (nm) | $\Delta\nu_{St}$ ($cm^{-1}$) | $\phi_{fl}$ | $\tau$ (ns) | $k_{fl} \cdot 10^{-7}$ ($s^{-1}$) | $k_{nr} \cdot 10^{-7}$ ($s^{-1}$) |
|---|---|---|---|---|---|---|---|---|
| **1 (Cu460)** | | | | | | | | |
| cyclohexane | 351.0 | 2.7 | 394.0 | 3110 | 0.93 | 2.83 | 32.8 | 2.47 |
| ethyl acetate | 360.5 | 2.4 | 415.5 | 3670 | 1.00 | 3.52 | 28.4 | 0.00 |
| acetone | 366.5 | 2.4 | 425.5 | 3785 | 0.80 | 3.70 | 21.6 | 5.41 |
| ethanol | 374.0 | 2.4 | 447.0 | 4365 | 0.70 | 3.41 | 20.5 | 8.80 |
| methanol | 375.0 | 2.4 | 453.0 | 4590 | 0.46 | 2.12 | 21.7 | 25.5 |
| trifluoroethanol | 386.5 | 2.5 | 462.0 | 4230 | 0.35 | 2.80 | 12.5 | 23.2 |
| water | 383.0 | 2.1 | 470.5 | 4855 | 0.01 | 0.36 | 2.78 | 275 |
| **2** | | | | | | | | |
| cyclohexane | 353.5 | 1.9 | 396.0 | 3035 | 0.98 | 2.85 | 34.4 | 0.70 |
| ethyl acetate | 357.0 | 1.8 | 418.5 | 4115 | 0.78 | 3.56 | 21.9 | 6.18 |
| acetone | 359.5 | 1.9 | 428.0 | 4450 | 0.42 | 2.73 | 15.4 | 21.2 |
| ethanol | 364.5 | 1.8 | 445.5 | 4990 | 0.08 | 0.29 (96%)<br>3.90 (4%) | - | - |
| methanol | 365.0 | 1.6 | 451.0 | 5225 | 0.05 | 0.10 (97%)<br>3.53 (3%) | - | - |
| trifluoroethanol | 378.5 | 1.5 | 458.5 | 4610 | 0.06 | 0.20 (97%)<br>4.21 (3%) | - | - |
| water | 347.5 | 1.1 | 471.0 | 7545 | 0.05 | 0.11 (76%)<br>4.66 (24%) | - | - |
| **3** | | | | | | | | |
| cyclohexane | 351.0 | 0.8 | 393.5 | 3075 | 1.00 | 2.90 | 34.5 | 0.00 |
| ethyl acetate | 359.0 | 0.7 | 415.5 | 3780 | 1.00 | 3.50 | 28.6 | 0.00 |
| acetone | 365.5 | 0.8 | 425.5 | 3860 | 1.00 | 3.73 | 26.8 | 0.00 |
| ethanol | 372.0 | 0.7 | 446.5 | 4485 | 0.67 | 3.42 | 19.6 | 9.66 |
| methanol | 376.0 | 0.7 | 454.0 | 4570 | 0.40 | 2.15 | 18.6 | 27.9 |
| trifluoroethanol | 386.5 | 0.7 | 458.0 | 4040 | 0.46 | 2.89 | 15.9 | 18.7 |
| water | 380.0 | 0.6 | 471.5 | 5105 | 0.01 | 0.36 | 2.78 | 275 |

**Table S2**. Photophysical properties of boron dipyrromethene PM546 and its monofluorinated derivative (**5**) in several solvents.

| | $\lambda_{ab}$ (nm) | $\varepsilon_{max}\cdot10^{-4}$ ($M^{-1}cm^{-1}$) | $\lambda_{fl}$ (nm) | $\Delta\nu_{St}$ ($cm^{-1}$) | $\phi_{fl}$ | $\tau$ (ns) | $k_{fl}\cdot10^{-8}$ ($s^{-1}$) | $k_{nr}\cdot10^{-8}$ ($s^{-1}$) |
|---|---|---|---|---|---|---|---|---|
| **4 (PM546)** | | | | | | | | |
| cyclohexane | 499.5 | 9.7 | 509.5 | 390 | 0.91 | 5.23 | 1.74 | 0.17 |
| ethyl acetate | 494.0 | 8.1 | 504.0 | 400 | 0.85 | 5.58 | 1.52 | 0.27 |
| acetone | 493.0 | 7.9 | 503.5 | 425 | 0.84 | 5.55 | 1.51 | 0.29 |
| ethanol | 495.0 | 8.1 | 505.0 | 400 | 0.85 | 5.52 | 1.54 | 0.27 |
| methanol | 492.5 | 8.2 | 503.5 | 445 | 0.81 | 5.58 | 1.45 | 0.34 |
| trifluoroethanol | 490.0 | 7.6 | 503.0 | 530 | 0.85 | 6.22 | 1.37 | 0.24 |
| **5** | | | | | | | | |
| cyclohexane | 511.0 | 3.1 | 522.0 | 410 | 0.81 | 6.25 | 1.30 | 0.30 |
| ethyl acetate | 504.0 | 2.7 | 514.5 | 405 | 0.80 | 6.47 | 1.23 | 0.31 |
| acetone | 502.5 | 2.5 | 516.0 | 520 | 0.76 | 6.60 | 1.15 | 0.36 |
| ethanol | 505.0 | 2.6 | 517.0 | 460 | 0.77 | 6.59 | 1.17 | 0.35 |
| methanol | 503.0 | 2.5 | 515.0 | 465 | 0.73 | 6.80 | 1.07 | 0.39 |
| trifluoroethanol | 502.5 | 2.4 | 514.0 | 445 | 0.72 | 7.56 | 0.95 | 0.37 |

**Table S3**. Photophysical properties of rhodamine 6G (Rh6G) and its monofluorinated (**7**) derivative in several solvents (not soluble in cyclohexane and ethyl acetate).

| | $\lambda_{ab}$ (nm) | $\varepsilon_{max}\cdot10^{4}$ ($M^{-1}cm^{-1}$) | $\lambda_{fl}$ (nm) | $\Delta\nu_{St}$ ($cm^{-1}$) | $\phi_{fl}$ | $\tau$ (ns) | $k_{fl}\cdot10^{-8}$ ($s^{-1}$) | $k_{nr}\cdot10^{-8}$ ($s^{-1}$) |
|---|---|---|---|---|---|---|---|---|
| **6 (Rh6G)** | | | | | | | | |
| acetone | 527.0 | 8.4 | 549.5 | 775 | 1.00 | 3.90 | 2.56 | 0.00 |
| ethanol | 530.0 | 9.1 | 551.5 | 735 | 0.77 | 3.90 | 1.97 | 0.59 |
| methanol | 528.0 | 8.7 | 549.0 | 725 | 0.93 | 4.06 | 2.28 | 0.14 |
| trifluoroethanol | 516.5 | 8.9 | 537.5 | 755 | 1.00 | 4.19 | 2.38 | 0.00 |
| water | 527.5 | 6.3 | 550.0 | 775 | 0.71 | 3.98 | 1.78 | 0.73 |
| **7** | | | | | | | | |
| acetone | 531.0 | 5.8 | 555.5 | 830 | 0.90 | 3.86 | 2.32 | 0.27 |
| ethanol | 533.5 | 5.9 | 556.5 | 775 | 0.83 | 3.83 | 2.17 | 0.44 |
| methanol | 531.5 | 6.1 | 555.5 | 810 | 0.84 | 3.94 | 2.13 | 0.41 |
| trifluoroethanol | 520.0 | 6.0 | 542.0 | 780 | 0.96 | 4.27 | 2.25 | 0.09 |
| water | 529.5 | 3.7 | 555.0 | 870 | 0.67 | 3.81 | 1.76 | 0.87 |

**Table S4**. Photophysical properties of Perylene Red and its monofluorinated derivative (**9**) in several solvents.

| | $\lambda_{ab}$ (nm) | $\varepsilon_{max}\cdot10^{-4}$ ($M^{-1}cm^{-1}$) | $\lambda_{fl}$ (nm) | $\Delta\nu_{St}$ ($cm^{-1}$) | $\phi_{fl}$ | $\tau$ (ns) | $k_{fl}\cdot10^{-7}$ ($s^{-1}$) | $k_{nr}\cdot10^{-7}$ ($s^{-1}$) |
|---|---|---|---|---|---|---|---|---|
| **8 (Per Red)** | | | | | | | | |
| cyclohexane | 558.5 | 4.7 | 587.0 | 870 | 1.00 | 5.64 | 18.3 | 0.00 |
| ethyl acetate | 568.2 | 4.9 | 597.5 | 865 | 1.00 | 6.16 | 16.2 | 0.00 |
| acetone | 569.5 | 4.8 | 602.0 | 950 | 0.99 | 6.33 | 15.6 | 0.21 |
| ethanol | 577.5 | 4.6 | 616.5 | 1095 | 0.90 | 6.21 | 14.4 | 1.68 |
| methanol | 577.0 | 4.7 | 617.0 | 1125 | 0.85 | 6.10 | 13.9 | 2.51 |
| trifluoroethanol | 590.0 | 5.0 | 631.0 | 1100 | 0.82 | 6.49 | 12.7 | 2.71 |
| **9** | | | | | | | | |
| cyclohexane | 547.0 | 5.6 | 573.0 | 830 | 0.97 | 5.39 | 18.1 | 0.48 |
| ethyl acetate | 554.0 | 5.4 | 584.5 | 940 | 0.89 | 5.92 | 15.0 | 1.86 |
| acetone | 555.0 | 5.3 | 590.0 | 1070 | 0.77 | 5.96 | 12.9 | 3.80 |
| ethanol | 561.5 | 5.3 | 603.0 | 1225 | 0.65 | 5.86 | 11.1 | 5.91 |
| methanol | 562.0 | 4.9 | 608.0 | 1345 | 0.64 | 5.71 | 11.3 | 6.24 |
| trifluoroethanol | 573.5 | 5.4 | 614.5 | 1165 | 0.54 | 5.80 | 9.28 | 7.96 |

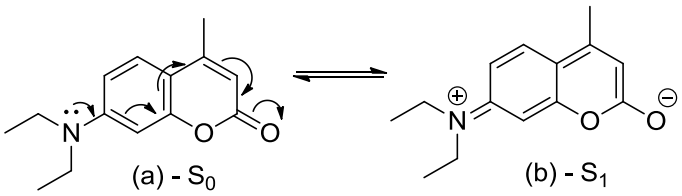


**Scheme S1**. Two main resonante structures of coumarine as result of the electronic coupling between the lone pair of the aromatic amine and the benzopyrone core.[1] (a) form prevails in the ground state, whereas (b) does in the excited state. The marked charge transfer character of the last one (push-pull from amine to carbonyl) explains the bathochromic shift in fluorescence as the solvent acidity increase (i.e., in water).

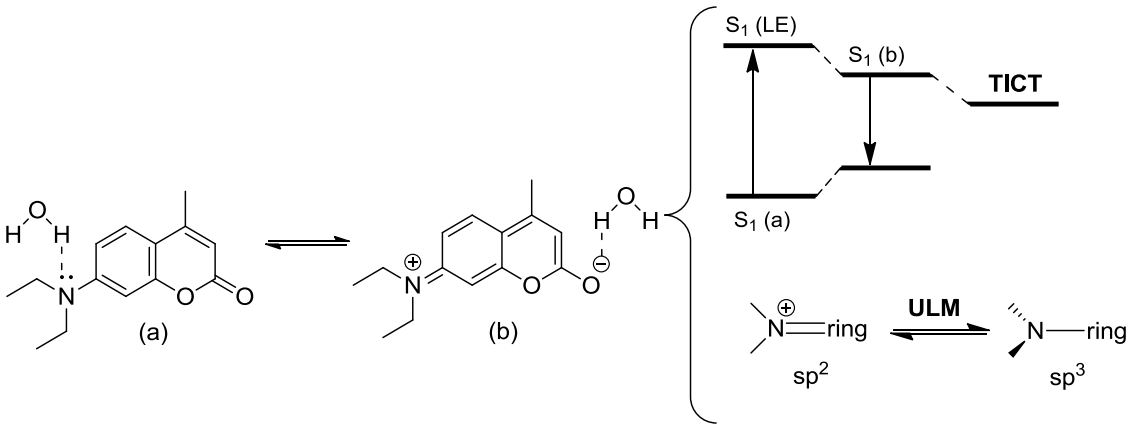


**Scheme S2**. Models which explain the increase of the non-radiative processes of coumarine in protic solvents where specific interaction with the negative charge placed at the oxygen are viable; intramolecular charge transfer as result of the twisting of the donor amine (TICT) and interconversion between the hybridization states of the amino (Umbrella Like Motion, ULM).

[1] López Arbeloa F, López Arbeloa I and López Arbeloa T 2001 *Handbook of Advanced Electronic and Photonic Materials and Devices* vol. 7 ed. H. S. Nalwa (New York: Academic Press) pp 209

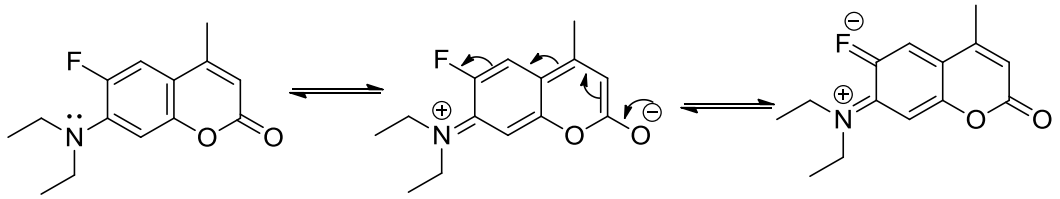

**Scheme S3**. Resonance structures once the fluorine is attached to the coumarine though the longitudinal horizontal axis in which the charge transfer takes place form the amino to the final carbonyl. Such structures are unavailable if the fluorine is presence in the transversal vertical axis.

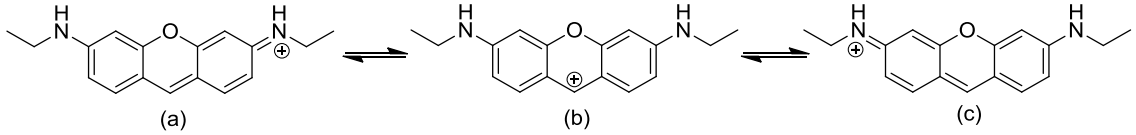


**Scheme S4.** Main resonance structures of rhodamine 6G.

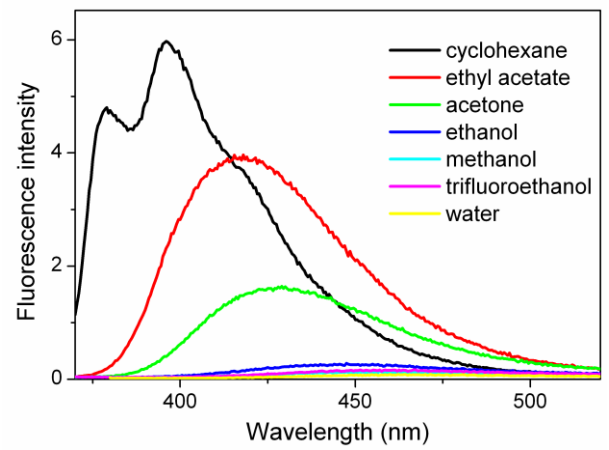


**Figure S1**. Evolution of the fluorescence spectra (normalized to the fluorescence quantum yield) with the solvent for compound **2**.

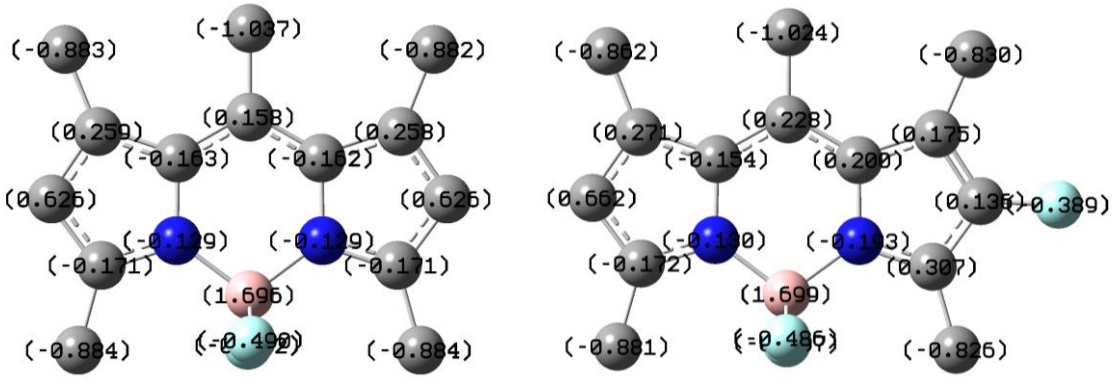


**Figure S2**. Mulliken charge distribution of PM546 and its monofluorinated derivative **5** in the ground state.

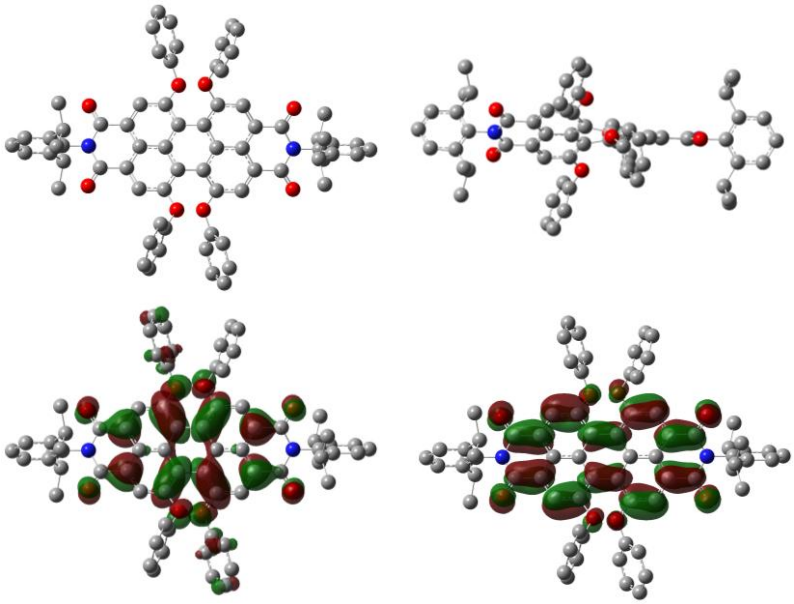


**Figure S3**. Optimized ground state geometry of perylene red in two different views and electronic density at the frontier orbitals HOMO and LUMO.

EurJOC European Journal of Organic Chemistry

FULL PAPER

DOI: 10.1002/ejoc.201200946

# Chlorinated BODIPYs: Surprisingly Efficient and Highly Photostable Laser Dyes

**Gonzalo Duran-Sampedro,[a] Antonia R. Agarrabeitia,[b] Inmaculada Garcia-Moreno,*[a] Angel Costela,[a] Jorge Bañuelos,[c] Teresa Arbeloa,[c] Iñigo López Arbeloa,[c] Jose Luis Chiara,*[d] and María J. Ortiz*[b]**

**Keywords:** Dyes/Pigments / Laser dyes / Photophysics / Fluorescence / Halogenation

A series of mono- to hexachlorinated BODIPY dyes have been prepared in good to excellent yields through the use of *N*-chlorosuccinimide as an inexpensive halogenating reagent. This library of chlorinated dyes allowed analysis in detail, from the experimental and theoretical points of view, of the dependency of the photophysical and optical properties of the dyes on the number and positions of the chlorine substituents on their BODIPY cores. Quantum mechanical calculations predict the regioselectivity of the halogenation reaction and explain why some positions are less prone to chlorination. The new chlorinated BODIPYs exhibit enhanced laser action with respect to their non-halogenated analogues, both in liquid solution and in the solid phase. In addition, chlorination is a facile and essentially costless protocol for overcoming important shortcomings exhibited by commercially available BODIPYs, which should favor their practical applications in optical and sensing fields.

## Introduction

In the past year alone, over 500 articles have been published on the synthesis and applications of 4-bora-3a,4a-diaza-*s*-indacene dyes, known as BODIPYs. The growing interest in these versatile fluorophores is due to their favorable spectroscopic properties, characterized by high absorption coefficients, high fluorescence quantum yields, high photostabilities, and low sensitivities to medium effects.[1] Currently, the development of new BODIPY dyes is driven by their potential applications as sensors in biology and in clinical diagnosis,[1g,2] as photosensitizers for photodynamic therapy (PDT),[3] and as laser generators,[1f,4] as well as for the manufacture of waveguides,[5] light-emitting diodes (OLEDs),[6] photovoltaic cells,[7] and electroluminescent devices,[6] in addition to the usual conventional applications of organic dyes. These and other emerging uses are conditioned by the emission wavelength, quantum yield, and stability of a given dye under the working conditions needed for each specific application; these can be particularly demanding, as is often the case with the new imaging techniques developed in optical microscopy that demand high-intensity laser irradiation.

The photophysical properties of a BODIPY dye are highly dependent on the substitution pattern of the indacene core, which allows the design of new dyes with improved optical properties ranging from the blue to the red region of the spectrum by appropriate selection of the electronic properties and positions of the substituents.[1] Core-halogenated BODIPYs are highly versatile starting materials for the modulation and optimization of these properties, facilitating the introduction of chemical diversity in the indacene nucleus through nucleophilic substitution of halogen[8] or through metal-catalyzed cross-coupling reactions.[2e,3m,4m,8l–8m,8o–8q,9] The chloro-BODIPYs have been the derivatives most widely used for this purpose, allowing the introduction of a wide range of C-, N-, O-, S-, Se-, and Te-based substituents.[4k,8a–8n,8p,9b,9e,9g,9s] Bromo- and iodo-BODIPYs have attracted interest in their own right as photosensitizers for solar hydrogen production[10] and as probes for PDT.[3] Iodine or bromine incorporation into the BODIPY core enhances intersystem crossing to the triplet excited state upon irradiation, as required for efficient singlet oxygen generation in PDT.

[a] Instituto Química-Física "Rocasolano", CSIC,
Serrano 119, 28006 Madrid, Spain
Fax: +34-915642431
E-mail: i.garcia-moreno@iqfr.csic.es
Homepage: http://www.iqfr.csic.es/ql/Web_QL/Laser_material.htm
[b] Departamento de Química Orgánica I, Facultad de Ciencias Químicas, Universidad Complutense,
28040, Madrid, Spain
Fax: +34-913944103
E-mail: mjortiz@quim.ucm.es
Homepage: http://www.ucm.es/info/quimorga/index_ENG.htm
[c] Departamento de Química Física, Universidad del País Vasco-EHU, Facultad de Ciencias y Tecnología,
Apartado 644, 48080 Bilbao, Spain
[d] Instituto de Química Orgánica General, CSIC,
Juan de la Cierva 3, 28006 Madrid, Spain
Fax: +34-915644853
E-mail: jl.chiara@iqog.csic.es
Homepage: http://www.iqog.csic.es/iqog/investigador/jose-luis-chiara-romero

Supporting information for this article is available on the WWW under http://dx.doi.org/10.1002/ejoc.201200946.

 © 2012 Wiley-VCH Verlag GmbH & Co. KGaA, Weinheim 

Conversely, in spite of the wide synthetic use of chloro-BODIPYs, their photophysical properties have scarcely been studied, possibly due to the expectation that chlorine substituents should impact negatively on both stability and fluorescence, owing to their high chemical reactivity and to the heavy atom effect.[11] Chlorine has, however, been reported to increase fluorescence in certain cases,[12] including some very recent examples of BODIPY dyes.[8d,8j,8m,9g,13] Accordingly, in this work we have synthesized a series of new BODIPY dyes bearing one to six chlorine atoms at different positions on the boradiazaindacene core (Scheme 1). This library of chlorinated BODIPYs allowed us to perform a detailed analysis, both from experimental and from theoretical points of view, of the dependency of the emitting properties of the dye on the number and positions of chlorine substituents on the BODIPY core. In the following section we describe the preparation of four different series of chlorinated BODIPY dyes together with a theoretical study of their structures and charge distributions, and finally we discuss the photophysical properties and laser behavior of the new dyes.

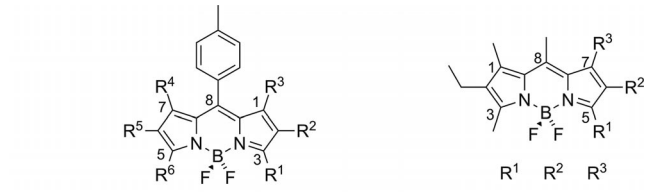

| | $R^1$ | $R^2$ | $R^3$ | $R^4$ | $R^5$ | $R^6$ |
|---|---|---|---|---|---|---|
| **1** | H | H | H | H | H | H |
| **2** | H | Cl | H | H | H | H |
| **3** | H | Cl | H | H | Cl | H |
| **4** | Cl | H | H | H | H | Cl |
| **5** | Cl | Cl | H | H | H | Cl |
| **6** | Cl | Cl | H | H | Cl | Cl |
| **7** | Cl | Cl | Cl | Cl | Cl | Cl |
| **8** | 4-$C_6H_4CHO$ | H | H | H | H | 4-$C_6H_4CHO$ |
| **9** | 4-$C_6H_4CHO$ | Cl | H | H | H | 4-$C_6H_4CHO$ |
| **10** | 4-$C_6H_4CHO$ | Cl | H | H | Cl | 4-$C_6H_4CHO$ |



| | $R^1$ | $R^2$ | $R^3$ |
|---|---|---|---|
| **11** | H | H | H |
| **12** | Cl | H | H |
| **13** | Cl | H | Cl |
| **14** | Cl | Cl | H |

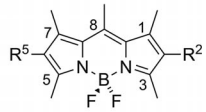

| | $R^2$ | $R^5$ |
|---|---|---|
| **15** | H | H |
| **16** | Cl | H |
| **17** | Cl | Cl |

Scheme 1. Core-chlorinated BODIPY dyes studied in this work and starting BODIPYs (**1**, **8**, **11**, **15**) used for their synthesis.

## Results and Discussion

### Synthesis

For the synthesis of the new chloro-BODIPYs we followed the three general strategies previously described for other halo-BODIPYs by electrophilic halogenation: a) direct halogenation of the unsubstituted BODIPY dye,[3c–3k,3m–3n,8o–8q,9c–9d,9f,9h,9o–9r,10,13a,14] b) halogenation of the dipyrromethane intermediate,[2e,8b,8e,8k,8n,9g,9l,9n,9t,15] and c) halogenation of the pyrrole precursors.[8j,8m,8p,9a,9e,9n]

The 2-mono-, 2,6-di-, 2,3,5-tri-, and 2,3,5,6-tretrachlorinated derivatives **2**, **3**, **5**, and **6**, respectively, were prepared by direct halogenation of BODIPY **1** with increasing amounts of *N*-chlorosuccinimide (NCS) as halogenating reagent (Scheme 2). Treatment of **1**[16] with NCS (2 equiv.) in THF at room temperature thus gave the 2-chloro-BODIPY **2**. No other monochlorinated derivatives were formed under the reaction conditions. Increasing the amount of NCS to 3 equiv. afforded the 2,6-dichloro-BODIPY **3** as major product (85%). Although it was possible to obtain the 2,3,5-trichloro derivative **5** by further increasing the amount of NCS to 4 equiv., the yield was low (32%), due to the concomitant formation of other polychlorinated products, including the 2,3,6-trichloro derivative, that could not be isolated pure. When 10 equiv. of NCS were used, the 2,3,5,6-tetrachloro-BODIPY **6** was obtained in 78% isolated yield. Use of larger amounts of NCS gave complex mixtures of polychlorinated products.

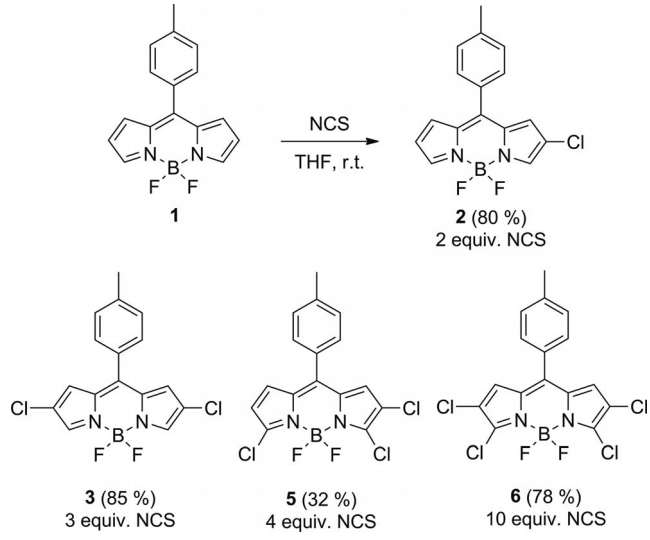


Scheme 2. Synthesis of BODIPYs **2**, **3**, **5**, and **6**.

For the preparation of 3,5-dichloro BODIPY **4**, we used the synthetic route described by Dehaen and Boens,[8b] starting from the corresponding dipyrromethane derivative **18**.[17] A similar strategy was employed for the synthesis of the hexachloro derivative **7** (Scheme 3), because this compound could not be isolated by direct halogenation of the BODIPY core, as mentioned above. Hexachlorination of **18**, requiring the use of a large excess (14 equiv.) of NCS at room temperature, was followed by oxidation of the chlorinated dipyrromethane with DDQ and subsequent treatment with $BF_3{\cdot}OEt_2$ in the presence of triethylamine to afford **7** in 30% overall yield.

Direct halogenation of BODIPY **11**[4l] gave a complex mixture of products that was very difficult to purify. In this case, halogenation of the pyrrole precursor was more appropriate (Scheme 4). 2-Acetylpyrrole was treated either with 1.1 or with 3 equiv. of NCS in THF at room temperature to give 2-acetyl-5-chloropyrrole (**19**)[8m,9e,18] or a mixture of 2-acetyl-3,5-dichloropyrrole (**20**) and 5-acetyl-2,3-dichloropyrrole (**21**),[18b] respectively, in moderate yields.

 © 2012 Wiley-VCH Verlag GmbH & Co. KGaA, Weinheim 

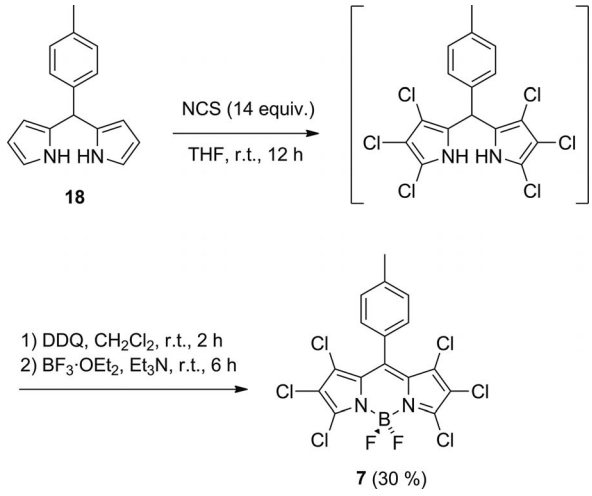


Scheme 3. Synthesis of hexachlorinated BODIPY **7**.

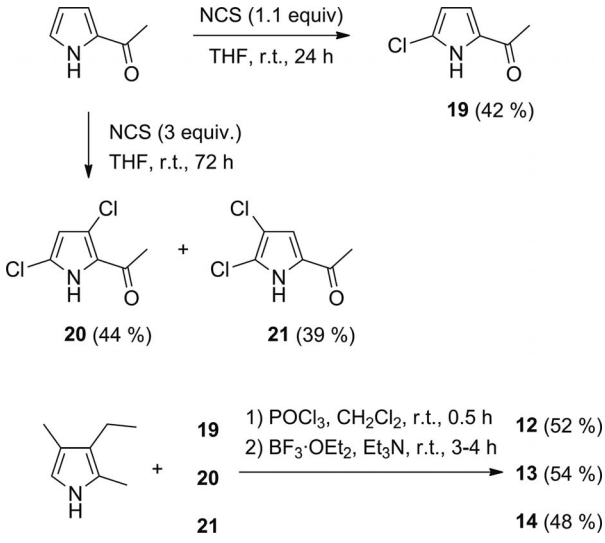


Scheme 4. Chlorination of 2-acetylpyrrole to generate BODIPY dyes **12**, **13**, and **14**.

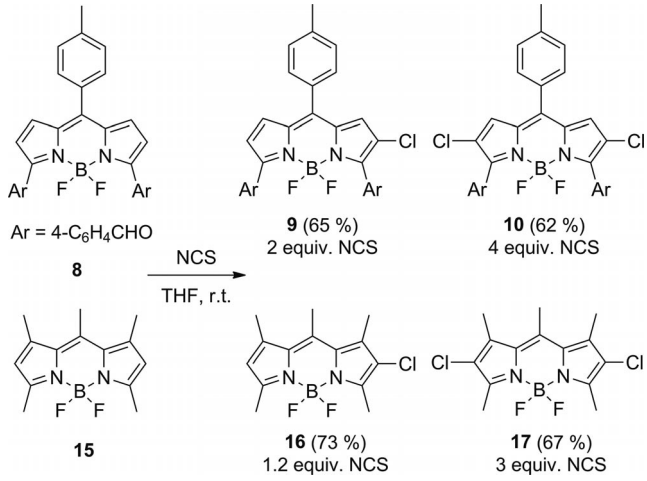


Scheme 5. Synthesis of BODIPYs **9**, **10**, **16**, and **17**.

Subsequent treatment of these pyrroles with 3-ethyl-2,4-dimethylpyrrole and phosphorus oxychloride, followed by treatment with $BF_3{\cdot}OEt_2$ in the presence of triethylamine, yielded the chlorinated BODIPY dyes **12** (52%), **13** (54%), and **14** (48%).

2-Chloro-BODIPY **9** and 2,6-dichloro-BODIPY **10** were obtained in good yields (62–65%) by direct chlorination of dye **8**[4k] with appropriate amounts of NCS (Scheme 5). A similar procedure was used for the preparation of compounds **16** (73%) and **17** (67%) starting from commercially available dye **15** (PM546, Scheme 5).

## Theoretical Study

We calculated the charge distributions (CHelpg) of the new BODIPYs with the objective of understanding the regioselectivities of the electrophilic halogenation reactions (Table 1 and Figures S1–S4 in the Supporting Information). The charge distribution map of, for instance, the parent non-halogenated compound **1** indicates that the BODIPY chromophore is most susceptible to electrophilic attack by chlorine (Table 1) at the 2- and the 6-positions, which have the highest negative charge, consistently with experimental observations in the synthesis of mono- and dichlorinated dyes **2** and **3**.

Table 1. Potential electrostatic map (red denotes negative and blue positive charge) of compound **1** and CHelpg charge distributions for the chromophoric carbon atoms susceptible to electrophylic attack by chlorine in the ground states of its chlorinated derivatives **2**–**7**. The full data, including the excited states, are listed in Figure S1 in the Supporting Information.

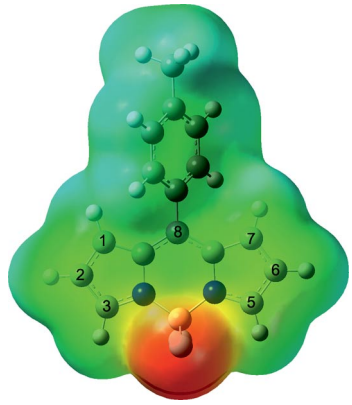


| Dye | BODIPY carbon atoms | | | | | |
|---|---|---|---|---|---|---|
| | **1** | **2** | **3** | **5** | **6** | **7** |
| **1** | –0.109 | –0.180 | 0.041 | 0.041 | –0.179 | –0.111 |
| **2** | –0.107 | –0.181 | 0.046 | 0.036 | 0.064 | –0.150 |
| **3** | –0.135 | 0.055 | 0.061 | 0.039 | 0.061 | –0.131 |
| **4** | –0.081 | –0.201 | 0.200 | 0.197 | –0.198 | –0.082 |
| **5** | –0.078 | –0.181 | 0.189 | 0.168 | 0.055 | –0.129 |
| **6** | –0.112 | 0.043 | 0.171 | 0.173 | 0.040 | –0.114 |
| **7** | 0.084 | 0.004 | 0.190 | 0.171 | 0.028 | 0.066 |

Upon substitution, the highly electronegative chlorine atom perturbs the charge distribution in the BODIPY framework, inducing a positive charge at the site of substitution and a negative charge at the adjacent carbon. As a

 © 2012 Wiley-VCH Verlag GmbH & Co. KGaA, Weinheim 

result, the positions most susceptible to further electrophilic substitution are now expected to be carbons 1 and 7 in preference to 3 and 5, according to their calculated charges. However, the opposite order of reactivity is observed for the chlorination reaction, probably as a consequence of the steric hindrance introduced by the tolyl substituent on the flanking CH carbons 1 and 7. Similar regioselectivity orders have been observed for stepwise brominations[8o] and iodinations[3n] of the same or closely related 8-arylated BODIPYs. In any case, use of large excesses of the halogenating reagents allows substitution at the 1- and the 7-positions.[8o]

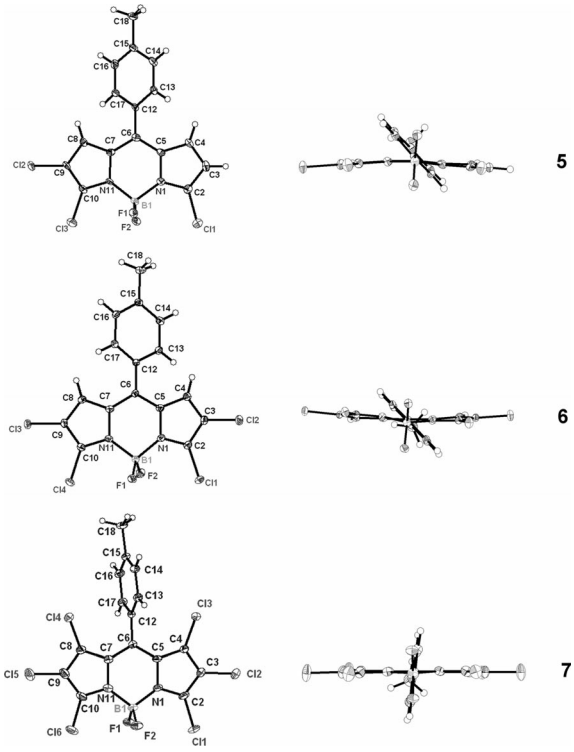


Figure 1. X-ray structures of BODIPY dyes **5**–**7**.

The optimized geometries predict that the 8-tolyl ring will be twisted with respect to the nearly planar indacene core, hampering electronic coupling between their electronic clouds. In all of the derivatives **2**–**6**, with free positions (1 and 7) adjacent to the aryl group, its rotation angle is about 55°, whereas the incorporation of chlorine at those positions (compound **7**) induces enough steric hindrance to twist the phenyl ring to a perpendicular disposition (89°) with respect to the chromophoric plane. These theoretical gas-phase predictions are in good agreement with the experimentally obtained (X-ray diffraction, solid state) geometries depicted in Figure 1. Indeed, the measured rotation angles are about 45° for compounds **5** and **6**, and 86° for derivative **7**. This concordance indicates that the calculated geometries are accurate.

## Photophysical and Lasing Properties

### Photophysics of Chlorinated 8-Tolyl-BODIPYs

The photophysical properties of this set of derivatives (Table 2) are governed by the presence of the tolyl unit at the *meso* position. In parent compound **1**, the absence of substituents at both *ortho* positions of the phenyl ring and/or the corresponding adjacent positions of the chromophoric system allows the unrestricted rotation of the aryl group.[19,20] Accordingly, the probability of internal conversion processes is greatly increased due to vibrational coupling, inducing drastic decreases both in fluorescence capability and in fluorescence lifetime, with respect to those exhibited by the fully unsubstituted BODIPY ($\phi \approx 0.90$ and $\tau \approx 7$–$8$ ns).[4o] In addition, the absence of the steric hindrance that would be required to constrain the phenyl ring in a perpendicular disposition could enable interaction with the BODIPY chromophore, distorting its planarity and further contributing to the nonradiative deactivation processes.[21,22]

Monochlorination of **1** at the 2-position and dichlorination at the 2- and 6-positions (dyes **2** and **3**, respectively) shift the spectral bands to lower energies and reduce the

Table 2. Photophysical properties of 8-tolyl-BODIPY (**1**) and its chlorinated derivatives **2**, **3**, and **5**–**7** in a common solvent (cyclohexane). The biexponential deconvolutions at the emission maxima are listed together with the amplitude-averaged lifetimes ($<\tau>$). The rate constants are calculated from these last values. The full photophysical data in several media are collected in Table S1 in the Supporting Information. The rate constants were calculated from the main lifetimes.

| Dye | $\lambda_{ab}$ [nm] | $\varepsilon_{max}$ (f) [$10^{-4}$ M$^{-1}$ cm$^{-1}$] | $\lambda_{fl}$ [nm] | $\phi$ | $\tau$ [ps] | $<\tau>$ [ps] | $<k_{fl}>$ [$10^{-8}$ s$^{-1}$] | $<k_{nr}>$ [$10^{-8}$ s$^{-1}$] |
|---|---|---|---|---|---|---|---|---|
| **1** | 500.5 | 6.9 (0.42) | 516.0 | 0.036 | 340<br>2285 (≈ 0 %) | 340 | 1.05 | 28.3 |
| **2** | 518.5 | 6.5 (0.42) | 534.5 | 0.093 | 845 (98%)<br>2255 (2%) | 873 | 1.06 | 10.4 |
| **3** | 538.0 | 1.4 (0.11) | 555.0 | 0.153 | 1320 (90%)<br>3860 (10%) | 1574 | 0.97 | 5.38 |
| **5** | 530.0 | 10.5 (0.50) | 542.0 | 0.56 | 2120 (12%)<br>4110 (88%) | 3871 | 1.44 | 1.13 |
| **6** | 546.5 | 8.3 (0.54) | 557.5 | 0.46 | 1180 (22%)<br>4720 (78%) | 3941 | 1.16 | 1.37 |
| **7** | 537.0 | 9.5 (0.46) | 548.5 | 0.45 | 1500 (10%)<br>2550 (90%) | 2445 | 1.84 | 2.25 |

 © 2012 Wiley-VCH Verlag GmbH & Co. KGaA, Weinheim 

absorption probabilities, particularly in the latter case. Such trends are attributable to the electron-withdrawing effect of the electronegative chlorine atom, which removes electron density from the BODIPY core. The fluorescence quantum yields and lifetimes of the new dyes increase significantly with chlorination (Figure 2) as a consequence of the induced drastic reduction in nonradiative deactivation processes (Table 2 and Table S1 in the Supporting Information). In fact, the nonradiative rate constant decreases by about 50% for each chlorine atom incorporated on the BODIPY core. Moreover, further chlorination at the 3- and 5-positions to afford the tri- and tetrachlorinated derivatives **5** and **6** gives rise to a further and significant modification of the photophysical behavior, revealing that halogenation gives entirely different results depending on the positions at which the chlorine atoms are incorporated. Chlorination at the 3- and 5-positions thus leads to an important increase in the absorption probability ($\varepsilon$ of dye **6** is six times higher than that of **3**), fluorescence quantum yield ($\phi$ of dye **6** is three times higher than that of **3**), and fluorescence lifetime, once more due to a drastic decrease in the nonradiative deactivation processes (Table 2 and Figure 2). In fact, the increases in the fluorescence capacities of dyes **5** and **6** cannot be associated with increases in the radiative rate constants, but with decreases in the nonradiative processes – $<k_{nr}>$ – varying from ca. $5 \times 10^8$ $s^{-1}$ in dichlorinated **3** to ca. $1.2 \times 10^8$ $s^{-1}$ in tri- and tetrachlorinated **5** and **6** (Table 2). Similar photophysical properties were reported by Boens et al. for compound **4**, with chlorine substituents at the 3- and 5-positions.[23] The same trends hold true for the fully chlorinated derivative **7**, although the spectral bands are in this case no longer shifted to lower energies, in spite of the larger number of chlorine atoms on the BODIPY core.

To provide an acceptable explanation for the dependence of the photophysical properties of these BODIPY derivatives on the numbers and positions of chlorine atoms, some considerations are to the point. Drexhage points out that C–H bond vibrations in the chromophore favor internal conversion processes and that the replacement of such bonds (e.g., by C–Cl bonds) should favor fluorescence emission.[24] However, such effects are rather small (i.e., <10%) and cannot explain the dependence of the fluorescence capacity on the position of the chlorine substituent in the BODIPY core. Charge transfer phenomena can also be ruled out because the photophysical properties are not very sensitive to the environment polarity (see Table S1 in the Supporting Information, in which the photophysical properties of the new dyes are analyzed as a function of the nature of the solvent). Moreover, electronic interaction between the phenyl ring and the chromophore as a consequence of the number of chlorine substituents can be discounted because the associated twist angles are almost the same in the different derivatives (around 55°, except in the case of the hexachlorinated compound **7**, in which this angle is 89°) and also in the different simulated solvents. The chlorination effect should therefore be related to its influence on the free motion of the 8-tolyl group, which is the key factor in the photophysics of this set of derivatives. A closer inspection of Table S1 in the Supporting Information reveals that the relationship between the fluorescence quantum yield and the degree of chlorination and anchoring position on the core is mainly governed by the probability of the nonradiative processes (internal conversion). The *meso* position in compound **1** is characterized by a high electronic density in the LUMO state and, consequently, it should be very sensitive to substituent effects.[4a] The removal of electronic density from the central position bearing the tolyl substituent by the electronegative chlorine substituents should thus be beneficial for the fluorescence capabilities of the chlorinated derivatives because it should significantly reduce the deleterious influence of the phenyl free rotation on their photophysics. In this way, the chlorinated derivatives show behavior similar to that previously observed for long-wavelength 8-tolyl-BODIPY dyes, in which electron density withdrawal from the chromophore core by extended π-conjugation through 3- and 5-aromatic substituents significantly reduced the influence of the free motion of the 8-tolyl group and led to highly efficient red-emitting BODIPYs.[4k] Although this effect is already

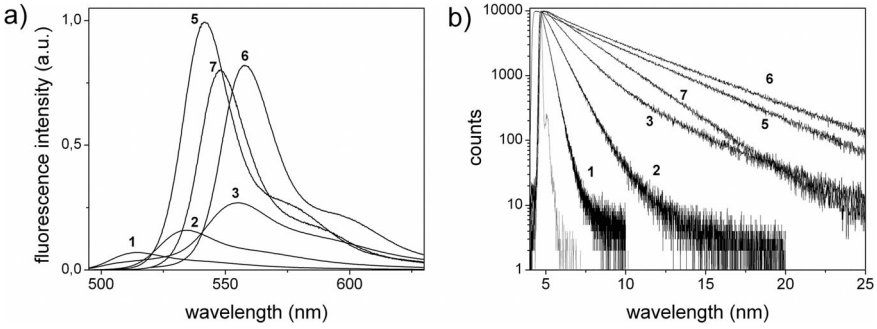


Figure 2. a) Fluorescence spectra of 8-tolyl-BODIPY (**1**) and its mono- (**2**), di- (**3**), tri- (**5**), tetra- (**6**), and hexachlorinated (**7**) derivatives, scaled by their fluorescence capabilities in cyclohexane, on excitation at the vibrational shoulder at lower energies. b) Corresponding fluorescence decay curves of these dyes.

 © 2012 Wiley-VCH Verlag GmbH & Co. KGaA, Weinheim 

achieved on incorporation of chlorine atoms at the 2- and 6-positions of the BODIPY core (compounds **2** and **3**), it becomes more relevant in dyes **4**–**7**, in which the 3- and 5-positions are also chlorinated.

This behavior is also confirmed by the biexponential character acquired by the fluorescence decay curves (monitored at the maximum of the emission spectrum) with chlorination. Whereas the fluorescence decay of the parent dye **1** is essentially a monoexponential curve characterized by a very short lifetime (<500 ps), monochlorination (dye **2**) already induces a biexponential decay, lengthening the short lifetime (ca. 800 ps) and giving rise to a longer one (ca. 2–3 ns). The contributions and durations of this component increase progressively with the number of chlorine atoms: from ca. 10% and 3.8 ns, respectively, in dye **3** up to ca. 80% and 4.7 ns, respectively, in tetrachlorinated dye **6**. This biexponential deconvolution was confirmed at different emission wavelengths, covering the whole fluorescence spectrum (see Table S2 in the Supporting Information). If the decay curves are monitored at the edges of the emission spectrum, the contributions of the short lifetimes are increased. Such biexponential behavior suggests the presence of two interconverting excited states. According to previously reported theoretical modeling of the excited states of 8-aryl-substituted BODIPYs, the phenyl ring can adopt two different conformations in the exited state: twisted and coplanar with respect to the BODIPY core, due to its unrestricted rotation.[21,22] Unfavorable steric interactions in the coplanar conformer cause an out-of-plane distortion of the indacene framework, this being a non-fluorescence state. The short (<1 ns) and the long (ca. 4 ns) components of these lifetimes should hence be assigned to fluorescence strongly reduced by the free motion of the 8-tolyl group, which makes electronic coupling between the phenyl group and the BODIPY core feasible, and to the normal emission of the BODIPY dye, because it reaches values typical of these chromophores, respectively.[4a] It seems that the emission bands of the coplanar states (poorly fluorescent) should be broader than those of the twisted states (mainly responsible for the fluorescence signal), explaining why the contributions of the short lifetimes to the decay curves are higher at the edges of the emission spectra. Similar trends have previously been reported for the decay curves of analogues bearing iodine atoms.[3n] In fact, the fluorescence capabilities of the chlorinated derivatives increase simultaneously with the contributions and lengthenings of this second components in the corresponding fluorescence decay curves (Figure 2), in accordance with lower populations or influence of the coplanar quenching excited states.

The simulated charge distributions (CHelpg) of all these chlorinated derivatives confirm the above hypothesis (Figure S1 in the Supporting Information). In general, the presence of the highly electronegative chlorine atom induces a charge redistribution in the BODIPY core, in which the carbon bonded to chlorine acquires a strong positive charge while the adjacent ones become more negatively charged and, consequently, the positive charges of the neighboring carbons are increased. Such effects are softened at the BODIPY carbon atoms further separated from the chlorinated one. As would be expected, the charge rearrangements induced by chlorination increase with the number of chlorine atoms, always being more significant in the excited states, in which the electronic motion is favored. In addition, substitution at the terminal positions of the delocalized π-systems (the 3- and 5-positions) favors electronic delocalization, especially in the excited states (Figure 3 and Supporting Information, Figure S1), efficiently removing the electronic density from the *meso* positions (in $S_1$ from 0.135 in compound **1** to 0.270 in tetrachlorinated **6**) and, consequently, significantly reducing the deleterious effect of the 8-tolyl motion on the photophysics. This "push-pull" effect[3n,16] causes the significant increases observed both in the absorptions and in the fluorescence probabilities of dyes **5**–**7**. Such charge rearrangement upon excitation should be the reason for the lack of correlation between the molar absorptions and the radiative deactivation rate constants.

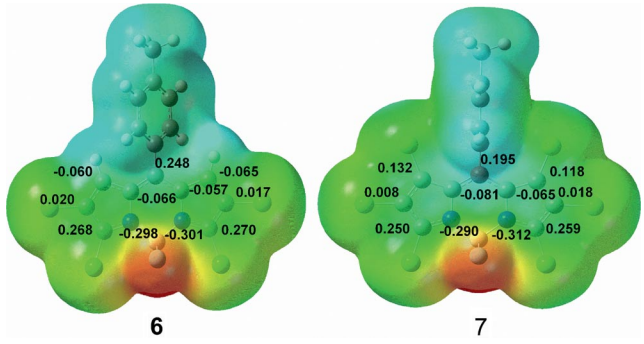


Figure 3. Potential electrostatic maps (red denotes negative and blue positive) together with the CHelpg charge distributions in the excited states for tetra- (**6**) and hexachlorinated (**7**) dyes. The whole charge distributions in ground and excited states are listed in Figure S1 in the Supporting Information.

At this point, it should be noted that, according to theoretical calculations, chlorination does not imply a significant modification in the dihedral angle of the 8-phenyl group with respect to the BODIPY plane (Figure 3, 55°). Therefore, the smaller influence of the free motion of the phenyl group on the photophysics of the chlorinated derivatives is only due to the significant reductions in the electronic charge density at the *meso* positions. On the other hand, the incorporation of chlorine atoms at the 1- and 7-positions of the BODIPY framework, adjacent to the tolyl group, has the opposite effect, concentrating electronic charge around the *meso* positions and enhancing the influence of aryl rotation. Indeed, a direct comparison of the charge distributions of compounds **7** and **6** indicates that the electronic charge at the *meso* position is less positive in the former (0.195 and 0.248, respectively, Figure 3). However, in the case of dye **7**, the steric hindrance induced by the chlorine atoms alters the orientation of the phenyl ring with respect to the indacene plane, and places it nearly perpendicular (Figures 1 and 3, 86° from X-ray and 89° from theoretical calculations, respectively). In this arrangement, the phenyl free motion is hindered and dye **7** exhibits a fluorescence capability similar to that of dye **6**.

 © 2012 Wiley-VCH Verlag GmbH & Co. KGaA, Weinheim 

### Photophysics of Chlorinated Red-Emitting-BODIPY Dyes

The above hypothesis about the electron-withdrawing effect of chlorine on the free rotation of the 8-aryl group was confirmed by analysis of the influence of chlorination on the photophysics of the red-emitting BODIPY **8** (Scheme 5<xshr5>), with the 3- and 5-positions substituted with *p*-formylphenyl groups.[4k] In this derivative **8**, which also bears a tolyl group at the *meso* position, the deleterious influence of this aryl free motion on the fluorescence emission is minimized by the delocalization of the π-system through the aromatic substituents at the 3- and 5-positions.[4k] Consequently, the chromophoric electronic density is removed from the *meso* position, explaining its high fluorescence quantum yield in relation to that of parent compound **1** (see the charge distributions in Figures S1 and S2 in the Supporting Information). Dye **8** was mono- (compound **9**) and dichlorinated (compound **10**) at the 2- and 6-positions (Scheme 5), as predicted by quantum mechanical calculations, which revealed that these positions have the highest negative charges in the chromophore and are hence the most susceptible to electrophilic attack (Figure S2 in the Supporting Information). The corresponding photophysical data in a common solvent are collected in Table S3 in the Supporting Information.

Figure 4 shows that chlorination of dye **8** induces further shifts of its bands to the red, as well as a decrease in the absorption probability in the dihalogenated derivative (from $3.3 \times 10^4$ M$^{-1}$cm$^{-1}$ in **8** to $1.1 \times 10^4$ M$^{-1}$cm$^{-1}$ in **10**). Moreover, the fluorescence quantum yields also decrease (from 0.54 to 0.42 upon the first halogenation to 0.39 after attachment of the second chlorine atom), through reductions in the radiative deactivation rate constants and increases in the internal conversion probabilities (Table S3 in the Supporting Information). In the previous set of derivatives **1**–**7**, the chlorine electron-withdrawing effect enhances the fluorescence emission by decreasing the internal conversion associated with the 8-tolyl motion. In the case of compounds **8**–**10**, however, such a nonradiative pathway is already counteracted by the aromatic substitution at the 3- and 5-positions, so the high electronegativity of the chlorine atom decreases the π-delocalization of the BODIPY through the 3- and 5-aromatic substituents, causing the observed reductions in the absorption and emission probabilities of dyes **9** and **10** with respect to the non-chlorinated dye **8**. Moreover, the further shifts of the spectral bands to lower energies upon chlorination imply that their excited and ground states are energetically closer and that, accordingly, the internal conversion processes are enhanced in terms of the energy gap law, which works well for dyes emitting in the red part of the visible.[25–28]

### Photophysics of Chlorinated Alkyl-BODIPY Dyes

To gain further insights into the effect of chlorination on the photophysics of BODIPY dyes, we studied cases of alkyl-substituted BODIPYs. We selected the previously reported compound **11**[4l] (Scheme 1) and the well-known commercial dye PM546 (**15**, Scheme 5).[29] The corresponding photophysical data in a common solvent are collected in Table 3.

Table 3. Photophysical properties of compounds **11** and **15** and of their mono- and dichlorinated derivatives (**12–14** and **16–17**, respectively) in cyclohexane. The full photophysical data in all the solvents studied are included in Tables S4 and S5, respectively, in the Supporting Information.

| Dye | $\lambda_{ab}$ [nm] | $\varepsilon_{max}$ (f) [$10^{-4}$ M$^{-1}$ cm$^{-1}$] | $\lambda_{fl}$ [nm] | ϕ | τ [ns] | $k_{fl}$ [$10^{-8}$ s$^{-1}$] | $k_{nr}$ [$10^{-8}$ s$^{-1}$] |
|---|---|---|---|---|---|---|---|
| **11** | 504.0 | 3.3 (0.22) | 515.0 | 0.96 | 5.46 | 1.75 | 0.07 |
| **12** | 510.5 | 5.1 (0.33) | 520.5 | 0.78 | 5.07 | 1.54 | 0.43 |
| **13** | 504.0 | 3.3 (0.27) | 526.0 | 0.57 | 3.95 | 1.44 | 1.09 |
| **14** | 521.0 | 3.3 (0.24) | 531.0 | 0.83 | 5.29 | 1.57 | 0.32 |
| **15** | 499.5 | 9.7 (0.50) | 512.0 | 0.91 | 5.23 | 1.74 | 0.17 |
| **16** | 512.0 | 5.5 (0.26) | 525.5 | 0.91 | 5.54 | 1.64 | 0.16 |
| **17** | 527.0 | 7.1 (0.34) | 542.5 | 0.87 | 5.65 | 1.54 | 0.23 |

In this set of derivatives the fluorescence decay curves are satisfactorily analyzed as monoexponentials, thus corroborating the influence of the aryl ring on the appearance of second exponentials for the derivatives **1**–**7** discussed above. The reference compound **11** is characterized by an asymmetric substitution pattern of the pyrroles, one being fully alkylated and the other fully unsubstituted. The incorporation of chlorine at the 5-position (compound **12**) increases the absorption probability, in accordance with the push-pull effect postulated above, but decreases the fluorescence capability of the dye. Both the reference dye **11** and

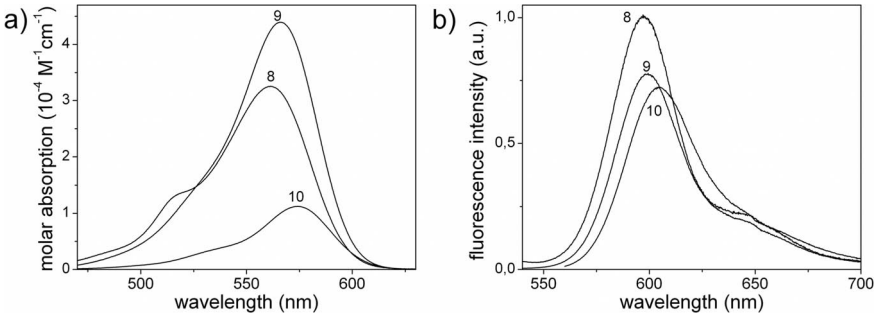


Figure 4. a) Absorption and b) fluorescence spectra of compound **8** and of its mono- (**9**) and dichlorinated (**10**) derivatives scaled by their molar absorptions and fluorescence abilities, respectively, in cyclohexane.

 © 2012 Wiley-VCH Verlag GmbH & Co. KGaA, Weinheim 

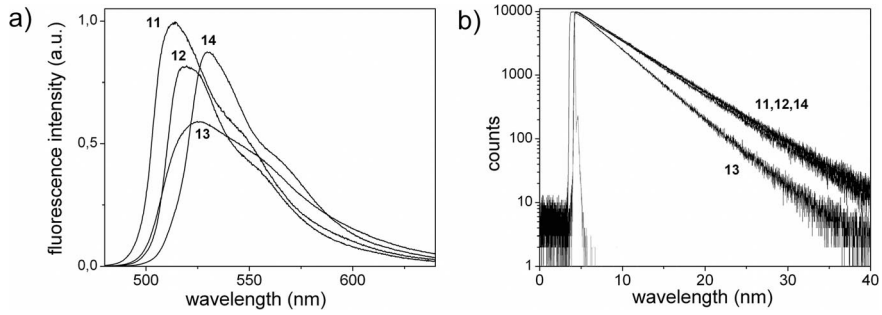


Figure 5. a) Fluorescence spectra of compound **11** and of its mono- (compound **12**) and dichlorinated derivatives **13** and **14**, scaled by their fluorescence capabilities in cyclohexane. b) Corresponding fluorescence decay curves of these dyes.

its monochlorinated derivative **12** exhibit only slight sensitivities to solvent (see Table S4 in the Supporting Information), with the fluorescence quantum yields decreasing only slightly on going from cyclohexane (0.96 for **11** and 0.78 for **12**) to 2,2,2-trifluoroethanol (0.75 for **11** and 0.55 for **12**). This could be attributable to the asymmetric substitution patterns of the pyrroles, with the alkylated ones behaving as electron donors and the unsubstituted or halogenated ones as electron acceptors, giving rise to asymmetric charge distributions between the pairs of pyrrole rings in the BODIPY frameworks that enhance nonradiative deactivation processes mainly in polar media.

Further halogenation produces entirely opposite results depending on the positions at which the chlorine is attached. Whereas chlorination at the 5- and 6-positions (compound **14**) causes a larger shift to lower energies and a slight recovery of the fluorescence capability (Figure 5), chlorination at the 5- and 7-positions (compound **13**) induces just the opposite effect (i.e., a shift to higher energies and a further reduction in the fluorescence capability). Such opposed tendencies are mainly related to nonradiative processes (Table 3), because the asymmetry in the pyrrole charge distribution mentioned above (Figure S3) is more pronounced upon substitution at the 7-position than at the 6-position.

In the case of dye PM546 (**15**), monochlorination (compound **16**) keeps the typical fluorescence quantum yield of the BODIPY chromophore, with values very close to unity (Table 3 and Supporting Information, Table S5). Dichlorination (compound **17**) produces more pronounced electron removal from the chromophore and a consequent slight decrease in the fluorescence ability, in good agreement with previous results reported for BODIPYs bearing electron acceptor moieties.[30] As discussed above, the 2- and 6-positions are not very sensitive to substituent effects (Figure S4 in the Supporting Information), so, apart from the expected spectral shift to lower energies, the optimal fluorescence behavior of this BODIPY is preserved upon chlorination.

## Lasing Properties

The lasing behavior of the *p*-tolyl chlorinated dyes **2**–**7** shows good correlation with their photophysical properties: the higher the fluorescence quantum yield, the higher the lasing efficiency, and the lower the nonradiative rate constant, the higher the lasing photostability.

Although the parent dye **1** does not lase, its chlorinated derivatives exhibit unexpected but highly efficient and photostable laser emission centered at ca. 575 nm when placed in a simple plane-plane nontunable resonator with a pump threshold energy of 0.8 mJ, a beam divergence of 5 mrad, and a pulse duration of 8 ns full-width at half maximum (FWHM). The dependence of the laser action of these new chlorinated derivatives on the corresponding dye concentrations was analyzed in ethyl acetate solutions by varying the optical densities from 8 to 30, while keeping all other experimental parameters constant. As an example, the results obtained for di- and trichlorinated dyes **3** and **5** are shown in Figure S5 in the Supporting Information.

Using the dye concentrations that optimized the laser efficiency of each derivative, we analyzed the dependence of their lasing properties both on the number and on the positions of the chlorine atoms attached to the chromophore. The laser efficiencies increase significantly with increasing chlorination of the BODIPY core, from 30% in monochlorinated dye **2** up to 60% in hexachlorinated dye **7** (Table 4). Consistently with the photophysical properties, chlorination at the 3- and 5-positions (dye **4**) enhances the laser efficiency with respect to that observed for dye **3**, which is also a dichlorinated derivative but with different regiochemistry (substituted at the 2- and 6-positions).[23]

The experimentally observable solvent effects on the dye laser action were analyzed in solutions of polar aprotic and polar protic solvents. No apolar solvents such as cyclohexane were used, due to the low solubilities of these new dyes, which prevented the production of solutions with the high dye concentrations required for laser operation under the pumping conditions selected in this work. Once again, photophysical and lasing properties are correlated: the higher the fluorescence quantum yields, the higher the lasing efficiencies. The laser actions of these chlorinated dyes in polar solvents such as acetone and methanol are thus less efficient than those registered in ethyl acetate. The *p*-tolyl chlorinated derivatives lase with high efficiencies, independently of the nature of the solvent (Table 4). These efficiencies are quite surprising in view of the low fluorescence quantum yields exhibited by these dyes (e.g., dye **2** lases with an efficiency of 28% in methanol in spite of having a fluorescent

 © 2012 Wiley-VCH Verlag GmbH & Co. KGaA, Weinheim 

Table 4. Lasing properties[a] of the new chlorinated derivatives of the *p*-tolyl BODIPY dye **1** in several solvents upon excitation at 532 nm.

| Dye | Data | EtOAc | MeOH | Acetone | $CH_2Cl_2$ |
|---|---|---|---|---|---|
| **2**[b] | $\lambda_l$ [nm] | 572 | 571 | 569 | 575 |
| | *Eff* [%] | 30 | 28 | 17 | 28 |
| | *I* [%] | 90 | | | |
| **3**[c] | $\lambda_l$ [nm] | 575 | 574 | 575 | 580 |
| | *Eff* [%] | 44 | 38 | 29 | 40 |
| | *I* [%] | 95 | | | |
| **4**[d] | $\lambda_l$ [nm] | 572 | 570 | 568 | 574 |
| | *Eff* [%] | 48 | 42 | 37 | 44 |
| | *I* [%] | 100 | | | |
| **5**[e] | $\lambda_l$ [nm] | 573 | 570 | 567 | 569 |
| | *Eff* [%] | 58 | 49 | 48 | 53 |
| | *I* [%] | 100 | | | |
| **6**[f] | $\lambda_l$ [nm] | 575 | 570 | 568 | 574 |
| | *Eff* [%] | 57 | 46 | 51 | 47 |
| | *I* [%] | 100 | | | |
| **7**[g] | $\lambda_l$ [nm] | 571 | 569 | 568 | 569 |
| | *Eff* [%] | 60 | 49 | 52 | 51 |
| | *I* [%] | 100 | | | |

[a] *Eff*: energy conversion efficiency. $\lambda_l$: peak wavelength of the laser emission. *I*: intensity of the dye laser output after 100000 pump pulses with respect to its initial intensity $I_0$. $I(\%) = (I/I_0) \times 100$, at 10 Hz repetition rate. [b] Dye concentration: $5 \times 10^{-3}$ M. [c] Dye concentration: $9 \times 10^{-4}$ M. [d] Dye concentration: $9 \times 10^{-4}$ M. [e] Dye concentration: $2 \times 10^{-3}$ M. [f] Dye concentration: $5 \times 10^{-4}$ M. [g] Dye concentration: $8 \times 10^{-4}$ M.

quantum yield of only 0.044). This behavior might be related to the short fluorescence lifetimes observed in the chlorinated derivatives, which lead to radiative rate constants similar to those observed in other BODIPY dyes.[4k,4l]

The lasing photostabilities of these dyes in ethyl acetate solutions were also analyzed by the protocol described in the Exp. Section. To compare the effect of chlorination on this laser parameter properly, the photostability of the parent dye **1** was also analyzed, because although it does not lase, it was possible to follow the evolution of its laser-induced fluorescence as a function of the number of pump pulses. The results are reported in Table 4 and, for purposes of clarity, the actual patterns of the fluorescence emissions of dyes **1**, **2**, and **6** under pumping at a repetition rate of 10 Hz are plotted in Figure 6. Once again, chlorination enhances the performances of these dyes: even monochlorinated **2** is more photostable than the parent compound **1**, and the photostabilities increase with the number of chlorine substituents in the BODIPY core. The tri-, tetra-, or hexachlorinated derivatives are thus highly photostable dyes, maintaining their initial laser outputs without sign of degradation after 100000 pumping pulses at 10 Hz repetition rate even under the drastic pumping conditions selected in this work. Once again, this laser behavior can be explained well in terms of the photophysics, because chlorination decreases the nonradiative rate constants significantly (Table 2) and, consequently, increases the laser lifetimes.

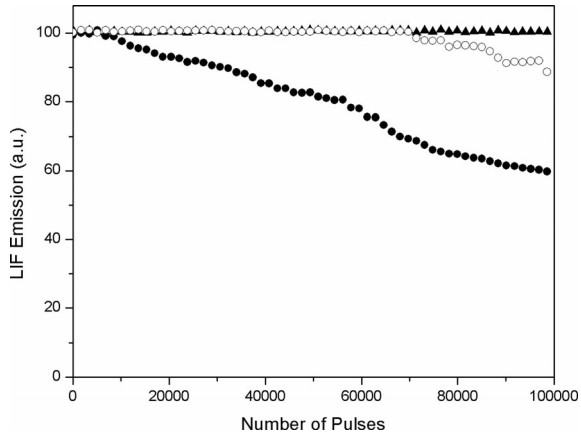


Figure 6. Normalized laser-induced fluorescence emissions as a function of the number of pump pulses for the dyes **1** (●), **2** (○), and **6** (▲) in ethyl acetate solutions. Pump laser wavelength, energy, and repetition rate: 532 nm, 5.5 mJ per pulse, and 10 Hz.

This enhancement of the laser behavior is also observed for all the other chlorinated BODIPY dyes **9** and **10** (derived from **8**), **12**–**14** (derived from **11**), and **16** and **17** (derived from **15**), when pumped under identical experimental conditions (Table 5). Dye **10**, for instance, exhibits a laser efficiency of 30% in ethyl acetate solution, which is a twofold increase with respect to its non-chlorinated parent dye **8**. The effect of chlorination on the laser actions of dyes **11** and **15** is outstanding. The low absorptions of parent dyes **11** and **15** at 532 nm preclude pumping at this standard wavelength. In fact, dye **11** has to be pumped at its maximum absorption wavelength (500 nm), increasing the technological complexity of the experimental setup and therefore limiting its applicability. The commercial dye PM546 (**15**) has to be pumped at a blue-shifted wavelength (355 nm), which is another standard wavelength used to induce laser emission from dye molecules. An advantage of chlorination of these dyes is the red-shifting of their absorption bands, allowing efficient pumping of the chlorinated derivatives at 532 nm, in the case of dye **11**, and even at

Table 5. Lasing properties of the new chlorinated BODIPY dyes in ethyl acetate solution pumped at 532 nm. For purposes of comparison, the corresponding data for the non-chlorinated dyes **8**, **11**, and **15**, evaluated under identical experimental conditions, are also included. Dye **11** was pumped at 500 nm and dyes **15** and **16** were pumped at 355 nm (data in parentheses).

| Laser data | Dyes<br>**8**[a] | **9**[b] | **10**[c] | **11**[d] | **12**[e] | **13**[e] | **14**[e] | **15**[f] | **16**[f(g)] | **17**[h] |
|---|---|---|---|---|---|---|---|---|---|---|
| *Eff* [%] | 14 | 28 | 30 | (34) | 38 | 46 | 36 | (23) | 40 (30) | 51 |
| $\lambda_l$ [nm] | 615 | 612 | 618 | (530) | 561 | 566 | 562 | (541) | 558 (556) | 562 |
| *I* [%] | 50 | 85 | 100 | (80) | 100 | 100 | 100 | (60) | 90 | 100 |

[a] Dye concentration: $1 \times 10^{-3}$ M. [b] $8 \times 10^{-4}$ M. [c] $1 \times 10^{-3}$ M. [d] $6 \times 10^{-4}$ M. [e] $15 \times 10^{-3}$ M. [f] $25 \times 10^{-3}$ M. [g] $3 \times 10^{-3}$ M. [h] $3.5 \times 10^{-3}$ M.

 © 2012 Wiley-VCH Verlag GmbH & Co. KGaA, Weinheim 

both standard wavelengths (355 and 532 nm) in the case of dye **15**. The monochlorinated derivative **12** thus lases at 561 nm with an efficiency of 38%, which increases to 46% for dichlorinated **13**. Similarly, monochlorinated **16** exhibits a highly efficient laser emission in ethyl acetate when pumped either in the UV or in the visible spectral regions. Whereas PM546 lases at 541 nm with an efficiency of 23% when pumped at 355 nm, its monochlorinated derivative **16** lases at 556 nm with an efficiency of 30% at the same pumping wavelength, which increases to 40% upon pumping at 532 nm.

Similar enhancement of the laser performances of dyes **8**, **11**, and **15** is also observed when the lasing properties of their chlorinated derivatives are analyzed as functions of the solvent (see Table S6 in the Supporting Information). In the same way, the photostabilities of these dyes are significantly improved by chlorination, the effect on the behavior of dye **8** being particularly remarkable; the laser output of **8** has decreased by 50% after 100000 pump pulses, but the presence of chlorine atoms is enough to maintain the laser emission at 100% of its initial value under the same experimental conditions.

Contrary to the behavior previously observed for the chlorinated derivatives of parent dye **1**, the laser data for chlorinated derivatives of **8**, **11**, and **15** do not correlate with their photophysical properties. In these dyes, the presence of chlorine induces significant increases in the laser actions (efficiencies and photostabilities) although, as discussed above, it has a deleterious effect on the photophysical properties (Tables S3–S5 in the Supporting Information) with the fluorescence quantum yields decreasing and the nonradiative rate constants increasing in relation to those registered for the non-chlorinated parent dyes.

A careful analysis of the results recorded with all the chlorinated BODIPY derivatives synthesized in this work suggests important questions about the influence of chlorine on the laser action of these dyes related to the following facts: a) a dye, such as tetrachlorinated **6**, with a fluorescence quantum yield in ethyl acetate as low as 0.39, exhibits a laser efficiency as high as 57%, b) a monochlorinated dye such as **12**, with a fluorescence quantum yield of 0.64, which is higher than that of **6**, exhibits a much lower laser efficiency (38%), c) monochlorinated laser dye **16**, with the highest fluorescence quantum yield (0.94), is not the most efficient laser dye of the series, and d) the good correlations established between the laser action and the photophysical properties of the chlorinated dyes derived from the parent compound **1** are not adhered to by the chlorinated dyes derived from compounds **8**, **11**, and **15**.

To gain deeper insight into the dependence of the laser behavior on chlorine substitution, we considered the effect of the polarization of the pump laser beam on the laser emissions of these new dyes, because the presence of an element as electronegative as chlorine should induce high dipole moments, the orientations of which would depend strongly on the number and positions of chlorine atoms on the BODIPY core. In the case of a dye molecule, the influence of polarization is determined mainly by the polarization of the exciting laser beam, the relative orientation of the transition moments in the dye molecule for the pumping and laser transitions, and the rotational diffusion-relaxation time. Matching the polarization of the pump laser to the preferred polarization of the gain medium can enhance the photon efficiency of the system. In contrast, if the applied field is not properly polarized or oriented with respect to the molecular dipole moment, the observed response will be reduced. To this end, the modules and orientations of the dipole moments of these molecules in the ground and excited states and the corresponding transition moments of absorption and emission were calculated (see Figures S6–S9 in the Supporting Information). The calculations showed that the transition moments of absorption and emission of the dye molecules studied are parallel to each other for excitation in the visible region of the spectrum because the same electronic transition is involved. The dye laser emissions were then measured as a function of the relative orientation between the polarization of the pumping radiation and that of the dye molecules. The pump laser was horizontally or vertically polarized by placing a combination of polarizer and $\lambda/2$ plate in the optical path. It was found that the tetrachlorinated dye **6**, which has a high dipole moment (11.230 D) totally aligned along (or parallel to) the transversal axis of the molecule, leads to a nonpolarized and highly efficient laser emission, regardless of the pump radiation being horizontally or vertically polarized.

With regard to dye **8**, its monochlorination to give **9** allows a better alignment of the molecular dipole moment along the transversal axis, reducing the twist angle of the dipole moment with respect to the axis induced by the *p*-formylphenyl substituent groups, which are disposed symmetrically, but slightly rotated with respect to the BODIPY core (Figure S8 in the Supporting Information) For this reason, dye **9** exhibits a nonpolarized laser emission with efficiency higher than that of its parent dye **8** and with a higher fluorescence quantum yield.

The influence of polarization on the laser actions of chlorinated dyes **12**, **14**, and **16** is more drastic, with dipole moments much lower and more rotated with respect to the transversal axis than those exhibited by the other chlorinated derivatives discussed previously (Figure S8 in the Supporting Information). Consequently, their laser emissions are highly polarized and, although efficient, are not as high as could be expected for dyes with the highest fluorescence quantum yields (0.78, 0.83, and 0.94, respectively).

The encouraging results registered with these new chlorinated dyes in the liquid phase led us to analyze the laser behavior of some of them when incorporated into solid-state matrices. The experiments were carried out with samples with those dye concentrations that had the highest lasing efficiencies in liquid solutions. MMA (methyl methacrylate) was chosen as the main monomeric component of the formulations because this ester mimics ethyl acetate, a solvent in which the studied dyes showed high lasing efficiencies. Broad-band and efficient laser emission, with beam divergence of ca. 5 mrad and pulse duration of ca. 5 ns FWHM, was registered for dyes **6** and **10** incorporated

 © 2012 Wiley-VCH Verlag GmbH & Co. KGaA, Weinheim 

as true solutions into the solid homopolymer PMMA (Table 6). No significant differences were observed in the wavelengths of the maximum laser emissions of each dye between their liquid and solid solutions. The dye-doped solid matrices exhibit high photostabilities, analyzed by monitoring the evolution of the laser outputs as a function of the number of pump pulses in the same position of the sample at a 10 Hz repetition rate. The lasing efficiencies of the solid materials (28% for **6** and 30% for **10**) are lower than those of the corresponding liquid solutions. Surface finishing of the solid samples in these experiments was not laser-grade, and higher lasing efficiencies would be expected with improved polishing.

Table 6. Laser properties of chlorinated BODIPY dyes **6** and **10** in PMMA pumped at 532 nm.

| Dye | [Dye] (M) | *Eff* [%] | $\lambda_l$ [nm] | *I* [%] |
|---|---|---|---|---|
| 6 | $5.0 \times 10^{-4}$ | 28 | 565 | 100 |
| 10 | $1.1 \times 10^{-3}$ | 30 | 614 | 95 |

## Conclusions

We have prepared a series of new mono- to hexachlorinated BODIPY dyes through three general synthetic strategies based on regioselective electrophilic chlorination with NCS as an inexpensive halogenating reagent. We have demonstrated that it is possible to control the degree of chlorination of the BODIPY core, which allows the synthesis of mono-, di-, and polychlorinated derivatives.

Quantum mechanical calculations can predict the positions at which chlorine will be incorporated and explain why some positions are less accessible to chlorination. Moreover, the positions at which the halogen is attached modulate the photophysical properties of the resulting BODIPYs. The fluorescence capacity of 8-tolyl-BODIPY or similar derivatives characterized by the presence of an aryl ring with unrestrained rotation can be tuned by the incorporation of appropriate substituents. In particular, the introduction of electron acceptor chlorine substituents at the 3- and 5-positions greatly increases the fluorescence capability of this compound. From a photophysical point of view, the chlorination of other BODIPYs leads to small reductions in fluorescence ability, but high fluorescence quantum yields are still obtained, making the use of these compounds as laser dyes possible.

The new chlorinated BODIPYs exhibit enhanced laser actions with respect to their non-halogenated analogues, both in liquid solution and in the solid phase. In fact, under demanding transversal pumping conditions, the presence of chlorine substituents allows lasing efficiencies as high as 60% to be reached, with high photostabilities. The surprisingly efficient laser actions from these newly chlorinated BODIPYs can be directly related to the improvement induced by chlorine in their photophysical properties and/or in their molecular dipole moments, increasing the modules and changing the orientations to match the polarization of the pump laser, which significantly enhances the photon efficiencies of the systems. In addition, chlorination is a facile and essentially costless protocol for overcoming important shortcomings exhibited by some commercial BODIPYs, such as low absorptions at standard laser pumping wavelengths and/or low photostabilities. In view of the easy synthetic assembly, and the large number of described BODIPY laser dyes, we are confident that this powerful approach can be extended to other dyes of this family, furthering their practical application in optical and sensing fields.[31]

## Experimental Section

**General:** Starting materials and reagents used in the preparation of BODIPYs are commercially available unless their synthesis is described. The solvents were dried and distilled before use. Spectral data for the known compounds were in accordance with the literature data. Flash column chromatography was performed with silica gel (Merck 60, 230–400 mesh). $^1$H and $^{13}$C NMR spectra were recorded with a Bruker Avance DPX 300 spectrometer (300 MHz for $^1$H and 75 MHz for $^{13}$C) and a Bruker Avance III spectrometer (700 MHz for $^1$H and 176 MHz for $^{13}$C). All spectra were recorded in $CDCl_3$. $^1$H chemical shifts are reported in ppm relative to tetramethylsilane ($\delta$ = 0.00 ppm) with use of the residual solvent signal as the internal reference. $^{13}$C chemical shifts are reported in ppm with $CDCl_3$ ($\delta$ = 77.67 ppm) as the internal standard. IR spectra ($cm^{-1}$) were recorded with a Bruker Tensor 27 FTIR spectrophotometer. Melting points were determined in open capillaries and are uncorrected. High-resolution mass spectra were determined by ESI with a FTMS Bruker APEX Q IV instrument and by EI with a Thermofisher MAT 95 XP.

BODIPY dyes **1**,[16] **4**,[8b,23] **8**,[4k] and **11**[4l] were synthesized by the methods described previously. BODIPY **15** was purchased from Lasing, S.A. and used as received.

**General Procedure for the Chlorination of BODIPY Core and Acetylpyrrole:** NCS in dry THF was slowly added at room temp. to a solution of starting material in dry THF and the reaction mixture was stirred for 12–72 h under argon. The solvent was removed and the mixture was diluted with EtOAc, washed with aqueous HCl (10%) and $H_2O$, dried with $MgSO_4$, filtered, and concentrated to dryness. The halogenated compounds were purified by flash chromatography on silica gel.

**General Procedure for the Synthesis of BODIPYs 12–14:** $POCl_3$ (1.1 equiv.) was added to a solution of chlorinated 2-acetylpyrrole (1 equiv.) in $CHCl_3$, and the mixture was stirred for 30 min at room temp. 3-Ethyl-2,4-dimethylpyrrole (1 equiv.) in $CHCl_3$ was then added and the resulting solution was stirred for 12 h at room temp. Triethylamine (1 equiv.) was added, followed by $BF_3{\cdot}Et_2O$ (1 equiv.), and the mixture was stirred for 3–4 h before being quenched with aqueous HCl (10%) and extracted with $CH_2Cl_2$. The organic extracts were washed with water, dried with $MgSO_4$, and filtered, and the solvents were evaporated to dryness. The dyes were isolated and purified by flash chromatography on silica gel.

**2-Chloro-4,4-difluoro-8-(4-tolyl)-4-bora-3a,4a-diaza-*s*-indacene (2):** BODIPY **1** (50 mg, 0.18 mmol) in dry THF (20 mL) and NCS (47 mg, 0.36 mmol) in dry THF (5 mL) were allowed to react for 12 h. Flash chromatography with hexane/EtOAc (98:2) afforded **2** (45 mg, 80%) as a green-orange solid; m.p. 171.8–172.0 °C. $^1$H NMR (700 MHz, $CDCl_3$): $\delta$ = 7.92 (s, 1 H, 5-H), 7.68 (s, 1 H, 3-

 © 2012 Wiley-VCH Verlag GmbH & Co. KGaA, Weinheim 

H), 7.39 (d, $J$ = 8.4 Hz, 2 H, 2′-H), 7.28 (d, $J$ = 8.4 Hz, 2 H, 3′-H), 6.95 (d, $J$ = 4.2 Hz, 1 H, 7-H), 6.74 (s, 1 H, 1-H), 6.52 (d, $J$ = 4.2 Hz, 1 H, 6-H), 2.41 (s, 3 H, $CH_3$) ppm. $^{13}C$ NMR (176 MHz, $CDCl_3$): $\delta$ = 147.8 (C-8), 145.8 (CH-5), 142.0 (C-4′), 139.7 (CH-3), 135.4 (C-7a), 133.2 (C-8a), 133.1 (CH-7), 130.6 (2×CH-2′), 130.5 (C-1′), 129.4 (2×CH-3′), 127.3 (CH-1), 121.5 (C-Cl), 119.3 (CH-6), 21.5 ($CH_3$) ppm. IR (neat): $\tilde{\nu}$ = 1548, 1405, 1364, 1259, 1105, 985 $cm^{-1}$. HRMS ($ESI^+$): calcd. for $[C_{16}H_{12}BClF_2N_2 + Na]^+$ 339.0648; found 339.0628.

**2,6-Dichloro-4,4-difluoro-8-(4-tolyl)-4-bora-3a,4a-diaza-*s*-indacene (3):** BODIPY **1** (40 mg, 0.14 mmol) in dry THF (15 mL) and NCS (56 mg, 0.42 mmol) in dry THF (5 mL) were allowed to react for 24 h. Flash chromatography with hexane/EtOAc (98:2) afforded **3** (39 mg, 85%) as an orange solid; m.p. 196.3–197.0 °C. $^1H$ NMR (700 MHz, $CDCl_3$): $\delta$ = 7.73 (s, 2 H, 3-H, and 5-H), 7.37 (d, $J$ = 8.4 Hz, 2 H, 2′-H), 7.29 (d, $J$ = 8.4 Hz, 2 H, 3′-H), 6.79 (s, 2 H, 1-H, and 7-H), 2.41 (s, 3 H, $CH_3$) ppm. $^{13}C$ NMR (176 MHz, $CDCl_3$): $\delta$ = 148.0 (C-8), 142.5 (C-4′), 141.8 and 141.7 (CH-3 and CH-5), 133.6 (C-7a and C-8a), 130.6 (2×CH-2′), 130.1 (C-1′), 129.6 (2×CH-3′), 128.6 and 128.5 (CH-1 and CH-7), 122.6 (C2-Cl and C6-Cl), 21.6 ($CH_3$) ppm. IR (neat): $\tilde{\nu}$ = 1550, 1484, 1358, 1261, 1112 $cm^{-1}$. HRMS ($ESI^+$): calcd. for $[C_{16}H_{11}BCl_2F_2N_2 + Na]^+$ 373.0258; found 373.0187.

**2,3,5-Trichloro-4,4-difluoro-8-(4-tolyl)-4-bora-3a,4a-diaza-*s*-indacene (5):** BODIPY **1** (90 mg, 0.32 mmol) in dry THF (15 mL) and NCS (171 mg, 1.28 mmol) in dry THF (10 mL) were allowed to react for 72 h. Flash chromatography with hexane/EtOAc (98:2) afforded **5** (40 mg, 32%) as an orange-red solid, together with an inseparable mixture of chlorinated products; m.p. 194.3–195.0 °C. $^1H$ NMR (700 MHz, $CDCl_3$): $\delta$ = 7.31 (d, $J$ = 8.4 Hz, 2 H, 2′-H), 7.27 (d, $J$ = 8.4 Hz, 2 H, 3′-H), 6.86 (d, $J$ = 4.2 Hz, 1 H, 7-H), 6.74 (s, 1 H, 1-H), 6.41 (d, $J$ = 4.2 Hz, 1 H, 6-H), 2.41 (s, 3 H, $CH_3$) ppm. $^{13}C$ NMR (176 MHz, $CDCl_3$): $\delta$ = 146.6 (C-8), 144.3 (C5-Cl), 142.0 (C-4′), 140.6 (C3-Cl), 134.1 (C-7a), 132.8 (CH-7), 131.1 (C-8a), 130.5 (2×CH-2′), 129.5 (2×CH-3′), 129.2 (C-1′), 127.2 (CH-1), 120.6 (C2-Cl), 119.6 (CH-6), 21.5 ($CH_3$) ppm. IR (neat): $\tilde{\nu}$ = 1554, 1387, 1258, 1107, 800 $cm^{-1}$. HRMS ($ESI^+$): calcd. for $[C_{16}H_{10}BCl_3F_2N_2 + Na]^+$ 406.9865; found 406.9834.

**2,3,5,6-Tetrachloro-4,4-difluoro-8-(4-tolyl)-4-bora-3a,4a-diaza-*s*-indacene (6):** BODIPY **1** (65 mg, 0.23 mmol) in dry THF (20 mL) and NCS (308 mg, 2.3 mmol) in dry THF (10 mL) were allowed to react for 48 h. Flash chromatography with hexane/EtOAc (98:2) afforded **6** (75 mg, 78%) as an orange-red solid; m.p. 231.0–231.8 °C. $^1H$ NMR (700 MHz, $CDCl_3$): $\delta$ = 7.30 (d, $J$ = 8.4 Hz, 2 H, 2′-H), 7.28 (d, $J$ = 8.4 Hz, 2 H, 3′-H), 6.79 (s, 2 H, 1-H and 7-H), 2.41 (s, 3 H, $CH_3$) ppm. $^{13}C$ NMR (176 MHz, $CDCl_3$): $\delta$ = 144.4 (C-8), 142.6 (C3-Cl and C5-Cl), 142.4 (C-4′), 131.4 (C-7a and C-8a), 130.5 (2×CH-2′), 129.6 (2×CH-3′), 128.9 (C-1′), 128.2 (CH-1 and CH-7), 121.6 (C2-Cl and C6-Cl), 21.5 ($CH_3$) ppm. IR (neat): $\tilde{\nu}$ = 1549, 1384, 1245, 1106 $cm^{-1}$. HRMS (EI): calcd. for $C_{16}H_9BCl_4F_2N_2$ 417.9579; found 417.9583.

**1,2,3,5,6,7-Hexachloro-4,4-difluoro-8-(4-tolyl)-4-bora-3a,4a-diaza-*s*-indacene (7):** NCS (3.38 g, 23.5 mmol) in dry THF (15 mL) was added slowly to a stirred solution of 5-(4-tolyl)dipyrromethane[17] (**18**, 400 mg, 1.69 mmol) in dry THF (30 mL), and the reaction mixture was heated at reflux under argon for 24 h. The solvent was removed, and DDQ (422 mg, 1.86 mmol) was added to the solution of the intermediate hexachlorodipyrromethane generated above in $CH_2Cl_2$ (50 mL). The mixture was stirred at room temp. for 1 h and triethylamine (1.5 mL, 8.4 mmol) was then added. After 10 min, $BF_3{\cdot}Et_2O$ (2 mL, 13.5 mmol) was added and the resulting solution was stirred for 24 h at room temp. The crude mixture was washed with $H_2O$, dried with $MgSO_4$, and filtered, and the solvents were evaporated to dryness. Purification by flash chromatography on silica gel with hexane/EtOAc (99:1) as eluent yielded **7** (245 mg, 30%) as a maroon solid; m.p. 275.1–276.0 °C. $^1H$ NMR (700 MHz, $CDCl_3$): $\delta$ = 7.26 (d, $J$ = 8.4 Hz, 2 H, 2′-H), 7.06 (d, $J$ = 8.4 Hz, 2 H, 3′-H), 2.40 (s, 3 H, $CH_3$) ppm. $^{13}C$ NMR (176 MHz, $CDCl_3$): $\delta$ = 143.7 (C-8), 142.5 (C-4′) 140.7 (C3-Cl and C5-Cl), 132.9 (C-7a and C-8a), 130.1 (2×CH-2′), 127.7 (2×CH-3′), 127.6 (C-1′), 126.3 (C1-Cl and C7-Cl), 121.4 (C2-Cl and C6-Cl), 21.6 ($CH_3$) ppm. IR (neat): $\tilde{\nu}$ = 1552, 1383, 1246, 1108 $cm^{-1}$. HRMS ($ESI^-$): calcd. for $[C_{16}H_7BCl_6F_2N_2 + CH_3OH - H]^+$ 518.8964; found 518.8926.

**2-Chloro-4,4-difluoro-3,5-bis(4-formylphenyl)-8-(4-tolyl)-4-bora-3a,4a-diaza-*s*-indacene (9):** BODIPY **8** (80 mg, 0.16 mmol) in dry THF (15 mL) and NCS (43 mg, 0.32 mmol) in dry THF (10 mL) were allowed to react for 48 h. Flash chromatography with hexane/EtOAc (9:1) afforded **9** (55 mg, 65%) as a red solid; m.p. 182.4–182.9 °C. $^1H$ NMR (700 MHz, $CDCl_3$): $\delta$ = 9.99 (s, 1 H, CHO), 9.95 (s, 1 H, CHO), 7.91 (d, $J$ = 8.4 Hz, 2 H, 4-formylphenyl), 7.90 (d, $J$ = 8.4 Hz, 2 H, 4-formylphenyl), 7.83 (d, $J$ = 8.4 Hz, 2 H, 4-formylphenyl), 7.79 (d, $J$ = 8.4 Hz, 2 H, 4-formylphenyl), 7.44 (d, $J$ = 8.4 Hz, 2 H, 4-tolyl), 7.32 (d, $J$ = 8.4 Hz, 2 H, 4-tolyl), 6.99 (d, $J$ = 4.2 Hz, 1 H, 7-H), 6.87 (s, 1 H, 1-H), 6.66 (d, $J$ = 4.2 Hz, 1 H, 6-H), 2.44 (s, 3 H, $CH_3$) ppm. $^{13}C$ NMR (176 MHz, $CDCl_3$): $\delta$ = 191.9 (CHO), 191.7 (CHO), 158.9 (C), 151.3 (C), 146.2 (C), 141.8 (C), 137.5 (C), 137.4 (2 C), 136.7 (C), 136.6 (C), 135.5 (C), 133.1 (CH), 131.1 (2×CH), 131.0 (C), 130.7 (2×CH), 130.0 (2×CH), 129.6 (2×CH), 129.4 (2×CH), 129.2 (2×CH), 127.8 (CH), 122.1 (C-Cl), 121.9 (CH) ppm. IR (neat): $\tilde{\nu}$ = 2926, 2860, 1702, 1542, 1260, 1073, 800 $cm^{-1}$. HRMS (EI): calcd. for $C_{30}H_{20}BClF_2N_2O_2$ 524.1272; found 524.1280.

**2,6-Dichloro-4,4-difluoro-3,5-bis(4-formylphenyl)-8-(4-tolyl)-4-bora-3a,4a-diaza-*s*-indacene (10):** BODIPY **8** (80 mg, 0.16 mmol) in dry THF (15 mL) and NCS (85 mg, 0.64 mmol) in dry THF (10 mL) were heated at reflux for 3 h. Flash chromatography with hexane/EtOAc (9:1) afforded **10** (55 mg, 62%) as a red solid; m.p. 211.3–211.8 °C. $^1H$ NMR (700 MHz, $CDCl_3$): $\delta$ = 9.98 (s, 2 H, 2×CHO), 7.87 (d, $J$ = 7.7 Hz, 4 H, 3′-H), 7.75 (d, $J$ = 7.7 Hz, 4 H, 2′-H), 7.44 (d, $J$ = 8.4 Hz, 2 H, 2′′-H), 7.34 (d, $J$ = 8.4 Hz, 2 H, 3′′-H), 6.93 (s, 2 H, 1-H and 7-H), 2.45 (s, 3 H, $CH_3$) ppm. $^{13}C$ NMR (176 MHz, $CDCl_3$): $\delta$ = 191.8 (2×CHO), 153.2 (C-3 and C-5), 146.4 (C-8), 142.2 (C-4′′), 136.8 (C-4′), 134.9 (C-1′), 133.4 (C-7a and C-8a), 130.9 (4 CH-2′), 130.6 (2×CH-2′′), 130.3 (C-1′′), 129.6 (2×CH-3′′), 129.2 (4 CH-3′), 129.1 (CH-1 and CH-7), 123.0 (C2-Cl and C6-Cl), 21.6 ($CH_3$) ppm. IR (neat): $\tilde{\nu}$ = 2924, 2856, 1700, 1540, 1268, 1219, 1144, 1070, 800, 768 $cm^{-1}$. HRMS ($ESI^-$): calcd. for $[C_{30}H_{19}BCl_2F_2N_2O_2 + CH_3OH - H]^+$ 589.1169; found 589.1234.

**Chlorination of Acetylpyrrole:** 2-Acetylpyrrole (200 mg, 1.83 mmol) in dry THF (30 mL) and NCS (269 mg, 2.01 mmol) in dry THF (30 mL) were allowed to react for 24 h at room temp. Flash chromatography with hexane/EtOAc (95:5) afforded 2-acetyl-5-chloropyrrole (**19**,[9e,18] 110 mg, 42%) as a colorless solid.

2-Acetylpyrrole (200 mg, 1.83 mmol) in dry THF (30 mL) and NCS (734 mg, 5.5 mmol) in dry THF (50 mL) were allowed to react for 72 h. Flash chromatography with hexane/EtOAc (95:5) afforded 2-acetyl-3,5-dichloropyrrole (**20**, 141 mg, 44%) as a colorless solid and 5-acetyl-2,3-dichloropyrrole (**21**,[18b] 125 mg, 39%) as a colorless solid.

**2-Acetyl-3,5-dichloropyrrole (20):** $^1H$ NMR (300 MHz, $CDCl_3$): $\delta$ = 10.09 (br. s, 1 H, NH), 6.07 (d, $J$ = 3.0 Hz, 1 H, 3-H), 2.51 (s, 3 H, $CH_3$) ppm. $^{13}C$ NMR (75 MHz, $CDCl_3$): $\delta$ = 186.7 (CO), 127.6

 © 2012 Wiley-VCH Verlag GmbH & Co. KGaA, Weinheim 

(C-2), 122.5 (C5-Cl), 119.7 (C3-Cl), 110.4 (CH), 28.1 ($CH_3$) ppm. IR (neat): $\tilde{\nu}$ = 3218, 1643, 1446, 1400, 761 $cm^{-1}$. HRMS (EI): calcd. for $C_6H_5Cl_2NO$ 176.9749; found 176.9751.

**5-Acetyl-2,3-dichloropyrrole (21):** $^1H$ NMR (300 MHz, $CDCl_3$): $\delta$ = 10.81 (br. s, 1 H, NH), 6.76 (d, $J$ = 2.7 Hz, 1 H, 4-H), 2.51 (s, 3 H, $CH_3$) ppm. $^{13}C$ NMR (75 MHz, $CDCl_3$): $\delta$ = 186.3 (CO), 128.0 (C-5), 120.5 (C2-Cl), 115.5 (CH), 110.5 (C3-Cl), 23.9 ($CH_3$) ppm. IR (neat): $\tilde{\nu}$ = 3218, 1643, 1447, 1399, 768 $cm^{-1}$. HRMS (EI): calcd. for $C_6H_5Cl_2NO$ 176.9749; found 176.9750.

**5-Chloro-2-ethyl-4,4-difluoro-1,3,8-trimethyl-4-bora-3a,4a-diaza-*s*-indacene (12):** 2-Acetyl-5-chloropyrrole (**19**,[9e,18] 91 mg, 0.63 mmol) in $CHCl_3$ (10 mL), $POCl_3$ (0.06 mL, 0.7 mmol), 3-ethyl-2,4-dimethylpyrrole (82 mg, 0.63 mmol) in $CHCl_3$ (10 mL), triethylamine (0.08 mL, 0.63 mmol), and $BF_3{\cdot}Et_2O$ (0.08 mL, 0.63 mmol) were allowed to react by the general procedure described above. Flash chromatography with hexane/$CHCl_3$ (5:5) afforded **12** (98 mg, 52%) as an orange solid; m.p. 171.2–171.7 °C. $^1H$ NMR (700 MHz, $CDCl_3$): $\delta$ = 6.90 (d, $J$ = 4.2 Hz, 1 H, 7-H), 6.20 (d, $J$ = 4.2 Hz, 1 H, 6-H), 2.51 (s, 3 H, $CH_3$), 2.44 (s, 3 H, $CH_3$), 2.35 (q, $J$ = 7.7 Hz, 2 H, $CH_2$), 2.26 (s, 3 H, $CH_3$), 0.99 (t, $J$ = 7.7 Hz, 3 H, $CH_3CH_2$) ppm. $^{13}C$ NMR (176 MHz, $CDCl_3$): $\delta$ = 161.1 (C), 140.7 (C), 138.6 (C), 135.7 (2 C), 134.0 (C), 133.1 (C), 122.8 (CH), 114.5 (CH), 17.1 ($CH_2$), 15.9 ($CH_3$), 14.5 ($CH_3$), 14.1 ($CH_3$), 13.1 ($CH_3$) ppm. IR (neat): $\tilde{\nu}$ = 1577, 1403, 1212, 1101, 771 $cm^{-1}$. HRMS (EI): calcd. for $C_{14}H_{16}BClF_2N_2$ 296.1060; found 296.1064.

**5,7-Dichloro-2-ethyl-4,4-difluoro-1,3,8-trimethyl-4-bora-3a,4a-diaza-*s*-indacene (13):** 2-Acetyl-3,5-dichloropyrrole (**20**, 90 mg, 0.50 mmol) in $CHCl_3$ (10 mL), $POCl_3$ (0.05 mL, 0.55 mmol), 3-ethyl-2,4-dimethylpyrrole (91 mg, 0.50 mmol) in $CHCl_3$ (10 mL), triethylamine (0.06 mL, 0.50 mmol), and $BF_3{\cdot}Et_2O$ (0.06 mL, 0.50 mmol) were allowed to react by the general procedure described above. Flash chromatography with hexane/EtOAc (98:2) afforded **13** (90 mg, 54%) as an orange solid; m.p. 193.1–193.6 °C. $^1H$ NMR (700 MHz, $CDCl_3$): $\delta$ = 6.21 (s, 1 H, 6-H), 2.72 (s, 3 H, $CH_3$), 2.51 (s, 3 H, $CH_3$), 2.36 (q, $J$ = 7.7 Hz, 2 H, $CH_2$), 2.31 (s, 3 H, $CH_3$), 1.00 (t, $J$ = 7.7 Hz, 3 H, $CH_3CH_2$) ppm. $^{13}C$ NMR (176 MHz, $CDCl_3$): $\delta$ = 162.2 (C), 141.7 (C), 139.8 (C), 137.0 (2 C), 135.0 (C), 133.2 (C), 127.2 (C), 126.4 (C), 115.6 (CH), 17.2 ($CH_2$), 16.3 ($CH_3$), 14.9 ($CH_3$), 14.4 ($CH_3$), 13.2 ($CH_3$) ppm. IR (neat): $\tilde{\nu}$ = 1568, 1417, 1375, 1194, 1084, 1031, 803 $cm^{-1}$. HRMS (EI): calcd. for $C_{14}H_{15}BCl_2F_2N_2$ 330.0668; found 330.0669.

**5,6-Dichloro-2-ethyl-4,4-difluoro-1,3,8-trimethyl-4-bora-3a,4a-diaza-*s*-indacene (14):** 5-Acetyl-2,3-dichloropyrrole (**21**, 90 mg, 0.50 mmol) in $CHCl_3$ (10 mL), $POCl_3$ (0.05 mL, 0.55 mmol), 3-ethyl-2,4-dimethylpyrrole (91 mg, 0.50 mmol) in $CHCl_3$ (10 mL), triethylamine (0.06 mL, 0.50 mmol) and $BF_3{\cdot}Et_2O$ (0.06 mL, 0.50 mmol) were allowed to react by the general procedure described above. Flash chromatography with hexane/EtOAc (95:5) afforded **14** (80 mg, 48%) as an orange solid; m.p. 187.3–187.8. $^1H$ NMR (700 MHz, $CDCl_3$): $\delta$ = 6.83 (s, 1 H, 7-H), 2.53 (s, 3 H, $CH_3$), 2.41 (s, 3 H, $CH_3$), 2.36 (q, $J$ = 7.7 Hz, 2 H, $CH_2$), 2.28 (s, 3 H, $CH_3$), 1.00 (t, $J$ = 7.7 Hz, 3 H, $CH_3CH_2$) ppm. $^{13}C$ NMR (176 MHz, $CDCl_3$): $\delta$ = 163.7 (C), 141.8 (C), 137.8 (C), 136.6 (2 C), 134.7 (C), 131.7 (C), 130.7 (C), 119.5 (CH), 116.2 (C), 17.1 ($CH_2$), 15.8 ($CH_3$), 14.4 ($CH_3$), 14.2 ($CH_3$), 13.3 ($CH_3$) ppm. IR (neat): $\tilde{\nu}$ = 1579, 1404, 1206, 1147, 1093, 1022, 801 $cm^{-1}$. HRMS (EI): calcd. for $C_{14}H_{15}BCl_2F_2N_2$ 330.0668; found 330.0670.

**2-Chloro-4,4-difluoro-1,3,5,7,8-pentamethyl-4-bora-3a,4a-diaza-*s*-indacene (16):** BODIPY **15** (60 mg, 0.23 mmol) in dry THF (15 mL) and NCS (37 mg, 0.28 mmol) in dry THF (5 mL) were allowed to react for 48 h. Flash chromatography with hexane/$CHCl_3$ (7:3) afforded **16** (50 mg, 73%) as an orange solid; m.p. 259.4–259.7 °C. $^1H$ NMR (700 MHz, $CDCl_3$): $\delta$ = 6.03 (s, 1 H, 6-H), 2.53 (s, 3 H, $CH_3$-C8), 2.46 (s, 6 H, $CH_3$-C3 and $CH_3$-C5), 2.36 (s, 3 H, $CH_3$-C7), 2.34 (s, 3 H, $CH_3$-C1) ppm. $^{13}C$ NMR (176 MHz, $CDCl_3$): $\delta$ = 156.0 (C-5), 148.3 (C-3), 142.8 (C-7), 141.7 (C-8), 134.1 (C-1), 132.7 (C-7a), 129.8 (C-8a), 122.1 (CH-6), 121.3 (C-Cl), 17.5 ($CH_3$-C7), 16.7 ($CH_3$-C8), 14.6 ($CH_3$-C5), 14.4 ($CH_3$-C1), 12.2 ($CH_3$-C3) ppm. IR (neat): $\tilde{\nu}$ = 1560, 1365, 1268, 1110 $cm^{-1}$. HRMS ($ESI^+$): calcd. for $[C_{14}H_{16}BClF_2N_2 + Na]^+$ 319.0961; found 319.0980.

**2,6-Dichloro-4,4-difluoro-1,3,5,7,8-pentamethyl-4-bora-3a,4a-diaza-*s*-indacene (17):** BODIPY **15** (50 mg, 0.19 mmol) in dry THF (15 mL) and NCS (76 mg, 0.57 mmol) in dry THF (10 mL) were allowed to react for 24 h. Flash chromatography with hexane/EtOAc (98:2) afforded **17** (42 mg, 67%) as an orange solid; m.p. 261.1–261.6 °C. $^1H$ NMR (700 MHz, $CDCl_3$): $\delta$ = 2.56 (s, 3 H, $CH_3$-C8), 2.48 (s, 6 H, $CH_3$-C3 and $CH_3$-C5), 2.35 (s, 3 H, $CH_3$-C1 and $CH_3$-C7) ppm. $^{13}C$ NMR (176 MHz, $CDCl_3$): $\delta$ = 150.7 (C-3 and C-5), 142.2 (C-8), 135.8 (C-1 and C-7), 130.4 (C-7a and C-8a), 122.4 (2 × C-Cl), 17.1 ($CH_3$-C8), 14.6 ($CH_3$-C1 and $CH_3$-C7), 12.3 ($CH_3$-C3 and $CH_3$-C5) ppm. IR (neat): $\tilde{\nu}$ = 1560, 1362, 1270, 1111 $cm^{-1}$. HRMS (EI): calcd. for $C_{14}H_{15}BCl_2F_2N_2$ 330.0668; found 330.0668.

**Preparation of Solid Polymeric Samples:** Solid matrices of PMMA incorporating some of the new fluorinated BDP dyes as true solutions were prepared essentially as described elsewhere.[4d] An appropriate amount of the dye was dissolved in pure MMA, which was polymerized to yield the materials named dye/PMMA. The solid samples were cast in a cylindrical shape, forming rods of 10 mm diameter and 10 mm length. A cut was made parallel to the axis of the cylinder to obtain a lateral flat surface of ca. 6 × 10 mm. This surface and the ends of the laser rods were prepared for lasing experiments with a grinding and polishing machine (Phoenix Beta 4000, Büehler) until optical-grade finishing. The planar grinding stage was carried out with a Texmet 1000 sand paper and 6 μm diamonds suspended in mineral oil as abrasive. The final polishing stage was carried out with a G-Tuch Microcloth and a cloth disk Mastertex with 1 μm diamonds in mineral oil.

**Photophysical Properties:** Solvents for laser and photophysical studies were of spectroscopic grade (Merck, Aldrich, or Sigma) and were used without purification; those used in synthetic work were purified by standard methods. Other reagents were from commercial sources, and used as received. The commercial laser dyes Pyrromethene 546 (Exciton) was used as received with a purity >99% (checked by spectroscopic and chromatographic methods). The monomer MMA (Merck) was successively washed with aqueous NaOH (5%) and water, dried with $Na_2SO_4$, and distilled under reduced pressure. Other reagents were from commercial sources and were used as received. The photophysical properties were determined in diluted solutions (around $2 \times 10^{-6}$ M), prepared by adding the corresponding solvent (spectroscopic grade) to the residue from the appropriate amount of a concentrated stock solution in acetone, after vacuum evaporation of this solvent. UV/Vis absorption and fluorescence spectra were recorded with a Varian model CARY 4E spectrophotometer and a SPEX Fluorolog 3–22 spectrofluorimeter, respectively. Fluorescence quantum yields ($\phi$) were determined by use of diluted dye solutions of suitable commercial BODIPYs (PM567 and PM650, $\phi$ = 0.84 and 0.10, respectively).[4a] Radiative decay curves were registered by the time-correlated single-photon-counting technique (Edinburgh Instruments, model FL920, fitted with a Hamamatsu C4878 microchannel plate detector), with picosecond time-resolution. Fluorescence emission was

 © 2012 Wiley-VCH Verlag GmbH & Co. KGaA, Weinheim 

monitored at the maximum emission wavelength after excitation at 470 nm and 530 nm with a diode laser (PicoQuant, model LDH470 and LDH530) with 150 ps FWHM pulses. The fluorescence lifetime ($\tau$) was obtained after deconvolution of the instrumental response signal from the recorded decay curves by an iterative method. The goodness of the exponential fit was controlled by statistical parameters (chi-square, Durbin–Watson, and analysis of residuals). The radiative ($k_{fl}$) and nonradiative ($k_{nr}$) rate constants were calculated from the fluorescence quantum yield and lifetime; $k_{fl} = \phi/\tau$ and $k_{nr} = (1 - \phi)/\tau$. In the case of biexponential deconvolutions the amplitude-averaged lifetime – $<\tau>$ – was calculated as the sum of the products of each lifetime and their contibutions divided by 100. The corresponding rate constants were calculated from this average lifetime ($<k_{fl}>$ and $<k_{nr}>$).

**Laser Experiments:** Liquid solutions of dyes were placed in 1 cm optical path quartz cells carefully sealed to avoid solvent evaporation during experiments. The solutions of the newly synthesized dyes, as well as the solid samples, were transversely pumped at different wavelengths matching the maximum absorptions of the corresponding dyes: at 355 nm, with 5 mJ per pulse, 8 ns FWHM pulses from the third-harmonic of a Q-switched Nd:YAG laser (Spectron SL282G) and at 532 nm with 5.5 mJ, 6 ns FWHM pulses from a frequency-doubled Q-switched Nd:YAG laser (Monocrom OPL-10) at a repetition rate of 10 Hz. The exciting pulses were line-focused onto the cell, providing pump fluences on the active medium of 110 mJ cm$^{-2}$. The oscillation cavity (2 cm length) consisted of a 90% reflectivity aluminum mirror, with the lateral face of the cell as output coupler.

The photostabilities of the dyes were evaluated by irradiation of solutions in ethyl acetate (10 μL) under lasing conditions. Each solution was contained in a cylindrical Pyrex tube (1 cm height, 1 mm internal diameter) carefully sealed to avoid solvent evaporation during the experiments. Although the low optical quality of the capillary tube prevents laser emission from the dyes, information about photostabilities can be obtained by monitoring the decrease in laser-induced fluorescence intensity, excited transversally to the capillary tube, as a function of the number of pump pulses at 10 Hz repetition rate. The fluorescence emission was monitored perpendicular to the exciting beam, collected through an optical fiber, imaged onto the input slit of a monochromator (Acton Research corporation), and detected with a charge-coupled device (CCD, SpectruMM:GS128B). The fluorescence emission was recorded by feeding the signal to the boxcar (Stanford Research, model 250) for integration prior to digitization and processing by a computer. Each experience was repeated at least three times. The estimated error in the energy and photostability measurements was 10%.

**Computational Details:** All quantum mechanical calculations were performed with the aid of the Gaussian 03 package. Ground- and excited-state geometries were fully optimized by the Density Functional Theory (DFT) method (with use of B3LYP) and the Configuration Interaction Singles (CIS) ab initio method, respectively, with use of the double-valence basis set (6–31G). Absorption and fluorescence transitions were simulated by the time-dependent DFT (TD-DFT) method from the ground- and excited-state geometries, respectively.

**X-ray Crystallographic Data:** Crystals of BODIPYs **5**–**7** suitable for X-ray analysis were obtained by recrystallization from hexane. Crystal data were collected with an Agilent SuperNova Cu diffractometer and a CCD Atlas detector at 100 K.

CCDC-882023 (for **5**), -882022 (for **6**), and -882021 (for **7**) contain the supplementary crystallographic data for this paper. These data can be obtained free of charge from The Cambridge Crystallographic Data Centre via www.ccdc.cam.ac.uk/data_request/cif.

**Supporting Information** (see footnote on the first page of this article): copies of $^1$H and $^{13}$C NMR spectra of all new compounds, full photophysical and laser data for compounds **1**–**17** in different solvents, quantum mechanical simulations of their charge distributions and dipole moment orientations, and additional figures and tables mentioned in the article.

## Acknowledgments

This work was supported by the Ministerio de Economia y Competitividad (MAT2010-20646-C04-01, MAT2010-20646-C04-02, MAT2010-20646-C04-03, MAT2010-20646-C04-04, and TRACE 2009-0144), the Comunidad de Madrid and the European Social Fund (S2009/PPQ-1634 "AVANCAT"), and the Gobierno Vasco (project number IT339-10). The SGI/IZO-SGIker UPV-EHU is gratefully thanked for allocation of computational resources. G. D. thanks Ministerio de Economía y Competitividad for an FPI fellowship.

[1] a) A. Loudet, K. Burgess, *Chem. Rev.* **2007**, *107*, 4891–4932; b) R. Ziessel, G. Ulrich, A. Harriman, *New J. Chem.* **2007**, *31*, 496–501; c) G. Ulrich, R. Ziessel, A. Harriman, *Angew. Chem.* **2008**, *120*, 1202; *Angew. Chem. Int. Ed.* **2008**, *47*, 1184–1201; d) F. L. Arbeloa, J. Bañuelos, V. Martinez, T. Arbeloa, I. L. Arbeloa, *Trends Phys. Chem.* **2008**, *13*, 101–122; e) A. C. Benniston, G. Copley, *Phys. Chem. Chem. Phys.* **2009**, *11*, 4124–4131; f) M. Benstead, G. H. Mehl, R. W. Boyle, *Tetrahedron* **2011**, *67*, 3573–3601; g) N. Boens, V. Leen, W. Dehaen, *Chem. Soc. Rev.* **2012**, *41*, 1130–1172.

[2] a) R. E. Pagano, C.-S. Chen, *Ann. N. Y. Acad. Sci.* **1998**, *845*, 152–160; b) R. E. Pagano, R. Watanabe, C. Wheatley, M. Dominguez, *Methods Enzymol.* **2000**, *312*, 523–534; c) Y. Gabe, Y. Urano, K. Kikuchi, H. Kojima, T. Nagano, *J. Am. Chem. Soc.* **2004**, *126*, 3357–3367; d) Z.-N. Sun, H.-L. Wang, F.-Q. Liu, Y. Chen, P. K. H. Tam, D. Yang, *Org. Lett.* **2009**, *11*, 1887–1890; e) A. Ojida, T. Sakamoto, M.-A. Inoue, S.-H. Fujishima, G. Lippens, I. Hamachi, *J. Am. Chem. Soc.* **2009**, *131*, 6543–6548; f) P. Didier, G. Ulrich, Y. Mely, R. Ziessel, *Org. Biomol. Chem.* **2009**, *7*, 3639–3642; g) X. Qian, Y. Xiao, Y. Xu, X. Guo, J. Qian, W. Zhu, *Chem. Commun.* **2010**, *46*, 6418–6436; h) J. O. Escobedo, O. Rusin, S. Lim, R. M. Strongin, *Curr. Opin. Chem. Biol.* **2010**, *14*, 64–70.

[3] a) A. Gorman, J. Killoran, C. O'Shea, T. Kenna, W. M. Gallagher, D. F. O'Shea, *J. Am. Chem. Soc.* **2004**, *126*, 10619–10631; b) S. O. McDonnell, M. J. Hall, L. T. Allen, A. Byrne, W. M. Gallagher, D. F. O'Shea, *J. Am. Chem. Soc.* **2005**, *127*, 16360–16361; c) T. Yogo, Y. Urano, Y. Ishitsuka, F. Maniwa, T. Nagano, *J. Am. Chem. Soc.* **2005**, *127*, 12162–12163; d) S. Atilgan, Z. Ekmekci, A. L. Dogan, D. Guc, E. U. Akkaya, *Chem. Commun.* **2006**, 4398–4400; e) S. Erbas, A. Gorgulu, M. Kocakusakogullari, E. U. Akkaya, *Chem. Commun.* **2009**, 4956–4958; f) S. Ozlem, E. U. Akkaya, *J. Am. Chem. Soc.* **2009**, *131*, 48–49; g) S. H. Lim, C. Thivierge, P. Nowak-Sliwinska, J. Han, H. van den Bergh, G. Wagnières, K. Burgess, H. B. Lee, *J. Med. Chem.* **2010**, *53*, 2865–2874; h) N. Adarsh, R. R. Avirah, D. Ramaiah, *Org. Lett.* **2010**, *12*, 5720–5723; i) H. He, P.-C. Lo, S.-L. Yeung, W.-P. Fong, D. K. P. Ng, *Chem. Commun.* **2011**, *47*, 4748–4750; j) H. He, P.-C. Lo, S.-L. Yeung, W.-P. Fong, D. K. P. Ng, *J. Med. Chem.* **2011**, *54*, 3097–3102; k) S. G. Awuah, J. Polreis, V. Biradar, Y. You, *Org. Lett.* **2011**, *13*, 3884–3887; l) Y. Cakmak, S. Kolemen, S. Duman, Y. Dede, Y. Dolen,

 © 2012 Wiley-VCH Verlag GmbH & Co. KGaA, Weinheim 

B. Kilic, Z. Kostereli, L. T. Yildirim, A. L. Dogan, D. Guc, E. U. Akkaya, *Angew. Chem.* **2011**, *123*, 12143; *Angew. Chem. Int. Ed.* **2011**, *50*, 11937–11941; m) Y. Chen, J. Zhao, L. Xie, H. Guo, Q. Li, *RSC Adv.* **2012**, *2*, 3942–3953; n) M. J. Ortiz, A. R. Agarrabeitia, G. Duran-Sampedro, J. Bañuelos Prieto, T. Arbeloa Lopez, W. A. Massad, H. A. Montejano, N. A. García, I. Lopez Arbeloa, *Tetrahedron* **2012**, *68*, 1153–1162; o) S. Duman, Y. Cakmak, S. Kolemen, E. U. Akkaya, Y. Dede, *J. Org. Chem.* **2012**, *77*, 4516–4527.

[4] a) F. Lopez Arbeloa, J. Bañuelos Prieto, V. Martinez, T. Arbeloa, I. Lopez Arbeloa, *Int. Rev. Phys. Chem.* **2005**, *24*, 339–374; b) O. Garcia, R. Sastre, D. del Agua, A. Costela, I. Garcia-Moreno, *Chem. Mater.* **2006**, *18*, 601–602; c) M. Liras, J. Bañuelos Prieto, M. Pintado-Sierra, F. Lopez Arbeloa, I. Garcia-Moreno, A. Costela, L. Infantes, R. Sastre, F. Amat-Guerri, *Org. Lett.* **2007**, *9*, 4183–4186; d) I. Garcia-Moreno, F. Amat-Guerri, M. Liras, A. Costela, L. Infantes, R. Sastre, F. Lopez Arbeloa, J. Bañuelos Prieto, I. Lopez Arbeloa, *Adv. Funct. Mater.* **2007**, *17*, 3088–3098; e) O. Garcia, R. Sastre, D. del Agua, A. Costela, I. Garcia-Moreno, F. Lopez Arbeloa, J. Bañuelos Prieto, I. Lopez Arbeloa, *J. Phys. Chem. C* **2007**, *111*, 1508–1516; f) O. Garcia, L. Garrido, R. Sastre, A. Costela, I. Garcia-Moreno, *Adv. Funct. Mater.* **2008**, *18*, 2017–2025; g) A. Costela, I. Garcia-Moreno, M. Pintado-Sierra, F. Amat-Guerri, M. Liras, R. Sastre, F. Lopez Arbeloa, J. Bañuelos Prieto, I. Lopez Arbeloa, *J. Photochem. Photobiol. A: Chem.* **2008**, *198*, 192–199; h) M. Alvarez, A. Costela, I. Garcia-Moreno, F. Amat-Guerri, M. Liras, R. Sastre, F. Lopez Arbeloa, J. Bañuelos Prieto, I. Lopez Arbeloa, *Photochem. Photobiol. Sci.* **2008**, *7*, 802–813; i) A. Costela, I. Garcia-Moreno, M. Pintado-Sierra, F. Amat-Guerri, R. Sastre, M. Liras, F. Lopez Arbeloa, J. Bañuelos Prieto, I. Lopez Arbeloa, *J. Phys. Chem. A* **2009**, *113*, 8118–8124; j) I. Garcia-Moreno, D. Zhang, A. Costela, V. Martin, R. Sastre, Y. Xiao, *J. Appl. Phys.* **2010**, *107*, 073105; k) M. J. Ortiz, I. Garcia-Moreno, A. R. Agarrabeitia, G. Duran-Sampedro, A. Costela, R. Sastre, F. Lopez Arbeloa, J. Bañuelos Prieto, I. Lopez Arbeloa, *Phys. Chem. Chem. Phys.* **2010**, *12*, 7804–7811; l) J. Bañuelos Prieto, A. R. Agarrabeitia, I. Garcia-Moreno, I. Lopez-Arbeloa, A. Costela, L. Infantes, M. E. Perez-Ojeda, M. Palacios-Cuesta, M. J. Ortiz, *Chem. Eur. J.* **2010**, *16*, 14094–14105; m) Y. Xiao, D. Zhang, X. Qian, A. Costela, I. Garcia-Moreno, V. Martin, M. E. Perez-Ojeda, J. Bañuelos, L. Gartzia, I. Lopez Arbeloa, *Chem. Commun.* **2011**, *47*, 11513–11515; n) D. Zhang, V. Martin, I. Garcia-Moreno, A. Costela, M. E. Perez-Ojeda, Y. Xiao, *Phys. Chem. Chem. Phys.* **2011**, *13*, 13026–13033; o) J. Bañuelos, V. Martin, C. F. A. Gomez-Duran, I. J. Arroyo Cordoba, E. Peña-Cabrera, I. Garcia-Moreno, A. Costela, M. E. Perez-Ojeda, T. Arbeloa, I. Lopez Arbeloa, *Chem. Eur. J.* **2011**, *17*, 7261–7270.

[5] L. Cerdan, A. Costela, I. Garcia-Moreno, O. Garcia, R. Sastre, *Opt. Express* **2010**, *18*, 10247–10256.

[6] L. Bonardi, H. Kanaan, F. Camerel, P. Jolinat, P. Retailleau, R. Ziessel, *Adv. Funct. Mater.* **2008**, *18*, 401–413.

[7] a) S. Hattori, K. Ohkubo, Y. Urano, H. Sunahara, T. Nagano, Y. Wada, N. V. Tkachenko, H. Lemmetyinen, S. Fukuzumi, *J. Phys. Chem. B* **2005**, *109*, 15368–15375; b) S. Erten-Ela, M. D. Yilmaz, B. Icli, Y. Dede, S. Icli, E. U. Akkaya, *Org. Lett.* **2008**, *10*, 3299–3302; c) T. Rousseau, A. Cravino, T. Bura, G. Ulrich, R. Ziessel, J. Roncali, *Chem. Commun.* **2009**, 1673–1675; d) T. Rousseau, A. Cravino, T. Bura, G. Ulrich, R. Ziessel, J. Roncali, *J. Mater. Chem.* **2009**, *19*, 2298–2300; e) D. Kumaresan, R. P. Thummel, T. Bura, G. Ulrich, R. Ziessel, *Chem. Eur. J.* **2009**, *15*, 6335–6339; f) T. Rousseau, A. Cravino, E. Ripaud, P. Leriche, S. Rihn, A. De Nicola, R. Ziessel, J. Roncali, *Chem. Commun.* **2010**, *46*, 5082–5084; g) C. Y. Lee, J. T. Hupp, *Langmuir* **2010**, *26*, 3760–3765; h) S. Kolemen, Y. Cakmak, S. Erten-Ela, Y. Altay, J. Brendel, M. Thelakkat, E. U. Akkaya, *Org. Lett.* **2010**, *12*, 3812–3815; i) B.-S. Kim, B. Ma, V. R. Donuru, H. Liu, J. M. J. Frechet, *Chem. Commun.* **2010**, *46*, 4148–4150; j) T. Kiliçoglu, Y. S. Ocak, *Microelectron. Eng.* **2011**, *88*, 150–154; k) T. Bura, N. Leclerc, S. Fall, P. Lévêque, T. Heiser, R. Ziessel, *Org. Lett.* **2011**, *13*, 6030–6033.

[8] a) M. Baruah, W. Qin, R. A. L. Vallée, D. Beljonne, T. Rohand, W. Dehaen, N. Boens, *Org. Lett.* **2005**, *7*, 4377–4380; b) T. Rohand, M. Baruah, W. Qin, N. Boens, W. Dehaen, *Chem. Commun.* **2006**, 266–268; c) T. Rohand, J. Lycoops, S. Smout, E. Braeken, M. Sliwa, M. Van der Auweraer, W. Dehaen, W. M. De Borggraeve, N. Boens, *Photochem. Photobiol. Sci.* **2007**, *6*, 1061–1066; d) W. Qin, T. Rohand, W. Dehaen, J. N. Clifford, K. Driesen, D. Beljonne, B. Van Averbeke, M. Van der Auweraer, N. Boens, *J. Phys. Chem. A* **2007**, *111*, 8588–8597; e) L. Li, B. Nguyen, K. Burgess, *Bioorg. Med. Chem. Lett.* **2008**, *18*, 3112–3116; f) O. Dilek, S. L. Bane, *Tetrahedron Lett.* **2008**, *49*, 1413–1416; g) O. Dilek, S. L. Bane, *Bioorg. Med. Chem. Lett.* **2009**, *19*, 6911–6913; h) E. Fron, E. Coutiño-Gonzalez, L. Pandey, M. Sliwa, M. Van der Auweraer, F. C. De Schryver, J. Thomas, Z. Dong, V. Leen, M. Smet, W. Dehaen, T. Vosch, *New J. Chem.* **2009**, *33*, 1490–1496; i) W. Qin, V. Leen, W. Dehaen, J. Cui, C. Xu, X. Tang, W. Liu, T. Rohand, D. Beljonne, B. Van Averbeke, J. N. Clifford, K. Driesen, K. Binnemans, M. Van der Auweraer, N. Boens, *J. Phys. Chem. C* **2009**, *113*, 11731–11740; j) L. Jiao, C. Yu, M. Liu, Y. Wu, K. Cong, T. Meng, Y. Wang, E. Hao, *J. Org. Chem.* **2010**, *75*, 6035–6038; k) D. W. Domaille, L. Zeng, C. J. Chang, *J. Am. Chem. Soc.* **2010**, *132*, 1194–1195; l) S. Yin, V. Leen, S. Van Snick, N. Boens, W. Dehaen, *Chem. Commun.* **2010**, *46*, 6329–6331; m) V. Leen, T. Leemans, N. Boens, W. Dehaen, *Eur. J. Org. Chem.* **2011**, *23*, 4386–4396; n) S. C. Dodani, S. C. Leary, P. A. Cobine, D. R. Winge, C. J. Chang, *J. Am. Chem. Soc.* **2011**, *133*, 8606–8616; o) L. Jiao, W. Pang, J. Zhou, Y. Wei, X. Mu, G. Bai, E. Hao, *J. Org. Chem.* **2011**, *76*, 9988–9996; p) V. Leen, D. Miscoria, S. Yin, A. Filarowski, J. M. Ngongo, M. Van der Auweraer, N. Boens, W. Dehaen, *J. Org. Chem.* **2011**, *76*, 8168–8176; q) X. Li, S. Huang, Y. Hu, *Org. Biomol. Chem.* **2012**, *10*, 2369–2372.

[9] a) C.-W. Wan, A. Burghart, J. Chen, F. Bergström, L. B.-A. Johansson, M. F. Wolford, T. G. Kim, M. R. Topp, R. M. Hochstrasser, K. Burgess, *Chem. Eur. J.* **2003**, *9*, 4430–4441; b) T. Rohand, W. Qin, N. Boens, W. Dehaen, *Eur. J. Org. Chem.* **2006**, 4658–4663; c) L. Bonardi, G. Ulrich, R. Ziessel, *Org. Lett.* **2008**, *10*, 2183–2186; d) D. Zhang, Y. Wen, Y. Xiao, G. Yu, Y. Liu, X. Qian, *Chem. Commun.* **2008**, 4777–4779; e) V. Leen, E. Braeken, K. Luckermans, C. Jackers, M. Van der Auweraer, N. Boens, W. Dehaen, *Chem. Commun.* **2009**, 4515–4517; f) Ö. A. Bozdemir, O. Büyükcakir, E. U. Akkaya, *Chem. Eur. J.* **2009**, *15*, 3830–3838; g) S. Rihn, P. Retailleau, N. Bugsaliewicz, A. De Nicola, R. Ziessel, *Tetrahedron Lett.* **2009**, *50*, 7008–7013; h) Y. Cakmak, E. U. Akkaya, *Org. Lett.* **2009**, *11*, 85–88; i) R. Guliyev, A. Coskun, E. U. Akkaya, *J. Am. Chem. Soc.* **2009**, *131*, 9007–9013; j) O. A. Bozdemir, Y. Cakmak, F. Sozmen, T. Ozdemir, A. Siemiarczuk, E. U. Akkaya, *Chem. Eur. J.* **2010**, *16*, 6346–6351; k) C. Thivierge, J. Han, R. M. Jenkins, K. Burgess, *J. Org. Chem.* **2011**, *76*, 5219–5228; l) T. K. Khan, M. Ravikanth, *Tetrahedron* **2011**, *67*, 5816–5824; m) S. Niu, G. Ulrich, P. Retailleau, R. Ziessel, *Tetrahedron Lett.* **2011**, *52*, 4848–4853; n) V. Lakshmi, M. J. Ravikanth, *Org. Chem.* **2011**, *76*, 8466–8471; o) S. Rihn, M. Erdem, A. De Nicola, P. Retailleau, R. Ziessel, *Org. Lett.* **2011**, *13*, 1916–1919; p) Y. Hayashi, S. Yamaguchi, W. Y. Cha, D. Kim, H. Shinokubo, *Org. Lett.* **2011**, *13*, 2992–2995; q) L. Fu, F.-L. Jiang, D. Fortin, P. D. Harvey, Y. Liu, *Chem. Commun.* **2011**, *47*, 5503–5505; r) D. T. Chase, B. S. Young, M. M. Haley, *J. Org. Chem.* **2011**, *76*, 4043–4051; s) T. Sakida, S. Yamaguchi, H. Shinokubo, *Angew. Chem.* **2011**, *123*, 2328; *Angew. Chem. Int. Ed.* **2011**, *50*, 2280–2283; t) T. K. Khan, R. R. S. Pissurlenkar, M. S. Shaikh, M. Ravikanth, *J. Organomet. Chem.* **2012**, *697*, 65–73.

[10] R. P. Sabatini, T. M. McCormick, T. Lazarides, K. C. Wilson, R. Eisenberg, D. W. McCamant, *J. Phys. Chem. Lett.* **2011**, *2*, 223–227.

 © 2012 Wiley-VCH Verlag GmbH & Co. KGaA, Weinheim 

[11] a) J. C. Koziar, D. O. Cowan, *Acc. Chem. Res.* **1978**, *11*, 334–341; b) K. N. Solovyov, E. A. Borisevich, *Phys. Usp.* **2005**, *48*, 231–253.
[12] a) M. Furst, H. Kallmann, F. H. Brown, *J. Chem. Phys.* **1957**, *26*, 1321–1332; b) B. Abrams, Z. Diwu, O. Guryev, S. Aleshkov, R. Hingorani, M. Edinger, R. Lee, J. Link, T. Dubrovsky, *Anal. Biochem.* **2009**, *386*, 262–269; c) X.-F. Zhang, I. Zhang, L. Liu, *Photochem. Photobiol.* **2010**, *86*, 492–498.
[13] a) K. Krumova, G. Cosa, *J. Am. Chem. Soc.* **2010**, *132*, 17560–17569; b) T.-I. Kim, S. Park, Y. Choi, Y. Kim, *Chem. Asian J.* **2011**, *6*, 1358–1361.
[14] J.-H. Ye, G. Wang, C. Huang, Z. Hu, W. Zhang, Y. Zhang, *Synthesis* **2012**, *44*, 104–110.
[15] a) L. Li, J. Han, B. Nguyen, K. Burgess, *J. Org. Chem.* **2008**, *73*, 1963–1970; b) V. Lakshmi, M. Ravikanth, *Dalton Trans.* **2012**, *41*, 5903–5911.
[16] A. Cui, X. Peng, J. Fan, X. Chen, Y. Wu, B. Guo, *J. Photochem. Photobiol. A: Chem.* **2007**, *186*, 85–92.
[17] B. J. Littler, M. A. Miller, C.-H. Hung, R. W. Wagner, D. F. O'Shea, P. D. Boyle, J. S. Lindsey, *J. Org. Chem.* **1999**, *64*, 1391–1396.
[18] a) C.-T. Ho, Q. Z. Gin, K. N. Lee, J. T. Carlin, *J. Agric. Food Chem.* **1982**, *30*, 362–364; b) R. A. Rane, V. N. Telvekar, *Bioorg. Med. Chem. Lett.* **2010**, *20*, 5681–5685.
[19] Q. Zheng, G. Xu, P. N. Prasad, *Chem. Eur. J.* **2008**, *14*, 5812–5819.
[20] M. A. H. Alamity, A. C. Benniston, G. Copley, K. J. Elliot, A. Harryman, B. Stewart, Y.-G. Zhi, *Chem. Mater.* **2008**, *20*, 4024–4032.
[21] F. Li, S. I. Yang, Y. Ciringh, J. Seth, C. H. Martin III, D. L. Singh, D. Kim, R. R. Birge, D. F. Bocian, D. Holten, J. S. Lindsey, *J. Am. Chem. Soc.* **1998**, *120*, 10001–10017.
[22] H. L. Kee, C. Kirmaier, L. Yu, P. Thamyongkit, W. J. Youngblood, M. E. Calder, L. Ramos, B. C. Noll, D. F. Bocian, W. R. Scheidt, R. R. Birge, J. S. Lindsey, D. Holten, *J. Phys. Chem. B* **2005**, *109*, 20433–20443.
[23] W. Qin, T. Rohand, M. Baruah, A. Stefan, M. Van der Auweraer, W. Dehaen, N. Boens, *Chem. Phys. Lett.* **2006**, *420*, 562–568.
[24] K. H. Drexhage, in: *Dye Laser* (Ed.: F. P. Schäfer), 3rd ed. Springer, Berlin, **1990**.
[25] L. Biczók, T. Bérces, F. Márta, *J. Phys. Chem.* **1993**, *97*, 8895–8899.
[26] P. O. Andersson, M. Bachilo, R.-L. Chen, T. Gillbro, *J. Phys. Chem.* **1995**, *99*, 16199–16209.
[27] P. Hartmann, M. J. C. Leiner, S. Draxler, M. E. Lippitsch, *Chem. Phys.* **1996**, *207*, 137–146.
[28] C. E. M. Carvalho, I. M. Brinn, A. V. Pinto, M. C. F. R. Pinto, *J. Photochem. Photobiol. A: Chem.* **2000**, *136*, 25–33.
[29] F. López Arbeloa, T. López Arbeloa, I. López Arbeloa, *J. Photochem. Photobiol. A: Chem.* **1999**, *121*, 177–182.
[30] F. López Arbeloa, J. Bañuelos, V. Martínez, T. Arbeloa, I. López Arbeloa, *ChemPhysChem* **2004**, *5*, 1762–1771.
[31] The dyes described in this work and their utilization as laser dyes are covered by Spanish Patent Application no. 201230486, filed on 30th March, **2012**.

Received: July 17, 2012
Published Online: October 4, 2012

 © 2012 Wiley-VCH Verlag GmbH & Co. KGaA, Weinheim 

*Eur. J. Org. Chem.* **2012** · © WILEY-VCH Verlag GmbH & Co. KGaA, 69451 Weinheim, 2012 · ISSN 1434–193X

***SUPPORTING INFORMATION***

***DOI:*** 10.1002/ejoc.201200946
***Title:*** Chlorinated BODIPYs: Surprisingly Efficient and Highly Photostable Laser Dyes
***Author(s):*** Gonzalo Duran-Sampedro, Antonia R. Agarrabeitia, Inmaculada Garcia-Moreno,* Angel Costela, Jorge Bañuelos, Teresa Arbeloa, Iñigo López Arbeloa, Jose Luis Chiara,* María J. Ortiz*

**B. Additional Figures and Tables Mentioned in the Article.**

**Figure S1.** Charge distribution (CHelpg) in the chromophoric core of 8-tolyl-BODIPY (**1**) and its chlorinated derivatives **2-7** in the ground and excited state (bold numbers).

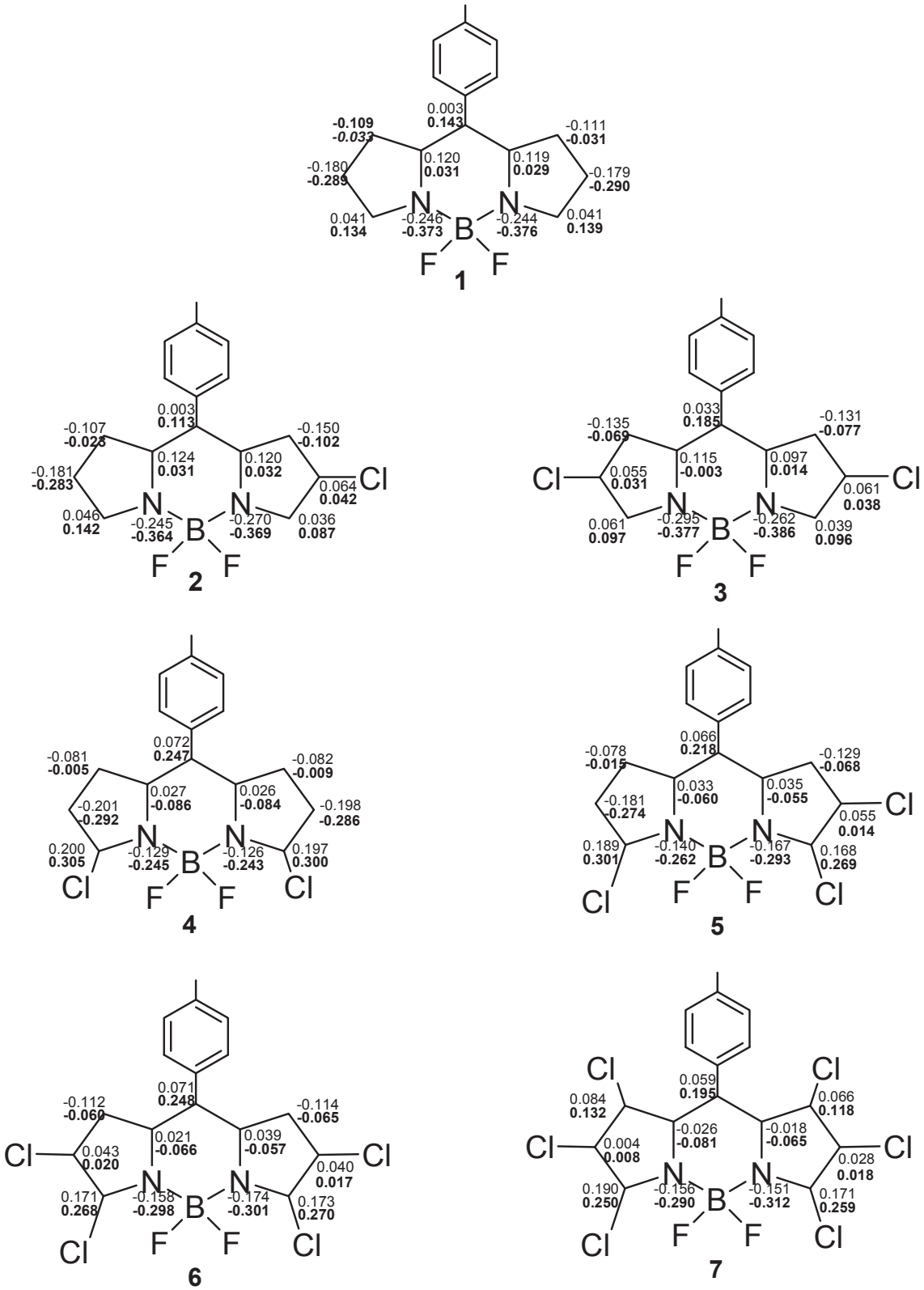

**Figure S2**. Charge distribution (CHelpg) in the chromophoric core of dye **8** and its mono- (**9**) and dichlorinated (**10**) derivatives in the ground and excited state (bold numbers).

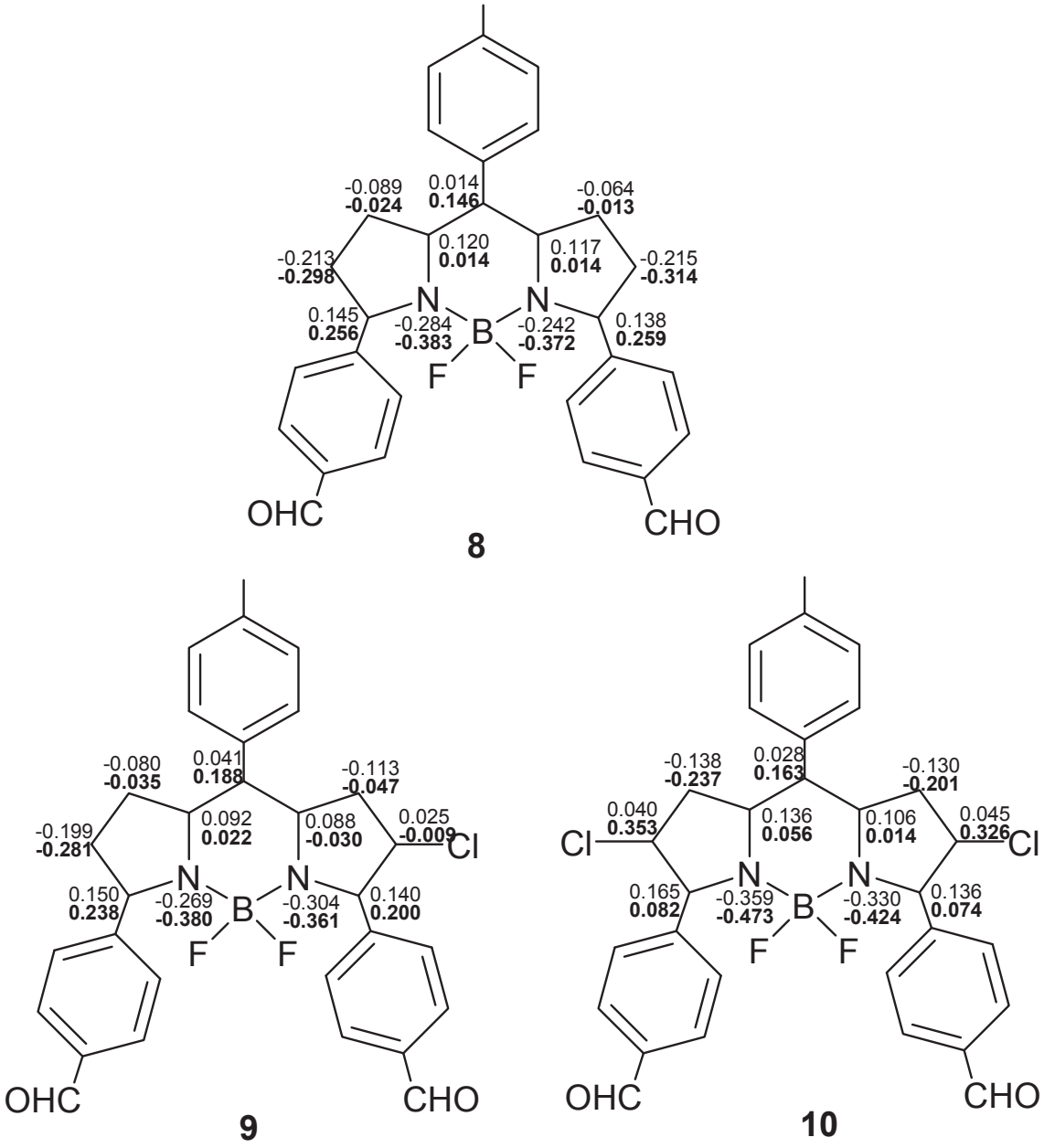

**Figure S3**. Charge distribution (CHelpg) in the chromophoric core of compound **11** and its mono- (**12**) and dichlorinated (**13** and **14**) derivatives in the ground and excited state (bold numbers).

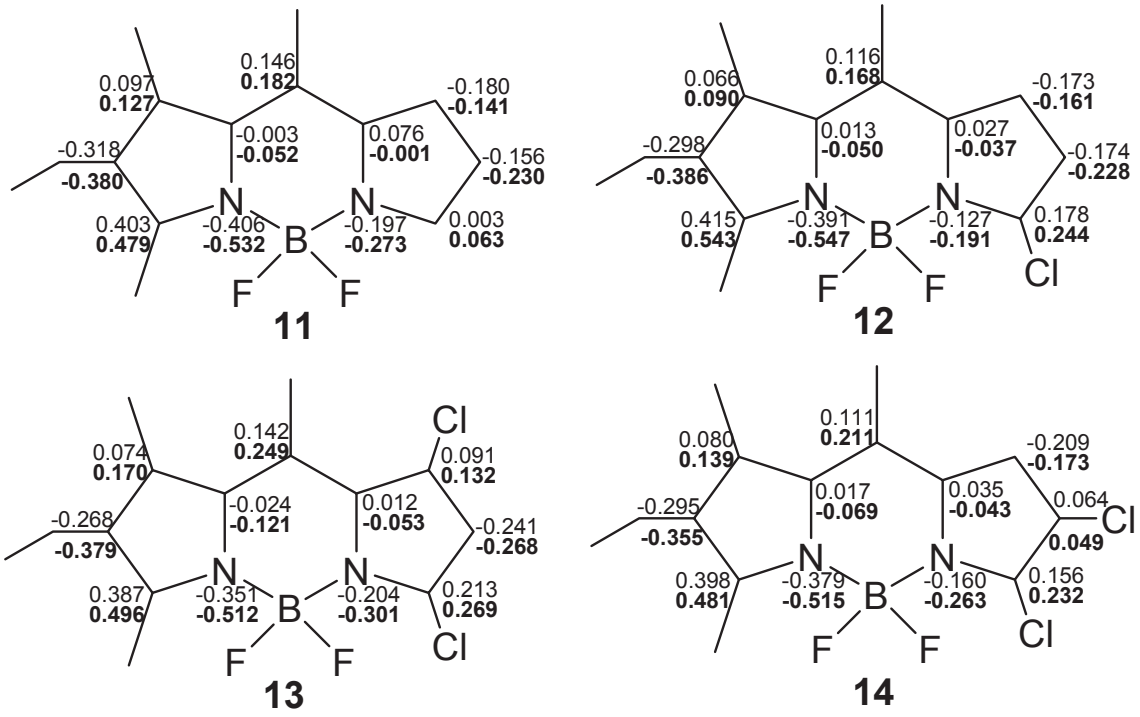

**Figure S4**. Charge distribution (CHelpg) in the chromophoric core of PM546 (**15**) and its mono- (**16**) and dichlorinated (**17**) derivatives in the ground and excited state (bold numbers).

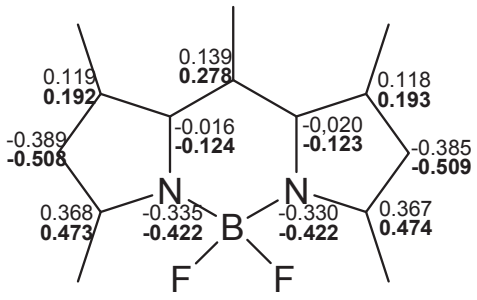


**15**

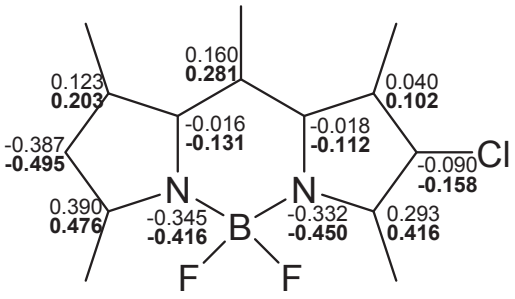


**16**

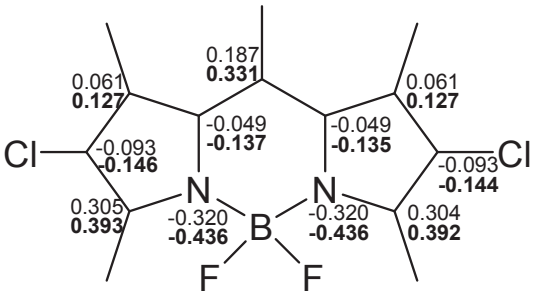


**17**

**Figure S5.** Lasing efficiencies of the new dyes **3** (dark bars) and **5** (grey bars) in ethyl acetate solution as function of the dye concentration.

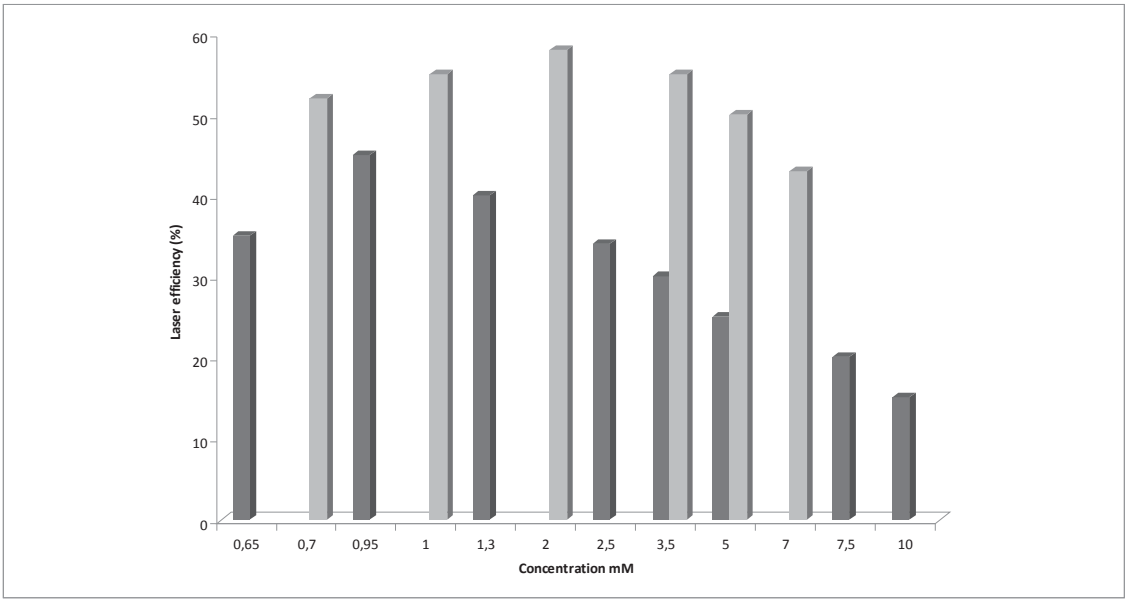

**Figure S6**. Dipole moment (μ, Debyes) orientation and values in the ground and first excited state of 8-tolyl-BODIPY **1** and its set of chlorinated derivatives **2-7**. The electric transition moment (M) magnitude and orientation for the $S_0$-$S_1$ transition is also included.

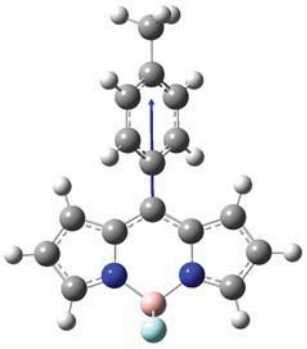

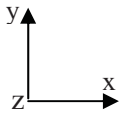


| **1** | x | y | z | Tot. |
|---|---|---|---|---|
| μ ($S_0$) | 0.029 | 7.272 | 0.043 | 7.273 |
| μ ($S_1$) | 0.015 | 8.213 | 0.026 | 8.213 |
| M | 2.948 | 0.004 | 0.241 | 2.957 |

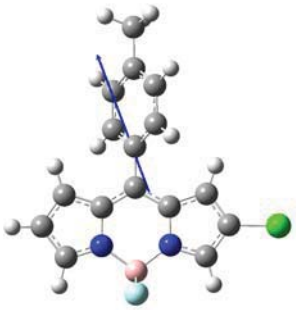

| **2** | x | y | z | Tot. |
|---|---|---|---|---|
| μ ($S_0$) | 0.911 | 7.961 | 0.472 | 8.034 |
| μ ($S_1$) | 1.181 | 9.003 | 0.121 | 9.081 |
| M | 2.965 | 0.614 | 0.138 | 3.031 |

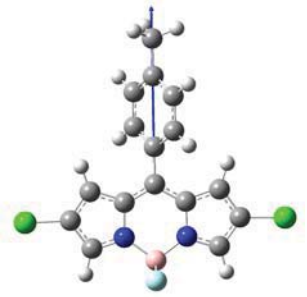

| **3** | x | y | z | Tot. |
|---|---|---|---|---|
| μ ($S_0$) | 0.180 | 7.839 | 0.242 | 7.845 |
| μ ($S_1$) | 0.739 | 8.820 | 0.162 | 8.852 |
| M | 3.093 | 0.256 | 0.090 | 3.104 |

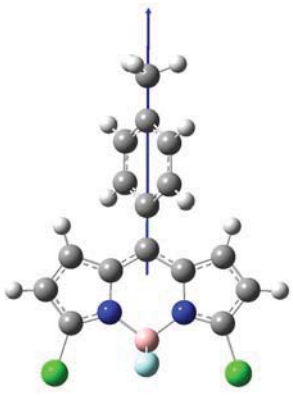

| **4** | x | y | z | Tot. |
|---|---|---|---|---|
| μ ($S_0$) | 0.020 | 9.834 | 0.031 | 9.830 |
| μ ($S_1$) | 0.008 | 11.312 | 0.028 | 11.310 |
| M | 3.130 | 0.003 | 0.166 | 3.134 |

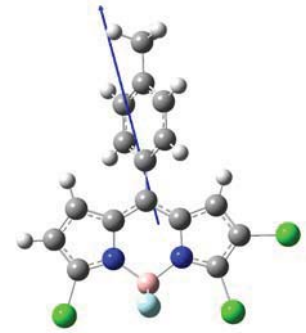

| **5** | x | y | z | Tot. |
|---|---|---|---|---|
| μ ($S_0$) | 1.551 | 9.928 | 0.055 | 10.048 |
| μ ($S_1$) | 1.819 | 11.445 | 0.062 | 11.589 |
| M | 3.201 | 0.214 | 0.113 | 3.210 |

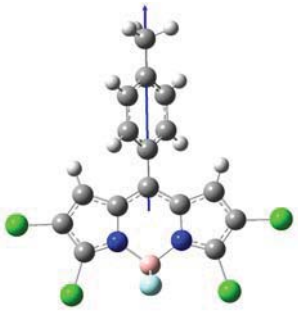

| **6** | x | y | z | Tot. |
|---|---|---|---|---|
| μ ($S_0$) | 0.176 | 9.714 | 0.021 | 9.710 |
| μ ($S_1$) | 0.069 | 11.236 | 0.032 | 11.230 |
| M | 3.288 | 0.027 | 0.084 | 3.290 |

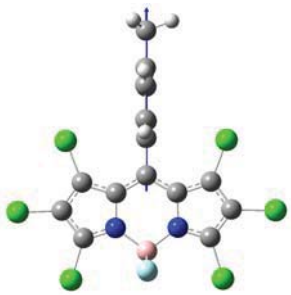

| **7** | x | y | z | Tot. |
|---|---|---|---|---|
| μ ($S_0$) | 0.119 | 6.603 | 0.000 | 6.604 |
| μ ($S_1$) | 0.181 | 7.950 | 0.000 | 7.952 |
| M | 3.510 | 0.064 | 0.000 | 3.510 |

**Figure S7**. Dipole moment (μ, Debyes) orientation and values in the ground and first excited state of dye **8** and its chlorinated derivatives **9** and **10**. The electric transition moment (M) magnitude and orientation for the $S_0$-$S_1$ transition is also included.

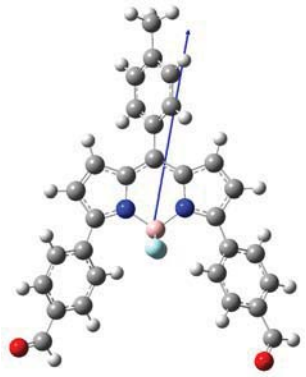

| **8** | x | y | z | Tot. |
|---|---|---|---|---|
| μ ($S_0$) | 2.283 | 12.291 | 1.905 | 12.647 |
| μ ($S_1$) | 3.082 | 12.686 | 2.002 | 13.208 |
| M | 3.810 | 0.126 | 0.100 | 3.813 |

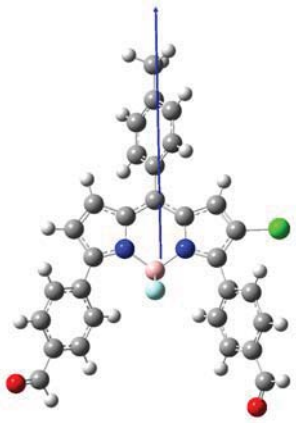

| **9** | x | y | z | Tot. |
|---|---|---|---|---|
| μ ($S_0$) | 1.715 | 11.605 | 0.935 | 11.768 |
| μ ($S_1$) | 1.682 | 11.932 | 1.324 | 12.115 |
| M | 3.638 | 0.873 | 0.096 | 3.745 |

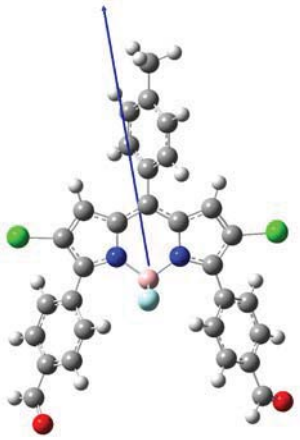

| **10** | x | y | z | Tot. |
|---|---|---|---|---|
| μ ($S_0$) | 1.643 | 11.640 | 0.675 | 11.775 |
| μ ($S_1$) | 2.235 | 12.108 | 0.907 | 12.345 |
| M | 3.678 | 0.118 | 0.034 | 3.680 |

**Figure S8**. Dipole moment (μ, Debyes) orientation and values in the ground and first excited state of dye **11** and its chlorinated derivatives **12-14**. The electric transition moment (M) magnitude and orientation for the $S_0$-$S_1$ transition is also included.

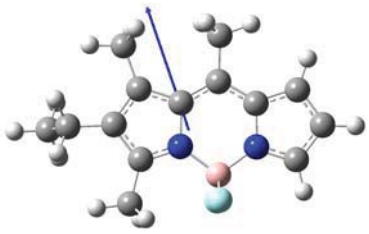

| **11** | x | y | z | Tot. |
|---|---|---|---|---|
| μ ($S_0$) | 1.974 | 5.286 | 0.016 | 5.643 |
| μ ($S_1$) | 1.941 | 6.295 | 0.479 | 6.605 |
| M | 3.178 | 0.310 | 0.133 | 3.196 |

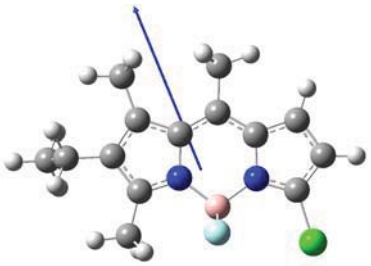

| **12** | x | y | z | Tot. |
|---|---|---|---|---|
| μ ($S_0$) | 4.278 | 5.779 | 0.064 | 7.191 |
| μ ($S_1$) | 4.436 | 7.016 | 0.009 | 8.301 |
| M | 3.156 | 0.826 | 0.178 | 3.264 |

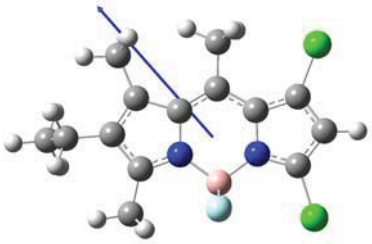

| **13** | x | y | z | Tot. |
|---|---|---|---|---|
| μ ($S_0$) | 4.084 | 4.979 | 0.147 | 6.442 |
| μ ($S_1$) | 4.175 | 5.967 | 0.441 | 7.296 |
| M | 3.309 | 0.235 | 0.125 | 3.319 |

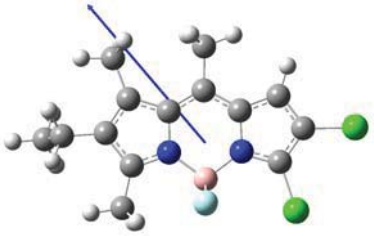

| **14** | x | y | z | Tot. |
|---|---|---|---|---|
| μ ($S_0$) | 5.956 | 5.761 | 0.087 | 8.289 |
| μ ($S_1$) | 6.526 | 6.962 | 0.331 | 9.548 |
| M | 3.293 | 0.483 | 0.121 | 3.330 |

**Figure S9**. Dipole moment (μ, Debyes) orientation and values in the ground and first excited state of PM546 (**15**) and its chlorinated derivatives **16** and **17**. The electric transition moment (M) magnitude and orientation for the $S_0$-$S_1$ transition is also included.

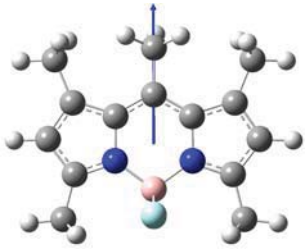

| **15** | x | y | z | Tot. |
|---|---|---|---|---|
| μ ($S_0$) | 0.018 | 5.145 | 0.205 | 5.149 |
| μ ($S_1$) | 0.001 | 6.156 | 0.396 | 6.169 |
| M | 3.227 | 0.001 | 0.001 | 3.227 |

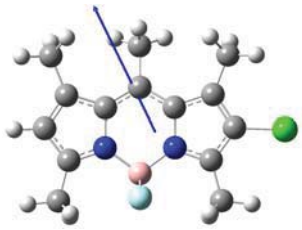

| **16** | x | y | z | Tot. |
|---|---|---|---|---|
| μ ($S_0$) | 2.691 | 5.196 | 0.152 | 5.854 |
| μ ($S_1$) | 2.98 | 6.272 | 0.032 | 6.951 |
| M | 3.297 | 0.015 | 0.055 | 3.297 |

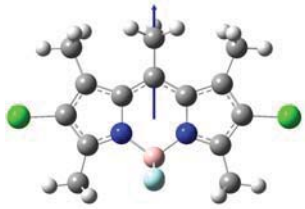

| **17** | x | y | z | Tot. |
|---|---|---|---|---|
| μ ($S_0$) | 0.000 | 5.214 | 0.077 | 5.210 |
| μ ($S_1$) | 0.000 | 6.346 | 0.115 | 6.347 |
| M | 3.372 | 0.000 | 0.000 | 3.372 |

**Table S1**. Photophysical data of compound **1** and its chlorinated derivatives **2**, **3**, **5**, **6**, and **7** in different solvents ranging from apolar (cyclohexane) to polar/aprotic (acetone and ethyl acetate) and polar/protic (ethanol, methanol and trifluoroethanol). The amplitude-averaged lifetime is calculated from the lifetimes of the biexponential deconvolution. The rate constants are calculated from this average lifetime.

| | $\lambda_{ab}$ (nm) | $\varepsilon_{max}$ (f) ($10^{-4}M^{-1}\cdot cm^{-1}$) | $\lambda_{fl}$ (nm) | $\phi$ | $\tau$ (ps) | $<\tau>$ (ps) | $<k_{fl}>$ ($10^{-8}$ $s^{-1}$) | $<k_{nr}>$ ($10^{-8}$ $s^{-1}$) |
|---|---|---|---|---|---|---|---|---|
| **1** | | | | | | | | |
| Cyclohexane | 500.5 | 6.9 (0.42) | 516.0 | 0.036 | 340<br>2285 (~ 0) | 340 | 1.05 | 28.3 |
| Ethyl acetate | 497.0 | 6.2 (0.39) | 514.5 | 0.024 | 235<br>1930 (~ 0) | 235 | 1.01 | 41.2 |
| Acetone | 496.5 | 6.1 (0.39) | 514.5 | 0.018 | 195<br>2755 (~ 0) | 195 | 0.92 | 50.1 |
| Ethanol | 497.5 | 6.2 (0.40) | 514.5 | 0.025 | 255<br>2850 (~ 0) | 255 | 0.99 | 38.5 |
| Methanol | 496.0 | 6.1 (0.40) | 513.5 | 0.018 | 200<br>3060 (~ 0) | 200 | 0.91 | 49.8 |
| $F_3$-ethanol | 493.0 | 5.6 (0.38) | 509.5 | 0.031 | 325<br>3495 (~ 0) | 325 | 0.96 | 30.0 |
| **2** | | | | | | | | |
| Cyclohexane | 518.5 | 6.5 (0.42) | 534.5 | 0.093 | 845 (98%)<br>2255 (2%) | 873 | 1.06 | 10.4 |
| Ethyl acetate | 511.5 | 5.6 (0.41) | 533.0 | 0.057 | 590 (98%)<br>2455 (2%) | 627 | 0.91 | 15.0 |
| Acetone | 510.5 | 5.4 (0.40) | 533.5 | 0.041 | 455 (98%)<br>1850 (2%) | 483 | 0.85 | 19.8 |
| Ethanol | 512.0 | 5.6 (0.40) | 533.0 | 0.058 | 595 (98%)<br>2275 (2%) | 628 | 0.92 | 15.0 |
| Methanol | 511.0 | 5.4 (0.40) | 533.0 | 0.044 | 480 (99%)<br>3340 (1%) | 508 | 0.86 | 18.8 |
| $F_3$-ethanol | 508.5 | 4.9 (0.38) | 531.0 | 0.074 | 860 (98%)<br>3350 (2%) | 910 | 0.81 | 10.2 |
| **3** | | | | | | | | |
| Cyclohexane | 538.0 | 1.4 (0.11) | 555.0 | 0.153 | 1320 (90%)<br>3860 (10%) | 1574 | 0.97 | 5.38 |
| Ethyl acetate | 530.0 | 1.3 (0.10) | 552.5 | 0.120 | 990 (90%)<br>3620 (10%) | 1253 | 0.96 | 7.02 |
| Acetone | 529.5 | 1.3 (0.19) | 552.5 | 0.076 | 760 (89%)<br>3650 (11%) | 1078 | 0.70 | 8.57 |
| Ethanol | 532.0 | 1.3 (0.10) | 553.0 | 0.133 | 1070 (89%)<br>3650 (11%) | 1354 | 0.98 | 6.40 |
| Methanol | 530.0 | 1.2 (0.11) | 552.0 | 0.092 | 850 (88%)<br>4960 (12%) | 1343 | 0.68 | 6.76 |
| $F_3$-ethanol | 528.5 | 1.1 (0.18) | 551.5 | 0.094 | 1480 (89%)<br>4710 (11%) | 1820 | 0.51 | 4.98 |

| | | | | | | | | |
|---|---|---|---|---|---|---|---|---|
| **5** | | | | | | | | |
| Cyclohexane | 530.0 | 10.5 (0.50) | 542.0 | 0.56 | 2120 (12%)<br>4110 (88%) | 3871 | 1.44 | 1.13 |
| Ethyl acetate | 523.0 | 7.7 (0.50) | 538.5 | 0.41 | 870 (26%)<br>3860 (74%) | 3082 | 1.33 | 1.91 |
| Acetone | 521.0 | 8.2 (0.49) | 538.0 | 0.39 | 1250 (13%)<br>3350 (87%) | 3077 | 1.27 | 1.98 |
| Ethanol | 523.0 | 8.4 (0.47) | 538.0 | 0.49 | 1720 (12%)<br>4100 (88%) | 3814 | 1.28 | 1.33 |
| Methanol | 521.5 | 8.2 (0.48) | 537.5 | 0.40 | 900 (18%)<br>3660 (82%) | 3163 | 1.26 | 1.89 |
| $F_3$-ethanol | 520.5 | 8.4 (0.50) | 536.5 | 0.56 | 2610 (10%)<br>5680 (90%) | 5373 | 1.04 | 0.82 |
| **6** | | | | | | | | |
| Cyclohexane | 546.5 | 8.3 (0.54) | 557.5 | 0.46 | 1180 (22%)<br>4720 (78%) | 3941 | 1.16 | 1.37 |
| Ethyl acetate | 535.0 | 7.7 (0.57) | 553.5 | 0.39 | 1080 (20%)<br>4610 (80%) | 3904 | 0.99 | 1.56 |
| Acetone | 536.5 | 7.7 (0.54) | 554.0 | 0.31 | 1160 (17%)<br>4390 (83%) | 3841 | 0.81 | 1.79 |
| Ethanol | 539.0 | 7.9 (0.50) | 553.0 | 0.38 | 1380 (19%)<br>5050 (81%) | 4352 | 0.87 | 1.42 |
| Methanol | 536.0 | 7.0 (0.51) | 552.5 | 0.28 | 920 (26%)<br>4750 (74%) | 3754 | 0.74 | 1.92 |
| $F_3$-ethanol | 537.0 | 7.1 (0.52) | 553.0 | 0.46 | 3550 (16%)<br>6560 (84%) | 6078 | 0.75 | 0.89 |
| **7** | | | | | | | | |
| Cyclohexane | 537.0 | 9.5 (0.46) | 548.5 | 0.45 | 1500 (10%)<br>2550 (90%) | 2445 | 1.84 | 2.25 |
| Ethyl acetate | 532.0 | 8.3 (0.48) | 546.5 | 0.41 | 1710 (15%)<br>2920 (85%) | 2738 | 1.49 | 2.15 |
| Acetone | 531.0 | 8.1 (0.46) | 546.5 | 0.37 | 1900 (6%)<br>2610 (94%) | 2567 | 1.44 | 2.45 |
| Ethanol | 532.0 | 6.3 (0.33) | 545.0 | 0.41 | 1930 (19%)<br>2960 (81%) | 2764 | 1.48 | 2.13 |
| Methanol | 531.0 | 4.3 (0.23) | 544.0 | 0.28 | 1290 (47%)<br>2710 (53%) | 2042 | 1.37 | 3.52 |
| $F_3$-ethanol | 529.5 | 8.1 (0.45) | 544.0 | 0.49 | 3770 (5%)<br>4720 (95%) | 4672 | 1.05 | 1.09 |

**Table S2**. Bi-exponential deconvolution of the fluorescence decay at different emission wavelengths upon excitation at 470 nm for compound **7** in diluted solutions of chloroform.

| $\lambda_{em}$ (nm) | $\tau$ (ns) | $<\tau>$ (ns) |
|---|---|---|
| 530 | 2.06 (37%)<br>3.00 (63%) | 2.65 |
| 540 | 2.16 (26%)<br>3.32 (74%) | 3.02 |
| 550 | 2.33 (17%)<br>3.40 (83%) | 3.21 |
| 560 | 2.19 (17%)<br>3.38 (83%) | 3.18 |
| 570 | 2.26 (33%)<br>3.42 (67%) | 3.03 |
| 580 | 1.97 (26%)<br>3.28 (74%) | 2.93 |

**Table S3.** Photophysical data of compound **8** and its chlorinated derivatives **9** and **10** in different solvents.

| | $\lambda_{ab}$ (nm) | $\varepsilon_{max}$ (f) ($10^{-4}M^{-1}cm^{-1}$) | $\lambda_{fl}$ (nm) | $\phi$ | $\tau$ (ns) | $k_{fl}$ ($10^{-8}$ $s^{-1}$) | $k_{nr}$ ($10^{-8}$ $s^{-1}$) |
|---|---|---|---|---|---|---|---|
| **8** | | | | | | | |
| Cyclohexane | 561.0 | 3.3 (0.30) | 597.5 | 0.54 | 3.68 | 1.46 | 1.25 |
| Ethyl acetate | 558.0 | 3.0 (0.28) | 599.0 | 0.57 | 3.67 | 1.55 | 1.17 |
| Acetone | 558.5 | 3.1 (0.30) | 599.5 | 0.51 | 3.48 | 1.46 | 1.41 |
| Ethanol | 559.0 | 3.1 (0.30) | 600.5 | 0.53 | 3.91 | 1.35 | 1.20 |
| Methanol | 557.0 | 3.1 (0.30) | 598.0 | 0.46 | 3.65 | 1.26 | 1.48 |
| $F_3$-ethanol | 551.5 | 3.0 (0.31) | 595.5 | 0.58 | 4.54 | 1.28 | 0.92 |
| **9** | | | | | | | |
| Cyclohexane | 566.0 | 4.4 (0.34) | 599.0 | 0.42 | 3.61 | 1.16 | 1.60 |
| Ethyl acetate | 559.5 | 4.0 (0.32) | 596.5 | 0.29 | 2.59 | 1.12 | 2.74 |
| Acetone | 558.0 | 4.0 (0.32) | 596.5 | 0.25 | 2.25 | 1.11 | 3.33 |
| Ethanol | 560.0 | 4.1 (0.34) | 597.5 | 0.29 | 2.78 | 1.04 | 2.55 |
| Methanol | 557.5 | 4.1 (0.34) | 595.5 | 0.22 | 2.28 | 0.96 | 3.42 |
| $F_3$-ethanol | 553.5 | 3.8 (0.35) | 595.5 | 0.36 | 3.92 | 0.92 | 1.63 |
| **10** | | | | | | | |
| Cyclohexane | 574.0 | 1.1 (0.09) | 605.0 | 0.39 | 3.60 | 1.08 | 1.70 |
| Ethyl acetate | 564.0 | 1.0 (0.08) | 599.5 | 0.22 | 2.17 | 1.03 | 3.58 |
| Acetone | 561.5 | 0.9 (0.08) | 599.0 | 0.19 | 1.92 | 1.02 | 4.19 |
| Ethanol | 565.0 | 1.0 (0.09) | 601.5 | 0.22 | 2.27 | 0.97 | 3.44 |
| Methanol | 562.5 | 1.0 (0.09) | 598.5 | 0.16 | 1.44 | 1.11 | 5.84 |
| $F_3$-ethanol | 561.0 | 0.9 (0.08) | 600.0 | 0.31 | 3.63 | 0.85 | 1.90 |

**Table S4.** Photophysical data of compound **11** and its chlorinated derivatives **12-14** in different solvents.

| | $\lambda_{ab}$ (nm) | $\varepsilon_{max}$ (f) ($10^{-4}M^{-1}cm^{-1}$) | $\lambda_{fl}$ (nm) | $\phi$ | $\tau$ (ns) | $k_{fl}$ ($10^{-8}$ $s^{-1}$) | $k_{nr}$ ($10^{-8}$ $s^{-1}$) |
|---|---|---|---|---|---|---|---|
| **11** | | | | | | | |
| Cyclohexane | 504.0 | 3.3 (0.22) | 515.0 | 0.96 | 5.46 | 1.75 | 0.07 |
| Ethyl acetate | 496.0 | 2.5 (0.23) | 512.5 | 0.84 | 5.57 | 1.50 | 0.28 |
| Acetone | 495.0 | 2.2 (0.20) | 512.5 | 0.79 | 5.66 | 1.39 | 0.37 |
| Ethanol | 497.0 | 2.5 (0.22) | 513.5 | 0.84 | 5.73 | 1.46 | 0.28 |
| Methanol | 495.5 | 2.5 (0.24) | 512.5 | 0.76 | 5.78 | 1.31 | 0.41 |
| $F_3$-ethanol | 492.0 | 1.9 (0.20) | 511.0 | 0.75 | 6.17 | 1.21 | 0.40 |
| **12** | | | | | | | |
| Cyclohexane | 510.5 | 5.1 (0.33) | 520.5 | 0.78 | 5.07 | 1.54 | 0.43 |
| Ethyl acetate | 501.5 | 3.7 (0.33) | 517.5 | 0.64 | 4.98 | 1.28 | 0.72 |
| Acetone | 499.5 | 3.3 (0.32) | 516.5 | 0.60 | 4.92 | 1.22 | 0.81 |
| Ethanol | 502.5 | 3.7 (0.32) | 518.0 | 0.64 | 5.15 | 1.24 | 0.70 |
| Methanol | 501.0 | 3.4 (0.31) | 517.0 | 0.60 | 5.12 | 1.17 | 0.78 |
| $F_3$-ethanol | 499.0 | 2.8 (0.30) | 516.0 | 0.55 | 5.47 | 1.00 | 0.82 |
| **13** | | | | | | | |
| Cyclohexane | 504.0 | 3.3 (0.27) | 526.0 | 0.57 | 3.95 | 1.44 | 1.09 |
| Ethyl acetate | 494.5 | 2.4 (0.26) | 522.0 | 0.41 | 3.33 | 1.23 | 1.77 |
| Acetone | 492.0 | 2.1 (0.25) | 522.0 | 0.34 | 3.05 | 1.11 | 2.16 |
| Ethanol | 495.5 | 2.4 (0.26) | 522.5 | 0.39 | 3.31 | 1.18 | 1.84 |
| Methanol | 493.0 | 2.2 (0.26) | 522.0 | 0.34 | 3.13 | 1.08 | 2.11 |
| $F_3$-ethanol | 491.0 | 2.0 (0.25) | 520.5 | 0.33 | 3.39 | 0.97 | 1.98 |
| **14** | | | | | | | |
| Cyclohexane | 521.0 | 3.3 (0.24) | 531.0 | 0.83 | 5.29 | 1.57 | 0.32 |
| Ethyl acetate | 505.5 | 2.3 (0.23) | 527.5 | 0.67 | 5.11 | 1.31 | 0.64 |
| Acetone | 502.0 | 2.0 (0.23) | 526.5 | 0.62 | 4.97 | 1.25 | 0.76 |
| Ethanol | 507.0 | 2.3 (0.23) | 527.5 | 0.67 | 5.21 | 1.28 | 0.63 |
| Methanol | 504.0 | 2.1 (0.23) | 527.0 | 0.63 | 5.16 | 1.22 | 0.72 |
| $F_3$-ethanol | 502.0 | 1.8 (0.21) | 527.5 | 0.61 | 5.68 | 1.07 | 0.68 |

**Table S5.** Photophysical data of compound **15** and its chlorinated derivatives **16** and **17** in different solvents.

| | $\lambda_{ab}$ (nm) | $\varepsilon_{max}$ (f) ($10^{-4}M^{-1}cm^{-1}$) | $\lambda_{fl}$ (nm) | $\phi$ | $\tau$ (ns) | $k_{fl}$ ($10^{-8}$ $s^{-1}$) | $k_{nr}$ ($10^{-8}$ $s^{-1}$) |
|---|---|---|---|---|---|---|---|
| **15** | | | | | | | |
| Cyclohexane | 499.5 | 9.7 (0.50) | 512.0 | 0.91 | 5.23 | 1.74 | 0.17 |
| Ethyl acetate | 494.0 | 8.1 (0.49) | 506.5 | 0.85 | 5.58 | 1.52 | 0.27 |
| Acetone | 493.0 | 7.9 (0.55) | 505.5 | 0.84 | 5.55 | 1.51 | 0.29 |
| Ethanol | 495.0 | 8.1 (0.49) | 507.0 | 0.85 | 5.52 | 1.54 | 0.27 |
| Methanol | 492.5 | 8.2 (0.48) | 505.5 | 0.81 | 5.58 | 1.45 | 0.34 |
| $F_3$-ethanol | 490.0 | 7.6 (0.47) | 502.5 | 0.85 | 6.22 | 1.37 | 0.24 |
| **16** | | | | | | | |
| Cyclohexane | 512.0 | 5.5 (0.26) | 525.5 | 0.91 | 5.54 | 1.64 | 0.16 |
| Ethyl acetate | 504.0 | 4.6 (0.25) | 519.0 | 0.94 | 5.81 | 1.62 | 0.10 |
| Acetone | 502.0 | 4.3 (0.24) | 518.5 | 0.87 | 5.94 | 1.46 | 0.22 |
| Ethanol | 505.0 | 4.6 (0.24) | 519.5 | 0.89 | 5.95 | 1.49 | 0.18 |
| Methanol | 503.0 | 4.3 (0.25) | 518.5 | 0.83 | 6.11 | 1.35 | 0.28 |
| $F_3$-ethanol | 502.0 | 4.1 (0.23) | 518.0 | 1.0 | 6.72 | 1.49 | 0.0 |
| **17** | | | | | | | |
| Cyclohexane | 527.0 | 7.1 (0.34) | 542.5 | 0.87 | 5.65 | 1.54 | 0.23 |
| Ethyl acetate | 517.5 | 6.0 (0.32) | 535.5 | 0.78 | 5.88 | 1.32 | 0.37 |
| Acetone | 515.5 | 5.6 (0.31) | 535.0 | 0.77 | 5.99 | 1.28 | 0.38 |
| Ethanol | 518.0 | 6.0 (0.31) | 536.5 | 0.76 | 5.94 | 1.28 | 0.40 |
| Methanol | 517.0 | 5.6 (0.32) | 535.5 | 0.79 | 6.09 | 1.30 | 0.34 |
| $F_3$-ethanol | 517.0 | 5.3 (0.30) | 535.5 | 0.73 | 6.59 | 1.10 | 0.41 |

**Table S6.** Lasing properties of the new chlorinated BODIPY dyes in different solvents pumped at 532 nm. For comparison purposes, the corresponding data of the non-chlorinated dyes **8**, **11**, and **15** evaluated under identical experimental conditions are also included. Dye **11** was pumped at 500 nm and dyes **15** and **16** were pumped at 355 nm (data in parentheses).

| Dye | Data | EtOAc | MeOH | Acetone | $CH_2Cl_2$ |
|---|---|---|---|---|---|
| **8**[a] | $\lambda_l$ (nm) | 615 | | 615 | 617 |
| | Eff (%) | 14 | | 14 | 10 |
| **9**[b] | $\lambda_l$ (nm) | 612 | 612 | 613 | 621 |
| | Eff (%) | 18 | 17 | 18 | 19 |
| **10**[c] | $\lambda_l$ (nm) | 618 | 610 | 614 | 621 |
| | Eff (%) | 30 | 21 | 23 | 25 |
| **11**[d] | $\lambda_l$ (nm) | (530) | (532) | (530) | |
| | Eff (%) | (34) | (30) | (28) | |
| **12**[e] | $\lambda_l$ (nm) | 561 | | 561 | 584 |
| | Eff (%) | 38 | | 19 | 35 |
| **13**[e] | $\lambda_l$ (nm) | 566 | | 565 | 570 |
| | Eff (%) | 46 | | 34 | 37 |
| **14**[e] | $\lambda_l$ (nm) | 562 | | 562 | 564 |
| | Eff (%) | 36 | | 19 | 30 |
| **15**[f] | $\lambda_l$ (nm) | (541) | | (545) | (547) |
| | Eff (%) | (23) | | (14) | (10) |
| **16**[f(g)] | $\lambda_l$ (nm) | 558 (556) | | (556) | 556 (556) |
| | Eff (%) | 40 (30) | | (20) | 32 (27) |
| **17**[h] | $\lambda_l$ (nm) | 562 | 560 | 570 | 563 |
| | Eff (%) | 51 | 44 | 38 | 49 |

[a,b,c,d,e,f,g,h] Dye concentrations: $1 \times 10^{-3}$ M, $8 \times 10^{-4}$ M, $1 \times 10^{-3}$ M, $6 \times 10^{-4}$ M; $15 \times 10^{-3}$ M; $25 \times 10^{-3}$ M, $3 \times 10^{-3}$ M; $3.5 \times 10^{-3}$ M, respectively.

Dyes **8**, **12**, **13**, **14**, **15** and **16** exhibited low solubility in methanol avoiding from producing too highly concentrated solutions required for the laser experiments under the pumping conditions selected in the present work.

Tetrahedron 68 (2012) 1153–1162

Contents lists available at SciVerse ScienceDirect

Tetrahedron

journal homepage: www.elsevier.com/locate/tet

# Synthesis and functionalization of new polyhalogenated BODIPY dyes. Study of their photophysical properties and singlet oxygen generation

Maria J. Ortiz [a,*], Antonia R. Agarrabeitia [a], Gonzalo Duran-Sampedro [a], Jorge Bañuelos Prieto [b], Teresa Arbeloa Lopez [b], Walter A. Massad [c], Hernán A. Montejano [c], Norman A. García [c], Iñigo Lopez Arbeloa [b]

[a] Departamento de Química Orgánica I, Facultad de Ciencias Químicas, Universidad Complutense, 28040 Madrid, Spain
[b] Departamento de Química Física, UPV-EHU, Apartado 644, 48080 Bilbao, Spain
[c] Departamento de Química, Universidad Nacional de Río Cuarto, 5800 Río Cuarto, Argentina

ARTICLE INFO

*Article history:*
Received 8 September 2011
Received in revised form 7 November 2011
Accepted 23 November 2011
Available online 28 November 2011

*Keywords:*
Polyiodinated BODIPYs
Electrophilic substitution reactions
Nucleophilic substitution reactions
Cross-coupling
Singlet oxygen generation

ABSTRACT

A theoretical and experimental study on the iodination of BODIPY dyes with different degrees of substitution has been developed. Polyhalogenated BODIPYs synthesized in this work are the first examples of this type of dyes with more than two halogen atoms in the BODIPY core and they can be selectively functionalized. Surprisingly, the position in which halogen is attached has a marked effect in the photophysical properties and modulates the fluorescence capacity of the resulting BODIPY. These iodinated BODIPYs are efficient singlet oxygen generators.

© 2011 Elsevier Ltd. All rights reserved.

## 1. Introduction

Along the last years the number of contributions in the literature about 4,4-difluoro-4-bora-3a,4a-diaza-*s*-indacene (BODIPY) dyes has increased exponentially, due to their advantageous photophysical properties, such as a high fluorescence quantum yield, low triplet–triplet absorption, and high photostability.[1] In addition, these dyes present a high number of applications.[2] The contributions directed at modifying the structure using new synthetic procedures have grown clearly in a similar way. In general, most synthetic routes are focused on the introduction of suitable substituents at an appropriate position of the indacene core, in most cases to extend the conjugation and to optimize their spectroscopic properties. Typical approaches to this problem include: Knoevenagel-type condensation of methyl-substituted BODIPYs,[1,3] nucleophilic substitution,[1,4] Liebeskind–Srögl reaction[5] or palladium coupling reactions (Sonogashira, Suzuki…).[1,3i,4f,6] Halogenated BODIPYs are the most useful building blocks for these synthetic strategies.[1,4,6]

In addition, halogenated BODIPY dyes can find applications as probes for photodynamic therapy (PDT), a noninvasive methodology for the treatment of malignant tumours and age related macular degeneration. The treatment requires a combined application of a photosensitizer and light of a wavelength matched to the $\lambda_{max}$ of the photosensitizer in order to generate cytotoxic reactive oxygen species (e.g., $^1O_2$) that eradicate tumours via cellular damage, via vasculature damage and, possibly, by response of the immune system.[7] The generation of reactive oxygen species requires the population of the triplet state of the dye. BODIPYs do not undergo efficient intersystem crossing to the triplet excited state. However, the presence of heavy atoms increases the quantum yield of intersystem crossing. Thus, it has been shown that iodine or bromine incorporation into the BODIPY nucleus enhanced intersystem crossing and a few promising sensitizers for use in PDT have been reported in the last few years as an alternative to the porphyrin-based photosensitizers.[8]

There are three different ways to achieve halogenated BODIPYs: halogenation of the pyrrole ring,[6a,9] halogenation of the dipyrromethane precursors[4a,10] or electrophilic substitution reactions on the BODIPY dye previously synthesized.[1,6c–e,g,8b–g,11] The latter reactions have been studied,[1] showing that positions 2 and 6 of the BODIPY core are the most susceptible to electrophilic attack. However, there is not a definitive study on the regioselectivity in

* Corresponding author. Tel.: +34 913 944 309; fax: +34 913 944 103; e-mail address: mjortiz@quim.ucm.es (M.J. Ortiz).

0040-4020/$ – see front matter © 2011 Elsevier Ltd. All rights reserved.
doi:10.1016/j.tet.2011.11.070

these reactions for unsubstituted BODIPYs. In most cases studied some of the other positions are blocked by substituents, although the bromination with NBS of a 1,3,5,7-unsubstituted BODIPY has been described recently,[12] providing mono- and dibrominated BODIPYs at the 2- and 6-positions with high regioselectivity. In this study none of the regioisomeric products, such as α-bromo-BODIPYs, were detected in the reaction mixture, even when an excess of the brominating agent was used.[12]

Based on this background, in this work we report a novel theoretical, experimental, and photophysical study on the iodination of a series of BODIPYs **1**–**3** with different degrees of substitution (Fig. 1). In addition, we have carried out a preliminary study of the selective functionalization and singlet oxygen generation of some of these halogenated BODIPYs.

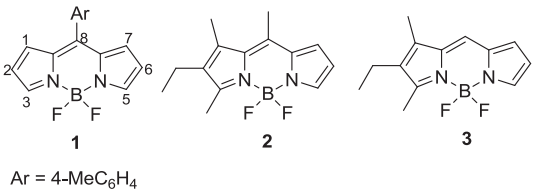


**Fig. 1.** Chemical structures of the BODIPY dyes **1**–**3**.

## 2. Results and discussion

### 2.1. Theoretical study

The mesomeric structures of the BODIPY core indicate that the 2- and 6-positions have the lower positive charge, so they should be most susceptible to electrophilic attack.[1] In this work, a computational study on compounds **1**–**3** gives the Mulliken charge distribution and the electrostatic potential map shown in Fig. 2. The electronic charge distribution of these BODIPY dyes is characteristic of a cyanine-like delocalized π-system[13] (Fig. 2, and Figs. 1S–3S in ESI).

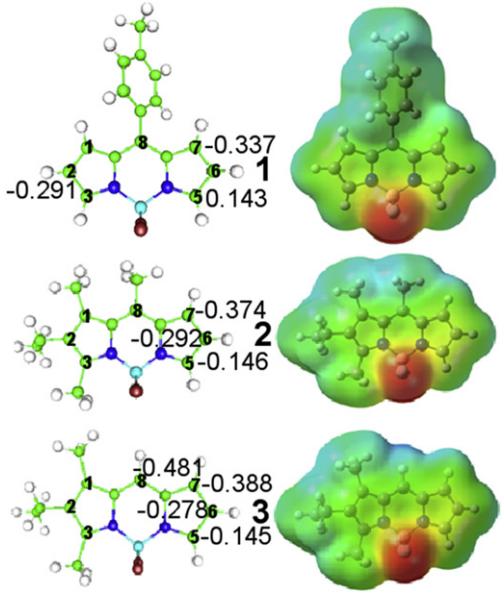


**Fig. 2.** Electrostatic potential map (blue-positive and red-negative) and Mulliken charge of BODIPYs **1**–**3**.

According to the values shown in Fig. 2, for dye **1**, positions 1- and 7 are the most favourable for an electrophilic attack. However, in order to predict the iodination site steric interactions should also be taken into account. Thus, there is a considerable sterical hindrance at 1- and 7-positions, due to the bulky phenyl group at *meso*-position, and also to the large size of the iodine atom, avoiding the incorporation of iodine at those sites.

Therefore, the combination of electronic and steric factors predicts that positions 2 and 6 are the most favourable for electrophilic substitution in compound **1**. The presence of the halogen atom modifies the charge distribution as shown in the ESI (Fig. 1S, ESI). Successive iodinations should occur on the most negative charged carbons, but taking into account that the adjacent positions of the phenyl group in compound **1** are inaccessible to iodine due to steric factors.

The sterical hindrance at positions 1 and 7 in compound **1** is not present in alkyl-substituted BODIPY **2** and **3**. As a consequence, the iodination should be controlled by electronic factors, meaning that the reaction should take place at the positions with the highest negative charge. At a first sight, all the free positions are susceptible to be iodinated. However, the electrostatic potential map shows a high positive density around the *meso* carbon (Fig. 2), hampering the approach of the electrophilic iodine atom. Indeed, such effect should be clearer at 8-position since typically the dipole moment of BODIPYs is oriented along the transversal axis, with the negative charge density located in the fluorine atoms and the positive density centred at the *meso*-position. Thus, in BODIPY **3** the *meso*-position cannot be iodinated, although is free and the carbon is characterized by a negative charge (Fig. 3S, ESI). Therefore, it should be expected that 5- and 6-positions will be first iodinated in BODIPY **2** and **3**, since the halogen can easily come around, although they have lower negative charge than 7- and 8-position.

### 2.2. Synthesis

To test these hypotheses, we have synthesized BODIPY dyes **1**,[14] **2**[15] and **3**,[16] using the methods previously described, and we have investigated the iodination reactions of these compounds with ICl or $I_2$/$HIO_3$ by using different concentrations of the iodination reagents and at different reaction times. The products obtained in the halogenation reactions of these BODIPY dyes are shown in Fig. 3 and Table 1.

The experimental results show that is possible to obtain selectively mono-, di-, tri- and tetraiodinated products of BODIPYs **1**, **2** and **3**. These are the first examples of this type of dyes with more than two halogen atoms in the BODIPY core. Thus, iodination of these dyes with ICl in almost equimolecular ratio (Table 1, entries 1, 10 and 14), gives the monoiodo-BODIPYs **4a**, **5a** and **6a**, respectively, in high yield. When two and a half equivalents are used (Table 1, entries 2, 11 and 15), diiodo-BODIPYs **4b**, **5b**, **5c**, **6b** and **6c**, are obtained. These compounds can be separated easily by column chromatography. Compound **5b** is obtained with much lower yield than **6b** probably due to steric hindrance by the methyl group in the *meso*-position.

Although it is possible to obtain the triiodo derivative **4c** (Table 1, entry 3), the yield is low because it is always accompanied of diiodo **4b** and tetraiodo **4d** derivatives, furthermore, in this case it is hard to separate the isomers chromatographically. A mixture of polyhalogenated derivatives with iodide and chlorine (**4d**, **4e**, **4f** and **4g**) in different positions of the BODIPY **1** are obtained with higher ratios of reagents (Table 1, entries 4 and 5). Similarly, BODIPY dyes **2** and **3** give rise to trihalogenated derivatives **5d**, **5e**, **6d** and **6e**, respectively (Table 1, entries 12 and 16). The formation of chlorinated products is in agreement with bibliographic data[17] showing that the reaction of iodine chloride with aromatic compounds can lead to chlorinated and/or iodine derivatives depending on the reaction conditions.

To prevent the formation of chlorinated derivatives, we carried out the iodination reactions using $I_2$/$HIO_3$ as a halogenating agent

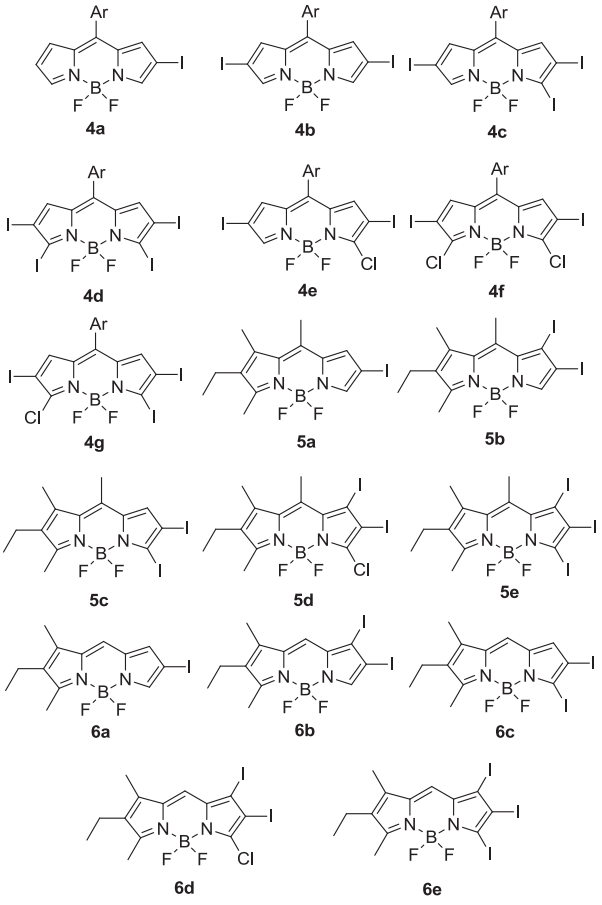


**Fig. 3.** Structures of the halogenated BODIPY dyes.

(Table 1, entries 6–9, 13 and 17). In these conditions, tetraiodo **4d** and triiodo derivatives **5e** and **6e** are obtained with good yields.

The data obtained indicate that, in principle, any free BODIPY position can undergo the electrophilic attack, which increase the synthetic utility of this reaction. Thus, whereas the 1- and 7-positions of BODIPY **1** do not undergo electrophilic substitution, due to the steric hindrance of the phenyl group, and then the halogenation occurs at the 2- and 6-positions, followed by the 3- and 5-positions. In the case of the BODIPY **2**, the electrophilic attack takes place in all positions, while in the BODIPY **3** the iodination reaction does not occur in the *meso*-position. The lack of iodination at this position is probably due to the high positive charge density at the *meso*-position, which prevents electrophilic substitution (Fig. 2).

**Table 1**
Reaction conditions and yields of isolated products of BODIPYs **1**–**3**

| Entry | Agent[a] | Ratio | *t* (min) | Products (yield, %)[d] |
|---|---|---|---|---|
| BODIPY **1** | | | | |
| 1 | A | 1:1[b] | 30 | **4a** (75) |
| 2 | A | 1:2.5[b] | 60 | **4a** (14), **4b** (72) |
| 3 | A | 1:3.5[b] | 120 | **4b** (22), **4c** (45), **4d** (8) |
| 4 | A | 1:4.5[b] | 180 | **4d** (10), **4e** (5), **4f** (21), **4g** (40) |
| 5 | A | 1:8[b] | 360 | **4d** (25), **4f** (24), **4g** (20) |
| 6 | B | 1:1:0.8[c] | 30 | **4a** (70) |
| 7 | B | 1:2.5:2[c] | 60 | **4a** (15), **4b** (69) |
| 8 | B | 1:3.5:3[c] | 60 | **4b** (15), **4c** (30), **4d** (30) |
| 9 | B | 1:4.5:4[c] | 180 | **4d** (64) |
| BODIPY **2** | | | | |
| 10 | A | 1:1.3[b] | 30 | **5a** (95) |
| 11 | A | 1:2.5[b] | 60 | **5a** (8), **5b** (10), **5c** (67) |
| 12 | A | 1:6[b] | 180 | **5c** (6), **5d** (35), **5e** (20) |
| 13 | B | 1:4.5:4[c] | 180 | **5c** (5), **5e** (48) |
| BODIPY **3** | | | | |
| 14 | A | 1:0.8[b] | 30 | **6a** (81) |
| 15 | A | 1:2.5[b] | 90 | **6a** (13), **6b** (34), **6c** (35) |
| 16 | A | 1:8[b] | 300 | **6d** (30), **6e** (35) |
| 17 | B | 1:5:4.5[c] | 300 | **6e** (54) |

[a] Halogenating reagent: A=ICl, B=$I_2$/$HIO_3$.
[b] Molar ratio BODIPY/ICl.
[c] Molar ratio BODIPY/$I_2$/$HIO_3$.
[d] Yield of isolated product.

## 2.3. Selective functionalization

The easily obtained polyhalogenated derivatives are valuable synthetic precursors for selective functionalization allowing the development of a variety of symmetric and asymmetric BODIPY compounds that are difficult to obtain by alternative procedures.[1,4,6] It is known that 3,5-dichloroBODIPY derivatives can undergo substitution of the chlorine atoms by a wide range of oxygen, carbon, nitrogen, and sulfur nucleophiles. Furthermore, the reaction conditions can be adjusted to obtain either mono- or disubstituted products.[1,4]

In this work, we have carried out nucleophilic substitution reactions of 2,3,5,6-tetraiodo BODIPY **4d** with 4-metoxyaniline, β-alanine and sodium diethyl malonate. In the first two cases only monosubstituted derivatives **7** and **8** were obtained, respectively, even when the reaction is carried out with an excess of the reagent and under reflux (Scheme 1).

These results contrast with those previously reported for the 3,5-dicloroderivatives[4] and a possible explanation could be that the presence of iodine atoms next to electron-donor groups increase the charge density of the system preventing the second nucleophilic substitution reaction to occur. To test this hypothesis, we treated compound **4d** with sodium diethyl malonate. Under these conditions, the mono and disubstituted BODIPY derivatives **9** and **10** were obtained. Furthermore, compound **9** afford the asymmetric derivative **11** by reaction with 4-methoxyaniline. In these cases, the absence of electron-donating groups allows the second $S_NAr$. The iodinated derivatives can be used in Pd-coupling reactions. Thus, a triplet Suzuki coupling reaction of **7** yielded the highly functionalized dye **12** (Scheme 1).

## 2.4. Photophysical properties

The photophysical properties of BODIPY **1** (Table 2, and Table 1S in ESI) are conditioned by the presence of the phenyl group at *meso*-position. It has been previously reported that the free rotation of such ring greatly increases the internal conversion processes and it can interact with the BODIPY core distorting the indacene planarity.[18] The absence of substituents at 1- and 7-positions enables the rotation of the phenyl ring (twisted 50° from the BODIPY plane).[19] Hence, compound **1** is characterized by a very low fluorescence quantum yield ($\phi$<0.04) and lifetime ($\tau$<700 ps). Successive iodination gives rise to a progressive bathochromic shift of the spectral bands (Table 2 and Fig. 4). In fact, the tetraiodinated derivative **4d** emits in the red region of the visible spectra (around 590 nm). The halogenation of the BODIPY core should induce a decrease in the fluorescence capacity due to the heavy atom effect, which increases the intersystem crossing probability (Fig. 4). This influence is observed for the monoiodo and the diiodo derivatives **4a** and **4b**, respectively. Surprisingly, further addition of iodine atoms to the BODIPY core leads to an increase in the intensities of the absorption and also in the fluorescence emission. For instance, the tetraiodinated derivative **4d** shows a very high molar absorption (around $11\times10^4\ M^{-1}\ cm^{-1}$, twice the non-iodinated BODIPY **1**) and even higher than other non-halogenated BODIPYs ($9\times10^4\ M^{-1}\ cm^{-1}$).[18b] Besides, the fluorescence quantum yield for compound **4d** is 0.1, much higher than 0.034, which is the value reported for the non-iodinated BODIPY **1**.[14]

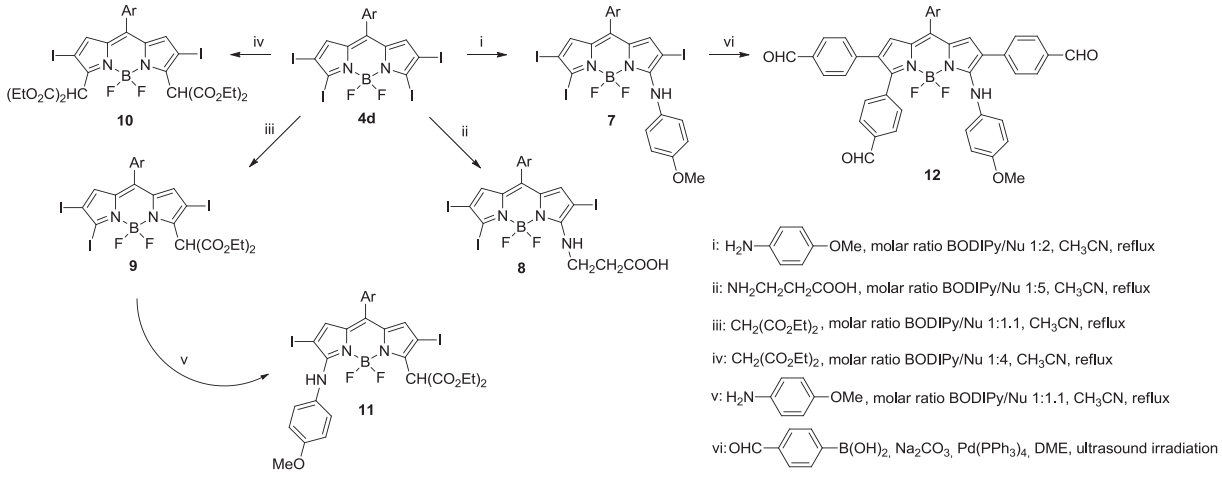


**Scheme 1.** Synthetic scheme for the preparation of BODIPY dyes **7**–**12**.

**Table 2**
Photophysical properties of BODIPY **1**, **2** and **3** and their iodinated derivatives in *c*-hexane. (The full data list for BODIPYs **1**, **2** and **3** series are included in Tables 1S, 3S and 4S in the ESI)

| | $\lambda_{ab}$ (nm) | $\varepsilon_{max}$ ($10^4$ $M^{-1}$ $cm^{-1}$) | $\lambda_{fl}$ (nm) | $\phi$ | $\tau$ (ps) |
|---|---|---|---|---|---|
| BODIPY **1** | | | | | |
| **1** | 500.5 | 6.9 | 516.0 | 0.036 | 323 |
| **4a** | 523.5 | 2.2 | 540.0 | 0.034 | 184 |
| **4b** | 548.5 | 4.3 | 567.5 | 0.012 | 117 |
| **4c** | 563.5 | 4.8 | 577.5 | 0.060 | 327 |
| **4d** | 581.0 | 11.6 | 593.0 | 0.099 | 678 |
| BODIPY **2** | | | | | |
| **2** | 504.0 | 3.3 | 515.0 | 0.96 | 5460 |
| **5a** | 517.5 | 4.6 | 532.0 | 0.13 | 560 |
| **5b** | 515.5 | 2.9 | 538.5 | 0.05 | 259 |
| **5c** | 532.0 | 9.8 | 546.0 | 0.20 | 1021 |
| **5e** | 531.5 | 1.7 | 554.5 | 0.10 | 331 |
| BODIPY **3** | | | | | |
| **3** | 512.5 | 2.9 | 517.5 | 0.70 | 5240 |
| **6a** | 528.0 | 6.3 | 538.5 | 0.11 | 489 |
| **6b** | 527.5 | 5.6 | 537.0 | 0.05 | 212 |
| **6c** | 542.0 | 7.6 | 550.5 | 0.26 | 1041 |
| **6e** | 543.5 | 6.9 | 551.5 | 0.07 | 358 |

Absorption ($\lambda_{ab}$) and fluorescence ($\lambda_{fl}$) wavelength of the maximum; molar absorption ($\varepsilon_{max}$) at the maximum wavelength; fluorescence quantum yield ($\phi$) and lifetime ($\tau$). Present lifetimes are the main component of the decay curve, which is analyzed as biexponential but with a negligible long lifetime.

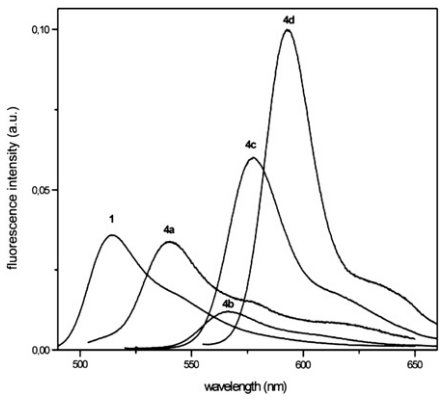


**Fig. 4.** Fluorescence spectra of BODIPY **1** and its iodinated derivatives **4a**–**d** in *c*-hexane, scaled by their fluorescence quantum yield.

Theoretical simulations of the absorption transition confirm the progressive bathochromic shift with the iodination degree and the enhancement of the absorption probability of **4d** with regard to the rest of derivatives (Table 2S, ESI). Compound **4d** shows a uniform charge distribution in the pyrrole moiety, whereas in the rest of the series it is more irregular (Fig. 1S, ESI). That means that the negative charge on nitrogen, and on positions 1-, 2- and 3, and their corresponding symmetrical ones, is nearly the same (around −0.255). Accordingly, the delocalization is improved, in concordance with the push–pull effect (substitution at the beginning and ending of the delocalized system).[14] Therefore, substitution at 3- and 5-positions counteracts in part the non-radiative processes (heavy atom effect and phenyl free rotation) improving the fluorescence efficiency of the dye. It seems that the iodine presence at those positions extents the chromophoric electronic density far away from the phenyl ring (Fig. 1S, ESI) diminishing the deleterious effect in fluorescence owing to its free motion.

On the other hand, the absence of the bulky phenyl group in BODIPY **2** and **3** leads to highly fluorescence molecules, as is characteristic of this dye family (Table 2, and Tables 3S–4S, ESI). The absorption probability is not very high due to the asymmetric substitution pattern, which leads to charge separation between the pyrroles (Fig. 2). The incorporation of an iodine atom at 6-position (**5a** and **6a**) implies a drastic decrease of the intensity of the fluorescence emission, which is attributed to the enhancement in the probability of intersystem crossing, as mentioned above (Table 2). However, further halogenation leads to entirely different results depending of the position in which the iodine is attached. The incorporation of a second iodine atom at position 7 (**5b** and **6b**) has a minimum effect on the wavelength of the absorption band position but induces a reduction of the intensity of the fluorescence emission, in agreement with the heavy atom effect. In contrast, the incorporation of a second iodine atom at position 5 (**5c** and **6c**) gives rise to a bathochromic spectral shift and increases the absorption probability and fluorescence efficiency (Table 2) in concordance with the push–pull effect. Again, the electronic distribution of **5c** and **6c** in the pyrrole rings is uniform (Figs. 2S–3S, ESI), in good agreement with the influence observed for the iodo-derivatives from BODIPY **1**. Therefore, the results obtained in the present study confirm that substitution at the ends of the delocalized π-system is advantageous for the fluorescence ability of the dye. In the triiodinated derivatives (**5e** and **6e**), the incorporation of iodine at 7- and 5-positions has the opposite influence in the photophysics of the dye. As a result, the effect of both iodine atoms is counteracted. That means, whereas substitution at 7-position should increase the intersystem crossing, without altering the band position,

substitution at 5-position should favour the fluorescence ability and give rise to a bathochromic shift. Consequently, their spectral bands are placed close to those of the diiodinated derivative (**5c** and **6c**) and their fluorescence capacity is similar to that of the monoiodinated ones (**5a** and **6a**) (Table 2). Indeed, the electronic distribution in the triiodinated derivatives is less uniform and the system is less aromatic (Figs. 2S–3S, ESI). Quantum mechanical simulation of the absorption transition nicely reproduces the shift of the band depending on the iodine position in the chromophore and describes qualitatively well the evolution of the absorption probability (Table 2S, ESI).

Finally, we should note the close correlation between the fluorescence quantum yield and the lifetime with both changing the number of halogens appended to BODIPY and the environmental properties. Such evolutions are controlled mainly by the non-radiative processes, thus the lower the fluorescence efficiency the faster the decay from the excited state.

Finally, we should note the close correlation between the fluorescence quantum yield and the lifetime with both changing the number of halogens appended to BODIPY and the environmental properties. Such evolutions are controlled mainly by the non-radiative processes, thus the lower the fluorescence efficiency the faster the decay from the excited state.

### 2.5. Singlet oxygen generation

Typically BODIPYs are characterized by very low triplet state population. However, iodinated derivatives **4**, **5** and **6** show low fluorescence yields mainly due to the triplet state population via the intersystem crossing process promoted by the so-called internal heavy atom effect.[2a,9a] Therefore they could be good singlet oxygen ($^1O_2$) generators after energy transfer from excited triplet state to ground state oxygen.

The transient absorption spectra of **4b** and **4d** dyes obtained by laser flash photolysis in MeCN solution were recorded in the range between 250 and 850 nm. The spectra of each dye present negative bands caused by depletion of the ground state, which are practically the same that the corresponding one for ground state absorption, revealing the lack of photoproduct generation under the selected laser experimental conditions. As a typical example, the case of **4b** is shown in Fig. 5.

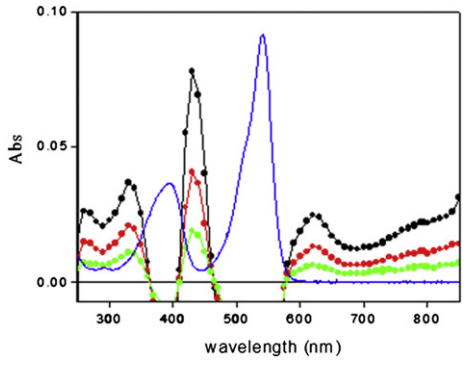


**Fig. 5.** Transient absorption spectra of **4b** in MeCN recorded at different times after the laser pulse: (○, 1 μs), (○, 4 μs), (○, 8 μs) and ground state absorption spectrum (▬).

The monoexponential decay of the spectrum for **4b** and **4d** is in agreement with the recovery in the bleaching regions. It worth noting that similar transient spectra were reported for the triplet state of others dipyrromethene dyes.[20] All these observations strongly suggest that the observed absorptions correspond to a unique transient species, which is assigned to the electronically excited triplet state of the dyes investigated.

We examined the ability of compounds **4b**–**d** with two or more atoms of iodine to generate $^1O_2$. This was done in $CH_3CN$ using 532 nm-excitation. The reference was Rose Bengal (RB) with a quantum yield $\Phi_{\Delta RB}$ for $^1O_2$ production of 0.71 determined in this work using perinaphthenone (PN) with $\Phi_{\Delta RB}$=1 as a reference compound (Fig. 4S, ESI). The results obtained are $\Phi_{\Delta \mathbf{4b}}$=0.83+7%, $\Phi_{\Delta \mathbf{4c}}$=0.86+9% and $\Phi_{\Delta \mathbf{4d}}$=0.87+6%, all these values are in the range of those exhibited by compounds recognized as efficient $^1O_2$ photosensitizer (Fig. 5S, ESI).

The results obtained show that the introduction of iodine atoms in 3 and/or 5 positions does not produce a significant increase in the efficiency of $^1O_2$ generation and they are in good agreement with those arising from the photophysical properties, showing that substitution at 3 or 5-position favours the fluorescence ability. It is clear that additional studies are needed to clarify the influence of the iodine atoms positions over the efficiency of singlet oxygen generation of these compounds. Nevertheless, the obvious consequence of the investigation described above is that these polyiodinated BODIPYs are efficient photosensitizers for the generation of $^1O_2$ and additionally they can be suitably functionalized at of 3- and 5-positions for their possible use as PDT agents.

## 3. Conclusion

We have demonstrated that it is possible to control the degree of iodination in the BODIPY core, which allows the synthesis of mono-, di- and polyiodinated derivatives. These are the first examples of this type of dyes with more than two halogen atoms in the BODIPY core. Moreover, considering the easy synthetic route of these polyhalogenated derivatives, the reaction could be extended to other dyes of this family, with different degrees of substitution. Another interesting observation in this study is that polyhalogenated compounds can be valuable synthetic precursors for the selective incorporation of the desired functional groups in a specific position of the BODIPY. Quantum mechanical calculations can predict the position in which iodine atoms will be incorporated and explain why some positions are inaccessible to the iodine atom. Moreover, the position in which halogen is attached modulates the photophysical properties of the resulting BODIPY. In general, substitution at 3- or 5-positions improves the absorption and fluorescence transition probability efficiency while in the rest of positions leads to an important reduction of the fluorescence ability owing to the heavy atom effect, which activates the intersystem crossing processes. Triplet state population via intersystem crossing leads to a high efficiency of **4b**–**d** as $^1O_2$ generators. Further work is in progress to complete the study over the triplet state (singlet oxygen generation and phosphorescence spectra) and finally to explore the applicability of these novel BODIPYs appropriately functionalized in PDT.

## 4. Experimental section

### 4.1. General

Starting materials and reagents used in the preparation of BODIPYs are commercially available unless synthesis is described. The solvents were dried and distilled, before use. Spectral data of the known compounds were in accordance with the literature data. Flash column chromatography was performed using silica gel Merck 60 (230–400 mesh). $^1H$ and $^{13}C$ NMR spectra were recorded with a Bruker Avance-DPX-300 spectrometer (300 MHz for $^1H$ and 75 MHz for $^{13}C$) and a Bruker Avance III spectrometer (700 MHz for $^1H$ and 176 MHz for $^{13}C$). The spectra were recorded in $CDCl_3$ or $CD_3OD$. $^1H$ NMR chemical shifts are reported in parts per million relative to tetramethylsilane ($\delta$=0.00 ppm), using the residual solvent signal as the internal reference. $^{13}C$ NMR chemical shifts are reported in ppm with $CDCl_3$ ($\delta$=77.67 ppm) as the internal standard. Chemical shift multiplicities are reported as s=singlet,

d=doublet, t=triplet, q=quartet and m=multiplet. IR spectra (in $cm^{-1}$) were recorded in a Bruker Tensor-27-FTIR spectrophotometer. Melting points were determined in open capillaries and are uncorrected. Mass spectra were registered by electron impact (EI) at 70 eV, by electrospray ionization (ESI) and by atmospheric pressure chemical injection (APCI) in a VGI2-250 spectrometer. High resolution mass spectra were determined by electrospray ionization in the positive mode ($ESI^+$) in an Accurate-Mass Q-TOF LC/MS 6520 (Agilent Technologies).

### 4.2. General procedure for the synthesis of halogenated BODIPYs

*4.2.1. Method A: iodination reaction with ICl.* To a solution of BODIPY in a $CH_2Cl_2$/MeOH mixture (1:1) was added dropwise a solution of ICl in MeOH. The BODIPY/ICl ratio is indicated in each case. This mixture was refluxed for 30–360 min. After cooling, the solvent was evaporated under vacuum. The crude product was dissolved in $CH_2Cl_2$, washed with $H_2O$, dried over $MgSO_4$, filtered and concentrated to dryness. The halogenated BODIPYs were purified by flash chromatography on silica gel (eluent hexane/EtOAc).

*4.2.2. Method B: iodination reaction with $I_2$/$HIO_3$.* Iodic acid dissolved in a minimum amount of water was added dropwise to a solution of BODIPY and iodine in EtOH. The BODIPY/$I_2$/$HIO_3$ ratio is indicated in each case. This mixture was refluxed for 30–300 min. After cooling, the solvent was evaporated under vacuum. The crude product was dissolved in $CH_2Cl_2$, washed with $H_2O$, dried over $MgSO_4$, filtered and concentrated to dryness. The halogenated BODIPYs were purified by flash chromatography on silica gel (eluent hexane/EtAcO).

### 4.3. Iodination reactions of BODIPYs 1–3

*4.3.1. BODIPY **1** with ICl (1:1).* According to the method A, BODIPY **1** (70 mg, 0.25 mmol) in $CH_2Cl_2$/MeOH (10 mL/10 mL) and ICl (41 mg, 0.25 mmol) in MeOH (5 mL) for 30 min were reacted. Flash chromatography using hexane/EtAcO (98:2) afforded, by order of elution, 4,4-difluoro-2-iodo-8-(4-tolyl)-4-bora-3a,4a-diaza-*s*-indacene (**4a**) (76 mg, 75%) as an orange solid and starting BODIPY **1** (10 mg, 14%).

*4.3.1.1. Compound **4a**.* Mp 166.2–166.8 °C; $^1H$ NMR (700 MHz, $CDCl_3$): $\delta$ 7.92 (1H, s, H-5), 7.76 (1H, s, H-3), 7.39 (2H, d, $J$=7.7 Hz, H-2′), 7.28 (2H, d, $J$=7.7 Hz, H-3′), 6.97 (1H, s, H-1), 6.96 (1H, d, $J$=4.2 Hz, H-7), 6.53 (1H, d, $J$=4.2 Hz, H-6), 2.41 (3H, s, $CH_3$); $^{13}C$ NMR (176 MHz, $CDCl_3$): $\delta$ 147.0 (C), 146.4 (CH), 145.6 (CH), 141.9 (C), 136.1 (CH), 135.8 (C), 135.1 (C), 133.1 (CH), 130.6 (CH), 129.4 (CH), 119.6 (CH), 70.8 (C–I), 21.5 ($CH_3$); IR (neat): 1539, 1258, 1111 $cm^{-1}$; MS ($APCI^-$) $m/z$ (%): 408 ($M^-$, 100); HRMS-$ESI^+$: calcd for ($C_{16}H_{12}BF_2IN_2$+$H^+$) 409.0182 found 409.0178.

*4.3.2. BODIPY **1** with ICl (1:2.5).* According to the method A, BODIPY **1** (70 mg, 0.25 mmol) in $CH_2Cl_2$/MeOH (10 mL/10 mL) and ICl (102 mg, 0.63 mmol) in MeOH (5 mL) for 60 min were reacted. Flash chromatography using hexane/EtAcO (98:2) afforded, by order of elution, 4,4-difluoro-2,6-diiodo-8-(4-tolyl)-4-bora-3a,4a-diaza-*s*-indacene (**4b**) (96 mg, 72%) as a green solid and **4a** (14 mg, 14%).

*4.3.2.1. Compound **4b**.* Mp 210.0–210.7 °C; $^1H$ NMR (700 MHz, $CDCl_3$): $\delta$ 7.80 (2H, s, H-3 and H-5), 7.37 (2H, d, $J$=7.7 Hz, H-2′), 7.29 (2H, d, $J$=7.7 Hz, H-3′), 7.05 (2H, s, H-1 and H-7), 2.41 (3H, s, $CH_3$); $^{13}C$ NMR (176 MHz, $CDCl_3$): $\delta$ 147.1 (CH), 145.1 (C), 141.4 (C), 136.6 (CH), 134.9 (C), 129.5 (CH), 129.2 (C), 128.5 (CH), 71.1 (C–I), 20.5 ($CH_3$); IR (neat): 1539, 1254, 1114 $cm^{-1}$; MS (EI) $m/z$ (%): 534 ($M^+$, 100), 407 (7), 280 (22), 265 (18), 203 (10), 139 (10); HRMS-$ESI^+$: calcd for ($C_{16}H_{11}BF_2I_2N_2$+$H^+$) 534.9153 found 534.9146.

*4.3.3. BODIPY **1** with ICl (1:3.5).* According to the method A, BODIPY **1** (70 mg, 0.25 mmol) in $CH_2Cl_2$/MeOH (10 mL/10 mL) and ICl (142 mg, 0.87 mmol) in MeOH (5 mL) for 120 min were reacted. Flash chromatography using hexane/EtAcO (98:2) afforded, by order of elution, **4b** (29 mg, 22%), 4,4-difluoro-2,3,6-triiodo-8-(4-tolyl)-4-bora-3a,4a-diaza-*s*-indacene (**4c**) (74 mg, 45%) as a green solid and 4,4-difluoro-2,3,5,6-tetraiodo-8-(4-tolyl)-4-bora-3a,4a-diaza-*s*-indacene (**4d**) (16 mg, 8%) as a green solid.

*4.3.3.1. Compound **4c**.* Mp 253.2–253.7 °C; $^1H$ NMR (700 MHz, $CDCl_3$): $\delta$ 7.80 (1H, s, H-5), 7.34 (2H, d, $J$=8.1 Hz, H-2′), 7.27 (2H, d, $J$=8.1 Hz, H-3′), 7.00 (1H, s, H-1), 6.96 (1H, s, H-7), 2.40 (3H, s, $CH_3$); $^{13}C$ NMR (176 MHz, $CDCl_3$): $\delta$ 148.6 (CH), 143.4 (C), 142.3 (C), 139.3 (C), 137.8 (CH), 137.4 (CH), 135.9 (C), 130.5 (CH), 129.7 (C), 129.6 (CH), 115.1 (C–I), 90.2 (C–I), 72.8 (C–I), 21.6 ($CH_3$); IR (neat): 1536, 1237, 1089 $cm^{-1}$; MS ($APCI^-$) $m/z$ (%): 660 ($M^-$, 100), 602 (40), 585 (25), 533 (42); HRMS-$ESI^+$: calcd for ($C_{16}H_{10}BF_2I_3N_2$+$H^+$) 660.8119 found 660.8109.

*4.3.3.2. Compound **4d**.* Mp 283.2–284.0 °C; $^1H$ NMR (700 MHz, $CDCl_3$): $\delta$ 7.31 (2H, d, $J$=7.7 Hz, H-2′), 7.27 (2H, d, $J$=7.7 Hz, H-3′), 6.91 (2H, s, H-1 and H-7), 2.40 (3H, s, $CH_3$); $^{13}C$ NMR (176 MHz, $CDCl_3$): $\delta$ 142.2 (C), 140.5 (C), 139.3 (C), 137.5 (CH), 130.4 (CH), 129.6 (CH), 129.1 (C), 115.9 (C–I), 90.9 (C–I), 21.6 ($CH_3$); IR (neat): 1536, 1320, 1215, 1086 $cm^{-1}$; MS ($APCI^-$) $m/z$ (%): 786 ($M^-$, 100), 677 (50); HRMS-$ESI^+$: calcd for ($C_{16}H_9BF_2I_4N_2$+$H^+$) 786.7086 found 786.7080.

*4.3.4. BODIPY **1** with ICl (1:4.5).* According to the method A, BODIPY **1** (70 mg, 0.25 mmol) in $CH_2Cl_2$/MeOH (10 mL/10 mL) and ICl (183 mg, 1.12 mmol) in MeOH (5 mL) for 180 min were reacted. Flash chromatography using hexane/EtAcO (98:2) afforded, by order of elution, 3-chloro-4,4-difluoro-2,6-diiodo-8-(4-tolyl)-4-bora-3a,4a-diaza-*s*-indacene (**4e**) (7 mg, 5%) as a green solid, 3,5-dichloro-4,4-difluoro-2,6-diiodo-8-(4-tolyl)-4-bora-3a,4a-diaza-*s*-indacene (**4f**) (32 mg, 21%) as a green solid, 3-chloro-4,4-difluoro-2,5,6-triiodo-8-(4-tolyl)-4-bora-3a,4a-diaza -*s*-indacene (**4g**) (69 mg, 40%) as a green solid and **4d** (20 mg, 10%).

*4.3.4.1. Compound **4e**.* Mp 259.8–260.3 °C; $^1H$ NMR (700 MHz): $\delta$ 7.79 (1H, s, H-5), 7.34 (2H, d, $J$=7.7 Hz, H-2′), 7.29 (2H, d, $J$=7.7 Hz, H-3′), 7.05 (1H, s, H-1), 7.01 (1H, s, H-7), 2.41 (3H, s, $CH_3$); $^{13}C$ NMR (176 MHz): $\delta$ 148.1 (C–Cl and CH), 144.5 (C), 142.4 (C), 138.4 (CH), 137.2 (CH), 135.7 (C), 135.0 (C), 130.6 (CH), 129.6 (CH), 129.4 (C), 76.3 (C–I), 72.4 (C–I), 21.6 ($CH_3$); IR (neat): 1373, 1239, 1046 $cm^{-1}$; MS ($APCI^-$) $m/z$ (%): 568 ($M^-$, 100), 549 (30), 473 (40), 441 (35); HRMS-$ESI^+$: calcd for ($C_{16}H_{10}BClF_2I_2N_2$+$H^+$) 568.8763 found 568.8759.

*4.3.4.2. Compound **4f**.* Mp 253.6–254.1 °C; $^1H$ NMR (700 MHz): $\delta$ 7.31 (2H, d, $J$=7.7 Hz, H-2′), 7.28 (2H, d, $J$=7.7 Hz, H-3′), 7.00 (2H, s, H-1 and H-7), 2.41 (3H, s, $CH_3$); $^{13}C$ NMR (176 MHz): $\delta$ 148.2 (C–Cl), 142.9 (C), 142.3 (C), 137.9 (CH), 134.8 (C), 130.5 (CH), 129.6 (CH), 129.0 (C), 76.6 (C–I), 21.5 ($CH_3$); IR (neat): 1542, 1363, 1233, 1100 $cm^{-1}$; MS ($APCI^-$) $m/z$ (%): 602 ($M^-$, 100), 583 (22), 507 (28), 475 (28); HRMS-$ESI^+$: calcd for ($C_{16}H_9BCl_2F_2I_2N_2$+$H^+$) 602.9373 found 602.9369.

*4.3.4.3. Compound **4g**.* Mp 260.0–260.5 °C; $^1H$ NMR (700 MHz): $\delta$ 7.31 (2H, d, $J$=7.7 Hz, H-2′), 7.28 (2H, d, $J$=7.7 Hz, H-3′), 7.00 (1H, s, H-7), 6.92 (1H, s, H-1), 2.41 (3H, s, $CH_3$); $^{13}C$ NMR (176 MHz): $\delta$ 148.6 (C–Cl), 142.3 (C), 141.7 (C), 139.1 (C), 138.1 (CH), 137.4 (CH), 135.0 (C), 130.5 (CH), 129.6 (CH), 129.1 (C), 115.3 (C–I), 90.6 (C–I), 77.2 (C–I), 21.6 ($CH_3$); IR (neat): 1542, 1224, 1094 $cm^{-1}$; MS ($APCI^-$)

*m*/*z* (%): 694 ($M^-$, 75), 585 (100), 439 (50); HRMS-ESI$^+$: calcd for ($C_{16}H_9BClF_2I_3N_2+H^+$) 694.7730 found 694.7721.

*4.3.5. BODIPY **1** with ICl (1:8).* According to the method A, BODIPY **1** (60 mg, 0.21 mmol) in $CH_2Cl_2$/MeOH (10 mL/10 mL) and ICl (272 mg, 1.68 mmol) in MeOH (5 mL) for 360 min were reacted. Flash chromatography using hexane/EtAcO (98:2) afforded, by order of elution, **4f** (30 mg, 24%), **4g** (29 mg, 20%) and **4d** (39 mg, 25%).

*4.3.6. BODIPY **1** with $I_2$/$HIO_3$ (1:1:0.8).* According to the method B, BODIPY **1** (83 mg, 0.29 mmol), $I_2$ (74 mg, 0.29 mmol) in EtOH (20 mL) and $HIO_3$ (41 mg, 0.23 mmol) for 30 min were reacted. Flash chromatography using hexane/EtAcO (98:2) afforded **4a** (83 mg, 70%) and starting BODIPY **1** (16 mg, 19%).

*4.3.7. BODIPY **1** with $I_2$/$HIO_3$ (1:2.5:2).* According to the method B, BODIPY **1** (83 mg, 0.29 mmol), $I_2$ (185 mg, 0.73 mmol) in EtOH (20 mL) and $HIO_3$ (102 mg, 0.58 mmol) for 60 min were reacted. Flash chromatography using hexane/EtAcO (98:2) afforded **4b** (107 mg, 69%) and **4a** (18 mg, 15%).

*4.3.8. BODIPY **1** with $I_2$/$HIO_3$ (1:3.5:3).* According to the method B, BODIPY **1** (73 mg, 0.26 mmol), $I_2$ (231 mg, 0.91 mmol) in EtOH (20 mL) and $HIO_3$ (137 mg, 0.78 mmol) for 60 min were reacted. Flash chromatography using hexane/EtAcO (95:5) afforded, by order of elution, **4b** (21 mg, 15%), **4c** (51 mg, 30%) and **4d** (61 mg, 30%).

*4.3.9. BODIPY **1** with $I_2$/$HIO_3$ (1:4.5:4).* According to the method B, BODIPY **1** (70 mg, 0.25 mmol), $I_2$ (286 mg, 1.12 mmol) in EtOH (20 mL) and $HIO_3$ (176 mg, 1 mmol) for 180 min were reacted. Flash chromatography using hexane/EtAcO (95:5) afforded **4d** (126 mg, 64%).

*4.3.10. BODIPY **2** with ICl (1:1:3).* According to the method A, BODIPY **2** (60 mg, 0.23 mmol) in $CH_2Cl_2$/MeOH (10 mL/10 mL) and ICl (49 mg, 0.30 mmol) in MeOH (5 mL) for 30 min were reacted. Flash chromatography using hexane/EtAcO (98:2) afforded 2-ethyl-4,4-difluoro-6-iodo-1,3,8-trimethyl-4-bora-3a,4a-diaza-*s*-indacene (**5a**) (85 mg, 95%) as an orange solid. Mp 160.2–160.7 °C; $^1$H NMR (300 MHz): $\delta$ 7.39 (1H, s, H-5), 6.95 (1H, s, H-7), 2.49 (3H, s, $CH_3$–C8), 2.40 (3H, s, $CH_3$–C3), 2.34 (2H, q, $J$=7.6 Hz, $CH_2CH_3$), 2.25 (3H, s, $CH_3$–C1), 0.98 (3H, t, $J$=7.6 Hz, $CH_3CH_2$); $^{13}$C NMR (75 MHz): $\delta$ 162.8 (C), 142.0 (C), 139.7 (CH), 138.9 (C), 136.2 (C), 135.3 (C), 134.7 (C), 127.6 (CH), 67.0 (C–I), 17.1 ($CH_2$), 16.4 ($CH_3$), 14.4 ($CH_3$), 14.2 ($CH_3$), 13.3 ($CH_3$); IR (neat): 1561, 1177 cm$^{-1}$; MS (ESI$^-$): 387 [M–H]$^-$; HRMS-ESI$^+$: calcd for ($C_{14}H_{16}BF_2IN_2+H^+$) 389.0499 found 389.0491.

*4.3.11. BODIPY **2** with ICl (1:2.5).* According to the method A, BODIPY **2** (63 mg, 0.24 mmol) in $CH_2Cl_2$/MeOH (10 mL/10 mL) and ICl (97 mg, 0.6 mmol) in MeOH (5 mL) for 60 min were reacted. Flash chromatography using hexane/EtAcO (98:2) afforded, by order of elution, 2-ethyl-4,4-difluoro-6,7-diiodo-1,3,8-trimethyl-4-bora-3a,4a-diaza-*s*-indacene (**5b**) (8 mg, 10%) as an orange solid, 2-ethyl-4,4-difluoro-5,6-diiodo-1,3,8-trimethyl-4-bora-3a,4a-diaza-*s*-indacene (**5c**) (83 mg, 67%) as a red solid and **5a** (8 mg, 8%).

*4.3.11.1. Compound **5b**.* Mp 201.5–202.0 °C; $^1$H NMR (700 MHz): $\delta$ 7.49 (1H, s, H-5), 2.87 (3H, s, $CH_3$–C3), 2.45 (3H, s, $CH_3$–C8), 2.36 (2H, q, $J$=7.7 Hz, $CH_2$), 2.30 (3H, s, $CH_3$–C1), 1.00 (3H, t, $J$=7.7 Hz, $CH_3CH_2$); $^{13}$C NMR (176 MHz): $\delta$ 163.1 (C), 142.8 (C), 140.3 (C), 139.0 (CH), 137.1 (C), 135.6 (C), 132.6 (C), 89.8 (C–I), 85.5 (C–I), 18.7 ($CH_3$), 17.2 ($CH_2$), 15.3 ($CH_3$), 14.3 ($CH_3$), 13.5 ($CH_3$); IR (neat): 1567, 1370, 1221, 1072 cm$^{-1}$; MS (APCI$^-$) *m*/*z* (%): 514 ($M^-$, 50), 513 (100); HRMS-ESI$^+$: calcd for ($C_{14}H_{15}BF_2I_2N_2+H^+$) 514.9466 found 514.9458.

*4.3.11.2. Compound **5c**.* Mp 223.6–224.1 °C; $^1$H NMR (700 MHz): $\delta$ 6.96 (1H, s, H-7), 2.52 (3H, s, $CH_3$–C3), 2.37 (3H, s, $CH_3$–C8), 2.35 (2H, q, $J$=7.7 Hz, $CH_2$), 2.25 (3H, s, $CH_3$–C1), 1.00 (3H, t, $J$=7.7 Hz, $CH_3CH_2$); $^{13}$C NMR (176 MHz): $\delta$ 163.8 (C), 141.9 (C), 138.8 (C), 136.9 (C), 136.6 (C), 134.8 (C), 128.3 (CH), 100.2 (C–I), 84.3 (C–I), 17.2 ($CH_2$), 15.8 ($CH_3$), 14.4 ($CH_3$), 14.2 ($CH_3$), 13.4 ($CH_3$); IR (neat): 1582, 1318, 1200, 1236 cm$^{-1}$; MS (EI) *m*/*z* (%): 514 ($M^+$, 98), 499 (100); HRMS-ESI$^+$: calcd for ($C_{14}H_{15}BF_2I_2N_2+H^+$) 514.9466 found 514.9451.

*4.3.12. BODIPY **2** with ICl (1:6).* According to the method A, BODIPY **2** (75 mg, 0.29 mmol) in $CH_2Cl_2$/MeOH (10 mL/10 mL) and ICl (282 mg, 1.74 mmol) in MeOH (5 mL) for 180 min were reacted. Flash chromatography using hexane/EtAcO (98:2) afforded, by order of elution, **5c** (9 mg, 6%), 3-chloro-6-ethyl-1,2-diiodo-5,7,8-trimethyl-4-bora-3a,4a-diaza-*s*-indacene (**5d**) (55 mg, 35%) as an orange solid and 2-ethyl-5,6,7-triiodo-1,3,8-trimethyl-4-bora-3a,4a-diaza-*s*-indacene (**5e**) (37 mg, 20%) as a red solid.

*4.3.12.1. Compound **5d**.* Mp 275.1–275.6 °C; $^1$H NMR (700 MHz): $\delta$ 2.84 (3H, s, $CH_3$–C5), 2.47 (3H, s, $CH_3$–C8), 2.36 (2H, q, $J$=7.7 Hz, $CH_2$), 2.29 (3H, s, $CH_3$–C7), 1.00 (3H, t, $J$=7.7 Hz, $CH_3CH_2$); $^{13}$C NMR (176 MHz): $\delta$ 163.5 (C), 142.5 (C), 138.9 (C), 137.6 (C), 137.5 (C–Cl), 135.4 (C), 132.6 (C), 90.0 (C–I), 89.5 (C–I), 19.1 ($CH_3$), 17.3 ($CH_2$), 15.3 ($CH_3$), 14.3 ($CH_3$), 13.5 ($CH_3$); IR (neat): 1566, 1369, 1186, 1088 cm$^{-1}$; MS (APCI$^-$) *m*/*z* (%): 548 ($M^-$, 98), 456 (30), 421 (100); HRMS-ESI$^+$: calcd for ($C_{14}H_{14}BClF_2I_2N_2+H^+$) 548.9076 found 548.9066.

*4.3.12.2. Compound **5e**.* Mp 235.6–236.1 °C; $^1$H NMR (700 MHz): $\delta$ 2.78 (3H, s, $CH_3$–C3), 2.46 (3H, s, $CH_3$–C8), 2.34 (2H, q, $J$=7.7 Hz, $CH_2$), 2.27 (3H, s, $CH_3$), 0.98 (3H, t, $J$=7.7 Hz, $CH_3CH_2$); $^{13}$C NMR (176 MHz): $\delta$ 163.1 (C), 142.2 (C), 140.3 (C), 138.8 (C), 138.1 (C), 137.1 (C), 100.4 (C–I), 97.8 (C–I), 93.7 (C–I), 19.1 ($CH_3$), 17.2 ($CH_2$), 15.3 ($CH_3$), 14.3 ($CH_3$), 13.8 ($CH_3$); IR (neat): 1610, 1332, 1250, 1120, 1098 cm$^{-1}$; MS (APCI$^+$): 663 ([M+Na]$^+$, 100), 607 (30); HRMS-ESI$^+$: calcd for ($C_{14}H_{14}BF_2I_3N_2+H^+$) 640.8432 found 640.8420.

*4.3.13. BODIPY **2** with $I_2$/$HIO_3$ (1:4.5:4).* According to the method B, BODIPY **2** (85 mg, 0.32 mmol) in $CH_2Cl_2$/MeOH (10 mL/10 mL) and ICl (366 mg, 1.44 mmol) in MeOH (5 mL) for 120 min were reacted. Flash chromatography using hexane/EtAcO (98:2) afforded, by order of elution, **5c** (8 mg, 5%) and **5e** (98 mg, 48%).

*4.3.14. BODIPY **3** with ICl (1:0.8).* According to the method A, BODIPY **3** (70 mg, 0.28 mmol) in $CH_2Cl_2$/MeOH (10 mL/10 mL) and ICl (36 mg, 0.22 mmol) in MeOH (5 mL) for 30 min were reacted. Flash chromatography using hexane/EtAcO (98:2) afforded 2-ethyl-4,4-difluoro-6-iodo-1,3-dimethyl-4-bora-3a,4a-diaza-*s*-indacene (**6a**) (85 mg, 81%) as an orange solid and starting BODIPY **1** (10 mg, 14%).

*4.3.14.1. Compound **6a**.* Mp 174.4–174.8 °C; $^1$H NMR (700 MHz): $\delta$ 7.41 (1H, s, H-5), 6.96 (1H, s, H-8), 6.80 (1H, s, H-7), 2.49 (3H, s, $CH_3$–C3), 2.33 (2H, q, $J$=7.7 Hz, $CH_2$), 2.10 (3H, s, $CH_3$–C1), 1.00 (3H, t, $J$=7.7 Hz, $CH_3CH_2$); $^{13}$C NMR (176 MHz): $\delta$ 165.9 (C), 142.2 (C), 140.8 (CH), 136.9 (C), 136.0 (C), 133.2 (C), 129.8 (CH), 122.0 (CH), 67.1 (C–I), 17.3 ($CH_2$), 14.1 ($CH_3$), 13.6 ($CH_3$), 9.6 ($CH_3$); IR (neat): 1601, 1368, 1346, 1140, 1090 cm$^{-1}$; MS (APCI$^-$) *m*/*z* (%): 374 ($M^-$, 70), 359 (100), 339 (20); HRMS-ESI$^+$: calcd for ($C_{13}H_{14}BF_2IN_2+H^+$) 375.0343 found 375.0335.

*4.3.15. BODIPY **3** with ICl (1:2.5).* According to the method A, BODIPY **3** (70 mg, 0.28 mmol) in $CH_2Cl_2$/MeOH (10 mL/10 mL) and ICl (114 mg, 0.7 mmol) in MeOH (5 mL) for 90 min were reacted. Flash chromatography using hexane/EtAcO (98:2) afforded, by order of elution, 2-ethyl-4,4-difluoro-6,7-diiodo-1,3-dimethyl-4-bora-3a,4a-diaza-*s*-indacene (**6b**) (48 mg, 34%) as an orange solid,

2-ethyl-4,4-difluoro-5,6-diiodo-1,3-dimethyl-4-bora-3a,4a-diaza-*s*-indacene (**6c**) (49 mg, 35%) as a red solid and **6a** (14 mg, 13%).

*4.3.15.1. Compound* ***6b***. Mp 226.7–227.3 °C; $^1$H NMR (300 MHz): $\delta$ 7.45 (1H, s, H-5), 6.95 (1H, s, H-8), 2.48 (3H, s, $CH_3$–C3), 2.35 (2H, q, $J$=7.5 Hz, $CH_2$), 2.15 (3H, s, $CH_3$–C1), 1.02 (3H, t, $J$=7.5 Hz, $CH_3CH_2$); $^{13}$C NMR (75 MHz): $\delta$ 167.0 (C), 142.7 (C), 140.5 (CH), 138.0 (C), 136.6 (C), 134.9 (C), 122.6 (CH), 94.0 (C–I), 80.8 (C–I), 17.4 ($CH_2$), 14.0 ($CH_3$), 13.8 ($CH_3$), 9.7 ($CH_3$); IR (neat): 1613, 1241, 1183, 1120, 1073, 982 cm$^{-1}$; MS (APCI$^+$) $m/z$ (%): 500 ($M^+$, 50), 481 (100), 374 (98); HRMS-ESI$^+$: calcd for ($C_{13}H_{13}BF_2I_2N_2$+$H^+$) 500.9304 found 500.9311.

*4.3.15.2. Compound* ***6c***. Mp 222.4–222.8 °C; $^1$H NMR (700 MHz): $\delta$ 6.81 (1H, s, H-8), 6.78 (1H, s, H-7), 2.51 (3H, s, $CH_3$–C3), 2.34 (2H, q, $J$=7.7 Hz, $CH_2$), 2.09 (3H, s, $CH_3$–C1), 1.01 (3H, t, $J$=7.7 Hz, $CH_3CH_2$); $^{13}$C NMR (176 MHz): $\delta$ 166.8 (C), 142.0 (C), 137.0 (C), 136.5 (C), 130.6 (CH), 120.0 (CH), 102.0 (C–I), 84.8 (C–I), 17.4 ($CH_2$), 14.1 ($CH_3$), 13.7 ($CH_3$), 9.6 ($CH_3$); IR (neat): 1615, 1322, 1265, 1138, 1109 cm$^{-1}$; MS (APCI$^+$) $m/z$ (%): 500 ($M^+$, 15), 481 (80), 374 (100), 361 (45); HRMS-ESI$^+$: calcd for ($C_{13}H_{13}BF_2I_2N_2^+$) 499.9226 found 499.9233.

*4.3.16. BODIPY* ***3*** *with ICl (1:8).* According to the method A, BODIPY **3** (70 mg, 0.28 mmol) in $CH_2Cl_2$/MeOH (10 mL/10 mL) and ICl (364 mg, 2.24 mmol) in MeOH (5 mL) for 300 min were reacted. Flash chromatography using hexane/EtAcO (98:2) afforded, by order of elution, 3-chloro-6-ethyl-4,4-difluoro-1,2-diiodo-5,7-dimethyl-4-bora-3a,4a-diaza-*s*-indacene (**6d**) (45 mg, 30%) as an orange solid and 2-ethyl-4,4-difluoro-5,6,7-triiodo-1,3-dimethyl-4-bora-3a,4a-diaza-*s*-indacene (**6e**) (61 mg, 35%) as a red solid.

*4.3.16.1. Compound* ***6d***. Mp 256.1–256.6 °C; $^1$H NMR (700 MHz): $\delta$ 6.86 (1H, s, H-8), 2.48 (3H, s, $CH_3$–C5), 2.33 (2H, q, $J$=7.7 Hz, $CH_2$), 2.13 (3H, s, $CH_3$–C7), 1.01 (3H, t, $J$=7.7 Hz, $CH_3$–$CH_2$); $^{13}$C NMR (176 MHz): $\delta$ 167.2 (C), 142.4 (C), 138.8 (C–Cl), 137.7 (C), 136.9 (C), 134.6 (C), 121.6 (CH), 94.3 (C–I), 84.2 (C–I), 17.4 ($CH_2$), 14.0 ($CH_3$), 13.8 ($CH_3$), 9.7 ($CH_3$); IR (neat): 1617, 1373, 1238, 1139, 1020, 972 cm$^{-1}$; MS (APCI$^+$) $m/z$ (%): 534 ($M^+$, 15), 515 (100), 408 (40), 359 (75), 223 (65); HRMS-ESI$^+$: calcd for ($C_{13}H_{12}BClF_2I_2N_2$+$H^+$) 534.8920 found 534.8911.

*4.3.16.2. Compound* ***6e***. Mp 262.3–262.8 °C; $^1$H NMR (700 MHz): $\delta$ 6.82 (1H, s, H-8), 2.51 (3H, s, $CH_3$–C3), 2.36 (2H, q, $J$=7.7 Hz, $CH_2$), 2.15 (3H, s, $CH_3$–C1), 1.03 (3H, t, $J$=7.7 Hz, $CH_3CH_2$); $^{13}$C NMR (176 MHz): $\delta$ 167.7 (C), 142.4 (C), 138.7 (C), 138.0 (C), 137.1 (C), 121.1 (CH), 100.5 (C–I), 97.9 (C–I), 93.6 (C–I), 17.4 ($CH_2$), 14.0 ($CH_3$), 13.8 ($CH_3$), 9.7 ($CH_3$); IR (neat): 1616, 1235, 1133, 1089 cm$^{-1}$; MS (APCI$^+$) $m/z$ (%): 626 ($M^-$, 100); HRMS-ESI$^+$: calcd for ($C_{13}H_{12}BF_2I_3N_2$+$H^+$) 626.8276 found 626.8269.

*4.3.17. BODIPY* ***3*** *with $I_2$/$HIO_3$ (1:5:4.5).* According to the method B, BODIPY **3** (110 mg, 0.44 mmol) in $I_2$ (559 mg, 2.20 mmol) in EtOH (20 mL) and $HIO_3$ (348 mg, 1.98 mmol) for 300 min were reacted. Flash chromatography using hexane/EtAcO (98:2) afforded **6e** (149 mg, 54%).

### 4.4. Selective functionalization. General procedure

A solution of halogenated BODIPY and nucleophilic reagent in $CH_3CN$ (20 mL) was refluxed for 1–8 h under argon atmosphere. After that time, the solvent was removed under reduced pressure and the resulting mixture was dissolved in EtAcO and washed with $H_2O$. The extract was dried over $MgSO_4$, filtered and concentrated to dryness. The product was purified by flash chromatography on silica gel (eluent hexane/EtOAc).

### 4.5. Synthesis of 4,4-difluoro-2,3,6-triiodo-5-(4-methoxyphenylamino)-8-(4-tolyl)-4-bora-3a,4a-diaza-*s*-indecene (7)

BODIPY **4d** (40 mg, 0.05 mmol) and 4-methoxyaniline (13 mg, 0.1 mmol) in $CH_3CN$ (20 mL) were refluxed for 8 h. Flash chromatography using hexane/EtAcO (95:5) afforded BODIPY **7** (31 mg, 77%) as a purple solid. Mp 213.4–213.9 °C; $^1$H NMR (700 MHz, $CDCl_3$): $\delta$ 8.03 (1H, s, NH), 7.25 (2H, d, $J$=8.4 Hz, H-2′), 7.21 (2H, d, $J$=8.4 Hz, H-3′), 7.12 (2H, d, $J$=8.4 Hz, H-3″), 7.11 (1H, s, H-7), 6.86 (2H, d, $J$=8.4 Hz, H-2″), 6.52 (1H, s, H-1), 3.77 (3H, s, $OCH_3$), 2.36 (3H, s, $CH_3$); $^{13}$C NMR (176 MHz, $CDCl_3$): $\delta$ 159.6 (C), 157.0 (C), 144.9 (CH), 140.2 (C), 137.7 (C), 134.3 (C), 131.1 (C), 130.1 (CH), 129.3 (CH), 129.2 (CH), 128.6 (CH), 127.9 (C), 114.5 (CH), 96.0 (C–I), 83.9 (C–I), 66.8 (C–I), 55.6 ($OCH_3$), 21.4 ($CH_3$); IR (neat): 3363, 1583, 1249, 1091 cm$^{-1}$; MS (APCI$^-$) $m/z$ (%): 659 ($M^-$–122, 10), 558 (100), 508 (20), 340 (35); HRMS-ESI$^+$: calcd for ($C_{23}H_{17}BF_2I_3N_3O$+$H^+$) 781.8647 found 781.8638.

### 4.6. Synthesis of 3-(2-carboxyethylamino)-4,4-difluoro-2,5,6-triiodo-8-(4-tolyl)-4-bora-3a,4a-diaza-*s*-indecene (8)

BODIPY **4d** (60 mg, 0.08 mmol) and 3-aminopropanoic acid (40 mg, 0.46 mmol) in $CH_3CN$ (20 mL) were refluxed for 4 h. Flash chromatography using hexane/EtAcO (98:2) afforded BODIPY **8** (44 mg, 77%) as an orange solid. Mp >300 °C; $^1$H NMR (700 MHz, $CD_3OD$): $\delta$ 7.22 (4H, s, H-2′ and H-3′), 7.04 (1H, s, H-1), 6.20 (1H, s, H-7), 4.08 (2H, t, $J$=6.3 Hz, $NHCH_2$), 2.50 (2H, t, $J$=6.3 Hz, $CH_2COOH$), 2.33 (3H, s, $CH_3$); $^{13}$C NMR (176 MHz, $CD_3OD$): $\delta$ 177.6 (COOH), 159.3 (C), 141.8 (CH), 139.4 (C), 136.7 (C), 135.9 (C), 130.7 (C), 129.9 (CH), 128.8 (CH), 126.3 (C), 124.4 (CH), 91.2 (C–I), 81.6 (C–I), 72.8 (C–I), 41.6 ($NHCH_2$), 35.5 ($CH_2COOH$), 20.0 ($CH_3$); IR (neat): 3350, 1740, 1570, 1254, 1091 cm$^{-1}$; HRMS-ESI$^-$: calcd for ($C_{19}H_{15}BF_2I_3N_3O_2$–$H^+$) 745.8290 found 745.8300.

### 4.7. Synthesis of 3-diethoxycarbonylmethyl-4,4-difluoro-2,5,6-triiodo-8-(4-tolyl)-4-bora-3a,4a-diaza-*s*-indecene (9)

BODIPY **4d** (130 mg, 0.16 mmol), diethyl malonate (0.03 mL, 0.18 mmol) and NaH (6 mg, 0.25 mmol) in $CH_3CN$ (20 mL) were refluxed for 1 h. Flash chromatography using hexane/EtAcO (9:1) afforded BODIPY **9** (96 mg, 71%) as a pink solid. Mp 178.3–178.8 °C; $^1$H NMR (700 MHz, $CDCl_3$): $\delta$ 7.34 (2H, d, $J$=8.4 Hz, H-2′), 7.27 (2H, d, $J$=8.4 Hz, H-3′), 7.06 (1H, s, H-1), 6.91 (1H, s, H-7), 5.53 (1H, s, $CH(CO_2Et)_2$), 4.24 (4H, q, $J$=7.0 Hz, $OCH_2CH_3$), 2.40 (3H, s, $CH_3$), 1.25 (6H, t, $J$=7.0 Hz, $OCH_2CH_3$); $^{13}$C NMR (176 MHz, $CDCl_3$): $\delta$ 165.0 (COO), 152.2 (C), 143.0 (C), 142.2 (C), 139.8 (CH), 139.1 (C), 137.3 (CH), 135.4 (C), 130.5 (C), 129.6 (CH and C), 114.3 (C–I), 90.1 (C–I), 77.0 (C–I), 62.7 ($OCH_2CH_3$), 52.1 ($CH(CO_2Et)_2$), 21.6 ($CH_3$), 14.1 ($OCH_2CH_3$); IR (neat): 1761, 1740, 1570, 1251, 1089 cm$^{-1}$; HRMS-ESI$^+$: calcd for ($C_{23}H_{20}BF_2I_3N_2O_4$+$Na^+$) 840.8514 found 840.8499.

### 4.8. Synthesis of 3,5-bis(diethoxycarbonylmethyl)-4,4-difluoro-2,6-diiodo-8-(4-tolyl)-4-bora-3a,4a-diaza-*s*-indecene (10)

BODIPY **4d** (50 mg, 0.06 mmol), diethyl malonate (0.04 mL, 0.26 mmol) and NaH (3 mg, 0.13 mmol) in $CH_3CN$ (20 mL) were refluxed for 1 h. Flash chromatography using hexane/EtAcO (98:2) afforded BODIPY **10** (40 mg, 73%) as a purple solid. Mp 212.3–212.8 °C; $^1$H NMR (300 MHz, $CDCl_3$): $\delta$ 7.36 (2H, d, $J$=8.1 Hz, H-2′), 7.28 (2H, d, $J$=8.1 Hz, H-3′), 7.05 (2H, s, H-1 and H-7), 5.48 (2H, s, $CH(CO_2Et)_2$), 4.23 (8H, q, $J$=7.2 Hz, $OCH_2CH_3$), 2.41 (3H, s, $CH_3$), 1.24 (12H, t, $J$=7.2 Hz, $OCH_2CH_3$); $^{13}$C NMR (176 MHz, $CDCl_3$): $\delta$ 165.1 (COO), 151.2 (C), 145.3 (C), 142.2 (C), 139.5 (CH), 135.1 (C), 130.6 (CH), 129.9 (C), 129.5 (CH), 76.2 (C–I), 62.6 ($OCH_2CH_3$), 52.1

($CH(CO_2Et)_2$), 21.5 ($CH_3$), 14.0 ($OCH_2CH_3$); IR (neat): 1760, 1743, 1580, 1255, 1090 $cm^{-1}$; HRMS-ESI$^-$: calcd for ($C_{30}H_{31}BF_2I_2N_3O-H^+$) 849.0163 found 849.0185.

### 4.9. Synthesis of 3-diethoxycarbonylmethyl-4,4-difluoro-2,6-diiodo-5-(4-methoxyphenylamino)-8-(4-tolyl)-4-bora-3a,4a-diaza-*s*-indecene (11)

BODIPY **9** (30 mg, 0.04 mmol) and 4-methoxyaniline (7 mg, 0.05 mmol) in $CH_3CN$ (20 mL) were refluxed for 2 h. Flash chromatography using hexane/EtAcO (8:2) afforded BODIPY **11** (20 mg, 70%) as a red solid. Mp 162.1–162.6 °C; $^1$H NMR (700 MHz, $CDCl_3$): $\delta$ 7.89 (1H, s, NH), 7.28 (2H, d, $J$=8.4 Hz, H-2′), 7.21 (2H, d, $J$=8.4 Hz, H-3′), 7.12 (1H, s, H-7), 7.11 (2H, d, $J$=8.4 Hz, H-3″), 6.86 (2H, d, $J$=8.4 Hz, H-2″), 6.62 (1H, s, H-1), 5.37 (1H, s, $CH(CO_2Et)_2$), 4.24 (8H, q, $J$=7.0 Hz, $OCH_2CH_3$), 3.77 (3H, s, $OCH_3$), 2.37 (3H, s, $CH_3$), 1.25 (12H, t, $J$=7.0 Hz, $OCH_2CH_3$); $^{13}$C NMR (176 MHz, $CDCl_3$): $\delta$ 166.4 (COO), 159.5 (C), 156.7 (C), 144.8 (CH), 140.1 (C), 139.2 (C), 133.9 (C), 133.4 (C), 133.0 (C), 130.5 (C), 130.2 (CH and CH), 129.2 (CH), 129.1 (CH), 128.0 (C), 114.5 (CH), 70.3 (C–I), 65.9 (C–I), 62.2 ($OCH_2CH_3$), 55.6 ($OCH_3$), 52.0 ($CH(CO_2Et)_2$), 21.4 ($CH_3$), 14.1 ($OCH_2CH_3$); IR (neat): 3363, 1765, 1740,1583, 1249, 1091 $cm^{-1}$; HRMS-ESI$^+$: calcd for ($C_{30}H_{28}BF_2I_2N_3O+Na^+$) 836.0077 found 836.0081.

### 4.10. Synthesis of 4,4-difluoro-2,3,6-(4-formylphenyl)-5-(4-methoxyphenylamino)-8-(4-tolyl)-4-bora-3a,4a-diaza-*s*-indecene (12)

BODIPY **7** (30 mg, 0.04 mmol) was dissolved in DME (20 mL). 4-Formylphenyl boronic acid (36 mg, 0.24 mmol) and $Na_2CO_3$ (13 mg, 0.12 mmol) were added in the presence of a catalytic amount of tetrakis(triphenylphosphine)palladium (3 mg, 0.0006 mmol). The reaction mixture was stirred under ultrasound irradiation for 5 h at 75 °C with a power of 720 W. After addition of $H_2O$ (50 mL), the organic layer was extracted with EtOAc, dried over $MgSO_4$, filtered and concentrated to dryness. Flash chromatography using hexane/EtOAc (95:5) afforded BODIPY **12** (57 mg, 46% yield) as a purple solid. Mp 190.6–191.1 °C; $^1$H NMR (700 MHz, $CDCl_3$): $\delta$ 10.0 (1H, s, CHO), 9.83 (1H, s, CHO), 9.78 (1H, s, CHO), 7.99 (1H, br s, NH), 7.86 (2H, d, $J$=8.3 Hz, 2CH), 7.69 (2H, d, $J$=8.1 Hz, 2CH), 7.60 (2H, d, $J$=8.3 Hz, 2CH), 7.44 (2H, d, $J$=7.9 Hz, 2CH), 7.43 (2H, d, $J$=8.3 Hz, 2CH), 7.28 (2H, d, $J$=7.9 Hz, 2CH), 7.14 (2H, d, $J$=8.3 Hz, 2CH), 7.03 (2H, d, $J$=8.1 Hz, 2CH), 6.99 (1H, s, CH), 6.76 (1H, s, CH), 6.69 (2H, d, $J$=8.8 Hz, 2CH), 6.39 (2H, d, $J$=8.8 Hz, 2CH), 3.53 (3H, s, $OCH_3$), 2.41 (3H, s, $CH_3$); $^{13}$C NMR (176 MHz, $CDCl_3$): $\delta$ 190.9 (CHO), 190.8 (CHO), 190.7 (CHO), 157.0 (C), 155.3 (C), 142.9–124.4 (C and CH), 120.5 (CH), 113.1 (CH), 54.4 ($OCH_3$), 20.4 ($CH_3$); IR (neat): 3370, 2854, 2732, 1698, 1597, 1449, 1205, 1099 $cm^{-1}$; MS (APCI$^-$) $m/z$ (%): 715 ($M^-$, 100), 666 (60), 576 (10); HRMS-ESI$^+$: calcd for ($C_{44}H_{32}BF_2N_3O_4+H^+$) 716.2534 found 716.2530.

### 4.11. Photophysical properties

*4.11.1. Photophysics.* Diluted BODIPY solutions were prepared by adding the corresponding solvent after evaporation of an adequate amount of a concentrated solution in acetone. Absorption and fluorescence spectra were recorded on a Varian model Cary 4E spectrophotometer and an SPEX Fluorolog 3-22 spectrofluorimeter, respectively. The fluorescence spectra were corrected from the wavelength dependence of the detector sensibility. Fluorescence quantum yield was determined using an adequate commercial BODIPY (PM567 and PM597)[18b] as reference. Radiative decay curves were registered with the time correlated single-photon counting technique (Edinburgh Instruments, model FL920, with picosecond resolution). Excitation was performed with a 470 nm diode laser and a 575 nm LED, both purchased by Picoquant. The emission was monitorized at the maximum emission wavelength. The fluorescence lifetime was obtained from the slope after deconvolution of the instrument response signal. The goodness of the deconvolution was controlled by the chi-squared statistical parameter and from the analysis of the residuals. Radiative and non-radiative rate constants were calculated as follows; $k_{fl}=\phi/\tau$ and $k_{nr}=(1-\phi)/\tau$.

*4.11.2. Computational details.* Ground state geometries and charge distributions were calculated at the Density Functional Theory using the hybrid method B3LYP, together with the lanl2dz basis set, especially parameterized to describe heavy atoms (i.e., iodine). Absorption transition was simulated by the Time Dependent method from the ground state.

### 4.12. Singlet oxygen generation

Individual argon-saturated solutions of **4b** and **4d** $Abs_{532}$ ca. 0.1 were irradiated with a flash photolysis apparatus. A nanosecond Nd/YAG laser system (Spectron) at 532 nm was used for excitation, employing a 150-W Xenon lamp as a source for the analyzing light. The detection system comprised a PTI monochromator and a red-extended photomultiplier (Hamamatsu R666). The signal, acquired and averaged by a digital oscilloscope (Hewlett–Packard 54504A), was transferred via an HPIB parallel interface to a PC where it was analyzed and stored.

The efficiency of $O_2(^1\Delta_g)$ production by **4b**, **4c** and **4d** in $CH_3CN$ was determined by the comparative method already described.[21,22] The initial intensities of the emission decay curves at 1270 nm ($I_0$) were determined for air-equilibrated solutions ($Abs_{532}$ ca. 0.2) as a function of laser fluence ($L_E$). The output at 532 nm of the already mentioned Spectron Nd/Yag laser was employed as the excitation source. $L_E$ was varied using neutral density filters. $\Phi_\Delta$ values for **4b** and **4d** were obtained by comparison of the slopes of the linear plots $I_0$ versus $L_E$ with that of a reference compound, all with absorbance matched solutions at 532 nm. The reference was Rose Bengal (RB) with a $\Phi_{\Delta RB}$=0.71 for $O_2(^1\Delta_g)$ generation determined in this work. For the determination of $\Phi_{\Delta RB}$ the already described technique was employed with emission at 355 nm. Perinaphthenone (PN), with $\Phi_{\Delta PN}$=1 in MeCN, was utilized as reference (Fig. 4S, ESI).[23]

The detection of $O_2(^1\Delta_g)$ phosphorescence was determined using a previously described system.[24] Briefly, a Nd/YAG laser (Spectron) was used for the excitation (532 nm) of the sensitizer RB ($Abs_{532}$=0.4), and the emitted radiation $O_2(^1\Delta_g)$ phosphorescence at 1270 nm was detected at right angles using an amplified Judson J16/8Sp germanium detector, after passing through two Wratten filters. The output of the detector was coupled to a digital oscilloscope and to a personal computer for the signal processing. Usually, six shots were needed for averaging, so as to achieve a good signal to noise ratio, from which the $I_0$ value was obtained.

### Acknowledgements

This work was supported by Projects MAT2007-65778-C02-02, MAT2010-20646-C04-02 and 04 of the Spanish MICINN, GR35/10-A of the UCM/BSCH and S-PE09UN61 of Gobierno Vasco.

### Supplementary data

These data include copies of $^1$H and $^{13}$C NMR spectra for all compounds, tables and figures of photophysical properties and singlet oxygen generation. Supplementary data associated

with this article can be found in the online version, at doi:10.1016/j.tet.2011.11.070. These data include MOL files and InChiKeys of the most important compounds described in this article.

## References and notes


1. Loudet, A.; Burgess, K. *Chem. Rev.* **2007**, *107*, 4891–4932.
2. (a) Ziessel, R.; Ulrich, G.; Harriman, A. *New J. Chem.* **2007**, *31*, 496–501; (b) Ulrich, G.; Ziessel, R.; Harriman, A. *Angew. Chem., Int. Ed.* **2008**, *47*, 1184–1201; (c) Benniston, A. C.; Copley, G. *Phys. Chem. Chem. Phys.* **2009**, *11*, 4124–4131; (d) Benstead, M.; Mehl, G. H.; Boyle, R. W. *Tetrahedron* **2011**, *67*, 3573–3601; (e) Boens, N.; Leen, V.; Dehaen, W. *Chem. Soc. Rev.* **2012**, , doi:10.1039/C1CS15132K Advance Article.
3. (a) Ziessel, R.; Ulrich, G.; Harriman, A.; Alamiry, M. A. H.; Stewart, B.; Retailleau, P. *Chem.—Eur. J.* **2009**, *15*, 1359–1369; (b) Kumaresan, D.; Thummel, R. P.; Bura, T.; Ulrich, G.; Ziessel, R. *Chem.—Eur. J.* **2009**, *15*, 6335–6339; (c) Barin, G.; Yilmaz, M. D.; Akkaya, E. U. *Tetrahedron Lett.* **2009**, *50*, 1738–1740; (d) Buyukcakir, O.; Bozdemir, O. A.; Kolemen, S.; Erbas, S.; Akkaya, E. U. *Org. Lett.* **2009**, *11*, 4644–4647; (e) Lee, J.-S.; Kang, N.-Y.; Kim, Y. K.; Samanta, A.; Feng, S.; Kim, H. K.; Vendrell, M.; Park, J. H.; Chang, Y.-T. *J. Am. Chem. Soc.* **2009**, *131*, 10077–10082; (f) Kolemen, S.; Cakmak, Y.; Erten-Ela, S.; Altay, Y.; Brendel, J.; Thelakkat, M.; Akkaya, E. U. *Org. Lett.* **2010**, *12*, 3812–3815; (g) Bozdemir, O. A.; Guliyev, R.; Buyukcakir, O.; Selcuk, S.; Kolemen, S.; Gulseren, G.; Nalbantoglu, T.; Boyaci, H.; Akkaya, E. U. *J. Am. Chem. Soc.* **2010**, *132*, 8029–8036; (h) Bura, T.; Retailleau, P.; Ziessel, R. *Angew. Chem., Int. Ed.* **2010**, *49*, 6659–6663; (i) Kolemen, S.; Bozdemir, O. A.; Cakmak, Y.; Barin, G.; Erten-Ela, S.; Marszalek, M.; Yum, J.-H.; Zakeeruddin, S. M.; Nazeeruddin, M. K.; Grätzel, M.; Akkaya, E. U. *Chem. Sci.* **2011**, *2*, 949–954; (j) Bura, T.; Retailleau, P.; Ulrich, G.; Ziessel, R. *J. Org. Chem.* **2011**, *76*, 1109–1117.
4. (a) Rohand, T.; Baruah, M.; Qin, W.; Boens, N.; Dehaen, W. *Chem. Commun.* **2006**, 266–268; (b) Rohand, T.; Lycoops, J.; Smout, S.; Braeken, E.; Sliwa, M.; Van der Auweraer, M.; Dehaen, W.; De Borggraeve, W. M.; Boens, N. *Photochem. Photobiol. Sci.* **2007**, *6*, 1061–1066; (c) Li, L.; Nguyen, B.; Burgess, K. *Bioorg. Med. Chem. Lett.* **2008**, *18*, 3112–3116; (d) Fron, E.; Coutiño-Gonzalez, E.; Pandey, L.; Sliwa, M.; Van der Auweraer, M.; De Schryver, F. C.; Thomas, J.; Dong, Z.; Leen, V.; Smet, M.; Dehaen, W.; Vosch, T. *New J. Chem.* **2009**, *33*, 1490–1496; (e) Qin, W.; Leen, V.; Dehaen, W.; Cui, J.; Xu, C.; Tang, X.; Liu, W.; Rohand, T.; Beljonne, D.; Van Averbeke, B.; Clifford, J. N.; Driesen, K.; Binnemans, K.; Van der Auweraer, M.; Boens, N. *J. Phys. Chem. C* **2009**, *113*, 11731–11740; (f) Jiao, L.; Yu, C.; Liu, M.; Wu, Y.; Cong, K.; Meng, T.; Wang, Y.; Hao, E. *J. Org. Chem.* **2010**, *75*, 6035–6038; (g) Leen, V.; Leemans, T.; Boens, N.; Dehaen, W. *Eur. J. Org. Chem.* **2011**, *23*, 4386–4396.
5. (a) Peña-Cabrera, E.; Aguilar-Aguilar, A.; González-Domínguez, M.; Lager, E.; Zamudio-Vázquez, R.; Godoy-Vargas, J.; Villanueva-García, F. *Org. Lett.* **2007**, *9*, 3985–3988; (b) Han, J.; Gonzalez, O.; Aguilar-Aguilar, A.; Peña-Cabrera, E.; Burgess, K. *Org. Biomol. Chem.* **2009**, *7*, 34–36; (c) Lager, E.; Liu, J.; Aguilar-Aguilar, A.; Tang, B. Z.; Peña-Cabrera, E. *J. Org. Chem.* **2009**, *74*, 2053–2058.
6. (a) Wan, C.-W.; Burghart, A.; Chen, J.; Bergström, F.; Johansson, LB.-A.; Wolford, M. F.; Kim, T. G.; Topp, M. R.; Hochstrasser, R. M.; Burgess, K. *Chem. Eur. J.* **2003**, *9*, 4430–4441; (b) Rohand, T.; Qin, W.; Boens, N.; Dehaen, W. *Eur. J. Org. Chem.* **2006**, 4658–4663; (c) Bonardi, L.; Ulrich, G.; Ziessel, R. *Org. Lett.* **2008**, *10*, 2183–2186; (d) Zhang, D.; Wen, Y.; Xiao, Y.; Yu, G.; Liu, Y.; Qian, X. *Chem. Commun.* **2008**, 4777–4779; (e) Bozdemir, Ö. A.; Büyükcakir, O.; Akkaya, E. U. *Chem.—Eur. J.* **2009**, *15*, 3830–3838; (f) Rihn, S.; Retailleau, P.; Bugsaliewicz, N.; De Nicola, A.; Ziessel, R. *Tetrahedron Lett.* **2009**, *50*, 7008–7013; (g) Cakmak, Y.; Akkaya, E. U. *Org. Lett.* **2009**, *11*, 85–88; (h) Guliyev, R.; Coskun, A.; Akkaya, E. U. *J. Am. Chem. Soc.* **2009**, *131*, 9007–9013; (i) Bozdemir, O. A.; Cakmak, Y.; Sozmen, F.; Ozdemir, T.; Siemiarczuk, A.; Akkaya, E. U. *Chem.—Eur. J.* **2010**, *16* 6346–6351; (j) Ortiz, M. J.; Garcia-Moreno, I.; Agarrabeitia, A. R.; Duran-Sampedro, G.; Costela, A.; Sastre, R.; López Arbeloa, F.; Bañuelos Prieto, J.; López Arbeloa, I. *Phys. Chem. Chem. Phys.* **2010**, *12*, 7804–7811; (k) Thivierge, C.; Han, J.; Jenkins, R. M.; Burgess, K. *J. Org. Chem.* **2011**, *76*, 5219–5228; (l) Khan, T. K.; Ravikanth, M. *Tetrahedron* **2011**, *67*, 5816–5824; (m) Niu, S.; Ulrich, G.; Retailleau, P.; Ziessel, R. *Tetrahedron Lett.* **2011**, *52*, 4848–4853.
7. (a) Dolmans, D. E. J. G. J.; Fukumura, D.; Jain, R. K. *Nat. Rev. Cancer* **2003**, *3*, 380–387; (b) Brown, S. B.; Brown, E. A.; Walker, I. *Lancet Oncol.* **2004**, *5*, 497–508; (c) Henderson, B. W.; Gollnick, S. O. In *CRC Hanboock of Organic Photochemistry and Photobiology*; CRC: New York, NY, 2004; Chapter 145, pp 1–25; (d) Jori, G. In *CRC Hanboock of Organic Photochemistry and Photobiology*; CRC: New York, NY, 2004; Chapter 146, pp 1–10; (e) Dougherty, T. J.; Levy, J. G. In *CRC Hanboock of Organic Photochemistry and Photobiology*; CRC: New York, NY, 2004; Chapter 147, pp 1–17; (f) Berg, K. In *Photodynamic Therapy at the Cellular Level*; Research Signpost: Kerala, India, 2007; Chapter 1, pp 1–16; (g) Krasnovsky, A. A., Jr. In *Photodynamic Therapy at the Cellular Level*; Research Signpost: Kerala, India, 2007; Chapter 2, pp 17–63; (h) Armesto, D.; Sastre, R. In *Aplicaciones recientes de la luz en medicina, medio ambiente y nuevos materiales*; Editorial Complutense: España, 2010; Chapter 2, pp 35–59.
8. (a) Gorman, A.; Killoran, J.; O'Shea, C.; Kenna, T.; Gallagher, W. M.; O'Shea, D. F. *J. Am. Chem. Soc.* **2004**, *126*, 10619–10631; (b) McDonnell, S. O.; Hall, M. J.; Allen, L. T.; Byrne, A.; Gallagher, W. M.; O'Shea, D. F. *J. Am. Chem. Soc.* **2005**, *127*, 16360–16361; (c) Yogo, T.; Urano, Y.; Ishitsuka, Y.; Maniwa, F.; Nagano, T. *J. Am. Chem. Soc.* **2005**, *127*, 12162–12163; (d) Atilgan, S.; Ekmekci, Z.; Dogan, A. L.; Guc, D.; Akkaya, E. U. *Chem. Commun.* **2006**, 4398–4400; (e) Erbas, S.; Gorgulu, A.; Kocakusakogullari, M.; Akkaya, E. U. *Chem. Commun.* **2009**, 4956–4958; (f) Ozlem, S.; Akkaya, E. U. *J. Am. Chem. Soc.* **2009**, *131*, 48–49; (g) Lim, S. H.; Thivierge, C.; Nowak-Sliwinska, P.; Han, J.; van den Bergh, H.; Wagnières, G.; Burgess, K.; Lee, H. B. *J. Med. Chem.* **2010**, *53*, 2865–2874; (h) Adarsh, N.; Avirah, R. R.; Ramaiah, D. *Org. Lett.* **2010**, *12*, 5720–5723; (i) He, H.; Lo, P.-C.; Yeung, S.-L.; Fong, W.-P.; Ng, D. K. P. *Chem. Commun.* **2011**, 4748–4750; (j) He, H.; Lo, P.-C.; Yeung, S.-L.; Fong, W.-P.; Ng, D. K. P. *J. Med. Chem.* **2011**, *54*, 3097–3102; (k) Awuah, S. G.; Polreis, J.; Biradar, V.; You, Y. *Org. Lett.* **2011**, *13*, 3884–3887.
9. (a) Leen, V.; Braeken, E.; Luckermans, K.; Jackers, C.; Van der Auweraer, M.; Boens, N.; Dehaen, W. *Chem. Commun.* **2009**, 4515–4517; (b) Morrison, M. D.; Hanthorn, J. J.; Pratt, D. A. *Org. Lett.* **2009**, *11*, 1051–1054.
10. (a) Jiao, L.; Li, J.; Zhang, S.; Wei, C.; Hao, E.; Vicente, M. G. H. *New J. Chem.* **2009**, *33*, 1888–1893; (b) Rao, M. R.; Mobin, S. M.; Ravikanth, M. *Tetrahedron* **2010**, *66*, 1728–1734.
11. (a) Algi, F.; Cihaner, A. *Org. Electron.* **2009**, *10*, 453–458; (b) He, H.; Ng, D. K. P. *Org. Biomol. Chem.* **2011**, *9*, 2610–2613; (c) Sabatini, R. P.; McCormick, T. M.; Lazarides, T.; Wilson, K. C.; Eisenberg, R.; McCamant, D. W. *J. Phys. Chem. Lett.* **2011**, *2*, 223–227.
12. Hayashi, Y.; Yamaguchi, S.; Cha, W. Y.; Kim, D.; Shinokubo, H. *Org. Lett.* **2011**, *13*, 2992–2995.
13. Fabian, J.; Hartmann, H. *Light Absorption of Organic Colorants*; Springer: Berlin, 1980.
14. Cui, A.; Peng, X.; Fan, J.; Chen, X.; Wu, Y.; Guo, B. *J. Photochem. Photobiol. A-Chem.* **2007**, *186*, 85–92.
15. Bañuelos-Prieto, J.; Agarrabeitia, A. R.; García-Moreno, I.; López-Arbeloa, I.; Costela, A.; Infantes, L.; Pérez-Ojeda, M. E.; Palacios-Cuesta, M.; Ortiz, M. J. *Chem.—Eur. J.* **2010**, *16*, 14094–14105.
16. Vos de Wael, E.; Pardoen, J. A.; van Koeveringe, J. A.; Lugtenburg, J. *Recl. Trav. Chim. Pays-Bas* **1977**, *96*, 306–309.
17. (a) Hubig, S. M.; Jung, W.; Kochi, J. K. *J. Org. Chem.* **1994**, *59*, 6233–6244; (b) Eberson, L.; Hartshorn, M. P.; Radner, F.; Persson, O. *J. Chem. Soc., Perkin Trans. 2* **1998**, 59–70; (c) Chaikovskii, V. K.; Filimonov, V. D. *Russ. J. Org. Chem.* **2001**, *37*, 1130–1133.
18. (a) Li, F.; Yang, S. I.; Ciringh, Y.; Seth, J.; Martin, C. H., III; Singh, D. L.; Kim, D.; Birge, R. R.; Bocian, D. F.; Holten, D.; Lindsey, J. S. *J. Am. Chem. Soc.* **1998**, *120*, 10001–10017; (b) López Arbeloa, F.; Bañuelos, J.; Martínez, V.; Arbeloa, T.; López Arbeloa, I. *Int. Rev. Phys. Chem.* **2005**, *24*, 339–374; (c) Kee, H. L.; Kirmaier, C.; Yu, L.; Thamyongkit, P.; Youngblood, W. J.; Calder, M. E.; Ramos, L.; Noll, B. C.; Bocian, D. F.; Scheidt, W. R.; Birge, R. R.; Lindsey, J. S.; Holten, D. *J. Phys. Chem. B* **2005**, *109*, 20433–20443; (d) Alamiry, M. A. H.; Benniston, A. C.; Copley, G.; Elliott, K. J.; Harriman, A.; Stewart, B.; Zhi, Y.-G. *Chem. Mater.* **2008**, *20*, 4024–4032.
19. (a) Chen, J.; Burghart, A.; Derecskei-Kovacs, A.; Burgess, K. *J. Org. Chem.* **2000**, *65*, 2900–2906; (b) Zheng, Q.; Xu, G.; Prasad, P. N. *Chem.—Eur. J.* **2008**, *14*, 5812–5819; (c) Vu, T. T.; Badré, S.; Dumas-Verdes, C.; Vachon, J.-J.; Julien, C.; Audebert, P.; Senotrusova, E. Y.; Schmidt, E. Y.; Trofimov, B. A.; Pansu, R. B.; Clavier, G.; Méallet-Renault, R. *J. Phys. Chem. C* **2009**, *113*, 11844–11855.
20. Montejano, H. A.; Amat-Guerri, F.; Costela, A.; García-Moreno, I.; Liras, M.; Sastre, R. *J. Photochem. Photobiol. A-Chem.* **2006**, *181*, 142–146.
21. Gutiérrez, I.; Bertolotti, S. G.; Biasutti, M. A.; Soltermann, A. T.; García, N. A. *Can. J. Chem.* **1997**, *75*, 423–428.
22. Wilkinson, F.; Helman, W. P.; Ross, A. B. *J. Phys. Chem. Ref. Data* **1993**, *22*, 113–262.
23. Netto-Ferreira, J. C.; Lhiaubet-Vallet, V.; da Silva, A. R.; da Silva, A. M.; Ferreira, A. B. B.; Miranda, M. A. *J. Braz. Chem. Soc.* **2010**, *21*, 966–972.
24. Massad, W. A.; Bertolotti, S. G.; Romero, M.; García, N. A. *J. Photochem. Photobiol. B-Biol.* **2005**, *80*, 130–138.

**Supporting Information**

# Synthesis and functionalization of new polyhalogenated BODIPY dyes. Study of photophysical properties and singlet oxygen generation

**Maria J. Ortiz,*[a] Antonia R. Agarrabeitia,[a] Gonzalo Duran-Sampedro,[a] Jorge Bañuelos Prieto,[b] Teresa Arbeloa Lopez,[b] Walter A. Massad,[c] Hernán A. Montejano,[c] Norman A. García[c] and Iñigo Lopez Arbeloa[b]**

[a]*Departamento de Quimica Organica I, Facultad de Ciencias Quimicas, Universidad Complutense, 28040 Madrid, Spain.*
[b]*Departamento de Quimica Fisica, UPV-EHU, Apartado 644, 48080 Bilbao, Spain.*
[c]*Departamento de Quimica, Universidad Nacional de Río Cuarto, 3.5800 Río Cuarto, Argentina.*

*mjortiz@quim.ucm.es*

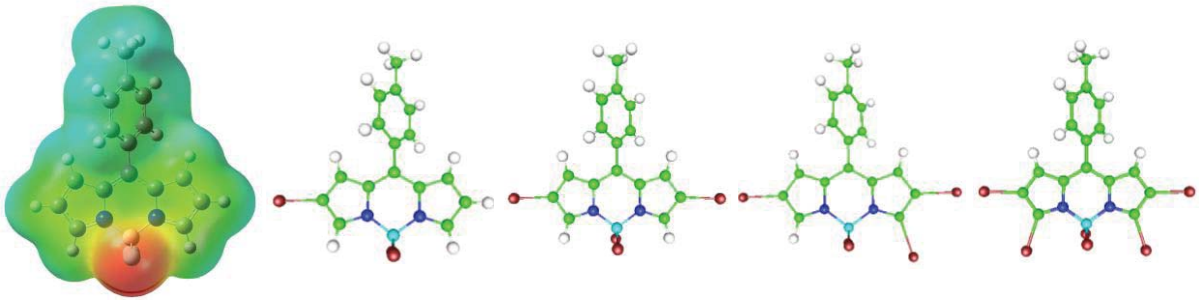

**BODIPY 1** **4a** **4b** **4c** **4d**

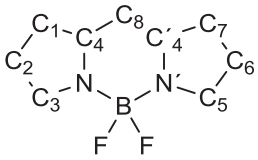


| Atom | 1 | 4a | 4b | 4c | 4d |
|---|---|---|---|---|---|
| **C1** | -0.337 | -0.258 | -0.255 | -0.255 | -0.250 |
| **C2** | -0.291 | -0.347 | -0.350 | -0.349 | -0.249 |
| **C3** | -0.143 | -0.093 | -0.089 | -0.087 | -0.265 |
| **C4** | 0.251 | 0.247 | 0.249 | 0.254 | 0.224 |
| **C´4** | 0.251 | 0.253 | 0.249 | 0.219 | 0.224 |
| **C5** | -0.143 | -0.139 | -0.089 | -0.265 | -0.265 |
| **C6** | -0.291 | -0.289 | -0.350 | -0.251 | -0.249 |
| **C7** | -0.337 | -0.334 | -0.255 | -0.259 | -0.250 |
| **C8** | 0.174 | 0.173 | 0.172 | 0.174 | 0.175 |
| **N** | -0.217 | -0.214 | -0.215 | -0.218 | -0.194 |
| **N´** | -0.217 | -0.217 | -0.215 | -0.191 | -0.194 |

**Figure 1S.** Mulliken electronic charge distribution in the ground state of the iodinated derivatives of BODIPY **1**, together with the electrostatic potential map of the reference compound (blue-positive and red-negative).

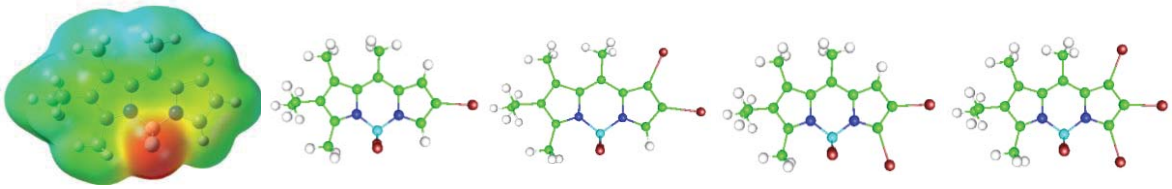

**BODIPY 2** **5a** **5b** **5c** **5e**

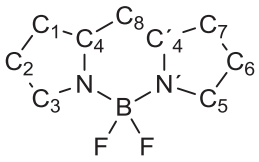


| Atom | 2 | 5a | 5b | 5c | 5e |
|---|---|---|---|---|---|
| **C1** | 0.114 | 0.115 | 0.113 | 0.113 | 0.125 |
| **C2** | 0.208 | 0.208 | 0.208 | 0.208 | 0.208 |
| **C3** | 0.178 | 0.180 | 0.183 | 0.182 | 0.187 |
| **C4** | 0.235 | 0.240 | 0.219 | 0.245 | 0.227 |
| **C´4** | 0.319 | 0.312 | 0.465 | 0.280 | 0.418 |
| **C5** | -0.146 | -0.093 | -0.091 | -0.269 | -0.264 |
| **C6** | -0.292 | -0.343 | -0.264 | -0.244 | -0.176 |
| **C7** | -0.374 | -0.300 | -0.454 | -0.296 | -0.441 |
| **C8** | 0.161 | 0.161 | 0.164 | 0.163 | 0.162 |
| **N** | -0.262 | -0.263 | -0.255 | -0.265 | -0.257 |
| **N´** | -0.213 | -0.211 | -0.219 | -0.185 | -0.197 |

**Figure 2S.** Mulliken electronic charge distribution in the ground state of the iodinated derivatives of BODIPY **2**, together with the electrostatic potential map of the reference compound (blue-positive and red-negative).

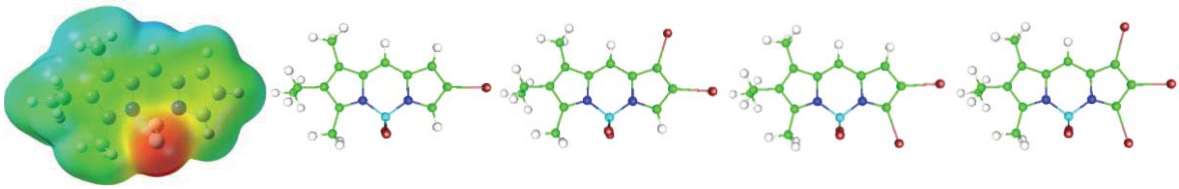

**BODIPY 3** **6a** **6b** **6c** **6e**

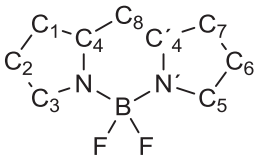


| Atom | 3 | 6a | 6b | 6c | 6e |
|---|---|---|---|---|---|
| **C1** | 0.105 | 0.105 | 0.099 | 0.102 | 0.097 |
| **C2** | 0.212 | 0.212 | 0.208 | 0.209 | 0.213 |
| **C3** | 0.182 | 0.184 | 0.187 | 0.187 | 0.190 |
| **C4** | 0.374 | 0.380 | 0.394 | 0.389 | 0.398 |
| **C´4** | 0.490 | 0.479 | 0.604 | 0.451 | 0.562 |
| **C5** | -0.145 | -0.093 | -0.105 | -0.266 | -0.272 |
| **C6** | -0.278 | -0.319 | -0.281 | -0.218 | -0.192 |
| **C7** | -0.388 | -0.324 | -0.417 | -0.325 | -0.403 |
| **C8** | -0.481 | -0.478 | -0.459 | -0.482 | -0.461 |
| **N** | -0.272 | -0.272 | -0.273 | -0.276 | -0.277 |
| **N´** | -0.234 | -0.229 | -0.231 | -0.202 | -0.204 |

**Figure 3S.** Mulliken electronic charge distribution in the ground state of the iodinated derivatives of BODIPY **3**, together with the electrostatic potential map of the reference compound (blue-positive and red-negative).

**Table 1S.** Photophysical properties of the 8-tolylBODIPYs and its iodinated derivatives (serie 1) in diluted apolar (cyclohexane), polar (ethyl acetate and acetone) and protic (ethanol, methanol and trifluoroethanol) solutions. Absorption ($\lambda_{ab}$) and fluorescence ($\lambda_{fl}$) wavelength, molar absorption ($\varepsilon_{max}$) fluorescence quantum yield ($\phi$) and lifetime ($\tau$).The lifetimes herein listed are those of the main component of the decay curve, however the decay curves are better fitted considering an additional long lifetime, but with a nearly negligible contribution (< 1 %).

| | c-hexane | Ethyl acetate | Acetone | Ethanol | Methanol | F3-EtOH |
|---|---|---|---|---|---|---|
| **BODIPY 1** | | | | | | |
| $\lambda_{ab}$ (nm) | 500.5 | 497.0 | 496.5 | 497.5 | 496.0 | 493.0 |
| $\varepsilon_{max}$($10^4 M^{-1}cm^{-1}$) | 6.9 | 6.2 | 6.1 | 6.2 | 6.1 | 5.6 |
| $\lambda_{fl}$ (nm) | 516.0 | 514.5 | 514.5 | 514.5 | 513.5 | 509.5 |
| $\phi$ | 0.036 | 0.024 | 0.018 | 0.025 | 0.018 | 0.031 |
| $\tau$ (ps) | 340 | 237 | 196 | 253 | 197 | 323 |
| $k_{fl}$ ($10^8$ $s^{-1}$) | 1.05 | 1.01 | 0.92 | 0.99 | 0.91 | 0.96 |
| $k_{nr}$ ($10^8$ $s^{-1}$) | 28.3 | 41.2 | 50.1 | 38.5 | 49.8 | 30.0 |
| **BODIPY 4a** | | | | | | |
| $\lambda_{ab}$ (nm) | 523.5 | 517.0 | 516.5 | 518.0 | 516.5 | 513.0 |
| $\varepsilon_{max}$($10^4 M^{-1}cm^{-1}$) | 2.2 | 1.9 | 1.9 | 1.8 | 1.7 | 1.7 |
| $\lambda_{fl}$ (nm) | 540.0 | 543.0 | 546.0 | 547.0 | 546.5 | 538.5 |
| $\phi$ | 0.034 | 0.011 | 0.008 | 0.010 | 0.008 | 0.009 |
| $\tau$ (ps) | 184 | 82 | 60 | 70 | 63 | 69 |
| $k_{fl}$ ($10^8$ $s^{-1}$) | 1.85 | 1.34 | 1.33 | 1.43 | 1.27 | 1.30 |
| $k_{nr}$ ($10^8$ $s^{-1}$) | 52.5 | 120.6 | 165.0 | 143.0 | 127.9 | 143.6 |
| **BODIPY 4b** | | | | | | |
| $\lambda_{ab}$ (nm) | 548.5 | 542.0 | 542.0 | 544.0 | 542.0 | 539.0 |
| $\varepsilon_{max}$($10^4 M^{-1}cm^{-1}$) | 4.3 | 3.7 | 3.4 | 3.6 | 3.5 | 3.4 |
| $\lambda_{fl}$ (nm) | 567.5 | 569.5 | 573.0 | 573.0 | 572.0 | 567.5 |
| $\phi$ | 0.012 | 0.007 | 0.005 | 0.006 | 0.005 | 0.006 |
| $\tau$ ( ps) | 117 | 69 | 57 | 65 | 57 | 72 |
| $k_{fl}$ ($10^8$ $s^{-1}$) | 1.02 | 1.01 | 0.88 | 0.92 | 0.88 | 0.83 |
| $k_{nr}$ ($10^8$ $s^{-1}$) | 84.4 | 143.9 | 174.5 | 152.9 | 174.5 | 138.0 |
| **BODIPY 4c** | | | | | | |
| $\lambda_{ab}$ (nm) | 563.5 | 556.5 | 553.0 | 559.0 | 557.5 | 553.0 |
| $\varepsilon_{max}$($10^4 M^{-1}cm^{-1}$) | 4.8 | 3.4 | 3.2 | 3.6 | 3.5 | 3.6 |
| $\lambda_{fl}$ (nm) | 577.5 | 578.5 | 578.0 | 582.0 | 580.0 | 576.0 |
| $\phi$ | 0.060 | 0.034 | 0.020 | 0.026 | 0.025 | 0.022 |
| $\tau$ ( ns) | 327 | 207 | 142 | 196 | 179 | 185 |
| $k_{fl}$ ($10^8$ $s^{-1}$) | 1.83 | 1.64 | 1.41 | 1.32 | 1.39 | 1.19 |
| $k_{nr}$ ($10^8$ $s^{-1}$) | 28.7 | 46.6 | 69.0 | 49.7 | 54.5 | 52.8 |
| **BODIPY 4d** | | | | | | |
| $\lambda_{ab}$ (nm) | 581.0 | 573.5 | 571.0 | 577.0 | 574.5 | 569.0 |
| $\varepsilon_{max}$($10^4 M^{-1}cm^{-1}$) | 11.6 | 8.0 | 7.1 | 9.0 | 8.5 | 8.4 |
| $\lambda_{fl}$ (nm) | 593.0 | 591.5 | 591.0 | 595.0 | 593.5 | 588.0 |
| $\phi$ | 0.099 | 0.073 | 0.058 | 0.067 | 0.061 | 0.059 |
| $\tau$ ( ns) | 678 | 533 | 469 | 498 | 477 | 503 |
| $k_{fl}$ ($10^8$ $s^{-1}$) | 1.46 | 1.37 | 1.23 | 1.34 | 1.28 | 1.17 |
| $k_{nr}$ ($10^8$ $s^{-1}$) | 13.3 | 17.4 | 20.0 | 18.7 | 19.7 | 18.7 |

**Table 2S.** Theoretical prediction (time dependent method combined with the B3LYP hybrid method and the lanl2dz basis set specially parameterized for heavy atoms, like iodine) of the absorption properties of BODIPY **1**, **2** and **3** and their corresponding iodinated derivatives. $\Delta E_{ab}$ is the absorption energy gap and f is the oscillator strength accounting for the absorption transition probability.

| | **1** | **4a** | **4b** | **4c** | **4d** |
|---|---|---|---|---|---|
| $\Delta E_{ab}$ (eV) | 3.09 | 2.71 | 2.55 | 2.52 | 2.46 |
| f | 0.37 | 0.22 | 0.27 | 0.36 | 0.45 |
| | **2** | **5a** | **5b** | **5c** | **5e** |
| $\Delta E_{ab}$ (eV) | 3.02 | 2.79 | 2.78 | 2.71 | 2.70 |
| f | 0.37 | 0.33 | 0.27 | 0.45 | 0.45 |
| | **3** | **6a** | **6b** | **6c** | **6e** |
| $\Delta E_{ab}$ (eV) | 2.98 | 2.72 | 2.72 | 2.66 | 2.66 |
| f | 0.37 | 0.31 | 0.24 | 0.44 | 0.46 |

**Table 3S.** Photophysical properties of the asymmetric 8-methylBODIPYs and its iodinated derivatives (serie 2). The halogenated derivatives need of a second long lived component in the fluorescence decay curve but with very low contribution (< 1 %).

| | c-hexane | Ethyl acetate | Acetone | Ethanol | Methanol | F3-EtOH |
|---|---|---|---|---|---|---|
| **BODIPY 2** | | | | | | |
| $\lambda_{ab}$ (nm) | 504.0 | 496.0 | 495.0 | 497.0 | 495.5 | 492.0 |
| $\varepsilon_{max}(10^4 M^{-1}cm^{-1})$ | 3.3 | 2.5 | 2.2 | 2.5 | 2.5 | 1.9 |
| $\lambda_{fl}$ (nm) | 515.0 | 512.5 | 512.5 | 5134.5 | 512.5 | 511.0 |
| $\phi$ | 0.96 | 0.84 | 0.79 | 0.84 | 0.76 | 0.75 |
| $\tau$ (ps) | 5460 | 5570 | 5660 | 5730 | 5780 | 6170 |
| $k_{fl}$ ($10^8$ $s^{-1}$) | 1.75 | 1.50 | 1.39 | 1.46 | 1.31 | 1.21 |
| $k_{nr}$ ($10^8$ $s^{-1}$) | 0.07 | 0.28 | 0.37 | 0.28 | 0.41 | 0.40 |
| **BODIPY 5a** | | | | | | |
| $\lambda_{ab}$ (nm) | 517.5 | 504.5 | 502.5 | 506.0 | 503.5 | 499.5 |
| $\varepsilon_{max}(10^4 M^{-1}cm^{-1})$ | 4.6 | 3.5 | 3.2 | 3.4 | 3.3 | 2.7 |
| $\lambda_{fl}$ (nm) | 532.0 | 531.5 | 532.5 | 534.0 | 533.5 | 530.5 |
| $\phi$ | 0.130 | 0.097 | 0.087 | 0.095 | 0.086 | 0.075 |
| $\tau$ (ps) | 560 | 460 | 410 | 440 | 420 | 420 |
| $k_{fl}$ ($10^8$ $s^{-1}$) | 2.32 | 2.11 | 2.12 | 2.37 | 2.04 | 1.78 |
| $k_{nr}$ ($10^8$ $s^{-1}$) | 15.5 | 19.6 | 22.2 | 20.5 | 21.7 | 22.0 |
| **BODIPY 5b** | | | | | | |
| $\lambda_{ab}$ (nm) | 515.5 | 506.0 | 502.5 | 505.5 | 503.5 | 497.0 |
| $\varepsilon_{max}(10^4 M^{-1}cm^{-1})$ | 2.9 | 2.2 | 1.7 | 2.2 | 2.1 | 1.9 |
| $\lambda_{fl}$ (nm) | 538.5 | 533.0 | 533.0 | 534.0 | 533.5 | 530.5 |
| $\phi$ | 0.050 | 0.031 | 0.024 | 0.021 | 0.020 | 0.019 |
| $\tau$ ( ps) | 259 | 160 | 127 | 125 | 122 | 147 |
| $k_{fl}$ ($10^8$ $s^{-1}$) | 1.93 | 1.93 | 1.89 | 1.68 | 1.64 | 1.29 |
| $k_{nr}$ ($10^8$ $s^{-1}$) | 36.6 | 60.5 | 76.8 | 78.3 | 80.3 | 66.7 |
| **BODIPY 5c** | | | | | | |
| $\lambda_{ab}$ (nm) | 532.0 | 518.5 | 515.5 | 520.0 | 518.0 | 511.5 |
| $\varepsilon_{max}(10^4 M^{-1}cm^{-1})$ | 9.8 | 6.4 | 5.8 | 6.4 | 6.1 | 4.8 |
| $\lambda_{fl}$ (nm) | 546.0 | 544.5 | 544.5 | 548.0 | 546.0 | 542.5 |
| $\phi$ | 0.20 | 0.15 | 0.13 | 0.16 | 0.13 | 0.11 |
| $\tau$ ( ns) | 1021 | 893 | 820 | 939 | 882 | 779 |
| $k_{fl}$ ($10^8$ $s^{-1}$) | 1.96 | 1.68 | 1.58 | 1.70 | 1.47 | 1.41 |
| $k_{nr}$ ($10^8$ $s^{-1}$) | 7.83 | 9.51 | 10.6 | 8.94 | 10.6 | 11.4 |
| **BODIPY 5e** | | | | | | |
| $\lambda_{ab}$ (nm) | 531.5 | 521.0 | 517.5 | 522.0 | 519.5 | 511.5 |
| $\varepsilon_{max}(10^4 M^{-1}cm^{-1})$ | 1.7 | 1.2 | 1.0 | 1.2 | 1.2 | 0.9 |
| $\lambda_{fl}$ (nm) | 554.5 | 552.0 | 551.5 | 554.0 | 552.5 | 548.5 |
| $\phi$ | 0.10 | 0.072 | 0.046 | 0.061 | 0.051 | 0.040 |
| $\tau$ ( ns) | 331 | 241 | 206 | 221 | 214 | 210 |
| $k_{fl}$ ($10^8$ $s^{-1}$) | 3.02 | 2.98 | 2.23 | 2.76 | 2.38 | 1.90 |
| $k_{nr}$ ($10^8$ $s^{-1}$) | 27.2 | 38.5 | 46.3 | 42.4 | 44.3 | 45.7 |

**Table 4S.** Photophysical properties of the asymmetric BODIPYs and its iodinated derivatives (serie 3). The decay curves of halogenated derivatives require the consideration of a second exponential characterized by a long lifetime, but with nearly negligible contribution (< 1 %). Hence, here are only listed the lifetime of the main component of the decay curve.

| | c-hexane | Ethyl acetate | Acetone | Ethanol | Methanol | F3-EtOH |
|---|---|---|---|---|---|---|
| **BODIPY 3** | | | | | | |
| $\lambda_{ab}$ (nm) | 512.5 | 505.0 | 503.5 | 505.5 | 504.5 | 494.5 |
| $\varepsilon_{max}(10^4 M^{-1}cm^{-1})$ | 2.9 | 2.1 | 1.9 | 2.0 | 1.9 | 1.5 |
| $\lambda_{fl}$ (nm) | 517.5 | 516.5 | 516.0 | 517.0 | 516.5 | 515.5 |
| $\phi$ | 0.70 | 0.69 | 0.65 | 0.69 | 0.60 | 0.49 |
| $\tau$ (ps) | 5240 | 5170 | 5170 | 5370 | 5300 | 5430 |
| $k_{fl}$ ($10^8$ $s^{-1}$) | 1.33 | 1.33 | 1.25 | 1.28 | 1.13 | 0.90 |
| $k_{nr}$ ($10^8$ $s^{-1}$) | 0.57 | 0.60 | 0.67 | 0.58 | 0.75 | 0.94 |
| **BODIPY 6a** | | | | | | |
| $\lambda_{ab}$ (nm) | 528.0 | 513.0 | 509.5 | 514.0 | 511.5 | 504.0 |
| $\varepsilon_{max}(10^4 M^{-1}cm^{-1})$ | 6.3 | 4.2 | 3.9 | 4.2 | 4.9 | 3.3 |
| $\lambda_{fl}$ (nm) | 538.5 | 540.5 | 541.0 | 543.0 | 542.5 | 540.0 |
| $\phi$ | 0.113 | 0.078 | 0.063 | 0.070 | 0.069 | 0.050 |
| $\tau$ (ps) | 489 | 362 | 317 | 349 | 324 | 308 |
| $k_{fl}$ ($10^8$ $s^{-1}$) | 2.31 | 2.15 | 1.98 | 2.00 | 2.12 | 1.62 |
| $k_{nr}$ ($10^8$ $s^{-1}$) | 18.1 | 25.4 | 29.5 | 26.6 | 28.7 | 30.8 |
| **BODIPY 6b** | | | | | | |
| $\lambda_{ab}$ (nm) | 527.5 | 515.0 | 509.0 | 517.5 | 513.0 | 501.0 |
| $\varepsilon_{max}(10^4 M^{-1}cm^{-1})$ | 5.6 | 3.6 | 3.4 | 3.5 | 3.5 | 3.0 |
| $\lambda_{fl}$ (nm) | 537.0 | 539.5 | 544.0 | 541.5 | 541.5 | 538.0 |
| $\phi$ | 0.050 | 0.023 | 0.019 | 0.018 | 0.016 | 0.015 |
| $\tau$ ( ps) | 212 | 116 | 97 | 90 | 87 | 110 |
| $k_{fl}$ ($10^8$ $s^{-1}$) | 2.35 | 1.98 | 1.96 | 2.00 | 1.84 | 1.36 |
| $k_{nr}$ ($10^8$ $s^{-1}$) | 44.8 | 84.2 | 101.1 | 109.1 | 113.1 | 89.5 |
| **BODIPY 6c** | | | | | | |
| $\lambda_{ab}$ (nm) | 542.0 | 528.0 | 524.5 | 529.0 | 526.5 | 520.0 |
| $\varepsilon_{max}(10^4 M^{-1}cm^{-1})$ | 7.6 | 5.4 | 4.9 | 5.3 | 5.2 | 4.5 |
| $\lambda_{fl}$ (nm) | 550.5 | 551.5 | 552.5 | 555.0 | 552.0 | 548.0 |
| $\phi$ | 0.26 | 0.19 | 0.16 | 0.20 | 0.17 | 0.12 |
| $\tau$ ( ns) | 1041 | 836 | 753 | 943 | 848 | 676 |
| $k_{fl}$ ($10^8$ $s^{-1}$) | 2.49 | 2.27 | 2.12 | 2.12 | 2.00 | 1.77 |
| $k_{nr}$ ($10^8$ $s^{-1}$) | 7.11 | 9.68 | 11.1 | 8.48 | 9.78 | 13.0 |
| **BODIPY 6e** | | | | | | |
| $\lambda_{ab}$ (nm) | 543.5 | 532.0 | 528.0 | 536.0 | 531.5 | 523.0 |
| $\varepsilon_{max}(10^4 M^{-1}cm^{-1})$ | 6.9 | 3.9 | 4.1 | 4.0 | 3.9 | 3.1 |
| $\lambda_{fl}$ (nm) | 551.5 | 553.5 | 553.0 | 557.0 | 554.0 | 550.5 |
| $\phi$ | 0.065 | 0.037 | 0.029 | 0.037 | 0.032 | 0.021 |
| $\tau$ ( ns) | 358 | 236 | 198 | 244 | 220 | 180 |
| $k_{fl}$ ($10^8$ $s^{-1}$) | 1.81 | 1.56 | 1.46 | 1.51 | 1.45 | 1.16 |
| $k_{nr}$ ($10^8$ $s^{-1}$) | 26.1 | 40.8 | 49.0 | 39.4 | 44.0 | 54.4 |

***Determination of the quantum yield for singlet molecular oxygen ($O_2(^1\Delta_g)$) generation ($\Phi_\Delta$) by time resolved phosphorescence detection (TRPD).***

It is known[1] that the value of $O_2(^1\Delta_g)$ phosphorescence emission at zero time ($I_0$) contains information about $\Phi_\Delta$. For a specific sensitizer and solvent $I_0$, depends linearly on Laser fluence ($E_0$) through expression (1)

$I_0 = \text{slope} \cdot E_0$ (1)

where slope can be considered as a proportionality constant which accounts for electronic and geometric characteristics of the detection system and solvent properties. Hence, a reference is needed for calibration. Measurements of sample and reference under identical experimental conditions, constant characteristics of irradiation wavelength and matched absorbances allows the evaluation of $\Phi_\Delta$.

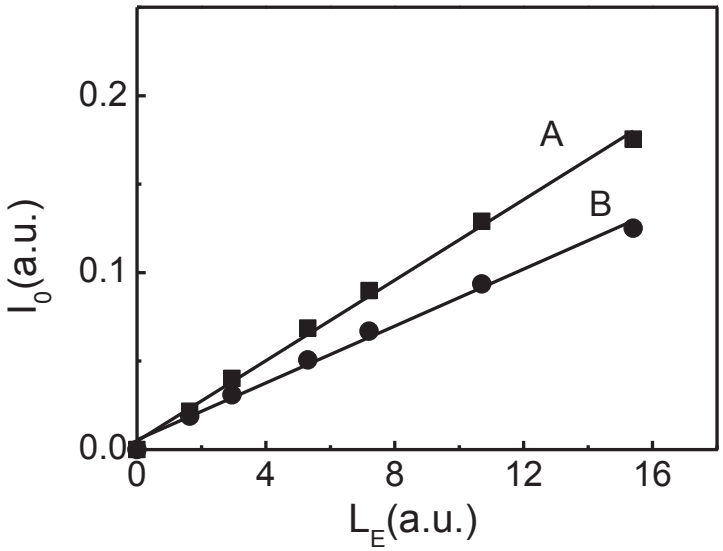


**Figure 4S.** Laser fluence ($E_0$) dependence on the amplitude of $O_2(^1\Delta_g)$ phosphorescence emission at zero time ($I_0$) in MeCN. A: PN; B: RB.

1 a) Gutiérrez, I.; Bertolotti, S.; Biasutti, M. A.; Soltermann, A. T.; García, N. A. *Can. J. Chem*., **1997**, *75*, 423-428; b) Schmidt, R.; Afshari, E. *J. Phys. Chem*. **1990**, *94*, 4377-4378.

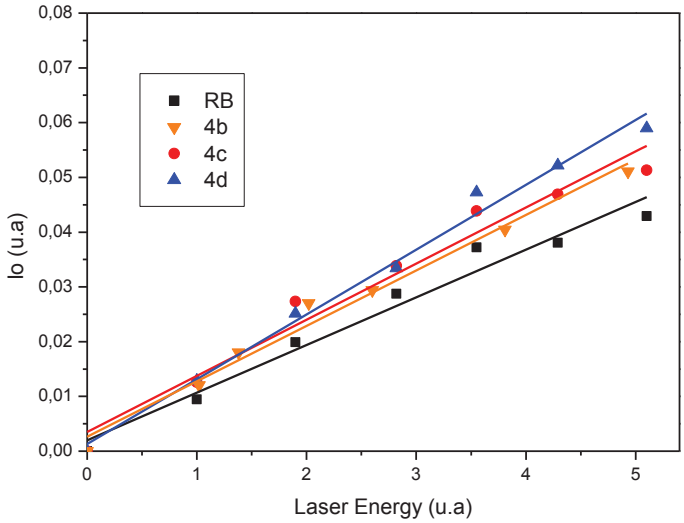


**Figure 5S.** Laser fluence ($E_0$) dependence on the amplitude of $O_2(^1\Delta_g)$ phosphorescence emission at zero time ($I_0$) in MeCN.

View Article Online / Journal Homepage / Table of Contents for this issue



Published on 25 May 2010. Downloaded by UNIVERSIDAD COMPLUTENSE MADRID on 18/02/2015 11:51:58.

# Red-edge-wavelength finely-tunable laser action from new BODIPY dyes†

M. J. Ortiz,*[a] I. Garcia-Moreno,[b] A. R. Agarrabeitia,[a] G. Duran-Sampedro,[a] A. Costela,[b] R. Sastre,[c] F. López Arbeloa,[d] J. Bañuelos Prieto[d] and I. López Arbeloa[d]

*Received 4th December 2009, Accepted 24th March 2010*
*First published as an Advance Article on the web 25th May 2010*
**DOI: 10.1039/b925561c**

New BODIPY dyes with two 4-formylphenyl, 4-(2,2-dimethoxycarbonylvinyl)phenyl and 4-(2,2-dicyanovinyl)phenyl groups at the 3- and 5-positions have been successfully designed and synthesized *via* palladium-catalyzed coupling reaction or Knoevenagel-type condensations. Structural modification of the BODIPY core *via* conjugation-extending residues significantly affects the spectroscopy and photophysical properties of the BODIPY fluorophore. These substituents cause the largest bathochromic shift in both absorption and emission spectra, which are shifted toward the red compared to its 4-phenylsubstituted analogue. Additionally, the fluorescence quantum yields and the Stokes shifts are also significantly higher than the corresponding phenyl-substituted dye. New BODIPY dyes have a high laser photostability, superior to that of commercial dyes with laser emission in the same spectral region, such as Perylene Red and Rhodamine 640. The substitution introduced in these derivatives allows to obtain tunable laser emission with a bandwidth of 0.15 $cm^{-1}$ and a tuning range of up to 50 nm. So with these three dyes it is possible to cover the spectral range 590–680 nm in a continuous way and with stable laser emission and small linewidth.

## 1. Introduction

The development of new fluorescent BODIPY dyes has become a booming area of research due to the potential applications of these dyes, for their use as sensors in biology and in clinical diagnosis, photosensitizers for photodynamic therapy, laser generators, waveguides, manufacture of light emitting diodes (OLED), photovoltaic cells and electroluminescent devices including also the usual conventional applications of organic dyes.[1] All these and other emerging applications are conditioned by the emission wavelength, quantum yield and stability of the dyes under the working conditions required for each specific application.

In particular, BODIPYs are one of the most used laser dyes family as active media of tunable dye lasers in the green–yellow visible region of the electromagnetic spectrum due to their high lasing efficiency and photostability, high fluorescence quantum yield, low rate constant of intersystem crossing and large molar absorption coefficient.[1a,c]

The photophysical properties of these dyes can be modulated to some extent incorporating the adequate substitution in the molecular structure of the parent BODIPY chromophore. Thus, the design of long-wavelength BODIPY dyes has especially attracted attention in the last years. Red-shifts of the optical spectra can be realized by substitution with aryl, vinyl, styryl, ethynylphenyl, fused aryl groups at the core or inserting heteroatoms at different positions of the chromophore (aza-BODIPY).[1a,c,2]

Recently, the synthesis of 3,5-dichloro-4,4-difluoro-8-(4-tolyl)-4-bora-3a,4a-diaza-*s*-indacene (**1**) has been described.[3] In the present work, we have carried out the synthesis, photophysical and lasing characterization of new 8-tolyl-substituted boradiazaindacenes (**2–4**) with absorption and emission spectra shifted towards longer wavelengths by extending the conjugation of the BODIPY core at the 3,5-positions (see Fig. 1).

The photophysical properties of these compounds have been compared with other 8-tolyl-substituted BODIPYs, and in addition, the behaviour of commercial dyes with laser emission in the same spectral region, such as Rhodamine

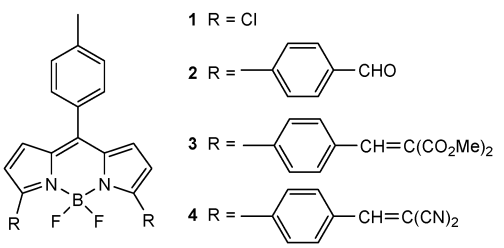


**Fig. 1** Chemical structures of the BODIPY dyes **1–4**.

[a] *Departamento de Quimica Organica I, Facultad de Ciencias Quimicas, Universidad Complutense, 28040-Madrid, Spain. E-mail: mjortiz@quim.ucm.es*
[b] *Instituto de Quimica-Fisica "Rocasolano" (IQFR), CSIC, Serrano 119, 28006-Madrid, Spain*
[c] *Instituto de Ciencia y Tecnologia de Polimeros (ICTP), CSIC, Juan de la Cierva 3, 28006-Madrid, Spain*
[d] *Departamento de Quimica Fisica, UPV-EHU, Apartado 644, 48080 Bilbao, Spain*

† Electronic supplementary information (ESI) available: Synthesis, characterization and electron density maps of dyes. See DOI: 10.1039/b925561c

 This journal is © the Owner Societies 2010

View Article Online

Published on 25 May 2010. Downloaded by UNIVERSIDAD COMPLUTENSE MADRID on 18/02/2015 11:51:58.

640 and Perylene Red was analyzed under the same pumping conditions. The present results suggest that the inclusion of *para* substituted phenyl groups at 3 and 5 positions of the 8-tolyl-BODIPY gives rise to an extended red emission, characterized by higher fluorescence capacity and a larger Stokes shift than other red-sensitive dyes. All these factors contribute to the laser behaviour of these new red emitting BODIPY, which lase with good efficiency and higher photostability than other commercial dyes lasing in the same spectral region.

## 2. Experimental

### 2.1 Materials

Starting materials and reagents used in the preparation of BODIPY dyes **1–4** are commercially available unless the synthesis is described. The solvents were dried and distilled, before use.

The commercial laser dye Rhodamine 640 (laser grade, Exciton) was used as received with a purity >99% (checked by spectroscopic and chromatographic methods). Perylene Red (BASF Lumogen Red 305) was first used as received with a purity of only 90% (checked by spectroscopic and chromatographic methods). Then, the dye purity was improved up to 99% through flash column chromatography based on silica with hexane–ethyl acetate 95/5 v/v proportion as eluent, to remove the *N*-methyl-2-pyrrolidone, identified by $^1$H-NMR as the principal impurity. Solvents for laser studies were of spectroscopic grade (Merck, Aldrich or Sigma) and were used without purification.

### 2.2 Synthesis of BODIPY 1-4

BODIPYs **2–4** were synthesized from 3,5-dichloro-4,4-difluoro-8-(4-tolyl)-4-bora-3a,4a-diaza-*s*-indacene (**1**).[3] Compound **1** was synthesized by a method previously described.[3] Their spectroscopic data are in agreement with those previously described ($^1$H NMR spectra is shown in the ESI, page 5).†

### 2.3 Characterization of the new dyes

Spectral data of the known compounds were in accordance with the literature data. Flash column chromatography was performed using silica gel Merck 60 (230–400 mesh). $^1$H and $^{13}$C NMR spectra were recorded using a Bruker Avance-DPX-300 spectrometer (300 MHz for $^1$H and 75 MHz for $^{13}$C) and a Bruker Avance-AV-500 spectrometer (500 MHz for $^1$H and 125 MHz for $^{13}$C). All spectra were recorded in $CDCl_3$. $^1$H chemical shifts are reported in ppm relative to tetramethylsilane ($\delta$ = 0.00 ppm), using the residual solvent signal as internal reference. $^{13}$C chemical shifts are reported in ppm with $CDCl_3$ ($\delta$ = 77.67 ppm) as the internal standard. Chemical shift multiplicities are reported as *s* = singlet, *d* = doublet, *t* = triplet, *q* = quartet and *m* = multiplet. IR spectra (in cm$^{-1}$) were recorded in a Bruker Tensor-27-FTIR spectrophotometer. Melting points were determined in open capillaries and are uncorrected. Mass spectra were registered by electron impact at 70 eV in a VGI2-250 spectrometer. High resolution mass spectra were determined by electro spray ionization in the positive mode (ESI†) in a Accurate-Mass Q-TOF LC/MS 6520 (Agilent Technologies). Combustion analyses (C, H, N) were obtained on a LECO CHNS-932 apparatus at the Universidad Complutense de Madrid analysis services and were within 0.4% of the theoretical values.

### 2.4 Photophysical properties

The photophysical properties were registered in $3 \times 10^{-6}$ M solutions in different solvents, prepared by adding the corresponding solvent to the residue from the adequate amount of a *ca.* $10^{-3}$ M stock solution in acetone, after vacuum evaporation of the solvent. UV-Vis absorption and fluorescence spectra were recorded on a Cary 4E spectrophotometer and on a SPEX Fluorolog 3–22 spectrofluorimeter, respectively. Fluorescence quantum yields ($\phi$) were evaluated from corrected spectra, using a *ca.* $10^{-6}$ M solution of the commercial PM650 dye in ethanol ($\phi$ = 0.10)[4] as reference. Radiative decay curves were registered by the time correlated single-photon counting technique (Edinburgh Instruments, model FL920). Fluorescence emission was monitored at the maximum emission wavelength after excitation at 470 nm by means of a diode laser (PicoQuant, model LDH470) with 150 ps FWHM pulses. The fluorescence lifetime ($\tau$) was obtained after the deconvolution of the instrumental response signal from the recorded decay curves by means of an iterative method. The goodness of the exponential fit was controlled by statistical parameters (chi-square, Durbin-Watson and the analysis of the residuals). The rate constant of radiative ($k_{fl}$) and non-radiative ($k_{nr}$) deactivations were calculated by means of: $k_{fl} = \phi/\tau$ and $k_{nr} = (1\text{-}\phi)/\tau$.

The ground state geometry was optimized using the B3LYP method and the double valence basis set (6-31G) implemented in the Gaussian 03 software. The energy minimization process was performed without any geometrical restrictions, and was considered to be adequately concluded when the analysis of the vibrational frequencies did not give any negative frequency.

### 2.5 Laser experiments

Liquid solutions of dyes were contained in 1 cm optical-path quartz cells that were carefully sealed to avoid solvent evaporation during experiments. The liquid cells of the newly synthesized red-edge dyes were transversely pumped at 532 nm, with 5 mJ pulse$^{-1}$, 6 ns FWHM pulses from a frequency-doubled Q-switched Nd:YAG laser (Monocrom OPL-10) at a repetition rate of up to 10 Hz, and at 568 nm, with 5 mJ, 10 ns FWHM pulses from a Nd-YAG-pumped dye laser (Spectron SL800 with an ethyl acetate solution of PM567). The exciting pulses were line-focused onto the lateral flat surface of the solid samples, providing pump fluences on the active medium of 180 mJ cm$^{-2}$. The oscillation cavity (2 cm length) consisted of a 90% reflectivity aluminium mirror, with the end face of the sample as output coupler.

For pumping at 532 nm, the concentrations of new BODIPY **2**, **3** and **4** were $9 \times 10^{-4}$ M, $8 \times 10^{-4}$ M and $3 \times 10^{-3}$ M, respectively, leading to solutions with an optical density of *ca.* 16. For pumping at 568 nm, the concentrations of **2**, **3** and **4** dyes were $9 \times 10^{-4}$ M, $4 \times 10^{-4}$ M and $2 \times 10^{-3}$ M, respectively, matching the optical density selected for irradiation at 532 nm.

View Article Online

Published on 25 May 2010. Downloaded by UNIVERSIDAD COMPLUTENSE MADRID on 18/02/2015 11:51:58.

The photostability of each dye was evaluated by irradiating under lasing conditions at 532 nm 10 μL of a solution in ethyl acetate. The solutions were contained in a cylindrical Pyrex tube (1-cm height, 1-mm internal diameter) carefully sealed to avoid solvent evaporation during the experiments. Monitoring of sample photolysis was carried out by recording the laser-induced fluorescence emission, excited transversally to the capillary with the same pump pulses from the Nd:YAG laser used for producing dye laser emission, as a function of the pump pulses at 10 Hz repetition rate. The fluorescence emission was monitored perpendicular to the exciting beam, collected by an optical fiber, and imaged onto the input slit of a monochromator (Acton Research corporation) and detected with a charge-coupled device (CCD) (SpectruMM:GS128B). The fluorescence emission was recorded by feeding the signal to the boxcar (Stanford Research, model 250) to be integrated before being digitized and processed by a computer. Each experience was repeated at least three times. The estimated error of the energy measurements was 10% and the experimental error in the photostabilty measurements was estimated to be on the order of 7%. Details of the experimental setup can be found elsewhere.[5,6]

Narrow-linewidth laser emission and tuning ranges of dye solutions were obtained by placing the samples in a home-made Shoshan-type oscillator[7] consisting of full-reflecting aluminium back and tuning mirrors, and a 2400 lines $mm^{-1}$ holographic grating in grazing incidence, with outcoupling *via* the grating zero order. Wavelength tuning was accomplished by rotation of the tuning mirror. Tuning mirror and grating (both from Optometrics) were 5 cm wide and the angle of incidence on the grating was 88.5°. Laser linewidth was measured with a Fabry-Perot etalon (IC Optical Systems) with a free spectral range of 15.9 GHz.

## 3. Results and discussion

### 3.1 Synthesis

BODIPY fluorophore can be easily functionalized at the 3- and 5-positions with two 4-formylphenyl groups by palladium-catalyzed coupling reaction of the 3,5-dichloro-4,4-difluoro-8-(4-tolyl)-4-bora-3a,4a-diaza-*s*-indacene (**1**)[3] using the Suzuki reaction. In these conditions, BODIPY derivative **2** was obtained (see Scheme 1). Compound **2** was transformed in the dimethoxycarbonylvinyl and dicyanovinyl-substituted fluorophores **3** and **4**, respectively, by Knoevenagel condensation (see Scheme 1). Suzuki coupling for the formation of aryl-substituted dye **2** was carried out under microwave or ultrasonic irradiation. Thus, **1** was treated with 2.5 equivalents of 4-formylphenylboronic acid under microwave irradiation for 30 min at 150 °C with a power of 200 W affording the diarylated derivative **2** (46%). When the reaction was run under ultrasonic irradiation at 75 °C with a power of 720 W, longer time (15 h) and 6 equivalents of boronic acid were required, affording **2** in 50% yield. Subsequently, BODIPY **3** was obtained with a 47% yield, from diaryl-substituted dye **2** with dimethyl malonate in the presence of $TiCl_4$. Similarly, the Knoevenagel reaction of compound **2** and malononitrile in the presence of β-alanine and acetic acid led to the formation of **4** (21%).

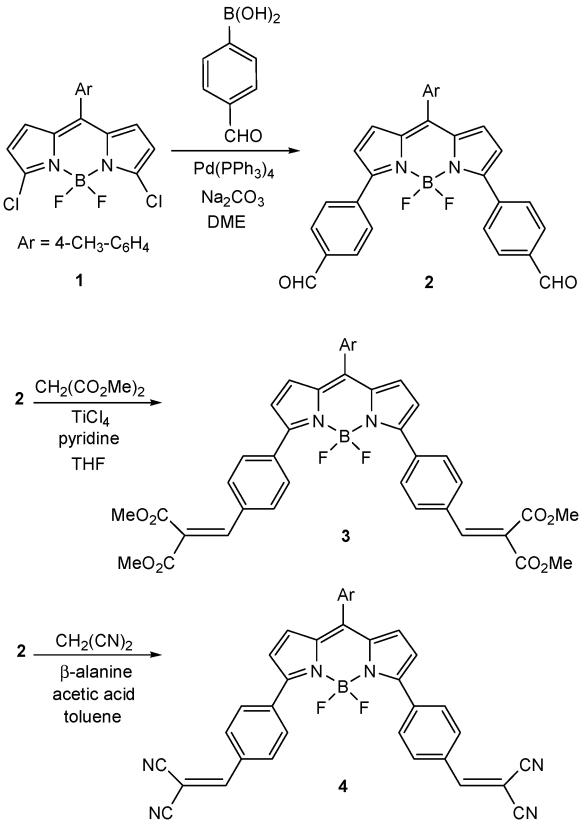


**Scheme 1** Synthetic routes of derivatives **2–4** from **1**.

### 3.2 Photophysical properties

The new BODIPYs **2–4** present absorption and fluorescence bands at around $\lambda_{ab} \approx 550–575$ nm and $\lambda_{fl} \approx 595–625$ nm (see Fig. 2), shifted toward the red spectral region with respect to other alkyl-substituted BODIPY dyes with absorption and fluorescence bands at the green/yellow spectral region.[8] The absorption and fluorescence bands of the new dyes are well separated from each other, leading to a relatively large Stokes shift ($\Delta\nu_{St} \approx 1200–1800$ $cm^{-1}$), about 3 times higher than that of typical alkyl-BODIPY derivatives. Fluorescent dyes with large Stokes shifts are of special interest in photonics because the loss of emission intensity by reabsorption effects, one of the main factors contributing to the losses in the resonator cavity of a dye laser, is reduced. The new dyes are also characterized by broad spectral bands, mainly for dye **4** (fwhm ≈ 2200 $cm^{-1}$).

Quantum mechanical calculations predict that the $S_0$–$S_1$ transition of these new BODIPYs, responsible for these Vis absorption and emission bands, involves the HOMO and LUMO molecular orbitals. The electronic density of these orbitals is illustrated in Fig. 3 for the specific case of **4** (see ESI page 12 for similar electronic clouds obtained to compound **2** and **3**).† As can be observed, the electronic π-system is not only localized in the BODIPY core but is also extended through the aromatic ring of the substituents at the 3- and 5-position, mainly in the excited state. This high delocalization

 This journal is © the Owner Societies 2010

View Article Online

Published on 25 May 2010. Downloaded by UNIVERSIDAD COMPLUTENSE MADRID on 18/02/2015 11:51:58.

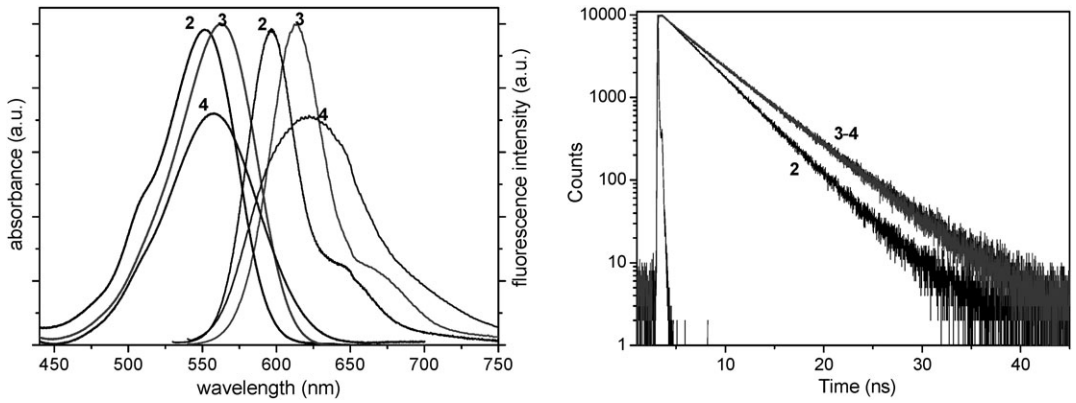


**Fig. 2** Absorption (normalized to emission spectrum), fluorescence spectra (scaled by their fluorescence quantum yield), and fluorescence decay curves of dyes **2**, **3** and **4** in trifluoroethanol.

in the electronic π-system should be responsible for the large spectral red shifts observed for these dyes.

Many of the reported red-emitting BODIPYs are achieved by the incorporation of delocalized substituents, bearing sometimes electron donor groups, usually at 3 and 5 positions of the chromophoric core.[9] The resonant interaction between such functional groups and the π-system of the BODIPY core provides a merocyanine like chromophore where electronic density could be shifted from the donor substituent to the BODIPY core leading to the formation of a charge transfer state, which quenches efficiently the fluorescent emission mainly in polar media.[10] In our case, the presence of electron acceptor groups at 3 and 5 positions causes a strong red shift, however such charge transfer states are not formed. In fact, and as discussed below, both the fluorescence quantum yield and the lifetime of dyes **2**, **3**, and **4** are nearly solvent independent. Therefore, the cyanine like delocalization typical of BODIPY is kept, as shown in Fig. 3, where the electronic density is extended through the whole molecule.

The optimized geometry in the ground state shows a nearly planar BODIPY core, with the phenyl unit at the *meso* 8-position twisted 51° and the aromatic rings at 3,5 positions twisted around 30°, with respect to the dipyrromethene plane. Upon excitation, the electronic distribution is extended to the vinyl group at *para* position of the phenyl substituents at 3 and 5 positions. Consequently the fluorescence band is more extended into the red, explaining the above commented large Stokes shift of these compounds. These red displacements are more prominent for dyes **3** and **4** than for dye **2** (see Fig. 2), probably because of the presence of vinyl groups in the former dyes and stronger electron withdrawing units at the *para*-phenyl position (methoxycarbonyl or cyano *versus* formaldehyde).

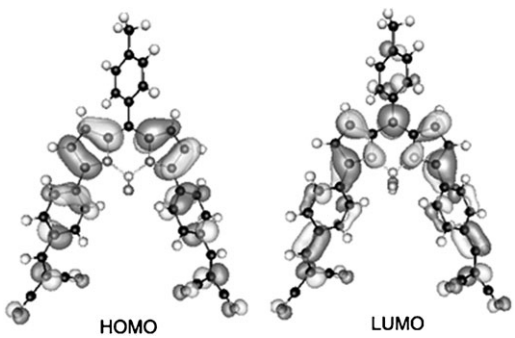


**Fig. 3** Electronic density maps of the HOMO and LUMO orbitals for dye **4**.

Fluorescence decay curves of **2–4** are analyzed as mono-exponential decays (see Fig. 2), and the fluorescence lifetimes are evaluated from the corresponding slopes. The photophysical parameters of BODIPYs **2–4** in several solvents are summarized in Table 1. The fluorescence quantum yield and lifetime ($\phi \approx 0.40$–$0.65$, and $\tau \approx 3.5$–$5.0$ ns, respectively) of these compounds are relatively high, in spite of the red emission of these dyes. In fact, systems with low $S_1$–$S_0$ energy have low fluorescent capacities because the non-radiative deactivation processes are favoured *via* a rapid internal conversion mechanism.[11] The increase in the internal conversion is probably the most critical issue to develop successfully efficient red emitting dyes. However, present red-emitting BODIPY dyes are characterized by a relative low non-radiative rate constant ($k_{nr} < 1.5 \times 10^8\ s^{-1}$) and a relative high fluorescence rate constant ($k_{fl} \approx 1.3 \times 10^8\ s^{-1}$, in spite of the low absorption probability, molar absorption $\varepsilon_{max} \approx 1$–$3 \times 10^4\ M^{-1}\ cm^{-1}$). Moreover, it has previously been probed that these dyes with a pendant phenyl group at the *meso* 8-position can enhance the internal conversion process *via* a rotational motion of the phenyl group, reducing the fluorescence efficiency.[2b,12] In the present cases, such a mechanism seems to have a minor effect, probably due to the high delocalization of the chromophoric π-system through the aromatic substituents at 3 and 5 positions.

In general, compound **4**, bearing cyano groups, presents the lowest fluorescent efficiency while dyes **2** and **3** show the highest $\phi$ value. The presence of electron withdrawing cyano groups induces a decrease in the $k_{fl}$ value, which is correlated with a lower absorption probability in BODIPY **4**. A more proper assignation of a decrease in the fluorescence probability should be made on the basis of the $k_{fl}/\nu$,[3] since the Einstein spontaneous emission is proportional to the fluorescence frequency. Again, it is confirmed that dye **4** bearing a cyano group has a lower fluorescence emission probability. Although this reduction in the fluorescence ability will reduce the lasing efficiency of this compound, its high Stokes shift would decrease the losses in the resonator cavity favouring its laser action.

View Article Online

Published on 25 May 2010. Downloaded by UNIVERSIDAD COMPLUTENSE MADRID on 18/02/2015 11:51:58.

**Table 1** Photophysical properties of dyes **2**, **3** and **4** in apolar (c-hexane), polar (acetone and ethyl acetate) and polar/protic solvents (ethanol, methanol and $F_3$-ethanol); absorption ($\lambda_{ab}$) and fluorescence ($\lambda_{fl}$) wavelength (±0.5 nm), molar absorption ($\varepsilon_{max}$, ± 0.1 × $10^4$ $M^{-1}$ $cm^{-1}$), fluorescence quantum yield ($\phi$ ± 0.05) and lifetime ($\tau$, ± 0.05 ns), radiative ($k_{fl}$, $10^8$ $s^{-1}$) and non-radiative ($k_{nr}$, $10^8$ $s^{-1}$) rate constants, and Stokes shift ($\Delta\nu_{St}$, $cm^{-1}$)

| Solvent | $\lambda_{ab}$ | $\varepsilon_{max}$ | $\lambda_{fl}$ | $\phi$ | $\tau$ | $k_{fl}$ | $k_{nr}$ | $\Delta\nu_{St}$ |
|---|---|---|---|---|---|---|---|---|
| **Dye 2** | | | | | | | | |
| $F_3$-ethanol | 551.5 | 3.0 | 595.5 | 0.58 | 4.54 | 1.28 | 0.92 | 1365 |
| Methanol | 557.0 | 3.1 | 598.0 | 0.46 | 3.65 | 1.26 | 1.48 | 1225 |
| Ethanol | 559.0 | 3.1 | 600.5 | 0.53 | 3.91 | 1.35 | 1.20 | 1250 |
| Acetone | 558.5 | 3.1 | 599.5 | 0.51 | 3.48 | 1.46 | 1.41 | 1225 |
| Ethyl acetate | 558.0 | 3.0 | 599.0 | 0.57 | 3.67 | 1.55 | 1.17 | 1240 |
| c-Hexane[a] | 561.0 | 3.3 | 597.5 | 0.54 | 3.68 | 1.46 | 1.25 | 1080 |
| **Dye 3** | | | | | | | | |
| $F_3$-ethanol | 562.5 | 1.8 | 613.5 | 0.59 | 4.98 | 1.18 | 0.82 | 1470 |
| Methanol | 570.0 | 1.9 | 618.5 | 0.60 | 4.56 | 1.31 | 0.88 | 1380 |
| Ethanol | 573.5 | 1.9 | 621.0 | 0.62 | 4.67 | 1.33 | 0.81 | 1330 |
| Acetone | 572.5 | 1.9 | 620.0 | 0.61 | 4.61 | 1.32 | 0.84 | 1345 |
| Ethyl acetate | 572.0 | 1.9 | 620.0 | 0.64 | 4.56 | 1.40 | 0.79 | 1355 |
| c-Hexane[a] | 575.5 | 1.8 | 618.0 | 0.56 | 4.39 | 1.27 | 1.00 | 1190 |
| **Dye 4** | | | | | | | | |
| F3-ethanol | 558.0 | 0.6 | 622.0 | 0.42 | 4.80 | 0.87 | 1.21 | 1845 |
| Methanol | 564.0 | 0.7 | 623.0 | 0.41 | 4.53 | 0.90 | 1.30 | 1675 |
| Ethanol | 566.0 | 0.6 | 625.0 | 0.47 | 4.59 | 1.02 | 1.15 | 1665 |
| Acetone | 565.5 | 0.6 | 625.0 | 0.44 | 4.80 | 0.92 | 1.16 | 1690 |
| Ethyl acetate | 563.0 | 0.6 | 617.5 | 0.54 | 4.66 | 1.16 | 0.98 | 1570 |
| c-Hexane[a] | 572.0 | 0.4 | 622.5 | 0.53 | 4.63 | 1.14 | 1.01 | 1420 |

[a] Not fully soluble.

The inclusion of *p*-substituted-phenyl groups at 3,5 positions results in more polar BODIPY dyes reducing their solubility in apolar media (*i.e.* c-hexane). The solvent effect on the photophysics of these new dyes (see Table 1) is the typical one observed in many alkyl-BODIPY dyes,[8] for instance: hypsochromic shifts of the spectral bands with the solvent polarity/acidity; a nearly solvent independent fluorescence quantum yield, and a progressive increase of the fluorescence lifetime and Stokes shift with the solvent's acidity and polarity. These BODIPYs have low solubility in apolar media. Anyway, their photophysics in such media (c-hexane, dioxane, dietilether and THF) was also registered (data in c-hexane included in Table 1, data in the rest of solvents not shown) for comparison. The results are consistent with the above commented evolutions with the solvent properties, corroborating the absence of any quenching charge transfer state in polar media and the maintenance of the cyanine like electronic π-system delocalization, in spite of the incorporation of electron withdrawing groups (aldehide, ester and cyano).

The photophysical behaviour of the new red emitting dyes **2**, **3** and **4** is compared with other structurally related 8-tolyl-BODIPYs found in the literature,[13] (see Fig. 4). The unsubstituted 8-tolyl-BODIPYs present a very low fluorescence quantum yield (see Fig. 4), attributed to an important internal conversion deactivation *via* the rotational motion of the pendant 8-aryl group.[2b,12] Besides, red-emitting dyes present low fluorescence capacity because the low $S_0$–$S_1$ energy gap favours the internal conversion processes.[11] However, the incorporation of 3,5-phenyl groups in 8-tolyl-BODIPY not only leads to a large red shift, but also to a progressive enhancement of the fluorescence quantum yield (see Fig. 4). Experimental results suggest that the internal conversion of 8-tolyl-BODIPYs is drastically reduced when aryl groups are incorporated at 3 and 5 positions of BODIPY core. The π-electronic delocalization through these groups induces a double bond character to the linking BODIPY-phenyl bonds, reducing the rotational motion of these aryl groups. Moreover, this extended π-system also reduces the electronic density at the *meso* 8-carbon of the BODIPY-core, mainly in the excited state (see Fig. 3), decreasing the effect of the 8-aryl rotation on the internal conversion of these dyes. The fluorescence bands of the new dyes **2**, **3** and **4** are more extensively red-shifted with a higher fluorescence quantum yield because the presence of adequate *para*-substituents at the 3,5-phenyl groups favours the delocalization of the π-system through these moieties, increasing their fluorescence ability.

Therefore, the present red-emitting BODIPY dyes show an important fluorescence capacity in the red part of the visible region and are promising candidates to be used as active media for developing an efficient red-dye laser.

### 3.3 Lasing properties

An ethyl acetate solution of derivative **2** transversely pumped at 532 nm with 5 mJ $pulse^{-1}$ in a simple plane–plane non-tunable resonator emits broad-linewidth laser light at 615 nm, with an efficiency (Eff, percentage of the excitation energy converted into laser emission) of 14%. The extension of the conjugation at 3,5-BODIPY positions, red-shifts effectively the wavelength of the laser emission up to 37 nm, although with a significant decrease in the laser efficiency of dyes **3** and **4** (see Table 2). The laser-pump of the new dyes at a wavelength (568 nm) near their absorption maxima improves the laser efficiency which increases for a factor of up to 5 with respect to that registered under excitation at 532 nm (see Table 2).

The lasing characteristics observed in concentrated solutions of the new BODIPY dyes show good correlation with their photophysical properties in dilute solution. The presence of 3,5-dimethoxycarbonylvinyl- and dicyanovinyl substituents induced spectral red-shifts in the absorption and fluorescent bands similar to those observed in the lasing emission. A slight decrease in the $k_{fl}$ value of dye **4** with respect to dye **2** (by a factor of ca 1.4) could suggest a diminution in the laser action, although not so significant reduction of the laser efficiency.

The actual effect of the solvent on the dye laser emissions was analyzed in solutions of apolar, polar nonprotic, and polar protic solvents at the dye concentrations that optimized the corresponding laser efficiency of each derivative. The results are summarized in Table 2. The low solubility of these new dyes in some common solvents prevents attaining the concentrated solutions required for laser experiments and, consequently, the correlation with the photophysical properties. However, some interesting tendencies can be derived from these experimental results: higher laser efficiencies of dye **2** are reached for polar aprotic solvents such as ethyl acetate and acetone. However, the very polar protic nature of the solvents (2,2,2-trifluoroethanol and methanol) improved the laser efficiencies of dyes **3** and **4** with respect to the values registered in apolar media. As previously discussed for commercial BODIPY dyes,[14] the behaviour of the new BODIPY derivatives in different solvents confirms the difficulty in understanding and predicting laser action on the basis of the

 This journal is © the Owner Societies 2010

View Article Online

Published on 25 May 2010. Downloaded by UNIVERSIDAD COMPLUTENSE MADRID on 18/02/2015 11:51:58.

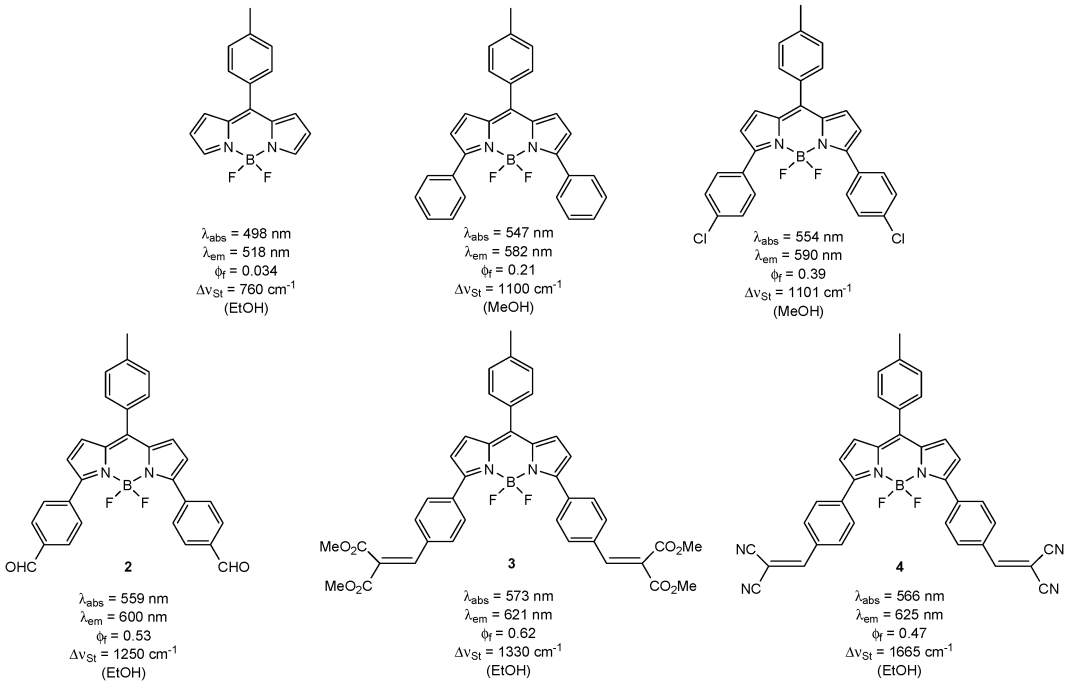


**Fig. 4** Chemical structures of 8-tolyl-BODIPYs susbtituted at 3 and 5 positions from the literature[13] and compounds **2–4** synthetized in this work.

**Table 2** Maximum wavelength of the laser emission ($\lambda_l$) and lasing efficiency (Eff) of the new BODIPY dyes in several solvents under excitation at 532 nm and, within parentheses, at 568 nm

| Dye | Data | THF | EtOAc | Acetone | $CH_2Cl_2$ | $F_3$-EtOH | MeOH |
|---|---|---|---|---|---|---|---|
| **2**[a] | $\lambda_l$/nm | 619 (620) | 615 (615) | 615 (613) | 617 | | |
| | Eff (%) | 11 (16) | 14 (20) | 14 (20) | 10 | | |
| **3**[b] | $\lambda_l$/nm | 636 (632) | 632 (628) | | | 625 | 628 (626) |
| | Eff (%) | 2 (8) | 2 (10) | | | 6 | 11 (17) |
| **4**[c] | $\lambda_l$/nm | 646 (659) | 648 (654) | 652 | | 655 (657) | 648 |
| | Eff (%) | 2 (5) | 4 (8) | 3 | | 5 (11) | 3 |

[a] Dye concentrations at 532 nm: $9 \times 10^{-4}$ M and at 568 nm: $9 \times 10^{-4}$ M. [b] Dye concentrations at 532 nm: $8 \times 10^{-4}$ M and at 568 nm: $4 \times 10^{-4}$ M. [c] Dye concentrations at 532 nm: $3 \times 10^{-3}$ M and at 568 nm: $2 \times 10^{-3}$ M.

polarity/polarizability or H-bond donor/acceptor ability or both liquid media, at least for dyes with a complex molecular structure.

The photostability (evolution of the emission with the number of pump pulses at 10 Hz) of each dye was evaluated by irradiating under lasing conditions 10 μL of a solution in ethyl acetate contained in capillary tubes carefully sealed to avoid solvent evaporation during experiments. The concentrations of laser dyes were adjusted so that the laser action was optimum in all cases. Although the optical quality of the capillary prevents laser emission from the dyes, information about their photostabilities can be obtained by monitoring the decrease in laser-induced fluorescence intensity perpendicular to the exciting beam, under transversal excitation of the capillary, as a function of the number of pump pulses. The results obtained from the dyes are plotted in Fig. 5.

Under 532 nm pumping, the new derivatives **3** and **4** result in being highly photostable, with the emission dropping by less than 20 and 10%, respectively, with respect to the initial value after 100 000 pump pulses, while the derivative **2** experiences a faster photodegradation process, losing up to 40% of its fluorescence emission.

In order to put the present results in proper perspective, the lasing parameters of two well-known dyes lasing at the same wavelengths as the dyes studied herein were also measured in liquid solutions at 532 nm under similar conditions. Perylene Red, used as received, in ethyl acetate solution ($5 \times 10^{-4}$ M) lases at 614 nm with an efficiency of 20%, while after purification the conversion efficiency of this dye increases to 26%. Rhodamine 640 ($1 \times 10^{-3}$ M) lases in the same spectral region with higher efficiency (40%) but exhibiting a dual laser emission, at 620 and 650 nm, due to reabsorption/reemission phenomena and inhomogeneous spectral broadening.[15] For comparison, the lasing photostabilities obtained under the above described experimental conditions for commercial dyes Perylene Red and Rhodamine 640 are also included in Fig. 5. The commercial dyes exhibit lasing efficiencies higher than those obtained with the new BODIPY derivatives described here, although with lower photostabilities: the initial fluorescence emission of Rhodamine 640 drops to 45% of its initial value after 60 000 pump pulses while the purified Perylene Red maintains a 70% of its initial emission after 100 000 pump pulses.

View Article Online

Published on 25 May 2010. Downloaded by UNIVERSIDAD COMPLUTENSE MADRID on 18/02/2015 11:51:58.

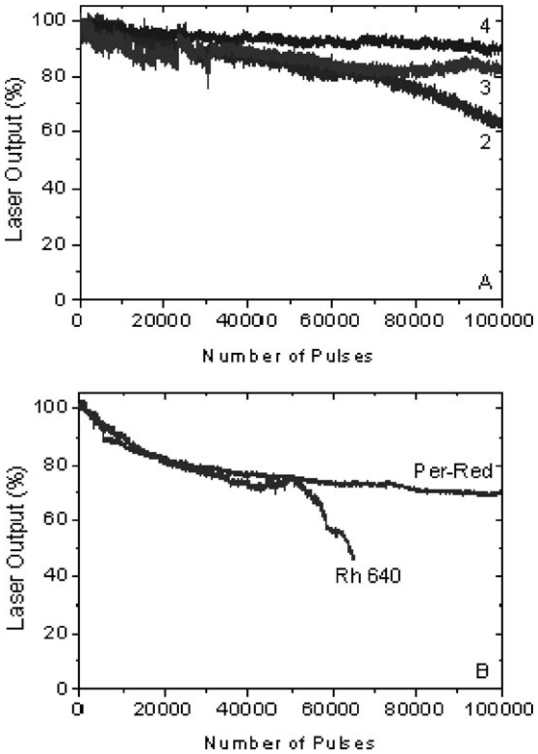


**Fig. 5** Normalized laser-induced fluorescence emission as a function of the number of pump pulses for the following dye solutions: (A) new BDP dyes **2**, **3** and **4** in ethyl acetate solution; and (B) **Per-Red** in ethyl acetate and **Rh640** in ethanol. Pump laser wavelength, energy and repetition rate: 532 nm, 5.5 mJ pulse$^{-1}$ and 10 Hz.

The tuning capability, one of the most important features of laser dyes, was determined for the new BODIPY dyes by placing their liquid solutions in the grazing-incidence grating tunable resonator. Tunable laser emission with a linewidth of the order of 0.15 cm$^{-1}$ and a tuning range of up to 50 nm was thus recorded, and the spectral region 590–680 nm can be continuously covered with narrow-linewidth and stable laser radiation by using the three dyes (see Fig. 6).

## 4. Conclusions

We have successfully designed and synthesized new BODIPY dyes to achieve large spectral red-shifts with particularly useful photophysical properties. The position of the emission band can be modulated by the type of substituent attached to the BODIPY core. All the red emitting dyes presented in this work are characterized by a high fluorescence capacity since the coupling between the electronic clouds of the pyrromethene core and the 3,5-aryl groups reduces the rotational motion of the phenyl groups. Besides, the new dyes exhibit large Stokes shift, which could also improve their fluorescence ability from a technological point of view. The new BODIPY dyes lase with good efficiency and high photostability, allowing a wavelength finely tunable over a wide range (590–680 nm) with a narrow-linewidth. Considering the easy synthetic build-up, the wide variety of possible substituents and the large number of described BODIPY laser dyes, this powerful approach could

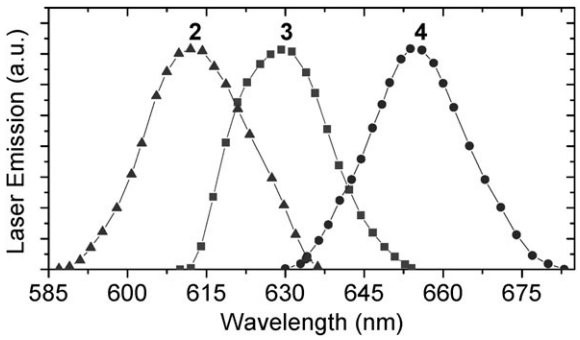


**Fig. 6** Laser tunability of new **2**, **3**, and **4** BDP dyes in ethyl acetate solutions. The solid lines in the tuning curves represent guidelines for the eyes.

be extended to other dyes of this family, with practical applications in optical and sensing fields.

## Acknowledgements

This research was financed by the Spanish MICINN (Project MAT2007-65778-C02-01 and -02 and Project CTQ2008-02820) and Universidad Complutense of Madrid (Project GR58/08). We acknowledge support provided by the Centro de Resonancia Magnetica of the Universidad Complutense de Madrid.

## References

1 (*a*) A. Loudet and K. Burgess, *Chem. Rev.*, 2007, **107**, 4891–4932; (*b*) R. Ziessel, G. Ulrich and A. Harriman, *New J. Chem.*, 2007, **31**, 496–501; (*c*) G. Ulrich, R. Ziessel and A. Harriman, *Angew. Chem., Int. Ed.*, 2008, **47**, 1184–1201; (*d*) S. Ela-Erten, M. D. Yilmaz, B. Icli, I. Dede, S. Icli and E. U. Akkaya, *Org. Lett.*, 2008, **10**, 3299–3302; (*e*) S. Ozlem and E. U. Akkaya, *J. Am. Chem. Soc.*, 2009, **131**, 48–49; (*f*) R. Ziessel, G. Ulrich, A. Harriman, M. A. H. Alamiry, B. Stewart and P. Retailleau, *Chem.–Eur. J.*, 2009, **15**, 1359–1369.

2 (*a*) A. Burghart, H. Kim, M. B. Welch, L. H. Thoresen, J. Reibenspies and K. Burgess, *J. Org. Chem.*, 1999, **64**, 7813–7819; (*b*) J. Chen, A. Burghart, A. Derecskei-Kovacsand and K. Burgess, *J. Org. Chem.*, 2000, **65**, 2900–2906; (*c*) B. Turfan and E. U. Akkaya, *Org. Lett.*, 2002, **4**, 2857–2859; (*d*) A. Coskun and E. U. Akkaya, *J. Am. Chem. Soc.*, 2005, **127**, 10464–10465; (*e*) For a recent review, see: A. B. Descalzo, H. J. Xu, Z. Shen and K. Rurack, *Ann. N. Y. Acad. Sci.*, 2008, **1130**, 164–171.

3 W. Qin, T. Rohand, M. Baruah, A. Stefan, M. Van der Auweraer, W. Dehaen and N. Boens, *Chem. Phys. Lett.*, 2006, **420**, 562–568.

4 F. López Arbeloa, J. Bañuelos, V. Martínez, T. Arbeloa and I. López Arbeloa, *ChemPhysChem*, 2004, **5**, 1762–1771.

5 A. Costela, I. García-Moreno, D. del Agua, O. García and R. Sastre, *J. Appl. Phys.*, 2007, **101**, 073110–073121.

6 A. Costela, I. Garcia-Moreno, C. Gomez, R. Sastre, F. Amat-Guerri, M. Liras, F. Lopez Arbeloa, J. Bañuelos Prieto and I. Lopez Arbeloa, *J. Phys. Chem. A*, 2002, **106**, 7736–7742.

7 I. Soshan, N. N. Danon and U. J. Oppenheim, *Appl. Phys.*, 1977, **48**, 2295–2299.

8 F. López Arbeloa, J. Bañuelos, V. Martínez, T. Arbeloa and I. López Arbeloa, *Int. Rev. Phys. Chem.*, 2005, **24**, 339–374.

9 (*a*) Z. Dost, S. Atilgan and E. U. Akkaya, *Tetrahedron*, 2006, **62**, 8484–8488; (*b*) W. Qin, T. Rohand, W. Dehaen, J. N. Clifford, K. Driesen, D. Beljonne, B. V. Averbeke, M. V. Auweraer and N. Boens, *J. Phys. Chem. A*, 2007, **111**, 8588–8697; (*c*) K. Umezawa, Y. Nakamura, H. Makino, D. Citterio and K. Suzuki, *J. Am. Chem. Soc.*, 2008, **130**, 1550–1551; (*d*) D. Zhang, Y. Wen, Y. Xiao, G. Yu, Y. Liu and X. Qian, *Chem. Commun.*, 2008, 4777–4779; (*e*) B. Ventura, G. Marconi,

 This journal is © the Owner Societies 2010

View Article Online

Published on 25 May 2010. Downloaded by UNIVERSIDAD COMPLUTENSE MADRID on 18/02/2015 11:51:58.

M. Bröring, R. Krüger and L. Flamigni, *New J. Chem.*, 2009, **33**, 428–438.

10 (*a*) L. G. S. Brooker, *J. Am. Chem. Soc.*, 1965, **87**, 937–938; (*b*) L. G. S. Brooker, A. C. Craig, D. W. Heseltine, P. W. Jenkins and L. L. Lincoln, *J. Am. Chem. Soc.*, 1965, **87**, 2443–2450; (*c*) J. Fabian and H. Hartmann, *Light Absorption of Organic Colorants*, Springer-Verlag, Berlin, 1980; (*d*) N. Tyutyulkov, J. Fabian, A. Melhorn, F. Dietz and A. Tadjer, *Polymethine Dyes: Strcuture and Properties*, St. Kliment Ohridski University Press, Sofia, 1991.

11 (*a*) P. O. Andersson, S. M. Bachilo, R.-L. Chen and T. Gillbro, *J. Phys. Chem.*, 1995, **99**, 16199–16209; (*b*) C. E. Carvalho, I. M. Brinn, A. V. Pinto and M. C. Pinto, *J. Photochem. Photobiol., A*, 2000, **136**, 25–33; (*c*) J. Bañuelos, F. López Arbeloa, V. Martínez, T. Arbeloa, F. Amat-Guerri, M. Liras and I. López Arbeloa, *Chem. Phys. Lett.*, 2004, **385**, 29–35.

12 (*a*) S. Badré, V. Monnier, R. Méallet-Renault, C. Dumas-Verdes, E. Y. Schmidt, A. I. Mikhaleva, G. Levi, A. Ibanez, B. A. Trofimov and R. B. Pansu, *J. Photochem. Photobiol., A*, 2006, **183**, 238–246; (*b*) Q. Zheng, G. Xu and P. N. Prasad, *Chem.–Eur. J.*, 2008, **14**, 5812–5819; (*c*) M. Alvarez, A. Costela, I. García-Moreno, F. Amat-Guerri, M. Liras, R. Sastre, F. López Arbeloa, J. Bañuelos and I. López Arbeloa, *Photochem. Photobiol. Sci.*, 2008, **7**, 802–813.

13 (*a*) T. Rohand, W. Qin, N. Boens and W. Dehaen, *Eur. J. Org. Chem.*, 2006, 4658–4663; (*b*) A. Cui, X. Peng, J. Fan, X. Chen, Y. Wu and B. Guo, *J. Photochem. Photobiol., A*, 2007, **186**, 85–92.

14 J. Bañuelos Prieto, F. López Arbeloa, V. Martínez Martínez, T. López Arbeloa and I. López Arbeloa, *J. Phys. Chem. A*, 2004, **108**, 5503–5508.

15 I. García-Moreno, A. Costela, M. Pintado-Sierra, V. Martín and R. Sastre, *J. Phys. Chem. B*, 2009, **113**, 10611–10618.

This journal is © The Owner Societies 2010

## Supporting Information

# Red-Edge Wavelength-Finely Tunable Laser Action from New Bodipy Dyes

**M. J. Ortiz,[*a] I. Garcia-Moreno,[b] A. R. Agarrabeitia,[a] G. Duran-Sampedro,[a] A. Costela,[b] R. Sastre,[c] F. López Arbeloa,[d] J. Bañuelos Prieto[d] and I. López Arbeloa[d]**

[a]*Departamento de Quimica Organica I (DQO), Facultad de Ciencias Quimicas, Universidad Complutense, 28040 Madrid, Spain.*
[b]*Instituto de Quimica-Fisica "Rocasolano" (IQFR), CSIC, Serrano 119, 28006 Madrid, Spain.*
[c]*Instituto de Ciencia y Tecnologia de Polimeros (ICTP), CSIC, Juan de la Cierva 3, 28006 Madrid, Spain.*
[d]*Departamento de Quimica Fisica, UPV-EHU, Apartado 644, 48080 Bilbao, Spain.*

*mjortiz@quim.ucm.es*

**Table of Contents** **Page**





PRIVILEGED DOCUMENT FOR REVIEW PURPOSES ONLY

**Synthesis of BODIPY 1-4.**

**Synthesis of 4,4-Difluoro-3,5-bis(*p*-formylphenyl)-8-(4-tolyl)-4-bora-3a,4a-diaza-*s*-indacene (2)**. Compound **2** was synthesized from **1**[1] in Suzuki cross-coupling reaction under both microwave and ultrasonic irradiation conditions.

Suzuki cross-coupling reaction under microwave irradiation: Compound **1** (87 mg, 0.25 mmol) was dissolved in DME (20 mL). *p*-Formylphenyl boronic acid (95 mg, 0.63 mmol) and $Na_2CO_3$ (79 mg, 0.75 mmol) were added in the presence of a catalytic amount of tetrakis(triphenylphosphine)palladium (8.6 mg, 0.008 mmol). The reaction mixture was stirred under microwave irradiation for 30 min at 150 ºC with a power of 200 W and 20 atm. After addition of $H_2O$ (50 mL), the organic layer was extracted with EtOAc, dried over $MgSO_4$, filtered and concentrated to dryness. Flash chromatography using hexane/EtOAc (8:2) afforded compound **2** (57 mg, 46% yield) as dark red crystals. M.p. 142.8-143.3 ºC; $^1$H NMR (300 MHz, $CDCl_3$): δ 9.97 (2 H, s, CHO), 7.95 (4 H, d, $J$ = 8.4 Hz, aromatic), 7.85 (4 H, d, $J$ = 8.4 Hz, aromatic), 7.43 (2 H, d, $J$ = 8.1 Hz, aromatic), 7.30 (2 H, d, $J$ = 8.1 Hz, aromatic), 6.93 (2 H, d, $J$ = 4.2 Hz, pyrrole), 6.63 (2 H, d, $J$ = 4.2 Hz, pyrrole), 2.43 (3 H, s, $CH_3$); $^{13}$C NMR (75 MHz, $CDCl_3$): δ 191.8 (CHO), 157.2 (C=N), 141.3, 138.2, 137.1, 136.5, 131.7, 131.1, 130.8, 130.1, 129.6, 129.3, 125.6, 121.3 (aromatic and C=C), 21.6 ($CH_3$); IR (neat): 2853, 2734 (CHO), 1699 (C=O), 1540 cm$^{-1}$; MS *m*/*z* (%): 490 ($M^+$, 61), 283 (100), 255 (95), 157 (47); HR-MS-ESI$^+$: calcd for ($C_{30}H_{21}BF_2N_2O_2$+$H^+$) 491.1700 found 491.1733; HPLC (reverse phase $C_{18}$ column, $CH_3CN$-$H_2O$ 9:1, flow rate 2 mL min$^{-1}$, $\lambda_{anal}$ 550 nm): $R_t$ = 1.94 min (98% purity).

Suzuki cross-coupling reaction under ultrasound irradiation: Compound **1** (48 mg, 0.14 mmol), 4-formylphenyl boronic acid (126 mg, 0.84 mmol), $Na_2CO_3$ (89 mg, 0.84 mmol) and a catalytic amount of tetrakis(triphenylphosphine)palladium (10 mg, 0.009 mmol) were stirred under ultrasound irradiation for 15 h at 75 ºC with a power of 720 W. Flash chromatography using hexane/EtOAc (8:2) afforded compound **2** (44 mg, 50% yield).

**Synthesis of 4,4-Difluoro-3,5-bis(*p*-2,2-dimetoxycarbonylvinylphenyl)-8-(4-tolyl)-4-bora-3a,4a-diaza-*s*-indacene (3)**. To a solution of $TiCl_4$ (1.0 M in $CH_2Cl_2$) (0.8 mL, 0.8 mmol) in 30 mL of dry THF at 0 ºC and under an argon atmosphere, were added



PRIVILEGED DOCUMENT FOR REVIEW PURPOSES ONLY

dropwise a solution of compound **2** (46 mg, 0.09 mmol) and dimethyl malonate (29 mg, 0.22 mmol) in dry THF. The reaction mixture was stirred at 0 ºC for 30 min and then, a solution of pyridine (0.12 mL, 1.4 mmol) in dry THF was added. The reaction was stirred at RT for 24 h before being quenched with $H_2O$ and extracted with ether. The combined organic phases were washed with $H_2O$, saturated $NaHCO_3$ solution and brine. The extract was dried over $MgSO_4$, filtered and concentrated to dryness. Flash chromatography using hexane/EtOAc (8:2) afforded compound **3** (34 mg, 47%) as dark blue crystals. M.p. 135.0-135.5 ºC; $^1$H NMR (300 MHz, $CDCl_3$): δ 7.93 (4 H, d, $J$ = 8.4 Hz, aromatic), 7.79 (2 H, s, 2 CH=C), 7.50 (6 H, m, aromatic), 7.37 (2 H, d, $J$ = 6.8 Hz, aromatic), 6.97 (2 H, d, $J$ = 4.3 Hz, pyrrole), 6.69 (2 H, d, $J$ = 4.3 Hz, pyrrole), 3.88 (12 H, s, 4 $CH_3O$), 2.53 (3 H, s, $CH_3$); $^{13}$C NMR (75 MHz, $CDCl_3$): 167.0 (COO), 164.5 (COO), 157.6 (C=N), 142.1, 134.6, 133.7, 131.3, 130.7, 129.9, 129.4, 129.1, 126.1, 121.1 (aromatic and CH=C), 52.8 ($CH_3O$), 52.7 ($CH_3O$), 21.5 ($CH_3$); IR (neat): 1732, 1682 (C=O), 1597 (C=C) cm$^{-1}$; MS *m*/*z* (%): 718 ($M^+$, 100), 59 (32); HR-MS-ESI$^+$: calcd for $C_{40}H_{33}BF_2N_2O_8$ $(M+NH_4)^+$ 736.2643 found 736.2642; HPLC (reverse phase $C_{18}$ column, $CH_3CN$-$H_2O$ 9:1, flow rate 2 mL min$^{-1}$, $\lambda_{anal}$ 500 nm): $R_t$ = 2.53 min (99% purity).

**Synthesis of 4,4-Difluoro-3,5-bis(*p*-2,2-dicyanovinylphenyl)-8-(4-tolyl)-4-bora-3a,4a-diaza-*s*-indacene (4)**. A mixture of compound **2** (52 mg, 0.09 mmol), malononitrile (14.5 mg, 0.22 mmol), *β*-alanine (6 mg, 0.06 mmol) and 6 mL acetic acid in 30 mL of toluene was refluxed for 24 h. The $H_2O$ generated during the condensation was azeotropically removed by using a Dean Stark trap. The mixture was then cooled, diluted with EtOAc, and washed with $H_2O$. The organic layer was dried over $MgSO_4$, filtered and concentrated to dryness. Flash chromatography using hexane/EtOAc (8:2) afforded compound **4** (13 mg, 21%) as dark blue crystals. M.p. 140.2-140.7 ºC; $^1$H NMR (500 MHz, $CDCl_3$): δ 7.98 (4 H, d, $J$ = 8.5 Hz, aromatic), 7.91 (4 H, d, $J$ = 8.5 Hz, aromatic), 7.70 (2 H, s, 2 CH=C), 7.44 (2 H, d, $J$ = 8.0 Hz, aromatic), 7.31 (2 H, d, $J$ = 8.0 Hz, aromatic), 6.96 (2 H, d, $J$ = 4.2 Hz, pyrrole), 6.68 (2 H, d, $J$ = 4.2 Hz, pyrrole), 2.44 (3 H, s, $CH_3$); $^{13}$C NMR (125 MHz, $CDCl_3$): 159.1 ($\underline{C}H=C(CN)_2$), 159.0 ($\underline{C}H=C(CN)_2$), 156.8 (C=N), 145.1, 141.9, 138.5, 137.9, 132.4, 131.9, 131.8, 131.5, 131.3, 131.1, 131.0, 130.8, 129.7, 128.7, 121.9 (aromatic), 114.1 (CN), 113.0 (CN), 83.6 (2 $(CN)_2\underline{C}=CH$), 21.5 ($CH_3$); IR (neat): 2229 (CN), 1538 cm$^{-1}$; MS *m*/*z* (%): 586



PRIVILEGED DOCUMENT FOR REVIEW PURPOSES ONLY

($M^+$, 100), 306 (40), 219 (28), 131 (41), 69 (79), 55 (51); HPLC (reverse phase $C_{18}$ column, $CH_3CN$-$H_2O$ 9:1, flow rate 2 mL $min^{-1}$, $\lambda_{anal}$ 570 nm): $R_t$ = 2.57 min (98% purity).

**Combustion Analysis Data**

| Compd | Molecular Formula | Calculated | | | Found | | |
|---|---|---|---|---|---|---|---|
| | | C | H | N | C | H | N |
| **1** | $C_{16}H_{11}BCl_2F_2N_2$ | 54.75 | 3.16 | 7.98 | 54.72 | 3.19 | 7.68 |
| **2** | $C_{30}H_{21}BF_2N_2O_2$ | 73.49 | 4.32 | 5.71 | 73.18 | 4.59 | 5.52 |
| **3** | $C_{40}H_{33}BF_2N_2O_8$ | 66.86 | 4.63 | 3.90 | 66.64 | 4.53 | 3.82 |
| **4** | $C_{36}H_{21}BF_2N_6$ | 73.74 | 3.61 | 14.33 | 73.57 | 3.53 | 14.18 |



PRIVILEGED DOCUMENT FOR REVIEW PURPOSES ONLY

## Electronic density maps of the HOMO and LUMO orbitals for dyes 2 and 3

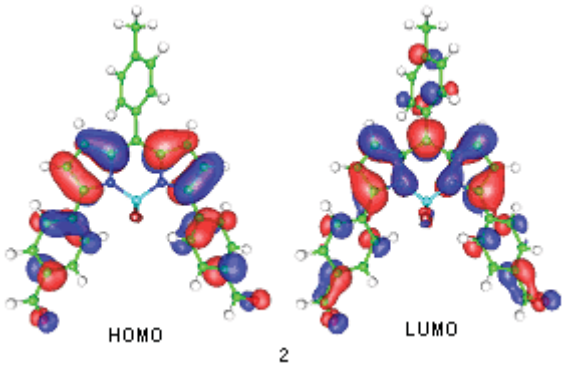


2

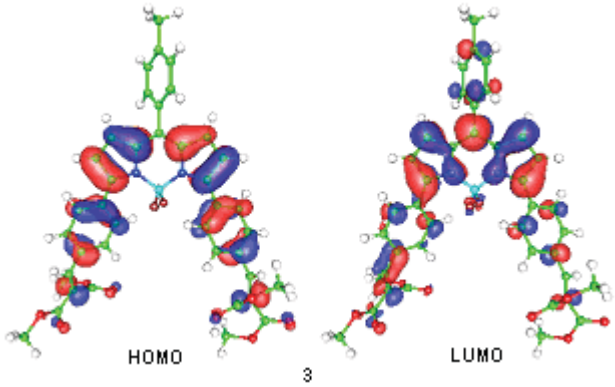


3



PRIVILEGED DOCUMENT FOR REVIEW PURPOSES ONLY

This journal is © The Owner Societies 2010

## References

**1** W. Qin, T. Rohand, M. Baruah, A. Stefan, M. Van der Auweraer, W. Dehaen, N. Boens, *Chem. Phys. Lett*. 2006, **420**, 562-568.



PRIVILEGED DOCUMENT FOR REVIEW PURPOSES ONLY

ADVANCED FUNCTIONAL MATERIALS
www.afm-journal.de



# Carboxylates versus Fluorines: Boosting the Emission Properties of Commercial BODIPYs in Liquid and Solid Media

*Gonzalo Durán-Sampedro, Antonia R. Agarrabeitia, Luis Cerdán, M. Eugenia Pérez-Ojeda, Angel Costela, Inmaculada García-Moreno,* Ixone Esnal, Jorge Bañuelos, Iñigo López Arbeloa, and María J. Ortiz**

**A new and facile strategy for the development of photonic materials is presented that fufills the conditions of being efficient, stable, and tunable laser emitters over the visible region of spectrum, with the possibility of being easily processable and cost-effective. This approach uses poly(methyl methacrylate) (PMMA) as a host for new dyes with improved efficiency and photostability synthesized. Using a simple protocol, fluorine atoms in the commercial (4,4-difluoro-4-bora-3a,4a-diaza-s-indacene) (*F*-BODIPY) by carboxylate groups. The new *O*-BODIPYs exhibit enhanced optical properties and laser behavior both in the liquid and solid phases compared to their commercial analogues. Lasing efficiencies up to 2.6 times higher than those recorded for the commercial dyes are registered with high photostabilities since the laser output remain at 80% of the initial value after 100 000 pump pulses in the same position of the sample at a repetition rate of 30 Hz; the corresponding commercial dye entirely loses its laser action after only 12 000 pump pulses. Distributed feedback laser emission is demonstrated with organic films incorporating new *O*-BODIPYs deposited onto quartz substrates engraved with appropriated periodical structures. These dyes exhibit laser thresholds up to two times lower than those of the corresponding parent dyes with lasing intensities up to one order of magnitude higher.**

## 1. Introduction

Presently, the development of photonic materials fulfilling the conditions of being efficient, stable and tunable emitters over the visible region of the electromagnetic spectrum, with the possibility of being easily processable, and cost-effective, is an area of active research driven by the wide range of possible practical applications. Over the last years, a vast amount of work has been carried out on materials engineering, designing and synthesizing semiconductor polymers and organic, hybrid and inorganic systems nano- and mesostructured, doped with organic dyes and quantum dots.[1] Nevertheless, despite this extensive activity up to now none of the obtained materials happens to meet all the above requirements at the same time.

Our research group has contributed greatly to this effort, developing solid state dye lasers (SSDL) both in bulk matrices and waveguiding thin films, on the basis of organic and/or hybrid materials doped with dyes with emission covering the spectral region from 550 up to 730 nm.[2] Albeit we have demonstrated lasing efficiencies as high as 60% in some particular case, the materials we have developed exhibit on average efficiencies of about 30% with photostabilities that being higher than those reported by other researchers, demand nonetheless an improvement in order to guarantee the implementation of these materials in practical applications. In addition, our work has shown that there is not an universal material that optimizes the lasing behavior of all the different dyes, but that a specific dye/host combination is needed for each chromophore, which is determined by the photophysical and photochemical chromophore's properties.

Here, we propose a new and facile strategy for the development of laser materials economically affordable with optimized emission properties in the visible region of the spectrum. This approach implies the utilization of a commercial polymer (poly(methyl methacrylate), PMMA) competitive in cost and easily processable, as host for dyes with improved efficiency and photostability. The chromophores are new derivatives of a

G. Durán-Sampedro, Prof. A. R. Agarrabeitia, Prof. M. J. Ortiz
Departamento de Química Orgánica I
Facultad de Ciencias Químicas
Universidad Complutense
28040, Madrid, Spain
E-mail: mjortiz@quim.ucm.es
Dr. L. Cerdán, M. E. Pérez-Ojeda, Prof. A. Costela, Prof. I. García-Moreno
Departamento de Sistemas de Baja Dimensionalidad
Superficies y Materia Condensada
Instituto Quimica-Fisica "Rocasolano"
C.S.I.C., Serrano 119, 28006 Madrid, Spain
E-mail: i.garcia-moreno@iqfr.csic.es
I. Esnal, Dr. J. Bañuelos, Prof. I. López Arbeloa
Departamento de Química Física
Facultad de Ciencias y Tecnología
Universidad del País Vasco-EHU
Apartado 644, E-48080-Bilbao, Spain

**DOI: 10.1002/adfm.201300198**


© 2013 WILEY-VCH Verlag GmbH & Co. KGaA, Weinheim

single family of commercial dyes obtained following a simple and general synthesis protocol, which exhibits high reaction yields. The selected family of dyes was that of the so-called *F*-BODIPYs (4,4-difluoro-4-bora-3a,4a-diaza-*s*-indacene), developed in the late 1980s and early 1990s by Boyer and co-workers, because they exhibit high fluorescence quantum yields, intense absorption, and tunable emission wavelength[3] as well as high chemical versatility to be functionalized.[2b,4] Currently, these dyes have numerous applications such as fluorescent probes in biological systems, photosensitizers for photodynamic therapy, and as materials for incorporation into electroluminescent devices.[5]

Among the numerous modifications in the BODIPY core, the replacement of one or both of the fluorine atoms in *F*-BODIPYs has become an active area. Thus, a wide variety of BODIPY dyes have been synthesized via fluorine displacement by alkyl or aryl derivatives (*C*-BODIPY),[5a–c,6] ethynyl groups (*E*-BODIPY),[5a–c,6e,7] and alkoxy or aryloxy derivatives (*O*-BODIPY),[5a–c,6c,6f–g,8] including *O*-chelated BODIPYs.[9] In addition, new types of boron modifications as borenium cations,[10] *CN*-BODIPY,[6a] *H*-BODIPY[10] and *Cl*-BODIPY,[6d,6g–h] have also been reported.

In one recent publication the authors evaluated the replacement of one or both of the fluorine atoms in 4,4-difluoro-1,3,5,7-tetramethyl-4-bora-3a,4a-diaza-*s*-indacene by acetoxy (AcO) groups in order to study the effect of an electron-withdrawing carboxylate on the boron atom in BODIPY, and they found that mono- and di-AcO substituted BODIPYs exhibited excellent fluorescence quantum yields and photostabilities.[11] Furthermore, the AcO modification on boron resulted in significantly improved water solubility, which is highly desirable for biological applications.[11] In another report about the stability of the BODIPY fluorophore under acidic and basic conditions, a 4,4-dichloroacetoxy BODIPY was formed when 4,4-dimetoxi-2,6-diethyl-1,3,5,7-tetramethyl-4-bora-3a,4a-diaza-*s*-indacene was mixed with an excess of dichloroacetic acid in $CH_2Cl_2$.[6f] However, no fluorescence study of this compound was explored.

Based on these observations, in the present work we report the synthesis and emission properties characterization of a library of *O*-BODIPYs **1**–**10** (**Figure 1**) from commercially available BODIPYs, in which two carboxylate (acetoxy or trifluoroacetoxy) groups are connected to the boron center in the place of the fluorine atoms. It is shown that these dyes are highly fluorescent and exhibit enhanced laser action with respect to their *F*-BODIPY analogues, both in liquid solution and solid phase. To investigate in depth the influence of the acetoxy substitutions on the BODIPY emission properties we have also synthesized, as a proof of concept, new *O*-BODIPYs via fluorine displacement by other carboxylate groups with different electronic character such as acryloyloxy, propioloyloxy, methoxy, or 4-nitrophenoxy groups (**11–14**).

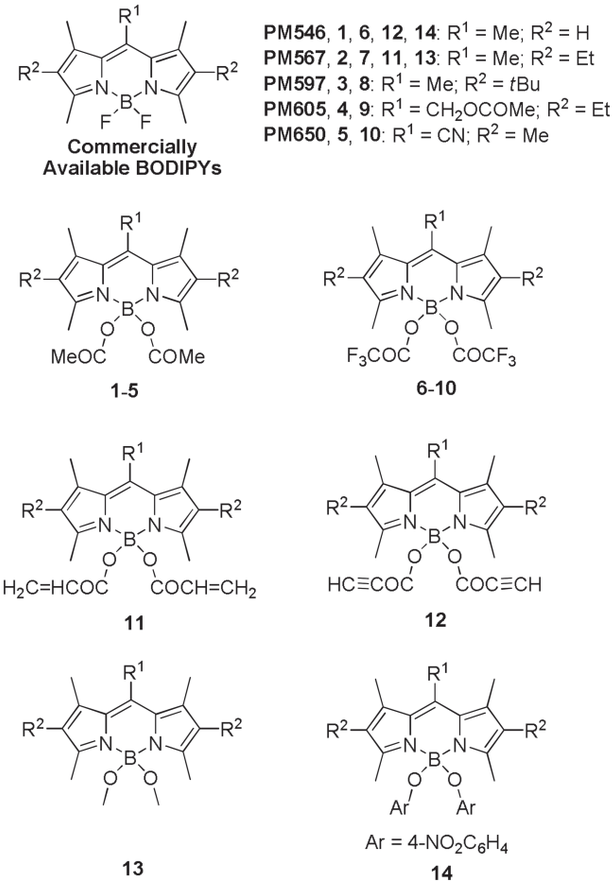


**Figure 1.** Molecular structures of dyes synthesized herein and their parent dyes.

## 2. Results and Discussion

### 2.1. Synthesis

BODIPY dyes **1**–**14** were successfully obtained from commercially available dyes[12] PM546, PM567, PM597, PM605 and PM650 through nucleophilic substitution reactions of fluorine atoms in the $BF_2$-group. Thus, 4,4-diacetoxy BODIPYs **1**,**2**,**4** and **5** were prepared with moderate yields by treating 20 equiv of TMSOAc with 1 equiv of PM546, PM567, PM605 or PM650, respectively, in presence of 3-4 equiv of $AlCl_3$ as Lewis acid (method A). In all these cases the monosubstituted derivative is not isolated. The dye **3** could not be synthesized by this method, so that an alternative procedure (method B) was used for their preparation involving the generation in situ of TMSOAc from acetic acid and TMSCl, in the absence of $AlCl_3$. Method B was also used in the synthesis of 4,4-bis(trifluoroacetoxy) BODIPYs **6**,**7** and **9** by adding of $TMSOCOCF_3$, generated in situ from trifluoroacetic acid and TMSCl, to the BODIPYs PM546, PM567 and PM605, respectively. 4,4-Bis(acryloyloxy) BODIPY **11** was prepared by reacting of PM567 with $TMSOCOCH=CH_2$, generated in situ from acrylic acid and TMSCl (method B), and this same method was used in the preparation of **12** from PM546 with propargylic acid and TMSCl. **Scheme 1** shows the synthesis of the dyes **2**,**7** and **11** from commercial BODIPY PM567.

Surprisingly, treatment of PM597 with $TMSOCOCF_3$ in 1,2-dichloroethane resulted in a mixture of **15** (10%) and **6** (22%) by loss of one or both *terc*butyl groups present in the starting compound (**Scheme 2**). Therefore, we were decided to develop an alternative procedure (method C). Thus, BODIPY**8**


© 2013 WILEY-VCH Verlag GmbH & Co. KGaA, Weinheim

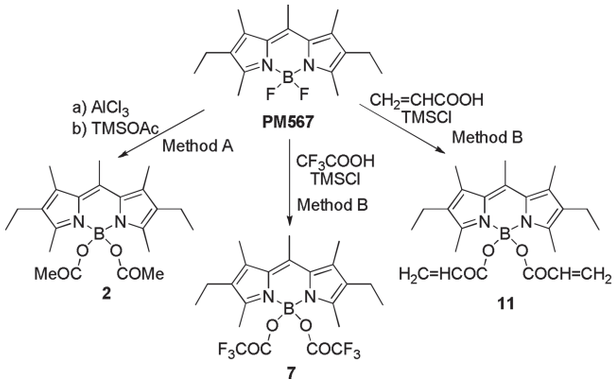


**Scheme 1.** Synthetic routes of derivatives **2**, **7**, and **11** from parent dye PM567.

was achieved by treatment of BODIPY PM597 with $AlCl_3$ in 1,2-dichloroethane and subsequent addition of $TMSOCOCF_3$, generated in situ as above (Scheme 2). Similarly, compound **10** was successfully obtained from PM650 with moderate yield.

In addition, two other analogues, 4,4-dimethoxy **13**,[6f] and 4,4-bis(4-nitrophenyl) **14** were synthetized according to procedure described in the literature or through the method A mentioned above.

### 2.2. Photophysical Properties

The selected commercial BODIPY laser dyes span a wide region of the visible spectrum; hence, the emission can be tuned from the green-yellow to the red as it is illustrated in **Figure 2**. The progressive bathochromic shift of the spectral bands is due to inductive donor effects of the alkyl groups at positions 2 and 6 (PM567 and PM597 vs PM546) or the electron withdrawing character of methylenacetoxy (PM605) or cyano (PM650) groups at position 8, which lead to a net stabilization of the LUMO molecular orbital.[4a] Except for the PM650 derivative, where a fluorescence quenching intramolecular charge transfer state is operative,[4a] these BODIPYs outstand by their bright and stable emission. For this reason, the set of derivatives from PM650 will be discussed later on.

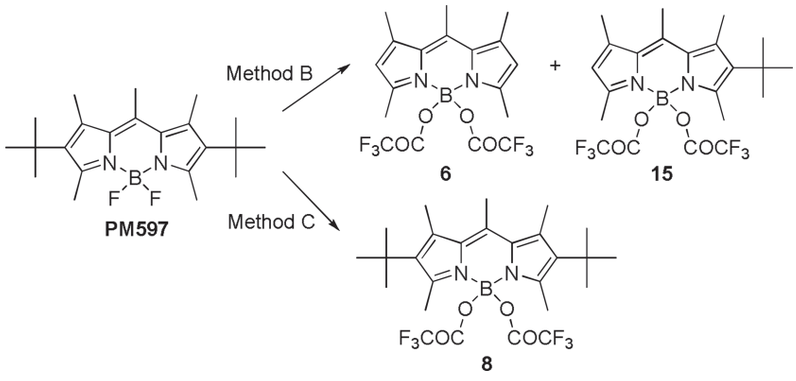


**Scheme 2.** Synthetic routes of derivatives **6**, **8**, and **15** from parent dye PM597.

At first sight, the replacement of the fluorine atoms by alcoxy or aryloxy derivatives should have minor influence on the photophysical properties of the chromophore since the $BF_2$ group does not take part in the delocalized $\pi$-system and acts as a bridge to keep the planarity and rigidity of the indacene core. For this reason, as is shown in **Table 1**, the positions of the spectral bands of the new *O*-BODIPYs are almost those of their respective *F*-BODIPY counterparts. Besides, the solvent effect on the photophysical properties follows the normal trends previously described for *F*-BODIPYs (Table S1–S4 in the Supporting Information); i.e., small hypsochromic spectral shifts with the solvent polarity and low dependency of the fluorescence quantum yield with the solvent characteristics.

Moreover, and as a common rule except for the dyes **13** and **14** that will be discussed later on, the fluorescence quantum yield and lifetime of the new *O*-BODIPYs increase with respect to the commercial ones, ameliorating the emission properties of the commercial *F*-BODIPYs, which were considered as a benchmark in fluorescence and laser behavior in the middle energetic part of the visible spectrum (Table 1).[6b,11] The enhancement of the emission properties of the *O*-BODIPYs depends on the electronic character of the carboxylate groups connected to the boron center in the following manner: while the fluorine displacement by the electron withdrawing acetoxy group (**1-4**) maintains or slightly improves the high fluorescent ability of the BODIPYs, a further increase in the electron acceptor character of the substituent via the inclusion of trifluoroacetoxy groups (**6–9**) leads to an even more significant improvement on the fluorescence quantum yield, which reaches nearly the unit in some solvents. Moreover, the same statement holds true for the attachment of other electron withdrawing carboxylate groups, such as acryloyloxy (**11**) or propioloyloxy (**12**).

It is noteworthy to remark the important improvement achieved in the fluorescent efficiency of PM597 through the replacement of fluorine atoms by carboxylate groups, thus, its fluorescence quantum yield increases from 0.43 up to 0.58 and 0.76 for its **3** and **8** *O*-BODIPYs derivatives, respectively (Table 1). The photophysical properties of the parent PM597 are controlled by the sterical hindrance induced by the *tert*-butyl groups at positions 2 and 6, which twists the planarity of the chromophore leading to an increase of both the internal conversion probability and the Stokes shift with respect to other planar BODIPYs such as, for instance, PM567. The **3** and **8** derivatives exhibit lower non-radiative rate constant than PM597, which could be related to the influence of the carboxylate group in the molecular geometry.

Overall, quantum mechanics calculations predict that the carboxylates are symmetrically disposed up and down the indacene core, both in the ground and excited state (**Figure 3**). Whereas the planarity of most of the *O*-BODIPYs remains the same regarding to their parent *F*-BODIPYs, a slight increase in the planarity is predicted for the PM597 derivatives since the dihedral angles, accounting for the pyrrole disposition with respect to the central ring, increase in around 3° in the excited state. However,


© 2013 WILEY-VCH Verlag GmbH & Co. KGaA, Weinheim

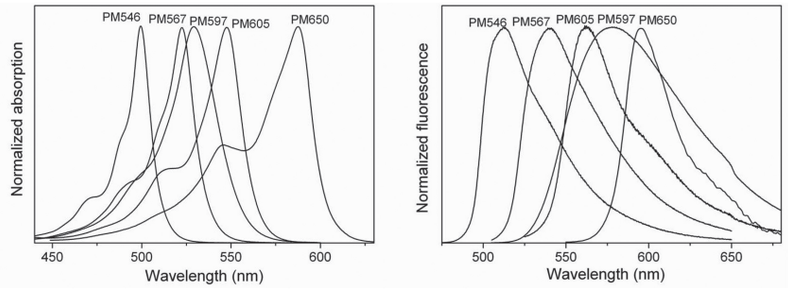


**Figure 2.** Normalized absorption and fluorescence spectra of commercial *F*-BODIPYs in a common solvent (cyclohexane).

such enhancement seems to be not strong enough to explain the important reduction observed in the internal conversion processes upon displacement of fluorine by carboxylate in the PM597 dye.

On the other hand, the photophysics behavior of the new *O*-BODIPY dyes depends strongly on the electronic character of the carboxylates substituent. Thus, the replacement of fluorine in PM567 by an electron donor methoxy group (**13**) has the opposite effect on the photophysical behavior with respect to that induced by electron withdrawing carboxylates since the presence of the–$OCH_3$ groups leads to a small reduction in the fluorescence quantum yield of the chromophore.

The opposite influence of the carboxy groups in the fluorescence quantum yield depending on their electronic character was analyzed in terms of the charge distribution in the corresponding excited states (Figure S1–S4 in the Supporting Information). In fact, the linkage of carboxylates to the boron atom implies a rearrangement in the chromophoric charge distribution, as it is reflected for PM567 in Figure 3. The acetoxy group behaves as an electron acceptor group (Hammet parameter, $\sigma_p = 0.31$).[13] Thus, its attachment to the boron leads to an increase of the positive charge in this last atom, while the oxygen acquires a negative charge much higher than of the fluorine in the corresponding *F*-BODIPYs. Such trend is more pronounced as the electron withdrawing character of the carboxylate substituent increases, for instance, in the case of the trifluoroacetoxy group ($\sigma_p$ = 0.46). However, the replacement of fluorine atoms by electron donor methoxy groups ($\sigma_p$ = –0.27) leads to the opposite behavior; the positive charge in the boron atom decrease and the oxygen results less negatively charged (Figure 3).

This rearrangement of the electronic charges around the boron atom determines the charge distribution of the chromophore (usually described as a cyclic cyanine). In fact, the negative charge of the aromatic nitrogen atoms decreases upon the presence of carboxylate groups (Figure 3 and Figure S1–S4 in the Supporting Information). This trend suggests that the electron lone pair is less localized in the nitrogen and tends to be more delocalized through the cyanine system. Furthermore, the charge alternation is softened, which is also indicative of higher delocalization. In addition, the aromatic character of the chromophore can be roughly evaluated by means of the Bond Length Alternation (BLA) parameter, which is defined as the difference between the average carbon-carbon bond lengths of alternative single and double bonds in the chromophoric $\pi$-system.[14] Regarding the corresponding values for

**Table 1.** Photophysical properties of commercial *F*-BODIPYs (PM546, PM567, PM597 and PM605) and their corresponding *O*-BODIPYs in cyclohexane; absorption ($\lambda_{ab}$) and fluorescence ($\lambda_{fl}$) wavelength at the maximum, Stokes shift ($\Delta\nu_{St}$), molar absorption at the maximum ($\varepsilon_{max}$), fluorescence quantum yield ($\varphi$) and lifetime ($\tau$), and radiative ($k_{fl}$) and non-radiative ($k_{nr}$) rate constants. The full photophysical data in several media are collected in the Supporting Information (Table S1–S4).

| | $\lambda_{ab}$ [nm] | $\varepsilon_{max}$ [$10^{-4}M^{-1}cm^{-1}$] | $\lambda_{fl}$ [nm] | $\Delta\nu_{St}$ [$cm^{-1}$] | $\varphi$ | $\tau$ [ns] | $k_{fl}$ [$10^{-8}$ $s^{-1}$] | $k_{nr}$ [$10^{-8}$ $s^{-1}$] |
|---|---|---|---|---|---|---|---|---|
| PM546 | 499.5 | 9.7 | 509.5 | 400 | 0.91 | 5.23 | 1.74 | 0.17 |
| **1** | 501.0 | 9.5 | 508.0 | 275 | 0.91 | 5.40 | 1.68 | 0.17 |
| **6** | 502.0 | 10.2 | 509.5 | 295 | 0.95 | 5.52 | 1.72 | 0.10 |
| **12** | 502.0 | 8.2 | 511.0 | 350 | 0.99 | 5.62 | 1.76 | 0.02 |
| **14** | 499.5 | 11.6 | 511.0 | 450 | 0.89 | 5.94 | 1.50 | 0.18 |
| PM567 | 522.5 | 9.3 | 537.0 | 520 | 0.88 | 5.60 | 1.57 | 0.21 |
| **2** | 522.0 | 8.5 | 537.0 | 535 | 0.84 | 5.71 | 1.47 | 0.28 |
| **7** | 525.5 | 7.8 | 541.5 | 565 | 0.94 | 6.25 | 1.50 | 0.10 |
| **11** | 523.5 | 8.1 | 541.0 | 620 | 0.90 | 5.98 | 1.50 | 0.17 |
| **13** | 522.0 | 8.0 | 539.5 | 620 | 0.81 | 5.64 | 1.44 | 0.34 |
| PM597 | 529.0 | 8.1 | 571.0 | 1395 | 0.43 | 3.91 | 1.10 | 1.46 |
| **3** | 530.5 | 7.0 | 573.0 | 1400 | 0.58 | 4.58 | 1.27 | 0.92 |
| **8** | 532.5 | 5.4 | 571.0 | 1265 | 0.76 | 5.99 | 1.27 | 0.40 |
| PM605 | 547.5 | 8.6 | 561.0 | 435 | 0.74 | 6.27 | 1.18 | 0.41 |
| **4** | 548.5 | 8.0 | 563.0 | 470 | 0.76 | 6.37 | 1.19 | 0.38 |
| **9** | 551.0 | 7.8 | 564.0 | 420 | 0.80 | 6.99 | 1.14 | 0.28 |


© 2013 WILEY-VCH Verlag GmbH & Co. KGaA, Weinheim

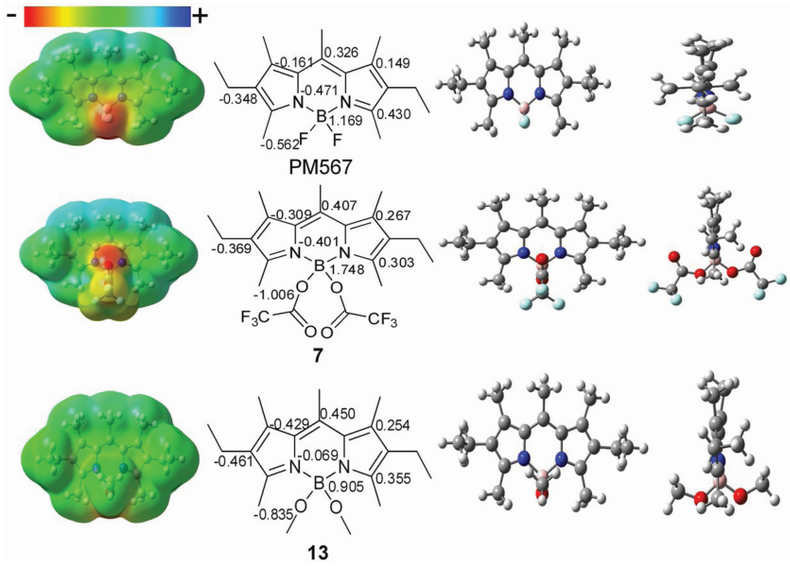


**Figure 3.** Electrostatic potential maps, ChelpG charge distribution (the corresponding data for the symmetrical counterpart in the chromophore are not included) in the excited state and the corresponding excited state geometries (at two different views) for PM567 dye and its derivatives **7** (trifluoroacetoxy) and **13** (methoxy). The electronic density distributions for all the derivatives are collected in Figure S1–S5 in the Supporting Information.

the *F*-BODIPYs and their respective *O*-BODIPYs, listed in Figure S1-S4 in the Supporting Information, the BLA parameter for dyes bearing acetoxy groups remains similar to that of their parent BODIPY (i.e., compound **2** (0.0227) vs PM567 (0.0222), in Figure S2, Supporting Information), but decreases for the derivatives bearing trifluoroacetoxy groups (i.e., compound **7** (0.0192) in Figure S2, Supporting Information). This tendency of the BLA parameter points out a higher aromaticity of the chromophore induced by the presence of electron withdrawing carboxylates, in good concordance with the enhancement of the fluorescence quantum yield experimentally observed. However, the presence of methoxy groups with electron donor character leads to an enhancement in the BLA parameter (0.0260 for compound **13** in Figure S2, Supporting Information) in line with the recorded decrease in the fluorescence efficiency. This evolution is even more pronounced for the PM597 derivatives **3** and **8** (0.0225, 0.0217 and 0.0181, respectively in Figure S3 in the Supporting Information). This fact, together with the slight increase in its planarity, could explain why this dye is the most sensitive system to the fluorine replacement by carboxylates.

On the other hand, aryloxy groups (4-nitrophenoxy) have also been attached to the boron of PM546 (compound **14**), replacing the fluorine atoms. While in apolar solvents the fluorescence efficiency keeps similar to the parent PM546 (Table 1), an increase in the polarity of the surrounding environment implies a progressive decrease of the fluorescence quantum yield, becoming almost negligible in the most polar solvents (from 0.89 in c-hexane to 0.05 in $F_3$-ethanol, Table S1 in the Supporting Information). At the same time, as is reflected in **Figure 4**, the fluorescence decay gets faster and eventually biexponential with a dominating lifetime of 0.18 ns, which reaches a contribution higher than 97% in $F_3$-ethanol (Table S1 in the Supporting Information). The presence of such fast lifetime indicates the presence of an extra non-radiative deactivation pathway, which is getting a higher influence as the solvent polarity increases and leads to very low fluorescence quantum yield in those media, in contrast to the rest of related *O*-BODIPYs where the fluorescence efficiency remains almost constant regardless of the solvent properties. Such fluorescence quenching in compound **14** and mainly in polar media suggests the activation of an intramolecular charge transfer (ICT) state from the BODIPY core to the nitro group, which is characterized by its strong electron withdrawing ability ($\sigma_p$ = 0.78). In fact, the presence of ICT states induced by the direct attachment of nitro groups to the BODIPY core have been previously reported.[15] Therefore, although we have concluded before that the replacement of fluorine by electron withdrawing alcoxys

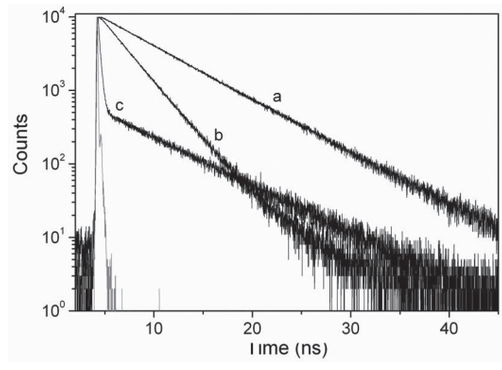


**Figure 4.** Fluorescence decay curves of compound **14** in a) cylochexane, b) methanol, and c) trifluoroethanol.


© 2013 WILEY-VCH Verlag GmbH & Co. KGaA, Weinheim

**Table 2.** Photophysical properties of the PM650 and its corresponding *O*-BODIPYs (**5** and **10**) in cyclohexane and methanol. The full photophysical data in several media are collected in Supporting Information (Table S5).

| | $\lambda_{ab}$ [nm] | $\varepsilon_{max}$ [$10^{-4}M^{-1}cm^{-1}$] | $\lambda_{fl}$ [nm] | $\Delta\nu_{St}$ [$cm^{-1}$] | $\varphi$ | $\tau$ [ns] | $k_{fl}$ [$10^{-8}$ $s^{-1}$] | $k_{nr}$ [$10^{-8}$ $s^{-1}$] |
|---|---|---|---|---|---|---|---|---|
| PM650 | | | | | | | | |
| c-hexane | 589.5 | 5.3 | 599.5 | 290 | 0.36 | 4.67 | 0.77 | 1.37 |
| Methanol | 587.5 | 4.1 | 609.0 | 605 | 0.060 | 1.29 | 0.46 | 7.29 |
| **5** | | | | | | | | |
| c-hexane | 588.5 | 4.5 | 600.5 | 340 | 0.39 | 5.19 | 0.75 | 1.17 |
| Methanol | 589.0 | 3.7 | 610.0 | 585 | 0.073 | 1.54[a)] | 0.47 | 6.02 |
| **10** | | | | | | | | |
| c-hexane | 591.0 | 3.8 | 599.0 | 225 | 0.47 | 5.99 | 0.78 | 0.88 |
| Methanol | 591.0 | 2.7 | 609.5 | 515 | 0.11 | 2.23 | 0.49 | 3.99 |

[a)]Main component (>98%) of the biexponential fit of the decay.

ameliorates the fluorescence of the dye, if the electron acceptor capacity of these substituent groups is too high, it could give rise to an extra non-radiative pathway (ICT), which quenches the fluorescence emission mainly in polar media.

Whereas all the above commented *F*-BODIPYs, were characterized by a bright fluorescence regardless of the media, the emission properties of the PM650 are limited by the presence of an ICT state induced by the electron withdrawing cyano group ($\sigma_p$ = 0.66) attached at position 8 (in a similar way to compound **14**).[4a] Thus, the fluorescence efficiency of this fluorophore, especially in polar solvents, is lower than that exhibited by other commercial BODIPYs (**Table 2** and Figure S5 in the Supporting Information). Furthermore, it was previously reported the unstability of PM650 dye in certain solvents (most of them characterized as electron donors)[16] since its solutions were completely bleached after some hours or days, depending of the solvent nature, as result of a specific interaction of the cyano group and those solvents. For this reason, all data listed for the derivatives of PM650 have been registered just after sample preparation.

In general, the replacement of the fluorine by carboxylates in PM650 follows the above commented trends for alkylated BODIPYs; thus, the presence of acetoxy (**5**) and mainly trifluoroacetoxy (**10**) improves the fluorescence capacity of the dye (Table 2). However, the presence of the quenching ICT process limits the fluorescence performance of these derivatives in polar media, and, although the fluorescence quantum yield is ameliorated it is still too low (around 0.1 in methanol in the best case, Table S5 in the Supporting Information) to achieve good laser performance. Whereas the presence of such quenching ICT state is harmful for the laser performance, it enables to apply PM650 and their O-BODIPYs derivatives as polarity sensors. The stabilization of the ICT state depends markedly of the solvent polarity, thus, the polarity of the surrounding environment can be monitored by means of the decrease in the fluorescence efficiency in such media or the change in the fluorescence colour (followed just with a naked eye) if the ICT state emits.[17] On the other hand, compounds **5** and **10** show also a lack of stability, even more pronounced than in the parent commercial PM650 and after few hours most of the solutions are bleached. Overall, the HOMO molecular orbital is stabilized when changing from *F*-BODIPYs to *O*-BODIPYs. Nevertheless, the carbon of the cyano gets a higher positive charge (from 0.463 in PM650 to 0.511 and 0.516 in compounds **5** and **10**, respectively, Figure S5 in theSupporting Information), whereas the nitrogen gets a slight higher negative charge. Therefore, the specific interaction of the cyano (through its carbon) with electron donor solvents should be more feasible in the *O*-BODIPYs, explaining its lower chemical stability than the reference PM650.

Summarizing, the replacement in the BODIPY core of fluorine atoms by electron withdrawing carboxylates is a good strategy to improve the fluorescence behavior, since it leads to more aromatic chromophores and, consequently, an enhanced laser action both in liquid and solid phase is expected.

### *2.2.1. pH-Dependence and Solubility Studies*

To accomplish the characterization of the new *O*-BODIPYs their pH stability and water solubility were carefully studied. As a proof of concept, we detail the results achieved for the derivatives **1** and **6** related to the behavior exhibited by their parent dye PM546, under otherwise identical experimental conditions. The pH-dependence experiments of the BODIPY fluorophores **1** and **6** reveals that theses BODIPYs were less degraded in acidic and basic conditions than the commercial PM546 (Figure S6 in the Supporting Information). This behavior could be understand taking into account that the $BF_2$ bridge is the most labile position of the BODIPY and, consequently, it could be the most suitable position to be attacked by acids or bases. It seems that the charge redistribution around the boron atom (increase of its positive charge) upon the replacement of fluorine by carboxylates strengthens the ionic B–N bond leading to dyes more robust to extreme pHs. In fact, theoretical calculations predict a slight decrease in such bond length (except for PM650) from ≈1.54 to 1.51 induced by the presence of trifluoroacetoxy groups.

Moreover, a solubility study was carried out with the BODIPYs above mentioned. The results obtained show that compounds **1** and **6** are more soluble in water than the parent


© 2013 WILEY-VCH Verlag GmbH & Co. KGaA, Weinheim

**Table 3** Lasing properties of commercial *F*-BODIPYs and their new derivatives at the dye concentrations that optimize their laser action in ethyl acetate solutions. [c]: dye concentration; Eff: lasing efficiency (ratio between the energy of the laser output and the pump energy incident on the sample surface); $\lambda_l$: peak wavelength of the laser emission; Intensity of the laser-induced fluorescence emission ($I_n$) after *n* pump pulses for dyes in ethyl acetate solution $\lambda_{exc}$: pumping wavelength.

| | $\lambda_{exc}$ = 355 nm, 5 Hz | | | | | $\lambda_{exc}$ = 532 nm, 10 Hz | | | | | | | | | | | | | |
|---|---|---|---|---|---|---|---|---|---|---|---|---|---|---|---|---|---|---|---|
| | PM546 | **1** | **6** | **12** | **14** | PM567 | **2** | **7** | **11** | **13** | PM597 | **3** | **8** | PM605 | **4** | **9** | PM650 | **5** | **10** |
| [c]/mM | 2.5 | 3.8 | 7.5 | 2.5 | 2.5 | 1.5 | 1.5 | 0.6 | 1.5 | 9 | 0.5 | 0.9 | 0.9 | 0.6 | 0.6 | 0.6 | 0.9 | 1.4 | 0.5 |
| Eff (%) | 23 | 43 | 53 | 59 | 16 | 48 | 63 | 68 | 65 | 59 | 53 | 59 | 65 | 55 | 60 | 67 | 35 | 50 | 55 |
| $\lambda_l$/nm | 541 | 544 | 541 | 542 | 541 | 566 | 566 | 562 | 563 | 565 | 588 | 586 | 587 | 586 | 591 | 592 | 657 | 655 | 661 |
| $I_n$ (%) [a] | 60 | 100 | 100 | 100 | 50 | 17 | 98 | 100 | 90 | 30 | 85 | 100 | 100 | 20 | 65 | 91 | 80 | 30 | 50 |
| n/1000 | 100 | 100 | 100 | 100 | 100 | 100 | 100 | 100 | 100 | 100 | 100 | 100 | 100 | 40 | 70 | 100 | 100 | 50 | 70 |

[a] $I_n$ (%) = 100 ($I_n/I_0$), with $I_0$ being the initial intensity.

PM546. Thus, while the PM546 is hydrophobic and it is not soluble in water, the dyes **1** and **6** exhibit 20 and 35 μg/mL, respectively, solubility in water, which is an important additional advantage of *O*-BODIPYs, in terms of their biological applications.

## 2.3. Lasing Properties

### *2.3.1. Liquid Phase*

According to the absorption properties of the new BODIPYs (Table 1 and 2), their lasing properties were studied under pumping at 355 nm (dyes **1**,**6**,**12** and **14**, analogues of PM546) and 532 nm (all the other derivatives). Under our experimental conditions (transversal excitation and strong focusing of the incoming pump radiation) the concentration of the dyes should be in the millimolar range, to ensure total absorption of the pump radiation within the first millimeter at most of the solution, in order to obtain an emitted beam with near-circular cross-section and optimize the lasing efficiency (ratio between the energy of the dye laser output and the pump energy incident on the sample surface). To determine the dye concentration that optimizes the laser emission for the different derivatives, first the dependence of their laser emission on the corresponding dye concentrations was analyzed in ethyl acetate by varying the optical densities from 4 to 40, while keeping all the other experimental parameters constant. **Table 3** summarizes the concentrations that produced the highest lasing efficiencies in each case as well as the corresponding lasing wavelengths. It can be appreciated in Table 3 that in all cases the lasing efficiency of the derivatives is higher than that of the commercial parent dye, with the highest lasing efficiencies being obtained in the derivatives incorporating trifluoroacetoxy groups (**6–10**).

Following the photophysical analysis, the actual effect of the solvent on the dye laser action was analyzed in solutions of polar protic and polar aprotic solvents. Although the photophysical studies showed that the new derivatives exhibited their highest fluorescence capacity when dissolved in apolar solvent*c*-hexane, the low solubility of the synthesized *O*-BODIPYs in this solvent prevented preparation of solutions of the dyes in *c*-hexane at the concentration required for laser experiments under the pumping conditions selected in the present work. In all the other solvents, each dye was dissolved at the concentration that was found to optimize its emission in ethyl acetate (that is, the concentrations tabulated in Table 3).

In **Table 4** are presented the lasing properties of the new *O*-BODIPYs as a function of the solvent, together with those of the corresponding parent dyes. The lasing behavior of the new compounds is in good agreement with their photophysical properties (Table S1–S5 in the Supporting Information). In the acetoxy derivatives **1–4** the photophysics changes little in the different solvents and so does the lasing efficiency, which nevertheless improves in general that of the parent dyes, in accordance with the improvement of the fluorescence capacity of those derivatives with respect to the parent dyes.

As discussed in the previous section, the inclusion of the trifluoroacetoxy groups in the BODIPYs further enhanced the fluorescence capacity of the parent dyes. Correspondingly, derivatives **6–9** exhibit consistently higher lasing efficiencies

**Table 4.** Lasing efficiencies for the commercial *F*-BODIPY dyes and their new derivatives in different solvents. $\lambda_{exc}$: pumping wavelength.

| Solvent | $\lambda_{exc}$ = 355 nm | | | | | $\lambda_{exc}$ = 532 nm | | | | | | | | | | | | | |
|---|---|---|---|---|---|---|---|---|---|---|---|---|---|---|---|---|---|---|---|
| | PM546 | **1** | **6** | **12** | **14** | PM567 | **2** | **7** | **11** | **13** | PM597 | **3** | **8** | PM605 | **4** | **9** | PM650 | **5** | **10** |
| $F_3$-ethanol[a] | | 39 | 47 | 40 | | 30 | 47 | 49 | 45 | 39 | 56 | 54 | 58 | 51 | 57 | 61 | 27 | 33 | 38 |
| Methanol | | 45 | 58 | 49 | 5 | 34 | 54 | 58 | 53 | 48 | 54 | 52 | 60 | 55 | 58 | 60 | 12 | 27 | 31 |
| Ethanol | | 44 | 56 | 50 | 7 | 36 | 52 | 59 | 57 | 51 | 51 | 52 | 59 | 56 | 60 | 64 | | 21 | 25 |
| Ethyl acetate | 23 | 43 | 53 | 59 | 16 | 48 | 63 | 68 | 61 | 59 | 53 | 59 | 65 | 55 | 60 | 67 | 35 | 50 | 55 |
| Acetone | 14 | 37 | | 52 | 14 | 36 | 55 | 57 | 60 | 55 | 50 | 53 | 60 | 57 | 59 | 65 | 31 | 44 | 49 |

[a] $F_3$-ethanol: 2,2,2,-trifluoroethanol


© 2013 WILEY-VCH Verlag GmbH & Co. KGaA, Weinheim

than compounds **1**–**4**. In the compounds **7**–**9**, the highest lasing efficiencies (an impressive 65-67%) are obtained in ethyl acetate, which is the solvent where those dyes have the highest quantum yield and radiative rate constant as well as the lowest nonradiative rate constant. In compound **6**, the highest quantum yield and radiative rate constant and the lowest nonradiative rate constant are achieved in methanol, and thus it is in this solvent where the highest lasing efficiency (58%) is observed.

The derivatives of PM567 with acryloyloxy (**11**) and methoxy (**13)** groups do not improve the lasing efficiencies demonstrated with the trifluoroacetoxy derivative **7**, in accordance with their lower fluorescence quantum yields and higher nonradiative rate constants, albeit compound **11** improves slightly de emission efficiency of derivative **2**, also in agreement with the slightly better photophysical parameters of**11** as compared with **2** (Table S2 in the Supporting Information). In the group of dyes pumped at 355 nm, compound **12**, derivative of PM546 incorporating propiloyloxy groups, exhibits much higher lasing efficiencies than the parent dye and the other derivatives, with the exception of compound **6**, which has better laser emission in polar protic solvents. This behavior reflects the photophysical properties: as can be seen in Table S1 in the Supporting Information, in polar protic solvents **6** has higher quantum yields and lower nonradiative constants than **12**, but the contrary happens in polar aprotic solvents. Compound **14**, on the other hand, is the one with the poorest lasing performance as a result of the fluorescence quenching processes discussed above, when considering the photophysical properties of the new derivatives.

Regarding dye PM650 and its derivatives **5** and **10**, as we have discussed in the previous section their emission properties are limited by the presence of an ICT state, which results in low fluorescence quantum yields in polar media. As a result their lasing efficiencies are lower than those of the other compounds pumped at 532 nm. As seen in Table S5 (Supporting Information), the fluorescence performance of these dyes is somewhat improved in polar aprotic solvents, which correlates with their higher lasing efficiencies in ethyl acetate and acetone, as compared with those observed in $F_3$-ethanol, methanol and ethanol.

An important parameter for any practical application of the dye lasers is their lasing photostability under repeated pumping. In Table 3 are collected data on the decrease of the laser-induced fluorescence intensity, under transversal excitation of capillary containing dye solutions in ethyl acetate (see Experimental Section), after a given number *n* of pump pulses, for both the commercial dyes and their derivatives synthesized in the present work. Dye PM546 and its derivatives **1** and **6** were pumped at 355 nm and 5 Hz repetition rate. All the other dyes were pumped at 532 nm and 10 Hz repetition rate. The pump energy was in all cases 5 mJ.

It has to be remarked that all the newly synthesized *O*-BODIPYs are more photostable than the corresponding *F*-BODIPYs, with the exception of **14** and derivatives of PM650, which lower stability reflects their lower chemical stability, due to the mechanism discussed above, when analyzing their photophysical properties.

### *2.3.2. Bulk Solid State*

The excellent laser performance exhibited by the new dyes in liquid solution led us to explore their behavior as photonic materials, either in bulk as SSDLs or incorporated into waveguiding structures. To this end, as a proof of concept, we chose dye PM567 as reference with which to compare the laser behavior of derivatives **2** and **7** under identical experimental conditions. As matrix material we chose PMMA because it mimics ethyl acetate, the solvent in which those dyes exhibited the highest lasing efficiencies in liquid solution (Table 4). The dye concentration in the matrix was that which optimized the lasing efficiency in ethyl acetate (Table 3). We have seen in previous work[18] that the covalent bonding of the chromophore to the polymeric matrix improves significantly the dye photostability because new channels are open to dissipate the excess energy released to the medium as heat. To check out the effect of this mechanism in the present case, PMMA matrices were also prepared incorporating dye **11**, which is an *O*-derivative of PM567 with acrylic bonds that allow the covalent bonding of the dye to the polymeric chains.

**Table 5.** Lasing properties of dyes incorporated in solid PMMA matrices. Eff: lasing efficiency; $\lambda_l$: peak laser emission wavelength; $I_n$(%): intensity of the laser output after *n* pump pulses in the same position of the sample, $I_n(\%) = 100(I_n/I_0)$, where $I_0$ is the initial intensity.

| Dye | Eff [%] | $\lambda_l$ [nm] | $I_{100000}$ [%][a)] | $I_n$ [%][b)] | *n* |
|---|---|---|---|---|---|
| PM567 | 34 | 566 | 30 | 0 | 12000 |
| **2** | 49 | 568 | 80 | 0 | 40000 |
| **7** | 56 | 568 | 100 | 80 | 100000 |
| **11** | 47 | 567 | 100 | 0 | 100000 |

[a)]Pumping at 10 Hz; [b)]Pumping at 30 Hz.

**Table 5** collects the lasing performance of the different dyes. The lasing efficiencies of the new materials based on PMMA doped with*O*-BODIPYs enhance significantly those recorded with the commercial PM567 and correlate with those obtained in liquid solution, with the efficiency of dye **7** being the highest and being maintained the relationship: Eff (PM567) < Eff (**11**) < Eff (**2**) < Eff (**7**). These efficiencies are lower than those obtained in liquid solution, probably due to the fact that the finishing of the surface of the solid samples relevant to the laser operation was not laser-grade, so that higher efficiencies are to be expected with laser-grade surfaces.

To assess the photostability of the new materials we followed the evolution of their laser emission under repeated pumping in the same position of the sample at 10 Hz repetition rate. All the three derivatives demonstrated a much higher photostability than the parent dye PM567 (Table 5). After 100 000 pump pulses, the emission of compound **2** dropped by 20%, but the lasing intensity of both derivatives **7** and **11** remained constant at the initial level. Trying to distinguish more clearly the photostability behavior of the different dyes, we decided to subject the dyes to more drastic pumping conditions. We had demonstrated in previous work that the accumulation of heat into polymeric SSDLs increases significantly with the pumping repetition rate, resulting in a decrease in the lasing photostability.[19] Consequently, we proceeded to pump the SSDLs at 30 Hz repetition rate. The results are collected in the last two columns of Table 5. To facilitate comparison of the results obtained in a more intuitive way, the actual evolution of the


© 2013 WILEY-VCH Verlag GmbH & Co. KGaA, Weinheim

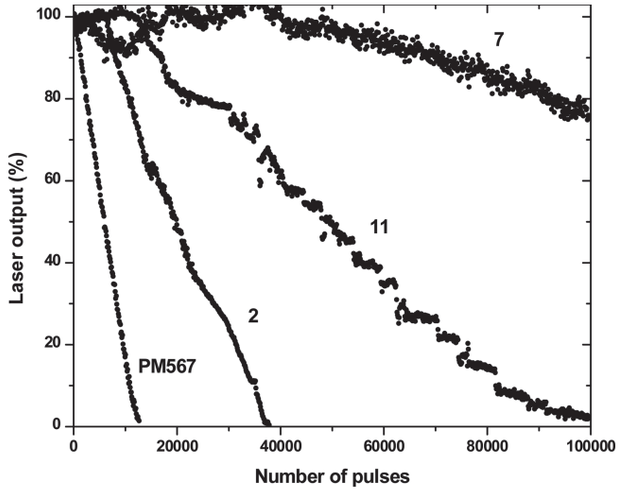


**Figure 5.** Normalized laser output as a function of the number of pump pulses in the same position of the sample of parent dye PM567 and its derivatives **2**, **7** and **11**. Pump energy and repetition rate: 3.5 mJ pulse$^{-1}$ and 30 Hz, respectively.

laser emission of the different dyes at 30 Hz repetition rate is showed in **Figure 5**.

Compound **11** being covalently bonded to the polymeric chains improves the heat dissipation and, consequently, the lasing photostability with respect to dye **2**, which is merely solved into the matrix. However, the highest photostability is achieved with PMMA doped with dye **7**, with a drop in its emission intensity of just 20% after 100,000 pump pulses. These unexpected results can be understood in the light of the photophysics of compounds **7** and **11** (Table S2 in the Supporting Information). While the fluorescence quantum yield and radiative rate constant of compound **7** in ethyl acetate are just somewhat higher than those of compound **11**, the nonradiative rate constant of **7** is much lower than that of **11**. That means that the energy not converted into laser emission, which appears in the medium as heat, is much lower in **7** than in **11**, which more than compensates the higher dissipation rates in the matrix doped with the covalently bonded dye **11**.

### *2.3.3. Thin Films*

In the previous section, we have studied the laser properties of the newly synthesized dyes operated as conventional two-mirror lasers. Nevertheless, there has been significant work over the last few years exploring the development of organic thin film lasers based on dye doped polymers because of their potential applications as coherent light sources suitable for integration in optoelectronic and disposable spectroscopic and sensing devices.[1d] In order to explore the suitability of the newly synthesized dyes for integrated devices, we implemented distributed feedback (DFB) lasers, the most common resonator type for organic thin film lasers.[1a]

In DFB lasers, light propagating in a waveguide mode of the organic film is Bragg-scattered by a wavelength-scale periodic modulation of the refractive index in the film, substrate, or both, to create a diffracted wave propagating in the counter propagating waveguide mode. The propagating and counter propagating modes will destructively interfere with each other at a given wavelength to create a photonic stopband at which light propagation is forbidden. This optical gap, whose width depends on the refractive index contrast of the periodic modulation, is centered at a wavelength $\lambda_B$, satisfying the Bragg condition, $m\lambda_B = 2\, n_{eff}\Lambda$, where $m$ is an integer that represents the order of the diffraction, $n_{eff}$ is the effective refractive index of the waveguide, which represents a geometrical average of the refractive indices of the three layers of the waveguide, and $\Lambda$ is the period of the modulation.[1a] Working with the second order $m = 2$, the resonant wavelength is equal to $n_{eff}\Lambda$, and light is diffracted out of the surface of the film perpendicular to the plane of the waveguide. That is, the second-order structure provides a surface-emitted output coupling of the laser light via first-order diffraction while providing in-plane feedback via second-order diffraction (Figure S7a in Supporting Information).

The fundamental transverse electric ($TE_0$) propagating mode in a waveguide 1 μm thick with refractive index 1.4900 (PMMA), deposited onto a quartz substrate ($n = 1.456$), experiences an effective refractive index $n_{eff} \approx 1.477$, as calculated with a waveguide mode solver,[20] in the range 550-600 nm. Hence, if dye doped PMMA thin films are deposited on substrates with modulation periods $\Lambda_1 = 386$ nm and $\Lambda_2 = 400$ nm, second-order photonic stopbands centered at $\lambda_{B1} \approx 570$ nm and $\lambda_{B2} \approx 590$ nm, respectively, will be obtained. As $\lambda_{B1}$ and $\lambda_{B2}$ match the emission windows of the PM567 and PM597 families, respectively, we choose these dyes to implement the DFB lasers.

Two compounds of each family were chosen, the commercial compounds as the references and the derivatives with trifluoroacetoxy groups (compounds **7** and **8**), which showed the best laser performances both in liquid and bulk media. In order to better compare the laser performances, the dye concentrations were selected to render similar absorbance (Abs ≈ 0.055) at the pumping wavelength (532 nm), enough to provide the needed gain while avoiding the undesirable effects of dye aggregation.

In agreement with the estimated Bragg resonant wavelengths, when the devices were pumped well above threshold DFB laser emission was obtained around 570 nm, for samples with PM567 and **7**, and around 590 nm, for samples with PM597 and **8** (**Figure 6**a).

Explicitly, the laser peaks were centered at 569.3 nm for PM567, 571.6 nm for **7**, 589.3 nm for PM597 and 590.4 nm for **8**. The differences in the emission wavelengths between each group of samples have its origin in the slight differences in the sample thicknesses, which modifies the effective refractive index$n_{eff}$ and, in turn, the resonant wavelength.

Figure 6b,c show the dependence of the DFB emission intensity on the pump intensity for the samples doped with PM567 derivatives and PM597 derivatives, respectively. At low pump intensities there is just fluorescence and the emission grows linearly. Once the threshold is reached, the intensity of the emission grows superlinearly with the pump intensity, and the emission linewidth collapses to a mere 0.2 nm (Figure 6a). From the data in Figure 6b it is seen that the sample with **7** not only has a lower laser threshold than that with PM567 (1.7 against 2.5 kW cm$^{-2}$) but presents an output intensity up to an order of magnitude higher, in agreement with the results


© 2013 WILEY-VCH Verlag GmbH & Co. KGaA, Weinheim

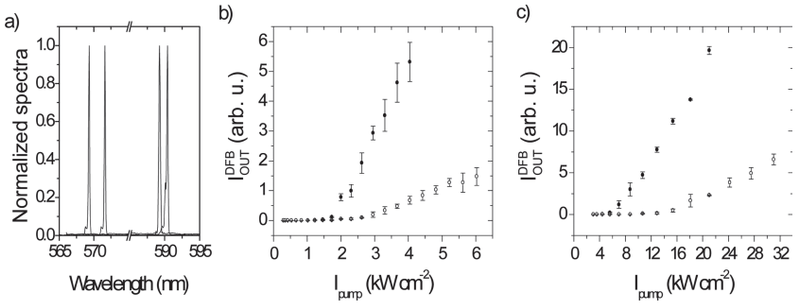


**Figure 6.** a) From left to right, DFB laser spectra of commercial PM567, derivative **7**, commercial PM597 and derivative **8** doped in PMMA. b) Output intensity as a function of pump intensity for commercial PM567 35 mM (hollow circles) and derivative **7** 25 mM (filled circles) doped in PMMA. c) Output intensity as a function of pump intensity for commercial PM597 25 mM (hollow circles) and derivative **8** 30 mM (filled circles) doped in PMMA.

observed in bulk media. Analogous results are obtained when comparing the samples with **8** and PM597 (Figure 6c). In this case the sample with **8** presents a laser threshold of 6 kW cm$^{-2}$, to be compared to the 14.5 kW cm$^{-2}$ needed to excite laser emission in the sample with PM597.

## 3. Experimental Section

BODIPY dyes PM546, PM567, PM597, PM605 and PM650 were purchased from Lasing, S. A. and used as received.[12] New BODIPYs **1–12** and **14** were synthesized by modification of methods previously described.[8a,11] Compound **13**[6f] was synthetized according to procedure described in the literature.

Characterization of the new dyes as well as quantum mechanical simulations, preparation of laser samples, methods followed to analyze the photophysical and laser properties in liquid and solid phase and procedures to pH and solubility studies are described in detail in the Supporting Information.

## 4. Conclusions

The development of *O*-BODIPYs from commercial dyes is a successful strategy to obtain optimized laser dyes. The replacement of the fluorines by electron acceptor carboxylate groups ameliorate the fluorescence efficiency, reaching in some cases values around 100%; hence, these novel BODIPYs would be promising candidates to achieve tunable lasers at different regions of the visible with improved performance. To confirm this possibility, the lasing performance of the new derivatives in liquid solution and solid state was assessed and compared with that of the parent dyes.

The lasing efficiencies of the new compounds correlate well with their photophysical properties: all the derivatives exhibit a lasing efficiency higher than that of the commercial parent dye (except **14**, derivative of PM546 with aryloxy groups, in agreement with its lower fluorescence capability), with the highest lasing efficiencies being obtained in the derivatives incorporating trifluoroacetoxy groups.

To assess the laser behavior of the new dyes in solid state, dye PM567 and its derivatives **2**, **7**, and **11** were incorporated into solid matrices of PMMA. The lasing efficiencies of the *O*-BODIPYs were in all cases higher than that of the parent dye, and correlate with those obtained in liquid solution. Thus, the highest efficiency, 56%, was obtained with compound **7**. Compound **7** also exhibited a very high lasing stability, with the laser emission remaining at 80% of its initial value after 100 000 pump pulses in the same position of the sample at 30 Hz repetition rate.

DFB laser emission was demonstrated with organic films incorporating trifluoroacetoxy derivatives **7** and **8**, deposited onto quartz substrates engraved with appropriated periodical structures. Both derivatives exhibited laser thresholds lower than those of the parent dyes as well lasing intensities up to one order of magnitude higher. In view of the easy synthetic assembly, and the large number of described BODIPY laser dyes, we are confident that this powerful approach can be extended to other dyes of this family, furthering their practical application in optical and sensing fields.[21]

## Supporting Information

Supporting Information is available from the Wiley Online Library or from the author.

## Acknowledgements

This work was supported by Projects MAT2010-20646-C04-01, MAT2010-20646-C04-02, MAT2010-20646-C04-04 and TRACE 2009-0144 of the Spanish Ministerio de Ciencia e Innovación (MICINN), actually Spanish Ministerio de Economia y Competitividad (MINECO). I.E. thanks the Gobierno Vasco for a predoctoral contract IT339-10. L.C., M.E.P.-O. and G.D.-S. thank MICINN for a predoctoral scholarship (FPI, cofinanced by Fondo Social Europeo).

Received: January 17, 2013
Revised: February 6, 2013
Published online: March 26, 2013

[1] a) I. D. W. Samuel, G. A. Turnbull, *Chem. Rev.* **2007**, *107*, 1272; b) H. Zou, S. Wu, J. Shen, *Chem. Rev.* **2008**, *108*, 3893; c) D. Bera, L. Qian, T.-K. Tseng, P. H. Holloway, *Materials* **2010**, *3*, 2260; d) C. Grivas, M. Pollnau, *Laser Photonics Rev.* **2012**, *6*, 419.

[2] a) A. Costela, I. García-Moreno, R. Sastre, in *Tunable Laser Applications*, (Ed: F. J. Duarte), CRC Press, Boca Raton, FL**2009**, Ch. *3*, pp 97–120; b) O. García, L. Garrido, R. Sastre, A. Costela, I. García-Moreno, *Adv. Funct. Mater.* **2008**, *18*, 2017; c) O. García, R. Sastre, I. García-Moreno, V. Martín, A. Costela, *J. Phys. Chem. C* **2008**, *112*, 14710; d) I. García-Moreno, A. Costela, V. Martín, M. Pintado-Sierra, R. Sastre, *Adv. Funct. Mater.* **2009**, *19*, 2547; e) A. Costela, I. García-Moreno, L. Cerdán, V. Martín, O. García, R. Sastre, *Adv. Mater.* **2009**, *21*, 4163; f) L. Cerdán, A. Costela, I. García-Moreno, O. García, R. Sastre, D. Muñoz, J. de Abajo, *Macromol. Chem. Phys* **2009**, *210*, 1624; g) R. Sastre, V. Martín, L. Garrido, J. L. Chiara, B. Trastoy, O. García, A. Costela, I. García-Moreno, *Adv. Funct. Mater.* **2009**, *19*, 3307; h) E. Enciso, A. Costela,


© 2013 WILEY-VCH Verlag GmbH & Co. KGaA, Weinheim

I. García-Moreno, V. Martín, R. Sastre, *Langmuir* **2010**, *26*, 6154; i) L. Cerdán, A. Costela, I. García-Moreno, O. García, R. Sastre, *Opt. Express* **2010**, *18*, 10247; j) V. Martín, J. Bañuelos, E. Enciso, I. López Arbeloa, A. Costela, I. García-Moreno, *J. Phys. Chem. C* **2011**, *115*, 3926; k) M. E. Pérez-Ojeda, C. Thivierge, V. Martín, A. Costela, K. Burgess, I. García-Moreno, *Opt. Mater. Express* **2011**, *1*, 243; l) M. E. Pérez-Ojeda, B. Trastoy, I. López Arbeloa, J. Bañuelos, A. Costela, I. García-Moreno, J. L. Chiara, *Chem. Eur. J* **2011**, *17*, 13258; m) L. Cerdán, A. Costela, G. Durán-Sampedro, I. García-Moreno, M. Calle, J. de Abajo, G. A. Turnbull, *J. Mater. Chem.* **2012**, *22*, 8938; n) L. Cerdán, A. Costela, I. García-Moreno, *Org. Electron.* **2012**, *13*, 1463; o) L. Cerdán, A. Costela, I. García-Moreno, J. Bañuelos, I. López Arbeloa, *Laser Phys. Lett.* **2012**, *9*, 426; p) L. Cerdán, E. Enciso, V. Martín, J. Bañuelos, I. López Arbeloa, A. Costela, I. García-Moreno, *Nat. Photonics* **2012**, *6*, 621; q) L. Cerdán, A. Costela, G. Durán-Sampedro, I. García-Moreno, *Appl. Phys. B* **2012**, *108*, 839.

[3] a) T. G. Pavlopoulos, M. Shah, J. H. Boyer, *Appl. Opt.* **1988**, *27*, 4998; b) M. Shah, K. Thangaraj, M. L. Soong, L. T. Wolford, J. H. Boyer, I. R. Politzer, T. G. Pavlopoulos, *Heteroatom. Chem.* **1990**, *1*, 389; c) T. G. Pavlopoulos, J. H. Boyer, M. Shah, K. Thangaraj, M. L. Soong, *Appl. Opt.* **1990**, *29*, 3885; d) T. G. Pavlopoulos, J. H. Boyer, K. Thangaraj, G. Sathyamoorthi, M. P. Shah, M. L. Soong, *Appl. Opt* **1992**, *31*, 7089; e) J. H. Boyer, A. M. Haag, G. Sathyamoorthi, M. L. Soong, K. Thangaraj, T. G. Pavlopoulos, *Heteroatom. Chem* **1993**, *4*, 39.

[4] a) F. Lopez Arbeloa, J. Bañuelos, V. Martinez, T. Arbeloa, I. Lopez Arbeloa, *Int. Rev. Phys. Chem.* **2005**, *24*, 339; b) O. Garcia, R. Sastre, D. del Agua, A. Costela, I. Garcia-Moreno, *Chem. Mater.* **2006**, *18*, 601; c) I. Garcia-Moreno, F. Amat-Guerri, M. Liras, A. Costela, L. Infantes, R. Sastre, F. Lopez Arbeloa, J. Bañuelos Prieto, I. Lopez Arbeloa, *Adv. Funct. Mater.* **2007**, *17*, 3088; d) A. Costela, I. Garcia-Moreno, M. Pintado-Sierra, F. Amat-Guerri, R. Sastre, M. Liras, F. Lopez Arbeloa, J. Bañuelos Prieto, I. Lopez Arbeloa, *J. Phys. Chem. A* **2009**, *113*, 8118; e) M. J. Ortiz, I. Garcia-Moreno, A. R. Agarrabeitia, G. Duran-Sampedro, A. Costela, R. Sastre, F. Lopez Arbeloa, J. Bañuelos Prieto, I. Lopez Arbeloa, *Phys. Chem. Chem. Phys.* **2010**, *12*, 7804; f) J. Bañuelos Prieto, A. R. Agarrabeitia, I. Garcia-Moreno, I. Lopez-Arbeloa, A. Costela, L. Infantes, M. E. Perez-Ojeda, M. Palacios-Cuesta, M. J. Ortiz, *Chem. Eur. J.* **2010**, *16*, 14094; g) Y. Xiao, D. Zhang, X. Qian, A. Costela, I. Garcia-Moreno, V. Martin, M. E. Perez-Ojeda, J. Bañuelos, L. Gartzia, I. Lopez Arbeloa, *Chem. Commun.* **2011**, *47*, 11513; h) J. Bañuelos, V. Martin, C. F. A. Gomez-Duran, I. J. Arroyo Cordoba, E. Peña-Cabrera, I. Garcia-Moreno, A. Costela, M. E. Perez-Ojeda, T. Arbeloa, I. Lopez Arbeloa, *Chem. Eur. J.* **2011**, *17*, 7261; i) G. Duran-Sampedro, A. R. Agarrabeitia, I. Garcia-Moreno, A. Costela, J. Bañuelos, T. Arbeloa, I. López Arbeloa, J. L. Chiara, M. J. Ortiz, *Eur. J. Org. Chem.* **2012**, *32*, 6335.

[5] a) A. Loudet, K. Burgess, *Chem. Rev.* **2007**, *107*, 4891; b) R. Ziessel, G. Ulrich, A. Harriman, *New J. Chem.* **2007**, *31*, 496; c) G. Ulrich, R. Ziessel, A. Harriman, *Angew. Chem. Int. Ed.* **2008**, *47*, 1184; d) F. L. Arbeloa, J. Bañuelos, V. Martinez, T. Arbeloa, I. L. Arbeloa, *Trends Phys. Chem.* **2008**, *13*, 101; e) A. C. Benniston, G. Copley, *Phys. Chem. Chem. Phys.* **2009**, *11*, 4124; f) M. Benstead, G. H. Mehl, R. W. Boyle, *Tetrahedron* **2011**, *67*, 3573; g) N. Boens, V. Leen, W. Dehaen, *Chem. Soc. Rev.* **2012**, *41*, 1130; h) S. G. Awuah, Y. You, *RSC Adv.* **2012**, *2*, 11169; i) A. Kamkaew, S. H. Lim, H. B. Lee, L. V. Kiew, L. Y. Chung, K. Burgess, *Chem. Soc. Rev.* **2013**, *42*, 77.

[6] a) L. Li, B. Nguyen, K. Burgess, *Bioorg. Med. Chem. Lett.* **2008**, *18*, 3112; b) C. Bonnier, W. E. Piers, A. Al-Sheikh Ali, A. Thompson, M. Parvez, *Organometallics* **2009**, *28*, 4845; c) S. M. Crawford, A. Thompson, *Org. Lett.* **2010**, *12*, 1424; d) T. W. Hudnall, T.-P. Lin, F. P. Gabbaï, *J. Fluorine Chem.* **2010**, *131*, 1182; e) G. Ulrich, S. Goeb, A. De Nicola, P. Retailleau, R. Ziessel, *J. Org. Chem.* **2011**, *76*, 4489; f) L. Yang, R. Simionescu, A. Lough, H. Yan, *Dyes Pigments* **2011**, *91*, 264; g) T. Lundrigan, S. M. Crawford, T. S. Cameron, A. Thompson, *Chem. Commun.* **2012**, *48*, 1003; h) T. Lundrigan, A. Thompson, *J. Org. Chem.* **2012**, *78*, 757.

[7] a) L. Bonardi, G. Ulrich, R. Ziessel, *Org. Lett.* **2008**, *10*, 2183; b) A. Nagai, J. Miyake, K. Kokado, Y. Nagata, Y. Chujo, *J. Am. Chem. Soc.* **2008**, *130*, 15276; c) A. Harriman, L. Mallon, R. Ziessel, *Chem. Eur. J.* **2008**, *14*, 11461; d) T. Rousseau, A. Cravino, T. Bura, G. Ulrich, R. Ziessel, J. Roncali, *Chem. Commun.* **2009**, 1673; e) A. Harriman, L. J. Mallon, K. J. Elliot, A. Haefele, G. Ulrich, R. Ziessel, *J. Am. Chem. Soc.* **2009**, *131*, 13375; f) J.-H. Olivier, A. Haefele, P. Retailleau, R. Ziessel, *Org. Lett.* **2010**, *12*, 408; g) T. Bura, P. Retailleau, R. Ziessel, *Angew. Chem. Int. Ed.* **2010**, *49*, 6659; h) T. Bura, R. Ziessel, *Org. Lett.* **2011**, *13*, 3072; i) S. Rihn, M. Erdem, A. De Nicola, P. Retailleau, R. Ziessel, *Org. Lett.* **2011**, *13*, 1916; j) S. Zhu, N. Dorh, J. Zhang, G. Vegesna, H. Li, F.-T. Luo, A. Tiwari, H. Liu, *J. Mater. Chem.* **2012**, *22*, 2781; k) J.-S. Lu, S.-B. Ko, N. R. Walters, S. Wang, *Org. Lett.* **2012**, *14*, 5660.

[8] a) C. Tahtaoui, C. Thomas, F. Rohmer, P. Klotz, G. Duportail, Y. Mély, D. Bonnet, M. Hibert, *J. Org. Chem.* **2007**, *72*, 269; b) Y. Tokoro, A. Nagai, Y. Chujo, *Tetrahedron Lett.* **2010**, *51*, 3451; c) C. A. Wijesinghe, M. E. El-Khouly, N. K. Subbaiyan, M. Supur, M. E. Zandler, K. Ohkubo, S. Fukuzumi, F. D'Souza, *Chem. Eur. J.* **2011**, *17*, 3147; d) B. Brizet, A. Eggenspiller, C. P. Gros, J. M. Barbe, C. Goze, F. Denat, P. D. Harvey, *J. Org. Chem.* **2012**, *77*, 3646.

[9] a) A. K. Parhi, M.-P. Kung, K. Ploessl, H. F. Kung, *Tetrahedron Lett.* **2008**, *49*, 3395; b) C. Ikeda, S. Ueda, T. Nabeshima, *Chem. Commun.* **2009**, 2544; c) A. Kubo, Y. Minowa, T. Shoda, K. Takeshita, *Tetrahedron Lett.* **2010**, *51*, 1600; d) S. Rausaria, A. Kamadulski, N. P. Rath, L. Bryant, Z. Chen, D. Salvemini, W. L. Neumann, *J. Am. Chem. Soc.* **2011**, *133*, 4200; e) Y. Tomimori, T. Okujima, T. Yano, S. Mori, N. Ono, H. Yamada, H. Uno, *Tetrahedron* **2011**, *67*, 3187.

[10] a) C. Bonnier, W. E. Piers, M. Parvez, T. S. Sorensen, *Chem. Commun.* **2008**, 4593; b) C. Bonnier, W. E. Piers, M. Parvez, *Organometallics* **2011**, *30*, 1067.

[11] X.-D. Jiang, J. Zhang, T. Furuyama, W. Zhao, *Org. Lett.* **2012**, *14*, 248.

[12] Laser grade, Exciton. They were used as received with a purity >99%.

[13] C. Hansch, A. Leo, R. W. Taft, *Chem. Rev.* **1991**, *91*, 165.

[14] G. Bourhill, J.-L. Brédas, L-T. Cheng, S. R. Marder, F. Meyers, J. W. Perry, B. G. Tiemann, *J. Am. Chem. Soc.* **1994**, *116*, 2619.

[15] I. Esnal, J. Bañuelos, I. López Arbeloa, A. Costela, I. García-Moreno, M. Garzón, A. R. Agarrabeitia, M. J. Ortiz, *RSC Adv.* **2013**, *3*, 1547.

[16] J. Bañuelos, T. Arbeloa, M. Liras, V. Martinez, F. López Arbeloa, *J. Photochem. Photobiol. A* **2006**, *184*, 298.

[17] a) A. P. de Silva, H. Q. N. Gunaratne, T. Gunnlaugsson, A. J. M. Huxley, C. P. McCoy, J. T. Rademacher, T. E. Rice, *Chem. Rev.* **1997**, *97*, 1515; b) K. Rurack, U. Resch-Genger, *Chem. Soc. Rev.* **2002**, *31*, 116; c) H. Sunahara, Y. Urano, H. Kojima, T. Nagano, *J. Am. Chem. Soc.* **2007**, *129*, 5597; d) J. Bañuelos, I. J. Arroyo-Cordoba, I. Valois-Escamilla, A. Alvarez-Hernández, E. Peña-Cabrera, R. Hu, B. Z. Tang, I. Esnal, V. Martínez, I. López Arbeloa, *RSC Adv.* **2011**, *1*, 677.

[18] A. Costela, I. García-Moreno, R. Sastre, *Phys. Chem. Chem. Phys.* **2003**, *5*, 4745.

[19] a) A. Costela, I. García-Moreno, D. del Agua, O. García, R. Sastre, *Appl. Phys. Lett.* **2004**, *85*, 2160; b) A. Costela, I. García-Moreno, D. del Agua, O. García, R. Sastre, *J. Appl. Phys.* **2007**, *101*, 073110.

[20] Online 1D multilayer slab waveguide mode solver by Dr. Manfred Hammer. http://wwwhome.math.utwente.nl/_hammer/oms.html (accessed March 2013).

[21] M. J. Ortiz, A. R. Agarrabeitia, M. Garzón Sanz, I. García-Moreno, A. Costela, G. Durán-Sampedro, Spanish Patent Application no. 201200871, **2012**.


© 2013 WILEY-VCH Verlag GmbH & Co. KGaA, Weinheim

Copyright WILEY-VCH Verlag GmbH & Co. KGaA, 69469 Weinheim, Germany, 2013.

ADVANCED FUNCTIONAL MATERIALS

# Supporting Information

for *Adv. Funct. Mater.*, DOI: 10.1002/adfm.201300198

# Carboxylates versus Fluorines: Boosting the Emission Properties of Commercial BODIPYs in Liquid and Solid Media

*Gonzalo Durán-Sampedro, Antonia R. Agarrabeitia, Luis Cerdán, M. Eugenia Pérez-Ojeda, Angel Costela, Inmaculada García-Moreno,* Ixone Esnal, Jorge Bañuelos, Iñigo López Arbeloa, and María J. Ortiz**

## Table of Contents

## General

*Synthesis:* Starting materials and reagents used in the preparation of BODIPYs are commercially available unless synthesis is described. The solvents were dried and distilled, before use. Spectral data of the known compounds were in accordance with the literature data. Flash column chromatography was performed using silica gel Merck 60 (230-400 mesh). $^{1}H$ and $^{13}C$ NMR spectra were recorded with a Bruker Avance-DPX-300 spectrometer (300 MHz for $^{1}H$ and 75 MHz for $^{13}C$) and Bruker Avance III spectrometer (700 MHz for $^{1}H$ and 176 MHz for $^{13}C$). All spectra were recorded in $CDCl_3$. $^{1}H$ chemical shifts are reported in ppm relative to tetramethylsilane ($\delta$ = 0.00 ppm), using the residual solvent signal as the internal reference. $^{13}C$ chemical shifts are reported in ppm with $CDCl_3$ ($\delta$ = 77.67 ppm) as the internal standard. Chemical shift multiplicities are reported as s = singlet, d = doublet, t = triplet, q = quartet and m = multiplet. IR spectra (in $cm^{-1}$) were recorded in a Bruker Tensor-27-FTIR spectrophotometer. High resolution mass spectra were determined by EI in a Thermofisher MAT 95 XP.

*Photophysical properties*: The photophysical properties were registered in diluted solutions (around $2\times10^{-6}$ M), prepared by adding the corresponding solvent to the residue from the adequate amount of a concentrated stock solution in acetone, after vacuum evaporation of this solvent. UV-Vis absorption and fluorescence spectra were recorded on a Varian model CARY 4E spectrophotometer and a SPEX Fluorolog 3-22 spectrofluorimeter, respectively. The fluorescence spectra were corrected from the wavelength dependence of the detector sensibility. Fluorescence quantum yield ($\phi$) was obtained using a methanolic solution of the corresponding commercial BODIPY as reference.[1,2,3,4,5] Radiative decay curves were registered with the time correlated single-photon counting technique (Edinburgh Instruments, model FL920) using a microchannel plate detector (Hamamatsu C4878), with picosecond time resolution (~ 20 ps). Fluorescence emission was monitored at the maximum emission wavelength after excitation at 470 nm and 530 nm by means of a diode laser (PicoQuant, model LDH470 and LDH530) with 150 ps FWHM pulses. The fluorescence lifetime ($\tau$) was obtained from the slope after the deconvolution of the instrumental response signal from the recorded decay curves by means of an iterative method. The goodness of the exponential fit

[1] F. López Arbeloa, T. López Arbeloa, I. López Arbeloa, I. García-Moreno, A. Costela, R. Sastre, F. Amat-Guerri, *Chem. Phys.* **1998**, *236*, 331.
[2] J. Bañuelos, F. López Arbeloa, V. Martínez, T. Arbeloa, I. López Arbeloa, *J. Phys. Chem. A* **2004**, *108*, 5503.
[3] F. López Arbeloa, T. López Arbeloa, I. López Arbeloa, *J. Photochem. Photobiol. A* **1999**, *121*, 177.
[4] A. Costela, I. García-Moreno, C. Gómez, R. Sastre, F. Amat-Guerri, M. Liras, F. López Arbeloa, J. Bañuelos, I. López Arbeloa, *J. Phys. Chem. A* **2002**, *106*, 7736.
[5] F. López Arbeloa, J. Bañuelos, V. Martínez, T. Arbeloa, I. López Arbeloa, *ChemPhysChem* **2004**, 5,1762.

was controlled by statistical parameters (chi-square, Durbin-Watson and the analysis of the residuals). The radiative ($k_{fl}$) and non-radiative deactivation ($k_{nr}$) rate constants were calculated as $k_{fl} = \phi/\tau$ and $k_{nr} = (1-\phi)/\tau$, respectively.

*Theoretical calculations*: Ground state geometry was optimized by the hybrid DFT method B3LYP, using the double-valence basis set (6-31G), whereas the first excited state optimized geometry was achieved by the *ab initio* CIS method, at the same basis set. The geometry was considered as a minimum of energy after the analysis of the frequencies did not yield any negative value. The charge distribution was analyzed with the CHelpG method. All the calculations were performed in the Gaussian 09 software running in the "arina" informatic cluster of the UPV/EHU.

*pH-dependence experiments:* They were carried out, following the procedure previously described,[6] by monitoring the change of absorbance at 494 nm of $10^{-5}$ M the dye (**1**, **6**, or PM546) in DMSO/$H_2O$ (1:1, v/v) in the pH range from 1-14 after 16 h at room temperature.

*Solubility experiments:* They were carried out by UV absorbance analysis. A powder of PM546, BODIPY **1**, or **6**, was shaken in water under ultrasonic irradiation at room temperature with a power of 720 W for 72 h. After filtration, UV absorbance of the aqueous solution was compared with that of a standard solution of the sample in DMSO/$H_2O$.[6]

*Preparation of solid samples and thin films*: The dyes were incorporated into the solid matrices following the procedure previously described.[4] The solid monolith samples were cast in a cylindrical shape, forming rods of 10 mm diameter and 10 mm length. A cut was made parallel to the axis of the cylinder to obtain a lateral flat surface of ≈6 mm × 10 mm. This surface as well as the ends of the laser rods was prepared for lasing experiments by using a grinding and polishing machine (Phoenix Beta 4000, Buehler) until optical-grade finish.[4]

To implement the DFB lasers, PMMA in proportion 50 mg/mL and dyes at concentration (with respect to the polymer) in the range 2.5-3.5 × $10^{-2}$M were solved in chloroform. Thin films ~1 μm thick were spin coated (1000 rpm, 30 seconds) onto quartz substrates engraved with 1D sinusoidal or squared-profile DFB structures with periods $\Lambda_1$=386 nm and $\Lambda_2$=400 nm, respectively, and depths *d*~100 nm, which resonant wavelengths matched the corresponding dye emission windows.

*Laser experiments*: Liquid solutions of dyes were contained in 1 cm optical-path rectangular quartz cells carefully sealed to avoid solvent evaporation during experiments. The

[6] X.-D. Jiang, J. Zhang, T. Furuyama, W. Zhao, *Org. Lett.* **2012**, *14*, 248.

liquid solutions were transversely pumped either at 355 nm, with 5 mJ, 8 ns FWHM pulses from the third-harmonic of a *Q*-switched Nd:YAG laser (Spectron SL282G) or at 532 nm, with 5 mJ, 6 ns FWHM pulses from a frequency-doubled *Q*-switched Nd:YAG laser (Monocrom OPL-10), at a repetition rate of up to 10 Hz. The lasing properties of the solid samples were studied under pumping at 532 nm with pulses from the OPL-10 laser, and their photostability was assessed at 30 Hz repetition rate with 3.5 mJ, 10 ns FWHM pulses from a diode-pumped, frequency-doubled, *Q*-switched Nd:YAG laser (Monocrom HALAZEN 532-12).

The exciting pulses were line-focused onto the cell or the lateral flat surface of the solid rods, providing pump fluences on the active medium in the range 110 - 180 mJ/cm$^2$. The oscillation cavity (2 cm length) consisted of a 90% reflectivity aluminum mirror, with the lateral face of the cell or the solid sample as output coupler.

The photostability of the dyes in liquid solution was evaluated by irradiating under lasing conditions 10 μL of a solution in ethyl acetate. The solutions were contained in a cylindrical Pyrex tube (1 cm height, 1 mm internal diameter) carefully sealed to avoid solvent evaporation during the experiments. Although the low optical quality of the capillary tube prevents laser emission from the dyes, information about photostabilities can be obtained by monitoring the decrease in laser-induced fluorescence intensity, excited transversally to the capillary tube, as a function of the number of pump pulses at a given repetition rate. The fluorescence emission was monitored perpendicular to the exciting beam, collected by an optical fiber, and imaged onto the input slit of a monochromator (Acton Research corporation) and detected with a charge-coupled device (CCD) (SpectruMM:GS128B). The fluorescence emission was recorded by feeding the signal to the boxcar (Stanford Research, model 250) to be integrated before being digitized and processed by a computer. Each experience was repeated at least three times. The photostability of the solid samples was measured by following the evolution of their laser emission under repeated pumping in the same position of the sample at 30 Hz repetition rate. The estimated error in the energy and photostability measurements was 10%.

In the DFB laser experiments (**Figure S7b**), the thin film samples were optically pumped at 532 nm with 20 ns full width at half maximum (FWHM) pulses from a frequency-doubled *Q*-switched Nd:YAG laser (Lotis TII SL-2132), operated at 15 Hz repetition rate. The pump radiation was vertically polarized and parallel to the DFB structure grooves, which allowed controlling the pulse energy incident on the sample by insertion into the pump beam path of a half-wave plate (HWP) and a linear polarizer (LP) set with its polarization axis

vertical. By rotating the HWP the linear polarization of the input beam is rotated out of the horizontal, and the pump beam is blocked more or less by the LP, depending on the rotation angle introduced by the HWP. Pump energy was measured with a calibrated Laser Energy Meter (QE 12LP-S-MB-DO, Gentec). The light incident on the sample arrived at an angle of about 34° from the normal to the surface, and was focused onto that surface by means of a spherical lens ($f$ = +15 cm), rendering an elliptical pump spot with major and minor axis of about 245 μm and 185 μm, respectively. The sample was placed on vertical and horizontal translation stages to allow precise positioning.

The normal to the film DFB laser emission was collected with a 5-cm focal length spherical lens, focused onto a fiber bundle and detected with a spectrograph/monochromator (Spectrapro-300i Acton Research) equipped with a thermoelectrically cooled CCD detector (SpectruMM:GS 128B). A shortwave Cut-off filter (CF) (OptoSigma, cut-off at 540 nm) was placed before the fibre bundle to avoid any scattered pump light entering the spectrograph. Neutral density filters were used to avoid CCD detector saturation. All the measurements were averaged over 15 pulses.

## Synthesis of BODIPYs

**General procedure A**. To a solution of BODIPY (1 equiv) in dry $CH_2Cl_2$ was added aluminium chloride (2-4 equiv) under an argon atmosphere and the mixture resulting was refluxed for 5-10 min. Then, trimethylsilylacetate (TMSOAc) (20 equiv) or 4-nitrophenol (5 equiv) was added and the mixture was refluxed until the complete consumption of the starting material was observed by TLC. Water was added, and the solution was extracted with $CH_2Cl_2$, dried over $MgSO_4$, filtered and concentrated to dryness. The compounds were purified by flash chromatography on silica gel.

**General procedure B**. To a solution of carboxylic acid (20 equiv) in 1,2-dichloroethane was added TMSCl (24 equiv) at room temperature under an argon atmosphere. The mixture was stirred at 90 ºC for 16 h and then was transferred *via* cannula to a flask containing a solution of BODIPY (1 equiv) in 1,2-dichloroethane and stirred at 90 ºC until the complete consumption of the starting material was observed by TLC. Water was added, and the solution was extracted with $CH_2Cl_2$, washed with a solution of $NaHCO_3$ and water, dried over $MgSO_4$, filtered and concentrated to dryness. The compounds were purified by flash chromatography on silica gel.

**General procedure C.** To a solution of carboxylic acid (20 equiv) in 1,2-dichloroethane was added TMSCl (24 equiv) at room temperature under an argon atmosphere and the mixture was stirred at 90 ºC for 16 h. Moreover, to a solution of BODIPY (1 equiv) in 1,2-dichloroethane was added aluminium chloride (2-4 equiv) under an argon atmosphere and the mixture resulting was refluxed for 5-10 min. Then, the first solution was transferred *via* cannula to a flask containing the BODIPY in the presence of $AlCl_3$ and the mixture was stirred at 90 ºC until the complete consumption of the starting material was observed by TLC. Water was added, and the solution was extracted with $CH_2Cl_2$, dried over $MgSO_4$, filtered and concentrated to dryness. The compounds were purified by flash chromatography on silica gel.

**4,4-Diacetoxy-1,3,5,7,8-pentamethyl-4-bora-3a,4a-diaza-*s*-indacene (1):**

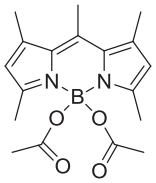

According to the general procedure A, BODIPY PM546 (216 mg, 0.82 mmol) in dry $CH_2Cl_2$ (20 mL) and $AlCl_3$ (437 mg, 3.28 mmol) for 5 min were reacted. TMSOAc (2.4 mL, 14.4 mmol) was added and the mixture was refluxed for 30 min. Flash chromatography using hexane/EtOAc (7:3) afforded **1** (100 mg, 36%) as an orange solid. $^1$H NMR (300 MHz, $CDCl_3$): $\delta$ 5.94 (2H, s, H-2 and H-6), 2.57 (3H, s, $CH_3$), 2.34 (12H, s, 4 $CH_3$), 1.92 (6H, s, 2 $CH_3$); $^{13}$C NMR (75 MHz, $CDCl_3$): $\delta$ 171.3 (CO), 151.2 (C), 142.4 (C), 140.8 (C), 133.7 (C), 121.4 (CH), 30.9 ($CH_3$), 17.6 ($CH_3$), 16.7 ($CH_3$), 14.4 ($CH_3$); IR (neat): 1752, 1557, 1510, 1371, 1266, 1207, 1031, 989 cm$^{-1}$; HRMS-EI: calcd for ($C_{18}H_{23}BN_2O_4$) 342.1750 found 342.1753.

**4,4-Diacetoxy-2,6-diethyl-1,3,5,7,8-pentamethyl-4-bora-3a,4a-diaza-*s*-indacene (2):**

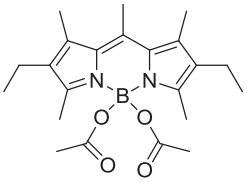

According to the general procedure A, BODIPY PM567 (40 mg, 0.13 mmol) in dry $CH_2Cl_2$ (20 mL) and $AlCl_3$ (51 mg, 0.39 mmol) for 10 min were reacted. TMSOAc (0.38 mL, 2.5 mmol) was added and the mixture was refluxed for 30 min. Flash chromatography using hexane/EtOAc (9:1) afforded,.by order of elution, BODIPY567 recovered (4 mg, 10%) and **2**

(25 mg, 48%) as an orange solid $^{1}$H NMR (300 MHz, $CDCl_3$): $\delta$ 2.60 (3H, s, $CH_3$), 2.31 (6H, s, 2 $CH_3$), 2.29 (4H, q, $J$ = 7.5 Hz, 2 $CH_2$), 2.26 (6H, s, 2 $CH_3$), 1.91 (6H, s, 2 $CH_3$), 0.94 (6H, t, $J$ = 7.5 Hz, 2 $\underline{CH_3}CH_2$); $^{13}$C NMR (75 MHz, $CDCl_3$): $\delta$ 171.2 (CO), 149.4 (C), 140.1 (C), 136.5 (C), 133.2 (C), 132.0 (C), 23.1 ($CH_3$), 17.3 ($CH_2$), 14.8 ($CH_3$), 14.7 ($CH_3$), 12.3 ($CH_3$); IR (neat): 1717, 1554, 1468, 1187, 1136, 981 cm$^{-1}$; HRMS-EI: calcd for ($C_{22}H_{31}BN_2O_4$) 398.2371 found 398.2372.

**4,4-Diacetoxy-2,6-di-*terc*butyl-1,3,5,7,8-pentamethyl-4-bora-3a,4a-diaza-*s*-indacene (3):**

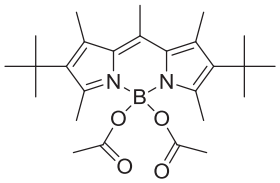

According to the general procedure B, acetic acid (0.19 mL, 10 mmol) in 1,2-dichloroethane (15 mL) and TMSCl (1.04 mL, 12 mmol) were reacted. After, this mixture and BODIPY PM597 (174 mg, 0.5 mmol) in 1,2-dichloroethane (5 mL) were refluxed for 6 h. Flash chromatography using hexane/EtOAc (9:1) afforded **3** (43 mg, 19%) as a red solid. $^{1}$H NMR (300 MHz, $CDCl_3$): $\delta$ 2.58 (3H, s, $CH_3$), 2.50 (6H, s, 2 $CH_3$), 2.40 (6H, s, 2 $CH_3$), 1.90 (6H, s, 2 $CH_3$), 1.31 (18H, s, 6 $CH_3$); $^{13}$C NMR (75 MHz, $CDCl_3$): $\delta$ 170.8 (CO), 149.4 (C), 140.6 (C), 137.4 (C), 136.4 (C), 134.6 (C), 33.2 (C), 32.2 ($CH_3$), 23.1 ($CH_3$), 19.9 ($CH_3$), 18.0 ($CH_3$), 16.4 ($CH_3$); IR (neat): 1720, 1544, 1264, 1191, 1030, 981, 738 cm$^{-1}$; HRMS-EI: calcd for ($C_{26}H_{39}BN_2O_4$) 454.3002 found 454.3000.

**4,4-Diacetoxy-8-acetoxymethyl-2,6-diethyl-1,3,5,7-pentamethyl-4-bora-3a,4a-diaza-*s*-indacene (4):**

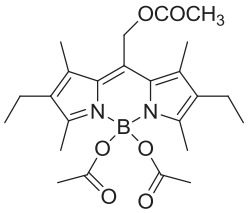


According to the general procedure A, BODIPY PM605 (50 mg, 0.13 mmol) in dry $CH_2Cl_2$ (20 mL) and $AlCl_3$ (71 mg, 0.53 mmol) for 10 min were reacted. TMSOAc (0.4 mL, 2.66 mmol) was added and the mixture was refluxed for 30 min. Flash chromatography using hexane/EtOAc (95:5) afforded **4** (22 mg, 36%) as an orange solid.$^{1}$H NMR (300 MHz, $CDCl_3$): $\delta$ 5.31 (2H, s, $CH_2O$), 2.33 (6H, s, 2 $CH_3$), 2.27 (4H, q, $J$ = 7.5 Hz, 2 $\underline{CH_2}CH_3$), 2.19 (6H, s, 2 $CH_3$), 2.07 (3H, s, $CH_3$), 1.93 (6H, s, 2 $CH_3$), 0.95 (6H, t, $J$ = 7.5 Hz, 2 $\underline{CH_3}CH_2$);

$^{13}$C NMR (75 MHz, $CDCl_3$): $\delta$ 171.8 (CO), 171.4 (CO), 152.9 (C), 137.1 (C), 134.3 (C), 133.7 (C), 132.9 (C), 59.0 ($CH_2O$), 23.4 ($CH_3$), 21.2 ($CH_3$), 17.8 ($CH_2$), 15.1 ($CH_3$), 13.4 ($CH_3$), 13.0 ($CH_3$); IR (neat): 1727, 1562, 1196, 1028, 982, 806 cm$^{-1}$; HRMS-EI: calcd for ($C_{24}H_{33}BN_2O_6$) 456.2430 found 456.2428.

**4,4-Diacetoxy-8-cyano-1,2,3,5,6,7-hexamethyl-4-bora-3a,4a-diaza-*s*-indacene (5):**

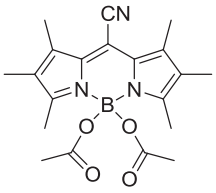


According to the general procedure A, BODIPY PM650 (50 mg, 0.17 mmol) in dry $CH_2Cl_2$ (20 mL) and $AlCl_3$ (66 mg, 0.5 mmol) for 10 min were reacted. TMSOAc (0.5 mL, 3.32 mmol) was added and the mixture was refluxed for 60 min. Flash chromatography using hexane/EtOAc (9:1) afforded **5** (18 mg, 28%) as a golden yellow solid.$^1$H NMR (300 MHz, $CDCl_3$): $\delta$ 2.35 (6H, s, 2 $CH_3$), 2.32 (6H, s, 2 $CH_3$), 1.93 (6H, s, 2 $CH_3$), 1.83 (6H, s, 2 $CH_3$); $^{13}$C NMR (75 MHz, $CDCl_3$): $\delta$ 171.6 (CO), 155.4 (C), 138.7 (C), 133.9 (C), 128.3 (C), 115.2 (C), 104.2 (C), 22.9 ($CH_3$), 13.0 ($CH_3$), 11.9 ($CH_3$), 9.1 ($CH_3$); IR (neat): 2220, 1716, 1557, 1186, 959, 768 cm$^{-1}$; HRMS-EI: calcd for ($C_{20}H_{24}BN_3O_4$) 381.1860 found 381.1864.

**4,4-Bis(trifluoroacetoxy)-1,3,5,7,8-pentamethyl-4-bora-3a,4a-diaza-*s*-indacene (6):**

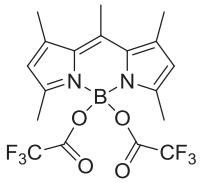


According to the general procedure B, trifluoroacetic acid (1.54 mL, 20 mmol) in 1,2-dichloroethane (15 mL) and TMSCl (2.08 mL, 24 mmol) were reacted. After, this mixture and BODIPY PM546 (262 mg, 1 mmol) in 1,2-dichloroethane (5 mL) were refluxed for 1 h.Flash chromatography using hexane/EtOAc (95:5) afforded **6** (144 mg, 32%) as an orange solid. $^1$H NMR (300 MHz, $CDCl_3$): $\delta$ 6.04 (2H, s, H-2 and H-6), 2.62 (3H, s, $CH_3$), 2.39 (6H, s, 2 $CH_3$), 2.31 (6H, s, 2 $CH_3$); $^{13}$C NMR (75 MHz, $CDCl_3$): $\delta$ 156.3 (q, $^2J_{CF}$ = 41.2 Hz, CO), 152.5 (C), 143.1 (C), 142.8 (C), 133.4 (C), 122.3 (CH), 114.8 (q, $^1J_{CF}$ = 289.8 Hz, $CF_3$), 17.5 ($CH_3$), 16.7 ($CH_3$), 14.0 ($CH_3$); $^{19}$F NMR (282 MHz, $CDCl_3$): $\delta$ -76.64 (m, $CF_3$); IR (neat): 1768, 1561, 1506, 1393, 1200, 1160, 974 cm$^{-1}$; HRMS-EI: calcd for ($C_{18}H_{17}BF_6N_2O_4$) 450.1180 found 450.1181.

**4,4-Bis(trifluoroacetoxy)-2,6-diethyl-1,3,5,7,8-pentamethyl-4-bora-3a,4a-diaza-*s*-indacene (7):**

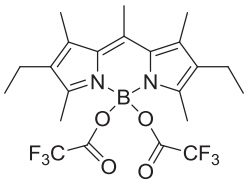

According to the general procedure B, trifluoroacetic acid (0.48 mL, 6.2 mmol) in 1,2-dichloroethane (15 mL) and TMSCl (0.67 mL, 7.5 mmol) were reacted. After, this mixture and BODIPY PM567 (100 mg, 0.31 mmol) in 1,2-dichloroethane (5 mL) were refluxed for 6 h.Flash chromatography using hexane/EtOAc (95:5) afforded **7** (31 mg, 20 %) as a yellow-orange solid. $^{1}$H NMR (700 MHz, $CDCl_3$): $\delta$ 2.62 (3H, s, $CH_3$), 2.29 (4H, q, $J$ = 7.7 Hz, 2 $CH_2$), 2.29 (6H, s, 2 $CH_3$), 2.26 (6H, s, 2 $CH_3$), 0.95 (6H, t, $J$ = 7.7 Hz, 2 $\underline{CH_3}CH_2$); $^{13}$C NMR (176 MHz, $CDCl_3$): $\delta$ 156.3 (q, $^{2}J_{CF}$ = 42.2 Hz, CO), 150.5 (C), 141.2 (C), 138.6 (C), 133.3 (C), 133.0 (C), 114.8 (q, $^{1}J_{CF}$ = 286.9 Hz, $CF_3$), 17.3 ($CH_2$), 17.2 ($CH_3$), 14.7 ($CH_3$), 14.6 ($CH_3$), 12.0 ($CH_3$); $^{19}$F NMR (282 MHz, $CDCl_3$): $\delta$ -76.75 (m, $CF_3$); IR (neat): 1763, 1546, 1206, 1155, 977, 772 cm$^{-1}$; HRMS-EI: calcd for ($C_{22}H_{25}BF_6N_2O_4$) 506.1810 found 506.1808.

**4,4-Bis(trifluoroacetoxy)-2-*terc*butyl-1,3,5,7,8-pentamethyl-4-bora-3a,4a-diaza-*s*-indacene (15):**

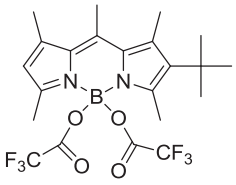

According to the general procedure B, trifluoroacetic acid (0.75 mL, 10 mmol) in 1,2-dichloroethane (15 mL) and TMSCl (1.04 mL, 12 mmol) were reacted. After, this mixture and BODIPY PM597 (187 mg, 0.5 mmol) in 1,2-dichloroethane (5 mL) were refluxed for 2 h. Flash chromatography on silica gel using hexane/EtOAc (97:3) afforded, by order of elution, **15** (25 mg, 10%) as an orange solid and **6** (50 mg, 22%).

*Compound **15***: $^{1}$H NMR (700 MHz, $CDCl_3$): $\delta$ 6.00 (1H, s, H-6), 2.62 (3H, s, $CH_3$), 2.47 (6H, s, 2 $CH_3$), 2.37 (3H, s, $CH_3$), 2.28 (3H, s, $CH_3$), 1.32 (9H, s, 3 $CH_3$); $^{13}$C NMR (176 MHz, $CDCl_3$): $\delta$ 156.1 (q, $^{2}J_{CF}$ = 40.5 Hz, CO), 152.0 (C), 150.8 (C), 142.0 (C), 141.3 (C), 141.1 (C), 138.2 (C), 134.0 (C), 133.4 (C), 122.1 (CH), 114.8 (q, $^{1}J_{CF}$ = 286.9 Hz, $CF_3$), 33.2 (C), 31.9 (3 $CH_3$), 18.1 ($CH_3$), 18.0 ($CH_3$), 17.8 ($CH_3$), 16.3 ($CH_3$), 14.0 ($CH_3$); $^{19}$F NMR (282 MHz, $CDCl_3$): $\delta$ -76.02 (m, $CF_3$); IR (neat): 1765, 1560, 1510, 1390, 1190, 974 cm$^{-1}$; HRMS-

EI: calcd for ($C_{22}H_{25}BF_6N_2O_4$) 506.1810 found 506.1812.

**4,4-Bis(trifluoroacetoxy)-2,6-di-*terc*butyl-1,3,5,7,8-pentamethyl-4-bora-3a,4a-diaza-*s*-indacene (8):**

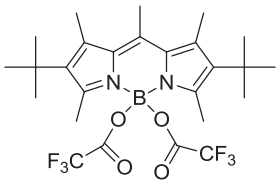

According to the general procedure C, trifluoroacetic acid (0.2 mL, 2.68 mmol) in 1,2-dichloroethane (10 mL) and TMSCl (3.2 mL solution 1 M in dichloromethane, 3.2 mmol) were reacted. After, this mixture and BODIPY PM597 (50 mg, 0.13 mmol) in presence of $AlCl_3$ (54 mg, 0.40 mmol) in 1,2-dichloroethane (10 mL) were refluxed for 10 min. Flash chromatography using hexane/EtOAc (95:5) afforded **8** (17 mg, 22%) as a red solid. $^1$H NMR (700 MHz, $CDCl_3$): $\delta$ 2.61 (3H, s, $CH_3$), 2.44 (6H, s, 2 $CH_3$), 2.43 (6H, s, 2 $CH_3$), 1.31 (18H, s, 6 $CH_3$); $^{13}$C NMR (176 MHz, $CDCl_3$): $\delta$ 154.8 (q, $^2J_{CF}$ = 42.2 Hz, CO), 149.2 (C), 140.2 (C), 138.6 (C), 136.7 (C), 133.3 (C), 113.7 (q, $^1J_{CF}$ = 286.9 Hz, $CF_3$), 32.1 (C), 30.9 ($CH_3$), 18.7 ($CH_3$), 17.1 ($CH_3$), 15.1 ($CH_3$); $^{19}$F NMR (282 MHz, $CDCl_3$): $\delta$ -77.37 (m, $CF_3$); IR (neat): 1760, 1566, 1500, 1397, 1192, 965; HRMS-EI: calcd for ($C_{26}H_{33}BF_6N_2O_4$) 562.2435 found 562.2437.

**4,4-Bis(trifluoroacetoxy)-8-acetoxymethyl-2,6-diethyl-1,3,5,7-pentamethyl-4-bora-3a,4a-diaza-*s*-indacene (9):**

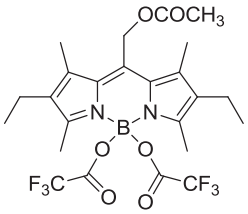

According to the general procedure B, trifluoroacetic acid (0.41 mL, 5.3 mmol) in 1,2-dichloroethane (15 mL) and TMSCl (0.55 mL, 24 mmol) were reacted. After, this mixture and BODIPY PM605 (100 mg, 0.266 mmol) in 1,2-dichloroethane (5 mL) were refluxed for 4 h.Flash chromatography using hexane/EtOAc (9:1) afforded **9** (33 mg, 22%) as a red solid. $^1$H NMR (300 MHz, $CDCl_3$): $\delta$ 5.30 (2H, s, $CH_2O$), 2.29 (4H, q, $J$ = 7.5 Hz, 2 $\underline{CH_2}CH_3$), 2.28 (6H, s, 2 $CH_3$), 2.22 (6H, s, 2 $CH_3$), 2.09 (3H, s, $CH_3$), 0.96 (6H, t, $J$ = 7.5 Hz, 2 $\underline{CH_3}CH_2$); $^{13}$C NMR (75 MHz, $CDCl_3$): $\delta$ 171.1 ($\underline{CO}CH_3$), 156.7 (q, $^2J_{CF}$ = 41.3 Hz, $\underline{CO}CF_3$), 154.0 (C), 139.2 (C), 134.9 (C), 134.1 (C), 133.5 (C), 115.1 (q, $^1J_{CF}$ = 286.7 Hz, $CF_3$), 58.5 ($CH_2O$), 21.1

($CH_3$), 17.6 ($CH_2$), 14.8 ($CH_3$), 13.3 ($CH_3$), 12.6 ($CH_3$); $^{19}$F NMR (282 MHz, $CDCl_3$): $\delta$ -76.62 (m, $CF_3$); IR (neat): 1755, 1500, 1202, 1159, 974 $cm^{-1}$; HRMS-EI: calcd for ($C_{24}H_{27}BF_6N_2O_6$) 564.1863 found 564.1866.

**4,4-Bis(trifluoroacetoxy)-8-cyano-1,2,3,5,6,7-hexamethyl-4-bora-3a,4a-diaza-*s*-indacene (10):**

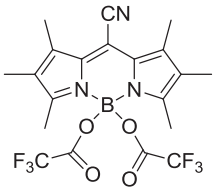


According to the general procedure C, trifluoroacetic acid (0.26 mL, 3.32 mmol) in 1,2-dichloroethane (10 mL) and TMSCl (4 mL solution 1 M in dichloromethane, 4 mmol) were reacted. After, this mixture and BODIPY PM650 (50 mg, 0.17 mmol) in presence of $AlCl_3$ (66 mg, 0.5 mmol) in 1,2-dichloroethane (10 mL) were refluxed for 90 min.Flash chromatography using hexane/$CHCl_3$ (8:2) afforded **10** (30 mg, 37%) as a purple solid. $^1$H NMR (700 MHz, $CDCl_3$): $\delta$ 2.38 (6H, s, 2 $CH_3$), 2.29 (6H, s, 2 $CH_3$), 1.87 (6H, s, 2 $CH_3$); $^{13}$C NMR (176 MHz, $CDCl_3$): $\delta$ 156.6 (C), 156.4 (q, $^2J_{CF}$ = 42.2 Hz, CO), 141.0 (C), 133.5 (C), 129.5 (C), 114.6 (q, $^1J_{CF}$ = 286.9 Hz, $CF_3$), 114.4 (C), 104.5 (C), 12.8 ($CH_3$), 11.9 ($CH_3$), 9.1 ($CH_3$); $^{19}$F NMR (282 MHz, $CDCl_3$): $\delta$ -76.58 (m, $CF_3$); IR (neat): 2225, 1773, 1555, 1467, 1386, 1199, 1157, 1022, 963, 769 $cm^{-1}$; HRMS-EI: calcd for ($C_{20}H_{18}BF_6N_3O_4$) 489.1289 found 489.1299.

**4,4-Bis(acryloyloxy)-2,6-diethyl-1,3,5,7,8-pentamethyl-4-bora-3a,4a-diaza-*s*-indacene (11):**

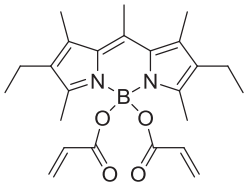


According to the general procedure B, acrylic acid (0.43 mL, 6.3 mmol) in 1,2-dichloroethane (20 mL) and TMSCl (0.95 mL, 7.5 mmol) were reacted. After, this mixture and BODIPY PM567 (100 mg, 0.31 mmol) in 1,2-dichloroethane (5 mL) were refluxed for 18 h. Flash chromatography using hexane/EtOAc (9:1) afforded **11** (38 mg, 29%) as an orange solid. $^1$H NMR (300 MHz, $CDCl_3$): $\delta$ 6.26 (2H, dd, $J$ = 17.1 and 1.8 Hz, 2 $\underline{CH_2}$=CH), 6.06 (2H, dd, $J$ = 17.1 and 10.2 Hz, 2 $\underline{CH}$=$CH_2$), 5.63 (2H, dd, $J$ = 10.2 and 1.8 Hz, 2 $\underline{CH_2}$=CH), 2.62 (2H, s,

$CH_3$), 2.27-2.24 (16H, m, 4 $CH_3$ and 2 $CH_2$), 0.92 (6H, t, $J$ = 7.5 Hz, 2 $CH_3$); $^{13}$C NMR (75 MHz, $CDCl_3$): $\delta$ 166.1 (COO), 149.7 (C), 140.5 (C), 136.5 (C), 133.2 (C), 132.0 (C), 131.2 (CH=$CH_2$), 129.4 ($CH_2$=CH), 17.3 ($CH_2$) 14.8 ($CH_3$), 14.7 ($CH_3$), 12.4 ($CH_3$) 12.3 ($CH_3$); IR (neat): 1726, 1628, 1548, 1371, 1192, 955 cm$^{-1}$; HRMS-EI: calcd for ($C_{24}H_{31}BN_2O_4$) 422.2374 found 422.2379.

**4,4-Bis(propioloyloxy)-1,3,5,7,8-pentamethyl-4-bora-3a,4a-diaza-*s*-indacene (12):**

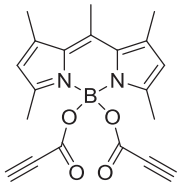

According to the general procedure B, propiolic acid (0.25 mL, 4 mmol) in 1,2-dichloroethane (20 mL) and TMSCl (4.8 mL, 1 M in dichloromethane, 4.8 mmol) were reacted. After, this mixture and BODIPY PM546 (50 mg, 0.2 mmol) in 1,2-dichloroethane (5 mL) were refluxed for 48 h. Flash chromatography using hexane/EtOAc (7:3) afforded **12** (32 mg, 44%) as an orange solid. $^1$H NMR (300 MHz, $CDCl_3$): $\delta$ 5.98 (2H, s, H-2 and H-6), 2.62 (2H, s, 2 CH≡C), 2.57 (3H, s, $CH_3$), 2.38 (6H, s, 2 $CH_3$), 2.35 (6H, s, 2 $CH_3$); $^{13}$C NMR (75 MHz, $CDCl_3$): $\delta$ 151.0 (C), 150.8 (C), 141.5 (C), 140.7 (C), 132.4 (C), 120.8 (CH), 76.2 (C≡C), 71.0 (C≡C), 16.5 ($CH_3$), 15.7 ($CH_3$), 13.5 ($CH_3$); IR (neat): 3230, 2101, 1695, 1563, 1467, 1263, 982, 828 cm$^{-1}$; HRMS-EI: calcd for ($C_{20}H_{19}BN_2O_4$) 362.1434 found 362.1439.

**4,4-Bis(4-nitrophenoxy)-1,3,5,7,8-pentamethyl-4-bora-3a,4a-diaza-*s*-indacene (14):**

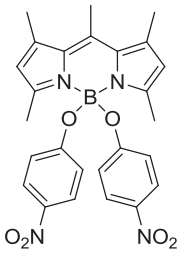

According to the general procedure A, BODIPY PM546 (100 mg, 0.38 mmol) in dry $CH_2Cl_2$ (20 mL) and $AlCl_3$ (101 mg, 0.76 mmol) for 5 min were reacted. 4-Nitrophenol (265 mg, 1.9 mmol) in $CH_2Cl_2$ (5 mL) was added and the mixture was stirred at room temperature for 12 h. Flash chromatography using hexane/EtOAc (7:3) afforded **15** (124 mg, 65%) as a green solid.$^1$H NMR (300 MHz, $CDCl_3$): $\delta$ 7.90 (4H, d, $J$ = 9.0 Hz, 4 CH), 6.47 (4H, d, $J$ = 9.0 Hz, 4 CH), 5.96 (2H, s, H-2 and H-6), 2.71 (3H, s, $CH_3$), 2.43 (6H, s, 2 $CH_3$), 2.34 (6H, s, 2 $CH_3$); $^{13}$C NMR (75 MHz, $CDCl_3$): $\delta$ 162.3 (C), 154.8 (C), 142.6 (C), 141.6 (C), 140.7 (C), 132.5

(C), 125.9 (CH), 122.8 (CH), 118.0 (CH), 17.7 ($CH_3$), 16.6 ($CH_3$), 14.9 ($CH_3$); IR (neat): 1556, 1499, 1277, 1184, 981, 803 $cm^{-1}$; HRMS-EI: calcd for ($C_{26}H_{25}BN_4O_6$) 500.1864 found 500.1866.

**Table S1**. Full photophysical data of PM546 and its *O*-BODIPYs

| | PM546 | | | | | | **1** | | | | | |
|---|---|---|---|---|---|---|---|---|---|---|---|---|
| | c-hex | Ethyl Ac | Acetone | EtOH | MetOH | $F_3$-etoh | c-hex | Ethyl Ac | Acetone | EtOH | MetOH | $F_3$-etoh |
| $\lambda_{ab}$ (nm) | 499.5 | 494.0 | 493.0 | 495.0 | 492.5 | 490.0 | 501.0 | 496.0 | 496.0 | 496.0 | 495.0 | 493.0 |
| $\varepsilon_{max}$ ($10^{-4}M^{-1}cm^{-1}$) | 9.7 | 8.1 | 7.9 | 8.1 | 8.2 | 7.6 | 9.5 | 8.1 | 7.8 | 8.0 | 7.7 | 7.0 |
| $\lambda_{fl}$ (nm) | 509.5 | 504.0 | 503.5 | 505.0 | 503.5 | 503.0 | 508.0 | 506.0 | 505.0 | 505.0 | 504.5 | 502.0 |
| $\Delta\nu_{St}$ ($cm^{-1}$) | 400 | 400 | 430 | 400 | 455 | 515 | 275 | 400 | 360 | 360 | 380 | 365 |
| $\phi$ | 0.91 | 0.85 | 0.84 | 0.85 | 0.81 | 0.85 | 0.91 | 0.86 | 0.88 | 0.88 | 0.85 | 0.85 |
| $\tau$ (ns) | 5.23 | 5.58 | 5.55 | 5.52 | 5.58 | 6.22 | 5.40 | 5.63 | 5.76 | 5.88 | 6.15 | 6.84 |
| $k_{fl}$ ($10^{-8}$ $s^{-1}$) | 1.74 | 1.52 | 1.51 | 1.54 | 1.45 | 1.37 | 1.68 | 1.53 | 1.53 | 1.50 | 1.38 | 1.24 |
| $k_{nr}$ ($10^{-8}$ $s^{-1}$) | 0.17 | 0.27 | 0.29 | 0.27 | 0.34 | 0.24 | 0.17 | 0.25 | 0.21 | 0.20 | 0.24 | 0.22 |
| | **6** | | | | | | **12** | | | | | |
| | c-hex | Ethyl Ac | Acetone | EtOH | MetOH | $F_3$-etoh | c-hex | Ethyl Ac | Acetone | EtOH | MetOH | $F_3$-etoh |
| $\lambda_{ab}$ (nm) | 502.0 | 498.0 | 497.5 | 498.0 | 497.0 | 494.0 | 502.0 | 498.0 | 497.5 | 498.5 | 497.5 | 493.5 |
| $\varepsilon_{max}$ ($10^{-4}M^{-1}cm^{-1}$) | 10.2 | 8.4 | 8.3 | 8.4 | 8.3 | 6.6 | 8.2 | 7.1 | 6.9 | 6.9 | 6.8 | 6.3 |
| $\lambda_{fl}$ (nm) | 509.5 | 507.5 | 507.0 | 507.5 | 506.0 | 503.0 | 511.0 | 507.0 | 507.0 | 507.5 | 506.0 | 503.5 |
| $\Delta\nu_{St}$ ($cm^{-1}$) | 295 | 375 | 375 | 375 | 360 | 360 | 350 | 355 | 375 | 355 | 340 | 400 |
| $\phi$ | 0.95 | 0.90 | 0.90 | 0.91 | 0.91 | 0.89 | 0.99 | 0.93 | 0.93 | 0.90 | 0.90 | 0.86 |
| $\tau$ (ns) | 5.52 | 5.97 | 6.12 | 6.07 | 6.37 | 6.97 | 5.62 | 6.03 | 6.23 | 6.21 | 6.51 | 7.02 |
| $k_{fl}$ ($10^{-8}$ $s^{-1}$) | 1.72 | 1.51 | 1.47 | 1.50 | 1.43 | 1.28 | 1.76 | 1.54 | 1.49 | 1.45 | 1.38 | 1.22 |
| $k_{nr}$ ($10^{-8}$ $s^{-1}$) | 0.10 | 0.17 | 0.16 | 0.15 | 0.14 | 0.16 | 0.02 | 0.12 | 0.11 | 0.16 | 0.15 | 0.20 |

| | **14** | | | | | |
|---|---|---|---|---|---|---|
| | c-hex | Ethyl Ac | Acetone | EtOH | MetOH | $F_3$-etoh |
| $\lambda_{ab}$ (nm) | 499.5 | 495.5 | 494.5 | 495.5 | 494.5 | 493.5 |
| $\varepsilon_{max}$ ($10^{-4}M^{-1}cm^{-1}$) | 11.6 | 10.0 | 9.8 | 9.7 | 9.6 | 9.2 |
| $\lambda_{fl}$ (nm) | 511.0 | 508.0 | 506.0 | 507.0 | 506.0 | 504.0 |
| $\Delta\nu_{St}$ ($cm^{-1}$) | 450 | 495 | 460 | 460 | 460 | 420 |
| $\phi$ | 0.89 | 0.83 | 0.80 | 0.51 | 0.33 | 0.05 |
| $\tau$ (ns) | 5.94 | 6.34 | 6.14 | 4.04 | 2.65 (99%)<br>5.87 (1%) | 0.18 (97%)<br>6.59 (3%) |
| $k_{fl}$ ($10^{-8}$ $s^{-1}$) | 1.50 | 1.31 | 1.30 | 1.26 | *1.24* | *2.78* |
| $k_{nr}$ ($10^{-8}$ $s^{-1}$) | 0.18 | 0.27 | 0.33 | 1.21 | *2.53* | *52.8* |

c-hex: cyclohexane; Ethyl Ac: ethyl acetate; EtOH: etanol; MetOH: methanol; $F_3$-etoh; 2,2,2-trifluoroethanol
*italic* – the rate constants were calculated from the main lifetime

**Table S2**. Full photophysical data of PM567 and its *O*-BODIPYs

| | PM567 | | | | | | **2** | | | | | |
|---|---|---|---|---|---|---|---|---|---|---|---|---|
| | c-hex | Ethyl Ac | Acetone | EtOH | MetOH | $F_3$-etoh | c-hex | Ethyl Ac | Acetone | EtOH | MetOH | $F_3$-etoh |
| $\lambda_{ab}$ (nm) | 522.5 | 516.5 | 516.0 | 518.0 | 516.0 | 516.0 | 522.0 | 520.0 | 519.5 | 520.0 | 519.0 | 517.5 |
| $\varepsilon_{max}$ ($10^{-4}M^{-1}cm^{-1}$) | 9.3 | 8.0 | 8.0 | 8.1 | 7.9 | 7.1 | 8.5 | 7.9 | 7.5 | 7.5 | 7.5 | 6.5 |
| $\lambda_{fl}$ (nm) | 537.0 | 531.5 | 532.0 | 532.5 | 531.5 | 535.0 | 537.0 | 534.0 | 534.0 | 534.0 | 534.0 | 532.0 |
| $\Delta\nu_{St}$ ($cm^{-1}$) | 520 | 550 | 580 | 540 | 560 | 700 | 535 | 505 | 520 | 505 | 540 | 530 |
| $\phi$ | 0.88 | 0.84 | 0.83 | 0.84 | 0.81 | 0.82 | 0.84 | 0.83 | 0.84 | 0.77 | 0.79 | 0.79 |
| $\tau$ (ns) | 5.60 | 5.78 | 5.92 | 6.09 | 6.10 | 6.94 | 5.71 | 5.95 | 6.14 | 6.29 | 6.54 | 7.40 |
| $k_{fl}$ ($10^{-8}$ $s^{-1}$) | 1.57 | 1.45 | 1.40 | 1.38 | 1.33 | 1.18 | 1.47 | 1.39 | 1.37 | 1.22 | 1.21 | 1.07 |
| $k_{nr}$ ($10^{-8}$ $s^{-1}$) | 0.21 | 0.28 | 0.29 | 0.26 | 0.31 | 0.26 | 0.28 | 0.28 | 0.26 | 0.36 | 0.32 | 0.28 |
| | **7** | | | | | | **11** | | | | | |
| | c-hex | Ethyl Ac | Acetone | EtOH | MetOH | $F_3$-etoh | c-hex | Ethyl Ac | Acetone | EtOH | MetOH | $F_3$-etoh |
| $\lambda_{ab}$ (nm) | 525.5 | 521.5 | 521.5 | 521.5 | 521.0 | 518.0 | 523.5 | 520.0 | 520.0 | 520.0 | 519.5 | 518.0 |
| $\varepsilon_{max}$ ($10^{-4}M^{-1}cm^{-1}$) | 7.8 | 6.7 | 6.5 | 6.6 | 6.5 | 6.6 | 8.1 | 7.2 | 7.1 | 7.0 | 8.4 | 6.4 |
| $\lambda_{fl}$ (nm) | 541.5 | 536.5 | 538.0 | 537.0 | 537.0 | 535.0 | 541.0 | 537.0 | 536.5 | 536.0 | 535.5 | 534.0 |
| $\Delta\nu_{St}$ ($cm^{-1}$) | 565 | 540 | 590 | 545 | 565 | 620 | 620 | 610 | 590 | 575 | 575 | 580 |
| $\phi$ | 0.94 | 0.93 | 0.91 | 0.90 | 0.88 | 0.82 | 0.90 | 0.85 | 0.88 | 0.84 | 0.81 | 0.78 |
| $\tau$ (ns) | 6.25 | 6.75 | 6.95 | 6.84 | 7.14 | 7.61 | 5.98 | 6.27 | 6.48 | 6.57 | 6.86 | 7.45 |
| $k_{fl}$ ($10^{-8}$ $s^{-1}$) | 1.50 | 1.38 | 1.31 | 1.31 | 1.23 | 1.08 | 1.50 | 1.36 | 1.36 | 1.28 | 1.18 | 1.05 |
| $k_{nr}$ ($10^{-8}$ $s^{-1}$) | 0.10 | 0.10 | 0.13 | 0.15 | 0.17 | 0.24 | 0.17 | 0.24 | 0.19 | 0.24 | 0.28 | 0.30 |

| | **13** | | | | | |
|---|---|---|---|---|---|---|
| | c-hex | Ethyl Ac | Acetone | EtOH | MetOH | $F_3$-etoh |
| $\lambda_{ab}$ (nm) | 522.0 | 517.5 | 517.0 | 518.5 | 517.5 | 516.5 |
| $\varepsilon_{max}$ ($10^{-4}M^{-1}cm^{-1}$) | 8.0 | 7.4 | 7.5 | 6.9 | 7.3 | 6.8 |
| $\lambda_{fl}$ (nm) | 539.5 | 535.5 | 535.5 | 536.5 | 536.0 | 535.5 |
| $\Delta\nu_{St}$ ($cm^{-1}$) | 620 | 650 | 670 | 650 | 665 | 685 |
| $\phi$ | 0.81 | 0.73 | 0.75 | 0.77 | 0.75 | 0.74 |
| $\tau$ (ns) | 5.64 | 5.67 | 5.80 | 6.20 | 6.38 | 7.40 |
| $k_{fl}$ ($10^{-8}$ $s^{-1}$) | 1.44 | 1.29 | 1.29 | 1.24 | 1.18 | 1.00 |
| $k_{nr}$ ($10^{-8}$ $s^{-1}$) | 0.34 | 0.48 | 0.43 | 0.37 | 0.39 | 0.35 |

c-hex: cyclohexane; Ethyl Ac: ethyl acetate; EtOH: etanol; MetOH: methanol; $F_3$-etoh; 2,2,2-trifluoroethanol

**Table S3**. Full photophysical data of PM597 and its *O*-BODIPYs

| | PM597 | | | | | | **3** | | | | | |
|---|---|---|---|---|---|---|---|---|---|---|---|---|
| | c-hex | Ethyl Ac | Acetone | EtOH | MetOH | $F_3$-etoh | c-hex | Ethyl Ac | Acetone | EtOH | MetOH | $F_3$-etoh |
| $\lambda_{ab}$ (nm) | 529.0 | 523.0 | 522.5 | 524.0 | 523.0 | 521.5 | 530.5 | 526.0 | 526.5 | 525.5 | 525.0 | 524.0 |
| $\varepsilon_{max}$ ($10^{-4}M^{-1}cm^{-1}$) | 8.1 | 7.7 | 7.4 | 7.6 | 7.6 | 7.0 | 7.0 | 6.8 | 6.6 | 6.4 | 6.6 | 5.9 |
| $\lambda_{fl}$ (nm) | 571.0 | 562.5 | 563.5 | 563.0 | 561.0 | 561.0 | 573.0 | 567.0 | 567.0 | 566.0 | 566.0 | 564.0 |
| $\Delta\nu_{St}$ ($cm^{-1}$) | 1395 | 1330 | 1395 | 1315 | 1305 | 1355 | 1400 | 1375 | 1355 | 1360 | 1380 | 1355 |
| $\phi$ | 0.43 | 0.47 | 0.46 | 0.43 | 0.42 | 0.43 | 0.58 | 0.60 | 0.64 | 0.64 | 0.63 | 0.67 |
| $\tau$ (ns) | 3.91 | 4.31 | 4.34 | 4.09 | 4.21 | 4.64 | 4.58 | 5.40 | 5.77 | 5.86 | 5.98 | 6.95 |
| $k_{fl}$ ($10^{-8}$ $s^{-1}$) | 1.10 | 1.09 | 1.06 | 1.05 | 1.00 | 0.93 | 1.27 | 1.11 | 1.11 | 1.09 | 1.05 | 0.96 |
| $k_{nr}$ ($10^{-8}$ $s^{-1}$) | 1.46 | 1.23 | 1.24 | 1.39 | 1.38 | 1.23 | 0.92 | 0.74 | 0.62 | 0.61 | 0.62 | 0.47 |
| | **8** | | | | | | | | | | | |
| | c-hex | Ethyl Ac | Acetone | EtOH | MetOH | $F_3$-etoh | | | | | | |
| $\lambda_{ab}$ (nm) | 532.5 | 528.0 | 527.5 | 527.5 | 526.5 | 525.5 | | | | | | |
| $\varepsilon_{max}$ ($10^{-4}M^{-1}cm^{-1}$) | 5.4 | 5.1 | 4.9 | 5.1 | 5.0 | 4.2 | | | | | | |
| $\lambda_{fl}$ (nm) | 571.0 | 567.0 | 566.0 | 567.0 | 567.0 | 564.0 | | | | | | |
| $\Delta\nu_{St}$ ($cm^{-1}$) | 1265 | 1300 | 1290 | 1320 | 1355 | 1300 | | | | | | |
| $\phi$ | 0.76 | 0.78 | 0.75 | 0.74 | 0.73 | 0.71 | | | | | | |
| $\tau$ (ns) | 5.99 | 6.58 | 6.87 | 6.51 | 6.63 | 7.02 | | | | | | |
| $k_{fl}$ ($10^{-8}$ $s^{-1}$) | 1.27 | 1.18 | 1.09 | 1.14 | 1.10 | 1.01 | | | | | | |
| $k_{nr}$ ($10^{-8}$ $s^{-1}$) | 0.40 | 0.33 | 0.36 | 0.40 | 0.41 | 0.41 | | | | | | |

c-hex: cyclohexane; Ethyl Ac: ethyl acetate; EtOH: etanol; MetOH: methanol; $F_3$-etoh; 2,2,2-trifluoroethanol

**Table S4**. Full photophysical data of PM605 and its *O*-BODIPYs

| | PM605 | | | | | | **4** | | | | | |
|---|---|---|---|---|---|---|---|---|---|---|---|---|
| | c-hex | Ethyl Ac | Acetone | EtOH | MetOH | $F_3$-etoh | c-hex | Ethyl Ac | Acetone | EtOH | MetOH | $F_3$-etoh |
| $\lambda_{ab}$ (nm) | 547.5 | 543.0 | 542.5 | 544.5 | 543.0 | 545.5 | 548.5 | 546.0 | 546.0 | 546.5 | 545.5 | 546.5 |
| $\varepsilon_{max}$ ($10^{-4}M^{-1}cm^{-1}$) | 8.6 | 7.5 | 7.2 | 7.5 | 7.4 | 6.4 | 8.0 | 7.4 | 7.2 | 7.0 | 7.0 | 6.4 |
| $\lambda_{fl}$ (nm) | 561.0 | 558.0 | 557.5 | 560.0 | 559.0 | 562.5 | 563.0 | 561.0 | 560.0 | 561.0 | 563.5 | 564.0 |
| $\Delta\nu_{St}$ ($cm^{-1}$) | 435 | 500 | 500 | 510 | 520 | 550 | 470 | 490 | 460 | 475 | 585 | 570 |
| $\phi$ | 0.74 | 0.73 | 0.70 | 0.66 | 0.62 | 0.58 | 0.76 | 0.74 | 0.71 | 0.69 | 0.66 | 0.66 |
| $\tau$ (ns) | 6.27 | 6.64 | 6.86 | 6.56 | 6.65 | 7.85 | 6.37 | 6.98 | 7.24 | 7.19 | 7.42 | 8.34 |
| $k_{fl}$ ($10^{-8}$ $s^{-1}$) | 1.18 | 1.10 | 1.02 | 1.00 | 0.93 | 0.74 | 1.19 | 1.06 | 0.98 | 0.96 | 0.89 | 0.79 |
| $k_{nr}$ ($10^{-8}$ $s^{-1}$) | 0.41 | 0.41 | 0.44 | 0.52 | 0.57 | 0.54 | 0.38 | 0.37 | 0.40 | 0.43 | 0.46 | 0.41 |

| | **9** | | | | | |
|---|---|---|---|---|---|---|
| | c-hex | Ethyl Ac | Acetone | EtOH | MetOH | $F_3$-etoh |
| $\lambda_{ab}$ (nm) | 551.0 | 548.5 | 548.0 | 548.5 | 548.0 | 549.0 |
| $\varepsilon_{max}$ ($10^{-4}M^{-1}cm^{-1}$) | 7.8 | 6.8 | 6.7 | 6.7 | 6.6 | 6.1 |
| $\lambda_{fl}$ (nm) | 564.0 | 563.5 | 564.5 | 566.5 | 564.0 | 565.5 |
| $\Delta\nu_{St}$ ($cm^{-1}$) | 420 | 485 | 535 | 580 | 520 | 530 |
| $\phi$ | 0.80 | 0.78 | 0.74 | 0.72 | 0.70 | 0.67 |
| $\tau$ (ns) | 6.99 | 7.57 | 7.77 | 7.53 | 7.43 | 8.52 |
| $k_{fl}$ ($10^{-8}$ $s^{-1}$) | 1.14 | 1.03 | 0.95 | 0.95 | 0.94 | 0.79 |
| $k_{nr}$ ($10^{-8}$ $s^{-1}$) | 0.28 | 0.29 | 0.33 | 0.37 | 0.40 | 0.39 |

c-hex: cyclohexane; Ethyl Ac: ethyl acetate; EtOH: etanol; MetOH: methanol; $F_3$-etoh; 2,2,2-trifluoroethanol

**Table S5**. Full photophysical data of PM650 and its *O*-BODIPYs

| | PM650 | | | | | | 5 | | | | | |
|---|---|---|---|---|---|---|---|---|---|---|---|---|
| | c-hex | Ethyl Ac | Acetone | EtOH | MetOH | $F_3$-etoh | c-hex | Ethyl Ac | Acetone | EtOH | MetOH | $F_3$-etoh |
| $\lambda_{ab}$ (nm) | 589.5 | 588.0 | 588.0 | 588.5 | 587.5 | 590.0 | 588.5 | 589.0 | 590.0 | 589.5 | 589.0 | 590.5 |
| $\varepsilon_{max}(10^{-4}M^{-1}cm^{-1})$ | 5.3 | 4.2 | 3.5 | 4.0 | 4.1 | 3.8 | 4.5 | 4.0 | 3.8 | 3.9 | 3.7 | 3.1 |
| $\lambda_{fl}$ (nm) | 599.5 | 603.0 | 606.0 | 608.0 | 609.0 | 614.5 | 600.5 | 606.0 | 609.0 | 609.5 | 610.0 | 615.0 |
| $\Delta\nu_{St}$ ($cm^{-1}$) | 290 | 435 | 510 | 540 | 605 | 675 | 340 | 475 | 530 | 560 | 585 | 675 |
| $\phi$ | 0.36 | 0.15 | 0.11 | 0.099 | 0.060 | 0.040 | 0.39 | 0.15 | 0.11 | 0.10 | 0.073 | 0.044 |
| $\tau$ (ns) | 4.67 | 2.37 | 1.81 | 1.64 | 1.29 | 1.14 | 5.19 | 2.82 | 2.05(95%)<br>4.30(5%) | 1.92(98%)<br>5.05(2%) | 1.54(98%)<br>5.70(2%) | 1.14(98%)<br>6.78(2%) |
| $k_{fl}$ ($10^{-8}$ $s^{-1}$) | 0.77 | 0.63 | 0.61 | 0.60 | 0.46 | 0.35 | 0.75 | 0.53 | *0.54* | *0.52* | *0.47* | *0.38* |
| $k_{nr}$ ($10^{-8}$ $s^{-1}$) | 1.37 | 3.59 | 4.92 | 5.49 | 7.29 | 8.42 | 1.17 | 3.01 | *4.34* | *4.69* | *6.02* | *8.38* |
| | **10** | | | | | | **16** | | | | | |
| | c-hex | Ethyl Ac | Acetone | EtOH | MetOH | $F_3$-etoh | c-hex | Ethyl Ac | Acetone | EtOH | MetOH | $F_3$-etoh |
| $\lambda_{ab}$ (nm) | 591.0 | 592.0 | 593.0 | 592.0 | 591.0 | 592.5 | 590.0 | 590.0 | 590.0 | 590.0 | 589.0 | 591.0 |
| $\varepsilon_{max}(10^{-4}M^{-1}cm^{-1})$ | 3.8 | 3.0 | 2.8 | 2.9 | 2.7 | 2.4 | 6.4 | 5.4 | 5.2 | 5.3 | 5.1 | 4.3 |
| $\lambda_{fl}$ (nm) | 599.0 | 607.0 | 610.5 | 609.5 | 609.5 | 613.5 | 600.0 | 606.5 | 608.5 | 609.5 | 610.5 | 614.0 |
| $\Delta\nu_{St}$ ($cm^{-1}$) | 225 | 420 | 485 | 485 | 515 | 580 | 280 | 460 | 515 | 540 | 600 | 635 |
| $\phi$ | 0.47 | 0.22 | 0.17 | 0.15 | 0.11 | 0.08 | 0.34 | 0.16 | 0.12 | 0.11 | 0.081 | 0.050 |
| $\tau$ (ns) | 5.99 | 3.50 | 2.85 | 2.62 | 2.23 | 1.84 | 4.43 | 2.56 | 1.99 | 1.86 | 1.42 | 1.10 |
| $k_{fl}$ ($10^{-8}$ $s^{-1}$) | 0.78 | 0.63 | 0.60 | 0.57 | 0.49 | 0.43 | 0.77 | 0.63 | 0.60 | 0.59 | 0.57 | 0.45 |
| $k_{nr}$ ($10^{-8}$ $s^{-1}$) | 0.88 | 2.23 | 2.91 | 3.24 | 3.99 | 5.00 | 1.49 | 3.28 | 4.42 | 4.78 | 6.47 | 8.64 |

c-hex: cyclohexane; Ethyl Ac: ethyl acetate; EtOH: etanol; MetOH: methanol; $F_3$-etoh; 2,2,2-trifluoroethanol
*italic* – the rate constants were calculated from the main lifetime.

**Figure S1**. CHelpG charge distribution of the PM546 and its *O*-derivatives (**1**, **6** and **12**) in the excited state. The Bond Length Alternation (BLA) parameter is also included.

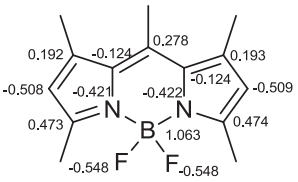


PM546
BLA = 0.0245

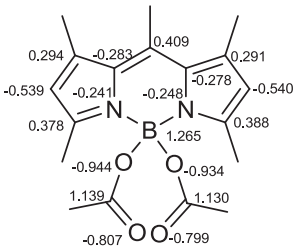


**1**
BLA = 0.0251

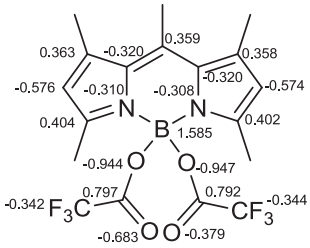


**6**
BLA = 0.0218

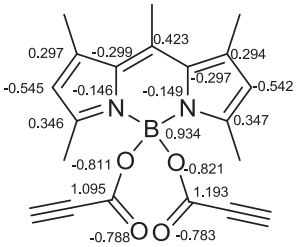


**12**
BLA = 0.0240

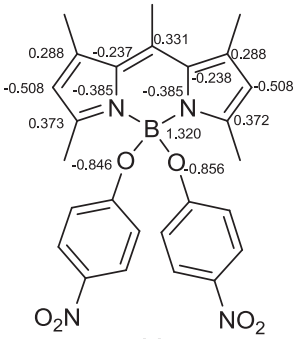


**14**
BLA = 0.0253

**Figure S2**. CHelpG charge distribution of the PM567 and its *O*-derivatives (**2**, **7**, **11** and **13**) in the excited state. The Bond Length Alternation (BLA) parameter is also included.

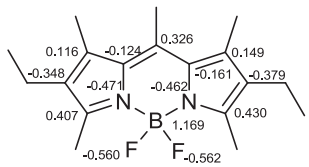


PM567
BLA = 0.0222

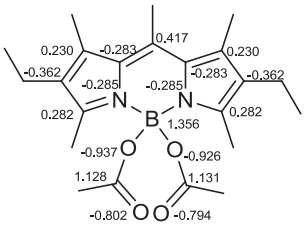


**2**
BLA = 0.0227

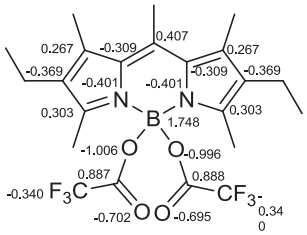


**7**
BLA = 0.0192

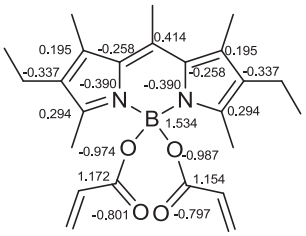


**11**
BLA =0.0225

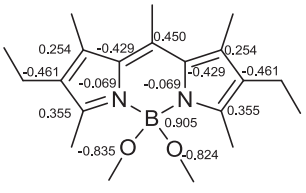


**13**
BLA = 0.0260

**Figure S3**. CHelpG charge distribution of the PM597 and its *O*-derivatives (**3** and **8**) in the excited state. The Bond Length Alternation (BLA) parameter is also included.

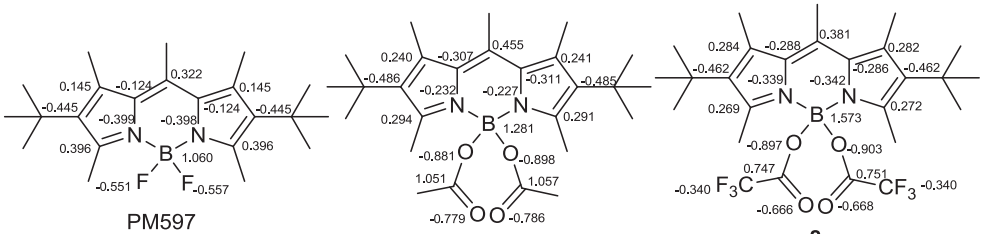


**Figure S4**. CHelpG charge distribution of the PM605 and its *O*-derivatives (**4** and **9**) in the excited state. The Bond Length Alternation (BLA) parameter is also included.

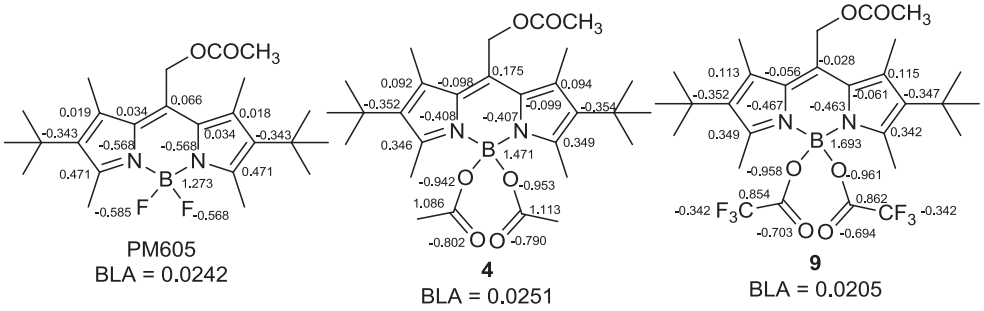


**Figure S5**. CHelpG charge distribution of the PM650 and its *O*-derivatives (**5** and **10**) in the excited state. The Bond Length Alternation (BLA) parameter is also included.

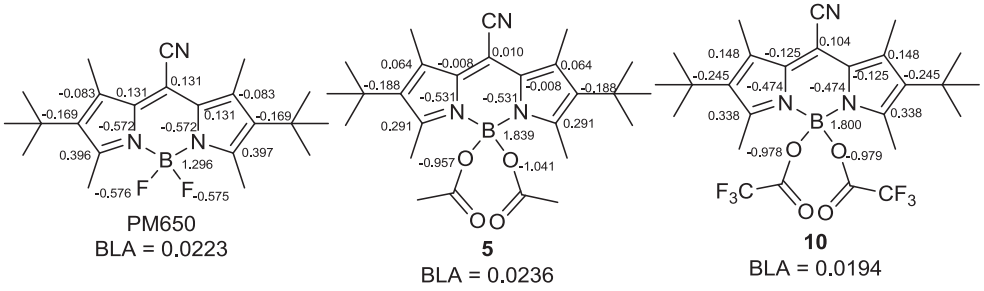

ChemPubSoc Europe

DOI: 10.1002/chem.201303579

CHEMISTRY A European Journal Full Paper

Laser Chemistry

# First Highly Efficient and Photostable *E* and *C* Derivatives of 4,4-Difluoro-4-bora-3a,4a-diaza-*s*-indacene (BODIPY) as Dye Lasers in the Liquid Phase, Thin Films, and Solid-State Rods

Gonzalo Duran-Sampedro,[a] Ixone Esnal,[c] Antonia R. Agarrabeitia,[a] Jorge Bañuelos Prieto,[c] Luis Cerdán,[b] Inmaculada García-Moreno,*[b] Angel Costela,[b] Iñigo Lopez-Arbeloa,[c] and María J. Ortiz*[a]

**Abstract:** A new library of *E*- and *C*-4,4-difluoro-4-bora-3a,4a-diaza-*s*-indacene (BODIPY) derivatives has been synthesized through a straightforward protocol from commercially available BODIPY complexes, and a systematic study of the photophysical properties and laser behavior related to the electronic properties of the B-substituent group (alkynyl, cyano, vinyl, aryl, and alkyl) has been carried out. The replacement of fluorine atoms by electron-withdrawing groups enhances the fluorescence response of the dye, whereas electron-donor groups diminish the fluorescence efficiency. As a consequence, these compounds exhibit enhanced laser action with respect to their parent dyes, both in liquid solution and in the solid phase, with lasing efficiencies under transversal pumping up to 73% in liquid solution and 53% in a solid matrix. The new dyes also showed enhanced photostability. In a solid matrix, the derivative of commercial dye PM597 that incorporated cyano groups at the boron center exhibited a very high lasing stability, with the laser emission remaining at the initial level after 100000 pump pulses in the same position of the sample at a 10 Hz repetition rate. Distributed feedback laser emission was demonstrated with organic films that incorporated parent dye PM597 and its cyano derivative. The films were deposited onto quartz substrates engraved with appropriate periodical structures. The *C* derivative exhibited a laser threshold lower than that of the parent dye as well as lasing intensities up to three orders of magnitude higher.

## Introduction

Tunable lasers are an important tool in a wide variety of fields such as spectroscopy, photochemistry, material diagnosis, medicine, or integrated optical devices. Organic dye molecules offer clear advantages over other commercially available multiwavelength laser sources such as low cost, ample spectral coverage over the visible region of the electromagnetic spectrum, and high conversion efficiency.[1]

Among the numerous classes of highly fluorescent dyes used as the active media of tunable lasers, the family of difluoroboron dipyrromethene complexes, or BODIPYs, is one with the highest potential.[2] Their development has acquired great importance in the last two decades owing to the excellent and easily modulated photophysical properties of these fluorophores.[3] As a consequence, they are also intensively applied as fluorescent probes in biological systems, photosensitizers for photodynamic therapy, and as materials for incorporation into electroluminescent devices.[2a,4]

The incorporation of appropriate functional groups into the chromophore could lead to new photophysical processes or large spectral shifts; therefore, depending on the desired application, one should carefully choose the kind of substituents and the position in which they will be incorporated into the BODIPY. A strategy that causes a substantial increase of the potential applications of the chromophore BODIPY is the substitution of fluorine atoms.[3a–c] Thus, a wide variety of new BODIPYs have been synthesized by means of fluorine displacement by alkyl or aryl groups (*C*-BODIPYs), ethynyl groups (*E*-BODIPYs), and alkoxy or aryloxy groups (*O*-BODIPYs).[5] The introduction of these functional groups leads to an increase in the Stokes shift as well as to the improved chemical and photochemical stability of these fluorophores, thereby opening the way to a new class of highly luminescent dyes.

[a] G. Duran-Sampedro, Prof. A. R. Agarrabeitia, Prof. M. J. Ortiz
Departamento de Quimica Organica I
Facultad de Ciencias Quimicas, Universidad Complutense
28040 Madrid (Spain)
Fax: (+34) 913944103
E-mail: mjortiz@quim.ucm.es

[b] Dr. L. Cerdán, Prof. I. García-Moreno, Prof. A. Costela
Instituto de Quimica-Fisica "Rocasolano" (IQFR), CSIC
Serrano 119, 28006 Madrid (Spain)
Fax: (+34) 915642431
E-mail: i.garcia-moreno@iqfr.csic.es

[c] I. Esnal, Dr. J. Bañuelos Prieto, Prof. I. Lopez-Arbeloa
Departamento de Quimica Fisica, UPV-EHU
Apartado 644, 48080 Bilbao (Spain)

Supporting information for this article is available on the WWW under http://dx.doi.org/10.1002/chem.201303579.


© 2014 Wiley-VCH Verlag GmbH & Co. KGaA, Weinheim

Despite the considerable volume of work on the synthesis and applications of this type of fluorophores, there are few reports on their optical and lasing properties.[5c,d] In this field, our research group has described the synthesis and characterization of the emission properties of a set of *O*-BODIPYs in which two carboxylate groups are connected to the boron center in place of the fluorine atoms. It was shown that these dyes are highly fluorescent and exhibit enhanced laser action with respect to their *F*-BODIPY analogues, both in liquid solution and the solid phase.[5c]

Considering these results, in the present work we have synthesized a new library of *E*- and *C*-BODIPY derivatives (named **1**–**7** in Scheme 1) from the commercially available BODIPYs and we have carried out a systematic study of their photophysical properties and laser behavior related to the electronic properties of the B-substituent group (alkynyl, cyano, vinyl, aryl, and alkyl). As far as we know, there is only one precedent on lasing performance of *E*-BODIPYs by Ray et al. in which it is revealed that this substitution at the boron center does not significantly improve the laser efficiency but enhances the photostability owing to their lower reaction rates with $^1O_2$ and lower $^1O_2$ generation capacity.[5d] However, the new BODIPY derivatives synthesized herein through a straightforward protocol exhibit lasing efficiencies up to four times higher than those recorded for the corresponding commercial dyes with high photostability in the liquid phase, the bulk solid state, and in thin films.

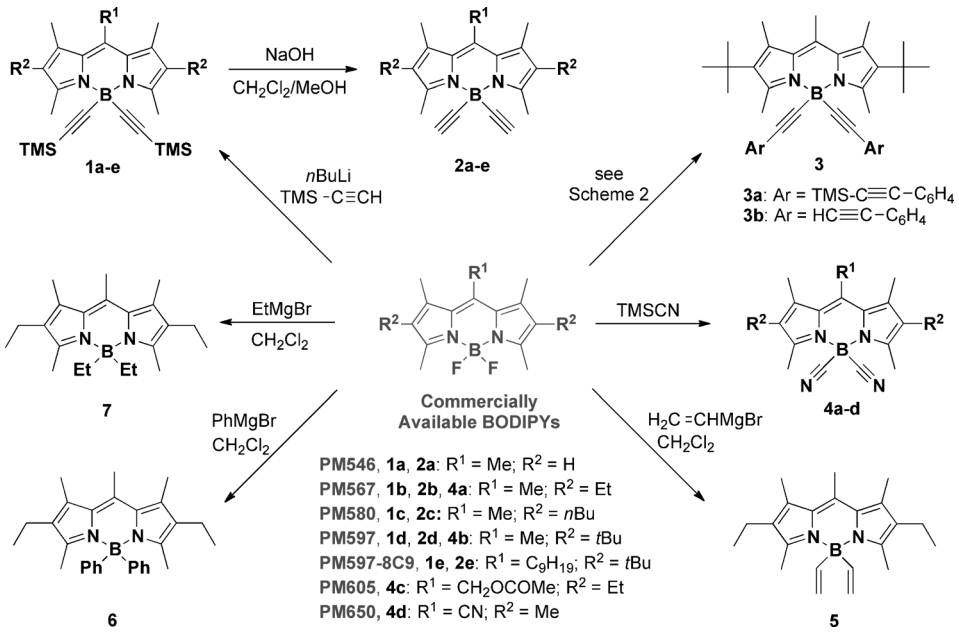


**Scheme 1.** Molecular structures of commercial dyes and their analogues **1**–**7** synthesized in this work.

## Results and Discussion

BODIPY dyes **1**–**7** were successfully obtained from commercially available dyes PM546, PM567, PM580, PM597, PM597-8C9, PM605, and PM650 with organolithium, Grignard reagents, or trimethylsilyl cyanide (TMSCN) as nucleophilic agents depending upon the desired change in the boron atom. BODIPY derivatives **1b**,[6] **2b**,[6] and **6**[7] were synthesized by the methods previously described. Dyes **1a**–**e** were prepared in good yield by the introduction of two trimethylsilylacetylene units by using an excess amount of the corresponding organolithium derivative, generated in situ from trimethylsilylacetylene and *n*-butyllithium. No monosubstituted derivatives were formed under the reaction conditions. Removal of the trimethylsilyl groups using an excess amount of NaOH afforded **2a**–**e** as the major products. Only compound **2a** was obtained in addition to a small percentage of the monoprotected derivative.

The reaction of PM597 with mono-TMS-protected 1,4-diethynylbenzene **8** gave *E*-BODIPY **3a** in good yield. The removal of the TMS protection yielded a mixture of dideprotected derivative **3b** (80%) and monodeprotected derivative **3c** (15%), which were separated by means of flash chromatography on silica (Scheme 2).

Replacement of the fluorine atoms by cyano groups (compounds **4a**–**d**) was carried out by the reaction of BODIPY with TMSCN in the presence of $AlCl_3$ as Lewis acid (compounds **4a**

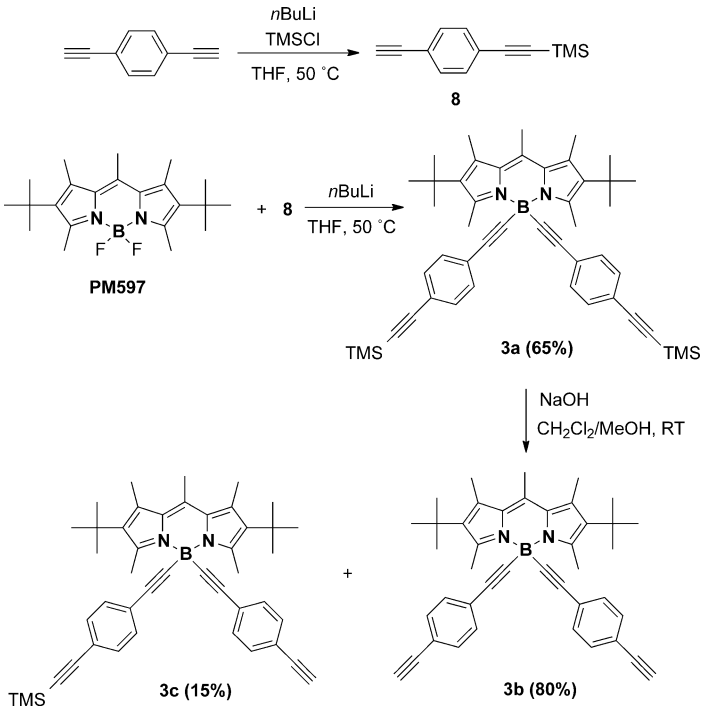


**Scheme 2.** Synthesis of BODIPYs **3a**–**c**.


© 2014 Wiley-VCH Verlag GmbH & Co. KGaA, Weinheim

and **4c**) or in the absence of $AlCl_3$ (compounds **4b** and **4d**) in 82 to 85% yield, except for **4d**, which was obtained in 25% isolated yield.

Furthermore, the use of an excess amount of Grignard reagents (vinylmagnesium bromide or ethylmagnesium bromide) led to rapid substitution of the fluorine atoms and allowed the preparation of compounds **5** and **7**, respectively, in moderate yield.

### Photophysical properties

The commercial *F*-BODIPYs that bear linear alkyl groups (PM546, PM567, and PM580) set themselves apart by their high fluorescence performance (approaching 100% in Figure 1 and Table S1 in the Supporting Information), although the fluorescence capacity of the BODIPYs depends on the functionalization of the core. Thus, the presence of methylenacetoxy at the *meso* position (PM605) reduces the radiative deactivation probability owing to its electron-withdrawing character, whereas the *tert*-butyl groups (PM597 and PM597-8C9) enhance the nonradiative pathways owing to the geometrical distortion induced by the sterical hindrance to accommodate such bulky groups. The most noteworthy case is the appearance of a quenching intramolecular charge transfer (ICT) state by the grafting of the cyano at the central position (PM650).[8]

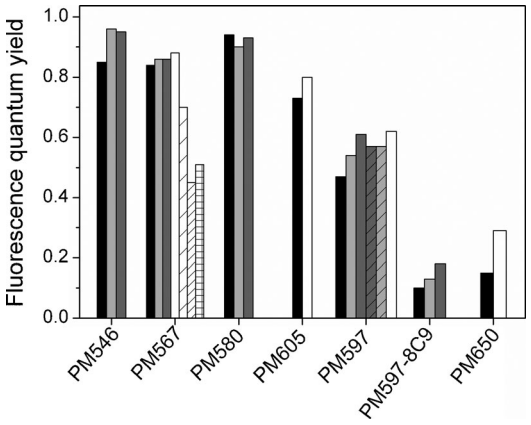


**Figure 1.** Fluorescence quantum yield in ethyl acetate of the commercial *F*-BODIPYs (black) and their corresponding *E*-BODIPYs bearing acetylene (**2a**–**e**, grey, striped if phenyl is also grafted, **3b**), acetylene TMS (**1a**, **1c**–**e**, light grey, striped upon addition of a phenyl, **3a**), and *C*-BODIPYs bearing a cyano (**4a**–**d**, white), vinyl (**5**, sparse stripe), ethyl (**7**, dense stripe), and phenyl group (**6**, grid).

The replacement of fluorine atoms in the above BODIPYs by acetylenes (**2a**–**e**) does not have a great impact on the photophysics of the chromophore (Figure 1). The fluorescence quantum yields of the resulting *E*-BODIPYs remain high (set of derivatives from PM546, PM567, and PM580), or at least similar to their corresponding counterpart (PM597). Moreover, the addition of trimethylsilyl (**1a**, **1c**, and **1d**), aryl (**3b**), or both (**3a**) onto the triple bond has a minor effect. These results are reasonable keeping in mind that the boron atom does not take part in the delocalized $\pi$ system but acts as a bridge unit to infer rigidity onto the whole structure. Indeed, opposite results (high bathochromic shifts and reduced fluorescence quantum yields) have been reported for acetylene groups directly attached to the core at the 2- and 6-positions.[9]

Nevertheless, the electronic character of the group anchored to the boron atom plays a key role in the fluorescence performance of the resulting *E*- and *C*-BODIPY (Figure 1). Such an effect can be easily discussed by considering the set of derivatives from PM567. The acetylene group behaves like a weak electron acceptor (Hammet parameter $\sigma_p^+ = 0.18$). A further increase in such behavior through the presence of cyano groups ($\sigma_p^+ = 0.66$) results in an improvement in the fluorescence behavior (see compounds **4a**–**4d** in their respective series in Figure 1). Such an enhancement is especially noticeable in PM650 since the fluorescence quantum yield increases from 0.15 to 0.29. It is possible that the two cyano groups linked to the boron atom counteract the charge separation induced by the *meso*-cyano substitution to hamper the population of the ICT state. However, a withdrawing character that is too strong could damage the fluorescence performance, which is what happens in *O*-BODIPYs that bear nitro groups ($\sigma_p^+ = 0.74$) owing to the activation of ICT processes.[5c]

By contrast, the presence of electron-donor groups, such as phenyl rings ($\sigma_p^+ = -0.18$), leads to a decrease in the fluorescence quantum yield and lifetime (Figure 1). Moreover, this compound (**6**) exhibits a high Stokes shift (1350 versus 550 $cm^{-1}$ in PM567) as a result of a bathochromic shift of the fluorescence band (Figure 2). Such a trend suggests a high geometrical rearrangement upon excitation, which enables the energy relaxation and the consequent loss of fluorescence emission. In addition, the optimized excited-state geometry points to the high steric hindrance induced by the two rings attached to the boron (Figure S1 in the Supporting Information). As a result, the two phenyl groups are placed orthogonally and the chromophore is distorted (deviation from planarity up to 25°). This lack of planarity enhances the internal conversion and explains the recorded lower fluorescence performance for compound **6**.

Similar trends are observed with the unsaturation degree of the alkyl chains attached to the boron atom. A change from acetylene (compound **2b**) to vinyl (**5**) and to ethyl (**7**) implies a reversal of the electronic behavior from electron donor to acceptor ($\sigma_p^+ = 0.18$, $-0.16$, and $-0.30$, respectively). Accordingly, the fluorescence quantum yield and lifetime decrease in the same fashion (Figures 1 and 2). In fact, in the *C*-BODIPY that bears ethyl (compound **7**), the Stokes shift is quite high (1115 $cm^{-1}$) as a consequence of the shift of the fluorescence band towards lower energies. Again, the optimized excited-state geometry confirms the geometrical distortion (up to 23°; Figure S2 in the Supporting Information) to be the main pathway for nonradiative deactivation.

The quantum mechanical calculations (Table 1) reproduce the experimental features well. Indeed, the absorption and fluorescence spectra signatures are satisfactorily predicted theoretically. Both compounds **6** and **7** stand out through an emission shifted to lower energies and a higher Stokes shift as result of an important change in the geometry upon excita-


© 2014 Wiley-VCH Verlag GmbH & Co. KGaA, Weinheim

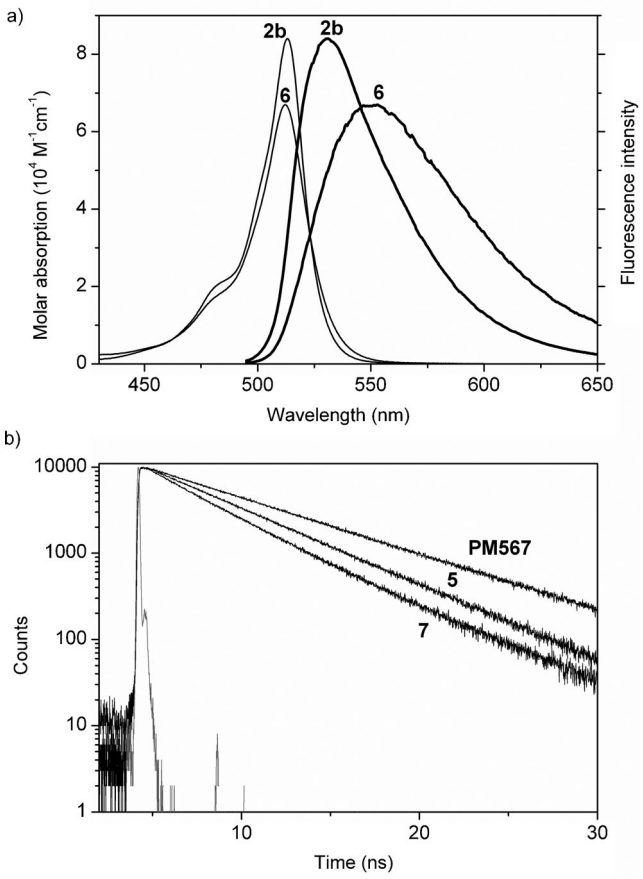


**Figure 2.** a) Absorption and normalized fluorescence (bold) spectra in ethyl acetate of PM567 derivatives bearing acetylene (**2b**) and phenyl (**6**) groups. b) Fluorescence decay curves of PM567 derivatives bearing vinyl (**5**) and ethyl (**7**) groups.

**Table 1.** Theoretical simulation (TD-B3LYP) of the absorption and fluorescence transition of representative *C*-BODIPYs: absorption ($\Delta E_{ab}$) and fluorescence ($\Delta E_{fl}$) energy gap, and Stokes shift ($\Delta \nu_{St}$).

| | $\Delta E_{ab}$ [eV] | $\Delta E_{fl}$ [eV] | $\Delta \nu_{St}$ [$cm^{-1}$] |
|---|---|---|---|
| PM567 | 2.91 | 2.87 | 380 |
| **2b** | 2.94 | 2.89 | 445 |
| **6** | 2.92 | 2.77 | 1210 |
| **5** | 2.95 | 2.88 | 580 |
| **7** | 2.99 | 2.83 | 1265 |
| PM597 | 2.87 | 2.73 | 1170 |
| PM597-8C9 | 2.84 | 2.62 | 1795 |

tion. Such theoretically suggested loss of planarity correlates well with the evolution of the nonradiative rate constant (Table S1 in the Supporting Information).

To address the opposite influence of the electron donor (harmful to the fluorescence capacity) and acceptor (slightly beneficial) groups, which are attached to boron in the *E*- and *C*-BODIPYs, we simulated the charge-density distribution in some selected compounds (Figure S3 in the Supporting Information). In a previous study on *O*-BODIPYs, we concluded that although the boron atom does not take part in the delocalized $\pi$ system, its substitution determines the charge distribution through the whole chromophore and hence the aromaticity of the $\pi$ system (evaluated by the bond-length alternation (BLA) parameter;[10] data included in Figure S3 in the Supporting Information).

The presence of acetylene groups leads to a higher positive charge in the boron atom and a slightly lower charge alternation through the core, with little influence on the aromaticity (similar BLA and fluorescence capacity to their corresponding reference *F*-BODIPYs). An increase in the electron-donor ability of the substituent (cyano groups) implies a strong rearrangement of the charge distribution, which results in a more aromatic chromophore, as reflected in the BLA parameter (i.e., 0.023 for compound **4a**), which is the lowest among all the BODIPYs reported herein. Accordingly, the derivatives with a cyano group at the boron atom (**4a**–**4d**) yield the highest fluorescence capacity. However, a progressive increase in the electron-donor ability of the substituent (from acetylene to ethyl) results in less aromatic dyes (BLA = 0.027, 0.029, and 0.031 for compounds **2b**, **5**, and **7**, respectively), which is in agreement with the registered lower fluorescence efficiencies. Especially remarkable is the asymmetric disposition of the phenyl rings in compound **6**. This should be a consequence of the steric hindrance between their *ortho*-hydrogen and the methyl groups in the 3- and 5-positions Figure S1 in the Supporting Information). As a result, one of the rings acquires a high positive charge (Figure S3 in the Supporting Information) and leads to a less aromatic dye (BLA = 0.028), thereby reducing the fluorescence capacity.

Whereas the lengthening of the alkyl chain (from ethyl to butyl) at the 2- and 6-positions of PM567 to yield PM580 has a minor effect on the photophysical properties, important changes are noticed when the aliphatic chain is enlarged (from one methylene to nine) at the 8-position of PM597 to yield PM597-8C9 (Figure 1 and Table S1 in the Supporting Information). The photophysical properties of PM597 were controlled by the steric hindrance induced by the *tert*-butyl groups, which leads to a loss of planarity in the chromophore. As consequence, the nonradiative rate constant (from $0.28\times10^8$ $s^{-1}$ in PM567 to $1.23\times10^8$ $s^{-1}$ in PM597) and the Stokes shift (from 550 to 1330 $cm^{-1}$, respectively) increased significantly. These trends seem to be more evident upon grafting a linear chain at the 8-position, because the nonradiative rate ($k_{nr}$) enhances up to $7.9\times10^8$ $s^{-1}$, thereby reducing the fluorescence quantum yield and lifetime (0.10 and 1.14 ns). In addition, the Stokes shift increases up to 2330 $cm^{-1}$ as a result of a stronger bathochromic shift in the fluorescence band (placed at 595 nm, also theoretically predicted in Table 1).

The optimized geometries show that the linear chain in PM597-8C9 adopts a linear disposition, far away from the indacene core (Figure S1 in the Supporting Information). However, its presence seems to enhance the steric hindrance and a drastic geometrical rearrangement takes place after excitation. As a result, the chromophore geometry is highly distorted and a deviation of planarity up to 30° is predicted. Overall, such loss of planarity implies lower aromaticity, but surprisingly, the opposite happens in the compounds that bear 2,6-*tert*-butyl. In fact, the BLA parameters suggest that these compounds


© 2014 Wiley-VCH Verlag GmbH & Co. KGaA, Weinheim

**Table 2.** Lasing efficiencies of commercial BODIPY dyes and their *C*-BODIPY derivatives in different solvents at the dye concentrations that optimize their laser action of solutions in ethyl acetate ($\lambda_{exc}$: pumping wavelength).

| Solvent | $\lambda_{exc}=355$ nm | | | | | | | | | | $\lambda_{exc}=532$ nm | | | | | | | | | | | | | | | | | |
|---|---|---|---|---|---|---|---|---|---|---|---|---|---|---|---|---|---|---|---|---|---|---|---|---|---|---|---|---|
| | PM546 | **1a** | **2a** | PM567 | **1b** | **2b** | **4a** | **5** | **6** | **7** | PM580 | **1c** | **2c** | PM597 | **1d** | **2d** | **3a** | **3b** | **4b** | PM597-8C9 | **1e** | **2e** | PM605 | **4c** | PM650 | **4d** | PM650–F–CN |
| EtOAc | 23 | 58 | 52 | 48 | 67 | 60 | 68 | 54 | 60 | 30 | 57 | 65 | 63 | 53 | 70 | 63 | 73 | 68 | 73 | 55 | 62 | 59 | 55 | 68 | 35 | 45 | 36 |
| Acetone | 14 | 56 | 49 | 36 | 65 | 57 | 65 | 45 | 56 | 25 | 57 | 63 | 62 | 50 | 67 | 62 | 71 | 65 | 70 | 52 | 59 | 56 | 57 | 69 | 31 | 40 | 30 |
| MeOH | | | | 34 | 58 | 54 | 61 | | 52 | | 51 | 61 | 57 | 54 | 63 | 59 | 69 | 63 | 68 | 47 | 59 | 54 | 55 | 66 | 12 | 30 | 22 |
| EtOH | 18 | 58 | 50 | 36 | 62 | **56** | 63 | 44 | 54 | 27 | | | | 51 | 65 | 61 | 69 | 60 | 67 | | | | 56 | 67 | | | |
| $F_3$–EtOH | | | | | | | | | | | | | | 56 | 63 | 57 | 70 | 62 | 65 | | | | 51 | 61 | 27 | 38 | 28 |
| $CH_2Cl_2$ | | | | | | | | | | | 50 | 61 | 59 | | | | | | | 50 | 60 | 56 | | | | | |
| THF | | | | | | | | | | | 59 | 66 | 64 | | | | | | | | | | | | | | |

(PM597 and PM597-8C9) become more aromatic as the excited-state distortion increases (BLA of 0.022 and 0.019, respectively). These evolutions have been previously reported and explained in terms of the "loose-bolt" or Brunings–Corwin effect, in which the lower planarity by constrained geometries implies a lower resonance energy, thereby placing the excited and ground states energetically closer.[11] Therefore, the strong bending of the chromophore in the excited state should be the reason for the important shift of the emission band towards higher energies and, at the same time, the reason for the reduction of the fluorescence efficiency in those compounds that bear *tert*-butyl groups at the 2- and 6-positions (PM597 and mainly PM597-8C9). In these dyes, further replacement of the fluorine atoms by acetylene (**1e**, **2e**) slightly ameliorates the fluorescence capacity, in line with the previously discussed *E*- and *C*-BODIPYs.

## Lasing properties

### *Liquid phase*

According to their absorption properties, the lasing properties of PM546 and its derivatives **1a** and **2a** were studied under pumping at 355 nm, whereas all the other dyes studied here were pumped at 532 nm. The dye concentrations in the lasing studies are in the millimolar range, as required by our experimental conditions of transversal excitation and strong focusing of the incoming pump radiation. In this way, the pump radiation is totally absorbed within the first millimeter of the solution to obtain an emitted laser beam with a near-circular cross-section.

To optimize the laser action, for the different dyes we first analyzed the dependence of their laser emission on dye concentration in ethyl acetate. The results obtained by varying the dye concentrations over the range 0.3 to 10 mM, depending on the dye, while keeping all the other experimental parameters constant, are collected in Table S2 in the Supporting Information. In all cases the dyes followed the typical behavior, with the lasing efficiency (defined as the ratio between the energy of the dye laser output and the pump energy incident on the sample surface) first increasing with dye concentration until a maximum value is reached. Increasing the dye concentration beyond this point results in a decrease in the lasing efficiency that can be related to reabsorption/reemission processes, which become increasingly important as the dye concentration rises. The optimum value of the dye concentration thus determined was then used to prepare dye solutions in a number of polar protic and polar aprotic solvents to analyze the effect of the nature of the solvent on the laser properties of the different derivatives. The results obtained are collected in Table 2.

The observed lasing efficiencies within the different families of *E*- and *C*-BODIPYs correlate well with their photophysical properties, determined in more diluted solutions (Tables S1 and S2 in the Supporting Information): higher lasing efficiency corresponds in general to a lower nonradiative rate constant. The few exceptions to this general rule (i.e., in the PM580 family) can be understood in terms of the effect of the much higher dye concentration in the solutions utilized in the laser experiments.

The lasing properties of the new dyes follow a dependence on the solvent character similar to that exhibited by the commercial ones, with the lasing efficiencies being higher in polar aprotic solvents than in polar protic ones. It can be seen in Table 2 that, with the exception of dye **7**, in all cases the lasing efficiency of the derivatives is higher than that of the commercial parent dye. The highest lasing efficiencies were obtained with the derivatives that incorporate cyano groups (compounds **4a**–**d**), which is in agreement with their photophysical behavior discussed above. The improvement in their fluorescence capacity was owing to the action of the cyano group counteracting the charge separation as a result of the increased electron-donor ability of the cyano substituent. The effect of the unsaturation degree of the alkyl chains attached to the boron atom, discussed in detail above, is also clearly indicated by the lasing data. Thus, the change from acetylene (compound **2b**) to vinyl (**5**) and to ethyl (**7**), which produces a reversal of the electronic behavior from electron donor to acceptor as well as an increased geometrical distortion in the excited-state geometry of those compounds, takes place in accord with a decrease in the lasing efficiency following the sequence Eff(**2b**) > Eff(**5**) > Eff(**7**) (Table 2).

An important parameter for any practical application of dye lasers is their lasing photostability under repeated pumping. Table 3 collects the data on the decrease in the laser-induced fluorescence intensity under transversal excitation of a capillary that contains dye solutions in ethyl acetate (see the Experi-


© 2014 Wiley-VCH Verlag GmbH & Co. KGaA, Weinheim

**Table 3.** Intensity of the laser-induced fluorescence emission ($I$) after 100000 pump pulses for dyes in ethyl acetate solution.

| | $\lambda_{exc}=355$ nm | | | $\lambda_{exc}=532$ nm | | | | | | | | | | | | | | | | | | | | | |
|---|---|---|---|---|---|---|---|---|---|---|---|---|---|---|---|---|---|---|---|---|---|---|---|---|---|
| | PM546 | **1a** | **2a** | PM567 | **1b** | **2b** | **4a** | **6** | **7** | PM580 | **1c** | **2c** | PM597 | **1d** | **2d** | **3a** | **3b** | **4b** | PM597-8C9 | **1e** | **2e** | PM605 | **4c** | PM650 | **4d** |
| $I$ [%][a] | 60 | 92 | 76 | 17 | 55 | 70 | 100 | 100 | 50 | 48 | 84 | 70 | 85 | 100 | 94 | 65 | 72 | 100 | 30[b] | 100 | 100 | 20[c] | 100 | 80 | 75 |

[a] $I$ [%] = 100 ($I/I_0$), with $I_0$ being the initial intensity. [b] After 60000 pump pulses. [c] After 40000 pump pulses.

mental Section) after a given number ($n$) of pump pulses for both the commercial dyes and their derivatives synthesized in the present work. Dye PM546 and its derivatives **1a** and **2a** were pumped at 355 nm and at 5 Hz repetition rate. All the other dyes were pumped at 532 nm and at a 10 Hz repetition rate. The pump energy was 5 mJ in all cases. Dyes **4a**–**c**, which exhibited the highest lasing efficiencies and the best photophysical behavior, also were the most photostable, with their laser-induced fluorescence emission remaining at the initial level after 100000 pump pulses. This stability is significantly higher than that of the corresponding commercial dyes (PM567, PM597, and PM605). Compound **4d**, which is the derivative of the *meso*-cyano-substituted dye PM650, exhibits lower photostability than **4a**–**c**, thereby reflecting the presence of the ICT state in PM650 with its harmful effects on laser performance and stability.[8]

### *Bulk solid state*

The excellent laser performance exhibited by the new dyes in liquid solution led us to explore their behavior as photonic materials, either in bulk as solid-state dye lasers (SSDLs) or incorporated into thin-film structures. First, we analyzed the laser behavior of the dyes incorporated into bulk solid samples cast in a cylindrical shape, thereby forming rods 10 mm in diameter and 10 mm in length (for more details, see the Supporting Information). The dyes chosen to perform this study were **4a**–**4c** because of their excellent lasing properties in liquid solution, and their behavior as SSDLs was compared with the corresponding parent dyes PM567, PM597, and PM605, respectively. As matrix material we chose poly(methylmethacrylate) (PMMA) because it mimics ethyl acetate, the solvent in which those dyes produced the highest lasing efficiencies (Table 2). In addition, PMMA has very high transparency, high laser damage threshold, very good chemical compatibility with the chosen dyes, and, most importantly from a practical point of view, the final production costs would be low owing to its cheapness. The dye concentration in the matrix was that which optimized the lasing efficiency in ethyl acetate (Table S2 in the Supporting Information).

Table 4 contains the lasing performance of the selected dyes. The lasing efficiencies of the *C*-BODIPYs enhanced significantly those obtained with the corresponding commercial parent dyes, and correlate with those obtained in liquid solution, with the efficiency of dye **4b** being the highest. These efficiencies are lower than those obtained in liquid solution, probably owing to the fact that the finishing of the surface of the solid samples relevant to the laser operation was not laser-grade, so that higher efficiencies are to be expected with laser-grade surfaces.

**Table 4.** Lasing properties of dyes incorporated into solid PMMA matrices.[a]

| Dye | Eff [%] | $\lambda_l$ [nm] | $I_n$ [%] | $n$ |
|---|---|---|---|---|
| PM567 | 34 | 566 | 30 | 100000 |
| **4a** | 49 | 568 | 96 | 100000 |
| PM597 | 36 | 585 | 85 | 100000 |
| **4b** | 53 | 588 | 100 | 100000 |
| PM605 | 37 | 595 | 0 | 65000 |
| **4c** | 51 | 597 | 80 | 100000 |

[a] Eff: lasing efficiency; $\lambda_l$: peak laser emission wavelength; $I_n$ [%]: intensity of the laser output after $n$ pump pulses in the same position of the sample; $I_n$ [%] = 100 × ($I_n/I_0$), with $I_0$ being the initial intensity.

To assess the photostability of the new materials, we followed the evolution of their laser emission under repeated pumping in the same position of the sample at a repetition rate of 10 Hz. All three derivatives demonstrated a much higher photostability than the parent dyes, with dye **4b**, which has a laser emission that remains at the initial level after 100000 pump pulses in the same position of the sample, exhibiting the best behavior once again. These results show that the newly developed *C*-BODIPYs are excellent candidates to achieve SSDLs with greatly improved performance.

### *Thin films*

As a proof of concept, we also assessed the laser properties of the new BODIPYs operated as dye-doped polymer thin-film lasers, since over the last few years there has been a growing interest in the development of these types of devices because of their potential applications as coherent light sources suitable for integration in spectroscopic and sensing devices.[12]

Given the outstanding laser properties shown by derivative **4b** both in liquid and the solid state, we decided to choose this dye and its parent dye PM597 as reference to develop the thin-film laser. The host matrix was PMMA. Thin films approximately 800–850 nm thick were prepared from solution by solving adequate amounts of dye and PMMA in chloroform, and the resulting solutions were spin-coated onto quartz substrates. The complete details on the sample preparation and evaluation can be found in the Supporting Information.

To obtain sufficient pump absorption and gain in the thin films, dye concentrations were selected to render an absorbance of 0.08 at the pump wavelength (532 nm). This means concentrations of 19 and 23 mM for PM597 and derivative **4b**,


© 2014 Wiley-VCH Verlag GmbH & Co. KGaA, Weinheim

respectively. Such high concentrations are prone to give rise to self-quenching[13] (mirrored as band displacements and reduction in fluorescence quantum yield and extinction coefficients) and aggregate formation[11] (appearance of new absorption bands). To assess the extent of both phenomena, the absorption and emission spectra of both dyes were collected (Figure 3). Even at these high dye concentrations, the absorption and fluorescence spectra are redshifted by 2.5 and 0.5 nm, respectively, with respect to the ones registered with the dilute solutions, whereas the band shapes are unchanged (i.e., there are no new spectral features; compare Figures 2a and 3a). Nevertheless, the extinction coefficients of PM597 and derivative **4b** are reduced from 7.7 and $6.7\times10^4$ м$^{-1}$cm$^{-1}$ ($2\times10^{-6}$ м in EtOAc) to approximately 6.2 and $5.2\times10^4$ м$^{-1}$cm$^{-1}$ (≈20 мм in PMMA), respectively. The fluorescence quantum yield was not measured for the thin films, so it cannot be compared with the one in dilute solutions, but it will be arguably lower in the thin films. The previous facts indicate that dyes PM597 and derivative **4b** will suffer from a certain amount of self-quenching (but no aggregation) in the thin films, but we will see that it is not enough to prevent laser action from taking place.

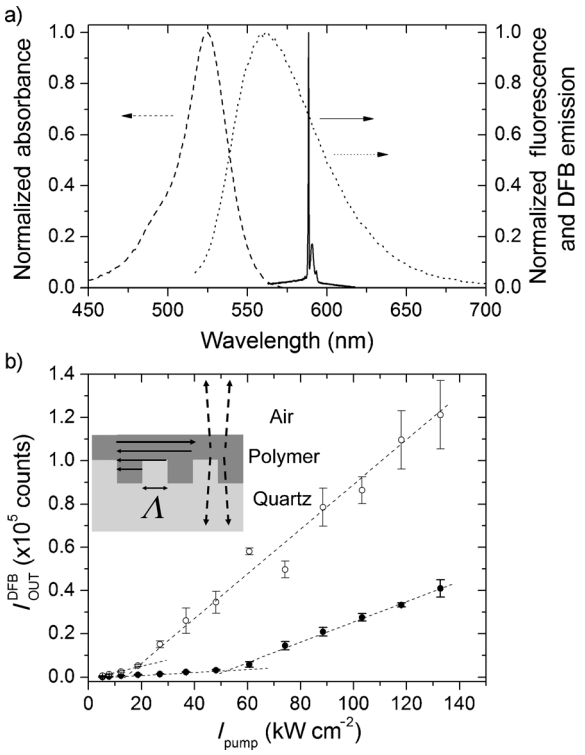


**Figure 3.** a) Absorption (dashed line), fluorescence ($\lambda_{exc}=500$ nm, dotted line), and laser spectra (solid line) of derivative **4b** (23 мм) doped in PMMA. b) DFB output intensity as a function of pump intensity from thin films of commercial PM597 19 мм (filled circles) and derivative **4b** (23 мм; hollow circles) doped in PMMA. Inset: sketch of DFB laser. The arrows represent in-plane feedback owing to second-order diffraction (solid arrows) and out-coupled laser emission owing to first-order diffraction (dashed arrow).

To obtain resonant oscillation within the thin film, we made use of distributed feedback (DFB) owing to Bragg scattering in periodic structures (Figure 3b, inset).[14] The emission wavelength ($\lambda_{DFB}$) in DFB lasers is given by the Bragg condition $m\cdot\lambda_{DFB}\approx2n_{eff}\cdot\Lambda$, in which $m$ is the diffraction order in which the device operates, $n_{eff}$ is the effective refractive index experienced by the propagating mode, and $\Lambda$ is the period of the refractive index modulation (Figure 3b, inset). By working with the second-order $m=2$, $\lambda_{DFB}\approx n_{eff}\cdot\Lambda$, the second-order diffraction provides in-plane feedback, and the laser light is diffracted out of the surface of the film perpendicular to the plane of the waveguide through first-order diffraction (Figure 3b, inset). The fundamental transverse electric ($TE_0$) propagating mode in waveguides approximately 800–850 nm thick with a refractive index of 1.4900 (PMMA), deposited onto a quartz substrate ($n=1.456$), experiences an effective refractive index $n_{eff}=1.472$.[15] By taking into account that the resonant wavelength must be in the emission window of the selected dyes ($\lambda_{DFB}\approx590$ nm), a substrate with modulation period $\Lambda=400$ nm was used. For the present experiments, the quartz substrate was scribed by e-beam lithography[16] with a squared grating (Figure 3b, inset) of period $\Lambda=400$ nm, a duty cycle of 50%, and a depth of 100 nm. These waveguides might sustain a second propagating mode, the fundamental transverse magnetic ($TM_0$) mode, which does not participate in the laser process. We have excited the samples with the pump polarization parallel to the grating grooves so that the transition dipole moment of the emitting molecules and the grating wave vector (which is perpendicular to the grooves and parallel to the structure) fully overlap. This way the laser threshold of the $TE_0$ mode is maximally reduced.[17]

By pumping the devices well above the threshold ($I_{pump}=130$ kW cm$^{-2}$), DFB laser emission with a linewidth of approximately 0.2 nm centered at 587.6 (PM597) and 588.5 nm (derivative **4b**) was obtained (Figure 3a), which is in agreement with the Bragg resonant wavelength expected for the chosen corrugated substrate and film thickness. The difference in the emission wavelengths is consistent with the slight changes in the sample thicknesses (≈±50 nm) owing to the deposition process, which modifies the effective refractive index $n_{eff}$ and, in turn, the resonant wavelength.

Figure 3b shows the dependence of the DFB laser intensity on the pump intensity (light/light curve) for the samples doped with PM597 (filled circles) and derivative **4b** (hollow circles). From this plot one can determine the laser thresholds, which are the points in which there is a change in slope in the light/light curve. From the data in Figure 3b it can be seen that derivative **4b** not only has a lower DFB laser threshold than the parent dye (20 versus 55 kW cm$^{-2}$) but presents a threefold enhancement in the output intensity when pumped well above threshold ($I_{pump}=130$ kW cm$^{-2}$), which is in agreement with the results obtained in bulk and liquid media.

## Conclusion

We have successfully designed and synthesized new *E*- and *C*-BODIPYs through a straightforward protocol from the commercially available BODIPYs. The experimental trends of the fluorescence efficiencies with the electron-donor/-acceptor properties of the susbtituents (Hammet parameter) at the boron


© 2014 Wiley-VCH Verlag GmbH & Co. KGaA, Weinheim

atom are properly rationalized by means of theoretical calculations in terms of the charge distribution and aromaticity (BLA) and excited-state geometry. Accordingly, the replacement of fluorine atoms by electron-acceptor moieties improves the fluorescence performance of commercial BODIPYs, whereas the electron-donor ones are harmful and lead to distorted geometries that enhance the nonradiative relaxation pathways.

The newly synthesized *E*- and *C*-BODIPYs exhibit enhanced laser action with respect to their parent dyes, both in liquid and in the solid phase, with the lasing properties correlating well with their photophysical behavior. The highest lasing efficiencies, up to 73% in the liquid phase and up to 53% in solid matrix under demanding transversal pumping conditions, were obtained with the derivatives that incorporated cyano groups at the boron center. These same derivatives also proved to be the most photostable, with stabilities significantly higher than that of the corresponding commercial dyes. Particularly relevant was the behavior of dye **4b** in solid matrix, which exhibited a very high lasing stability, with the laser emission remaining at the initial level after 100000 pump pulses in the same position of the sample at 10 Hz repetition rate.

DFB laser emission was demonstrated with organic films that incorporated parent dye PM597 and its derivative **4b**, deposited onto quartz substrates engraved with appropriate periodical structures. Derivative **4b** exhibited a laser threshold lower than that of the parent dye as well as lasing intensities up to three orders of magnitude higher.

These results show that the newly developed *E*- and *C*-BODIPYs are excellent candidates to achieve SSDLs with much improved performance.

## Experimental Section

BODIPY dyes PM546, PM567, PM580, PM597, P597-8C9, PM605, and PM650 were purchased from Exciton and used as received (purity $>99\%$). Experimental procedures, characterization, and NMR spectra of the new dyes as well as quantum mechanical simulations, preparation of laser samples, and methods followed to analyze the photophysical and laser properties in the liquid and solid phase are described in detail in the Supporting Information.

## *Acknowledgements*

This work was supported by the Ministerio de Economia y Competitividad (projects MAT2010-20646-C04-01, MAT2010-20646-C04-02, and MAT2010-20646-C04-04) and Gobierno Vasco (project IT339-10), which is also thanked by I.E. for a contract (SPE12UN140 and SPE13UN). G.D.-S thanks the MICINN for a predoctoral scholarship (FPI, cofinanced by Fondo Social Europeo).

**Keywords:** donor–acceptor systems · dyes/pigments · laser chemistry · photophysics · polymers

[1] a) *Dye Laser Principles* (Eds.: F. J. Duarte, L. W. Hillman), Academic Press, New York, **1990**; b) *Tunable Lasers Handbook* (Ed.: F. J. Duarte), Academic Press, New York, **1995**; c) *Tunable Laser Applications*, 2nd ed. (Ed.: F. J. Duarte), CRC, Boca Ratón, **2009**; d) I. D. W. Samuel, G. A. Turnbull, *Chem. Rev.* **2007**, *107*, 1272–1295.

[2] a) M. Benstead, G. H. Mehl, R. W. Boyle, *Tetrahedron* **2011**, *67*, 3573–3601; b) Y. Xiao, D. Zhang, X. Qian, A. Costela, I. Garcia-Moreno, V. Martin, M. E. Perez-Ojeda, J. Bañuelos, L. Gartzia, I. Lopez Arbeloa, *Chem. Commun.* **2011**, *47*, 11513–11515; c) J. Bañuelos, V. Martin, C. F. A. Gómez-Duran, I. J. Arroyo Cordoba, E. Peña-Cabrera, I. Garcia-Moreno, A. Costela, M. E. Pérez-Ojeda, T. Arbeloa, I. López Arbeloa, *Chem. Eur. J.* **2011**, *17*, 7261–7270; d) G. Duran-Sampedro, A. R. Agarrabeitia, I. Garcia-Moreno, A. Costela, J. Bañuelos, T. Arbeloa, I. López Arbeloa, J. L. Chiara, M. J. Ortiz, *Eur. J. Org. Chem.* **2012**, 6335–6358.

[3] a) T. Bura, P. Retailleau, R. Ziessell, *Angew. Chem.* **2010**, *122*, 6809–6813; *Angew. Chem. Int. Ed.* **2010**, *49*, 6659–6663; b) C. Thivierge, A. Loudet, K. Burgess, *Macromolecules* **2011**, *44*, 4012–4015; c) C. A. Osorio-Martínez, A. Urías-Benavides, C. F. A. Gómez-Durán, J. Bañuelos, I. Esnal, I. López Arbeloa, E. Peña-Cabrera, *J. Org. Chem.* **2012**, *77*, 5434–5438; d) Y. Yang, Q. Guo, H. Chen, Z. Zhou, Z. Guo, Z. Shen, *Chem. Commun.* **2013**, *49*, 3940–3942.

[4] a) A. Loudet, K. Burgess, *Chem. Rev.* **2007**, *107*, 4891–4932; b) R. Ziessel, G. Ulrich, A. Harriman, *New J. Chem.* **2007**, *31*, 496–501; c) G. Ulrich, R. Ziessel, A. Harriman, *Angew. Chem.* **2008**, *120*, 1202–1219; *Angew. Chem. Int. Ed.* **2008**, *47*, 1184–1201; d) F. L. Arbeloa, J. Bañuelos, V. Martinez, T. Arbeloa, I. L. Arbeloa, *Trends Phys. Chem.* **2008**, *13*, 101–122; e) A. C. Benniston, G. Copley, *Phys. Chem. Chem. Phys.* **2009**, *11*, 4124–4131; f) N. Boens, V. Leen, W. Dehaen, *Chem. Soc. Rev.* **2012**, *41*, 1130–1172; g) S. G. Awuah, Y. You, *RSC Adv.* **2012**, *2*, 11169–11183; h) A. Kamkaew, S. H. Lim, H. B. Lee, L. V. Kiew, L. Y. Chung, K. Burgess, *Chem. Soc. Rev.* **2013**, *42*, 77–88.

[5] For example, see: a) S.-L. Niu, C. Massif, G. Ulrich, P.-Y. Renard, A. Romieu, R. Ziessel, *Chem. Eur. J.* **2012**, *18*, 7229–7242; b) A. Kaloudi-Chantzea, N. Karakostas, F. Pitterl, C. P. Raptopoulou, N. Glezos, G. Pistolis, *Chem. Commun.* **2012**, *48*, 12213–12215; c) G. Durán-Sampedro, A. R. Agarrabeitia, L. Cerdán, M. E. Pérez-Ojeda, A. Costela, I. García-Moreno, I. Esnal, J. Bañuelos, I. López Arbeloa, M. J. Ortiz, *Adv. Funct. Mater.* **2013**, 23, 4195–4205 and references cited therein; d) K. K. Jagtap, N. Shivran, S. Mula, D. B. Naik, S. K. Sarkar, T. Mukherjee, D. K. Maity, A. K. Ray, *Chem. Eur. J.* **2013**, *19*, 702–708; e) R. Ziessel, G. Ulrich, A. Haefele, A. Harriman, *J. Am. Chem. Soc.* **2013**, *135*, 11330–11344.

[6] C. Goze, G. Ulrich, R. Ziessel, *Org. Lett.* **2006**, *8*, 4445–4448.

[7] L. Yang, R. Simionescu, A. Lough, H. Yan, *Dyes Pigm.* **2011**, *91*, 264–267.

[8] F. Lopez Arbeloa, J. Bañuelos, V. Martinez, T. Arbeloa, I. Lopez Arbeloa, *Int. Rev. Phys. Chem.* **2005**, *24*, 339–374.

[9] I. Garcia-Moreno, L. Wang, A. Costela, J. Bañuelos, I. Lopez Arbeloa, Y. Xiao, *ChemPhysChem* **2012**, *13*, 3923–3931.

[10] G. Bourhill, J. L. Bredas, L. T. Cheng, S. R. Marder, F. Meyers, J. W. Perry, B. G. Tiemann, *J. Am. Chem. Soc.* **1994**, *116*, 2619–2620.

[11] a) L. J. E. Hofer, R. J. Grabenstetter, E. O. Wiig, *J. Am. Chem. Soc.* **1950**, *72*, 203–209; b) M. Dekhtyar, W. Rettig, M. Sczepan, *Phys. Chem. Chem. Phys.* **2000**, *2*, 1129–1136; c) J. Bañuelos Prieto, F. López Arbeloa, V. Martínez, T. Arbeloa, I. López Arbeloa, *J. Phys. Chem. A* **2004**, *108*, 5503–5508; d) A. Costela, I. García-Moreno, M. Pintado-Sierra, F. Amat-Guerri, R. Sastre, M. Liras, F. López Arbeloa, J. Bañuelos Prieto, I. López Arbeloa, *J. Phys. Chem. A* **2009**, *113*, 8118–8124.

[12] C. Grivas, M. Pollnau, *Laser Photonics Rev.* **2012**, *6*, 419–462.

[13] F. López Arbeloa, T. López Arbeloa, I. López Arbeloa, I. García-Moreno, A. Costela, R. Sastre, F. Amat-Guerri, *Chem. Phys.* **1998**, *236*, 331–341.

[14] T. T. Vu, M. Dvorko, E. Y. Schmidt, J.-F. Audibert, P. Retailleau, B. A. Trofimov, R. B. Pansu, G. Clavier, R. Méallet-Renault, *J. Phys. Chem. C* **2013**, *117*, 5373–5385.

[15] Online 1D multilayer slab waveguide mode solver by Dr. Manfred Hammer, http://wwwhome.math.utwente.nl/hammer/oms.html.

[16] G. A. Turnbull, A. Carleton, G. F. Barlow, A. Tahraouhi, T. F. Krauss, K. A. Shore, I. D. W. Samuel, *J. Appl. Phys.* **2005**, *98*, 023105.

[17] D. Wright, E. Brasselet, J. Zyss, G. Langer, W. Kern, *J. Opt. Soc. Am. B* **2004**, *21*, 944–950.

Received: September 10, 2013
Revised: November 18, 2013
Published online on January 22, 2014


© 2014 Wiley-VCH Verlag GmbH & Co. KGaA, Weinheim

CHEMISTRY
A EUROPEAN JOURNAL

# Supporting Information

© Copyright Wiley-VCH Verlag GmbH & Co. KGaA, 69451 Weinheim, 2014

## First Highly Efficient and Photostable *E* and *C* Derivatives of 4,4-Difluoro-4-bora-3a,4a-diaza-*s*-indacene (BODIPY) as Dye Lasers in the Liquid Phase, Thin Films, and Solid-State Rods

Gonzalo Duran-Sampedro,[a] Ixone Esnal,[c] Antonia R. Agarrabeitia,[a] Jorge Bañuelos Prieto,[c] Luis Cerdán,[b] Inmaculada García-Moreno,*[b] Angel Costela,[b] Iñigo Lopez-Arbeloa,[c] and María J. Ortiz*[a]

chem_201303579_sm_miscellaneous_information.pdf

## General

*Synthesis*: Starting materials and reagents used in the preparation of BODIPYs are commercially available unless synthesis is described. The solvents were dried and distilled, before use. Spectral data of the known compounds were in accordance with the literature data. Flash column chromatography was performed using silica gel Merck 60 (230-400 mesh). $^{1}H$ and $^{13}C$ NMR spectra were recorded with a Bruker Avance-DPX-300 spectrometer (300 MHz for $^{1}H$ and 75 MHz for $^{13}C$) and Bruker Avance III spectrometer (700 MHz for $^{1}H$ and 176 MHz for $^{13}C$). All spectra were recorded in $CDCl_3$. $^{1}H$ chemical shifts are reported in ppm relative to tetramethylsilane ($\delta$ = 0.00 ppm), using the residual solvent signal as the internal reference. $^{13}C$ chemical shifts are reported in ppm with $CDCl_3$ ($\delta$ = 77.67 ppm) as the internal standard. Chemical shift multiplicities are reported as s = singlet, d = doublet, t = triplet, q = quartet, m = multiplet and dd = double doublet. IR spectra (in $cm^{-1}$) were recorded in a Bruker Tensor-27-FTIR spectrophotometer. High resolution mass spectra were determined by EI in a Thermofisher MAT 95 XP.

BODIPYs **PM546**, **PM567**, **PM580**, **PM597**, **PM597-8C9**, **PM605** and **PM650** were purchased from Lasing, S. A.[1] BODIPY derivatives **1b**,[2] **2b**,[2] and **6**[3] were synthesized by the methods previously described.

*Photophysical properties*: The photophysical properties were registered in diluted solutions (around $2\times10^{-6}$ M), prepared by diluting a concentrated stock solution in ethyl acetate. UV-Vis absorption and fluorescence spectra were recorded on a Varian model CARY 4E spectrophotometer and a SPEX Fluorolog 3-22 spectrofluorimeter, respectively. The fluorescence spectra were corrected from the wavelength dependence of the detector sensibility. Fluorescence quantum yield ($\phi$) was obtained using an ethanolic solution of the corresponding commercial BODIPY as reference.[4] Radiative decay curves were registered with the time correlated single-photon counting technique (Edinburgh Instruments, model FL920) using a microchannel plate detector (Hamamatsu C4878), with picosecond time resolution (~ 20 ps). Fluorescence emission was monitored at the maximum emission wavelength after excitation at 470 nm and 530

[1] Laser grade, Exciton. They were used as received with a purity > 99%.
[2] C. Goze, G. Ulrich, R. Ziessel, *Org. Lett*. **2006**, *8*, 4445-4448.
[3] L. Yang, R. Simionescu, A. Lough, H. Yan, *Dyes and Pigments* **2011**, *91*, 264-267.
[4] F. López Arbeloa, J. Bañuelos, V. Martinez, T. Arbeloa, I. López Arbeloa, *Int. Rev. Phys. Chem*. **2005**, *24*, 339-374.

nm by means of a diode laser (PicoQuant, model LDH470 and LDH530) with 150 ps FWHM pulses. The fluorescence lifetime ($\tau$) was obtained from the slope after the deconvolution of the instrumental response signal from the recorded decay curves by means of an iterative method. The goodness of the exponential fit was controlled by statistical parameters (chi-square, Durbin-Watson and the analysis of the residuals). The radiative ($k_{fl}$) and non-radiative deactivation ($k_{nr}$) rate constants were calculated by means of: $k_{fl} = \phi/\tau$ and $k_{nr} = (1-\phi)/\tau$, respectively.

*Theoretical calculations*: Ground state geometry was optimized by the hybrid DFT method B3LYP, using the double-valence basis set (6-31G), whereas the first excited state optimized geometry was achieved by the *ab initio* CIS method, at the same basis set. The geometry was considered as a minimum of energy after the analysis of the frequencies did not yield any negative value. The charge distribution was analyzed with the CHelpG method. All the calculations were performed in the Gaussian 09 software running in the "arina" informatic clusted of the UPV/EHU.

*Preparation of solid samples and thin films*: The dyes were incorporated into the solid matrices following the procedure previously described.[5] The solid monolith samples were cast in a cylindrical shape, forming rods of 10 mm diameter and 10 mm length. A cut was made parallel to the axis of the cylinder to obtain a lateral flat surface of ≈6 mm × 10 mm. This surface as well as the ends of the laser rods was prepared for lasing experiments by using a grinding and polishing machine (Phoenix Beta 4000, Buehler) until optical-grade finish.

To implement the DFB lasers, PMMA in proportion 50 mg/mL and dyes at concentration (with respect to the polymer) in the range $2 \times 10^{-2}$ M were solved in chloroform. Thin films ~800-850 nm thick were spin coated (1000 rpm, 30 seconds) onto quartz substrates engraved with 1D squared-profile DFB structure with period $\Lambda$ = 400 nm, duty cycle 50% and depth 100 nm, which resonant wavelengths matched the corresponding dye emission windows.

*Laser experiments*: Liquid solutions of dyes were contained in 1 cm optical-path rectangular quartz cells carefully sealed to avoid solvent evaporation during the experiments. The liquid solutions were transversely pumped either at 355 nm, with 5 mJ, 8 ns FWHM pulses from the third-harmonic of a Q-switched Nd:YAG laser (Spectron SL282G) or at 532 nm, with 5 mJ, 6 ns FWHM pulses from a frequency-

[5] A. Costela, I. García-Moreno, C. Gómez, R. Sastre, F. Amat-Guerri, M. Liras, F. López Arbeloa, J. Bañuelos, I. López Arbeloa, *J. Phys. Chem. A* **2002**, *106*, 7736-7742.

doubled Q-switched Nd:YAG laser (Monocrom OPL-10), at a repetition rate of up to 10 Hz. The lasing properties of the solid samples were studied under pumping at 532 nm with pulses from the OPL-10 laser.

The exciting pulses were line-focused onto the cell or the lateral flat surface of the solid rods, providing pump fluences on the active medium in the range 110-180 mJ/cm$^2$. The oscillation cavity (2 cm length) consisted of a 90% reflectivity aluminum mirror, with the lateral face of the cell or the solid sample as output coupler.

The photostability of the dyes in liquid solution was evaluated by irradiating under lasing conditions 10 μL of a solution in ethyl acetate. The solutions were contained in a cylindrical Pyrex tube (1 cm height, 1 mm internal diameter) carefully sealed to avoid solvent evaporation during the experiments. Although the low optical quality of the capillary tube prevents laser emission from the dyes, information about photostabilities can be obtained by monitoring the decrease in laser-induced fluorescence intensity, excited transversally to the capillary tube, as a function of the number of pump pulses at a given repetition rate. The fluorescence emission was monitored perpendicular to the exciting beam, collected by an optical fiber, and imaged onto the input slit of a monochromator (Acton Research corporation) and detected with a charge-coupled device (CCD) (SpectruMM:GS128B). The fluorescence emission was recorded by feeding the signal to the boxcar (Stanford Research, model 250) to be integrated before being digitized and processed by a computer. Each experience was repeated at least three times. The photostability of the solid samples was measured by following the evolution of their laser emission under repeated pumping in the same position of the sample at 10 Hz repetition rate. The estimated error in the energy and photostability measurements was 10%.

In the DFB laser experiments, the thin film samples were optically pumped at 532 nm with 20 ns full width at half maximum (FWHM) pulses from a frequency-doubled Q-switched Nd:YAG laser (Lotis TII SL-2132), operated at 15 Hz repetition rate. The pump radiation was vertically polarized and parallel to the DFB structure grooves, which allowed controlling the pulse energy incident on the sample by insertion into the pump beam path of a half-wave plate (HWP) and a linear polarizer (LP) set with its polarization axis vertical. By rotating the HWP the linear polarization of the input beam is rotated out of the horizontal, and the pump beam is blocked more or less by the LP, depending on the rotation angle introduced by the HWP. Pump energy was measured with a calibrated Laser Energy Meter (QE 12LP-S-MB-DO, Gentec). The light incident

on the sample arrived at an angle of about 34° from the normal to the surface, and was focused onto that surface by means of a spherical lens (f = +15 cm), rendering an elliptical pump spot with major and minor axis of about 245 μm and 185 μm, respectively. The sample was placed on vertical and horizontal translation stages to allow precise positioning.

The normal to the film DFB laser emission was collected with a 5-cm focal length spherical lens, focused onto a fiber bundle and detected with the spectrograph/monochromator and CCD system above described. A shortwave Cut-off filter (CF) (OptoSigma, cut-off at 540 nm) was placed before the fibre bundle to avoid any scattered pump light entering the spectrograph. Neutral density filters were used to avoid CCD detector saturation. All the measurements were averaged over 15 pulses.

**Synthesis and Characterization of BODIPYs**

*General procedure A.* To a solution of trimethylsilylacetylene (8 equiv) in anhydrous THF was added *n*-butyllithium (8 equiv) at -78ºC under an argon atmosphere. The mixture was stirred at -78ºC for 1 h and at room temperature for half an hour. The resulting anion was then transferred *via* cannula to a degassed solution of the BODIPY (1 equiv) in anhydrous THF. The solution was stirred at room temperature until the complete consumption of the starting material was observed by TLC. Water was added, and the solution was extracted with $CH_2Cl_2$, dried over $MgSO_4$, filtered and concentrated to dryness. The compounds were purified by flash chromatography on silica gel.

*General procedure B.* To a solution of 4,4-bis(trimethylsilylethynyl) BODIPY (1 equiv) in $CH_2Cl_2$ (5 mL) was added a solution of NaOH (20 equiv) in MeOH (5 mL). The solution was stirred at room temperature until the complete consumption of the starting material was observed by TLC. Water was added, and the solution was extracted with $CH_2Cl_2$, dried over $MgSO_4$, filtered and concentrated to dryness. The compounds were purified by flash chromatography on silica gel.

General procedure C. To a solution of BODIPY (1 equiv) in dry $CH_2Cl_2$ was added aluminium chloride (2 equiv) under an argon atmosphere and the mixture resulting was refluxed for 10 min. Then, TMSCN (20 equiv) was added and the mixture was refluxed

until the complete consumption of the starting material was observed by TLC. Water was added, and the solution was extracted with $CH_2Cl_2$, dried over $MgSO_4$, filtered and concentrated to dryness. The compounds were purified by flash chromatography on silica gel.

*General procedure D.* To a solution of BODIPY (1 equiv) in 1,2-dichloroethane (15 mL) was added TMSCN (20 equiv) at room temperature under an argon atmosphere and the mixture was stirred at 90ºC for 16 h. Water was added, and the solution was extracted with $CH_2Cl_2$, washed with a solution of $NaHCO_3$ and water, dried over $MgSO_4$, filtered and concentrated to dryness. The compounds were purified by flash chromatography on silica gel.

*General procedure E.* A solution of alkylmagnesium bromide or phenylmagnesium bromide in THF (10 equiv) was added to a solution of BODIPY (1 equiv) in dry $CH_2Cl_2$ (10-15 mL) at 0ºC. The solution was stirred until the complete consumption of the starting material was observed by TLC. Water was added, and the solution was extracted with $CH_2Cl_2$ and washed successively with water and brine. The organic layer was dried over $MgSO_4$, filtered and concentrated to dryness. The compounds were purified by flash chromatography on silica gel.

***4,4-Bis(trimethylsilylethynyl)-1,3,5,7,8-pentamethyl-4-bora-3a,4a-diaza-s-indacene (1a)***

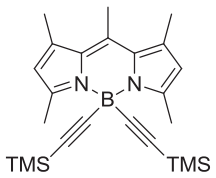


According to the general procedure A, trimethylsilylacetylene (0.43 mL, 3.04 mmol) in THF (10 mL) and *n*-butyllithium (1.9 mL, 1.6 M in hexane, 3.04 mmol) were reacted. Then, the resulting anion and **PM546** (100 mg, 0.38 mmol) were stirred for 10 min. Flash chromatography using hexane/EtOAc (98:2) afforded **1a** (142 mg, 89%) as an orange solid. $^1$H NMR (300 MHz, $CDCl_3$): $\delta$ = 6.01 (s, 2H, H-2 and H-6), 2.63 (s, 6H, 2 $CH_3$), 2.47 (s, 3H, $CH_3$), 2.33 (s, 6H, 2 $CH_3$), 0.01 (s, 18H, 6 $CH_3$); $^{13}$C NMR (75 MHz, $CDCl_3$): $\delta$ = 153.2 (C), 140.8 (C), 138.4 (C), 129.9 (C), 121.1 (CH), 17.4 ($CH_3$), 16.2 ($CH_3$), 15.5 ($CH_3$), 0.0 ($CH_3$), two C≡C not observed; IR (neat): 2950, 2918, 2110,

1548, 1240, 1183, 979, 825, 750 $cm^{-1}$; HRMS-EI: calcd for ($C_{24}H_{35}BN_2Si_2$) 418.2430 found 418.2433.

***4,4-Bis(trimethylsilylethynyl)-2,6-dibutyl-1,3,5,7,8-pentamethyl-4-bora-3a,4a-diaza-s-indacene (1c)***

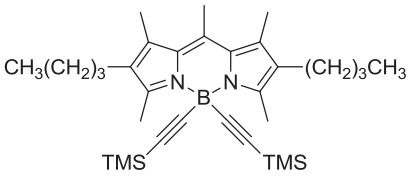


According to the general procedure A, trimethylsilylacetylene (0.3 mL, 2.16 mmol) in THF (10 mL) and *n*-butyllithium (1.3 mL, 1.6 M in hexane, 2.16 mmol) were reacted. Then, the resulting anion and **PM580** (100 mg, 0.27 mmol) were stirred for 10 min. Flash chromatography using hexane/EtOAc (99:1) afforded **1c** (100 mg, 70%) as an orange solid. $^1$H NMR (300 MHz, $CDCl_3$): $\delta$ = 2.60 (s, 6H, $2CH_3$), 2.48 (s, 3H, $CH_3$), 2.33 (t, $J$ = 7.2 Hz, 4H, $2CH_2$), 2.23 (s, 6H, $2CH_3$), 1.31. (m, 8H, $2CH_2$), 0.87 (t, $J$ = 6.9 Hz, 6H, $2CH_3$), 0.02 (s, 18H, $6CH_3$); $^{13}$C NMR (75 MHz, $CDCl_3$): $\delta$ = 151.8 (C), 139.0 (C), 133.9 (C), 130.5 (C), 129.6 (C), 99.7 (C≡C), 32.6 ($CH_2$), 23.6 ($CH_2$), 22.2 ($CH_2$), 16.9 ($CH_3$), 14.5 ($CH_3$), 13.7 ($CH_3$), 13.6 ($CH_3$), 0.0 ($CH_3$); IR (neat): 2957, 2922, 2854, 2123, 1550, 1244, 1180, 969, 835, 755 $cm^{-1}$; HRMS-EI: calcd for ($C_{32}H_{51}BN_2Si_2$) 530.3680 found 530.3681.

***4,4-Bis(trimethylsilylethynyl)-2,6-di-tertbutyl-1,3,5,7,8-pentamethyl-4-bora-3a,4a-diaza-s-indacene (1d)***

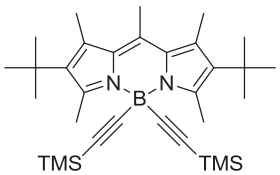


According to the general procedure A, trimethylsilylacetylene (0.3 mL, 2.16 mmol) in THF (10 mL) and *n*-butyllithium (1.3 mL, 1.6 M in hexane, 2.16 mmol) were reacted. Then, the resulting anion and **PM597** (100 mg, 0.27 mmol) were stirred for 20 min. Flash chromatography using hexane/EtOAc (98:2) afforded **1d** (90 mg, 63%) as a red solid. $^1$H NMR (300 MHz, $CDCl_3$): $\delta$ = 2.82 (s, 6H, $2CH_3$), 2.52 (s, 3H, $CH_3$), 2.40 (s, 6H, $2CH_3$), 1.38 (s, 18H, $6CH_3$), 0.04 (s, 18H, $6CH_3$); $^{13}$C NMR (75 MHz, $CDCl_3$): $\delta$ = 151.4 (C), 139.1 (C), 136.5 (C), 134.6 (C), 131.2 (C), 99.7 (C≡C), 33.0 (C), 31.8 ($CH_3$),

19.7 ($CH_3$), 18.6 ($CH_3$), 17.5 ($CH_3$), 0.0 ($CH_3$); IR (neat): 2956, 2925, 2150, 1549, 1264, 1194, 981, 833, 758 $cm^{-1}$; HRMS-EI: calcd for ($C_{32}H_{51}BN_2Si_2$) 530.3680 found 530.3684.

***4,4-Bis(trimethylsilylethynyl)-2,6-di-tertbutyl-1,3,5,7-tetramethyl-8-nonyl-4-bora-3a,4a-diaza-s-indacene (1e)***

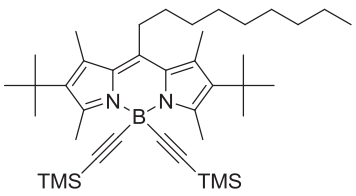


According to the general procedure A, trimethylsilylacetylene (0.23 mL, 1.6 mmol) in THF (10 mL) and *n*-butyllithium (1 mL, 1.6 M in hexane, 1.6 mmol) were reacted. Then, the resulting anion and PM597-8C9 (100 mg, 0.2 mmol) were stirred for 10 min. Flash chromatography using hexane/EtOAc (99:1) afforded **1e** (73 mg, 57%) as a red solid. $^1$H NMR (300 MHz, $CDCl_3$): $\delta$ = 2.96-2.91 (m, 2H, $CH_2$), 2.81 (s, 6H, $2CH_3$), 2.45 (s, 6H, $2CH_3$), 1.58 (m, 2H, $CH_2$), 1.37 (s, 18H, $6CH_3$), 1.21 (m, 12H, $6CH_2$), 0.82 (t, $J$ = 6.9 Hz, 3H, $CH_3$), 0.03 (s, 18H, $6CH_3$); $^{13}$C NMR (75 MHz, $CDCl_3$): $\delta$ = 151.6 (C), 144.4 (C), 136.6 (C), 134.6 (C), 129.5 (C), 32.9 (C), 32.0 ($CH_3$), 31.5 ($CH_2$), 31.3 ($CH_2$), 29.8 ($CH_2$), 29.2 ($CH_2$), 29.1 ($CH_2$), 28.9 ($CH_2$), 28.3 ($CH_2$), 22.3 ($CH_2$), 18.9 ($CH_3$), 16.4 ($CH_3$), 13.8 ($CH_3$), 0.0 ($CH_3$), two C≡C not observed; IR (neat): 2958, 2926, 2857, 2123, 1528, 1432, 1383, 1179, 976 $cm^{-1}$; HRMS-EI: calcd for ($C_{40}H_{67}BN_2Si_2$) 642.4930 found 642.4936.

***4,4-Bis[(4-(trimethylsilylethynyl)phenyl)ethynyl]-2,6-di-tertbutyl-1,3,5,7,8-penta methyl-4-bora-3a,4a-diaza-s-indacene (3a)***

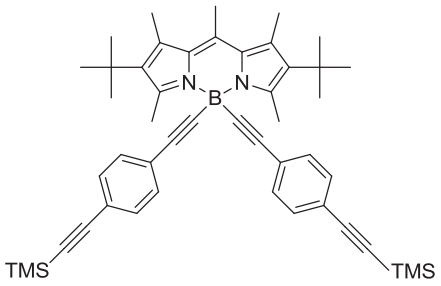


According to the general procedure A, [4-(trimethylsilylethynyl)phenyl]acetylene[6] (**8**) (278 mg, 1.6 mmol) in THF (10 mL) and *n*-butyllithium (1 mL, 1.6 M in hexane, 1.6

[6] Y. Cakmak, E. U. Akkaya, *Org. Lett*. **2009**, *11*, 85-88.

mmol) were reacted. Then, the resulting anion and **PM597** (75 mg, 0.2 mmol) were stirred for 10 min. Flash chromatography using hexane/EtOAc (99:1) afforded **3a** (95 mg, 65%) as a red solid. $^{1}$H NMR (300 MHz, $CDCl_3$): $\delta$ = 7.24-7.22 (m, 8H, phenyl), 2.93 (s, 6H, $2CH_3$), 2.56 (s, 3H, $CH_3$), 2.43 (s, 6H, $2CH_3$), 1.38 (s, 18H, $6CH_3$), 0.16 (s, 18H, $6CH_3$); $^{13}$C NMR (75 MHz, $CDCl_3$): $\delta$ = 151.7 (C), 139.8 (C), 137.2 (C), 135.7 (C), 131.7 (C), 131.6 (CH), 131.3 (CH), 125.7 (C), 121.4 (C), 105.1 (C≡C), 95.2 (C≡C), 33.4 (C), 32.2 ($CH_3$), 20.1 ($CH_3$), 18.9 ($CH_3$), 18.0 ($CH_3$), 0.0 ($CH_3$); IR (neat): 2955, 2360, 2153, 1538, 1114, 968, 834, 758 cm$^{-1}$; HRMS-EI: calcd for ($C_{48}H_{59}BN_2Si_2$) 730.4308 found 730.4310.

***4,4-Diethynyl-1,3,5,7,8-pentamethyl-4-bora-3a,4a-diaza-s-indacene (2a)***

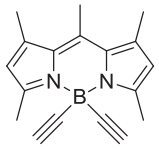


According to the general procedure B, BODIPY **1a** (142 mg, 0.34 mmol) in $CH_2Cl_2$ (5 mL) and NaOH (272 mg, 6.8 mmol) in MeOH (5 mL) for 4 days were reacted. Flash chromatography using hexane/EtOAc (99:1) gave, by order of elution, monodeprotected product **1f** (21 mg, 18%) as an orange solid and dideprotected product **2a** (73 mg, 78%) as an orange solid.

*Compound **2a***: $^{1}$H NMR (300 MHz, $CDCl_3$): $\delta$ = 6.05 (s, 2H, H-2 and H-6), 2.67 (s, 6H, $2CH_3$), 2.51 (s, 3H, $CH_3$), 2.35 (s, 6H, $2CH_3$), 2.11 (s, 2H, 2CH≡C); $^{13}$C NMR (75 MHz, $CDCl_3$): $\delta$ = 153.5 (C), 141.4 (C), 139.4 (C), 130.3 (C), 121.8 (CH), 82.8 (C≡C), 17.7 ($CH_3$), 16.6 ($CH_3$), 16.0 ($CH_3$); IR (neat): 3270, 2055, 1553, 1189, 990 cm$^{-1}$; HRMS-EI: calcd for ($C_{18}H_{19}BN_2$) 274.1640 found 274.1642.

*Compound **1f***:

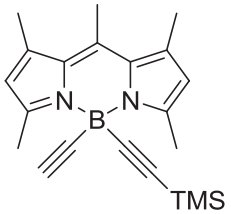


$^{1}$H NMR (300 MHz, $CDCl_3$): $\delta$ = 6.03 (s, 2H, H-2 and H-6), 2.65 (s, 6H, $2CH_3$), 2.50 (s, 3H, $CH_3$), 2.34 (s, 6H, $2CH_3$), 2.04 (s, 1H, CH≡C), 0.02 (s, 9H, $3CH_3$); $^{13}$C NMR (75 MHz, $CDCl_3$): $\delta$ = 153.2 (C), 141.0 (C), 138.8 (C), 130.0 (C), 121.4 (CH), 17.4 ($CH_3$), 16.3 ($CH_3$), 15.6 ($CH_3$), 0.0 ($CH_3$), C≡C not observed; IR (neat): 3267, 2180, 1545,

1467, 1199, 980, 835, 760 $cm^{-1}$; HRMS-EI: calcd for ($C_{21}H_{27}BN_2Si$) 346.2035 found 346.2037.

***4,4-Diethynyl-2,6-dibutyl-1,3,5,7,8-pentamethyl-4-bora-3a,4a-diaza-s-indacene (2c)***

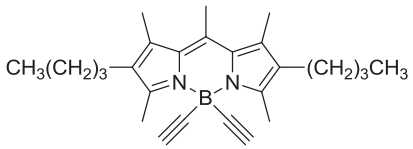


According to the general procedure B, BODIPY **1c** (144 mg, 0.27 mmol) in $CH_2Cl_2$ (5 mL) and NaOH (216 mg, 5.4 mmol) in MeOH (5 mL) for 4 days were reacted. Flash chromatography using hexane/EtOAc (98:2) afforded **2c** (65 mg, 62%) as an orange solid. $^1$H NMR (300 MHz, $CDCl_3$): $\delta$ = 2.65 (s, 6H, $2CH_3$), 2.54 (s, 3H, $CH_3$), 2.33 (t, $J$ = 7.2 Hz, 4H, $2CH_2$), 2.26 (s, 6H, $2CH_3$), 2.10 (s, 2H, 2CH≡C), 1.31 (m, 8H, $4CH_2$), 0.86 (t, $J$ = 7.2 Hz, 6H, $2CH_3$); $^{13}$C NMR (75 MHz, $CDCl_3$): $\delta$ = 152.1 (C), 139.6 (C), 134.9 (C), 131.3 (C), 130.0 (C), 82.7 (C≡C), 32.9 ($CH_2$), 24.0 ($CH_2$), 22.7 ($CH_2$), 17.3 ($CH_3$), 14.9 ($CH_3$), 14.1 ($CH_3$); IR (neat): 3274, 2952, 2920, 2853, 2058, 1553, 1477, 1189, 991, 948, 641 $cm^{-1}$; HRMS-EI: calcd for ($C_{26}H_{35}BN_2$) 386.2890 found 386.2896.

***4,4-Diethynyl-2,6-di-tertbutyl-1,3,5,7,8-pentamethyl-4-bora-3a,4a-diaza-s-indacene (2d)***

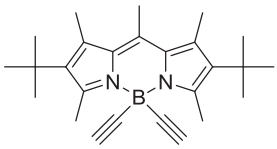


According to the general procedure B, BODIPY **1d** (90 mg, 0.17 mmol) in $CH_2Cl_2$ (5 mL) and NaOH (136 mg, 3.4 mmol) in MeOH (5 mL) for 4 days were reacted. Flash chromatography using hexane/EtOAc (98:2) afforded **2d** (59 mg, 90%) as a red solid. $^1$H NMR (300 MHz, $CDCl_3$): $\delta$ = 2.85 (s, 6H, $2CH_3$), 2.54 (s, 3H, $CH_3$), 2.41 (s, 6H, $2CH_3$), 2.11 (s, 2H, 2CH≡C), 1.36 (s, 18H, $6CH_3$); $^{13}$C NMR (75 MHz, $CDCl_3$): $\delta$ = 151.2 (C), 139.3 (C), 136.8 (C), 135.3 (C), 131.2 (C), 82.4 (C≡C), 33.0 (C), 31.9 ($CH_3$), 19.7 ($CH_3$), 18.6 ($CH_3$), 17.6 ($CH_3$); IR (neat): 3270, 2950, 2060, 1557, 1467, 1198, 963 $cm^{-1}$; HRMS-EI: calcd for ($C_{26}H_{35}BN_2$) 386.2890 found 386.2892.

***4,4-Diethynyl-2,6-di-tertbutyl-1,3,5,7-tetramethyl-8-nonyl-4-bora-3a,4a-diaza-s-indacene (2e)***

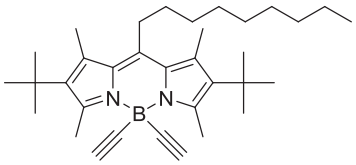

According to the general procedure B, BODIPY **1e** (70 mg, 0.11 mmol) in $CH_2Cl_2$ (5 mL) and NaOH (87 mg, 2.2 mmol) in MeOH (5 mL) for 4 days were reacted. Flash chromatography using hexane/EtOAc (99:1) afforded **2e** (33 mg, 60%) as a red solid. $^1$H NMR (300 MHz, $CDCl_3$): $\delta$ = 3.00-2.94 (m, 2H, $CH_2$), 2.86 (s, 6H, $2CH_3$), 2.47 (s, 6H, $2CH_3$), 2.11 (s, 2H, 2CH≡C), 1.58 (m, 2H, $CH_2$), 1.38 (s, 18H, $6CH_3$), 1.21 (m, 12H, $6CH_2$), 0.82 (t, $J$ = 6.9 Hz, 3H, $CH_3$); $^{13}$C NMR (75 MHz, $CDCl_3$): $\delta$ = 151.4 (C), 144.7 (C), 136.8 (C), 135.3 (C), 129.5 (C), 82.2 (C≡C), 32.9 (C), 32.0 ($CH_3$), 31.5 ($CH_2$), 31.4 ($CH_2$), 29.8 ($CH_2$), 29.2 ($CH_2$), 29.0 ($CH_2$), 28.9 ($CH_2$), 28.3 ($CH_2$), 22.3 ($CH_2$), 18.9 ($CH_3$), 16.4 ($CH_3$), 13.8 ($CH_3$); IR (neat): 3297, 2957, 2925, 2856, 2060, 1529, 1431, 1383, 1178, 976 cm$^{-1}$; HRMS-EI: calcd for ($C_{34}H_{51}BN_2$) 498.4140 found 498.4144.

***4,4-Bis[(4-ethynylphenyl)ethynyl]-2,6-di-tertbutyl-1,3,5,7,8-pentamethyl-4-bora-3a,4a-diaza-s-indacene (3b)***

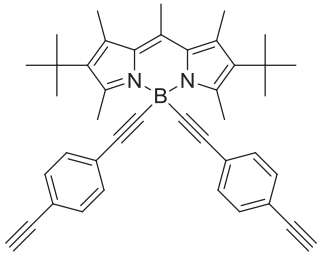

According to the general procedure B, BODIPY **3a** (90 mg, 0.12 mmol) in $CH_2Cl_2$ (5 mL) and NaOH (96 mg, 2.4 mmol) in MeOH (5 mL) for 4 days were reacted. Flash chromatography using hexane/EtOAc (99:1) afforded, by order of elution, monodeprotected product **3c** (12 mg, 15%) as a red solid and dideprotected product **3b** (56 mg, 80%) as a red solid.

*Compound **3b***: $^1$H NMR (300 MHz, $CDCl_3$): $\delta$ = 7.29-7.22 (m, 8H, phenyl), 3.03 (s, 2H, 2CH≡C), 2.93 (s, 6H, $2CH_3$), 2.56 (s, 3H, $CH_3$), 2.43 (s, 6H, $2CH_3$), 1.38 (s, 18H, $6CH_3$); $^{13}$C NMR (75 MHz, $CDCl_3$): $\delta$ = 151.7 (C), 139.8 (C), 137.2 (C), 135.7 (C), 131.7 (CH), 131.6 (C), 131.4 (CH), 126.1 (C),120.4 (C), 83.7 (C≡C), 78.1 (C≡CH),

33.4 (C), 32.2 ($CH_3$), 20.1 ($CH_3$), 18.9 ($CH_3$), 18.0 ($CH_3$); IR (neat): 3275, 2957, 2355, 2144, 1554, 1190, 1114, 967 $cm^{-1}$; HRMS-EI: calcd for ($C_{42}H_{43}BN_2$) 586.3515 found 586.3520.

*Compound **3c***:

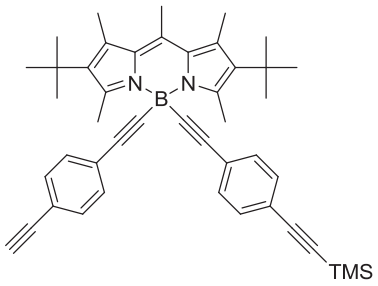


$^1$H NMR (300 MHz, $CDCl_3$): $\delta$ = 7.27-7.23 (m, 8H, phenyl), 3.04 (s, 1H, CH≡C), 2.94 (s, 6H, $2CH_3$), 2.57 (s, 3H, $CH_3$), 2.43 (s, 6H, $2CH_3$), 1.39 (s, 18H, $6CH_3$), 0.17 (s, 9H, $3CH_3$); $^{13}$C NMR (75 MHz, $CDCl_3$): $\delta$ = 151.7 (C), 139.8 (C), 137.2 (C), 135.7 (C), 131.7 (CH), 131.6 (C), 131.5 (CH), 131.4 (CH), 131.3 (CH), 126.1 (C), 125.7 (C), 121.5 (C), 120.4 (C), 105.1 (C≡C), 95.2 (C≡C), 83.7 (C≡C), 78.1 (C≡*C*H), 33.4 (C), 32.2 ($CH_3$), 20.1 ($CH_3$), 18.9 ($CH_3$), 18.0 ($CH_3$), 0.0 ($CH_3$); IR (neat): 3283, 2955, 2360, 2153, 1538, 1173, 1114, 968, 834, 758 $cm^{-1}$; HRMS-EI: calcd for ($C_{45}H_{51}BN_2Si$) 658.3910 found 658.3916.

***4,4-Dicyano-2,6-diethyl-1,3,5,7,8-pentamethyl-4-bora-3a,4a-diaza-s-indacene (4a)***

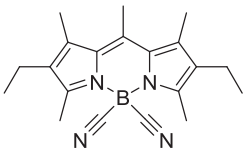


According to the general procedure C, PM567 (50 mg, 0.16 mmol) in dry $CH_2Cl_2$ (15mL) and aluminium chloride (42 mg, 0.32 mmol) were reacted. Then, TMSCN (0.42 mL, 3.20 mmol) was added and the mixture was refluxed for 10 min. Flash chromatography using hexane/EtOAc (95:5) afforded **4a** (44 mg, 84%) as an orange solid. $^1$H NMR (700 MHz, $CDCl_3$): $\delta$ = 2.59 (s, 9H, $3CH_3$), 2.39 (q, $J$ = 7.5 Hz, 4H, $2CH_2$), 2.32 (s, 6H, $2CH_3$), 1.00 (t, $J$ = 7.5 Hz, 6H, $2CH_3$); $^{13}$C NMR (176 MHz, $CDCl_3$): $\delta$ = 152.2 (C), 140.8 (C), 137.7 (C), 133.9 (C), 130.2 (C), 17.3 ($CH_2$), 17.2 ($CH_3$), 14.8 ($CH_3$), 14.7 ($CH_3$), 13.3 ($CH_3$), two CN not observed; IR (neat): 2959, 2214, 1549, 1476, 1190, 977 $cm^{-1}$; HRMS-EI: calcd for ($C_{20}H_{25}BN_4$) 332.2501 found 332.2507.

***4,4-Dicyano-2,6-di-tertbutyl-1,3,5,7,8-pentamethyl-4-bora-3a,4a-diaza-s-indacene (4b)***

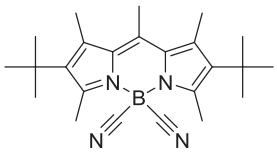

According to the general procedure D, PM597 (75 mg, 0.2 mmol) in 1,2-dichloroethane (15 mL) and TMSCN (0.53 mL, 4 mmol) were reacted. Flash chromatography using hexane/EtOAc (98:2) afforded **4b** (64 mg, 82%) as a red solid. $^{1}$H NMR (300 MHz, $CDCl_3$): $\delta$ = 2.68 (s, 6H, $2CH_3$), 2.54 (s, 3H, $CH_3$), 2.42 (s, 6H, $2CH_3$), 1.35 (s, 18H, $6CH_3$); $^{13}$C NMR (75 MHz, $CDCl_3$): $\delta$ = 152.4 (C), 140.4 (C), 138.5 (C), 137.9 (C), 132.2 (C), 33.3 (C), 32.0 ($CH_3$), 19.5 ($CH_3$), 17.8 ($CH_3$), 17.3 ($CH_3$), 17.2 ($CH_3$), two CN not observed; IR (neat): 2965, 2201, 1536, 1383, 1197, 977 cm$^{-1}$; HRMS-EI: calcd for ($C_{24}H_{33}BN_4$) 388.3565 found 388.3568.

***4,4-Dicyano-8-acetoxymethyl-2,6-diethyl-1,3,5,7-tetramethyl-4-bora-3a,4a-diaza-s-indacene (4c)***

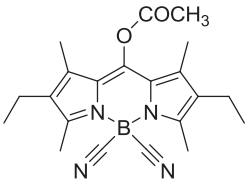

According to the general procedure C, PM605 (100 mg, 0.26 mmol) in dry $CH_2Cl_2$ (15mL) and aluminium chloride (70.7 mg, 0.53 mmol) were reacted. Then, TMSCN (0.7 mL, 5.3 mmol) was added and the mixture was refluxed for 20 min. Flash chromatography using hexane/EtOAc (95:5) afforded **4c** (88 mg, 85%) as a red solid. $^{1}$H NMR (300 MHz, $CDCl_3$): $\delta$ = 5.26 (s, 2H, $CH_2O$), 2.61 (s, 6H, $2CH_3$), 2.38 (q, $J$ = 7.5 Hz, 4H, $2CH_2$), 2.24 (s, 6H, $2CH_3$), 2.09 (s, 3H, $CH_3CO$), 1.01 (t, $J$ = 7.5 Hz, 6H, $2CH_3$); $^{13}$C NMR (75 MHz, $CDCl_3$): $\delta$ = 170.4 (COO), 155.3 (C), 138.0 (C), 135.1 (C), 132.7 (C), 130.8 (C), 57.9 ($CH_2O$), 20.6 ($CH_3$), 17.3 ($CH_2$), 14.6 ($CH_3$), 13.7 ($CH_3$), 12.9 ($CH_3$), two CN not observed; IR (neat): 2960, 2209, 1720, 1549, 1476, 1189, 985 cm$^{-1}$; HRMS-EI: calcd for ($C_{22}H_{27}BN_4O_2$) 390.2224 found 390.2227.

***4,4,8-Tricyano-1,2,3,5,6,7-hexamethyl-4-bora-3a,4a-diaza-s-indacene (4d)***

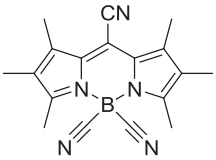

According to the general procedure D, PM650 (100 mg, 0.33 mmol) in 1,2-dichloroethane (15 mL) and TMSCN (0.9 mL, 6.64 mmol) were reacted. Flash chromatography using hexane/EtOAc (95:5) afforded **4d** (26 mg, 25%) as a purple solid. $^{1}$H NMR (300 MHz, $CDCl_3$): $\delta$ = 2.61 (s, 6H, $2CH_3$), 2.40 (s, 6H, $2CH_3$), 1.96 (s, 6H, $2CH_3$); $^{13}$C NMR (75 MHz, $CDCl_3$): $\delta$ = 158.9 (C), 140.7 (C), 130.9 (C), 130.5 (C), 114.5 (CN), 104.6 (C), 14.5 ($CH_3$), 12.3 ($CH_3$), 9.7 ($CH_3$), two B-CN not observed; IR (neat): 2920, 2856, 2212, 1555, 1466, 1184, 909 cm$^{-1}$; HRMS-EI: calcd for ($C_{18}H_{18}BN_5$) 315.1803 found 315.1807.

***4,4-Vinyl-2,6-diethyl-1,3,5,7,8-pentamethyl-4-bora-3a,4a-diaza-s-indacene (5)***

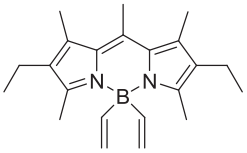

According to the general procedure E, vinylmagnesium bromide (1.8 mL, 0.7 M in THF, 1.26 mmol) and PM567 (100 mg, 0,31 mmol) in $CH_2Cl_2$ (10 mL) for 1 h were refluxed. Flash chromatography using hexane afforded **5** (43 mg, 41%) as an orange solid. $^{1}$H NMR (300 MHz, $CDCl_3$): $\delta$ = 6.36 (dd, $J$ = 19.5 and 12.9 Hz, 2H, $CH$=$CH_2$), 5.33 (dd, $J$ = 12.9 and 3.9 Hz, 2H, 2CH=$CH_2$), 4.90 (dd, $J$ = 19.5 and 3.9 Hz, 2H, 2CH=$CH_2$), 2.58 (s, 3H, $CH_3$), 2.35 (q, $J$ = 7.5 Hz, 4H, $2CH_3CH_2$), 2.28 (s, 6H, $2CH_3$), 2.22 (s, 6H, $2CH_3$), 0.94 (t, $J$ = 7.5 Hz, 6H, $2CH_3CH_2$); $^{13}$C NMR (75 MHz, $CDCl_3$): $\delta$ = 150.5 (C), 139.9 (C), 132.9 (C), 132.4 (C), 131.1 (C), 121.5 ($CH_2$=CH), 17.9 ($CH_3$), 17.8 ($CH_2$), 15.5 ($CH_3$), 15.2 ($CH_3$), 15.1 ($CH_3$), two $CH_2$=$CH$B not observed; IR (neat): 3044, 2963, 2929, 1555, 1179, 972 cm$^{-1}$; HRMS-EI: calcd for ($C_{22}H_{31}BN_2$) 334.2578 found 334.2574.

***2,4,4,6-Tetraethyl-1,3,5,7,8-pentamethyl-4-bora-3a,4a-diaza-s-indacene (7)***

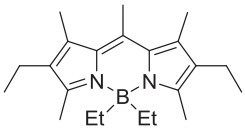


According to the general procedure E, ethylmagnesium bromide (1.7 mL, 0.9 M in THF, 1.57 mmol) and PM567 (50 mg, 0,157 mmol) in $CH_2Cl_2$ (15 mL) at room temperature for 1 h were reacted. Flash chromatography using hexane/EtOAc (98:2) afforded **7** (22 mg, 41%) as an orange solid. $^1$H NMR (300 MHz, $CDCl_3$): $\delta$ = 2.58 (s, 3H, $CH_3$), 2.35 (q, $J$ = 7.5 Hz, 4H, $2CH_3\mathit{CH_2}$), 2.34 (s, 6H, $2CH_3$), 2.29 (s, 6H, $2CH_3$), 0.97 (t, $J$ = 7.5 Hz, 6H, $2\mathit{CH_3}CH_2$), 0.74 (q, $J$ = 7.5 Hz, 4H, $2CH_3\mathit{CH_2}B$), 0.21 (t, $J$ = 7.5 Hz, 6H, $2\mathit{CH_3}CH_2B$); $^{13}$C NMR (75 MHz, $CDCl_3$): $\delta$ = 148.2 (C), 139.7 (C), 132.3 (C), 132.0 (C), 131.3 (C), 17.8 ($CH_3$), 17.6 ($CH_2$), 15.1 ($CH_3$), 15.0 ($CH_3$), 14.0 ($CH_3$), 9.4 ($CH_3$), two $CH_2B$ not observed; IR (neat): 2956, 1555, 1460, 1195, 987, 769 cm$^{-1}$; HRMS-EI: calcd for ($C_{22}H_{35}BN_2$) 338.2890 found 338.2894.

**Table S1.** Photophysical properties of the commercial *F*-BODIPYs and their corresponding *E*- and *C*-BODIPYs in diluted solutions of ethyl acetate (2μM); absorption ($\lambda_{ab}$) and fluorescence ($\lambda_{fl}$) wavelength, molar absorption ($\varepsilon_{max}$), Stokes shift ($\Delta\nu_{St}$), fluorescence quantum yield ($\phi$) and lifetime ($\tau$), radiative ($k_{fl}$) and non-radiative ($k_{nr}$) rate constants.

| | $\lambda_{ab}$ (nm) | $\varepsilon_{max}$ ($10^4 M^{-1}cm^{-1}$) | $\lambda_{fl}$ (nm) | $\Delta\nu_{St}$ ($cm^{-1}$) | $\phi$ | $\tau$ (ns) | $k_{fl}$ ($10^8$ $s^{-1}$) | $k_{nr}$ ($10^8$ $s^{-1}$) |
|---|---|---|---|---|---|---|---|---|
| **PM546** | 494.0 | 8.1 | 504.0 | 400 | 0.85 | 5.58 | 1.52 | 0.27 |
| **1a** | 493.5 | 5.5 | 504.0 | 420 | 0.96 | 5.78 | 1.66 | 0.07 |
| **2a** | 493.0 | 7.9 | 503.5 | 425 | 0.95 | 5.71 | 1.66 | 0.09 |
| **PM567** | 516.5 | 8.0 | 531.5 | 550 | 0.84 | 5.78 | 1.45 | 0.28 |
| **1b** | 513.5 | 7.4 | 530.5 | 625 | 0.86 | 5.97 | 1.44 | 0.23 |
| **2b** | 513.0 | 8.4 | 531.0 | 660 | 0.86 | 5.72 | 1.50 | 0.24 |
| **4a** | 515.5 | 6.7 | 530.5 | 550 | 0.88 | 6.32 | 1.39 | 0.19 |
| **5** | 510.0 | 8.4 | 531.5 | 795 | 0.70 | 4.89 | 1.43 | 0.61 |
| **6** | 512.0 | 6.9 | 550.0 | 1350 | 0.51 | 4.74 | 1.07 | 1.03 |
| **7** | 507.5 | 4.8 | 538.0 | 1115 | 0.45 | 4.05 | 1.11 | 1.36 |
| **PM580** | 518.5 | 8.5 | 536.5 | 650 | 0.94 | 5.93 | 1.58 | 0.10 |
| **1c** | 515.0 | 10.0 | 533.0 | 655 | 0.90 | 5.75 | 1.56 | 0.17 |
| **2c** | 514.5 | 11.3 | 532.5 | 655 | 0.93 | 5.68 | 1.64 | 0.12 |
| **PM605** | 543.0 | 7.5 | 558.0 | 500 | 0.73 | 6.64 | 1.10 | 0.41 |
| **4c** | 541.5 | 7.6 | 557.0 | 515 | 0.80 | 7.18 | 1.10 | 0.28 |
| **PM597** | 523.0 | 7.7 | 562.5 | 1330 | 0.47 | 4.31 | 1.09 | 1.23 |
| **1d** | 521.5 | 7.0 | 565.5 | 1490 | 0.54 | 5.19 | 1.04 | 0.89 |
| **2d** | 521.0 | 7.2 | 566.5 | 1540 | 0.61 | 5.41 | 1.13 | 0.72 |
| **3a** | 522.0 | 6.4 | 567.0 | 1520 | 0.57 | 5.23 | 1.09 | 0.82 |
| **3b** | 521.5 | 6.2 | 565.0 | 1475 | 0.57 | 5.21 | 1.09 | 0.82 |
| **4b** | 526.0 | 6.7 | 567.0 | 1375 | 0.62 | 5.78 | 1.07 | 0.66 |
| **PM597-8C9** | 523.0 | 8.6 | 595.5 | 2330 | 0.10 | 1.14 | 0.88 | 7.90 |
| **1e** | 520.5 | 8.2 | 606.0 | 2710 | 0.13 | 1.75 | 0.74 | 4.97 |
| **2e** | 519.5 | 7.0 | 604.5 | 2705 | 0.18 | 2.43 | 0.74 | 3.37 |
| **PM650** | 588.0 | 4.2 | 603.0 | 435 | 0.15 | 2.37 | 0.63 | 3.59 |
| **4d** | 587.0 | 4.7 | 602.0 | 425 | 0.29 | 4.59 | 0.63 | 1.55 |

**Table S2**. Lasing efficiencies of commercial BODIPY dyes and their *E*- and *C*-BODIPY derivatives as a function of the concentration in ethyl acetate. [c]: dye concentration; $\lambda_{exc}$: pumping wavelength; $\lambda_L$ = peak of the laser emission.

| [c] (mM) | $\lambda_{exc}$ = 355 nm | | | $\lambda_{exc}$ = 532 nm | | | | | | | | | | | | | | | | | | | | | | | |
|---|---|---|---|---|---|---|---|---|---|---|---|---|---|---|---|---|---|---|---|---|---|---|---|---|---|---|---|
| | PM546 | **1a** | **2a** | PM567 | **1b** | **2b** | **4a** | **5** | **6** | **7** | PM580 | **1c** | **2c** | PM597 | **1d** | **2d** | **3a** | **3b** | **4b** | PM597 -8C9 | **1e** | **2e** | PM605 | **4c** | PM650 | **4d** | PM650 -F-CN |
| | $\lambda_L \approx$ | | | $\lambda_L \approx$ 570 nm | | | | | | | $\lambda_L \approx$ 570 | | | $\lambda_L \approx$ 585 nm | | | | | | $\lambda_L \approx$ 610 nm | | | $\lambda_L \approx$ 595 nm | | $\lambda_L \approx$ 655 nm | | |
| 0.3 | | | | | | | | | | | | | | 50 | 60 | 57 | 65 | 59 | 58 | | | | 49 | 53 | 17 | | |
| 0.4 | | | | | | | | | | | | | | | | | | | | | | | 52 | 59 | | | |
| 0.5 | | | | | | | | | | | | | | 53 | 67 | 61 | 71 | 65 | 62 | | | | | | 25 | 35 | 24 |
| 0.6 | | | | | | | | | | | | | | | | | | | | | | | 55 | 63 | | | |
| 0.7 | | | | | | | | | | | | | | | | | | | | | | | | | 30 | 40 | 30 |
| 0.8 | | | | 38 | | | 64 | | | | 51 | 57 | 50 | 51 | 70 | 63 | 73 | 68 | 68 | 45 | 51 | 47 | 51 | 68 | | | |
| 0.9 | | | | | | | | | | | | | | | | | | | | | | | | | 35 | 45 | 36 |
| 1.0 | 18 | 40 | 40 | 43 | | | 67 | 40 | 47 | | 55 | 62 | 57 | 49 | 68 | 60 | 70 | 66 | 73 | 50 | 57 | 52 | | | | | |
| 1.5 | 21 | 48 | 47 | 48 | 60 | 50 | 68 | 49 | 54 | | 57 | 65 | 63 | 44 | 67 | 58 | 67 | 64 | 70 | 52 | 62 | 59 | 47 | 65 | 32 | 37 | 32 |
| 2.5 | 23 | 54 | 49 | 45 | 65 | 56 | 60 | 54 | 60 | 10 | 53 | 63 | 60 | 38 | 64 | 52 | 64 | 61 | 65 | 49 | 58 | 54 | 40 | 60 | | 26 | 22 |
| 3.5 | 20 | 58 | 52 | 49 | 67 | 60 | 55 | 52 | 58 | 20 | 50 | 61 | 57 | | 60 | 46 | 58 | 55 | 60 | | | | | | | | |
| 5.0 | 15 | 52 | 47 | 30 | 63 | 58 | 50 | 47 | 54 | 30 | 41 | 53 | 50 | | 51 | 39 | 53 | 43 | 53 | 44 | 52 | 48 | 25 | 35 | | | |
| 7.5 | | 41 | 44 | 25 | 52 | 54 | 40 | 38 | 50 | 23 | | | | | | | | | | 36 | 46 | 40 | | | | | |
| 10.0 | | 34 | 37 | | 47 | 52 | 31 | 26 | 47 | 13 | 30 | 39 | 30 | | | | | | | | | | | | | | |

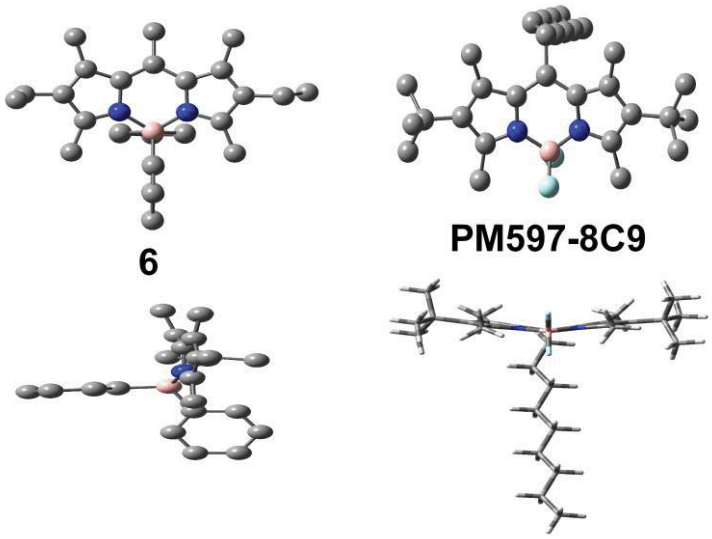


**Figure S1.** Optimized geometries in the excited state of compound **6** (front and side-view) and PM597-8C9 (front and view from the boron atom). The two different views are shown for a better clarity of the spatial disposition of the rings and linear chain, respectively.

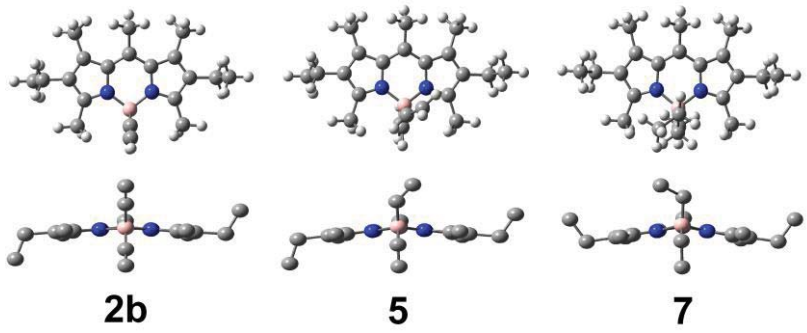


**Figure S2.** First excited state optimized geometries (CIS/6-31G) of compounds derived from PM567 **2b** (acetylene), **5** (vinyl) and **7** (ethyl). A view from the boron atom is also included for a better evaluation of the planarity of the chromophore.

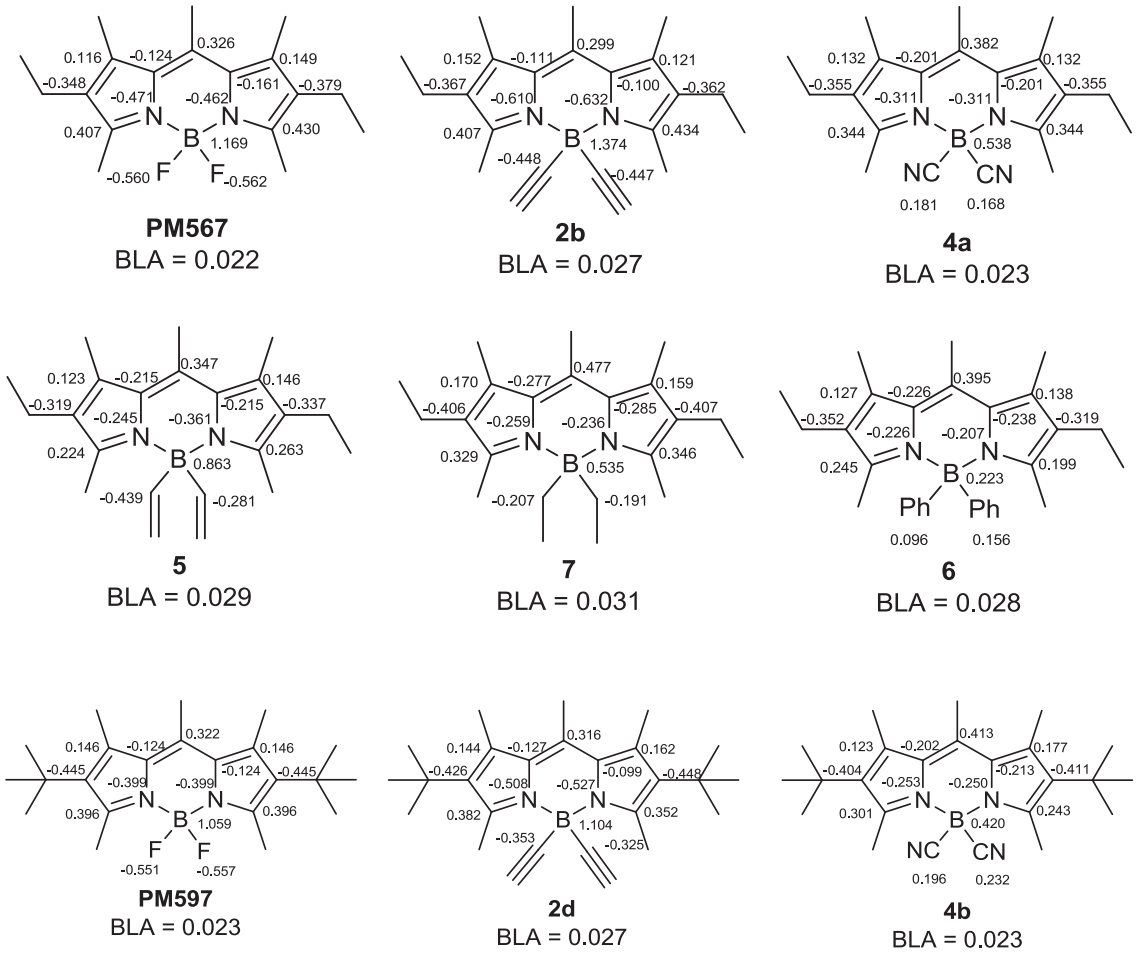


**Figure S3**. Excited state charge distribution (CHelpG) of representative *E*- and *C*-BODIPYs from PM567 and PM597.

Journal Name

Dynamic Article Links ►

Cite this: DOI: 10.1039/c0xx00000x

www.rsc.org/xxxxxx

ARTICLE TYPE

# Asymmetric BODIPY triad for panchromatic absorption and red-edge laser emission†

**Gonzalo Duran-Sampedro,[a] Antonia R. Agarrabeitia,[a] Inmaculada Garcia-Moreno,[b] Leire Gartzia-Rivero,[c] Santiago de la Moya,[a] Jorge Bañuelos,*[c] Íñigo López-Arbeloa,[c] and María J. Ortiz*[a]**

***Received (in XXX, XXX) Xth XXXXXXXXX 200X, Accepted Xth XXXXXXXXX 200X***

**DOI: 10.1039/b000000x**

**A rational design of an unprecedented asymmetric cassette triad based entirely on BODIPY chromophores allows efficient light harvesting over the UV-vis spectral region, leading to a bright and stable red-edge laser emission via efficient energy-transfer processes.**

Long wavelength (>600 nm) fluorescent dyes have found applications in a wide variety of fields, such as laser printing, information storage, displays and solar power conversion.[1] They have also proved to be useful tools in biomedical applications (including photodynamic therapies),[2] due mainly to the deeper penetration into tissues of this kind of light.[3] Although a number of long-wavelength emitting commercial dyes with reasonable efficiency are available,[4] these dyes have important drawbacks: low absorption at the standard pump wavelengths (355 and 532 nm) and/or poor photostability. One approach to overcome these drawbacks is the straightforward synthesis of energy transfer cassettes,[5] which has proved to be a powerful strategy in fields such as light-harvesting systems and sensors.[6] However, this approach has not been tried to date to develop panchromatic dyes with enhanced red-edge laser emission.

The rational design of a multichromophoric molecular system enabling an efficient cascade of excitation energy transfer (EET) processes is challenging, since the effectiveness of each individual EET event depends on the mutual separation and relative orientation of the involved donor and acceptors moieties. BODIPYs (4,4-difluoro-4-bora-3a,4a-diaza-s-indacenes) have demonstrated to be valuable scaffolds to design cascade-like EET architectures,[7] since they can be properly functionalized to assure strong absorption throughout the visible spectrum.[8] On the other hand, high efficiency of monochromatic emission beyond 650 nm can be obtained from certain conveniently-functionalized BODIPYs.[9] On the basis of this synthetic versatility of the BODIPY chromophores for designing energy-transfer systems, herein we came to report a straightforward, efficient and cost-effective synthetic protocol to produce an unprecedented panchromatic all-BODIPY cassette triad (**1** in Fig. 1) enabling highly efficient and stable laser emission at 665 nm.

The asymmetric molecular architecture of **1** is not trivial, at it was judiciously designed to get the desired photophysical property thought to the simpler synthetic route. Thus, its twisted architecture was selected to avoid supramolecular aggregation by π-π stacking interactions, which are known to have a deleterious effect on laser action. However, compared to symmetric BODIPY systems, which can be straightforwardly synthesized (*e.g.*, from pyrrole derivatives), a facile and scalable synthesis of low symmetric BODIPY analogues is still challenging.

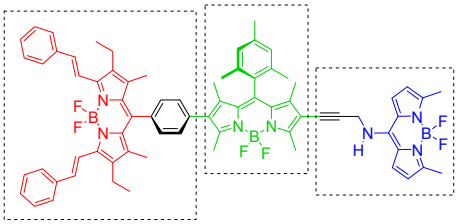

**1**

**Fig. 1.** Developed cassette triad. Key BODIPY moieties in different colours (spacers in black). Individual key synthetic building-block fragments inside dotted windows.

The lateral 8-aminoBODIPY moiety of **1** (blue fragment in Fig. 1) was selected as the short-wavelength donor due to the known strong absorption and highly efficient and stable emission in the blue-green spectral region exhibited by related individual BODIPYs (400-500 nm).[10] On the other hand, the central 8-mesitylBODIPY moiety (green moiety in Fig. 1) was chosen on the basis of its expected strong absorption and emission in the green-orange spectral region (490-600 nm),[11] which should allow the required dual behaviour of the central core inside the triad (donor and acceptor moiety), but also because the corresponding isolated BODIPY results a convenient synthetic building block to let its lateral asymmetric functionalization as shown later. Finally, the 3,5-distyrylBODIPY chromophore (red fragment in Fig. 1) was selected due to its likely strong absorption and high efficient emission in the red-edge spectral region (600-750 nm).[9] Moreover, the molecular assembly of the said moieties was addressed thought to relatively short and rigid spacers (twisted 1,4-phenylene‡ and 1,3-propynylidene) to get the desired photophysical property. Thus, the phenylene bridge results crucial to maintain the triad twisted, avoiding its aggregation. Besides, this twisted spacer should maintain the corresponding linked BODIPYs electronically isolated. Alternatively, the non-π-conjugated propynylidene spacer is key to keep the "blue" identity of the lateral 8-aminoBODIPY, maintaining the linked

chromophores isolated. The selection of the spacers take into account synthetic factors also, since they must allow the straightforward assembly of synthetically-accessible BODIPY-based building blocks, as mentioned below.

Thus, triad **1** was attained by the straightforward convergent synthetic route shown in Fig. 2, which was judiciously designed on the basis of using workable palladium-catalysed carbon-carbon coupling reactions (Sonogashira and Suzuki). Synthetically-accessible 2,6-diiodoBODIPY **3** (easily obtainable from accessible **2**),[12] is the key intermediate of the designed route, since it could be submitted to controlled (stepped) carbon-carbon coupling reaction towards the final desired triad. Thus, the Sonogashira coupling of **3** with the blue *N*-propargyl-8-aminoBODIPY **5** (obtained from commercial **4**[13] by using the methodology described by Peña *et al.*[10]) allowed the easy preparation of diad **6** (Fig. 2). On the other hand, submitting synthetically accessible **7**[14] to Knoevenagel-like reaction with benzaldehyde/$K_2CO_3$ (standard red-shifting distyryl functionalization of 3,5-dimethylBODIPYs[9]) allows obtaining boronic-ester-based red BODIPY **8**, which could be straightforwardly coupled to diad **6** by Suzuki reaction, to afford desired **1** (Fig. 2).

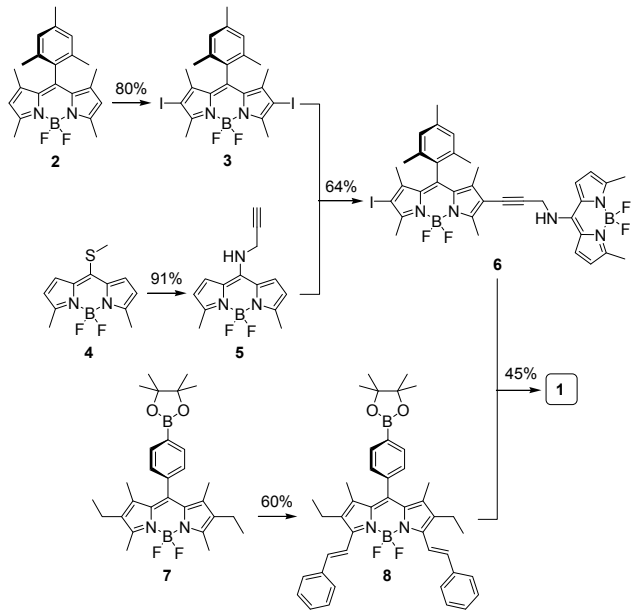


**Fig. 2.** Convergent synthetic route to **1** (yields over arrows; see ESI† for details).

As consequence of the mentioned rational design, the absorption spectrum of triad **1** (Fig. 3) resulted to be the sum of the bands of the involved individual chromophores. Accordingly, four strong absorption bands at 631, 536, 426 and 342 nm ($\varepsilon_{max}$ up to $10^5$ $M^{-1}cm^{-1}$, see Table S1 in ESI†), covering the whole near-ultraviolet-to-red spectral region were recorded. The three vis bands were assigned to the corresponding absorption of the electronically-isolated BODIPY chromophores of **1**, by comparing the absorption spectrum of **1** with those individually obtained from parent dyes **2**, **5** and **8** (Fig. 3). The observed red shift of the band at 536 nm, when compared with the obtained from **2**, is due to the conjugation of the central BODIPY core of **1** with the lateral phenylene spacer and, mainly, with the propynylidene one (see Fig. 3). On the other hand, the ultraviolet (UV) band at 342 nm results from the summed UV absorptions of the involved individual BODIPY chromophores, being the distyryl chromophore the main contributor (see Fig 3). Theoretical calculations conducted on **1** (B3LYP/6-31+g*, see ESI†) support also the claimed electronic isolation of chromophores, by predicting the involvement of molecular orbitals placed exclusively at each BODIPY fragment for the vis electronic transitions associated to each vis absorption band, (see Fig. 3). Therefore, the cassette-required selective excitation of chromophores should be possible in **1**.

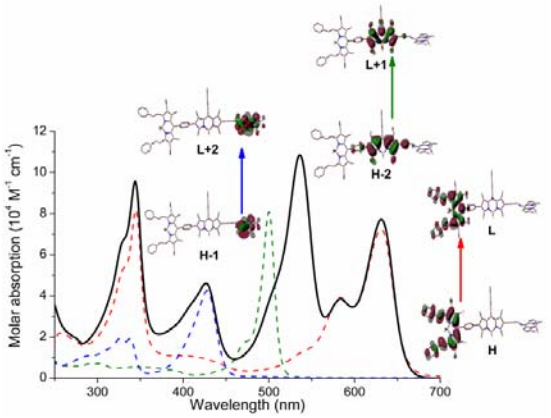


**Fig. 3.** Absorption spectra of **1** (solid line), **2** (green), **5** (blue) and **8** (red) in ethyl acetate, as well as computed molecular orbitals involved in each visible transition of **1**.

Indeed, the selective excitation of each chromophore in **1** leads to a strong red fluorescence from the distyryl fragment (645 nm, $\phi$ = 72%; see Table S1 in ESI†), regardless of the excitation wavelength along the whole UV-vis spectrum (Fig. 4). Therefore, efficient EET processes take place, as demonstrated also by the excitation spectra monitored at a long-enough wavelength (see Fig. 4), which matches with the absorption spectrum showing its characteristic four bands (*cf.*, Figs. 3 and 4).

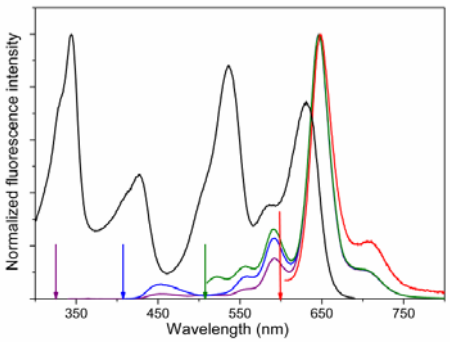


**Fig. 4.** Fluorescence spectra of **1** at different excitation wavelengths along the UV-vis (indicated by arrows), and excitation spectrum monitored at 700 nm (black).

The efficiencies of the EET processes occurring in **1** can be estimated from the quenching of the emission of the donor chromophores, lateral blue and central green, induced by the presence of the corresponding acceptor chromophores, central


This journal is © The Royal Society of Chemistry [year]

green and lateral red (see Fig. S1 and Table S1 in ESI†). Thus, the efficiency of the EET from the blue donor to the green acceptor resulted to be 99%, whereas the efficiency from the green donor to the final red acceptor was 91%. The intramolecular EETs between chromophores should obey a Förster-resonance energy-transfer (FRET) mechanism, being extremely efficient due to the involved separation distances and the notable spectral overlaps (especially high for the blue and green chromophores; see Fig. S2 in ESI†). Besides, a contribution of the through-bond energy transfer (TBET) mechanism should also be feasible in the hop from the central green chromophore to the red one, since the involved phenylene spacer could enable the required electronic connection through its π-conjugated orbitals. In fact, the calculated efficiency for this EET process is quite high, despite the lower spectral overlap existing for the green and red chromophores (Fig. S2 in ESI†). In contrast, such mechanism is less feasible in the hop from the lateral blue chromophore to the central one, owing to the involved methylene-bridge of the involved propynylidene spacer, which should reduce the electron-exchange probability.

The optimized photophysics of **1**, obtained from its carefully designed structure, results in enhanced laser behaviour as a laser dye when compared to those obtained individually from the parent monochromophoric dyes. Thus, this singular structure enables **1** to lase efficiently in the red spectral region under pumping either in the UV (355 nm) or in the vis (532 nm) spectral regions, due to the mentioned cassette behaviour, but also because the covalent binding of its three BODIPY chromophores leads to a significant increase in the absorptions, at both pumping wavelengths, when compared to those exhibited individually by the related monochromophoric parent dyes. This is a key factor from the point of view of the laser action, since it allows reducing significantly the required gain-media concentrations, avoiding consequently dye-solubility problems, or dye quenching and/or aggregation processes, all of them with detrimental effect on the laser emission. For instance, the new triad exhibits molar absorption coefficients of $9.5 \cdot 10^4$ and $11 \cdot 10^4$ $M^{-1}cm^{-1}$ at 355 and 532 nm, respectively, which are above those exhibited individually by the comparison parent dyes (see Fig. 3).

Under transversal pump conditions at 355 nm, broad-line-width laser emission, with pump threshold energy of ~0.6 mJ, divergence of 5 mrad and pulse duration of 8 ns full width at half maximum (FWHM), was obtained from a triad solution placed in a simple plane-plane non-tunable resonator (see ESI† for experimental details). In agreement with the photophysical behaviour, the cascade of EET processes inside triad **1** leads to a highly efficient (up to 49%) and monochromatic laser emission centered at 665 nm. This laser efficiency is much higher than that recorded from parent red BODIPY **8**, whose laser efficiency does not exceed the 30% value when pumped under identical experimental conditions, either at 355 nm or at 532 nm. These results could be related with the next facts: (a) the lower absorption of **8** at 532 nm, when compared to triad **1**, making necessary to increase significantly the dye concentration in the gain media to achieve the optimal pumping conditions, and (b) the energetic difference between absorbed (355 nm) and emitted (665 nm) photons, which makes the emission process to be energetically more favourable when taking place through to an EET cascade, as occurring in **1**.

Triad **1** exhibits also an excellent photostability, maintaining 100% of the initial emission intensity after 100000 pump pulses (see ESI† for experimental details). In order to put this result in a proper perspective, the lasing parameters of the commercial BODIPY dye PM650, lasing at the same wavelength obtained from **1**, were measured under identical experimental conditions. Noticeably and differently to **1**, PM650 could not be pumped at 355 nm, since its low absorption at this wavelength makes necessary dye concentrations upcoming the dye solubility limit. On the other hand, pumping PM650 ($2 \cdot 10^{-3}$ M in ethyl acetate) at 532 nm makes this dye to lase at 657 nm with 35% efficiency and a 38% lost of the initial laser-induced fluorescence intensity after 100000 pump pulses. Therefore, triad **1** outperforms the lasing properties of PM650, especially taking into account that PM650 was only pumped at the longer 532 nm wavelength; *i.e.*, with less energetic photons minimizing the energy released to the medium and, therefore, reducing the rate and extension of photodegradation process occurring when pumping with high-energy photons. Moreover, compared to PM650, triad **1** exhibits another important advantage, namely its high chemical stability in solution. Thus, PM650 has been reported to be highly unstable in certain solvents (most of them characterized as electron donors),[15] becoming completely bleached after some hours (or days in the best case), and implying that its solutions have to be used and characterized just after preparation.

In conclusion, we have developed a straightforward and cost-effective synthetic approach to attain an asymmetric all-BODIPY triad with panchromatic absorption and, simultaneously, efficient and photostable laser emission in the red-edge spectral region. The rational design of this molecular system ameliorates three key optical factors to improve its photonic applicability: four strong absorption bands with extinction absorption coefficients up to $10^5$ $M^{-1}cm^{-1}$, EET efficiency as high as 99%, and laser efficiency up to 49%, the latter being much higher than those exhibited by the parent red BODIPY mimicking the triad red chromophore, and by the commercial dye PM650, which is considered the bench-mark of the red-emitting BODIPY-based laser dyes.

Financial support from the MINECO (MAT2014-51937-C3-1-P, -2-P and -3-P) of Spain, UCM (GR3/14-910107 and -910150) and Gobierno Vasco (IT339-10) is gratefully acknowledged. L.G.-R. thanks UPV-EHU for a postdoctoral fellowship and G.D.-S thanks MINECO for predoctoral fellowships.

## Notes and references

[a] *Depto. de Química Orgánica I, Facultad de CC. Químicas, Universidad Complutense de Madrid, Ciudad Universitaria s/n, 28040, Madrid, Spain. E-mail: mjortiz@ucm.es*

[b] *Depto. de Sistemas de Baja Dimensionalidad, Superficies y Materia Condensada, Instituto de Química-Física "Rocasolano", C.S.I.C., Serrano 119, 28006 Madrid, Spain.*

[c] *Depto. de Química Física, Universidad del Pais Vasco-EHU, Apartado 644, 48080, Bilbao, Spain. E-mail: jorge.banuelos@ehu.es*

†Electronic Supplementary Information (ESI) available: Experimental, photophysical and computational details, characterization data and NMR spectra of the new compounds, as well as Figs. S1-S2 and Table S1. See DOI: 10.1039/b000000x/

‡Neighbouring methyl groups make the 1,4-phenylene spacer of triad **1** to be twisted, as it occurs in the phenyl group of related monochromophoric

BODIPYs. This effect is also shown in the computed triad structure (see Fig. 2).


1 (a) T. A. Fayed, in *Reviews in Fluorescence* (Ed. Geddes), C. D., Springer, New York, 2011; (b) *Tunable Laser Applications*, 2nd ed. (Ed. F. J. Duarte), CRC, New York 2009; (c) L. Bonardi, H. Kanaan, F. Camerel, P. Jolinat, P. Retailleau and R. Ziessel, *Adv. Funct. Mater*. 2008, **18**, 401; (d) O. A. Bozdemir, S. Erbas-Cakmak, O. O. Ekiz, A. Dana and E. U. Akkaya, *Angew. Chem. Int. Ed*., 2011, **50**, 10907.

2 (a) T. Yogo, Y. Urano, Y. Ishitsuka, F. Maniwa and T. Nagano, *J. Am. Chem. Soc*., 2005, **127**, 12162; (b) T. Myochin, K. Hanaoka, T. Komatsu, T. Terai and T. Nagano, *J. Am. Chem. Soc*., 2012, **134**, 13730.

3 R. Steiner in *Applied Laser Medicine* (Eds. H. P. Berlien and G. H. Müller), Sringer-Verlag, 2003.

4 *Lambdachrome Laser Dyes* (Ed. U. Backmann), Lambda Physik, 2000.

5 (a) D. McQuade, A. Pullen and T. Swager, *Chem. Rev.,* 2000, **100**, 2537; (b) A. Coskun and E. U. Akkaya, *J. Am. Chem. Soc*., 2005, **127**, 10464; (c) X. Zhang, Y. Xiao and X. Qian, *Org. Lett.,* 2008, **10**, 29; (d) Y. Xiao, D. Zhang, X. Qian, A. Costela, I. Garcia-Moreno, V. Martin, M. E. Perez-Ojeda, J. Bañuelos, L. Gartzia and I. Lopez Arbeloa, *Chem. Commun*., 2011, **47**, 11513; (e) L. Cerdan, E. Enciso, V. Martin, J. Bañuelos, I. Lopez Arbeloa, A. Costela and I. Garcia-Moreno*, Nature Photonics,* 2012, **6**, 621.

6 (a) J. Warnan, F. Buchet, Y. Pellegrin, E. Blart and F. Odobel, *Org. Lett*., 2011, **13**, 3944; (b) Y. Shi, R. B. M. Hill, J.-H. Yum, A. Duale, S. Barlow, M. Grätzel, S. R. Marder and M. K. Nazeeruddin, *Angew. Chem. Int. Ed.*, 2011, **50**, 6619; (c) N. C. Jeong, H.-J. Son, C. Prasittichai, C. Y. Lee, R. A. Jensen; O. K. Farha and J. T. Hupp, *J. Am. Chem. Soc.* 2012, **134**, 19820; (d) D. K. Panda, F. S. Goodson, S. Ray and S. Saha, *Chem. Commun*., 2014, **50**, 5358.

7 (a) J. Han, J. Jose, E. Mei and K. Burgess, *Angew. Chem. Int. Ed.,* 2007, **46**, 1684; (b) W. Lin, L. Yuan, Z. Cao, Y. Feng and J. Song, *Angew. Chem. Int. Ed.,* 2010, **49**, 375; (c) R. Ziessel, G. Ulrich, J. H. Oliver, T. Bura and A. Sutter, *Chem. Commun.,* 2010, **46**, 7978; (d) Y. Ueno, J. Jose, A. Loudet, C. Perez-Bolivar, P. Anzenbacher and K. Burgess, *J. Am. Chem. Soc.,* 2011, **133**, 51; (e) Y. Zhao, Y. Zhang, X. Lv, Y. Liu, M. Chen, P. Wang, J. Liu and W. Guo, *J. Mater. Chem.*, 2011, **21**, 13168; (f) Q. Huaulmé, E. Cece, A. Mirlouop and R. Ziessel, *Tetrahedron Lett*., 2014, **55**, 4953.

8 (a) S. Erten-Ela, M. D. Yilmaz, B. Icli, Y. Dede, S. Icli and E. U. Akkaya, *Org. Lett*., 2008, **10**, 3299; (b) K. Umezawa, Y. Nakamura, H. Makino, D. Citterio and K. Suzuki, *J. Am. Chem. Soc.,* 2008, **130**, 1550; (c) A. Haefele, C. Zedde, P. Retailleau, G. Ulrich and R. Ziessel, *Org. Lett.*, 2008, **12**, 1672; (d) S. Kolemen, O. A. Bozdemir, Y. Cakmak, G. Barin, S. Erten-Ela, M. Marszalek, Y.-H. Yum, S. M. Zakeeruddin, M. K. Nazeeruddin, M. Grátzel and E. U. Akkaya, *Chem. Sci.,* 2011, **2**, 949; (e) S. Zhu, J. Zhang, G. K. Vegesna, R. Pandey, F.-T. Luo, S. A. Green and H. Liu, *Chem. Commun.,* 2011, **47**, 3508; (f) C. Qin, A. Mirloup, N. Leclerc; A. Islam; A. El-Shafei, L. Han and R. Ziessel, *Adv. Ener. Mater*., 2014, **4**, 85; (g) S. Kuhri, V. Engelhardt, R. Faust and D. M. Guldi, *Chem. Sci.,* 2014, **5**, 2580.

9 H. Lu, J. Mack, Y. Yang and Z. Shen, *Chem. Soc. Rev.*, 2014, **43**, 4778.

10 (a) C. F. A. Gomez-Duran; I. Garcia-Moreno, A. Costela, V. Martin, R. Sastre, J. Bañuelos, F. Lopez Arbeloa, I. Lopez Arbeloa and E. Peña Cabrera, *Chem. Commun.,* 2010, **46**, 5103; (b) J. Bañuelos, V. Martin, C. F. A. Gomez-Duran, I. J. Arroyo Cordoba, E. Peña-Cabrera, I. Garcia-Moreno, A. Costela, M. E. Perez-Ojeda, T. Arbeloa and I. Lopez Arbeloa, *Chem. Eur. J*,. 2011, **17**, 7261.

11 (a) A. Loudet and K. Burgess, *Chem. Rev.*, 2007, **107**, 4891; (b) G. Ulrich, R. Ziessel and A. Harriman, *Angew. Chem. Int. Ed.*, 2008, **47**, 1184.

12 L. Fu, F.-L. Jian, D. Fortin, P. D. Harvey and Y. Liu, *Chem. Commun*., 2011, **46**, 5503.

13 Purchased from Cuántico de México.

14 M. Koepf, A. Trabolsi, M. Elhabiri, J. A. Wytko, D. Paul, A. M. Albrecht-Gary and J. Weiss, *Org. Lett.,* 2005, **7**, 1279.

15 J. Bañuelos, T. Arbeloa, M. Liras, V. Martinez and F. Lopez Arbeloa, *J. Photochem. Photobiol. A,* 2006, **184**, 298.



This journal is © The Royal Society of Chemistry [year]

**Supporting information for**

# Asymmetric BODIPY triad for panchromatic absorption and red-edge laser emission

Gonzalo Duran-Sampedro,[a] Antonia R. Agarrabeitia,[a] Inmaculada García-Moreno,[b] Leire Gartzia-Rivero,[c] Santiago de la Moya,[a] Jorge Bañuelos,*[,c] Íñigo López-Arbeloa,[c] and María J. Ortiz*[,a]

[a] *Depto. de Química Orgánica I, Facultad de CC. Químicas, Universidad Complutense de Madrid, Ciudad Universitaria s/n, 28040, Madrid, Spain.*
*E-mail:mjortiz@ucm.es*

[b] *Depto. de Sistemas de Baja Dimensionalidad, Superficies y Materia Condensada, Instituto de Química-Física "Rocasolano", C.S.I.C., Serrano 119, 28006 Madrid, Spain.*

[c] *Depto. de Química Física, Universidad del Pais Vasco-EHU, Apartado 644, 48080, Bilbao, Spain.*
*E-mail: jorge.banuelos@ehu.es*

## Table of contents

## 1. General

**Synthesis.** Common solvents were dried and distilled by standard procedures. All starting materials and reagents were obtained commercially and used without further purifications. Flash chromatography purifications were performed on silica gel 60 (60, 230-400 mesh ASTM). Thin-layer chromatography (TLC) was performed on silica gel plates (silica gel 60, F254, supported on aluminium). NMR spectra were recorded at 20 ºC and the residual solvent peaks were used as internal standards. FTIR spectra were obtained from neat samples using the ATR technique. High resolution mass spectrometry (HRMS) was performed using the EI technique.

**Photophysical properties.** The absorption and fluorescence spectra, as well as fluorescence decay curves, were recorded in diluted solutions (around $2 \cdot 10^{-6}$ M) of ethyl acetate. UV-Vis absorption and fluorescence spectra were recorded on a Varian model CARY 4E spectrophotometer and on an Edinburgh Instruments spectrofluorimeter (model FLSP 920), respectively. Fluorescence quantum yields ($\phi$) were obtained using coumarin 1 ($\phi$ = 0.75 in ethanol), PM546 ($\phi$ = 0.85 in ethanol) and cresyl violet ($\phi$ = 0.54 in ethanol) for the emission in the blue, green and red spectral region respectively. The values were calculated from corrected spectra (detector sensibility to the wavelength) and corrected by the refractive index of the solvent. Radiative decay curves were registered with the time correlated single-photon counting technique (Edinburgh Instruments, model FLSP920, with picosecond time-resolution). Fluorescence emission was monitored at the maximum emission wavelength after excitation at 410, 490 and 590 nm by means of a Femtopower 1060 Supercontinuum source (Fianium, SC-400-4-PP-03M) with 4 Watt pulse and a repetition rate of 10 MHz. The fluorescence lifetime ($\tau$) was obtained after the deconvolution of the instrumental response signal from the recorded decay curves by means of an iterative method. The goodness of the exponential fit was controlled by statistical parameters (chi-square, Durbin-Watson and the analysis of the residuals). The radiative ($k_{fl}$) and non-radiative ($k_{nr}$) rate constants were calculated from the fluorescence quantum yield and lifetime: $k_{fl} = \phi/\tau$; $k_{nr} = (1-\phi)/\tau$.

The EET efficiency was calculated as the decrease of the donor fluorescence quantum yield of the donor induced by the presence of the acceptor within the triad cassette **1** ($(1-\phi_D^0/\phi_D)\times 100$, where $\phi^0$ and $\phi$ denote the fluorescence quantum yields of the isolated donor and the donor linked-to-acceptor, respectively).

**Quantum mechanical calculations.** Ground state geometries were optimized at the Density Functional Theory (DFT) using the hybrid B3LYP method and the double valence basis set with diffuse and polarization functions (6-31+g*). The geometries were considered as energy minimum when the corresponding frequency analysis did not give any negative value. The absorption spectra were simulated by the Time Dependent (TD) method. All the calculations were performed using the Gaussian 09 software as implemented in the computational cluster “arina” of the UPV/EHU.

**Laser behaviour.** Liquid solutions of dyes were contained in 1 cm optical-path rectangular quartz cells carefully sealed to avoid solvent evaporation during the experiments. The liquid solutions were transversely pumped either at 355 nm, with 5 mJ, 8 ns FWHM pulses from the third-harmonic of a Q-switched Nd:YAG laser (Spectron SL282G) or at 532 nm, with 5 mJ, 6 ns FWHM pulses from a frequency-doubled Q-switched Nd:YAG laser (Monocrom OPL-10), at a repetition rate of up to 10 Hz.

The exciting pulses were line-focused onto the cell, providing pump fluences on the active medium in the range 110-180 mJ/cm$^2$. The oscillation cavity (2 cm length) consisted of a 90% reflectivity aluminium mirror, with the lateral face of the cell or the solid sample as output coupler.

The photostability of the dyes in liquid solution was evaluated by irradiating under lasing conditions 10 μL of a solution in ethyl acetate. The solutions were contained in a cylindrical Pyrex tube (1 cm height, 1 mm internal diameter) carefully sealed to avoid solvent evaporation during the experiments. Although the low optical quality of the capillary tube prevents laser emission from the dyes, information about photostabilities can be obtained by monitoring the decrease in laser-induced fluorescence intensity, excited transversally to the capillary tube, as a function of the number of pump pulses at a given repetition rate. The fluorescence emission was monitored perpendicular to the exciting beam, collected by an optical fibre, and imaged onto the input slit of a monochromator (Acton Research corporation) and detected with a charge-coupled device (CCD) (SpectruMM:GS128B). The fluorescence emission was recorded by feeding the signal to the boxcar (Stanford Research, model 250) to be integrated before being digitized and processed by a computer. Each experience was repeated at least three times. The estimated error in the energy and photostability measurements was 10%.

## 2. Synthetic procedures and characterization data

**Synthesis of 5:** Propargylamine (23 mg, 0.42 mmol) was added to a solution of thiomethylBODIPY **4**[1] (75 mg, 0.28 mmol) in dry $CH_2Cl_2$ (2 mL), and the mixture was stirred for 1 h at room temperature. Solvent removal under reduced pressure and purification by column chromatography on silica gel using hexane/$CH_2Cl_2$ (7/3) allow obtaining BODIPY **5** as a yellow solid (70 mg, 91%).

$^1$H NMR (300 MHz, $CDCl_3$) $\delta$ 6.79 (d, $J$ = 3.8 Hz, 2H), 6.21 (t, $J$ = 4.9 Hz, 1H, NH), 6.06 (d, $J$ = 3.9 Hz, 2H), 4.07 (dd, $J$ = 5.5 and 2.3 Hz, 2H, $CH_2$), 2.49 (s, 6H), 2.36 (t, $J$ = 2.3 Hz, 1H, C≡CH). $^{13}$C NMR (75 MHz, $CDCl_3$) $\delta$ 148.1, 144.7, 122.9, 119.9 (CH), 115.5 (CH), 77.0 (C≡CH), 74.6 (C≡CH), 36.3 ($CH_2$), 14.2 ($CH_3$). FTIR $\nu$ 3380, 2972, 2920, 2243, 1574, 1399, 1168, 1020 cm$^{-1}$. HRMS *m/z* 273.1239 (calcd for $C_{14}H_{14}BF_2N_3$ 273.1247).

**Synthesis of 6:** BODIPY **3**[2] (50 mg, 0.08 mmol), CuI (2 mg, 0.008 mmol) and $Pd(PPh_3)_4$ (0.8 mg, 8 μmol) were placed into a 50 mL two-neck round-bottom flask under argon atmosphere. Then, anhydrous THF (5 mL), anhydrous triethylamine (2.5 mL) and BODIPY **5** (66 mg, 0.24 mmol) were added, and the resulting mixture refluxed for 4 h. After reaction completion (TLC monitoring), the obtained mixture was concentrated under reduced pressure, and submitted to column chromatography on silica gel using hexane/$CH_2Cl_2$ (8/2) to obtain BODIPY **6** as an orange solid (40 mg, 64%).

$^1$H NMR (700 MHz, $CDCl_3$) $\delta$ 6.90 (broad s, 4H), 6.24 (t, $J$ = 5.2 Hz, 1H, NH), 6.10 (d, $J$ = 3.6 Hz, 2H), 4.53 (d, $J$ = 5.2 Hz, 2H, $CH_2$NH), 2.58 (s, 3H), 2.53 (s, 3H), 2.49 (s, 6H), 2.28 (s, 3H), 1.98 (s, 6H), 1.35 (s, 3H), 1.33 (s, 3H). $^{13}$C NMR (176 MHz, $CDCl_3$) $\delta$ 157.6, 157.5, 148.4, 145.1, 144.8, 144.4, 142.7, 139.3, 134.6, 131.5, 130.4, 129.3 (CH), 129.3, 123.0, 119.8 (CH), 115.4 (CH), 113.8, 88.6 (C≡C), 85.9 (C≡C), 79.0 (C-I), 37.8 ($CH_2$), 21.3 ($CH_3$), 19.5 ($CH_3$), 16.1 ($CH_3$), 15.8 ($CH_3$), 14.2 ($CH_3$), 13.7 ($CH_3$), 12.4 ($CH_3$). FTIR $\nu$ 3385, 2923, 2855, 2233, 1576, 1214, 1087 cm$^{-1}$. HRMS *m/z* 763.2146 (calcd for $C_{36}H_{36}B_2F_4IN_5$ 763.2138).

**Synthesis of 8:** Benzaldehyde (0.07 mL, 0.6 mmol) was added to a solution of BODIPY **7**[3] (100 mg 0.2 mmol) in dry DMF (3 mL) under argon atmosphere. Then, acetic

---

[1] Purchased from Cuántico de México

[2] L. Fu, F.-L. Jian, D. Fortin, P. D. Harvey and Y. Liu, *Chem. Commun.,* 2011, **46**, 5503.

[3] M. Koepf, A. Trabolsi, M. Elhabiri, J. A. Wytko, D. Paul, A. M. Albrecht-Gary and J. Weiss, *Org. Lett.,* 2005, **7**, 1279.

acid (6 drops) and piperidine (6 drops) were added, and the resulting mixture submitted to microwave irradiation (30 min, 150 ºC; 1 min pre-stirring). After solvent removal under reduced pressure, the crude product was submitted to column chromatography on silica gel using $CH_2Cl_2$ to give **8** as a deep purple solid (80 mg, 60%).

$^1$H NMR (700 MHz, $CDCl_3$): $\delta$ 7.86 (d, *J* = 7.8 Hz, 2H), 7.72 (d, *J* = 16.8 Hz, 2H, CH=CH), 7.56 (d, *J* = 7.5 Hz, 4H), 7.33 (appt, *J* = 7.5 Hz, 4H), 7.27 (d, *J* = 7.8 Hz, 2H), 7.24 (appt, *J* = 7.5 Hz, 2H), 7.17 (d, *J* = 16.8 Hz, 2H, CH=CH), 2.54 (q, *J* = 7.5 Hz, 4H), 1.33 (s, 12H), 1.25 (s, 6H), 1.09 (t, *J* = 7.5 Hz, 6H). $^{13}$C NMR (176 MHz, $CDCl_3$): $\delta$ 150.4, 139.2, 138.9, 138.8, 137.4, 135.9 (CH), 135.4 (CH), 133.9, 132.9, 128.7 (CH), 128.6 (CH), 128.0 (CH), 127.4 (CH), 120.1 (CH), 84.2 (C-O), 25.0 ($CH_3$), 18.4 ($CH_2$), 14.1 ($CH_3$), 11.7 ($CH_3$). FTIR $\nu$ 2965, 2926, 2871, 1611, 1575, 1396, 1178, 1043 cm$^{-1}$. HRMS *m/z* 682.3708 (calcd for $C_{43}H_{46}B_2F_2N_2O_2$ 682.3716).

**Synthesis of triad 1:** $K_2CO_3$ (11 mg, 0.08 mmol) was added to a solution of **6** (22 mg 0.029 mmol) and **8** (20 mg, 0.029 mmol) in toluene/ethanol/water (2:2:1, 10 mL), and argon flow passed through the obtained mixture for 30 min. Then, $Pd(PPh_3)_4$ (1.2 mg, 3 μmol) was added, and the resulting mixture refluxed for 8 h under argon atmosphere. After solvent removal under reduced pressure, the resulting mixture was submitted to column chromatography on silica gel using hexane/$CH_2Cl_2$ (5/5) to give **1** as a deep-purple solid (14 mg, 45%).

$^1$H NMR (300 MHz, $CDCl_3$) $\delta$ 7.72 (d, *J* = 16.8 Hz, 2H, CH=CH), 7.56 (d, *J* = 7.3 Hz, 4H), 7.36-7.22 (m, 11H), 7.18 (d, *J* = 16.8 Hz, 2H, CH=CH), 6.94 (d, *J* = 4.0 Hz, 2H), 6.92 (s, 2H), 6.26 (t, *J* = 5.4 Hz, 1H, NH), 6.13 (d, *J* = 4.0 Hz, 2H), 4.59 (d, *J* = 5.4 Hz, 2H, $\underline{CH_2}$NH), 2.58-2.51 (m, 16H), 2.28 (s, 3H), 2.07 (s, 6H), 1.38 (s, 3H), 1.30 (s, 3H), 1.29 (s, 6H), 1.09 (t, *J* = 7.5 Hz, 6H). $^{13}$C NMR (176 MHz, $CDCl_3$) $\delta$ 156.6, 156.2, 150.5, 144.8, 143.1, 143.0, 140.2, 139.2, 138.9, 138.3, 137.3, 136.1 (CH), 135.1, 134.7, 134.0, 133.9, 133.7, 133.0, 131.6, 130.9 (CH), 130.7, 129.4, 129.3 (CH), 128.8 (CH), 128.7 (CH), 128.6 (CH), 127.4 (CH), 120.0 (CH), 115.4 (CH), 88.3 (C≡C), 37.9 ($CH_2$NH), 21.3 ($CH_3$), 19.6 ($CH_3$), 18.4 ($CH_2$), 14.2 ($CH_3$), 14.1 ($CH_3$), 14.0 ($CH_3$), 13.6 ($CH_3$), 12.3 ($CH_3$), 12.0 ($CH_3$), 11.4 ($CH_3$). FTIR $\nu$ 3389, 2960, 2851, 2233, 1710, 1375, 1176, 1011, 965 cm$^{-1}$. HRMS (MALDI-TOF) 1191.5892 (calcd for $C_{73}H_{70}B_3F_6N_7$ 1191.5876).

## 3. Photophysical properties

**Table S1**. Photophysical properties of triad **1** and parent monochromophoric BODIPYs (**2**, **5** and **8**) in ethyl acetate: Absorption ($\lambda_{ab}$) and fluorescence ($\lambda_{fl}$) wavelengths, molar absorption coefficients ($\varepsilon_{max}$), fluorescence quantum yields ($\phi$) and lifetimes ($\tau$), as well as radiative ($k_{fl}$) and non-radiative ($k_{nr}$) rate constants.

| | $\lambda_{ab}$ (nm) | $\varepsilon_{max}\cdot10^{-4}$ ($M^{-1}$ $cm^{-1}$) | $\lambda_{fl}$ (nm) | $\phi$ | $\tau$ (ns) | $k_{fl}\cdot10^{-8}$ ($s^{-1}$) | $k_{nr}\cdot10^{-8}$ ($s^{-1}$) |
|---|---|---|---|---|---|---|---|
| **5** | 428.0 | 4.6 | 488.0 | 0.90 | 4.82 | 1.86 | 0.20 |
| **2** | 500.0 | 8.7 | 508.5 | 0.94 | 5.86 | 1.60 | 0.10 |
| **8** | 631.0 | 7.8 | 647.0 | 0.68 | 4.89 | 1.39 | 0.65 |
| **T-1** | 344.0 | 9.8 | - | - | - | - | - |
| | 426.0 | 4.8 | 450.5 | 0.01 | - | - | - |
| | 536.0 | 11.2 | 560.0 | 0.08 | - | - | - |
| | 631.0 | 8.0 | 645.0 | 0.72 | 5.23* | 1.37 | 0.53 |

*the same lifetime is recorded upon direct excitation ($\lambda_{exc}$ = 590 nm) or by exciting the triad blue chromophore ($\lambda_{exc}$ = 410 nm).

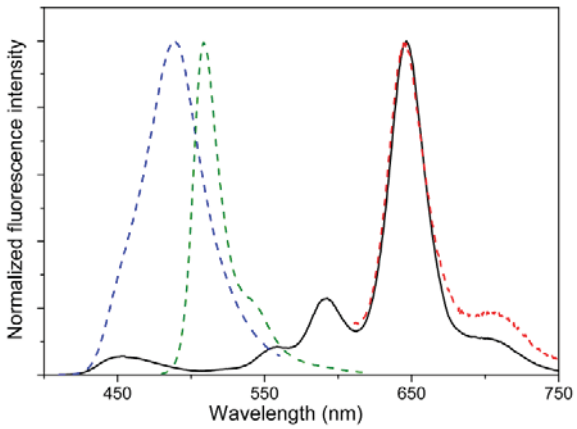


**Figure S1**. Fluorescence spectrum of **1** (black) upon excitation at the blue-edge of the visible spectrum. The corresponding fluorescence spectra of **2**, **5** and **8** (dashed green, blue and red, respectively) are included for comparison.

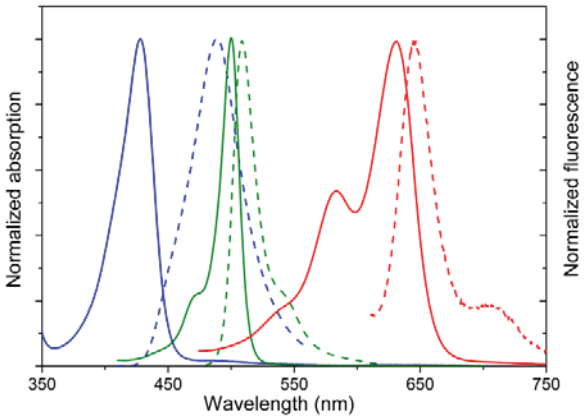


**Figure S2**. Absorption (solid) and fluorescence (dashed) spectra of compounds **5** (blue), **2** (green) and **8** (red) showing the required spectral overlap between the donor fluorescence and the acceptor absorption bands in the FRET formalism.

Published on 23 February 2015. Downloaded by Instituto de Quimica Fisica Rocasolano (IQFR) on 21/03/2015 10:46:16.

PCCP

PAPER

View Article Online
View Journal | View Issue

Cite this: *Phys. Chem. Chem. Phys.*, 2015, **17**, 8239

# Coumarin–BODIPY hybrids by heteroatom linkage: versatile, tunable and photostable dye lasers for UV irradiation†

I. Esnal,[a] G. Duran-Sampedro,[b] A. R. Agarrabeitia,[b] J. Bañuelos,*[a] I. García-Moreno,[c] M. A. Macías,[d] E. Peña-Cabrera,[d] I. López-Arbeloa,[a] S. de la Moya*[b] and M. J. Ortiz[b]

Received 13th January 2015,
Accepted 23rd February 2015

DOI: 10.1039/c5cp00193e

www.rsc.org/pccp

Linking amino and hydroxycoumarins to BODIPYs through the amino or hydroxyl group lets the easy construction of unprecedented photostable coumarin–BODIPY hybrids with broadened and enhanced absorption in the UV spectral region, and outstanding wavelength-tunable laser action within the green-to-red spectral region (~520–680 nm). These laser dyes allow the generation of a valuable tunable UV (~260–350 nm) laser source by frequency doubling, which is essential to study accurately the photochemistry of biological molecules under solar irradiation. The tunability is achieved by selecting the substitution pattern of the hybrid. Key factors are the linking heteroatom (nitrogen *vs.* oxygen), the number of coumarin units joined to the BODIPY framework and the involved linking positions.

## Introduction

Solar ultraviolet (UV) photons constitute one of the most ubiquitous and potent environmental carcinogens. For this reason, a great deal of work concerning the photophysics and photochemistry of the excited states created in key biomolecules (*e.g.*, nucleic acids) upon exposure to UV light is being conducted, since such states are at the beginning of the complex chain of biochemical events that culminates in photocarcinogenesis.[1] However, more accurate experiments are urgently needed to understand the dynamics of these excited states, which have been stymied by the lack of suitable laser sources providing efficient, stable and tunable UV radiation within the range of 250–350 nm. An attractive approach to overcome this drawback involves the design of new laser dyes with strong UV absorption and highly efficient and stable emission in the visible (Vis) spectral region (500–700 nm), since it constitutes the only way to generate, efficiently and without undesired re-absorption/re-emission processes, the required tunable UV laser radiation by frequency doubling, and even with ultra-short pumping pulses.

Since it is still difficult to judiciously design single laser dyes fulfilling the mentioned requirements, a powerful strategy is the construction of molecular energy-transfer arrays (coupled or cassette systems) able to undergo efficient excitation energy transfer (EET) from UV-absorbing donors to a covalently-linked Vis-emitting laser dye acting as the acceptor partner. To address this issue, we were prompted to develop unprecedented laser dyes featuring the direct covalent integration of UV-absorbing coumarin (1*H*-chromen-2-one) chromophores into Vis-emitting BODIPY (4,4-difluoro-4-bora-3*a*,4*a*-diaza-*s*-indacene) ones (Fig. 1).

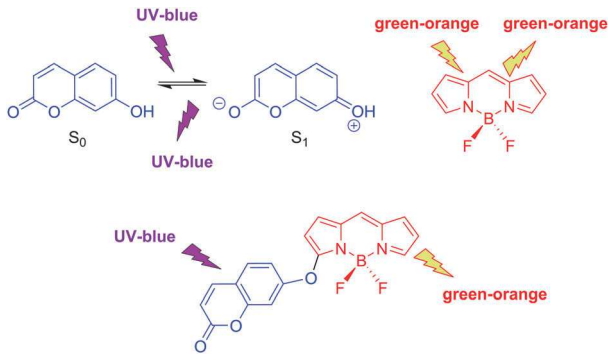


Fig. 1 Simple push-pull 7-hydroxycoumarin (blue) and BODIPY (red) chromophores, and a hybrid system based on them.

[a] *Depto. de Química Física, Universidad del Pais Vasco-EHU, Apartado 644, 48080, Bilbao, Spain. E-mail: jorge.banuelos@ehu.es*
[b] *Depto. de Química Orgánica I, Facultad de CC. Químicas, Universidad Complutense de Madrid, Ciudad Universitaria s/n, 28040, Madrid, Spain. E-mail: santmoya@ucm.es*
[c] *Depto. de Sistemas de Baja Dimensionalidad, Superficies y Materia Condensada, Instituto de Química-Física "Rocasolano", C.S.I.C., Serrano 119, 28006, Madrid, Spain*
[d] *Depto. de Química, Universidad de Guanajuato, Col. Noria Alta s/n, Guanajuato, 36050, Mexico*

† Electronic supplementary information (ESI) available: General experimental details, synthetic procedures and characterization data, Fig. S1–S5, Tables S1 and S2, as well as copies of the NMR spectra recorded from new compounds. See DOI: 10.1039/c5cp00193e

Published on 23 February 2015. Downloaded by Instituto de Quimica Fisica Rocasolano (IQFR) on 21/03/2015 10:46:16.

Coumarins are an interesting family of fluorescent dyes;[2] among them, amino and hydroxycoumarin derivatives (mainly 7-amino and 7-hydroxycoumarins) are especially significant because their photophysical signatures are ruled by internal charge transfer (ICT) upon light absorption (classic push-pull dyes, see Fig. 1),[3] which is valuable for developing certain applications (*e.g.*, fluorescent sensing by ICT modulation).[4] Moreover, simple amino and hydroxycoumarins are characterized by absorbing and emitting in the UV/blue-edge spectral region, taking the emission place with relatively large quantum yield,[5] which has been used for developing blue dye lasers.[2] However, coumarins are not as photostable as other common laser dyes, and they usually undergo bleaching under long UV pumping.[6]

On the other hand, BODIPYs constitute a recognized family of Vis-emitting dyes with noticeable utility in the development of a plethora of photonic tools,[7] due to their excellent photophysical properties, high solubility in organic solvents improving dyed-material processability (*e.g.*, in the preparation of organic films), and possibility of selective functionalization to finely modulate their physical properties.[7] The usually large molar-absorption coefficients ($\varepsilon$) and high fluorescence quantum yields ($\phi$) of BODIPYs have promoted their application as fluorescent dyes for lasing.[7d,8] On the other hand, the characteristic green/orange-edge emission of the BODIPY chromophore should be highly interesting for developing tunable UV lasers by frequency doubling. However, two important drawbacks limit this application: low absorption in the UV spectral region, and small Stokes shifts enabling undesired re-absorption/re-emission processes.

Despite the outstanding and spectrally-complementary photophysical properties of BODIPYs and coumarins, cassettes combining both chromophores are scarce.[9] Thus, the unique two molecular coumarin–BODIPY cassettes described up to now were attained by linking a naked coumarin (non aminated, nor hydroxylated) to a BODIPY chromophore, hence without heteroatom linkage.[9b] On the other hand, non-cassette coumarin–BODIPY hybrids obtained by fusing,[10a] or by linking through a hydrocarbonated spacer,[4,10b] both moieties are described to exhibit interesting photophysical properties (*e.g.*, ICT processes giving place to large Stokes shifts), which are useful for developing certain photonic tools.[4,10] It should be noted that none of these systems have been evaluated as laser dyes. Furthermore, challenging coumarin–BODIPY hybrids involving push-pull amino or hydroxycoumarins covalently linked to the BODIPY chromophore through the amino or hydroxyl heteroatom (note the possibility of ICT processes involving both chromophores) are unknown.

All the above mentioned prompted us to develop the latter coumarin–BODIPY hybrids (*e.g.*, see hybrid based on 7-hydroxycoumarin shown in Fig. 1). The main goals of these new molecular dyes should be: (1) a strong UV-blue absorption enabling an efficient green-orange fluorescence and laser, (2) the possibility of emission modulation by tuning ICT processes involving both chromophores[11] and, (3) enhanced photostability of the involved chromophores by its mutual covalent linkage,[8a,b] which is especially interesting in the case of the photounstable coumarin partner.

# Result and discussion

## Synthesis

For our purpose, we chose the coumarin–BODIPY structures shown in Fig. 2 (*i.e.*, **1–4dX** and **2–4mX**, with **X** = **A**, **B** or **C**). These structural designs were selected on the basis of synthetic accessibility, and possibility of cassette behavior (**1dX** case) or photophysics modulation by tuning ICT processes (rest of the cases).

Dicoumarin-substituted *O*-BODIPY **1dA** was straightforwardly obtained from commercial 2,6-diethyl-1,3,5,7,8-pentamethyl-BODIPY (PM567, **1**), a known strongly fluorescent green-emitting dye,[12] by $AlCl_3$ promoted substitution of fluorine[8c,13] by the corresponding coumarin (see Fig. 3). On the other hand, monocoumarin- and dicoumarin-substituted BODIPYs **2mX** and **2dX**, **3mX** and **3dX**, and **4mX** and **4dX** were obtained by controlled aromatic nucleophilic substitution in 3,5-dichloro-BODIPYs (mono or disubstitution),[14] using the corresponding coumarin (**AH**, **BH** or **CH**) as the nucleophile, and 3,5-dichloro-8-(*p*-tolyl)BODIPY (**2**),[14a] 3,5-dichloro-8-mesitylBODIPY (**3**)[15] or 3,5-dichloro-8-(trifluoromethyl)BODIPY (**4**)[14b] as the corresponding starting BODIPY. The latter dihaloBODIPYs were selected on the basis of their synthetic accessibility (Fig. 3), and the different stereoelectronic influence of their *meso* groups (R) in the photophysics of the BODIPY chromophore. On the other hand, the coumarins used as nucleophiles in the mentioned halogen (fluorine or chlorine) substitutions were commercial 7-hydroxy-4-methyl-2*H*-chomen-2-one (**AH**), 7-amino-4-methyl-2*H*-chromen-2-one (**BH**) and 4-hydroxy-2*H*-chromen-2-one (**CH**).

Chlorine substitutions on less-activated **2** and **3** (when compared to trifluoromethylated **4**) with less nucleophilic hydroxycoumarins **AH** and **CH** (when compared to aminocoumarin **BH**) required specific base catalysis (see Fig. 3). On the other hand, since highly activated **4** was tested to decompose under the employed basic conditions, chlorine substitutions on it (especially by using less activated hydroxycoumarins) were promoted by microwave (MW) irradiation (see Fig. 3). Finally, the synthesis of disubstituted derivatives (**2dX**) required stronger reaction conditions (*e.g.*, longer times; see ESI†) because the involved monosubstituted intermediates (**2mX**) are less activated than the

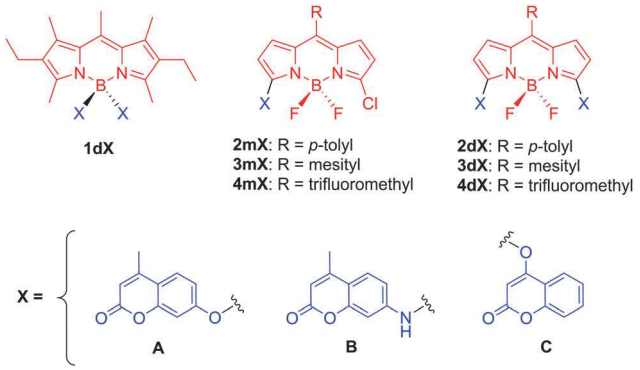


Fig. 2 Selected structural designs for coumarin–BODIPY hybrids (up, **X** = **A**, **B** or **C**), and corresponding coumarin moieties (down).

 This journal is © the Owner Societies 2015

Published on 23 February 2015. Downloaded by Instituto de Quimica Fisica Rocasolano (IQFR) on 21/03/2015 10:46:16.

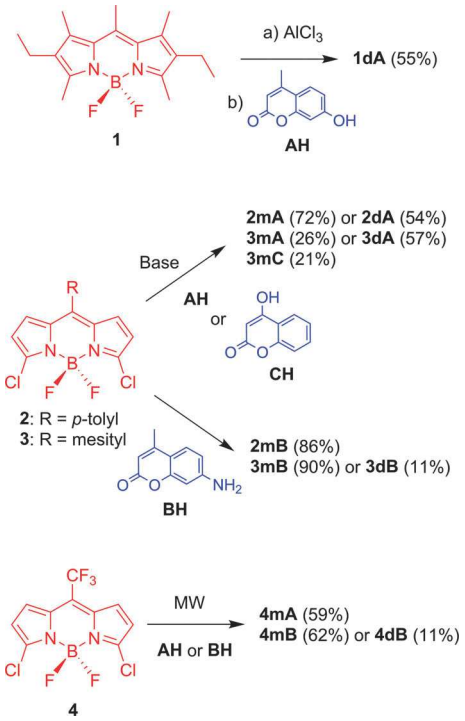


Fig. 3 Synthesis of coumarin–BODIPY hybrids (see ESI† for experimental details). Yields in parentheses.

corresponding starting dichloroBODIPYs. This fact is especially significant in the case of the amino derivatives (note the less electron-withdrawing effect of nitrogen when compared with oxygen), and explains the low yield when obtaining **3dB** (null in the case of **2dB**), and the use of MW irradiation for obtaining **4dB** (together with **4mB**) from **4** (see Fig. 3).

## Photophysics

The absorption spectrum of **1dA** was almost the sum of the absorptions of the individual chromophores involved in its molecular structure, as shown by its comparison with the spectra recorded for **1** and **AH** (double concentration for the latter since two coumarins are involved in **1dA**, see Fig. 4). Therefore, no noticeable electronic coupling between chromophores exists in **1dA**, at least at its ground state, as it was expected by the role of the linking boron in the BODIPY partner. Indeed, boron is an advisable linking position to develop molecular cassettes based on BODIPY, since it does not participate in the cyanine-like π-system of the BODIPY chromophore, but provides rigidity to it.[16] Theoretical calculations (B3LYP/6-31g) conducted on **1dA** (see ESI†) also support the claimed electronic isolation of chromophores. Thus, the conducted time dependent quantum mechanical simulation (see ESI†) predicts the involvement of molecular orbitals placed exclusively at the coumarin moiety, or at the BODIPY one, for the main electronic transitions associated with each absorption band (UV and Vis) of **1dA** (see Fig. S1 in ESI†). This photophysical result is also supported by electrochemical measurements (see ESI†). Thus, the oxidation and reduction waves recorded in the cyclic voltammogram of **1dA** match almost

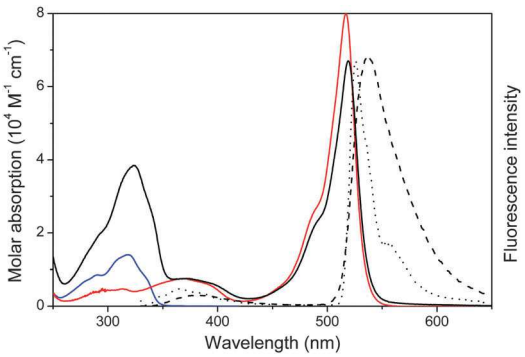


Fig. 4 Absorption spectra (bold) of **1dA** (black), **1** (red) and **AH** (blue), and normalized fluorescence spectra of **1dA** (dashed at room temperature; dotted at 77 K) upon UV irradiation (325 nm) in ethanol (see ESI† for experimental details).

perfectly with those registered for each individual parent molecules **1** and **AH** (see Fig. S2 in ESI†).

In this regime, very weak electronic-coupling limit, the cassette-required selective excitation of chromophores should be feasible. In fact, exciting the BODIPY or the coumarin chromophore in **1dA** (Vis or UV irradiation, respectively) leads to the typical fluorescent BODIPY signature (see Fig. 4). Noticeably, the characteristic high quantum yield of the BODIPY chromophore was maintained by UV excitation ($\phi$ = 82%, see Table S1 in ESI†). Moreover, the observed coumarin–BODIPY intramolecular EET process is highly efficient (approaching the 100%), as demonstrated by the residual emission from the coumarin chromophore, despite its direct excitation (see Fig. 4). The short donor–acceptor distance (~5 Å between chromophoric centers, as predicted theoretically) ensures a fast and efficient quenching of the donor by the EET to the acceptor BODIPY.

The EET in **1dA** should take place by the Förster resonance energy-transfer (FRET) mechanism,[17] taking into account: (1) the feasible spectral overlap of the emission transitions of the coumarin donor not only with the UV absorption transitions of the acceptor BODIPY (*e.g.*, $S_0 \rightarrow S_2$),[18] but also with the Vis ones, although in less extension (see Fig. S3 in ESI†); (2) the spatial proximity of the involved chromophores; (3) the lack of orbital overlap avoiding the electronic exchange required by the through-bond energy-transfer (TBET) mechanism,[19] due to the spacing imposed by the tetrahedral boron. Indeed, the EET efficiency of **1dA** was practically the same when decreasing the temperature, even at 77 K, where the electronic-exchange mechanism (an energy-activated process) is virtually nullified.[20] The hypsochromic shift and narrowing of the fluorescence signal upon freezing the sample (Fig. 4) is merely due to the low temperature, which lowers the relaxation of the excited state upon irradiation, and hinders the vibrational motion.

Regarding hybrids based on **2** (see Fig. 2), their fluorescence response is limited by the rotational free motion of the *p*-tolyl moiety, which drastically enhanced the probability of de-excitation by internal conversion ($\phi$ = 25% for **2**; see Fig. 5, and Table S1 in ESI†).[21] Linking hydroxycoumarin **AH** to BODIPY **2**, to generate

Published on 23 February 2015. Downloaded by Instituto de Quimica Fisica Rocasolano (IQFR) on 21/03/2015 10:46:16.

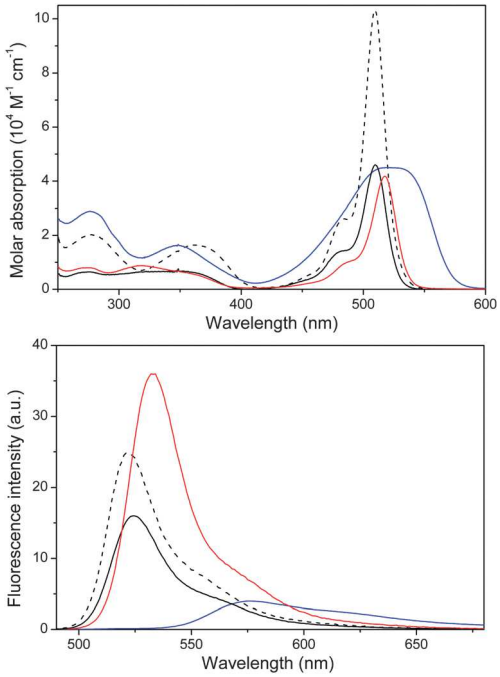


Fig. 5 Absorption (up) and fluorescence (down, upon Vis irradiation) spectra of **2** (dashed), **2mA** (black), **2mB** (blue) and **2dA** (red) in ethyl acetate (see ESI† for experimental details).

hybrid **2mA**, gives rise to a slight decrease in the quantum yield of the BODIPY emission upon Vis irradiation, but without noticeable changes in the shape and position of both the absorption and the emission band (*cf.* **2** and **2mA** in Fig. 5, and in Table S1 in ESI†). However, the replacement of the oxygen linkage of **2mA** by nitrogen in **2mB** decreases significantly the fluorescence ($\phi$ = 4%), shifts the spectral bands towards the red (mainly in fluorescence, up to ~55 nm), and broadens them (mainly in absorption); (see Fig. 5, and Table S1 in ESI†).

The mentioned effect observed in **2mB** must result from a strong electronic coupling between the aminocoumarin and the BODIPY due to the involved nitrogen linkage. Additionally, the nitrogen must promote an ICT process, from the coumarin to the BODIPY, due to its known electron-donating ability (note its +K conjugative effect). The ICT must be also favored by the electron-withdrawing effect exerted by the chlorine (strong −I inductive effect) on the BODIPY chromophore. Indeed, the computed frontier orbitals (B3LYP/6-31g; see ESI†) for amino-coumarin-based **2mB** are extended through the whole molecular structure (see Fig. S4 in ESI†), which supports an ICT process by the HOMO → LUMO transition. However, the frontier orbitals for hydroxycoumarin-based **2mA**, where the more-electronegative less-conjugative oxygen linkage is involved, shows that the coumarin–BODIPY electronic interaction is much weaker. In fact, the computed frontier orbitals for hybrid **2mA** are mainly located at the BODIPY core, with a small contribution of the oxygen atom (see Fig. S4 in ESI†). As a consequence of the transfer of electronic density from the coumarin fragment to the BODIPY moiety, not only the fluorescence efficiency decreases, but also the fluorescence lifetimes become faster (see data collected in Table S1 in ESI†). The ICT-character of the emitting state implies also an increase of the deactivation rate constants, especially the non-radiative one. Thus, the amino connection induces a more pronounced fluorescence-quenching than the oxygen linkage, due to the less electron-donor character of the latter. Likely, the higher charge-separation promoted in the former case further enhances the non-radiative deactivation probability.

Noticeably, linking an additional **AH** moiety in **2mA**, to generate hybrid **2dA**, boosts the fluorescence quantum up to 36%, producing also a modest red shift in both the absorption and the emission bands (see Fig. 5, and Table S1 in ESI†). In agreement with this observation, we have previously demonstrated that symmetrically substituting the 8-(*p*-tolyl)BODIPY chromophore with electronegative atoms at the C3 and C5 BODIPY positions ameliorates the negative effect produced by the aryl motion.[21] Noteworthily, the time dependent simulations of **2**, **2mA**, **2mB** and **2dA** (see Table S2 in ESI†) also predict the observed shifts of the absorption bands as a consequence of an increase in the HOMO energy. These agreements of the theoretical predictions with the experimental findings confirm the goodness of the conducted computations.

Although hybrids **2mA**, **2mB** and **2dA** are not able to work as real cassettes because the excitation energy is truly delocalized over both BODIPY and coumarin moieties, especially in nitrogen-linked **2mB** where the electron coupling is more important (*cf.* frontier orbitals in Fig. S4 in ESI†), the UV irradiation gives rise to the same Vis emission observed upon Vis irradiation, without detecting the emission signal from the coumarin. However, the observed EET cannot be adequately described by a FRET mechanism, due to the demonstrated high electronic interaction between coumarin and BODIPY moieties (highlighted also by the noticeable different absorption spectra for hybrids and corresponding individual chromophores; *cf.* the Vis absorptions of **2mB** and **2** in Fig. 5). Thus, the EET observed in these hybrids really lies in a coherent process, where the excitation oscillates back and forth between the donor coumarin and the acceptor BODIPY. In these cases, where an electronic mechanism takes place (strong coupling limit), the EET process is extremely fast and efficient.

Restricting the conformation motion of the phenyl ring in *meso*-arylBODIPYs, *via* the sterical hindrance induced by *ortho* methyl groups in the aryl moiety, is known to increase the BODIPY fluorescence by decreasing the probability of non-radiative deactivation pathways (*cf.* **2** and **3** in Table S1 in ESI†). Thus, mesityl-based hydroxycoumarin hybrids **3mA** and **3dA** are more fluorescent than the corresponding *p*-tolyl analogues **2mA** and **2dA**. Indeed, the fluorescence quantum yields of **3mA** and **3dA** are similar to those obtained for parent **3** (higher than 90%; see Fig. 6 and Table S1 in ESI†). The same effect is observed when the 7-hydroxycoumarin moiety of **3mA** is substituted by the 3-hydroxycoumarin moiety in **3mC** (see Table S1 in ESI†). However, the strong electronic interaction provided by the nitrogen linkage, when compared with the oxygen one, makes the aminocoumarin-based **3mB** to lose fluorescence ability ($\phi$ = 7%), probably due to the same ICT process invoked for **2mB**. Indeed, the absorption band of **3mB** is broader,

 This journal is © the Owner Societies 2015

Published on 23 February 2015. Downloaded by Instituto de Quimica Fisica Rocasolano (IQFR) on 21/03/2015 10:46:16.

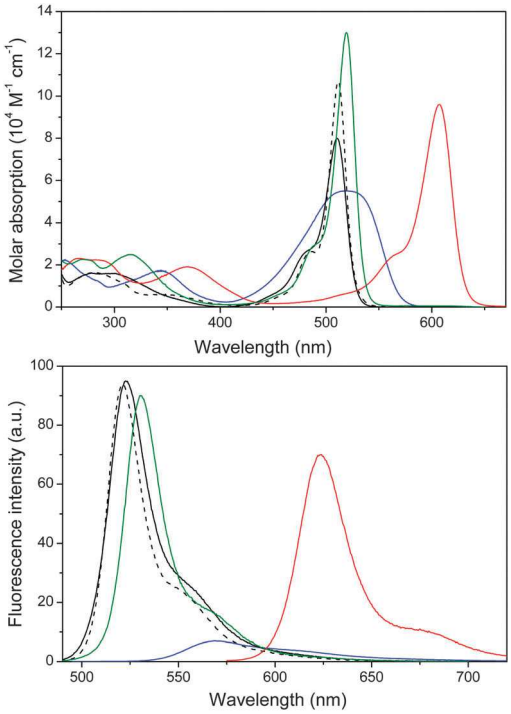


Fig. 6 Absorption (up) and fluorescence (bottom, upon Vis irradiation) spectra of **3** (dashed), **3mA** (black), **3mB** (blue) and **3dA** (green) and **3dB** (red) in ethyl acetate (see ESI† for experimental details).

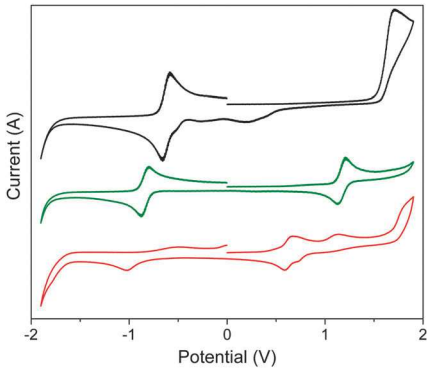


Fig. 7 Cyclic voltammograms of **3** (black), **3dA** (green) and **3dB** (red) in acetonitrile (see ESI† for experimental details).

the Stokes shift is larger, and the fluorescence lifetimes are shorter (*cf.* Fig. 5 and 6; see Table S1 in ESI†) than those recorded for **2mB**, due to the higher electronic interaction provided by the nitrogen linkage.

Switching off the ICT process of **3mB**, by introducing a second unit of aminocoumarin to generate **3dB** (note the suppression of the chlorine electronic effect), boosts the fluorescence efficiency ($\phi$ = 70%; see Fig. 6 and Table S1 in ESI†). Noticeably, a deep red shift of both the absorption and emission spectral bands is now observed, recovering such bands of the typical narrow shape (vibrational resolution) and Stokes shift of parent **3** (*cf.* **3**, **3mB** and **3dB** in Fig. 6, and in Table S1 in ESI†). This spectral shift was properly predicted by the time dependent simulation also (see Table S2 in ESI†). All these data demonstrate the lack of ICT in **3dB**, as well as the existence of an extended conjugation involving coumarins and BODIPY (see Fig. S5 in ESI†). Once again, the UV irradiation of **3dB** was tested to produce the same Vis emission that the obtained by Vis irradiation, showing that this coumarin–BODIPY hybrid could be a promising UV-pumped lasing dye with efficient emission in the orange-edge of the red region (623 nm, see Fig. 6) and, therefore, a promising UV-emitting lasing dye (*ca.* 310 nm) by frequency doubling.

A clear experimental proof of the strong electronic interaction between BODIPY and coumarin moieties in hybrids **3dA** and **3dB** is provided by their electrochemical behavior when compared with the exhibited by parent **3** in the same conditions (see Fig. 7). Thus, the oxidation potential decreases noticeably from 1.70 V for **3** (irreversible process), to 1.18 V and 0.63 V for **3dA** and **3dB**, respectively (reversible processes; a second oxidation wave at 1.13 V is additionally detected for **3dB**). Moreover, it is observed that the lower the oxidation potential, the closer are the cathodic and anodic peaks (see Fig. 7). These results suggest that the HOMO energy, which is related to the oxidation ability, is significantly higher for the hybrids, as a consequence of the electronic coupling. Therefore, the absorption energy gap, which is related to the separation between the cathodic and anodic peaks, is also significantly lower for the hybrids, in agreement with both the observed absorption red-shifts (see Fig. 6) and the computational predictions (see Table S2 in ESI†).

Regarding hybrids based on **4**, their photophysics are characterized by the marked red-shift of the spectral bands imposed by the *meso* trifluoromethyl group (*cf.* **2**, **3** and **4** in Table S1 in ESI†). Thus, the strong −I inductive effect exerted by the *meso* trifluoromethyl group must stabilize preferentially the LUMO state, since it is characterized by a high electronic density at the *meso* position, and differently to that occurring at the HOMO, where a node is placed at such position (*cf.* the HOMO and LUMO computed for **2** in Fig. S4 in ESI†). This fact must decrease the absorption energy gap, as supported by the conducted theoretical simulations (see Table S2 in ESI†), explaining the observed absorption shifts. However, the same effect should also boost undesired ICT processes from the coumarin to the BODIPY, mainly in the case of mono-aminocoumarin-based **4mB**, but also in mono-hydroxycoumarin-based **4mA**. In fact, **4mB** is observed to be not fluorescent, while **4mA** exhibits less fluorescence ($\phi$ = 40%) and faster lifetime than parent **4** (see Table S1 in ESI†).

Analogous to **3dB**, the double-aminocoumarin substitution of **4dB** enhances the fluorescence ability by decreasing the probability of the fluorescence-quenching ICT process (note the lack of the ICT-promoting chlorine), as well as pushes the spectral bands deeply toward the red region (*cf.* **4mA** and **4dB** in Fig. 8), by the establishment of an extended conjugation (*cf.* the computed energy gaps dated in Table S2 in ESI†). It must be noted that the high fluorescence efficiency ($\phi$ = 70%) of red-emitting (665 nm) **4dB**, joined to the tested viability of both UV or Vis excitation to record the same Vis emission, makes this dye potentially valuable as a red-emitting lasing dye, but also as a UV-emitting one (*ca.* 330 nm) by frequency doubling.

Published on 23 February 2015. Downloaded by Instituto de Quimica Fisica Rocasolano (IQFR) on 21/03/2015 10:46:16.

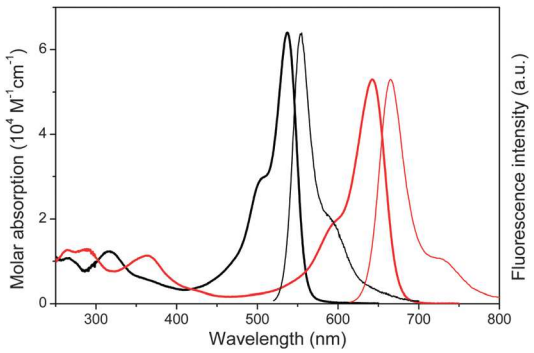


Fig. 8 Absorption (bold) and corresponding normalized fluorescence (thin, upon Vis irradiation) of **4mA** (black) and **4dB** (red) in ethyl acetate (see ESI† for experimental details).

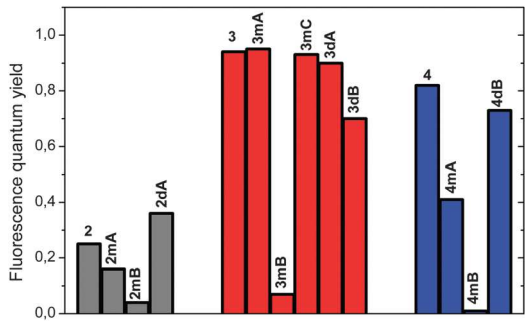


Fig. 9 Fluorescence efficiency of BODIPY–coumarin hybrids and corresponding parent BODIPYs in ethyl acetate (data from Table S1 in ESI†).

The fluorescence efficiency of the studied BODIPY–coumarin hybrids, together with the corresponding parent BODIPYs, is graphically compared in Fig. 9, showing that the most promising hybrids for our purpose (lasing by UV pumping) are **3mA**, **3mC**, **3dA**, **3dB** and **4dB**.

## Laser behavior

With the exception of non-fluorescent **4mB** (see Fig. 9), all the obtained coumarin–BODIPY dyes exhibited laser emission either by standard pumping in the UV (355 nm) as in the Vis (532 nm) spectral region. Moreover, coumarin–BODIPY hybridization led to a significant increase in the dye absorption at both pumping wavelengths. This is a key factor from the laser point of view, since it allows reducing significantly the required gain-media concentrations avoiding, consequently, solubility problems, or quenching and/or aggregation processes, all of them with detrimental effects on the laser emission. For instance, hybrid dye **3mB** exhibited molar absorption coefficients of $1.6 \times 10^4$ and $5.3 \times 10^4$ $M^{-1}$ $cm^{-1}$, at 355 and 532 nm, respectively, which are well above the coefficients exhibited by parent **3** ($0.6 \times 10^4$ $M^{-1}$ $cm^{-1}$ at both wavelengths).

Since this work is focused on the development of BODIPY laser dyes able to be UV pumped, we have deeply studied the laser behavior of the obtained coumarin–BODIPY hybrids under laser UV irradiation. To optimize the laser action, we analyzed first the dependence of the laser emission on the dye concentration, keeping constant the rest of the experimental parameters. Ethyl acetate solutions (1 cm path length) with optical densities within the range 1–35 were studied (see ESI†). Thus, under the experimental conditions (transversal excitation and strong focusing of the incoming pumping radiation), the concentration of the dye must be in the millimolar range to ensure total absorption of the pumping radiation over the first millimeter at most of the sample solution, in order to obtain an emitted beam with near-circular cross section optimizing the lasing efficiency, which is defined as the ratio between the energy of the laser output and the pumping energy incising on the sample surface.

Broad-line-width laser emission, with a pump threshold energy of ~0.6 mJ, divergence of 5 mrad and pulse duration of 8 ns full width at half maximum (FWHM), was obtained from all the fluorescent hybrid dyes when placed in a simple plane–plane non-tunable resonator. The lasing properties recorded at the optimal concentration for the studied coumarin–BODIPY hybrids and parent BODIPYs are shown in Table 1, showing good correlation with their photophysical properties: the higher the fluorescence quantum yield, the higher is the lasing efficiency; the longer the fluorescence wavelength, the "redder" is the lasing emission; the lower the non-radiative rate constant, the higher is the lasing photostability.

Hybrid dyes based on 3,5-dicoumarin-substituted BODIPY and involving oxygen linkers (**2dA** and **3dA**) achieved laser efficiencies up to 51%, which are much higher than those reached by the corresponding unsubstituted parent dyes **2** and **3** (see Table 1). In fact, the laser efficiency of **3** was poor under the selected laser conditions (28%), whereas **2** and **4** did not exhibit laser emission, but for different reasons. Thus, while the

Table 1 Lasing properties of coumarin–BODIPY hybrids and parent BODIPY dyes in ethyl acetate solution under transversal UV pumping at 335 nm (see ESI for experimental details)

| Dye | $[c]^a$/mM | Eff.$^b$ (%) | $\lambda^c$/nm | $I_n{}^d$ (%) | $n$/1000$^e$ |
|---|---|---|---|---|---|
| **1** | 12 | 20 | 575 | 0 | 6 |
| **1dA** | 2 | 45 | 565 | 25 | 50 |
| **2**$^f$ | — | — | — | — | — |
| **2mA** | 1 | 21 | 552 | 20 | 50 |
| **2mB** | 1 | 14 | 610 | 0 | 50 |
| **2dA** | 1 | 35 | 562 | 35 | 50 |
| **3** | 12 | 22 | 590 | 0 | 50 |
| **3mA** | 2 | 46 | 555 | 40 | 50 |
| **3mB** | 1 | 8 | 615 | 20 | 50 |
| **3mC** | 2 | 45 | 540 | 55 | 50 |
| **3dA** | 2 | 51 | 575 | 55 | 50 |
| **3dB** | 1 | 25 | 645 | 30 | 50 |
| **4**$^f$ | — | — | — | — | — |
| **4mA** | 1 | 30 | 615 | 35 | 50 |
| **4mB**$^f$ | — | — | — | — | — |
| **4dB** | 1 | 40 | 680 | 55 | 50 |

$^a$ Dye concentration optimizing its laser action in ethyl acetate solution. $^b$ Lasing efficiency, as the ratio between the energy of the laser output and the pump energy incident on the sample surface. $^c$ Peak wavelength for the laser emission. $^d$ Intensity decay for the laser-induced fluorescence emission after $n$ pumping pulses at a 10 Hz repetition rate, and measured as 100 ($I_n/I_0$) with $I_0$ being the initial intensity and $I_n$ the after $n$ pulses. $^e$ Number of pumping pulses. $^f$ Absence of laser emission under any lasing conditions at 335 nm.

 This journal is © the Owner Societies 2015

Published on 23 February 2015. Downloaded by Instituto de Quimica Fisica Rocasolano (IQFR) on 21/03/2015 10:46:16.

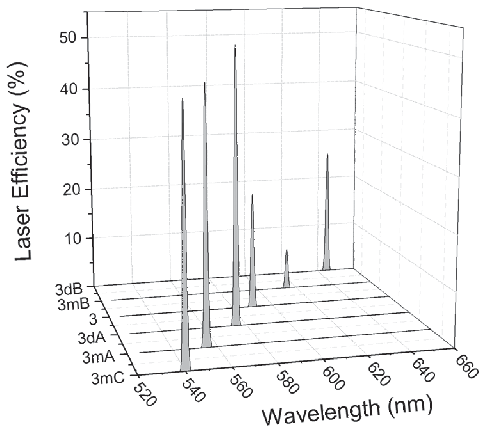


Fig. 10 Lasing emission spectra of BODIPY **3** and their coumarin–BODIPY hybrids **3mA**, **3mB**, **3mC**, **3dA** and **3dB** (data from Table 1).

laser behavior of **2** is due to its low fluorescence yield (see Fig. 9) preventing laser action, the absence of laser emission from **4** is only caused by its low absorption at the selected pumping UV wavelength. Thus, when **4** is pumped in the Vis region at 532 nm, efficient laser emission (68%) centered at 600 nm is recorded.

In the case of coumarin–**3** hybrids, the high laser efficiency recorded for the oxygen-linked monocoumarin hybrids **3mA** and **3mC** (*ca.* 45%; see Table 1) must be highlighted, which agrees well with their high fluorescence quantum yields (95% and 93%, respectively, see Fig. 9). More surprising was the peculiar behavior of other monocoumarin hybrids, such as **2mA**, **2mB** and **3mB**, because although they exhibited very low fluorescence quantum yields (4%, 16% and 7%, respectively; see Fig. 9), they not only presented laser emission but also with laser efficiencies as high as 21% (see Table 1). This fact can be explained by the ICT-character of the emitting states of these hybrids (see the Photophysics section), leading to: (a) high Stokes shift (up to 1700 $cm^{-1}$), which reduces re-absorption/re-emission processes and, thus, their deleterious effect in the laser action; (b) very short fluorescence lifetimes (below to 0.28 ns), which lead to radiative-rate constants similar to those observed for the other hybrid dyes; and (c) high dipole moments allowing the molecular alignment with respect to the polarization of the exciting laser beam to enhance the emission efficiency of the media.[22] The combination of all these factors in the same molecule (see Table S1 in ESI†) is the origin of the unique lasing properties exhibited by these hybrids.

Depending on the number and position of coumarin units joined to the BODIPY framework as well as on the nature of the linking heteroatom, the wavelength of the laser emission shifts towards the blue or towards the red with respect to the corresponding parent (unsubstituted) BODIPY. For instance, in the case of hybrids based on **3**, hydroxycoumarin hybridization (**3mA**, **3dA** and **3mC**) leads to noticeable hypsochromic shifts, whereas the aminocoumarin hybridization (**3mB** and **3dB**) does the opposite (*i.e.*, towards the red, see Table 1). Noticeably, the dye series based on **3** enables to reach wavelength-tunable laser action within the green-to-red spectral region (520–660 nm; see Fig. 10).

An important parameter for any practical application of the dye lasers is their lasing photostability under repeated pumping. Table 1 collects data on the decrease of the laser-induced fluorescence intensity of the studied coumarin–BODIPY hybrids and their corresponding parent BODIPYs and coumarins, under transversal excitation of capillary containing dye solutions after *n* pump pulses at 10 Hz repetition rate (see ESI†). It is well-known that coumarins are rather unstable dyes under laser irradiation. In fact, the studied coumarines lost their laser emission completely after just 6000 pump pulses under the selected experimental conditions. However, data in Table 1 demonstrate that the new coumarin–BODIPY hybrids became photostable laser dyes, enhancing significantly the photostability recorded for the corresponding parent BODIPYs.

This improvement of the photostability must be related to the excitation energy transfer from the coumarin moieties to the BODIPY core, which allows reducing the rate and extension of the photodegradation processes undergone by coumarins under UV laser irradiation. This behavior is widespread to all the herein developed hybrids, regardless of the acting EET mechanism: *via* FRET if the coumarins are linked to the BODIPY boron, or by electron coupling if they are directly anchored to the BODIPY chromophore. Once again, the dicoumarin-based hybrids involving oxygen as a linking atom became the most photostable, retaining up to 55% of the initial emission after 50 000 pumping pulses. In other words, albeit the photochemically unstable coumarin fragment is directly pumped, the fast transfer of the excitation energy to the BODIPY *via* electronic coupling provides an optimal laser performance over long exposure periods to irradiation.

## Conclusions

Unprecedented coumarin–BODIPY hybrids involving push-pull amino or hydroxycoumarins covalently linked to the BODIPY chromophore through to the amino or hydroxyl coumarin heteroatom could be straightforwardly attained from the corresponding coumarins and BODIPYs by nucleophilic halogen-substitution processes involving the boron or the C3/5 BODIPY position, and adjusting conveniently the reaction conditions to promote and control the substitution reactivity, which is especially important in the case of the hybrids based on 3-coumarin or 3,5-dicoumarin-substituted BODIPY involving oxygen as linkage.

The photophysical signatures of the obtained hybrid dyes are controlled by the type and number of coumarin units, as well as by the involved BODIPY linking position and coumarin linking heteroatom (N or O). Thus, boron is demonstrated to be an optimal linking site to promote BODIPY emission by UV irradiation *via* FRET, whereas the direct connection of the coumarin to the conjugated framework of the BODIPY chromophore allows a fine modulation of the spectroscopical properties of the dye. Thus, BODIPY double-substitution with aminocoumarins is recommended to avoid undesired ICT phenomena, and achieve bright emission pushed to the red edge, due to a strong resonant

Published on 23 February 2015. Downloaded by Instituto de Quimica Fisica Rocasolano (IQFR) on 21/03/2015 10:46:16.

interaction, whereas hydroxycoumarins are recommended for enhancing the fluorescence performance.

The developed fluorescent coumarin–BODIPY hybrid dyes undergo lasing with good efficiency and high stability, allowing wavelength finely tunable over a wide range (~520–700 nm). Moreover, their laser action is enhanced when compared with the corresponding parent dyes, and correlates well with their photophysics. The highest lasing efficiencies (up to 51% at 355 nm) were recorded from hybrids based on two hydroxycoumarin and 3,5-disubstituted BODIPY. These hybrids also proved to be the most photostable, with laser emission remaining up to 55% of its initial level after 50 000 pump pulses at a 10 Hz repetition rate.

The attainment of these novel hybrid dyes based on BODIPY and coumarin, with strong UV absorption and highly efficient and stable laser emission in the green-red spectral region, concerns one of the greatest challenges in the ongoing development of advanced photonic materials with relevant applications. In fact, these organic dyes are the only ones that allow, by frequency doubling, the generation of tunable UV (~260–350 nm) laser radiation with ultra-short pulses. Radiation with these characteristics is essential to analyze accurately the photochemistry of biological molecules, as important as nucleic acids, trying to understand their stability under solar radiation, since their excited states are known to be involved at the beginning of the complex biological events that culminates in photodamage, including photocarcinogenesis, a growing human health problem.

## Acknowledgements

Financial support from Spain (MINECO: MAT2010-20646-C04-01, 02 and -04) and Mexico (DAIP: 2014, and CONACyT: 123732I) is gratefully acknowledged. I. E. thanks Gobierno Vasco for a research contract (IT339-10). G. D.-S. thanks MINECO for a predoctoral FPI grant.

## Notes and references

1 For example, see: C. E. Crespo-Hernández, B. Cohen, P. M. Hare and B. Kohler, *Chem. Rev.*, 2004, **104**, 1977.

2 (*a*) in *Dye Lasers*, ed. F. P. Schäfer, Springer-Verlag, New York, 3rd edn, 1990; (*b*) in *Dye Laser Principles*, ed. F. J. Duarte and L. W. Hillman, Academic, New York, 1990; (*c*) F. López Arbeloa, I. López Arbeloa and T. López Arbeloa, in *Handbook of Advanced Electronic and Photonic Materials and Devices*, ed. H. S. Nalwa, Academic Press, San Diego, 2001, vol. 7; (*d*) F. J. Duarte, *Tunable Laser Optics*, Elsevier Academic, New York, 2003.

3 (*a*) J. Wang, S. Qian and J. Cui, *J. Org. Chem.*, 2006, **71**, 4308; (*b*) G. Signore, R. Nifosi, L. Albertazzi, B. Storti and R. Bizarri, *J. Am. Chem. Soc.*, 2010, **132**, 1276.

4 (*a*) S. Lin and W. S. Struve, *Photochem. Photobiol.*, 1991, **54**, 361; (*b*) X. Cao, W. Lin, Q. Yu and J. Wang, *Org. Lett.*, 2011, **13**, 6098; (*c*) Y. Qian, B. Yang, Y. Shen, Q. Du, L. Lin, J. Lin and H. Zhu, *Sens. Actuators, B*, 2013, **182**, 498; (*d*) A. K. Bhoi, S. K. Das, D. Majhi, P. K. Sahu, A. Nijamudheen, N. Anoop, A. Rahaman and M. Sarkar, *J. Phys. Chem. B*, 2014, **118**, 9926; (*e*) D. Majhi, S. K. Das, P. K. Sahu, S. M. Pratik, A. Kumar and M. Sarkar, *Phys. Chem. Chem. Phys.*, 2014, **16**, 18349.

5 (*a*) B. Wagner, *Molecules*, 2009, **14**, 210; (*b*) X. Liu, Z. Xu and J. M. Cole, *J. Phys. Chem. C*, 2013, **117**, 16584.

6 (*a*) G. Jones II, W. R. Jackson, C.-Y. Choi and W. R. Bergmark, *J. Phys. Chem.*, 1985, **89**, 294; (*b*) S. C. Guggenheimer, J. H. Boyer, K. Thangaraj, M. P. Shah, M. L. Soong and T. G. Pavlopoulos, *Appl. Opt.*, 1993, **32**, 3942.

7 (*a*) A. Loudet and K. Burgess, *Chem. Rev.*, 2007, **107**, 4891; (*b*) G. Ulrich, R. Ziessel and A. Harriman, *Angew. Chem., Int. Ed.*, 2008, **47**, 1184; (*c*) F. L. Arbeloa, J. Bañuelos, V. Martínez, T. Arbeloa and I. López Arbeloa, *Trends Phys. Chem.*, 2008, **13**, 101; (*d*) M. Benstead, G. H. Mehl and R. W. Boyle, *Tetrahedron*, 2011, **67**, 3573; (*e*) N. Boens, V. Leen and W. Dehaen, *Chem. Soc. Rev.*, 2012, **41**, 1130; (*f*) A. Kamkaew, S. H. Lim, H. B. Lee, L. V. Kiew, L. Y. Chung and K. Burgess, *Chem. Soc. Rev.*, 2013, **42**, 77; (*g*) A. Bessette and G. S. Hanan, *Chem. Soc. Rev.*, 2014, **43**, 3342; (*h*) H. Lu, J. Mack, Y. Yang and Z. Shen, *Chem. Soc. Rev.*, 2014, **43**, 4778.

8 (*a*) Y. Xiao, D. Zhang, X. Qian, A. Costela, I. García-Moreno, V. Martín, M. E. Pérez-Ojeda, J. Bañuelos, L. Gartzia and I. López-Arbeloa, *Chem. Commun.*, 2011, **47**, 11513; (*b*) L. Gartzia-Rivero, H. Yu, J. Bañuelos, I. López-Arbeloa, A. Costela, I. García-Moreno and Y. Xiao, *Chem. – Asian J.*, 2013, **8**, 3133; (*c*) G. Durán-Sampedro, A. R. Agarrabeitia, L. Cerdán, M. E. Pérez-Ojeda, A. Costela, I. García-Moreno, I. Esnal, J. Bañuelos, I. López Arbeloa and M. J. Ortiz, *Adv. Funct. Mater.*, 2013, **23**, 4195; (*d*) G. Durán-Sampedro, I. Esnal, A. R. Agarrabeitia, J. Bañuelos, L. Cerdan, I. García-Moreno, A. Costela, I. López Arbeloa and M. J. Ortiz, *Chem. – Eur. J.*, 2014, **20**, 2646.

9 (*a*) R. C. A. Keller, J. R. Silvius and B. De Kruijff, *Biochem. Biophys. Res. Commun.*, 1995, 508; (*b*) Y. Zhao, Y. Zhang, X. Lu, Y. Liu, M. Chen, P. Wang, J. Liu and W. Guo, *J. Mater. Chem.*, 2011, **21**, 13168.

10 (*a*) A. Y. Bochkov, I. O. Akchurin, O. A. Dyachenko and V. F. Traven, *Chem. Commun.*, 2013, **49**, 11653; (*b*) Z. Yang, Y. He, J.-H. Lee, N. Park, M. Suh, W.-S. Chae, J. Cao, X. Peng, H. Jung, C. Kang and J. S. Kim, *J. Am. Chem. Soc.*, 2013, **135**, 9181.

11 BODIPYs are known to undergo ICT processes with groups at the C3/5 position. For example, see: (*a*) X. Peng, J. Du, J. Fan, J. Wang, Y. Wu, J. Zhao, S. Sun and T. Xu, *J. Am. Chem. Soc.*, 2007, **129**, 1500; (*b*) E. Deniz, G. C. Isbasar, Ö. A. Bozdemir, T. L. Yildirim, A. Siemiarczuk and E. U. Akkaya, *Org. Lett.*, 2008, **10**, 3401.

12 F. López Arbeloa, J. Bañuelos, V. Martínez, T. Arbeloa and I. López Arbeloa, *Int. Rev. Phys. Chem.*, 2005, **24**, 339.

13 (*a*) C. Tahtaoui, C. Thomas, F. Tohmer, P. Klotz, G. Duportail, Y. Mèly, D. Bonnet and M. Hibert, *J. Org. Chem.*, 2007, **72**, 269; (*b*) E. M. Sánchez-Carnerero, F. Moreno, B. L. Maroto, A. R. Agarrabeitia, M. J. Ortiz, B. G. Vo, G. Muller and S. de la Moya, *J. Am. Chem. Soc.*, 2014, **136**, 3346.

 This journal is © the Owner Societies 2015

Published on 23 February 2015. Downloaded by Instituto de Quimica Fisica Rocasolano (IQFR) on 21/03/2015 10:46:16.

14 (*a*) T. Rohand, M. Baruah, W. Qin, N. Boens and W. Dehaen, *Chem. Commun.*, 2006, 266; (*b*) L. Li, B. Nguyen and K. Burgess, *Bioorg. Med. Chem. Lett.*, 2008, **18**, 3112; (*c*) Y. A. Volkova, B. Brizet, P. D. Harvey, A. D. Averin, C. Goze and F. Denat, *Eur. J. Org. Chem.*, 2013, 4270; (*d*) E. M. Sánchez-Carnerero, F. Moreno, B. L. Maroto, A. R. Agarrabeitia, J. Bañuelos, T. Arbeloa, I. López-Arbeloa, M. J. Ortiz and S. de la Moya, *Chem. Commun.*, 2013, **49**, 11641.

15 T. Sakida, S. Yamaguchi and H. Shinokubo, *Angew. Chem., Int. Ed.*, 2011, **50**, 2280.

16 For example see: (*a*) C. Goze, G. Ulrich and R. Ziessel, *J. Org. Chem.*, 2007, **72**, 313; (*b*) M. A. H. Alamiry, J. P. Hagon, A. Harriman, T. Bura and R. Ziessel, *Chem. Sci.*, 2012, **3**, 1041; (*c*) A. Kaloudi-Chantzea, N. Karakostas, F. Pitterl, C. P. Raptopoulou, N. Glezos and G. Pistolis, *Chem. Commun.*, 2012, **48**, 12213; (*d*) N. Karakostas, I. M. Mavridis, K. Seintis, M. Fakis, E. N. Koini, I. D. Petsalakis and G. Pistolis, *Chem. Commun.*, 2014, **50**, 1362; (*e*) E. M. Sánchez-Carnerero, L. Gartzia-Rivero, F. Moreno, B. L. Maroto, A. R. Agarrabeitia, M. J. Ortiz, J. Bañuelos, I. López-Arbeloa and S. de la Moya, *Chem. Commun.*, 2014, **50**, 12765.

17 (*a*) T. Förster, *Discuss. Faraday Soc.*, 1959, **27**, 7; (*b*) J. Fan, M. Hu, P. Zhan and X. Peng, *Chem. Soc. Rev.*, 2013, **114**, 11567.

18 A. Harriman, L. J. Mallon, S. Goeb, G. Ulrich and R. Ziessel, *Chem. – Eur. J.*, 2009, **15**, 4553.

19 S. Speiser, *Chem. Rev.*, 1996, **96**, 1953.

20 (*a*) J. Iehl, J. F. Nierengarten, A. Harriman, T. Bura and R. Ziessel, *J. Am. Chem. Soc.*, 2012, **134**, 988; (*b*) D. Bai, A. C. Benniston, J. Hagon, H. Lemmetyinen, N. V. Tkachenko, W. Clegg and R. W. Harrington, *Phys. Chem. Chem. Phys.*, 2012, **14**, 4447.

21 G. Duran-Sampedro, A. R. Agarrabeitia, I. García-Moreno, A. Costela, J. Bañuelos, T. Arbeloa, I. López Arbeloa, J. L. Chiara and M. J. Ortiz, *Eur. J. Org. Chem.*, 2012, 6335.

22 L. Cerdán, A. Costela, I. García-Moreno, J. Bañuelos and I. López-Arbeloa, *Laser Phys. Lett.*, 2012, **9**, 426.

Electronic Supplementary Material (ESI) for Physical Chemistry Chemical Physics.
This journal is © the Owner Societies 2015

**Supporting information for**

# Coumarin/BODIPY hybrids by heteroatom linkage: versatile, tunable and photostable dye lasers for UV irradiation

I. Esnal,[a] G. Duran-Sampedro,[b] A. R. Agarrabeitia,[b] J. Bañuelos,*[,a]
I. García-Moreno,[c] M. A. Macías,[d] E. Peña-Cabrera,[d] I. López-Arbeloa,[a]
S. de la Moya,*[,b] and M. J. Ortiz[b]

[a] *Depto. de Química Física, Universidad del Pais Vasco-EHU, Apartado 644, 48080, Bilbao, Spain.*

[b] *Depto. de Química Orgánica I, Facultad de CC. Químicas, Universidad Complutense de Madrid, Ciudad Universitaria s/n, 28040, Madrid, Spain.*

[c] *Depto. de Sistemas de Baja Dimensionalidad, Superficies y Materia Condensada, Instituto de Química-Física "Rocasolano", C.S.I.C., Serrano 119, 28006, Madrid, Spain.*

[d] *Depto. de Química, Universidad de Guanajuato, Col. Noria Alta s/n, Guanajuato, 36050, Mexico.*

*E-mail: jorge.banuelos@ehu.es, santmoya@ucm.es*

## Table of contents

# 1. General

## *Synthesis*

Common solvents were dried and distilled by standard procedures. All starting materials and reagents were obtained commercially and used without further purifications. Flash chromatography purifications were performed on silica gel 60 (60, 230-400 mesh ASTM). Thin-layer chromatography (TLC) was performed on silica gel plates (silica gel 60, F254, supported on aluminium). NMR spectra were recorded at 20 ºC and the residual solvent peaks were used as internal standards. Complex spin-system signals were additionally simulated by using MestRe-C.[1] FTIR spectra were obtained from neat samples using the ATR technique. High resolution mass spectrometry (HRMS) was performed using the EI technique.

## *Photophysics*

Standard abbreviations: Absorption maximum ($\lambda_{ab}$); fluorescence maximum ($\lambda_{fl}$); molar extinction coefficient at $\lambda_{ab}$ ($\varepsilon_{max}$); fluorescence quantum yield ($\phi$); mean fluorescence lifetime ($\tau$); Stokes, or pseudo-Stokes when indicated, shift ($\Delta\nu_{St}$). Absorption and fluorescence spectra, as well as fluorescence-decay curves, were recorded in diluted solutions (~$2\cdot10^{-6}$ M) of ethyl acetate (cut-off ~190 nm). UV-Vis absorption and fluorescence spectra were recorded on a Varian CARY 4E spectrophotometer and on an Edinburgh Instruments spectrofluorimeter (model FLSP 920), respectively. $\phi$ values were obtained using quinine sulfate ($\phi$ = 0.55, in 0.1N $H_2SO_4$) as reference for the UV coumarin-chromophore emission, and **1** ($\phi$ = 0.84 in ethanol), PM597 ($\phi$ = 0.43 in ethanol), PM605 ($\phi$ = 0.66 in ethanol) and Nile Blue ($\phi$ = 0.27 in methanol) for the Vis BODIPY-chromophore emission. These values were calculated from corrected fluorescence spectra (detector sensibility to the wavelength), and corrected by the refractive index of the solvent. Temperature-dependence measurements were performed using a liquid-hydrogen-cooled cryostat (Oxford), and an external electronic temperature-controller device for heating. Radiative-decay curves were registered with the time-correlated single-photon counting technique (Edinburgh Instruments FL920, with picosecond time-resolution). Fluorescence emission was monitored at $\lambda_{fl}$ upon direct

[1] MestRe-C: C. Cobas, J. Cruces and J. Sardina, MestRe-C, program version 2.3.

excitation at 470 nm and 530 nm by means of a diode laser (PicoQuant LDH470 and LDH530, respectively) with 150 ps full width at half maximum (FWHM) pulses. $\tau$ values were obtained after the deconvolution of the instrumental response signal from the recorded decay curves by means of an iterative method. The goodness of the exponential fit was controlled by statistical parameters (chi-square, Durbin-Watson and analysis of the residuals). The radiative ($k_{fl}$) and non-radiative ($k_{nr}$) rate constants were calculated from the fluorescence quantum yield and lifetime: $k_{fl} = \phi/\tau$; $k_{nr} = (1-\phi)/\tau$.

### *Electrochemistry*

Voltammograms (Metrohm Autolab) were recorded using a three-electrode set up with a platinum disk (diameter 3 mm) or layer (surface 8 mm x 7.5 mm) as the working electrode, a platinum wire as the counter electrode, and Ag/AgCl as the reference electrode. 0.1 M solution of tetrabutylammonium hexafluorophosphate ($TBAPF_6$) in dry acetonitrile was used as the electrolyte solvent. The studied compounds were dissolved in the solution to achieve a concentration of 0.5-1.0 mM. All redox potentials were reported vs. ferrocene, as the internal standard. The solutions were purged with argon and all the measurements were performed under argon.

### *Quantum mechanical calculations*

Ground state geometries were optimized at the Density Functional Theory (DFT) using the hybrid B3LYP method, and the double valence basis set (6-31g). The geometries were considered as energy minimum when the corresponding frequency analysis did not give any negative value. The absorption spectra were simulated by the Time-Dependent (TD) method. The solvent effect (ethyl acetate) was considered in the conducted theoretical simulations by means of the Polarizable Continuum Model (PCM). All the calculations were performed using the Gaussian 09[2] software as implemented in the computational cluster “arina” of the UPV/EHU.

---

[2] Gaussian 09: Frisch, M. J.; Trucks, G. W.; Schlegel, H. B.; Scuseria, G. E.; Robb, M. A.; Cheeseman, J. R.; Scalmani, G.; Barone, V.; Mennucci, B.; Petersson, G. A.; Nakatsuji, H.; Caricato, M.; Li, X.; Hratchian, H. P.; Izmaylov, A. F.; Bloino, J.; Zheng, G.; Sonnenberg, J. L.; Hada, M.; Ehara, M.; Toyota, K.; Fukuda, R.; Hasegawa, J.; Ishida, M.; Nakajima, T.; Honda, Y.; Kitao, O.; Nakai, H.; Vreven, T.; Montgomery, J. A., Jr.; Peralta, J. E.; Ogliaro, F.; Bearpark, M.; Heyd, J. J.; Brothers, E.; Kudin, K. N.; Staroverov, V. N.; Kobayashi, R.; Normand, J.; Raghavachari, K.; Rendell, A.; Burant, J. C.; Iyengar, S. S.; Tomasi, J.; Cossi, M.; Rega, N.; Millam, N. J.; Klene, M.; Knox, J. E.; Cross, J. B.; Bakken, V.; Adamo, C.; Jaramillo, J.; Gomperts, R.; Stratmann, R. E.; Yazyev, O.; Austin, A. J.; Cammi, R.; Pomelli, C.; Ochterski, J. W.; Martin, R. L.; Morokuma, K.; Zakrzewski, V. G.; Voth, G. A.; Salvador, P.; Dannenberg, J. J.; Dapprich, S.; Daniels, A. D.; Farkas, Ö.; Foresman, J. B.; Ortiz, J. V.; Cioslowski, J.; Fox, D. J. Gaussian, Inc., Wallingford CT, 2009.

### *Laser behavior*

Liquid solutions of dyes were contained in 1 cm optical-path rectangular quartz cells carefully sealed to avoid solvent evaporation during the experiments. These solutions were transversely pumped either at 355 nm, with 5 mJ, 8 ns FWHM pulses from the third-harmonic of a Q-switched Nd:YAG laser (Spectron SL282G) or at 532 nm, with 5 mJ, 6 ns full width at half maximum (FWHM) pulses from a frequency-doubled Q-switched Nd:YAG laser (Monocrom OPL-10), at a repetition rate of up to 10 Hz. The exciting pulses were line-focused onto the cell, providing pump fluencies on the active medium in the range 110-180 mJ/cm$^2$. The oscillation cavity (2 cm length) consisted of a 90% reflectivity aluminium mirror, with the lateral face of the cell or the solid sample as output coupler. The photostability of the dyes in liquid solution was evaluated by irradiating under lasing conditions 10 μL of ethyl acetate solution, contained in a cylindrical Pyrex capillary (1 cm height, 1 mm internal diameter) carefully sealed to avoid solvent evaporation during the experiments. Although the low optical quality of the capillary tube prevents from laser emission from the dye, information about dye photostability can be obtained by monitoring the decrease in the laser-induced fluorescence intensity, by exciting transversally the capillary, as a function of the number of pump pulses at a given repetition rate. The fluorescence emission was monitored perpendicular to the exciting beam, collected by an optical fiber, and imaged onto the input slit of a monochromator (Acton Research corporation) and detected with a charge-coupled device (CCD) (SpectruMM:GS128B). The fluorescence emission was recorded by feeding the signal to the boxcar (Stanford Research, model 250) to be integrated before being digitized and processed by a computer. Each experience was repeated at least three times. The estimated error in the energy and photostability measurements was 10%.

## 2. Synthetic procedures and characterization data

***General procedure A.*** To a solution of the corresponding starting BODIPY (1 equiv) and coumarin (1-6 equiv) in dry $CH_3CN$ (15 mL) was added $K_2CO_3$ (3-6 equiv), or NaH (4 equiv), and the resulting mixture refluxed until consumption of the starting BODIPY (TLC monitoring). The reaction was quenched by addition of water, and the organic layer extracted with $CH_2Cl_2$, dried over $MgSO_4$, filtered, and concentrated to dryness. The obtained hybrids were purified by flash chromatography on silica gel.

***General procedure B.*** A solution of the corresponding starting BODIPY (1 equiv) and coumarin (3-6 equiv) in dry $CH_3CN$ (3 mL) was placed in a sealed vessel, and reacted in a Biotage® Initiator Classic microwave synthesizer at 150 ºC for 3 h. EtOAc was then added, and the solution was washed with 10% aq HCl, or 10% aq NaOH, and water, dried over $MgSO_4$, filtered, and concentrated to dryness. The obtained hybrids were purified by flash chromatography on silica gel.

***General procedure C.*** To a solution of the corresponding BODIPY (1 equiv) in dry $CH_3CN$ (15 mL) was added coumarin (4-6 equiv), and the resulting mixture refluxed until consumption of the starting BODIPY (TLC monitoring). EtOAc was then added, and the solution washed with 10% aq HCl, or 10% aq NaOH, and water, dried over $MgSO_4$, filtered, and concentrated to dryness. The obtained hybrid were purified by flash chromatography on silica gel.

**Hybrid 1dA:** To a solution of BODIPY **1**[3] (50 mg, 0.16 mmol) in dry $CH_2Cl_2$ was added aluminium chloride (41.8 mg, 0.32 mmol) under an argon atmosphere, and the mixture resulting was refluxed for 10 min. Then, coumarin **AH** (111 mg, 0.63 mmol) was added and the mixture was refluxed for 30 min. Water was added, and the solution was extracted with $CH_2Cl_2$, dried over $MgSO_4$, filtered and concentrated to dryness. Flash chromatography using hexane/EtOAc (7:3) afforded **1dA** (60 mg, 55%) as an orange solid. $^1$H NMR (300 MHz, $CDCl_3$) $\delta$ 7.26 (d, *J* = 8.7 Hz, 2H), 6.61 (dd, *J* = 8.7 and 2.4 Hz, 2H), 6.17 (d, *J* = 2.4 Hz, 2H), 5.94 (d, *J* = 0.9 Hz, 2H), 2.72 (s, 3H), 2.34 (s, 12H), 2.24 (d, *J* = 0.9 Hz, 6H), 2.20 (q, *J* = 7.5 Hz, 4H), 0.83 (t, *J* = 7.5 Hz, 6H) ppm; $^{13}$C NMR (75 MHz, $CDCl_3$) $\delta$ 162.2 (C), 160.1 (C), 155.1 (C), 153.1 (C), 152.5 (C), 140.3 (C), 137.9 (C), 133.6 (C), 132.2 (C), 125.2 (CH), 116.6 (CH), 112.8 (C), 111.0 (CH), 105.1 (CH), 18.6 ($CH_3$), 17.3 ($CH_3$), 17.1 ($CH_2$), 14.8 ($CH_3$), 12.6 ($CH_3$) ppm; FTIR $\upsilon$ 2925, 1718, 1606, 1548, 1388,

[3] Laser grade, Exciton. It was used as received with a purity > 99%.

1190, 1138, 1068, 1002, 978 $cm^{-1}$; HRMS-EI *m/z* calcd for ($C_{38}H_{39}BN_2O_6$) 630.2900, found 630.2895.

**Hybrid 2mA:** According to the general procedure A, BODIPY **2**[4] (100 mg, 0.286 mmol), coumarin **AH** (49.5 mg, 0.286 mmol) and $K_2CO_3$ (118.5 mg, 0.858 mmol) were reacted for 24 h. Flash chromatography using hexane/EtOAc (95:5) afforded **2mA** (101 mg, 72%) as a red solid. $^1H$ NMR (300 MHz, $CDCl_3$) $\delta$ 7.60 (d, *J* = 9.3 Hz, 1H), 7.31 (d, *J* = 8.1 Hz, 2H), 7.24 (d, *J* = 8.1 Hz, 2H), 7.17-7.15 (m, 2H), 6.84 (d, *J* = 4.5 Hz, 1H), 6.67 (d, *J* = 4.2 Hz, 1H), 6.28 (d, *J* = 4.2 Hz, 1H), 6.20 (d, *J* = 1.2 Hz, 1H), 5.83 (d, *J* = 4.8 Hz, 1H), 2.38 (s, 6H) ppm; $^{13}C$ NMR (75 MHz, $CDCl_3$) $\delta$ 164.5 (C), 160.2 (C), 156.4 (C), 154.5 (C), 151.9 (C), 143.1 (C), 141.1 (C), 139.9 (C), 133.9 (CH), 132.8 (C), 130.5 (CH), 129.8 (CH), 129.6 (C), 129.3 (CH), 128.6 (C), 126.5 (CH), 118.1 (CH), 116.7 (C), 116.4 (CH), 114.6 (CH), 108.6 (CH), 105.9 (CH), 21.5 ($CH_3$), 18.8 ($CH_3$) ppm; FTIR $\upsilon$ 2918, 2850, 1727, 1710, 1582, 1509, 1418, 1255, 1097, 1017, 974 $cm^{-1}$; HRMS-EI *m/z* calcd for ($C_{26}H_{18}BClF_2N_2O_3$) 490.1065, found 490.1060.

**Hybrid 2dA:** According to the general procedure A, BODIPY **2**[4] (50 mg, 0.142 mmol), coumarin **AH** (150.5 mg, 0.85 mmol) and $K_2CO_3$ (117 mg, 0.85 mmol) in dry $CH_3CN$ (10 mL) were reacted for 24 h. Flash chromatography using hexane/EtOAc (7:3) afforded **2dA** (48 mg, 54%) as a red solid. $^1H$ NMR (300 MHz, $CDCl_3$) $\delta$ 7.56 (d, *J* = 9.3 Hz, 2H), 7.36 (d, *J* = 8.1 Hz, 2H), 7.26 (d, *J* = 8.1 Hz, 2H), 7.17-7.14 (m, 4H), 6.77 (d, *J* = 4.2 Hz, 2H), 6.19 (d, *J* = 1.2 Hz, 2H), 5.81 (d, *J* = 4.2 Hz, 2H), 2.40 (s, 3H), 2.37 (d, *J* = 1.2 Hz, 6H) ppm; $^{13}C$ NMR (75 MHz, $CDCl_3$) $\delta$ 161.7 (C), 160.4 (C), 157.4 (C), 154.6 (C), 151.9 (C), 143.0 (C), 140.8 (C), 130.9 (CH), 130.5 (CH), 130.0 (C), 129.2 (CH), 128.5 (C), 126.2 (CH), 117.5 (C), 116.0 (CH), 114.3 (CH), 107.9 (CH), 104.0 (CH), 21.5 ($CH_3$), 18.8 ($CH_3$) ppm; FTIR $\upsilon$ 2926, 1732, 1582, 1440, 1249, 1106, 978 $cm^{-1}$; HRMS-EI *m/z* calcd for ($C_{36}H_{25}BF_2N_2O_6$) 630.1772, found 630.1168.

**Hybrid 2mB:** According to the general procedure B, BODIPY **2**[4] (40 mg, 0.114 mmol) and coumarin **BH** (120 mg, 0.684 mmol) in dry $CH_3CN$ (15 mL) were reacted at 150 ºC for 3 h. Flash chromatography using hexane/EtOAc (8:2) afforded **2mB** (48 mg, 86%) as a red solid. $^1H$ NMR (300 MHz, $CDCl_3$) $\delta$ 8.14 (broad s, 1H, NH), 7.55 (d, *J* = 8.7 Hz, 1H), 7.30 (d, *J* = 8.1 Hz, 2H), 7.22 (d, *J* = 8.1 Hz, 2H), 7.15 (d, *J* = 2.1 Hz, 1H), 7.04 (dd, *J* = 8.7 and

[4] T. Rohand, M. Baruah, W. Qin, N. Boens and W. Dehaen, *Chem. Commun.*, 2006, 266.

2.1 Hz, 1H), 6.94 (d, *J* = 4.8 Hz, 1H), 6.51 (d, *J* = 4.8 Hz, 1H), 6.48 (d, *J* = 3.9 Hz, 1H), 6.20 (d, *J* = 3.9 Hz, 1H), 6.18 (d, *J* = 1.2 Hz, 1H), 2.38 (s, 3H), 2.37 (d, *J* = 1.2 Hz, 3H) ppm; $^{13}$C NMR (75 MHz, $CDCl_3$) $\delta$ 160.5 (C), 156.3 (C), 154.7 (C), 151.9 (C), 140.9 (C), 140.3 (C), 136.6 (C), 135.6 (CH), 133.6 (C), 132.4 (C), 132.3 (C), 130.4 (C), 130.3 (CH), 129.2 (CH), 126.2 (CH), 124.0 (CH), 116.9 (CH), 114.4 (CH), 114.0 (CH), 110.6 (CH), 107.9 (CH), 21.4 ($CH_3$), 18.7 ($CH_3$) ppm; FTIR $\upsilon$ 3353, 2922, 1728, 1709, 1579, 1470, 1383, 1100, 979 cm$^{-1}$; HRMS-EI *m/z* calcd for ($C_{26}H_{19}BClF_2N_3O_2$) 489.1225, found 489.1220.

**Hybrids 3mA and 3dA:** According to the general procedure A, BODIPY **3**[5] (50 mg, 0.132 mmol), coumarin **AH** (70 mg, 0.396 mmol) and $K_2CO_3$ (55 mg, 0.396 mmol) in dry $CH_3CN$ (10 mL) were reacted for 2 h. Flash chromatography using hexane/EtOAc (8:2) afforded, by order of elution, **3mA** (18 mg, 26%) as a red solid, and **3dA** (50 mg, 57%) as a red solid. **3mA**: $^1$H NMR (700 MHz, $CDCl_3$) $\delta$ 7.60 (d, *J* = 9.1 Hz, 1H), 7.23-7.20 (m, 2H), 6.88 (s, 2H), 6.59 (d, *J* = 4.2 Hz, 1H), 6.40 (d, *J* = 4.2 Hz, 1H), 6.23 (s, 2H), 6.22 (d, *J* = 4.2 Hz, 1H), 5.76 (d, *J* = 4.9 Hz, 1H), 2.39 (d, *J* = 1.4 Hz, 3H), 2.28 (s, 3H), 2.05 (s, 6H) ppm; $^{13}$C NMR (176 MHz, $CDCl_3$) $\delta$ 164.7 (C), 160.2 (C), 156.3 (C), 154.6 (C), 151.7 (C), 142.5 (C), 140.1 (C), 139.0 (C), 136.8 (C), 132.9 (C), 132.4 (CH), 130.0 (C), 128.4 (C), 128.2 (CH), 127.2 (CH), 126.3 (CH), 118.2 (C), 116.9 (CH), 116.6 (CH), 114.8 (CH), 108.9 (CH), 105.9 (CH), 21.1 ($CH_3$), 20.0 ($CH_3$), 18.8 ($CH_3$) ppm; FTIR $\upsilon$ 2924, 1734, 1573, 1436, 1354, 1261, 1104, 1025, 981, cm$^{-1}$; HRMS-EI *m/z* calcd for ($C_{28}H_{22}BClF_2N_2O_3$) 518.1378, found 518.1371. **3dA**: $^1$H NMR (300 MHz, $CDCl_3$) $\delta$ 7.57 (d, *J* = 9.6 Hz, 2H), 7.19-7.15 (m, 4H), 6.89 (s, 2H), 6.50 (d, *J* = 4.2 Hz, 2H), 6.19 (d, *J* = 1.2 Hz, 2H), 5.73 (d, *J* = 4.2 Hz, 2H), 2.37 (d, *J* = 1.2 Hz, 6H), 2.28 (s, 3H), 2.10 (s, 6H) ppm; $^{13}$C NMR (75 MHz, $CDCl_3$) $\delta$ 162.2 (C), 160.8 (C), 157.6 (C), 155.0 (C), 152.3 (C), 142.7 (C), 139.2 (C), 137.4 (C), 130.0 (CH), 129.1 (C), 128.9 (C), 128.6 (CH), 126.6 (CH), 118.0 (C), 116.5 (CH), 114.7 (CH), 108.5 (CH), 104.3 (CH), 21.5 ($CH_3$), 20.4 ($CH_3$), 19.2 ($CH_3$) ppm; FTIR $\upsilon$ 2921, 1732, 1573, 1429, 1258, 1106, 1011, 978 cm$^{-1}$; HRMS-EI *m/z* calcd for ($C_{38}H_{29}BF_2N_2O_6$) 658.2085, found 658.2075.

**Hybrid 3mB:** According to the general procedure B, BODIPY **3**[5] (50 mg, 0.132 mmol) and coumarin **BH** (70 mg, 0.396 mmol) in dry $CH_3CN$ (2.5 mL) were reacted at 150 ºC for 3 h. Flash chromatography using hexane/EtOAc (8:2) afforded **3mB** (62 mg, 90%) as a red

[5] T. Sakida, S. Yamaguchi and H. Shinokubo, *Angew. Chem. Int. Ed.*, 2011, **50**, 2280.

solid. $^{1}$H NMR (300 MHz, $CDCl_3$) $\delta$ 8.17 (broad s, 1H, NH), 7.55 (d, *J* = 8.4 Hz, 1H), 7.16 (d, *J* = 2.1 Hz, 1H), 7.05 (dd, *J* = 8.4 and 2.1 Hz, 1H), 6.87 (s, 2H), 6.67 (d, *J* = 4.8 Hz, 1H), 6.45 (d, *J* = 4.8 Hz, 1H), 6.18 (d, *J* = 1.2 Hz, 1H), 6.17 (d, *J* = 3.9 Hz, 1H), 6.12 (d, *J* = 3.9 Hz, 1H), 2.36 (d, *J* = 1.2 Hz, 3H), 2.27 (s, 3H), 2.04 (s, 6H) ppm; $^{13}$C NMR (75 MHz, $CDCl_3$) $\delta$ 160.8 (C), 157.0 (C), 155.1 (C), 152.2 (C), 141.2 (C), 139.0 (C), 137.4 (C), 137.3 (C), 135.9 (C), 134.8 (CH), 133.7 (C), 133.2 (C), 132.6 (C), 129.3 (C), 128.6 (CH), 126.5 (CH), 123.0 (CH), 117.4 (CH), 114.8 (CH), 114.5 (CH), 111.3 (CH), 108.5 (CH), 21.5 ($CH_3$), 20.3 ($CH_3$), 19.0 ($CH_3$) ppm; FTIR $\upsilon$ 3350, 2932, 1712, 1569, 1455, 1375, 1110, 989 cm$^{-1}$; HRMS-EI *m/z* calcd for ($C_{28}H_{23}BClF_2N_3O_2$) 517.1538, found 517.1530.

**Hybrid 3dB:** According to the general procedure B, BODIPY **3**[5] (50 mg, 0.132 mmol) and coumarin **BH** (92.5 mg, 0.528 mmol) in dry $CH_3CN$ (3 mL) were reacted at 150 ºC for 3 h. Flash chromatography using hexane/EtOAc (8:2) afforded, by order of elution, **3mB** (48 mg, 70%) as a red solid (see characterization data above), and **3dB** (10 mg, 11%) as a blue solid. $^{1}$H NMR (700 MHz, $CDCl_3$) $\delta$ 7.69 (broad s, 2H, 2NH), 7.47 (d, *J* = 8.4 Hz, 2H), 7.11 (d, *J* = 2.1 Hz, 2H), 6.99 (dd, *J* = 8.4 and 2.1 Hz, 2H), 6.88 (s, 2H), 6.46 (d, *J* = 4.2 Hz, 2H), 6.29 (d, *J* = 4.2 Hz, 2H), 6.11 (s, 2H), 2.35 (s, 6H), 2.29 (s, 3H), 2.09 (s, 6H) ppm; $^{13}$C NMR (176 MHz, $CDCl_3$) $\delta$ 160.9 (C), 155.0 (C), 152.1 (C), 150.4 (C), 142.6 (C), 138.3 (C), 137.2 (C), 134.5 (C), 129.8 (C), 129.5 (C), 128.9 (CH), 128.1 (CH), 125.9 (CH), 115.3 (C), 115.2 (CH), 112.8 (CH), 105.5 (CH), 105.4 (CH), 21.2 ($CH_3$), 19.9 ($CH_3$), 18.6 ($CH_3$) ppm; FTIR $\upsilon$ 3351, 2922, 1724, 1544, 1461, 1357, 1010, 977 cm$^{-1}$; HRMS-EI *m/z* calcd for ($C_{38}H_{31}BF_2N_4O_4$) 656.2404, found 656.2397.

**Hybrid 3mC:** According to the general procedure A, BODIPY **3**[5] (50 mg, 0.13 mmol), 4-hydroxycoumarin **CH** (85.5 mg, 0.53 mmol) and NaH (72.9 mg, 0.53 mmol) in dry $CH_3CN$ (15 mL) were reacted for 24 h. Flash chromatography using hexane/EtOAc (93:7) afforded **3mC** (14 mg, 21%) as an orange solid. $^{1}$H NMR (500 MHz, $CDCl_3$) $\delta$ 8.10 (dd, *J* = 8.1, 1.6 Hz, 1H), 7.67-7.63 (m, 1H), 7.41-7.38 (m, 2H), 6.98 (d, *J* = 0.4 Hz, 2H), 6.74 (d, *J* = 4.5 Hz, 1H), 6.63 (d, *J* = 4.3 Hz, 1H), 6.37 (d, *J* = 4.3 Hz, 1H), 6.24 (d, *J* = 4.5 Hz, 1H), 6.11 (s, 1H), 2.37 (s, 3H), 2.14 (s, 6H) ppm; $^{13}$C NMR (125 MHz, $CDCl_3$) $\delta$ 162.9 (C), 161.6 (C), 158.6 (C), 153.7 (C), 145.1 (C), 144.0 (C), 139.3 (C), 136.7 (C), 134.0 (C), 133.4 (CH), 130.9 (CH), 130.0 (CH), 129.5 (C), 128.4 (CH), 128.0 (C), 124.7 (CH), 123.6 (CH), 118.6 (CH), 116.8 (CH), 114.5 (C), 106.7 (CH), 97.5 (CH), 21.1 ($CH_3$), 20.0 ($CH_3$) ppm; FTIR $\upsilon$ 1725, 1629, 1594, 1570, 1541, 1520, 1437, 1419, 1381, 1355, 1330, 1286, 1231, 1183,

1110, 1086, 994 $cm^{-1}$; HRMS (FAB) *m/z* calcd. for $C_{27}H_{21}BClF_2N_2O_3$ $[M+H]^+$ 505.1302, found 505.1309.

**Hybrid 4mA:** According to the general procedure C, BODIPY **4**[6] (40 mg, 0.137 mmol) and coumarin **AH** (97 mg, 0.55 mmol) in dry $CH_3CN$ (15 mL) were reacted for 12 h. Flash chromatography using hexane/EtOAc (5:5) afforded, by order of elution, starting BODIPY **4** (10 mg, 25%), and **4mA** (37 mg, 59%) as a red solid. $^1H$ NMR (300 MHz, $C_3D_6O$) $\delta$ 7.86 (d, *J* = 8.7 Hz, 1H), 7.63-7.61 (m, 1H), 7.36 (d, *J* = 2.1 Hz, 1H), 7.31 (dd, *J* = 8.7 and 2.1 Hz, 1H), 7.16-7.14 (m, 1H), 6.47 (d, *J* = 4.2 Hz, 1H), 6.37 (d, *J* = 5.1 Hz, 1H), 6.25 (d, *J* = 1.2 Hz, 1H), 2.41 (d, *J* = 1.2 Hz, 3H) ppm; $^{13}C$ NMR (75 MHz, $C_3D_6O$) $\delta$ 171.0 (C), 160.3 (C), 156.5 (C), 156.0 (C), 153.5 (C), 140.3 (C), 137.0 (CH), 135.2 (C), 130.7 (C), 128.8 (CH), 127.5 (CH), 127.4 (C), 127.3 (q, *J* = 273.4 Hz, $CF_3$), 120.4 (C), 118.4 (CH), 117.7 (CH), 116.1 (CH), 113.1 (CH), 110.2 (CH), 19.0 ($CH_3$) ppm; FTIR $\upsilon$ 2923, 1691, 1567, 1444, 1247, 1108, 978 $cm^{-1}$; HRMS-EI *m/z* calcd for ($C_{20}H_{11}BClF_5N_2O_3$) 468.0471, found 468.0461.

**Hybrids 4mB and 4dB:** According to the general procedure C, BODIPY **4**[6] (32 mg, 0.11 mmol) and coumarin **BH** (192 mg, 0.66 mmol) in dry $CH_3CN$ (15 mL) were reacted for 16 h. Flash chromatography using hexane/EtOAc (8:2) afforded, by order of elution, **4mB** (32 mg, 62%) as a red solid, and **4dB** (4 mg, 11%) as a blue solid. **4mB**: $^1H$ NMR (700 MHz, $CDCl_3$) $\delta$ 8.50 (broad s, 1H, NH), 7.62 (d, *J* = 8.4 Hz, 1H), 7.47 (m, 1H), 7.19 (d, *J* = 2.1 Hz, 1H), 7.11 (dd, *J* = 8.4 and 2.1 Hz, 1H), 6.89 (m, 1H), 6.61 (d, *J* = 4.9 Hz, 1H), 6.27 (d, *J* = 4.2 Hz, 1H), 6.26 (s, 1H), 2.40 (s, 3H) ppm; $^{13}C$ NMR (176 MHz, $CDCl_3$) $\delta$ 160.0 (C), 159.2 (C), 154.5 (C), 151.5 (C), 139.2 (C), 135.6 (CH), 134.0 (C), 132.0 (C), 127.5 (C), 126.4 (CH), 122.6 (q, $^1J_{CF}$ = 274,6 Hz, $CF_3$), 122.5 (CH), 119.0 (q, $^2J_{CF}$ = 33.4 Hz, C), 118.5 (C), 118.2 (CH), 115.2 (CH), 115.1 (CH), 114.3 (CH), 110.0 (CH), 18.7 ($CH_3$) ppm; FTIR $\upsilon$ 3350, 2925, 1732, 1715, 1599, 1525, 1487, 1369, 1100, 983 $cm^{-1}$; HRMS-EI *m/z* calcd for ($C_{20}H_{12}BClF_5N_3O_2$) 467.0631, found 467.0623. **4dB**: $^1H$ NMR (700 MHz, $CDCl_3$) $\delta$ 7.80 (broad s, 2H, 2NH), 7.53 (d, *J* = 8.4 Hz, 2H), 7.22 (m, 2H), 7.12 (d, *J* = 2.1 Hz, 2H), 7.03 (dd, *J* = 8.4 and 2.1 Hz, 2H), 6.44 (d, *J* = 4.9 Hz, 2H), 6.16 (d, *J* = 1.4 Hz, 2H), 2.37 (d, *J* = 1.4 Hz, 6H) ppm; $^{13}C$ NMR (176 MHz, $CDCl_3$) $\delta$160.6 (C), 154.9 (C), 151.9 (C), 141.6 (C), 129.6 (CH), 127.0 (C), 126.1 (CH), 116.2 (C), 115.9 (CH), 113.6 (CH), 107.2 ~~(CH), 106.7 (CH), 18.7 ($CH_3$)~~, $CF_3$ not observed; FTIR $\upsilon$ 3354, 2930, 1730, 1710, 1589,

[6] L. Li, B. Nguyen and K. Burgess, *Bioorg. Med. Chem. Lett.*, 2008, **18**, 3112.

1536, 1477, 1355, 1108, 987 $cm^{-1}$; HRMS-EI *m/z* calcd for ($C_{30}H_{20}BF_5N_4O_4$) 606.1496, found 606.1489.

## 3. Photophysical, electrochemical and computational results (Figs. S1-S5 and Table S1-S2)

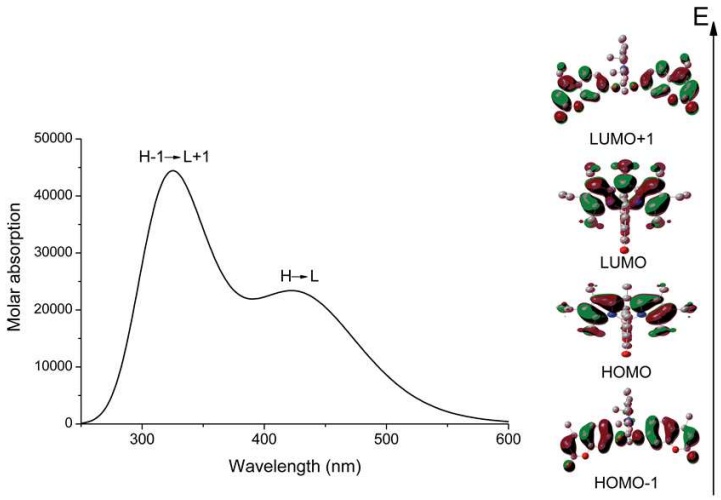


**Fig S1.** TD simulation of the of the absorption spectrum of **1dA** in acetone (B3LYP/6-31g//PCM) and corresponding contour maps of the molecular orbital involved in the electronic transitions (the TD method predicts accurately the UV transition of the coumarin, but, as it is known, overestimates the energy gap of the Vis transition and, in the case of the BODIPYs, underestimates also their transition probability).

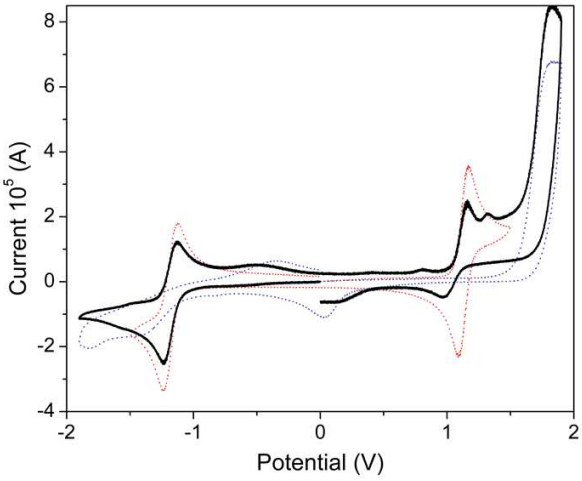


**Fig S2.** Cyclic voltammograms of **1dA** (solid black), **1** (dotted red) and **AH** (doted blue).

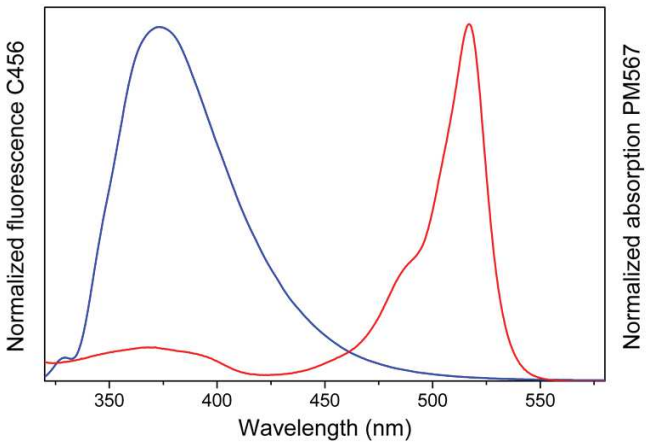


**Fig S3**. Spectral overlap between **AH** fluorescence (blue) and **1** absorption (red).

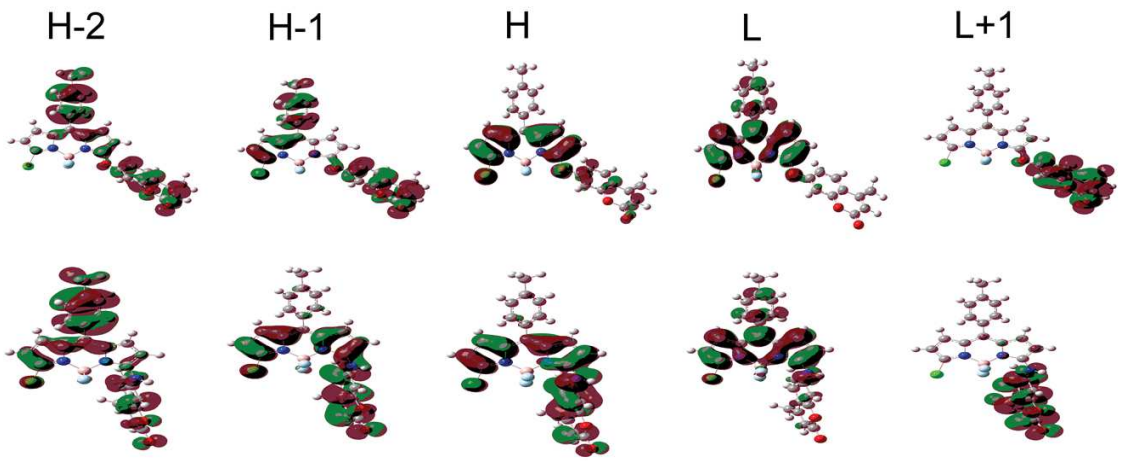


**Figure S4**. Computed frontier molecular orbitals (contour maps) of **2mA** (up) and **2mB** (down). H and L denotes HOMO and LUMO respectively.

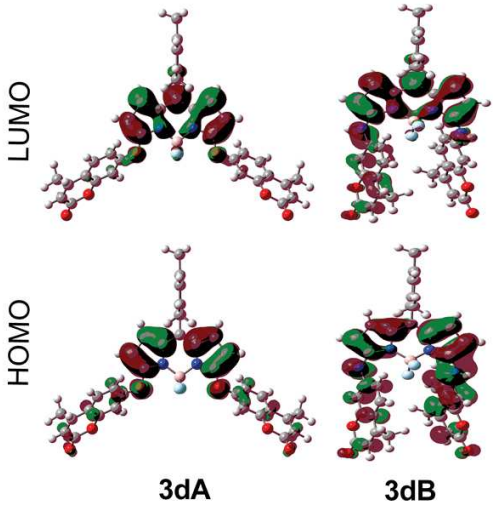


**Fig S5.** Computed HOMO and LUMO (contour maps) of **3dA** and **3dB**.

**Table S1**. Photophysical properties of coumarin/BODIPY hybrids **1dA**, **2mA**, **2mB**, **2dA**, **3mA**, **3mB**, **3mC**, **3dA**, **3dB**, **4mA**, **4mB** and **4dB**, and corresponding parent coumarins (**AH** and **BH**) and BODIPYs (**1**-**4**) in ethyl acetate. The fluorescence data were recorded upon excitation of the Vis absorption band.

| compound | $\lambda_{ab}$ (nm) | $\varepsilon_{max}$ ($10^4 M^{-1}cm^{-1}$) | $\lambda_{fl}$ (nm) | $\phi$ | $\tau$ (ns) | $k_{fl}$ ($10^8$ $s^{-1}$) | $k_{nr}$ ($10^8$ $s^{-1}$) | $\Delta\nu_{St}$ ($cm^{-1}$) |
|---|---|---|---|---|---|---|---|---|
| **AH*** | 323.0 | 1.4 | 380.0 | 0.28 | 1.2 | 2.3 | 6.0 | 4645 |
| **BH** | 340.0 | 2.0 | 400.0 | 0.82 | 2.89 | 2.8 | 0.62 | 4410 |
| **1** | 516.5 | 8.0 | 531.5 | 0.84 | 5.78 | 1.45 | 0.28 | 545 |
| **1dA** | 519.0<br>323.5 | 6.7<br>3.9 | 537.0 | 0.82 | 6.78 | 1.2 | 0.26 | 645 |
| **2** | 509.5 | 10.3 | 522.0 | 0.25 | 1.93 | 1.3 | 3.9 | 470 |
| **2mA** | 510.0 | 4.6 | 525.0 | 0.16 | 0.84 | 1.9 | 10.0 | 560 |
| **2mB** | 524.0 | 4.5 | 577.0 | 0.04 | 0.28 | 1.4 | 34.3 | 1750 |
| **2dA** | 517.5 | 4.2 | 532.0 | 0.36 | 1.56 | 2.3 | 4.1 | 525 |
| **3** | 511.5 | 10.7 | 521.5 | 0.94 | 5.90 | 1.6 | 0.10 | 375 |
| **3mA** | 510.5 | 8.0 | 522.5 | 0.95 | 4.48 | 2.1 | 0.11 | 450 |
| **3mB** | 519.5 | 5.5 | 569.0 | 0.07 | 0.28 (60%)<br>0.60 (40%) | 2.5 | 33.2 | 1675 |
| **3mC** | 510.5 | 7.5 | 521.5 | 0.93 | 5.02 | 1.8 | 0.14 | 415 |
| **3dA** | 519.5 | 13.0 | 530.0 | 0.90 | 3.78 | 2.4 | 0.26 | 380 |
| **3dB** | 607.0 | 9.6 | 623.5 | 0.70 | 3.83 | 1.8 | 0.78 | 435 |
| **4** | 545.0 | 6.8 | 552.0 | 0.82 | 6.77 | 1.2 | 0.26 | 230 |
| **4mA** | 537.0 | 6.4 | 555.0 | 0.41 | 2.81 | 1.5 | 2.1 | 605 |
| **4mB** | 520.5 | 3.7 | - | 0 | - | - | - | - |
| **4dB** | 642.5 | 5.3 | 665.0 | 0.73 | 2.50 | 2.9 | 1.1 | 525 |

*Data in ethanol.

**Table S2.** TD simulation (B3LYP/6-31g//PCM) of the electronic absorption transition (energy gap, $\Delta E_{ab}$, and oscillator strength, *f*) for the coumarin/BODIPY hybrids **2mA**, **2mB**, **2dA**, **3mA**, **3mB**, **3dA**, **3dB**, **4mA**, **4mB** and **4dB**, and the corresponding parent BODIPYs **2**-**4** in ethyl acetate.

| compound | $\Delta E_{ab}$ (eV) | *f* | compound | $\Delta E_{ab}$ (eV) | *f* | compound | $\Delta E_{ab}$ (eV) | *f* |
|---|---|---|---|---|---|---|---|---|
| **2** | 2.92 | 0.512 | **3** | 2.93 | 0.529 | **4** | 2.74 | 0.543 |
| **2mA** | 2.79 | 0.835 | **3mA** | 2.82 | 0.812 | **4mA** | 2.62 | 0.703 |
| **2mB** | 2.43 | 0.777 | **3mB** | 2.62 | 0.657 | **4mB** | 2.57 | 0.573 |
| **2dA** | 2.69 | 1.043 | **3dA** | 2.71 | 1.092 | **4dB** | 2.04 | 0.350 |
| | | | **3dB** | 2.28 | 0.321 | | | |